A NOVEL COMBINED PHAGE AND YEAST DISPLAY-BASED APPROACH TO DISCOVER BINDING DOMAINS FOR CAR T-CELL THERAPIES: FOCUS ON EBV-ASSOCIATED MALIGNANCIES

BY

ANTONIO JESÚS BARRENA DÍAZ, MSCI

THESIS SUBMITTED IN FULFILMENT OF THE REQUIREMENTS FOR THE DEGREE OF DOCTOR OF PHILOSOPHY

COLLEGE OF MEDICAL, VETERINARY AND LIFE SCIENCES

SCHOOL OF LIFE SCIENCES

UNIVERSITY OF GLASGOW

Funding a healthier future

MEDICAL RESEARCH SCOTLAND

JULY 2021

Abstract

It is estimated that more than 90% of the adult population worldwide is infected with the Epstein-Barr virus (EBV). The infection is associated with certain lymphomas and carcinomas, causing around 1% of all cancers and these are challenging to treat. Cancer immunotherapy is an approach to help the patient's body fight the disease by boosting antitumour immunity. A novel, cutting-edge immunotherapy treatment has been recently developed, among them the Chimeric Antigen Receptor T-cell therapy, also known as CAR T-cells.

CAR T-cells are modified T-cells designed to carry a gene coding for an artificial protein receptor (the CAR) able to recognise a specific tumour-associated antigen (TAA) and deliver a signal of T-cell activation by an HLA-independent interaction. The CAR can be designed in several ways by combining different domains obtained from existing proteins, including receptors expressed in T-cells and antibodies. The antigen-binding domain is the CAR domain able to interact with the TAA (typically on the target cell surface), triggering the activation singling cascade in the T-cells and thereby eliciting a T-cell response to the cancer cell. Single chain variable fragments (scFvs) are composite proteins derived from antibodies that have been commonly used as antigen-binding domains for CARs. Murine scFvs, formatted from existing murine antibodies obtained by mouse immunisation, have been used for the currently most successful CAR T-cell therapies, treating B-cell malignancies. However, mouse scFvs also increase the therapy's immunogenicity and have a negative outcome in efficacy and safety. Therefore, human scFvs are being used to develop new CAR T-cells therapies, and scFvs can be obtained from phage display libraries synthesised using B-cells from human donors.

In this research, a phage display library of human scFvs has been used to obtain scFvs to design CARs to treat EBV-associated malignancies. Three EBV TAAs, expressed in a wide range of EBV-associated malignancies, were selected to be targeted by the CARs: the human protein B7H4 and the viral proteins Latent membrane protein 1 (LMP1) and Latent membrane protein 2A (LMP2A). B7-H4 is a transmembrane immune checkpoint protein expressed on many cancer cells and tumour-associated macrophages. It acts to inhibit T-cell effector functions. LMP1 and LMP2A are viral proteins expressed on the plasma membrane of several EBV-

associated malignancies, such as Nasopharyngeal carcinoma, Hodgkin lymphoma, or Diffuse large B-cell lymphoma.

A novel combined phage and yeast display-based approach was developed to screen the phage display library. This new approach uses a yeast display platform as a source of antigen. The yeast express the membrane antigen on their surface, and the phage display library is panned against them. Then, after one or several rounds of phage selection and for the final steps of the selection, the system is flipped, and the selected pool of scFvs is expressed in the yeast display system. In these final steps, the yeast are exposed to adherent mammalian cells expressing the membrane antigen. The scFvs, on the surface of the yeast, bind to the antigen on the surface of the mammalian cells. The strength of interaction yeast-mammalian cells is boosted by avidity due to the high number of scFvs expressed on the surface of the yeast. This increases the chances of holding the binding yeast after several washes and washing off the non-binding yeast. This method helps to overcome phage display biases, limitations and, cost-effectively, allows the selection of scFvs. Using this new methodology, eleven anti-B7H4 scFvs were successfully isolated and one potential anti-LMP1 scFv. The anti-B7H4 scFvs show different strengths of interaction with B7H4, providing a diverse set of clones that can be used to explore the optimal affinity for an anti-B7H4 CAR T-cell therapy. Preliminary CAR constructs were designed using these novel isolated scFvs to perform functional characterisation. However, the expression of the CARs in a reporter T-cell line was challenging and their utility as CAR components remains to be determined. The next steps in this work will be to investigate the capacity of these scFvs to induce antigen-specific signalling in CAR format.

Table of contents

List of figures

List of tables

Acknowledgements

First and foremost, I would like to thank Medical Research Scotland for awarding me the studentship that funded this project, especially to Dr Alex M. Graham for always being available to help and support the students. Thanks also to TC Biopharm Ltd. for the economic contribution to this studentship.

I would like to thank my supervisor, Dr Joanna B. Wilson, for all the trust and guidance throughout these years and help in editing, correcting and finalising this thesis. I also truly appreciate her understanding in some difficult personal circumstances.

I would like to thank Lab 412/416 for a great environment, interesting meetings, and valuable feedback. Special thanks to Dr Marc Ciosi, for being always curious and helpful and provide me with the PCR custom buffer. Thanks also to Malak Ammar for the delicious baklavas and her help with CRISPR/Cas9.

I would like to thank Diane Vaughan from the flow cytometry core facility for her precious help with the FACS experiments. Also, a special mention to all the ladies in the autoclave room in the Davidson building. Thank you for your hard work to consistently provide glassware and medium.

I would like to dedicate this thesis to my family, especially my mother. Thanks for being a wonderful mother and for the unconditional love and care. To the memory of my grandparents, Julian and Dominga. For all these years of happiness in Brovales during my childhood. To my partner, Carmen, for being instrumental in building the person I am today and a future together. Thanks for supporting me in every decision and for your patience and love.

I want to conclude with this special dedication to an exceptional person that is no longer with us. Thank you for all these years of crazy parties and adventures, endless laughs, terrible hangovers and pure friendship. Thanks for being an example of generosity and strength. Thanks for your support and encouragement. You always knew I could achieve my goals. I could not wish for a better friend. This thesis seems like the end of a long way, and it is dedicated to you, Tomás Gomez Martín.

Author's declaration

I declare that the work presented in this thesis represents the original work carried out by the author in the laboratory of Dr Joanna B. Wilson and has not been previously submitted in any form for a higher degree. Where use has been made of materials or data provided by others, due acknowledgments have been made. This thesis is being submitted for the degree of Doctor of Philosophy at the University of Glasgow.

Antonio Jesús Barrena Díaz

July 2021

Abbreviations

˚C	Degree celsius
κVL	Kappa variable light chain
µg	Microgram
µl	Microlitre
µM	Micromolar
µm	Micrometre
aa	Amino acids
AAVS1	Associated virus integration site 1
ADCC	Antibody-dependent cellular cytotoxicity
ADCP	Antibody-dependent cellular phagocytosis
AIDS	Acquired immune deficiency syndrome
aka	Also known as
ALL	Acute lymphoblastic leukaemia
APC	Antigen presenting cells
aAPC	Artificial APC
BARTs	*Bam*HI A rightward transcripts
BCR	B-cell receptor
BL	Burkitt lymphoma
bp	Base pair
BSA	Bovine serum albumin
BTLA	B and T-lymphocyte attenuator
CAIX	Carbonic anhydrase IX
CAR	Chimeric antigen receptor
CDR	Complementarity-determining regions
CEA	Carcinoembryonic antigen
CFU	Colony-forming units
CHO	Chinese hamster ovary cells
CR2	Complement receptor type 2
CRISPR	Clustered regularly interspaced short palindromic repeats
crRNA	CRISPR RNA
CRS	Cytokine release syndrome
CTAR	C-terminal activating region
DAP	DNAX-activating protein
DC	Dendritic cells

dH_2O	Deionised water
DLBCL	Diffuse large B-cell lymphoma
DNA	Deoxyribonucleic acid
dNTPs	Deoxynucleoside triphosphates
EA	Early antigen
EBERs	Epstein–Barr virus-encoded small RNAs
EBNA	Epstein-Barr virus nuclear antigen
EBV	Epstein-Barr virus
ECL	Enhanced chemiluminescence
EGFRt	Truncated epidermal growth factor receptor
ELISA	Enzyme-linked immunosorbent assay
EMA	European medicines agency
ENKTCL	Nasal-type extranodal NK/T-cell lymphoma
FACS	Fluorescence-activated cell sorting
FBS	Foetal bovine serum
FDA	Food and drug administration
FRT	FLP recombination target
FVIII	Factor VIII
GA	Gastric adenocarcinoma
gRNA	Guide RNA
GC	Germinal centres
GCV	Ganciclovir
GFP	Green fluorescent protein
GMP	Good manufacturing practices
GVHD	Graft versus host disease
HAS	Human serum albumin
HDR	Homology-directed repair
HIV	Human immunodeficiency virus
HL	Hodgkin lymphoma
HLA	Human leukocyte antigen
HLH	Hemophagocytic lymphohistiocytosis
HR	Homologous recombination
HRP	Horseradish peroxidase enzyme
HSC	Hematopoietic stem cells
HSV-tk	Herpes simplex virus type 1 thymidine kinase
iCAR	Inhibitory CAR

iCasp9	Inducible caspase-9
IFT	Immunofluorescence antibody testing
IM	Infectious mononucleosis
IMGT	ImMunoGeneTics
iPSC	Induced pluripotent stem cells
IRF	Interferon regulatory factor
ITAM	Immunoreceptor tyrosine-based activation motif
Ig	Immunoglobulin
kb	Kilobase
kDa	Kilodalton
KIR	Killer-cell immunoglobulin-like receptor
LAT	Linker for activation of T-cells
Lck	Lymphocyte-specific protein tyrosine kinase
LEC	Lymphoepithelioma-like carcinoma
LMP	Latent membrane protein
lN2	Liquid nitrogen
M	Molar
mA	Milliampere
mAb	Monoclonal antibody
MAS	Macrophage activation syndrome
MCL	Mantle cell lymphoma
MFI	Mean fluorescent intensity
mg	Milligram
MHC	Major histocompatibility complex
MHRA	Medicines and healthcare products regulatory agency
MIZ-1	Myc-interacting DNA-binding zinc finger protein 1
ml	Millilitre
mM	Millimolar
MMEJ	Microhomology-mediated end joining
MOG	Myelin oligodendrocyte glycoprotein
MS	Multiple sclerosis
na	Not applicable
NFM	Non-fat milk powder
ng	Nanogram
NGS	Next-generation sequencing
NHEJ	Non-homologous end joining

NK	Natural killer
nM	Nanomolar
NPC	Nasopharyngeal carcinoma
NPM	Nucleophosmin
nt	Nucleotide
OD	Optical density
OND	Oligodeoxynucleotides
ORF	Open reading frame
PAM	Protospacer adjacent motif
pAgs	Phosphoantigens
PBMC	Peripheral blood mononuclear cells
PCR	Polymerase chain reaction
pRb	Retinoblastoma tumour suppressor protein
PTLD	Post-transplant lymphoproliferative disorders
RLUs	Relative light units
RNA	Ribonucleic acid
RNP	Ribonucleoprotein
rpm	Revolutions per minute
rSAP	Shrimp alkaline phosphatase
RT-PCR	Reverse transcription polymerase chain reaction
scFv	Single-chain variable fragment
SEAP	Secreted embryonic alkaline phosphatase
SPR	Surface plasmon resonance
synNotch	Synthetic Notch
TAA	Tumour associated antigen
TALEN	Transcription activator-like effector nucleases
TCR	T-cell receptor
TetR	Tet repressor protein
Tfh	T-follicular helper
TFS	Thermo Fisher scientific
TGFß	Transforming growth factor-beta
Th17	T-helper 17
TIDE	Tracking of indels by decomposition
Tm	Melting temperature
TLR	Toll-like receptor
TME	Tumour microenvironment

TNF	Tumour necrosis factor
TNP	Trinitrophenyl
tracrRNA	Trans-activating CRISPR RNA
TRADD	TNF receptor type 1-associated death domain protein
TRAF	TNF receptor associated factor
TRUCKs	T-cells redirected for universal cytokine killing
U	Units
v	Volume
V	Voltage
VCA	Virus capsid antigens
VH	Variable heavy chain
VHH	Variable heavy homodimers
VL	Variable light chain
vNAR	Variable new antigen receptor domain
w	Weight
W	Watt
wt	Wild type
xg	Times gravity
ZAP70	Zeta-chain-associated protein kinase 70
ZFN	Zinc finger nuclease

1. Introduction

1.1 Epstein-Barr virus

The Epstein-Barr virus (EBV), or human herpesvirus 4 (HHV-4), is one of the most common viruses in humans. Seroepidemiologic studies indicate that more than 90% of adults worldwide have been infected with EBV (1). The infection usually takes place during childhood, and then the virus persists as a latent and asymptomatic infection of B-cells. EBV was discovered in 1964 in a B-cell line obtained from a Burkitt lymphoma, which was the first established cell line from human lymphoma (2). Later studies with the EBV also provided the first evidence of cellular transformation by a viral infection, as such, EBV was the first human tumour-associated virus to be discovered (3).

EBV has a double-stranded DNA genome approximately 172 kilobase (kb) in length with 87 genes, including 11 latent genes (4). Among the proteins coded by latent genes, the latent membrane proteins (LMP1 and LMP2) and the Epstein-Barr virus nuclear antigens (EBNA1, EBNA2, EBNA-Leader protein, EBNA3A, EBNA3B and EBNA3C) have an important role in EBV infection and persistence. The viral genome also produces a group of non-coding RNAs which include the Epstein–Barr virus-encoded small RNAs (EBERs), the *Bam*HI A rightward transcripts (BARTs) miRNAs and the BHRF1 miRNAs. The early lytic protein BHRF1, an apoptosis regulator Bcl-2 homologue, is also expressed in some latently infected cells.

In its life cycle, the virus can switch between lytic and latent infections. Primary infection takes place in the oropharyngeal region. However, the early events of infection are poorly understood. Thorley-Lawson and Babcock proposed a model of EBV infection and persistence where EBV enters via saliva, crossing the epithelial barrier, into lymphoepithelial structures of the Waldeyer's ring (5,6). There, EBV infects naive B-cells and induces differentiation to blast cells through expression of the growth programme (known as latency 3). The blast cells undergo proliferative expansion and differentiation into resting memory B-cells. The resting memory B-cells enter the germinal centres (GC) and switch to the default programme (known as latency 2), expressing limited viral information to ensure survival of the infected cell and maintenance of the viral genome. Subsequently,

the infected resting memory B-cells leave the lymphoepithelium and go into the peripheral circulation. There, viral expression is further reduced entering the latency programme (comprising two stages known as latency 1 and latency 0), where the cells express minimal or no viral information. This allows the infected memory B-cell to avoid recognition by the immune system responses, being maintained as apparently normal memory cells. The non-coding RNAs are expressed in all the transcription stages, apart from the BHRF1 miRNAs, expressed only during the growth program, and a subset of BART miRNAs that are absent from the GC and memory compartments (table 1.1).

Latently infected cells can re-enter the lymphoepithelium from peripheral circulation where the default program is activated again in the GC. They can return to the peripheral circulation, where the latency programme is activated again, allowing the infecting cells to divide as memory B-cells. However, occasionally, a fraction of the infected cells fail to activate the default program in the lymphoepithelium and undergo terminal differentiation to become plasma cells, which initiates viral replication and the lytic cycle in the mucosal epithelium, expressing a total of 76 viral lytic genes (7). In this case, new viruses are produced by the infected cells and released by cell lysis into the saliva spreading the infection.

Table 1.1 EBV latency programmes as described by the Thorley-Lawson model of EBV infection and persistence.

Program	Latency	Site *in vivo*	Viral genes expressed
Growth	Latency 3	Tonsil naïve B-cells	EBNA1, EBNA2, EBNA-LP, EBNA3A, EBNA3B, EBNA3C, LMP1, LMP2, BHRF1, EBERs, BARTs and BHRF1 miRNAs
Default	Latency 2	Tonsil GC memory B-cells	EBNA1, LMP1, LMP2, EBERs and BARTs
Latency	Latency 1	Peripheral dividing memory B-cells	EBNA1, EBERs and BARTs
	Latency 0	Peripheral resting memory B-cells	EBERs and BARTs

EBV infection is lifelong, and the virus is never entirely eradicated. However, immune surveillance mechanisms keep this infection to a very in low grade (between 50 and less than 1 EBV genome copies per 10^6 periphery B-cells) (8). Despite EBV infection predominantly being asymptomatic, EBV infection is

associated with several diseases, including infectious mononucleosis (IM) and autoimmune diseases. Moreover, due to the transforming activity of the virus and the accumulation of cancer-promoting events in the cell, EBV infection is also associated with particular cancers where the presence of the virus in latency is an important factor for cell immortalisation. Each of these cancers typically shows a viral expression pattern of one of the latency programs (table 1.2).

Table 1.2 EBV-associated malignancies and EBV latency.

EBV-associated malignancies	EBV latent protein expression	Latency
Burkitt lymphoma	EBNA1	Latency 1
Nasal-type extranodal NK/T-cell lymphoma	EBNA1 and LMP2B*	-
Diffuse large B-cell lymphoma	EBNA1, LMP1 and LMP2	Latency 2
Hodgkin lymphoma	EBNA1, LMP1 and LMP2	Latency 2
Post-transplant lymphoproliferative disorder/lymphoma	EBNA1, EBNA2, EBNA-LP, EBNA3A, EBNA3B, EBNA3C, LMP1 and LMP2	Latency 3
AIDS-associated immunoblastic and primary central nervous system lymphoma	EBNA1, EBNA2, EBNA-LP, EBNA3A, EBNA3B, EBNA3C, LMP1 and LMP2	Latency 3
Gastric adenocarcinoma	EBNA1 and LMP2	-
Nasopharyngeal carcinoma	EBNA1, LMP1 and LMP2	Latency 2
Lymphoepithelioma-like carcinoma	EBNA1, LMP1 and LMP2	Latency 2
Leiomyosarcoma	EBNA1 and EBNA2	-

*LMP2B is expressed in the absence of LMP2A.

1.1.1 The EBV latent proteins

1.1.1.1 Latent membrane protein 1

The Latent membrane protein 1 (LMP1) (P03230, UniProtKB) is a viral protein expressed during latency 2 and 3 of EBV infection. It is comprised of 386 amino acids. Amino acids 1-24 form a short cytoplasmatic amino-terminal domain. Amino acids 25-186 form the transmembrane domain producing five loops (three extracellular in the case of plasma membrane localisation). Amino acids 187-386 form the C-terminal signalling domain (figure 1.1). LMP1 acts as a constitutively active receptor, mimicking the stimulation given by $CD4^+$ T-cells to B-cells through CD40-CD40L interaction and supporting the survival and proliferation of EBV-infected B-cells. It forms homo-oligomers in the membrane through the transmembrane domains, giving rise to signal transduction by the cytoplasmatic

C-terminal signalling domains (9). The interactions between transmembrane domains 3-6 and an FWLY motif in the transmembrane domain 1 and 2 mediate the oligomerisation needed for the signalling (10,11). Within the C-terminal signalling domain, there are three regions involved in cell signalling. The C-terminal activating region 1 (CTAR1) spans amino acids 194-232 and is responsible for the interaction of LMP1 with the cellular signalling molecules: Tumour necrosis factor (TNF) receptor associated factor (TRAF) 2 and TRAF3. The C-terminal activating region 2 (CTAR2) spans amino acids 351-386 and is accountable for the interaction with TRAF6 and TNF receptor type 1-associated death domain protein (TRADD). The C-terminal activating region 3 (CTAR3), amino acids 275-330, is responsible for the interaction with Ubc9 (12,13) and JAK3 (14) (figure 1.1). These three regions allow the activation by LMP1 of the signalling pathways NF-κB, MAPK/JNK, MAPK/ERK, P38 MAPK, PI3-K/AKT and IRF7. The activation of these signalling pathways is responsible for cell cycle progression, promotion of angiogenesis, inflammation and cell survival in B-cells and epithelial cells (15–17).

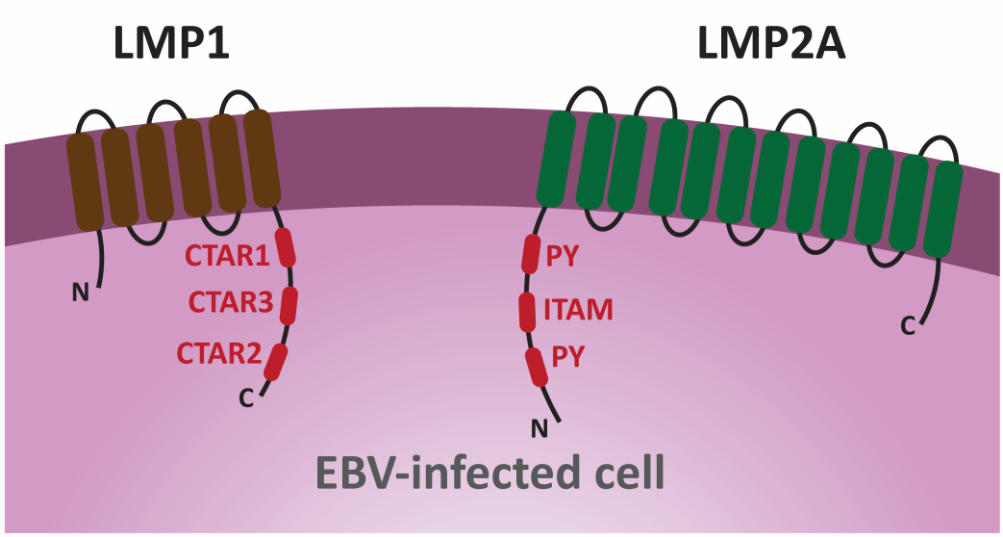

Figure 1.1 Diagrammatic representation of LMP1 and LMP2A shown in the plasma membrane of an EBV-infected cell. In brown LMP1 with its three extracellular loops and the C-terminal signalling tail with CTAR1, CTAR2 and CTAR3 in red. CTAR1, CTAR2 and CTAR3 allow the activation of NF-κB, MAPK/JNK, MAPK/ERK, P38 MAPK, PI3-K/AKT and IRF7. In green LMP2A with its six extracellular loops and the N-terminal signalling tail with the proline-rich PY and ITAM motifs in red. ITAM motif generates the BCR-like signalling through the recruitment of the cellular Lyn and Syk kinases and the PY motifs interact with E3 ubiquitin ligases.

1.1.1.2 Latent membrane protein 2

The Latent membrane protein 2 (LMP2) gene of EBV is expressed in latency 2 and 3 in EBV infection and produces two different transcripts from two separate

promoters: LMP2A and LMP2B, the latter differs from the former by the absence of the first exon. LMP2A (P13285-1, UniprotKB) is the longest isoform with 497 amino acids. Amino acids 1-119 form the amino-terminal signalling domain, amino acids 120-470 the twelve transmembrane domains with eleven loops (six extracellular in the case of plasma membrane localisation), and amino acids 471-497, the cytoplasmatic C-terminal domain (figure 1.1). LMP2A forms a homo-oligomeric complex due to the presence of a clustering signal located at the C-terminal domain (18,19). The formation of homo-oligomeric structures is required for LMP2A signalling activation. The isoform LMP2B (P13285-2, UniprotKB) lacks the amino-terminal signalling domain, encoded by exon 1 of LMP2A. LMP2B acts as a regulator of LMP2A activity by contributing to the formation of homo-oligomeric structures and inhibiting the phosphorylation of LMP2A (20). Signalling through LMP2A appears to mimic the B-cell receptor (BCR) signal (21,22). During an immune response in the germinal centres, EBV-infected B-cells undergo multiple rounds of antigen-driven proliferation and somatic hypermutation (5,23). The N-terminal cytoplasmatic domain of LMP2A has two proline-rich PY motifs and several phosphorylated tyrosine residues. Adjacent to the phosphorylated tyrosine residues, there is an immunoreceptor tyrosine-based activation motif (ITAM). Signalling via the ITAM motif generates the BCR-like signalling through the recruitment of the cellular Lyn and Syk kinases. The PY motifs also interact with E3 ubiquitin ligases, initiating ubiquitination-dependent proteasomal degradation of targeted cellular proteins (18,24,25). Together with the signalling of LMP1, LMP2A enhances the survival of EBV-infected B-cells in the competitive environment of the lymph nodes and promotes their differentiation into memory B-cells.

1.1.1.3 EBNAs

The EBV genome codes for six EBV nuclear antigens: EBNA1, EBNA2, EBNA-LP, EBNA3A, EBNA3B and EBNA3C.

It is involved in maintaining the viral episome in the cell and through replication and segregation (26) and contributes to the regulation of the expression of other latent genes. EBNA2 affects the host cell gene expression and has a central role in B-cell transformation. It induces the expression of the protooncogene *C-Myc* after infection, suggesting a critical role in the induction of B-cell proliferation

(27). It also acts as a transcriptional regulator of LMP1 and LMP2(28,29). EBNA-LP (aka EBNA5) cooperates with EBNA2 in the activation of the host cell and viral gene expression (30,31). The EBNA3 family is composed by EBNA3A (aka EBNA3), EBNA3B (aka EBNA4) and EBNA3C (aka EBNA6) and act as transcriptional regulators (32). EBNA3A and EBNA3C repress EBNA2 mediated transactivation (33). EBNA3A also prevents MIZ-1 (Myc-interacting DNA-binding zinc finger protein 1) from binding to its coactivator NPM (nucleophosmin), resulting in a transcription decrease of the cell cycle inhibitor CDKN2B (34). The role of EBNA3B is yet not clear, complete deletion from the EBV genome does not affect transformed B-cell growth *in vitro* (35), but the lack of EBNA3B promotes B-cell lymphomagenesis *in vivo* (36). EBNA3C can upregulate the expression of LMP1 and interact with pRb (retinoblastoma tumour suppressor protein) promoting cell transformation (37,38).

1.1.2 EBV-associated malignancies

The group of malignancies associated with EBV infection is comprised mostly of lymphomas but also carcinomas. It includes Burkitt lymphoma, diffuse large B-cell lymphoma, gastric adenocarcinoma, Hodgkin lymphoma, nasopharyngeal carcinoma, lymphoepithelioma-like carcinoma, nasal type extranodal NK/T-cell lymphoma, post-transplant lymphoproliferative disorder/lymphoma, acquired immune deficiency syndrome (AIDS)-associated immunoblastic and primary central nervous system lymphomas and leiomyosarcoma (39) (table 1.2).

EBV-associated malignancies vary in their typical age of onset, and the incidence varies with geographic location, environment and probably ethnicity. Poor hygiene and the high-density housing conditions more prevalent in developing countries, promote higher rates of primary infection in early life (1). The age of onset of the primary infection has potential relevance in the epidemiology of IM and EBV-associated cancers. Different patterns of expression of the EBV latent proteins have been observed in these malignancies, generally correlating with a specific latency program, however, there is some variability in this (table 1.2).

1.1.2.1 Burkitt lymphoma

Burkitt lymphoma (BL) is a B-cell lymphoma found in the germinal centre, generally presenting as oropharyngeal or abdominal tumour masses. BL cancers are classified into three types: endemic, sporadic, and AIDS-associated. Endemic BL is primarily a paediatric disease, strongly associated with malaria infection and prevalent in equatorial Africa and Papua New Guinea. Sporadic BL has a much lower incidence, wide age of onset range and worldwide occurrence. EBV is detected in 95% of endemic BL, but the association of EBV with sporadic cases is lower (5% to 10% EBV association). AIDS-related BL is more common in the general population, it occurs in the early stages of human immunodeficiency virus (HIV) immunosuppression, 30% to 40% of the cases are associated with EBV infection (40). BL is characterised by deregulation of c-Myc expression by a chromosomal translocation involving the *MYC* gene (location 8q24) and one of the three immunoglobulin loci. 80% of BL cases present the *MYC* translocation with the immunoglobulin heavy chain locus (14q32) and 20% with the kappa (2p12) or lambada (22q11) light chain loci (41–43).

1.1.2.2 Nasal-type extranodal NK/T-cell lymphoma

EBV infection is detected in approximately 90% of cases of nasal-type extranodal NK/T-cell lymphoma (ENKTCL). ENKTCL is relatively common in East Asia and Latin America, comprising around 3-10% of the non-Hodgkin lymphoma's cases, with onset in a wide range of ages. In Western countries, cases are uncommon, contributing less than 1% of the cases of non-Hodgkin lymphomas (44).

1.1.2.3 Diffuse large B-cell lymphoma

EBV infection is detected in 8-12% of all diffuse large B-cell lymphoma (DLBCL) in patients older than 50 years in Asian countries and less than 5% in Western countries. The median age for EBV-positive DLBCL is 71. It can affect young people, but the prevalence is low. EBV^+ status in DLBCL in the elderly patient is associated with poor prognosis, but this is not observed in younger patients (45–49). The main biological feature that differentiates EBV^+ DLBCL from EBV^- DLBCL is the activation of the NF-kB and JAK/STAT signalling pathways in the former (50,51).

1.1.2.4 Hodgkin lymphoma

Hodgkin lymphoma (HL) is a B-cell lymphoma characterised by the presence of Reed-Sternberg cells in an inflammatory environment. EBV infection has been detected in 40-50% of the cases of classical HL, but this proportion differs both geographically and with different sub-types. EBV infection has been detected in 100% of AIDS-related HL (52,53).

1.1.2.5 Post-transplant lymphoproliferative disorder/lymphoma

Post-transplant lymphoproliferative disorder/lymphoma (PTLD) comprises a group of diseases, primarily B-cell lymphomas, associated with induced immunosuppression, for example after organ transplantation. EBV infection is detected in 95% of these lymphomas. During immunosuppression, the immune system is unable to control EBV-infection and suppress viral loads. This is the primary contributing factor for the development of PTLD. In some cases, following the cessation of immunosuppression, regression of PTLD is observed. The risk of PTLD is elevated in patients that are negative for EBV infection before transplantation but where the transplant is EBV positive. PTLD is rare, but the incidence has risen with the increase in transplantation and the availability of novel immunosuppressive agents (54,55).

1.1.2.6 AIDS-associated immunoblastic and primary central nervous system lymphoma

AIDS-associated immunoblastic and primary central nervous system lymphomas are malignancies that can occur in the later stages of AIDS after HIV infection. EBV infection has been detected in approximately 90% of primary central nervous system lymphomas and up to 70% of immunoblastic lymphomas. No HIV infection is detected in these lymphomas, suggesting that there is not a direct involvement of HIV in the tumour development and that it is the consequent immunosuppression that is causal (56,57).

1.1.2.7 Gastric adenocarcinoma

Gastric adenocarcinoma (GA) represents 95% of the malignancies of the stomach, and it is the third leading cause of cancer deaths worldwide. EBV is detected only in approximately 10% of GA cases, but due to the prevalence, GA is one of the

most common EBV-associated malignancies. EBV^+ GA is two times more common in males than in females, but little is known about the epidemiology (58).

1.1.2.8 Nasopharyngeal carcinoma

Nasopharyngeal carcinoma (NPC) is a rare type of cancer affecting the nasopharynx (the upper part of the throat behind the nose) endemic in Southern China and Southeast Asia. While the incidence rate in most regions is <1 per 100,000 person-year, in Hong Kong the incidence is >20 cases per 100,000 person-year. Non-keratinizing NPC is the most common histological subtype comprising over 95% of NPC in high-incidence areas. In this subtype of NPC EBV is detected in 100% of the cases. Factors that influence NPC pathogenesis include EBV infection, but also environmental factors and genetic susceptibility. Among the environmental factors, consumption of salt-preserved fish and other preserve food, alcohol and smoking are noted risk factors. Regarding the genetic susceptibility, there is a strong association between NPC risk and the *HLA* (Human leukocyte antigen) loci and adjacent genes in the *MHC* (Major histocompatibility complex) region on chromosome 6p21 (59–61). HLA-A2, B14, B17 and B46 have been associated with increased NPC risk (62,63). HLA alleles leading to reduced ability to present EBV antigens may be linked with increase in risk for developing NPC. Furthermore, an NPC susceptibility locus containing the *HLA-A* region located between the D6S510 and D6S211 microsatellite markers has been identified (64).

1.1.2.9 Lymphoepithelioma-like carcinoma

Lymphoepithelioma-like carcinoma (LEC) is a rare malignancy with morphologic features like undifferentiated NPC, but it occurs outside of the nasopharynx. EBV infection has been detected in LEC of the stomach, salivary gland, lung and thymus. It also occurs at lower incidence in the skin, uterine cervix, tonsil, oral cavity, trachea, larynx, urinary bladder and vagina. The genetic and environmental factors associated with NPC may also influence the risk of developing EBV-associated LEC. The association of EBV with LEC is not well characterised (65).

1.1.2.10 Leiomyosarcoma

Leiomyosarcoma is a rare type of cancer that affects smooth muscle tissue. It typically occurs in the uterus, gastrointestinal tract and in soft tissues, where it is classified as cutaneous or subcutaneous. EBV infection has been detected in leiomyosarcomas of immunocompromised patients. However, leiomyosarcomas among immunocompetent individuals are EBV-negative. EBV is detected especially in the case of children with AIDS, and it is the second most common cancer in this patient group. HIV is not found in leiomyosarcoma tumour tissue, suggesting it is not directly related to carcinogenesis (66,67).

1.1.3 The immune response against EBV

The immune response against EBV infection involves innate, the adaptive cellular and the adaptive humoral immunity. In immunocompetent hosts, the immune system controls the infection during both lytic and latency programmes (68).

1.1.3.1 The cellular response to EBV infection

During primary infection, the lytic and latent proteins induce the expansion of EBV-specific $CD4^+$ and $CD8^+$ T-cells and the activation of Natural killer (NK) cells (68) (figure 1.2.A). Lytic peptides are the main drivers of the T-cell response, but latent peptides also trigger an antigen-specific T-cell response. The latent peptides belong predominantly to the EBNA3 family and less frequency to LMP2. LMP1-specific T-cell responses are very rare and strong EBNA-1-specific T-cell responses associated with specific HLA types have also been observed, but the frequency is low (69–71). After the T-cell response to EBV, a small population of memory T-cells persist as tissue-resident memory cells and circulating memory cells maintaining the immune surveillance and controlling the infection (72).

NK cells are characterised for their cytotoxicity against viral infected and tumour cells. The expansion of Killer-cell immunoglobulin-like receptor (KIR) negative NK cells during EBV infection have been described (73), but not the expansion of KIR^+ NK cells (74). The expression of CD94/NKG2 family receptors controls the activation (NKG2D, NKG2C, NKG2E, NKG2H and NKG2F) or inhibition (NKG2A, NKG2B) of the cytotoxic activity of NK cells. NKG2D homodimers recognize MICA/B, nonclassical MHC glycoproteins class I. NKG2A or NKG2C heterodimers

recognize HLA-E, which often presents classical MHC class I heavy chain signal peptides (75,76).

$CD8^+$ NK T-cells (NKT cells) displaying cytotoxicity against HL and NPC cells have been identified, suggesting that NKT cells can also restrict EBV-induced tumorigenesis (77). NKT cells recognise glycolipids presented on the non-classical MHC class I molecule CD1d by the Vα24-Jα18/Vß11 T-cell receptor (78,79). Data suggest that during EBV infection, CD1d ligands are expressed, and NKT cells could be a significant barrier in early innate control of EBV infection. Then, a downregulation of CD1d may allow circumvention of the NKT cell-mediated cytotoxicity (80).

T-cells of γδ subtype, specifically Vγ9Vδ2 and Vδ1, are also expanded when they are exposed *in vitro* to EBV-infected cells (81,82). Vγ9Vδ2 T-cells recognise diphosphate-containing metabolites, also named phosphoantigens (pAgs), in complex with the receptor BTN3A1. The nature of the interaction between the Vγ9Vδ2 T-cell receptor (TCR), pAgs and their receptors is still a matter of study (83). So far, it is known that the pAgs bind the B30.2 intracellular domain of BTN3A1 and then, the Vγ9Vδ2 TCR engages the BTN2A1–BTN3A1 complex via two different binding sites: the Vγ9 framework regions bind to BTN2A1, while the Complementarity-determining region 2 (CDR2) of the Vδ2 chain and the CDR3 of the Vγ9 possibly bind the BTN3A1 (84). Vγ9Vδ2 and Vδ1 T-cells also recognised target cells by the expression of the receptor NKG2D.

1.1.3.2 The humoral response to EBV infection

During EBV primary infection different individual antigen complexes are observed driving the humoral response. These complexes have been defined by Burkitt lymphoma cell-based immunofluorescence antibody testing (IFT). Antigen complexes could be formed by proteins and polypeptide fragments, protein–DNA/protein–RNA complexes, glycoproteins and glycolipids. The main antigen complexes that drive the humoral response during EBV primary infection are the virus capsid antigens (VCA), the early antigen complexes (EA) and the EBNA complexes. The VCA are composed of virion structural proteins. EA complexes are composed of regulatory proteins synthesised to allow the production of viral DNA, the virion structural proteins and membrane proteins. EBNA complexes consist of

different DNA-binding proteins (EBNA1, EBNA-LP, EBNA2, EBNA3A, EBNA3B and EBNA3C), but of these, the humoral response is dominated by EBNA1. The evolution of EBV-specific antibody response during primary infection, convalescence and latent infection and reactivation is well described (figure 1.2.B) (85,86).

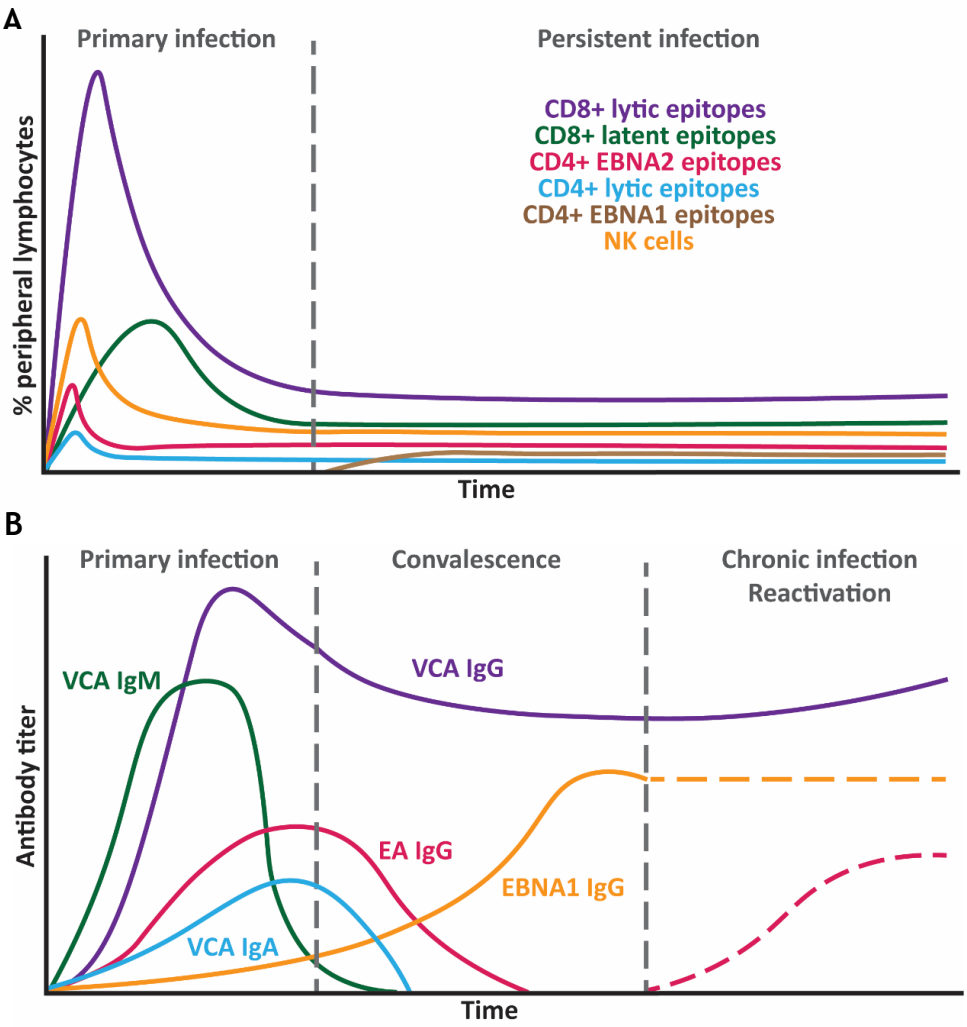

Figure 1.2 The immune response against EBV. A) Cellular response to EBV infection. Figure adapted from Taylor et al. 2015. B) Humoral response to EBV infection. The dashed lines for EBNA1 IgG indicate possible alteration in when developing chronic (loss) or malignant (gain) disease. For EA IgG indicates increase in chronic or malignant disease. Figure adapted from Middeldorp et al. 2015 (86).

1.1.3.3 Immune evasion strategies of EBV

The immune response can control EBV infection, but the virus is not eliminated and persists in a latent state. During the lytic cycle, EBV has developed strategies to overcome the immune response. During latency, EBV limits viral protein expression, which restricts the immune response. Furthermore, the expressed proteins also display immunomodulatory functions (87) (table 1.3).

Table 1.3 Immunomodulatory functions of EBV lytic and latent proteins.

EBV protein	Infection stage	Immunomodulatory functions*
BNLF2a	Lytic	Depletes peptides from the ER through inhibiting peptide transport
BGLF5	Lytic	HLA class I and class II downregulation Downregulates TLR2 and TLR9
BILF1	Lytic	Downregulates HLA class I
gp42	Lytic	Downregulates HLA class II
BZLF1	Lytic	Downregulates HLA class II Inhibits IFNα4 and IFNß promoters Inhibits NF-κB expression Reduces expression of TNFα and IFNγ receptor Favour type I IFN irresponsiveness Induces immunosuppressive TGFß expression
BRLF1	Lytic	Reduces expression of IRF3 and IRF7
BILF4	Lytic	Inhibits IRF7 to suppress IFNα production
BGLF4	Lytic	Inhibits IRF3 activity Reduces IFNß production Suppresses NF-κB activity
BPLF1	Lytic	Interferes with TLR- and LMP1-mediated NF-κB activation
BARF1	Lytic	Neutralises effects of CSF-1
BLLF3	Lytic	Compromises lymphocyte responses and proliferation Induces NF-κB activity through TLR2 Induces production of pro-inflammatory cytokines and IL-10
BCRF1	Lytic	Inhibits antiviral $CD4^+$ T-cell responses Inhibits co-stimulatory molecules on human monocytes
EBNA1	Latent	Inhibition of its translation and degradation Inhibition of the NF-κB pathway Modulation of STAT1 and TGFß pathways
ENBA2	Latent	Induces low level of IFNß production Inhibits production of selective ISGs Enhances STAT3 activity Upregulates IL-18 receptor
LMP1	Latent	Mimic CD40 signalling Induces type I IFN production Induces STAT1 and STAT2 activity Upregulates IRF7 Reduces TLR9 expression
LMP2A	Latent	Inhibits NF-κB activity Inhibits IL-6 production Induces NF-κB activity Accelerates turnover of IFN receptors
LMP2B	Latent	Accelerates turnover of IFN receptors

*Reviewed in Ressing et al. 2015 (87).

1.1.4 Current status of vaccination and therapies to treat EBV infection and EBV-associated diseases

The prevention of EBV infection would probably have a significant impact on public health, given the diversity of diseases linked to EBV infection. However, despite thorough research, there is still not clinically approved EBV vaccine able to prevent EBV infection of B-cell and epithelial cells or eliminate infected cells. Another strategy for EBV vaccination is the development of non-prophylactics vaccines to treat EBV-associated diseases (88).

1.1.4.1 Prophylactic EBV vaccination

A prophylactic vaccination has as a goal the induction of a neutralising antibody response against a pathogen or a toxin. In the case of EBV, T-cell immunity plays an essential role in restricting viral growth during primary exposure. Therefore, two different approaches have been tried for EBV prophylactic vaccination: vaccines directed to promote humoral immunity and vaccines directed to promote cellular immunity (89).

The main target for humoral prophylactic vaccination against EBV is the virion surface glycoprotein gp350. gp350 initiates virion attachment to the host B-cell by binding the Complement receptor type 2 (CR2) and facilitates the interaction of the viral protein gp42 to HLA class II, then triggering membrane fusion and the invasion of the cell. A gp350 deficient virus can still infect the cell, but this is less efficient. In a phase II clinical study with 181 seronegative adults and using recombinant gp350 purified from the supernatant of Chinese hamster ovary cells (CHO), 97% of the vaccinated group showed gp350 seroconversion and reduced incidence of IM compared to the placebo group. 8 of 90 individuals in the placebo group developed IM while only 2 of 86 did it in the sample group. However, these numbers cannot be considered as evidence of protection against asymptomatic infection. The study suggested that this vaccine is safe, but its formulation is a limitation, three doses were needed to generate a neutralising antibody response (90). A tetrameric gp350 formulation has shown improvement in the antibody titre compared to the monomeric formulation, also boosting T-cell immunity in preclinical studies (91).

Other approaches for EBV vaccination have been also studied. Vaccination with EBNA3 HLA-B8 restricted epitope was well tolerated and induced T-cell epitope-specific responses in phase I clinical trials. Nevertheless, all the vaccinated individuals were asymptomatically infected post-vaccination (92). Pavlova et al. generated EBV-like particles for EBV vaccination. These particles are created in mammalian cell lines expressing EBV genes but with no capacity to package the viral DNA into virions (93).

Importantly, once EBV infection is established, the humoral response has little influence in controlling the latently infected B-cells beyond EBV reactivation. It is also unlikely that a pre-existing T-cell immunity would have the capacity to prevent the establishment of latent infection, based on the low frequency of T-cells responding to EBV latent antigens.

1.1.4.2 Vaccine therapy to treat EBV-associated diseases

The potential of the EBV latent proteins to promote oncogenic transformation limit the use of the full-length versions in any EBV vaccine using coding DNA. Using truncated proteins or just epitopes is an approach to overcome this problem.

Dendritic cell (DC) based vaccines have been tested in clinical trials with LMP antigens for NPC patients. These vaccines consisted of the infusion of EBV peptide-pulsed monocyte-derived DC or adenovirus modified DC to express a truncated version of EBV antigens (94,95). Chia et al. tested their vaccine in sixteen patients with advance NPC, the vaccine was safely administered but the efficacy was limited. They observed induction of an LMP1 and LMP2 specific T-cell response *in vitro* with DC vaccination but fail to observe increase in the frequency of peripheral LMP1 and LMP2 specific T-cells in the patients (95). Furthermore, the difficulties in preparing DC vaccines (especially in mass format) make this approach impractical to treat NPC.

The use of recombinant antigens offers safety advantages compared to other approaches using coding DNA, but its efficacy depends on the capacity of the preparation to be efficiently taken and processed by antigen-presenting cells (APC). EBNA1 is expressed in all EBV-associated malignancies and it is the minimal EBV gene product able to drive oncogenicity (96). DC express endocytic receptors

to deliver antigens for HLA presentation to $CD8^+$ and $CD4^+$ T-cells. The receptor DEC-205 was used to deliver EBNA1 by the creation of a fusion protein with the C-terminus of the antibody heavy chain of anti-human DEC-205 (αDEC-E1) with the amino acids 400-641 of EBNA1. Immunisation of humanised mice with the fusion protein promoted DC-activation of EBNA1-specific $CD4^+$ and $CD8^+$ T-cell responses and induction of anti-EBNA1 antibodies. Nevertheless, the $CD4^+$ T-cell responses were prominent compared to the $CD8^+$ T-cell responses (97).

The incorporation of viral epitopes from LMP1, LMP2 or EBNA1 delivered by viral vectors may be more viable to treat EBV-associated malignancies. Due to its good safety profile and capacity to induce T-cell and B-cell responses in humans, the Modified Vaccinia Ankara (MVA), an attenuated strain of the vaccinia virus, has been used to test EBNA1 and LMP2 targeting vaccines. An MVA vaccine was designed to encode a fusion protein of the C-terminal half of the EBNA1 protein and the full-length LMP2 protein. Its safety and its capacity to expand both EBNA1- and LMP2-specific $CD4^+$ and $CD8^+$ T cells in NPC patients have been evaluated in two phase I clinical trials with encouraging results (98,99). Hui et al. treated 18 patients with three doses over a period of 9 weeks, 12 of 18 patients and 9 of 18 patients showed an increase in their IFN-γ response to EBNA1 and LMP2 respectively and response rates were higher in patients who received the highest dose. Hui et al. showed that the vaccine is both safe and immunogenic and they postulated that it could be used to maintain remission following primary treatment (98).

Furthermore, Rühl et al. found that adenoviral delivery of EBNA1 allowed higher $CD8^+$ T-cell stimulation than αDEC-E1 or MVA-encoding EBNA1. It was observed that heterologous prime-boost vaccinations for $CD4^+$ T-cell priming by either αDEC-E1 or MVA-encoding EBNA1 need to be combined with $CD8^+$ T-cell priming by EBNA1-encoding adenovirus to establish efficient long-term immune control of EBNA1-expressing lymphomas in mouse models, demonstrating that heterologous vaccination against EBNA1 is effective in treating $EBNA1^+$ T and B-cell lymphomas in the model systems (100).

1.1.4.3 T-cell therapy to treat EBV-associated diseases

T-cell immunity plays an important role in the control of EBV infection. EBV-associated malignant cells express viral proteins that contribute to the malignant transformation. Therefore, these viral proteins are potential targets for T-cell immunotherapy. The latent nuclear proteins EBNA1, EBNA2, EBNA3A, EBNA3B, EBNA3C and EBNALP are expressed intracellularly, and they are challenging to target adequately with an antibody-mediated therapy. However, they can be processed to peptides and be presented via the HLA class I and II molecules on the surface of infected cells. The membrane proteins LMP1 and LMP2 are located in the membranes of organelles and also the plasma membrane. They are also processed intracellularly into peptides and presented via in the HLA class I and II complexes. The EBV latent proteins are an attractive target for viral antigen-specific T-cells. Nevertheless, their recognition is dependent on HLA expression (101).

It has been reported that the infusion of peripheral lymphocytes from an EBV-positive donor contains enough EBV specific T-cells to induce complete responses (disappearance of all signs of cancer in response to treatment) in patients with donor-derived PTLD after allogeneic stem cell transplantation. However, this infusion also included large numbers of alloreactive T-cells and caused severe graft-versus-host disease (GVHD) (102). Infusing non-alloreactive EBV specific T-cells, generated by stimulating donor lymphocytes with EBV-transformed lymphoblastoid cells derived from donors, led to a complete response with no significant acute or chronic GVHD (103,104).

EBV-associated malignancies with EBV infection in latency 2, only express the viral proteins EBNA1 and LMP1 and LMP2. EBNA1 peptides are poorly presented by HLA Class I molecules because of the internal glycine-alanine repeats regions. These repeats inhibit translation and proteasomal degradation of EBNA1 by interfering the processing by the 19S proteasomal subunit, thus low levels of EBNA1 are expressed to maintain the viral genome while minimising the antigen presentation (105–109). Several peptides derived from LMP1 and LMP2 have been identified to be cognate in some HLA class I alleles, but the number of circulating LMP1 and LMP2 reactive T-cells in an individual is low. Treating latency 2 tumours with EBV specific T-cells is therefore challenging. Nevertheless, T-cells specific for LMP1

and LMP2 have been expanded and used for adoptive therapy in patients with different EBV-associated lymphomas with EBV infection in latency 2. From 21 patients with active EBV-associated lymphoma at the time of the infusion, 13 had clinical responses (improvement of the risk/benefit ratio in response to treatment), including 11 complete responses (110). LMP1 and LMP2 specific T-cells have also been engineered to express the dominant-negative transforming growth factor-beta type II receptor (dn-TGFßRII) and used to treat patients with relapsed HL (111,112). TGFß (transforming growth factor-beta) is secreted by these malignant cells and the stroma surrounding the tumorigenic cells, thereby promoting tumour growth and metastasis and inhibiting APCs and the effector function of T-cells and NK-cells (113). Expressing dn-TGFßRII would block signalling by all three TGFß isoforms in T-cells, avoiding the suppression of the T-cell immunosurveillance. 4 of the 7 patients evaluated in this clinical trial achieved clinical responses and 2 of them complete and ongoing response for more than four years. There was also one patient who had only a partial response to unmodified LMP1 and LMP2 specific T-cells (111).

EBV-associated malignancies with EBV infection in latency 1 only express the latent protein EBNA1, which is poorly presented by the HLA class I system, and therefore, the $CD8^+$ effector T-cells cannot carry out an effective cytotoxic action. However, EBNA1 contains numerous epitopes effective in the HLA class II (114). It has been shown that EBNA1 can also be presented by some specific HLA class I alleles (115). Therefore, EBNA1 can induce both $CD4^+$ helper and $CD8^+$ T-cells (116). Nevertheless, the clinical efficacy of expanded EBV specific T-cells has not been evaluated yet for BL.

Furthermore, there is increasing evidence of a role played by EBV in the pathogenesis of multiple sclerosis (MS) (117–119). In a clinical study treating progressive MS patients with *in vitro*-expanded autologous EBV-specific T-cells targeting EBNA1, LMP1 and LMP2, seven out of ten patients treated showed clinical improvement and no toxicities (120). This suggests that EBV-specific T-cells could also be used for treating MS.

1.1.4.4 Antibody therapy to treat EBV-associated diseases

LMP1 and LMP2A are the most suitable EBV proteins to be targeted with an antibody due to their location on the plasma membrane of the EBV-infected cell. However, both proteins have several transmembrane domains and small extracellular loops (figure 1.1). The development of antibodies targeting these extracellular loops is a challenging affair due to the low exposure of these loops on the cell. Therefore, antibodies targeting the complex peptide-HLA have been developed for targeting LMP1 and LMP2A, showing antitumor activity against EBV malignancies (121,122). These antibodies recognise specific cognate peptides in conjunction with specific HLAs, limiting their use to patients carrying these HLA alleles.

Two antibodies targeting extracellular loops of LMP1 and LMP2 have been developed, and their potential use as therapeutic tools revealed in preclinical studies (123–126). Chen et al. isolated, from a Fab phage display library previously developed by Jiao et al., an anti-LMP1 Fab targeting an extracellular loop of LMP1. The specific loop targeted by this antibody is unknown as they used in their phage selection a preparation composed of all three extracellular loops from LMP1. They also demonstrated that by conjugating this Fab with mitomycin C it could inhibit the growth rate of NPC xenografts in a mouse model (123,127). Cao et al. isolated from the same phage display library an anti-LMP2 Fab targeting an extracellular loop of LMP2. The specific loop is also unknown as the phage display selection was performed by panning with cells expressing LMP2A and the isolated clones screened by ELISA with a mix of polypeptides comprising all the extracellular loops of LMP2. They also show this Fab can inhibit the proliferation of LMP2A-positive NPC cells *in vitro* (125). Furthermore, Ammous-Boukhris et al. isolated from a peptide phage display library a peptide named B1.12, with amino acid sequence ACPLDLRSPCG, able to bind to the extracellular loop 1 of LMP1. NPC cells expressing LMP1 treated with B1.12 showed decreased cell viability and G0/G1 cell cycle arrest (128).

1.1.5 B7H4 as tumour associated antigen

B7H4 (aka B7S1, B7X or B7h.5) is encoded by the gene *VTCN1* and belongs to the B7 family of immunoregulatory proteins. The B7 family is a set of membrane

proteins with extracellular immunoglobulin-like domains, necessary for the interaction with their ligands (table 1.4). They are expressed in different cell types, including APC, T-cells, and tumour cells.

Table 1.4 B7 family proteins.

Name	Alternative name	Ligand
B7-1	CD80	CD28, CTLA-4
B7-2	CD86	CD28, CTLA-4
B7DC	PDCD1L2, PD-L2 and CD273	PD-1
B7H1	PD-L1 and CD274	PD-1
B7H2	ICOSL, B7RP1 and CD275	ICOS
B7H3	CD276	*Unknown*
B7H4	VTCN1	*Unknown*
B7H5	VISTA, Platelet receptor Gi24 and SISP1	*Unknown*
B7H6	NCR3L1	NKp30
B7H7	HHLA2	CD28H

B7H4 was identified in 2003 by three independent groups (129–131). While mouse B7H4 (Q7TSP5, UniprotKB) is a glycosyl-phosphatidylinositol-anchored membrane protein (130,132), human B7H4 (Q7Z7D3, UniprotKB) is described as a type I membrane protein. Despite this, the proteins share approximately 87% amino acid identity, and the functionality appears to be the same (129). Human B7H4 is a 282 amino acid protein that includes a signal peptide (amino acids 1-24), an extracellular domain (amino acids 25-259), a transmembrane domain (amino acids 260-280), and a short intracellular domain (amino acids 281 and 282). The extracellular domain is composed of two different immunoglobulin-like domains: Ig-like V-type 1 (amino acids 35-146) and Ig-like V-type 2 (amino acids 153-241) (figure 1.3).

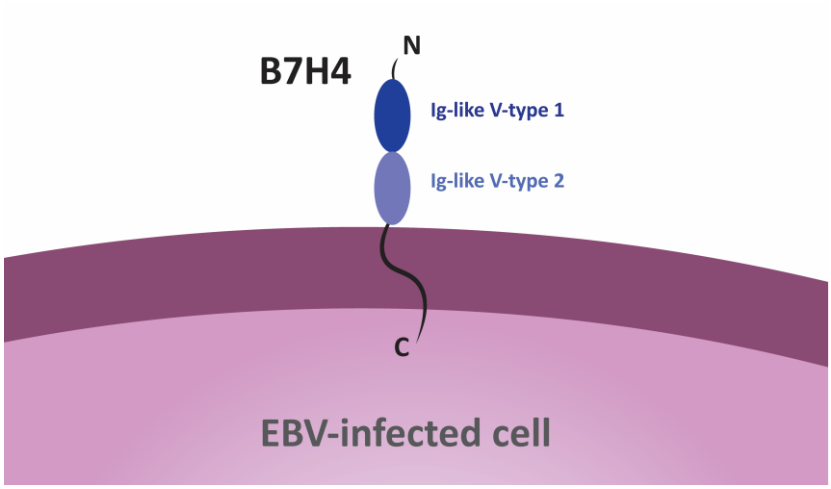

Figure 1.3 B7H4 in the plasma membrane of an expressing cell, in this case an EBV-infected cell. Domain Ig-like V-type 1 is believed to interact with the B7H4 unknown receptor.

An increase in the expression of B7H4 has been detected in multiple cancers, including: breast cancer, ovarian cancer, uterine endometrioid adenocarcinoma, prostate cancer, melanoma, oesophageal squamous cell carcinoma, gastric cancer, non-small cell lung cancer, pancreatic cancer, cervical carcinoma, oral squamous cell carcinoma, gallbladder carcinoma, non-Hodgkin lymphoma, pleural adenocarcinoma, hepatocellular carcinoma and colorectal cancer (133,134,143–149,135–142). Moreover, its expression has also been reported in an immunosuppressive population of macrophages present in tumour microenvironment (TME) (146,150,151). The protein termed B and T-lymphocyte attenuator (BTLA) has been proposed as the receptor for B7H4, but an interaction of recombinant soluble B7H4 with cells expressing BTLA could not be demonstrated (152,153). Therefore, the receptor for B7H4 has not yet been identified unambiguously. Nevertheless, it is accepted that the receptor is expressed on activated T-cells and has an immunoregulatory role (154) (figure 1.4).

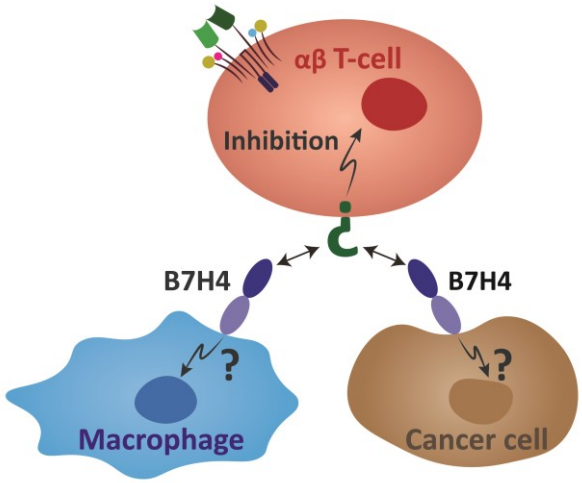

Figure 1.4 B7H4 expression and interaction with its receptor in the TME. APCs (tumours cells or macrophages) express B7H4 that interacts with its unknown receptor expressed on T-cells, delivering an inhibitory co-stimulation to the T-cell. Evidence of B7H4 signalling to the APC through this interaction has been also reported, but it is not well characterised yet.

B7H4 is considered an attractive target for possible antibody-related therapy. In 2014, a study revealed the crystal structure of the Ig-like V-type 1 domain of human B7H4. In this study, a mouse monoclonal antibody (mAb) against human B7H4, and cross-reactive with the Ig-like V-type 1 domain of mouse B7H4, was used for preclinical studies (clone 1H3). Clone 1H3 showed significant growth inhibition of B7H4 expressing tumours *in vivo* using an induced pulmonary metastasis mice model by injecting B7H4 expressing CT26 cells into BALB/c mice. The tumour growth inhibition activity of anti-B7H4 clone 1H3 was due to two different mechanisms of action: antibody-dependent cellular cytotoxicity (ADCC) and partial blocking of B7H4-mediated T-cell inhibition (155). Another mouse mAb targeting human B7H4 has been used conjugated to an anti-tumour agent (Clone h1D11 conjugated to monomethyl auristatin E). The studies with this drug-conjugated antibody showed durable tumour regression in triple-negative breast cancer cell lines and a patient-derived xenograft mouse model (156).

FPA150 is a human afucosylated IgG1 targeting human B7H4. Human IgGs are glycoproteins bearing a two N-linked biantennary complex-type oligosaccharide attached to Asn297 of the Fc and essential for antibody effector functions. Shields et al. described the impact of core oligosaccharide fucosylation in the capacity of the IgGs to bind the FcγRIIIa and its implications in ADCC (157). The fucose residue disrupts optimum intermolecular carbohydrate-carbohydrate interactions between the oligosaccharide linked to Asn297 of the Fc and the oligosaccharide

linked to Asn162 of the FcγRIIIa (158). FcγRIIIa have been proven a critical receptor to be activated for successful elimination of tumours through ADCC (159). Afucosylation is achieved by engineering the cell line producing the IgGs to avoid the presence of fucose sugar in the oligosaccharides present in the Fc region. CHO cells are frequently used for commercial production of therapeutic antibodies. The production of afucosylated IgG1 in CHO has been accomplished by establishing CHO cell lines with tetracycline-regulated expression of the enzyme GnTIII (160) or Knock-out of the gene *FUT8* (161), increasing the affinity of binding of the IgGs to the FcγRIIIa and therefore the ADCC activity. FPA150 redirects FcγRIIIa$^+$ effector cells (NK cells and macrophages) to eliminate B7H4 expressing tumour cells while at the same time blocks the inhibition by B7H4 of T-cells. FPA150 showed a favourable safety profile in a Phase 1a clinical trial (162,163).

1.1.5.1 B7H4 expression in EBV-associated malignancies

B7H4 could also be an attractive target to treat EBV-associated malignancies. Its expression is induced on B-cells infected with EBV *in vitro* and EBV-positive B-cell lines (figure 1.3). In patients, expression of B7H4 has been shown so far in EBV-associated DLBCL and NPC (164–166) and expression might extend to other EBV-malignancies. B7H4 expression was detected in the EBV-positive lymphoma cell lines Raji and IM-9, but was not on the EBV-negative lymphoma cell line Ramos (167). B7H4 expression has also been detected in NPC cell line, and its expression decreased by shRNA, leading to inhibit cell proliferation and invasion. shRNA downregulation of B7H4 induced cell cycle arrest and apoptosis through inactivation of p-JAK2 and p-STAT3, promotion of BAX and caspase-3 and reduction of Bcl-2, MMP-2 and MMP-9 (168).

B7H4 seems to function as both a ligand and a receptor (figure 1.4). Although there are only two amino acids comprising the intracellular domain, B7H4 induces Fas-mediated and caspase-dependent apoptosis of EBV-transformed B-cells (167). However, it is still not clear how B7H4 deliver its signal to the interior of the cell. The role of B7H4 in apoptosis inhibition was revealed by treating an EBV$^+$ DLBCL cell line with an anti-B7H4 antibody. The treatment reduced the phosphorylation of Erk1/2 and Akt, decreasing cell viability and enhancing apoptosis. This study established the role of B7H4 in activating Erk1/2 and Akt signalling pathways (165). Moreover, the engagement of B7H4 with anti-B7H4 antibody reduced the

growth of Raji and IM-9 cell lines, leading to cell cycle arrest at the G0-G1 phase in a dose and time-dependent manner, through down-regulation of the AKT pathway. This raises the possibility that the engagement of B7H4 could affect these signalling pathways in APCs (169).

1.2 Chimeric antigen receptor T-cell therapy

A chimeric antigen receptor (CAR) is an artificial membrane protein designed to combine functional protein domains from two entities: an antibody and membrane receptors, the latter typically expressed on αß T-cells (figure 1.5.A). At least four separated domains are fused to generate the chimera: an antigen-binding domain and a hinge domain (for dimerization) from an antibody, along with a transmembrane domain and intracellular signalling domains from a T-cell membrane receptor. Such a CAR has been typically expressed in αß T-cells introduced by retroviral transduction or the Sleeping Beauty transposon system (figure 1.5.B).

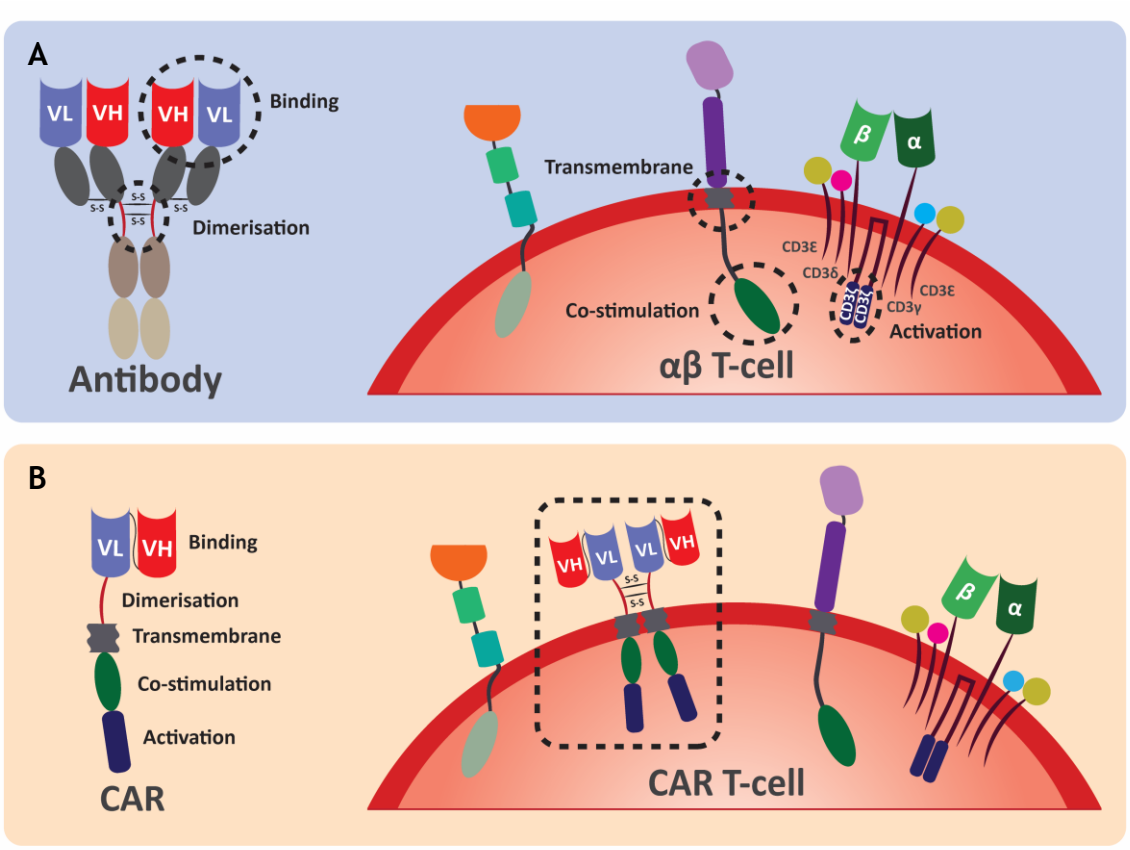

Figure 1.5 CAR design. A) Protein domains used to create a CAR. From an antibody, the binding domain, composed by the VH and the VL chains, and the hinge domain for dimerization by disulphide bridges are used. The dimerization domain could also be obtained from other proteins, for example, CD8. From the αβ T-cell, different domains from different receptors typically expressed in these cells are used. The activation domain typically is the CD3ζ chain of the TCR complex. The transmembrane

domain is obtained from T-cell co-stimulatory molecules, such as CD8 or CD28. The co-stimulation domains are also obtained from co-stimulatory molecules with a role in the regulation of T-cell activation, such as CD28 or 4-1BB. B) CAR structure and expression in T-cells. Depiction of the structure of a CAR chain composed by its different domains. The chains form CAR dimers when expressed in T-cells.

The objective of this approach is to deliver a signal of activation through the recognition of a specific antigen, and independent of MHC antigen presentation, to a T-cell. In so doing, it is aimed to generate a T-cell response to a specific antigen. As well as the specificity of each domain used in the CAR, several factors are critical for efficient CAR engagement and T-cell activation: the density of expression of the antigen in the target cell, the affinity of the binding domain for its target, the level of expression of the CAR, the position of the epitope in the target antigen and the length and flexibility of the hinge region (170–173).

1.2.1 CAR domains

A standard CAR is composed of an antigen-binding domain, a hinge domain, a transmembrane domain and an intracellular domain. Each of the four CAR components is considered below.

1.2.1.1 Antigen-binding domain

The antigen-binding domain has been selected by the interaction of antibody with the target (usually a protein), and therefore determines the specificity of the CAR. It is then designed to incorporate the antigen binding features to the CAR. The antigen-binding domain is located at the N-terminal end of the CAR molecule. This domain is commonly a single-chain variable fragment (scFv). An scFv is a fusion between the variable heavy chain (VH) region and the variable light chain (VL) region of the relevant antibody, connected with a linker peptide (174,175). There are two possible conformations for scFvs, with either the VH at or the VL at the N-terminal end. Other antigen-binding domains configurations have been used to create CARs, for example, VH-only CARs, nanobody-based CARs or NK receptor-based CARs (176–179).

1.2.1.2 Hinge domain

This region connects the antigen-binding domain with the transmembrane domain. It is involved in dimerization of the molecules and provides flexibility, but also defines the length, and therefore, the distance between the antigen-binding domain and the plasma membrane. Hinge regions obtained from CD8α, CD28 and IgGs (mainly IgG1, IgG2 and IgG4) have been used in CARs. A short distance to the plasma membrane is achieved using the hinge regions of CD8 and CD28. Medium and long hinge domains have been generated by incorporating to the hinge region plus the CH2 and CH3 domains from IgG1 and IgG4, either CH3 alone for a medium length, or both for a longer domain (180,181). The extracellular length of the CAR, together with the position of the target epitope, has been shown to be critical for the optimal delivery of an activation signal (182,183).

1.2.1.3 Transmembrane domain

The transmembrane domain links the extracellular domain of the CAR (binding domain and hinge region) to the intracellular domain (endodomain). The most common transmembrane domains used for CARs are derived from CD8α, CD28 and CD3ζ. The selection of a transmembrane domain for a CAR is considered in conjunction with the selected hinge domain and the endodomain. For example, for a CAR with a hinge region derived from CD8α, a CD8α-derived transmembrane domain is usually selected (184,185). In another example, a CAR receptor with a CD28-derived endodomain, a CD28-derived transmembrane domain and hinge region is chosen (186,187). Several publications have shown the use of interchangeable transmembrane domains. However, the transmembrane domain does provide an important contribution to the functionality of the CAR. It can affect its expression and localisation on the cell surface and impact the T-cell activation and function by altering the level of inflammatory cytokines produced upon activation or, in the case of non-standard transmembrane domains, provide new biological proprieties (179,188–190).

Moreover, Ying et al. demonstrated that altering the length of the CD8α derived hinge and the transmembrane domain could lead to the production of lower levels of cytokines, expression of higher levels of antiapoptotic molecules and slower cell proliferation. It translates in lower toxicity than the prototype CAR and the

same efficacy. The CAR T-cell with modified CD8α hinge and transmembrane domain were able to proliferate and differentiate into memory cells *in vivo* and produces a potent and durable anti-tumour response (191).

1.2.1.4 Intracellular domain (or endodomain)

The intracellular domain of a CAR is usually composed of several domains from different receptors. Two different groups of endodomains have been used in CARs: activation domains and co-stimulation domains. Activation domains deliver a signal to the CAR T-cell to activate its cytotoxic response against the target cell. The most common activation domain used in CARs is derived from CD3ζ. However, activation domains derived from the Fc receptor for IgE-γ (FcεRI) and the DNAX-activating protein 12 (DAP12) have also been used (192,193). Activation through CD3ζ, FcεRI and DAP12 depend on the phosphorylation of ITAMs (194). The engagement of the CAR with its ligand leads to phosphorylation of the ITAMs and induction of a signalling cascade resulting in the activation of the CAR T-cell (195).

Co-stimulation domains are usually derived from two protein families: the CD28 family receptors (CD28 and ICOS) and the tumour necrosis factor receptor superfamily (4-1BB, OX40 and CD27). Additionally, the DNAX-activating protein 10 (DAP10) and Toll-like receptor 2 (TLR2) have been used as co-stimulation domains in CARs. The signalling motifs present in the co-stimulatory domains provide a supportive signal to the ITAM signalling for T-cell activation (195).

1.2.2 CAR T-cell activation and co-stimulation

One single CAR can deliver several signals to the T-cell through the recognition of a ligand (the antigen). The majority of the CARs currently studied, and the ones already with clinical approval, have the CD3ζ activation signalling domain. For co-stimulation, choosing the right domain is vital for the efficacy and safety of the therapy. The most commonly used co-stimulatory domains are CD28 or 4-1BB.

1.2.2.1 T-cell activation through CD3ζ

The TCR is a heterodimer formed by the α and ß TCR chains with ligand binding specificity but without signal-transducing activity. The TCR is noncovalently associated with the signal-transducing subunits CD3γ, CD3δ and CD3ε and CD3ζ

(figure 1.6.A). CD3γ, CD3δ and CD3ε contain a single ITAM, while CD3ζ contains three in tandem. The TCR complex is composed by the TCR heterodimer, two CD3ε chains, one CD3γ, one CD3δ and two CD3ζ following the stoichiometry TCRαß–CD3εγ–CD3εδ–CD3ζζ. A total of ten ITAMs are present in the final complex, six of them in the CD3ζ homodimer. It is still unknown how all these ITAMs works together, or if they perform different signalling functions. The major event for T-cell activation occurs at the CD3ζ chains. Therefore, the CD3ζ chain is the most relevant subunit of the TCR complex for CAR design. Following TCR clustering by MHC-peptide recognition and coreceptor (CD4 or CD8) interaction with the MHC, the lymphocyte-specific protein tyrosine kinase (Lck) phosphorylates the TCR complex ITAMs, and these are then recognised by the two SH2 domains (phosphorylated tyrosine recognition domains) present in the Zeta-chain-associated protein kinase 70 (ZAP70). ZAP70 locates near the surface membrane of T-cells and its interaction with the phosphorylated ITAMs of the TCR complex leads to the phosphorylation of the transmembrane protein linker for activation of T-cells (LAT). Phosphorylated LAT then serves as a docking site to trigger the activation of serine-threonine kinases, including MAPK and PKC family proteins to activate the pathways NFAT, NF-κB, AP-1 and ATF-2 (196) (figure 1.6.A).

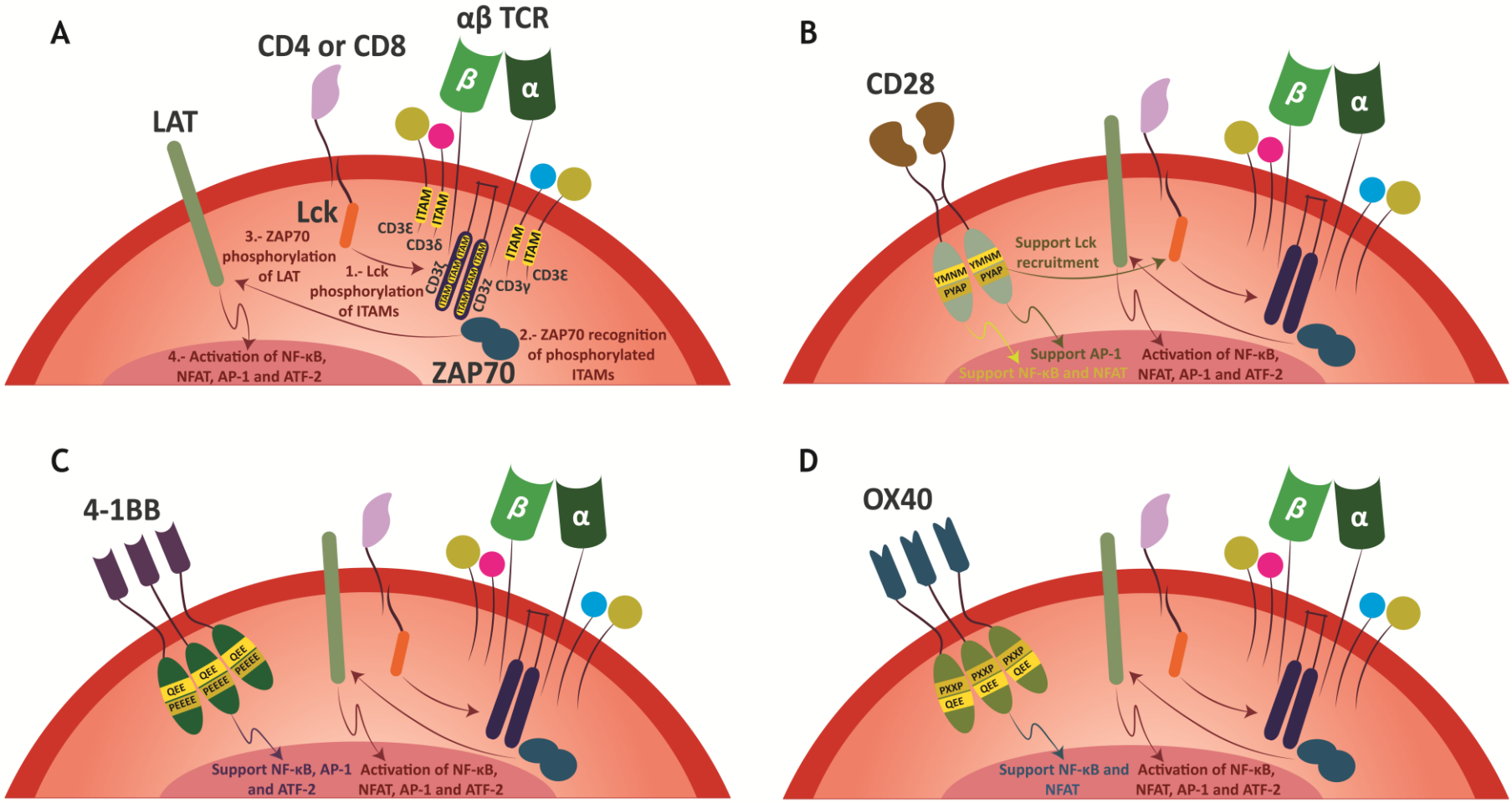

Figure 1.6. T-cell activation and co-stimulation. A) TCR activation cascade followed by HLA-peptide recognition. During MHC-peptide TCR activation, the TCR complex recognises the MHC-peptide complex and the coreceptor (CD4 or CD8) interacts with the MHC, leading to phosphorylation of the TCR ITAMs by Lck. Then, the phosphorylated ITAMs are recognised by ZAP70, leading to LAT phosphorylation and NF-κB, NFAT and AP-1 activation. B) CD28 co-stimulation of TCR signalling. In addition to MHC-peptide TCR activation, CD28 co-stimulation could be trigger by integration with CD80 and CD86. The YMNM and PYAP motifs trigger signalling that support NF-κB, NFAT and AP-1 activation. Furthermore, PYAP also supports the recruitment of Lck for TCR activation. C) 4-1BB co-stimulation of TCR signalling. 4-1BB co-stimulation could be trigger by integration with 4-1BBL. The two cytoplasmatic TRAF-binding motifs QEE and PEEEE trigger signalling that support NF-κB, AP-1 and ATF-2 activation. D) OX40 co-stimulation of TCR signalling. OX40 co-stimulation could be trigger by integration with OX40L. The cytoplasmatic TRAF-binding motif QEE trigger signalling that support NF-κB activation and the PI3K-binding motif PXXP support NFAT activation.

1.2.2.2 T-cell co-stimulation

The functional outcome of the TCR signalling is also determined by the signalling by the T-cell co-receptors (co-stimulatory and co-inhibitory receptors). There is a broad diversity of these receptors involved not only in TCR signalling regulation, but also in T-cell differentiation (197). So far, the most used co-stimulatory domains for CAR design have been CD28, 4-1BB, OX40 (198–200) (considered below), but novel co-stimulatory domains as ICOS, CD27, DAP10 and TLR2 have been also studied (195,201–204).

• CD28 co-stimulation

CD28 gives its name to a family of receptors that include CD28, CTLA4, BTLA, ICOS and PD1. CD28 is the receptor for the ligands CD80 (B7-1) and CD86 (B7-2). It is expressed as homodimer on $CD4^+$ and $CD8^+$ naive T-cells and its expression declines with the individual's age. During activation, some T-cells lose the expression of CD28. These $CD28^-$ T-cells are generally antigen-experienced and highly differentiated T-cells with heterogeneous functions (cell cytotoxicity or immune regulation).

CD80 and CD86 are induced by different stimuli in different cell types. The expression of CD86 is constitutive in APCs, and it is rapidly upregulated under stimuli, while CD80 is transiently expressed and slowly upregulated in activated APCs. CD80 and CD86 can also interact with CTLA-4, an immune checkpoint receptor upregulated after T-cell activation and involved in inhibiting further activation. CD80 and CD86 may have different biological functions due their difference in binding kinetics to CD28 and CTLA-4 and their differences in induction and expression on APCs. Some evidence suggests that CD80 could have preferential interaction to CTLA-4 over CD28 (205–207). Qureshi et al. 2011 suggested that CTLA-4 may capture CD80 and CD86 on the surface of the APCs by trans-endocytosis, a process where material created by one cell is endocytosed by a different cell, resulting in impairment of CD28 co-stimulation (208). Furthermore, CTLA-4 transmit an inhibitory signal to the cell, but the mechanism is still unclear. Some studies suggest that stimulation of CTLA-4 leads to TCR signalling attenuation and others modulation of cell motility and/or signalling through PI3 kinase (209,210).

CD28 modulates proliferation, differentiation and effector functions in T-cells. It has two cytoplasmic motifs, YMNM and PYAP. The YMNM motif is involved in the recruitment of the proteins PI3K, GRB2 and GADS. PI3K signalling leads to activation of NFAT and the adaptor proteins GRB2 and GADS to the activation of NF-κB. The PYAP motif is responsible for recruiting Lck, supporting NFAT activation. Moreover, it also recruits GRB2 for activation of AP-1 (211) (figure 1.6.B).

• 4-1BB co-stimulation

4-1BB (aka CD137), is a member of the tumour necrosis factor receptor (TNFR) family expressed on lymphoid cells and also in non-hematopoietic cells. In lymphoid cells, 4-1BB is expressed on activated T-cells and not expressed in naïve T-cells. 4-1BB is expressed to a higher extent on activated $CD8^+$ compared to activated $CD4^+$ T-cells. It recognises the homotrimer 4-1BB ligand (4-1BBL), expressed on activated APCs.

4-1BB is a co-stimulatory molecule with roles in expansion, effector function and development of memory T-cell phenotype. 4-1BB has two cytoplasmatic TRAF-binding motifs (QEE and PEEEE) for the interaction of TRAF1, TRAF2 and TRAF3 (212,213), leading to the activation of NF-κB, AP-1 and ATF-2 (figure 1.6.C).

• OX40 co-stimulation

OX40 (aka CD134), is a member of the TNFR family expressed on activated T-cells and not expressed in naïve T-cells. It recognises the homotrimer OX40 ligand (OX40L) expressed on activated APCs. OX40 has a cytoplasmatic TRAF-binding motif (QEE) for the interaction of TRAF2, TRAF3 and TRAF5. Mouse OX40 also contains a potential PI3K-binding motif (PXXP), but this motif is not observed in human OX40. However, human OX40 recruit PI3K by an unknown mechanism (214).

OX40 is a co-stimulatory molecule with roles in expansion, effector function and development of memory T-cell phenotype. OX40 co-stimulation leads to the activation of NF-κB and NFAT (214,215) (figure 1.6.D).

1.2.3 Conventional CAR T-cell therapy

Three approaches have been used in the design of conventional CAR therapies. The first design sought to induce antigen-dependent T-cell activation, giving rise to the first-generation of CARs. Subsequently, it was observed that for better antigen-dependent activation, a co-stimulation signal needed to be incorporated into the system, and the second-generation of CARs was developed. The third-generation of CARs seeks to boost the co-stimulation of second-generation CARs, increasing T-cell activation (figure 1.7).

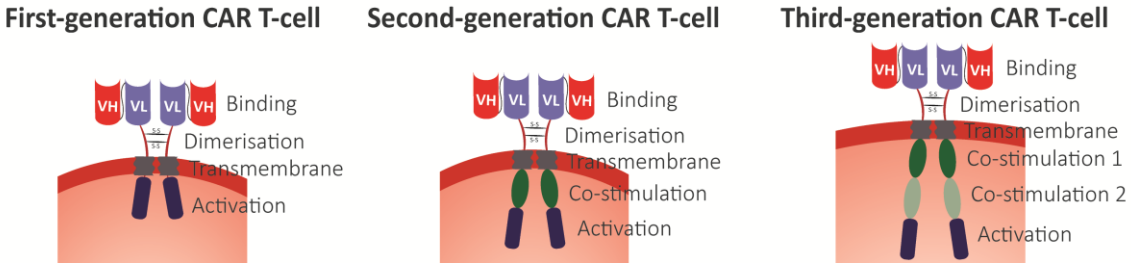

Figure 1.7 Conventional CAR T-cell therapy. The CAR used for the first-generation CAR T-cells comprises in its intracellular signalling domain the activation domain of CD3ζ, although FcRγ has been also used. For the second-generation, the intracellular signalling domain the CAR encloses the activation domain of CD3ζ plus a co-stimulatory domain. For the third-generation, two co-stimulation domains are used. Co-stimulation domains are obtained from the intracellular signalling domain of co-stimulatory receptors such as CD28, 4-1BB or OX40.

1.2.3.1 First-generation CAR T-cells

The first CAR, developed in 1989, named scFvRγ/ζ, was made using a scFv specific to the antigen trinitophenyl and fused to CD3ζ (216). In the same publication, another CAR design was reported using the γ chain of the antibody Fc receptor (FcRγ) instead of CD3ζ. This receptor was expressed in a cytotoxic T lymphocyte (CTL) hybridoma, which had no expression of the TCR/CD3 complex, demonstrating antigen-specific T-cell stimulation (216,217). However, first-generation CARs such as these, failed to promote T-cell proliferation and survival. It was concluded that this failure was because they lacked co-stimulatory signalling (figure 1.7).

1.2.3.2 Second-generation CAR T-cells

In 2003, a first-generation CAR anti-CD19 was used, and the T-cells were expanded in the presence of CD80 co-stimulation and IL-15. This was shown to eradicate Raji

(B-cell) tumour cells and persisted in the body in a xenograft mouse model. The anti-tumour activity was dependent on *in vivo* CD80-mediated co-stimulation, this was demonstrated with another xenograft model using $CD19^+$ NALM-6 pre-B-cells (cell line no expressing CD80 and CD86) comparing with CD80 transduced $CD19^+$ NALM-6 pre-B-cells (218). Consequently, second-generation CARs were designed by adding an intracellular co-stimulatory domain to the first-generation CAR (figure 1.7) (219–221). Different co-stimulatory domains have been used for second-generation CARs, each of them providing specific co-stimulation and conferring different biological properties to the CAR. Among them are CD28, CD134 (OX40), CD137 (4-1BB), CD27, ICOS and DAP10 (198,199,201,202,220,222,223). The efficacy of adding these co-stimulatory domains to second-generation CARs has been demonstrated in multiple preclinical studies using different cancer models (223–227).

Several clinical trials have been performed with second-generation CAR T-cell therapies targeting the tumour associated antigen (TAA) CD19 in paediatric (184,228–230) and adult patients (231–233). In 2017, the FDA (Food and Drug Administration) granted the first approval of second-generation autologous CAR T-cell therapy to treat acute lymphoblastic leukaemia (ALL). Tisagenlecleucel, aka CTL019 or Kymriah, targets CD19 with a CAR carrying the endodomains the CD3ζ and 4-1BB. 75 patients were treated with Tisagenlecleucel, and 60% of them had a complete response after 9 months follow up (184). In May 2018, the FDA granted a second approval using Tisagenlecleucel to treat relapsed or refractory DLBCL following a trial with 81 patients showing 32% patients with complete response after 9 months follow up (234). In October 2017, another second-generation autologous CAR T-cell therapy targeting CD19 with the endodomains CD3ζ and CD28, Axicabtagene ciloleucel aka as KTE-C19 or Yescarta, was approved by the FDA for DLBCL after a trial with 101 patients showing 58% complete response after 15 months follow up (186). In July 2020, the FDA granted approval for Brexucabtagene autoleucel, aka Tecartus, for the treatment of mantle cell lymphoma (MCL) in adults. Brexucabtagene autoleucel differs from Axicabtagene ciloleucel in the manufacturing process. Brexucabtagene autoleucel has an additional step to remove circulating tumour cells from immune cells (blood cell enrichment). This step is necessary for certain types of B-cell cancers. In February 2021, the FDA granted approval for Lisocabtagene maraleucel, aka Breyanzi.

Lisocabtagene maraleucel, which include a non-functional truncated epidermal growth factor receptor (EGFRt) co-expressed with the second-generation CAR. The objective is to reduce the number, or eliminate, the CAR T-cells using an antibody anti-EGFR after treatment. To date, all the approved CAR T-cell therapies target the TAA CD19.

1.2.3.3 Third-generation CAR T-cells

The third-generation CARs include the addition of an extra co-stimulatory domain to the second-generation CAR to contributing to signalling with additional stimulation and enhance T-cell activation through the CAR (figure 1.7). They have been shown to increase cytokine production and tumour growth inhibition in mice (173,200,235–237). In the design of a third-generation CAR, the distance of each endogenous domain to the plasma membrane and their configuration has an impact on T-cell activation. For example, a third-generation CAR with an intracellular domain consisting of CD28/OX40/CD3ζ has been shown to enhance the production of IL2 and IL10 (200), whereas the CAR CD28-CD3ζ-OX40 showed the opposite effect (238). This has also been shown with ICOS/4-1BB/CD3ζ compared with 4-1BB/ICOS/CD3ζ, where the fist configuration enhances the production of IL7 and IL10, while the second instead enhances the production of IL6 and IL13 (239). It is not clear why this happens, but the position in the CAR could have an impact on the ability of the intracellular domain to recruit the necessary protein to transmits the signalling correctly. DAP10 and TLR2 have also been used as co-stimulatory domain in third-generations CARs together with CD3ζ and CD28 endodomains, proving enhancement of the antitumor efficacy when compared with the second generation CARs (203,204).

1.2.4 Manufacture of clinical-grade CAR T-cell therapies

To safely treat patients with CAR T-cell therapies, they need to be manufactured under good manufacturing practices (GMP). GMP describes the standard required to satisfy the guidelines recommended by the regulatory agencies such the FDA in the United States, the European Medicines Agency (EMA) or Medicines and Healthcare products Regulatory Agency (MHRA) in United Kingdom. These agencies oversee the authorisation and licensing of manufacturing and distribution of pharmaceutical products. During the procedure, we can identify the following

steps: the collection of starting material, T-cell selection and activation, genetic modification, CAR T-cell expansion, formulation and cryopreservation (240–242) (figure 1.8).

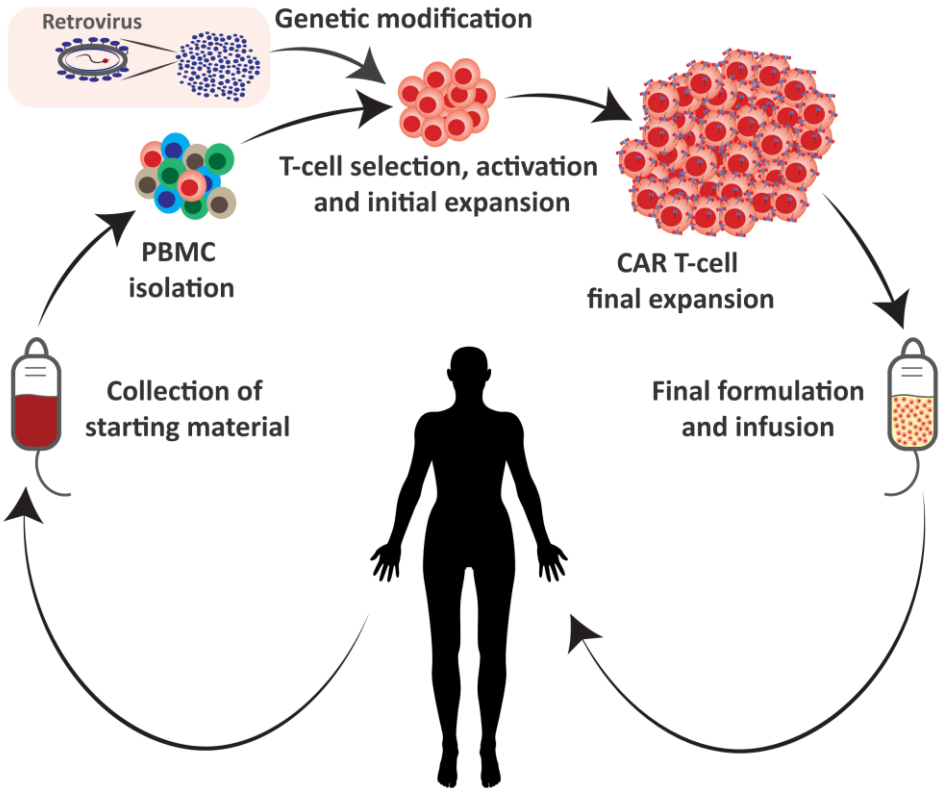

Figure 1.8 Manufacturing of clinical-grade autologous CAR T-cell therapies. The manufacturing of an autologous CAR T-cell therapy starts with the collection of blood from the patient and the isolation of the PBMC. These two steps are clusters in the process named leukapheresis and performed with an apheresis system. The cells are cryopreserved and shipped to the manufacturing facility, where the cells are selected, activated for initial expansion, and infected with a retrovirus that delivers the genetic material coding for the CAR to the cell. The infected T-cells (CAR T-cells) and the residual amount of non-infected T-cells are then expanded on a larger scale. Finally, the cells are washed and subjected to the establish quality checks before being cryopreserved and shipped back to the treatment centre to be infused into the patient bloodstream.

1.2.4.1 Collection of starting material

The currently approved CAR T-cell therapies use autologous material (i.e., cells derived from the patient) to avoid immune rejection of the modified cells. In adoptive therapy, the blood is collected from the patient and the peripheral blood mononuclear cells (PBMC) are isolated by apheresis. In some cases, the patient could have a low count of white blood cells due to the disease or previous treatments, negatively affecting the collection of a good quality starting material and the T-cell expansion (243–245). Early collection and cryopreservation could

ensure a good quality starting material, and the cells could be cryopreserved for 2.5 years before CAR T-cell therapy manufacturing.

Allogenic material (from donors) is also being used in clinical trials, and several technologies strive to improve the safety and efficacy of this approach. Allogenic therapies are often called “off-the-shelf”, and the main objective is to reduce the time consuming and costly process of developing individual treatments (246,247).

1.2.4.2 T-cell selection, activation and initial expansion

T-cells are enriched from the PBMC usually by depletion of other populations. Commonly, the entire population of T-cells ($CD3^+$ T-cells) is used for CAR T-cell therapies. Nevertheless, the possibility of using specific subsets of T-cells could improve the therapeutic effect and reduce toxicity (248,249).

To achieve *ex vivo* expansion of T-cells an activation signal through the TCR complex and a co-stimulation signal, usually through CD28 or by stimulation with IL-2, are required. This activation signal is typically given using clinical-grade beads coated with anti-CD3 and anti-CD28 (Tisagenlecleucel) (184), but anti-CD3 and IL2 stimulation is also used (Axicabtagene ciloleucel) (186).

EBV antigens can also be used to activate and expand viral-specific T-cells using EBV-transformed lymphoblastoid B-cell lines as APCs for T-cell stimulation. These cells are then modified with a CAR targeting the TAA of interest. This is an attractive approach for allogeneic CAR T-cell therapy, as TCRs restricted to EBV antigens have been shown to have a low incidence of GVHD (250,251). Furthermore, CAR-dependent activation and expansion of T-cells has been achieved using non-viable artificial APCs (aAPCs) presenting the TAA targeted by the CAR. This method of activation and initial expansion of T-cells is performed after the genetic modification with the CAR. aAPCs are genetically modified K562 cells (a human erythroleukemia cell line), designed to express co-stimulatory molecules such as CD86 or 4-1BBL and the TAA. The cells are lethally irradiated (hence non-viable) and used in co-culture with the CAR-modified T-cells. K562 cells lack expression of HLA-A and HLA-B, so T-cells are exclusively expanded through CAR stimulation (252).

1.2.4.3 CAR genetic modification of T-cells

Currently, the system for T-cell modification with CARs is using retroviral vectors to introduce the expression construct, although transposon/transposase systems have been also used. The use of elements randomly integrated into the cell genome like retrovirus or transposons leads to insertional mutagenesis and polyclonal preparations. The insertional mutagenesis can have an effect on CAR T-cell proliferation and persistence (253,254).

CAR T-cells have been mainly generated using two retroviral systems, γ-retroviral and lentiviral vectors. γ-retroviral vectors are highly efficient at infecting dividing cells while lentiviral vectors are also able to infect non-dividing cells. Both have the advantage of high and stable gene expression and have shown long-term safety when used in hematopoietic stem cells (HSC) and T-cell therapy. Both can pack ~3kb of insert (larger size leads to less efficient packaging). However, titer and transduction efficiency are typically lower in γ-retroviral vectors than lentiviral vectors. Retroviral vectors can also induce a moderate inflammatory reaction of target cells, even though the inflammatory potential is low (255–258).

Transposon/transposase systems require cell electroporation. Two main systems are being used for mammalian cells, Sleeping beauty and PiggyBac. These systems have the advantage of simple manufacture and reduced cost and immunogenicity compared to retroviral vectors. However, the integration of the genetic material is random, and there is a potential associated risk of oncogenesis. Furthermore, the unlikely but existing possibility of the integration of the transposase-encoding plasmid could result in the remobilisation of the inserted transposon. Even so, an Sleeping beauty transposon/transposase system with intermediate activity (transposase SB11) has shown long term safety and efficacy in CAR T-cell therapy (256,259,260).

Furthermore, the expression of the CAR constructs has been archived by mRNA electroporation, in this case the CAR T-cell are not genetically modified. mRNA electroporation leads to transient expression of the CAR for about one week. Hence the cell infusions must be repeated several times. This system has no associated immunogenicity and there is no genetic integration involved, therefore negligible risk of genotoxicity (261).

1.2.4.4 CAR T-cell final expansion

During the final CAR T-cell expansion, the number of cells is progressively increased. Therefore, the volume of the culture medium must increase accordingly. The characteristics of the final product are influenced by the CAR T-cell construct, the gene-editing system and the culture conditions during *ex vivo* T-cell expansion. Media supplementation with cytokines is an important factor influencing the cell phenotype in the final product. The optimal cytokine composition for CAR T-cell expansion is yet to be determined. Currently, IL2, IL7, IL15 are the main cytokines used. A combination of IL7 and IL15 show enhanced proliferation and a positive less differentiated phenotype compared to IL2 (262–265).

Different $CD4^+$ and $CD8^+$ populations, according to the level of T-cell differentiation, are evident after CAR T-cell expansion and before patient infusion: naïve CAR T-cells, stem-like memory CAR T-cells, central memory CAR T-cells, effector memory CAR T-cells, effector CAR T-cells and exhausted CAR T-cells (264,266) (table 1.5). The frequency of $CD8^+$ $CD45RA^+$ $CCR7^+$ T-cells (naïve and stem-like memory) correlates with CAR–T-cell expansion and a favourable outcome in patients with lymphoma (263). Exhausted CAR T-cells are characterised by a decrease in effector functions and an increase in the expression of inhibitory receptors, such as PD-1, LAG-3, CTLA4 and TIM3 (267). Their presence in the final formulation has a negative impact on the outcome of CAR T-cell therapies.

Table 1.5 $CD4^+$ and $CD8^+$ populations after CAR T-cell expansion.

Population*	CD45RA	CCR7	CD95	CD62L	IL2Rβ	LAG3	PD1
Naïve	+	+	-	+	-	-	-
Stem-like memory	+	+	+	+	+	-	-
Central memory	-	+	+	+	+	-	-
Effector memory	-	-	+	-	+	-	-
Effector	+	-	+	-	+	-	-
Exhausted	+	-	+	-	+	+	+

* Ordered from less differentiated (naïve) to more differentiated (exhausted).

1.2.4.5 Formulation and cryopreservation

After the final expansion, the cells must be washed, concentrated and suspended in an appropriate medium for intravenous infusion into the patient. The washing

is performed with 0.9% sodium chloride in water (isotonic saline). Then, the cells are suspended for cryopreservation in 0.9% isotonic saline supplemented with human serum albumin (HAS) and a cryopreservation agent, for example, CS10. CS10 is a DMSO based solution used for clinical-grade cell cryopreservation. PlasmaLyte A can also be used instead of 0.9% isotonic saline. The components of the cryopreservation media are optimised to maximise the cell viability. The infusion into patients of the required amount of DMSO for cryopreservation is safe (268,269).

1.2.4.6 Release tests

Different tests are necessary before releasing CAR T-cells for infusion (270). These tests differ with the manufacturing strategy, but all are aimed to ensure safety, purity and potency (241). For assessing the safety, the absence of bacteria, mycoplasma and endotoxin must be confirmed. With retroviral modified CAR T-cells, the number of copies inserted of the transgene and the presence of replication-competent viruses must also be assessed. For purity assessment, the percentage of $CD3^+$ cells, the percentage of CAR^+ T-cells and the residual tumour cells (in the case of autologous therapy) must be determined. The residual activation beads or residual aAPCs also need to be assessed. The potency must be defined *in vitro* by cytotoxicity assay or IFN-γ release assay (259,261,271).

1.2.4.7 Infusion into the patient

The number of CAR T-cells infused into the patient variates depending on the therapy. For example, a single dose of Tisagenlecleucel contains 0.6 to 6 x 10^8 CAR-positive viable T-cells, while the maximum single dose for Axicabtagen ciloleucel is 2 x 10^8 CAR-positive viable T-cells. In the case of Tisagenlecleucel, the single dose could be suspended in one to three infusion bags with volumes ranging from 10 ml to 50 ml. For Axicabtagen ciloleucel, just a single infusion bag is necessary with approximately 68 ml.

Previous lymphodepletion chemotherapy is given to patients in most CAR T-cell therapy protocols to create a favourable immune environment for adopting the infused CAR T-cells. Lymphodepletion leads to lymphocytopenia (low or null lymphocyte count in the bloodstream) that affects T-cells, B-cells and NK cells. Previous lymphodepletion treatment to the therapy could have multiple positive

effects. Lymphodepletion could lead to modification of the TME by reducing the number of T-reg cells and other tumour-promoting phenotypes. Also, it could alter the tumour phenotype by changes in the expression of costimulatory receptors or a decrease in the production of some metabolites. In addition, it decreases the therapy's immunogenicity and could remove endogenous cells that act as sinks for cytokines such IL2, IL7 or IL15. The negative aspect effects of lymphodepletion include the higher risk of infections and the toxicity associated with the lymphodepletion chemotherapy. Some of the chemotherapy agents used for lymphodepletion are cyclophosphamide and fludarabine (272).

1.2.5 CAR T-cell therapy-related side effects and toxicity

1.2.5.1 Cytokine release and macrophage activation syndromes

The most prevalent toxicity reported following the infusion of CAR T-cells resulted from a cytokine release syndrome (CRS). CRS symptoms result from the large and rapid release of cytokines into the blood associated with T-cell engagement and proliferation, such as IFNγ. CRS symptoms include nausea, headache, tachycardia, hypotension, rash and shortness of breath and can be fatal (273).

In addition to CRS, some patients receiving CAR T-cell therapy have also shown symptoms related to hemophagocytic lymphohistiocytosis (HLH), such as hepatosplenomegaly, liver dysfunction, coagulopathy, profound hyperferritinemia and hypofibrinogenemia. Whereas high level of IFN-γ are expected in CRS, the elevation of IL6, IL10 and GM-CSF in these patients are better explained by macrophage activation syndrome (MAS), a subset of HLH (274). IL6 is produced by macrophages, monocytes and DCs and can act via two signalling pathways, cis or trans-signalling. In the classic signalling, or cis-signalling pathway, IL6 binds to membrane-bound IL6R in complex with the gp130 dimer activating JAKs and STAT3 pathways. gp130 is ubiquitously expressed, whereas membrane-bound IL6R expression is restricted to immune cells. Cis-signalling results in B-cell activation, T-helper 17 (Th17) and T-follicular helper (Tfh) cell differentiation and $CD8^+$ T-cell proliferation. In the trans-signalling pathway, IL6 binds to soluble IL6R, forming a complex with a gp130 dimer potentially on the surface of all the cells. Trans-signalling has an impact at two different levels. In blood vessels, it leads to an increase of vascular permeability, monocyte and neutrophil recruitment and

vascular leaks. In the liver, an increase of ferritin, fibrinogen, hepcidin, serum amyloid A, C-reactive protein, thrombopoietin, complement C3 and decrease of albumin. IL6R blockade via mAb therapy has proven highly effective in treating MAS. In addition to cis and trans-signalling, IL6 also has a third model of signalling named trans-presentation. During trans-presentation, DCs produce IL6 and it binds to membrane-bound IL6R within the cell, therefore DCs present the complex IL6-IL6R on the surface to gp130-expressing T-cells, this presentation is required for priming of pathogenic Th17 cells. Anti-IL6 is unable to block this interaction, while anti-IL6R can block cis-signalling, trans-signalling and trans-presentation. Therefore, targeting the receptor instead of the ligand leads to more effective blockade of the pleiotropic activity of IL6 (275–278).

A direct relationship between the severity of CRS and MAS and the disease burden at the time of the CAR T-cell infusion was reported (232,279). Most patients who responded to the therapy exhibited at least mild CRS (high fever). Corticosteroids have also shown to rapidly reverse severe CRS without compromising the antitumor response (229,231,279–282). CRS and MAS have also been reported after administration of other immunotherapies such as infusion of therapeutic mAbs anti-CD3, anti-CD20, anti-CD28 or Blinatumomab (a bi-specific T-cell engager targeting CD19) and systemic infusion of IL2 (283–288).

1.2.5.2 Neurological toxicity

Neurological toxicity is the second significant side effect of CAR T-cell treatment and it is characterised by tremor, dysgraphia, mild difficulty with expressive speech, impaired attention, apraxia and mild lethargy (229,231,273,282). The causes are unclear, but it has been hypothesised that it could also be due to elevated cytokine levels. In some cases, it may have a different pathophysiology than CRS and requires different management. Similar symptoms were also reported with the treatment with Blinatumomab (289). Neurological toxicities during anti-CD19 CAR T-cell therapies could be enhanced by on-target off-tumour CAR T-cell activation. Parker et al. 2020 have shown expression of CD19 in human brain mural cells, a cell population critical for blood-brain-barrier integrity (290).

1.2.5.3 Anaphylaxis

Anaphylaxis is a severe and potentially life-threatening systemic reaction to a substance that has become an allergen (a substance that can cause allergic reactions). Tissues around the body release histamine and other molecules leading to breathing difficulties, fast heartbeat, confusion and anxiety and ultimately collapsing or losing consciousness, most likely through IgE antibodies specific to the CAR. Some of the CAR T-cell therapies in clinical trials use binding domains derived from murine antibodies, which could lead to humoral and cellular rejection of the CAR T-cells (291). IgEs anti-murine CAR crosslink the high-affinity receptor FcεRI expressed on the surface of mast cells and basophils leading to release of histamine, tryptase, carboxypeptidase A and proteoglycans. Humanisation of the murine binding domain is needed to avoid an anaphylactic reaction and improve persistence and efficacy (292). Another option is to use binding domains obtained from libraries of human antibodies created from human B-cells.

1.2.5.4 Insertional oncogenesis

During a gene therapy trial using HSC, γ-retroviral vector integration in the proximity of the *LMO2* proto-oncogene promoter lead to aberrant transcription and expression of LMO2, ultimately giving rise to T-cell transformation (293). No cases of transformation have been reported after infusion of CAR T-cells yet. The gene *LMO2* is silent in T-cells, making this locus an unlikely place for retroviral integration. However, there remains a risk of insertional mutagenesis and consequently transformation using such vectors. It is crucial to follow the patients involved in CAR T-cell therapies with this possibility in mind. Ultimately, it would be preferable if vectors could be designed to target and integrate to known safe sites such as the TCR itself.

1.2.5.5 Graft versus host disease and rejection

Trials with autologous patient-derived CAR T-cells have proven efficacious and to have clinical benefits. Nevertheless, establishing an “off-the-shelf” cell bank is an attractive solution to reduce the time of production, the cost of the treatment, avoid contamination with tumour cells and problems with patient T-cell dysfunction (246). There are two main issues in the use of allogenic CAR T-cells:

GVHD, where the donor cells attack the recipient tissues by recognition of recipient MHCs with their TCRs; and rejection, when the patient T-cells attack the CAR T-cells by recognition of the latter MHCs. Some approaches have been used to avoid GVHD and rejection. For example, the use of virus-specific allogeneic CAR T-cells or gene-edited allogeneic CAR T-cells with the knockout of their TCRs and MHC (247).

1.2.5.6 On-target off-tumour and off-target off-tumour antigen recognition

A signal of activation can be triggered through a CAR by three possible routes. During the on-target response, the CAR is activated by the antigen expressed on the tumour cell. This is the ideal situation for an effective antitumor activity without side effects. Alternatively, the off-target off-tumour response is a consequence of poor characterisation of the binding domain whereby a different antigen on a normal cell activates the CAR due to lack of specificity. With the on-target off-tumour response, the CAR is activated by the correct antigen, but this is also expressed in a normal cell which stimulates the CAR T-cell response. On-target off-tumour response is a common situation for CARs targeting human TAAs.

One of the first examples of on-target off-tumour toxicity in a CAR T-cell trial was reported using CAR T-cells against carbonic anhydrase IX (CAIX), overexpressed in renal cancer cells, to treat patients with renal cell carcinoma. After several CAR T-cell infusions liver toxicity developed, and a liver biopsy revealed the presence of CAIX expression on the bile duct epithelium(294). In another study, CAR T-cells targeting carcinoembryonic antigen (CEA) were used to treat patients with metastatic colorectal cancer, inducing severe transient inflammatory colitis due to the expression of CEA in intestinal crypt epithelial cells (295). Immunohistochemical staining for CEA in these biopsies demonstrated near-complete loss of CEA in the denuded colon specimens, but this protein was re-expressed in the regenerating tissue. Regarding the first approved CAR T-cell therapies targeting CD19 expressed on malignant B-cells, the treatment resulted in B-cell aplasia due to the recognition of CD19 also in normal B-cells (296).

CAR T-cell therapy also has shown toxicity in a preclinical study targeting B7H4 with second-generation CAR T-cells. Smith et al. 2016 saw tumour regression following infusion of anti-B7H4 CAR T-cell therapy in a preclinical mouse model,

but also lethal toxicity 6–8 weeks after therapy. Assessment of murine B7H4 expression distribution in different tissues showed expression in ductal and mucosal epithelial cells in normal tissues; the expression of B7H4 in human tissues is similar to mice. On-target off-tumour toxicity antigen recognition was established as the cause of toxicity. Smith et al. chose for their *in vivo* studies the murine scFv 3#68. Clone 3#68 showed high reactivity against moderate B7H4 expression *in vitro*, indicating high affinity of binding between 3#68 and B7H4 (297).

Chmielewski et al. 2004 showed that high affinity scFvs exhibit less discrimination than low affinity scFvs, between target cells with high or low antigen expression levels (298). Moreover, if the affinity of the CARs is compared with the affinity of TCRs, for TCRs there is a threshold of affinity where higher affinities does not translate to enhancement of the T-cell functionality (299). TCR affinity also correlates with the speed of the T-cell response, enhancing TCR affinity can accelerate the T-cell activation (300). Tuning the affinity of an scFv used in CAR T-cells seems to be critical for the efficacy and safety of the therapy.

Furthermore, Ghorashian et al. 2019 showed that low-affinity second-generation anti-CD19 CAR T-cells increased proliferation and cytotoxicity *in vitro* compared to CAR T-cells using the scFv previously used for Tisagenlecleucel and Axicabtagene ciloleucel. The clinical data showed that 12/14 patients with relapsed/refractory paediatric ALL achieved a complete response; the data were compared with the previously reported clinical study with second-generation anti-CD19 CAR T-cells. Enhanced CAR T-cell expansion compared with Tisagenlecleucel and good persistence was observed. No severe CRS was reported, although it needs to be interpreted with caution since 10/14 patients had a low disease burden (301).

In conclusion, adjusting the affinity of the binding domain for the target antigen could be an approach to discriminate malignant cells (overexpressing the antigen) from healthy cells (expressing physiological levels of antigen) (302–307). If T-cell activation is affected by the reduction of the binding affinity, a third-generation design to increase co-stimulation may be more suitable for these affinity tuned CARs, and an extra co-stimulatory domain can significantly improve their anti-

tumour cytotoxic function (308). Thus, onset toxicity may be avoided during anti-B7H4 CAR T-cell therapy by affinity tuning of the scFv.

1.2.6 Current limitations in CAR T-cell therapy

Second-generation anti-CD19 CAR T-cell are currently showing high efficacy in the treatment of relapsed B-cell malignancies (184,186,234). Therefore, CAR T-cell therapies are a promising approach to tackle haematological malignancies. However, there are some current limitations regarding the manufacture and distribution, the application in different type of cancers and the safety of the therapy.

1.2.6.1 Limitations regarding manufacture

The manufacture of autologous CAR T-cell therapies requires the collection by apheresis of PBMC from patients and its shipment to the manufacturing facility. There, a complicated procedure is necessary to obtain the final therapy, which finally needs to be cryopreserved and shipped to the hospital for subsequent infusion (240–242). The whole procedure requires between 17 and 22 days (Axicabtagen ciloleucel and Tisagenlecleucel, respectively). The current price of the therapy is also a handicap. In the USA, treatment with Tisagenlecleucel costs up to USD 475,000 and Axicabtagen ciloleucel USD 373,000 per patient. In Europe, the price is lower due to negotiations with the national health services but is nevertheless high (309,310).

Currently, patients treated with CAR T-cells therapies have been previously heavily pre-treated, and there is the possibility of not having enough time to wait for the manufacture of the therapy. Furthermore, the disease stage of the patient could also impact the quality of the starting material and lead to failures in meeting the transduction, cell number and phenotype criteria during manufacture (311,312).

Closed systems for cell therapy manufacturing are being developed to reduce the need for experienced researchers, expensive GMP facilities, time of production, delivery and costs. One example is the platform CliniMACS Prodigy (Miltenyi biotec), which has been used successfully for CAR T-cell therapy production and can be installed in the same hospital where the patient will receive the therapy,

or a laboratory nearby, allowing academic institutions to perform clinical trials with CAR T-cells (313–317).

Allogenic "off-the-shelf" CAR T-cell therapies could also be a game-changer to increase the flexibility of CAR T-cell therapies by reducing time, risk during production, availability and prices. Several technologies have been developed to improve the safety of allogeneic infusion of CAR T-cells with the objective to avoid GVHD and rejection (246,247,318).

1.2.6.2 Limitations regarding safety and scope of the therapy

One of the limitations of CAR T-cell therapies is the identification of suitable TAAs to be targeted by the therapy. The majority of the TAA proposed for CAR T-cell therapies are human proteins also expressed in healthy tissue. Therefore, there is a high probability of on-target off tumour recognition leading to toxicity.

A suitable TAA for CAR T-cell therapy would ideally be widely and stably expressed in the cancer cells to guarantee the efficacy of the therapy. It should also have a profile of clinically manageable and no lethal on-target off-tumour toxicities to ensure the safety of the therapy (319). These TAAs have restricted expression to a cell linage and this expression is conserved in malignancies. They do not seem to give a survival advantage to the tumour and offer a stable expression and safety profile. Some examples are the TAAs present in haematological malignancies such as CD19, CD20, CD22 and BCMA. The TAA CD19 is the chosen targeted for Tisagenlecleucel and Axicabtagen ciloleucel (indicated to treat B-cell malignancies) and widely and stable expressed during B-cell development. On-target off-tumour recognition of healthy cells expressing CD19 leads to long term B-cell aplasia that can be managed effectively by clinicians. Other CAR T-cell therapies targeting different TAA are being tested for haematological malignancies in clinical trials (table 1.6).

Table 1.6 Most common TAAs currently targeted in CAR T-cell clinical trials.

Malignancies	TAAs
Haematological malignancies	CD19, BCMA, CD20, CD22, CD30, CD33, CD123 and CD138.
Solid tumours	MSLN, GD2, GPC3, MUC1, CD38, EGFRvIII and CEA.

Expanding the use of CAR T-cells therapies to solid tumours is also one of the challenges for CAR T-cell therapies. The main issues to tackle are the effective infiltration, expansion and persistence of the CAR T-cells into a fibrotic tumour stroma with an immunosuppressive TME (320–322). Suitable TAAs need to be identified for the treatment of solid tumours with CAR T-cells. These TAAs are not usually expressed in the cell lineage but expressed during malignancies. The expression of these TAAs confer a survival advantage to the malignant cells by immunomodulation of the TME or increment of the growth rate. Some examples are PDL1, PDL2, B7H4, B7H3, Her2/neu or EGFRvIII. In these cases, a wide and stable expression of the TAA in all the malignant cells in the solid tumour is not always observed. However, CAR T-cells also trigger a complementary anti-tumour endogenous response within the TME (323). Several TAAs are being explored for solid tumours in clinical trials (table 1.6).

CAR T-cell therapies have proven to be more successful in haematological malignancies. Nevertheless, new approaches have been developed to increase the efficacy and safety in solid and haematological malignancies and to expand the scope to the second group of TAAs.

1.2.7 New generation of CAR T-cells to improve efficacy and flexibility

Different CAR T-cell technologies have been developed to boost the efficacy and flexibility of conventional CAR T-cell therapies (figure 1.9). The aims are developing approaches for an effective and wide use of CAR T-cells in haematological and solid malignancies and improve the safety and efficacy of allogeneic infusion.

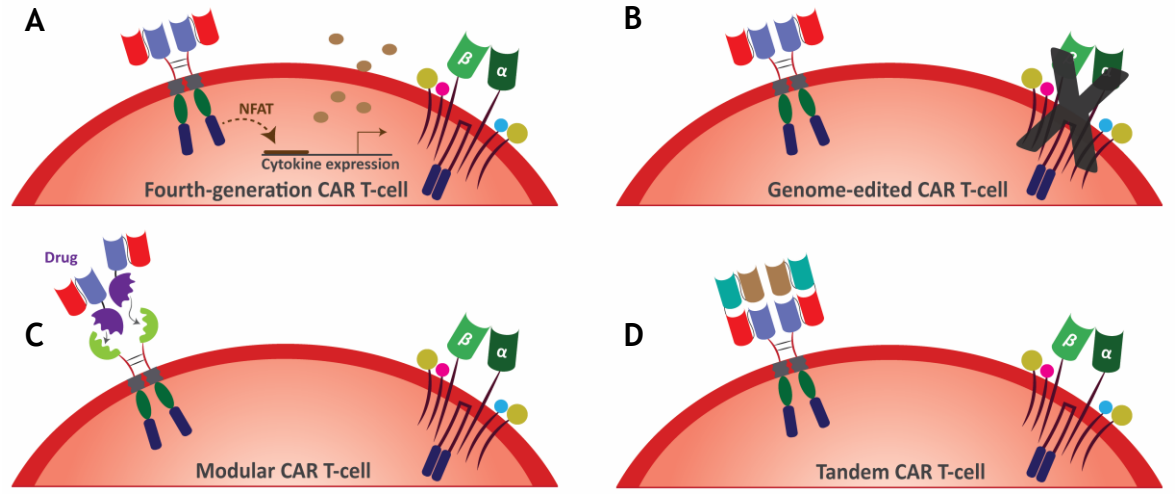

Figure 1.9 New generation of CAR T-cells to improve efficacy and flexibility. A) The fourth-generation of CAR T-cells use the signalling delivered by the CAR to activate the expression of factors to enhance expansion, persistence, anti-tumoral activity or migration into the TME. CAR T-cell directly expressing those factors are also considered fourth-generation CAR T-cells. B) The genome-edited CAR T-cells introduce additional genetic modifications to promote the knock-out of endogenous TCRs or HLAs to increase the safety of allogenic therapies or co-inhibitory receptors or transcription factors to improve efficacy. C) The CAR activation of modular CAR T-cells depends on a soluble drug (CAR-adaptor) that binds specifically to the modular CAR (modCAR), the drug contains the binding domain to the target antigen. D) Tandem CAR T-cells simultaneously target two or more TAAs by a CAR composed of two or more scFvs in tandem. For descriptions of the different elements in this figure, refer to figure 1.5.

1.2.7.1 Fourth-generation CAR T-cells

The fourth-generation CAR T-cells have the aim of reprogramming the TME to escape immunosuppression (figure 1.9.A). They are also known as armoured CARs or CAR T-cells redirected for universal cytokine killing (TRUCKs) and have been developed to include factors to enhance expansion, persistence, anti-tumoral activity or migration into the TME. CAR-TRUCK cells use NFAT activation upon CAR antigen recognition, to induce cytokine expression (genes encoded by a cassette). In another strategy, the cytokines are expressed with the CAR, separated by 2A "self-cleaving" peptides (18–22 amino acids long viral peptides that mediate cleavage of polypeptides in eukaryotic cells) (324). The cytokines IL7, IL12, IL15, IL18, IL21 and/or IL36γ have been expressed in CAR T-cells using these approaches (325–333). Co-expression of IL15 and IL21 in CAR T-cells targeting the TAA Glypican-3 have shown superior *ex-vivo* expansion and antitumor activity in xenograft model of hepatocellular carcinoma compared to CAR T-cell expressing IL15 or IL21 (334).

Furthermore, the expression of a constitutively activated IL7R increased persistence and antitumor activity in preclinical models (335). Moreover, a CAR has been designed with a truncated cytoplasmic domain of IL-2Rß to recruit STAT5 (induced by IL-2, IL7 and IL-15) and a STAT3-binding YXXQ motif (induced by IL21) able to deliver antigen-dependent JAK-STAT3/5 pathway activation, demonstrating superior antitumor effects with minimal toxicity in xenograft mouse models compared to conventional second-generation CAR (336).

Chemokines or their receptors have also been used in CAR T-cells to enhance their migration into the TME. The receptors CCR4, CCR2b, CXCR2 and CXCR1 have been co-expressed in CAR T-cells to make them respond to tumour-related chemokines (337–341). CAR T-cells have been engineered to express the chemokines CCL19, CCL5 and CXCL9, but their ability to interact with endogenous chemokine receptor needs to be taken in consideration (330,342).

CAR T-cells have also been modified to co-express co-stimulatory ligands such as 4-1BBL and CD40L to introduce extra CAR-independent co-stimulation (343,344). When 4-1BBL (naturally expressed on APCs) is co-expressed on CAR T-cell, it can stimulate 4-1BB on its surface and the surface of others CAR T-cells giving extra stimulation to a second-generation CAR with the endodomains CD3ζ and CD28. These CAR T-cells had increased tumour cytotoxicity and persistence and induced less PD-1 expression compared with the second-generation CAR(343). The co-expression of CD40L (expressed on activated T-cells) on CAR T-cells increased proliferation and secretion of proinflammatory Th1 cytokines and augmented the immunogenicity of patient-derived $CD40^+$ leukaemia cells(344). Moreover, dominant-negative receptors of PD1, TGF-ß receptor II and CD95 (FasR) have also been expressed on CAR T-cells. These dominant-negative variants lack the intracellular signalling domain and compete for the interaction with the ligand with the endogenous receptors to combat the immunosuppressive environment (345–347).

The use of chimeric IL4 receptors has also been explored in CAR T-cells. IL4 may be present in the TME to redirect the immune response to a Th2-type inflammation instead of the anti-tumour Th1. A chimeric IL4R, with the extracellular domain of IL4R and the intracellular domains of IL7R or IL21R, have been designed to take advantage of IL4 presence to deliver favourable signalling to the CAR T-cells

(348,349). This approach has also been explored with the extracellular domain of the co-inhibitory molecule PD1 and the intracellular domain of co-stimulatory CD28 (350).

1.2.7.2 Genome-edited CAR T-cells

New designs of CAR T-cells have introduced additional genetic modifications to promote the knock-out of endogenous TCRs, HLAs, co-inhibitory receptors or transcription factors related to cytotoxicity dysfunction (figure 1.9.B). Several clinical trials are being conducted with genome-edited CAR T-cells (351).

Knocking-out endogenous TCR and HLA is an approach to improve the performance of allogeneic CAR T-cell therapies. The knock-out of TCR and HLA class I have been achieved using a zinc finger nuclease (ZFN) (352,353). Also, Poirot et al. 2015 knocked-out the TCR, by disrupting the TCRα constant gene (*TRAC*), and CD52 using transcription activator-like effector nucleases (TALEN) and tested these CAR T-cells in a GVHD preclinical model. CD52 is expressed on mature lymphocytes and its function is not yet well understood (354). It is a common target used for lymphocyte depletion. CD52 was knocked-out by Poirot et al. 2015 in their allogenic CAR T-cells to be able to support their engraftment by depleting the T-cells before infusion. Treatment with alemtuzumab (an anti-CD52 therapeutic antibody) achieves T-cells depletion without affecting the gene-edited CAR T-cells (355).

The CRISPR (Clustered regularly interspaced short palindromic repeats)/Cas9 system has also been used to knock-out PD1, the TCR (gene *TRAC*), the HLA class I genes (gene *B2M*), LAG3, CTLA4, GM-CSF and TGF-β receptor II (356–364). Another approach using CRISPR/Cas9 is the development of CAR T-cells against TAAs expressed on T-cells, for example CD7. In this case, CD7 was knocked-out on the CAR T-cells to avoid CAR induced self-activation and anti-CAR T-cell cytotoxicity (mediated by the same CAR T-cells) (365). CRISPR/Cas9 can also be used to inactivate genes involved in the regulation of T-cell effector function or T-cell differentiation, such as *DGKA* and *PTPN2* (366,367).

Current targets for gene edited CAR T-cell are summarised in table 1.7. Other possible interesting genes to targets are *TET2* and the genes encoding the transcription factors NR4A and TOX (253,368,369).

Table 1.7 Genes edited in CAR T-cells.

Gene	Protein	Objective	Reference
CD52	Campath-1 antigen (CD52)	Lymphocyte depletion with Anti-CD52 before allogenic CAR T-cell infusion	355
TRAC	TCR α-chain constant region	Disruption of endogenous TCR expression for allogenic CAR T-cell therapy	355, 358, 359, 360
PDCD1	PD1(CD279)	Disruption of the inhibitory interactions with PDL1 and PDL2	356,357, 359,360
B2M	$ß_2$ microglobulin	Disruption of MHC class I molecules expression for allogenic CAR T-cell therapy	359, 360
LAG3	LAG3 (CD223)	Disruption of the inhibitory interactions with MHC class II	361
CTLA4	CTLA4 (CD152)	Disruption of the inhibitory interactions with CD80 and CD86	362
CSF2	GM-CSF	Control the development of inflammation and toxicities	363
TGFBR2	TGF-ß receptor II	Disruption of TGF-ß inhibitory stimulation	364
CD7	CD7	Development of Anti-CD7 CAR T-cells	365
DGKA	Diacylglycerol kinase α	Disruption of the negative regulation of CAR T-cell activation through the metabolism of diacylglycerol	366
PTPN2	Protein tyrosine phosphatase non-receptor type 2	Disruption of the negative regulation of CAR T-cell activation through by dephosphorylation of Lck	367

1.2.7.3 Modular CAR T-cells

The modular CAR T-cell technology, also known as universal CAR T-cell technology, aims to develop flexible CAR T-cell systems able to target different TAAs by separating the antigen-binding domain and the receptor into two different entities: the modular CAR (modCAR, to deliver the signal to the cell) and the CAR-adaptor (to recognise the TAA and interact with the modCAR) (figure 1.9.C). Therefore, "off-the-shelf" modCAR T-cells could be developed and used in

combination with a drug (the CAR-adapter) to target different TAAs. Several methodologies have been reported in this area. In most of them, the CAR-adaptor is based on antibodies or antibody fragments fused with domains or tags able to bind with high affinity to the extracellular domain of the modCAR and trigger the intracellular signal in the CAR T-cell (370). This tag in the CAR-adaptor can consist of a peptide, an antibody fragment or a coupled molecule. In the modCAR, the adaptor binding domain could also be an antibody fragment able to recognise the tag at the CAR-adaptor. However, other entities have also been used, for example, FcγRIIIa (CD16) (371). This technology can be used with antibodies already approved for clinical use. One limitation of this approach is the interaction with circulating antibodies, able to bind to the CD16 modCAR. To efficiently compete with circulating antibodies, glycoengineered antibodies with increased affinity to CD16 could be used as a CAR-adaptor.

Biotin-binding immunoreceptors (BBIR) have also used as tags in modCARs. BBIR have an avidin or streptavidin-based binding domain able to bind to biotinylated antibodies used as a CAR-adaptor (372,373). Furthermore, modCAR tags based on the leucine zipper AZip (zipCAR) have been designed to recognised CAR-adaptors labelled with the leucine zipper BZip (zipFv). This system has been named SUPRA (Split, universal and programmable) CAR T-cells (374).

1.2.7.4 Tandem CAR T-cells

CAR targeting simultaneously two or more TAAs have been designed to avoid tumour escape and relapse. Patients treated with anti-CD19 CAR T-cells therapies have shown a high rate of relapse. The main reason for relapse is the loss of expression of CD19 on the tumour cells (375). Bispecific Tandem CARs consist in two scFvs in tandem linked by a peptide (figure 1.9.D). Tandem CAR T-cells targeting CD19 in combination with HER2/neu, CD20, CD133, CD22 or BCMA have been developed (376–380). Furthermore, a bispecific Tandem CAR has been designed using the anti-HER2/neu scFv linked to IL13 mutein (IL13 with high affinity of binding to IL13Rα2). This CAR can simultaneously recognise HER2/neu and IL13Rα2 on the surface of the tumour cells (381). Tandem CARs could also be trispecific, a CAR has also been designed using the scaffold anti-HER2/neu scFv-IL13 mutein by adding an extra scFv targeting EphA2 (382). Some Tandem CARs

have been already tested in clinical trials, for example, targeting CD19/CD20 or BCMA/CD38 (383,384).

1.2.8 New generations of CAR T-cells to improve safety

As mentioned before, adjusting the affinity of the binding domain could have a significant effect on the discrimination of healthy cells and it could avoid on-target off-tumour activation of CAR T-cell (298,301–307). Furthermore, various techniques have been proposed to avert the side-effects related to on-target off-tumour responses and increase the safety of the therapy (figure 1.10).

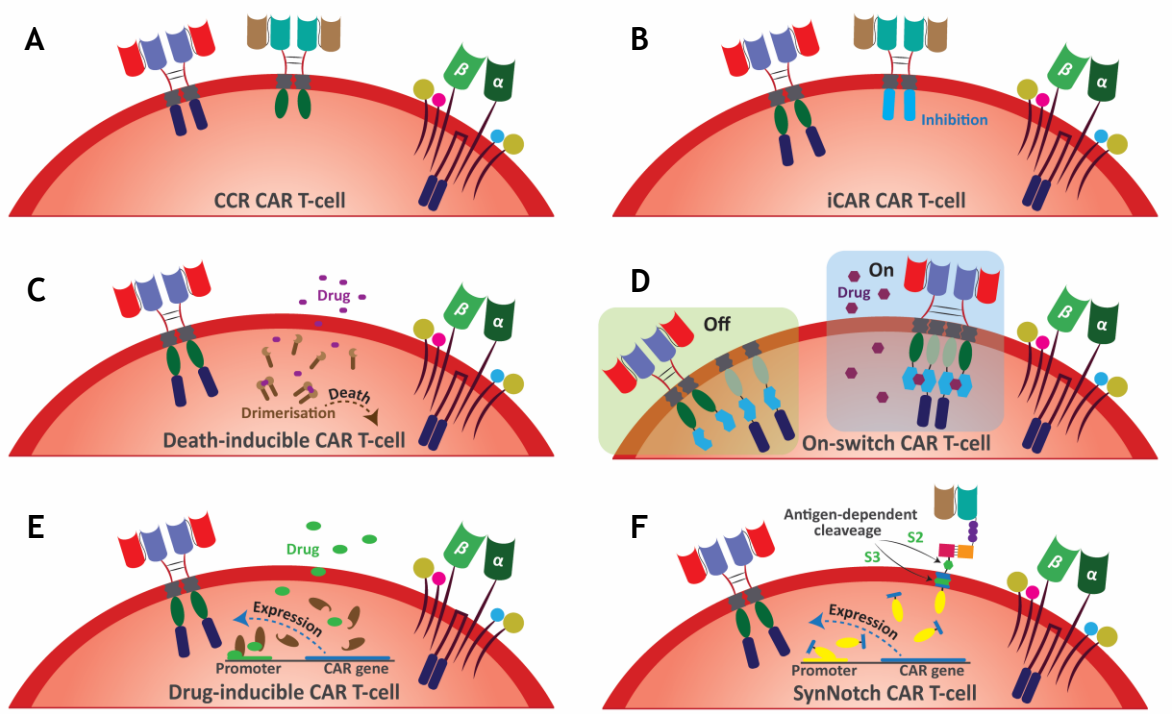

Figure 1.10 New generations of CAR T-cells to improve safety. A) Chimeric co-stimulatory receptor (CCR) CAR T-cells co-express two CARs recognising two different TAAs. One CAR delivers the activation signal while the other the co-stimulation, leading to full activation with cells expressing both TAAs. b) CAR T-cells with extra inhibitory CAR (iCAR CAR T-cells) co-express two CARs recognising two different TAAs (TAA1 and TAA2). One CAR delivers the activation and co-stimulation signals while the other provides an inhibitory signal, leading to the CAR T-cell activation with cells expressing TAA1 but not expressing TAA2. C) Death-inducible CAR T-cells co-express a suicide gene expressing a protein that can dimerise under the presence of a drug, leading to cell death. D) On-switch CAR T-cells co-express a CAR with a co-stimulation domain and a dimerization domain together with a membrane protein adaptor, with an activation domain and a dimerization domain (an extra co-stimulation domain can also be included). Under the presence of a drug, the CAR and the membrane adaptor dimerise forming a functional on-switch CAR. E) Drug-inducible CAR T-cells express the CAR only under the presence of a drug. F) Synthetic Notch CAR T-cells express a synthetic Notch receptor that recognise a first target protein (target 1) and induce the receptor cleavage in S2 and S3, releasing its intracellular domain. The cleaved intracellular domain induces the expression of a CAR targeting a second protein, in this case a TAA. The CAR is just expressed in presence of target 1. The Notch core region is composed by the heterodimerisation domain (pick and orange squares), the Lin12-Notch repeats (purple spheres) and the cleavage domains. For descriptions of the different elements in this figure, refer to figure 1.5.

1.2.8.1 CAR T-cell with a chimeric co-stimulatory receptor

The co-expression of two CARs recognising two different TAA (one delivering the activation and the other the co-stimulation signal) could lead to the activation of CAR T-cells in the context of cells overexpressing both TAAs, minimising targeting healthy cells. This co-stimulatory type receptor has been named Chimeric Co-stimulatory Receptor (CCR) (figure 1.10.A) (385).

1.2.8.2 CAR T-cells with extra inhibitory CAR

This approach employs the co-expression of two CARs, the CAR with activation signalling targeting a TAA and an inhibitory CARs (iCARs) with co-inhibition signalling (signalling for example from CTLA-4 or PD-1) targeting an antigen expressed on healthy cells but not on tumour cells (figure 1.10.B). However, appropriate targets for an iCAR need to be identified (386).

1.2.8.3 Death-inducible CAR T-cells

The introduction of suicide genes or elimination genes has been proposed to deplete CAR T-cells from the patient's body after treatment (figure 1.10.C). The integration of an inducible caspase-9 (iCasp9) is an exciting proposal. Caspase-9 is a pro-apoptotic molecule coded by the gene *CASP9*. iCasp9 comprises of a fusion protein between ΔCaspase9 (a caspase-9 without its caspase activation domain known as CARD) and the human FK506-F36V domain, aka FK506, binding protein domain (FKBP). FK506-F36V allows conditional dimerization of the fusion protein using Rimiducid (AP1903), an FKBP activator. ΔCaspase-9 is activated by dimerisation leading to rapid autocatalytic cleavage and the production of the two individual subunits of caspase-9 (p35/p12), which activate caspase-3 promoting apoptosis. A single dose of Rimiducid injected into patients could eliminate from the patient's body 90% of the modified T-cells in 30 minutes (387–390).

Herpes simplex virus type 1 thymidine kinase (HSV-tk) is a well characterised suicide gene (in combination with ganciclovir) that can also be used in CAR T-cell therapy (391). HSV-tk can phosphorylate nucleoside analogues such the drug ganciclovir (GCV), turning the drug into a toxic compound (GCV-triphosphate) leading to inhibition of DNA synthesis and cell death (392). The main disadvantage

compared with iCasp9 is the potential immunogenicity of the system (HSV-tk is a viral protein) and the slower cell killing rate.

A different approach is the co-expression of a cell surface antigen that can be targeted by a cytotoxic mAb. One example is the expression of CD20 that could be targeted with the clinical mAb Rituximab (393). In another example, a truncated version of human EGFR is targeted with the clinical mAb Cetuximab. The truncated human EGFR retains the transmembrane cell surface localisation and the conformational epitope recognised by Cetuximab (394).

1.2.8.4 On-switch CAR T-cells

Wu et al. 2015 have described an on-switch CAR T-cell system based on the combination of a CAR with a drug to trigger CAR T-cell activation in the presence of the drug and the target antigen (figure 1.10.D). The drug switch is based on the dimerization at the plasma cell membrane of two different subunits, the CAR and the adaptor, to form a full competent on-switch CAR composed by two CARs and two adaptors. The CAR consists of the antigen-binding domain, hinge domain, transmembrane domain, co-stimulatory domain and a drug-induced dimerization domain. The adaptor consists of a transmembrane domain, drug-induced dimerization domain and activation domain, with the possibility of also introducing co-stimulatory domains between the transmembrane domain and the drug-induced dimerization domain. The drug-induced dimerization domain at the CAR is the FKBP domain, also used in the iCasp9 system. The drug-induced dimerization domain at the adaptor is the T2089L mutant of FKBP (FRB*). FRB* heterodimerizes with FKBP in the presence of the rapamycin analogue AP21967, leading to the formation of the full competent on-switch CAR able to trigger antigen-dependent T-cell activation (395). Another strategy has been developed introducing the dimerization domains extracellularly between the binding domain and the hinge domain (396), providing a potentially promising strategy to boost the avidity of low-affinity CARs by crosslinking with AP21967.

1.2.8.5 Drug-inducible CAR T-cells

A tetracycline-inducible expression system has been used to control and modulate the expression of CARs in CAR T-cells (figure 1.10.E). This system consists of a Tet-responsive promoter that binds the Tet-On 3G transactivator protein in the

presence of doxycycline. The Tet-On 3G transactivator protein is expressed constitutively while the CAR is controlled by the Tet-responsive promoter. Doxycycline (a synthetic antibiotic derived from tetracycline) is added to induce the expression of the CAR. The Tet-On 3G system is highly sensitive to doxycycline with reduced basal expression compared with other tetracycline-inducible systems. Multiple intratumorally administration of doxycycline allowed the local expression of the anti-CD147 CAR and local antitumor activity in a xerograph model of hepatocellular carcinoma (397).

1.2.8.6 Synthetic Notch CAR T-cells

Synthetic Notch (synNotch) receptors are fusion proteins that use the singular transmembrane domain of Notch proteins (398). Notch family members are proteolytically induced receptors with an important role in embryonic development, controlling cell fate. In T-cells, Notch signalling is crucial during thymic T-cell development and remains important in peripheral T-cells (399). The engagement of a Notch receptor with its ligand leads to intramembrane proteolysis and release of the intracellular domain, which is a transcription factor that can then go into the nucleus to function (400).

SynNotch receptors use the intermembrane domain of a Notch receptor, a customised intracellular domain and an antigen-binding extracellular domain (398). The use of SynNotch receptors activates transcription in response to the recognition of specific antigens. Roybal et al. 2016 developed a new approach for CAR T-cell therapy based on the use of a synNotch receptor targeting the first antigen to control the expression of a CAR targeting a second antigen (figure 1.10.F). This receptor was configured with a binding domain (scFv), the Notch core region (compose by the Lin12-Notch repeats, the heterodimerization domains and the transmembrane domains) and the intracellular transcription factor (401). The Notch core region contains three cleavage domains: S1, S2 and S3. The cleavage of S1 occurs during protein maturation in the trans-Golgi, mediated by a furin-like convertase and giving rise to two subunits that then form a heterodimer at the plasma cell membrane. Interaction with the ligand leads to ADAM metalloprotease mediate cleave of S2, removing the extracellular fragment of the heterodimer. Then, the γ-secretase complex mediates the intracellular release of the transcription factor (S3) (402). The engagement of the synNotch receptor with

its antigen would lead to the release of the transcription factor able to induce the expression of the CAR. Therefore, the CAR would only be expressed in the presence of the first antigen (401).

A CAR targeting the TAA ROR1 has been used in xenograft models of $ROR1^+$ human tumours with synNotch receptors targeting EpCAM or B7H3. Anti-ROR1 CAR T-cell therapy induced lethal toxicity due to the expression of ROR1 in the bone marrow and splenic stromal cells. $ROR1^+$ stroma cells are $EpCAM^-$ and $B7H3^-$. To overcome the toxicity anti-EpCAM or anti-B7H3 synNotch receptors were used for local induction of anti-ROR1 CAR within the tumour. The strategy resulted in tumour regression without toxicity (403). Moreover, SynNotch receptors can be used to locally induce the expression of cytokines, T-cell differentiation, cell death or delivering of biological drugs (404).

1.2.9 Use of CAR in other cells

Aside from the αß T-cells, CARs have also been expressed in different cells such as T-reg cells, iPSC, NK cells, γδ T-cells and macrophages (table 1.8).

Table 1.8 Other CAR-modified cells and applications.

Other CAR-modified cells	Applications	References
CAR T-reg cells	Therapy to treat GVHD and inflammatory diseases	405-425
T-iPSC CAR T-cells	Allogenic therapy using cell lines as a source of starting material	426-432
CAR NK cells	Allogenic therapy based on the characteristic of NK cells	433
CAR NK-92 cells	Allogenic CAR NK cell therapy using a cell line as a source of starting material	433,435, 436, 437
CAR NKT cells	Allogenic therapy based on the characteristic of NKT cells	438, 439
CAR γδ T-cells	Allogenic therapy based on the characteristic of the γδ T-cells populations	442-449
CAR macrophages	Therapy based on the antigen-specific enhancement of macrophage phagocytosis	450

1.2.9.1 CAR T-reg cells

$CD4^+$ αß T-reg cells are immunosuppressive lymphocytes that can be engineered with a CAR to promote antigen-specific immunotolerance and homeostasis in inflammatory diseases or transplantations. Antigen-specific CAR T-reg cells usually carry a standard second-generation CAR. Although CAR T-reg cells can be induced *in vitro,* they are generally contaminated with effector T-cells. Therefore, the current expansion methodology for CAR T-reg cells uses T-reg cells purified from patients (autologous) or donors (allogenic) PBMC. Standardising a robust method for CAR T-reg cells expansion is challenging. Naïve T-reg cells can be isolated, stimulated with anti-CD3, anti-CD28 and IL2 to create a master product. Then, these cells are transduced with a CAR and expanded in the presence of IL2 (405). Furthermore, CAR transduced T-reg cells can be sorted to be expanded in the presence of donor's PBMC, anti-CD3 antibody and OND (oligodeoxynucleotides) (406) to stabilize $Helios^+$ $Foxp3^+$ cells (407).

Foxp3 is a crucial transcriptional regulator for the development and inhibitory function of Treg (408–410). Two population of $Foxp3^+$ Tregs cells can be differentiated based on the expression of the transcription factor Helios (encoded by the gene *IKZF2*). $Helios^+$ $Foxp3^+$ T-reg cells are thymic-derived T-reg cells while $Helios^-$ $Foxp3^+$ T-reg cells are induced in the periphery, around 70% of the T-reg cells in the periphery are $Helios^+$ $Foxp3^+$ T-reg cells (411,412). $Helios^+$ $Foxp3^+$ T-reg cells are the optimal subpopulation of T-reg cells for cellular therapy due to their capacity to produce effector cytokines and their stability of Foxp3 expression during *ex-vivo* expansion (407). A Foxp3 transgene has been used in CAR constructions to drive $CD4^+$ T-cell differentiation into T-reg cells (413).

Several antigens have been targeted with CAR T-reg cells in different diseases models (414). In transplantation, anti-HLA-A2 CAR T-reg cells have been used to treat GVHD and skin rejection showing promising results (415–417). In haemophilia A, a recessive X-linked coagulation disorder caused by a defect in the gene *F8*, Factor VIII (FVIII) has also been targeted, suppressing anti-FVIII antibody response (418). Anti-CEA CAR T-reg cells have also been used to treat colitis and asthmas being more effective than unmodified T-reg cells (419,420). In colitis disease models, CAR T-reg cells targeting trinitrophenyl (TNP) have also shown improved activity compared to T-reg cells (421,422). In multiple sclerosis, targeting the

myelin oligodendrocyte glycoprotein (MOG) have demonstrated improved disease suppression than unmodified T-reg cells (413). Most of these CARs are second-generation CAR with CD28 and CD3ζ intracellular domains (413,415–420), but the combination CD28 and FcRγ have also been used (421,422).

Dawson et al. 2020 compared ten different second-generation CARs with CD3ζ and different co-stimulation domains for CAR T-reg cells in a model of GVHD. They tested the intracellular signalling domains of CD28, CD28-Y173F (mutant with diminished PI3K pathway activity) (423), 4-1BB, OX40, ICOS, CTLA4, CTLA4-Y165G (mutant with increased cell surface expression) (424), PD1, TNFR2 and TNFRSF18 (aka GITR, glucocorticoid-induced TNFR-related protein). Second-generation CAR with CD3ζ and CD28 were superior to the other constructions, and they concluded that inclusion of CD28 in the construction was essential CAR T-reg cells function (425).

1.2.9.2 T-iPSC CAR T-cells

Induced pluripotent stem cells (iPSC) are very exciting platform for "off-the-shelf" CAR T-cells (426). iPSC are generated from a somatic cell by the introduction of genes coding for four specific transcription factors (Myc, Oct3/4, Sox2 and Klf4) (427). iPSC are immortal, and different iPSC lines can be established. Then, these cell lines can be used to be differentiated into any cell linage, including lymphocytes (428). T-iPSC, iPSC generated from peripheral T-cells, bear the TCR rearrangement of the parental cell (429,430). For example, a T-iPSC line has been generated from a virus-specific T-cell targeting the EBV antigen LMP2 (431). The use of a virus-specific T-iPSC for cell therapy is an interesting method to avoid GVHD (103,104). iPSCs also have the advantage that they can be easily genetically edited, resulting in a stable and invariant modified clonal line. Functional CAR T-cells targeting CD19 have been generated from T-iPSC, an anti-CD19 CAR T-iPSC line was established and differentiated into anti-CD19 T-iPSC CAR T-cells. Curiously, the phenotype acquired after differentiation by the anti-CD19 T-iPSC CAR T-cells was closer to a γδ T-cell rather than an αß T-cell, even though they carried an αß TCR. The acquisition of this phenotype was not related to the CAR modification, but may be the premature expression of the αß TCR during development (T-iPSC expresses αß TCR) could polarise the development toward the γδ-like lineages (432). Maturation of T-iPSC–derived T-cells need further

optimisation to be able to shape the differentiation to the desired phenotype. T-iPSC can also be genetically modified to include gene knock-out or expression of cytokines or chemokines, allowing easy establishment of T-iPSC lines with the most sophisticated CAR technology for redirecting phenotype, and could be used in "off-the-shelf" allogeneic CAR T-cell therapy.

1.2.9.3 CAR expression in NK, NK-92 and NKT cells

Preclinical studies have shown antitumor activity of CAR-modified NK cells, and several clinical trials are currently underway, most of them targeting the TAA CD19. Furthermore, the NK cell line NK-92 is being also used for CAR-modified NK cells clinical trial targeting CD19, CD7, CD33 and HER2/neu (433). NK-92 was established in 1994 from a 50-year-old male patient non-Hodgkin lymphoma and showed *in vitro* cytotoxicity against K562 and Daudi cells (434). For their use in patients, to overcome the handicap of their malignant origin, the NK-92 cells are irradiated to suppress proliferation but maintain the cytotoxic activity (435). Infusion of irradiated NK-92 cells in patients has been shown to be safe (436). No major rejection has been shown with NK-92 cells, but patients treated with NK-92 cells have normally been pre-treated and as consequence they may have some level of immunocompromise (437). CAR-modified NKT cells (aka CIK cells, cytokine-induced killer cells) have also shown efficacy in preclinical models (438,439).

1.2.9.4 CAR γδ T-cells

The γδ T-cells population is composed of functionally distinct subsets, each of them with different characteristics. They also share features typically present in the innate immunity repertoire. They express receptors usually present in NK cells and show tissue-specific localisation of oligoclonal subpopulations sharing the same TCR chains (440). Also, they can behave as APC by opsonisation of targets cells and upregulation of costimulatory molecules and HLA-DR (441).

γδ T-cells have also been modified to express CARs. Rischer et al. 2004 expanded and transduced Vγ9Vδ2 T-cells with a first-generation CAR. Two first-generation CARs were investigated: anti-GD2 CAR and anti-CD19 CAR. Target specific activation by the CAR and cytotoxicity against antigen-expressing tumour cells was shown. The capacity of γδ T-cells to be activated by pAgs was proposed as a tool

for *in vivo* selective re-expansion during cell therapy (442). Furthermore, a polyclonal population of γδ T-cells was modified to express a second-generation CAR targeting CD19, demonstrating their efficacy in a mouse xenograft model. These cells were defined as bispecific based on the concept of stimulation by the CAR and their polyclonal γδ TCRs (443).

Fisher et al. 2017 used Vγ9Vδ2 T-cells to express a co-stimulatory CAR with an endodomain derived from DAP10 to target the TAA GD2. The receptor NKG2D (expressed in NK cells and Vγ9Vδ2 T-cells) is a hexametric complex composed of an extracellular homodimer and two intracellular homodimers of DAP10. After the interaction with the ligands, phosphorylation of the tyrosine-based signalling motif YINM of DAP10 triggers cell-mediated cytotoxicity and cytokine production (444,445). They showed cytotoxic activity dependent on the double engagement of Vγ9Vδ2 TCR and CAR, and no activity when the receptors were engaged individually. This double engaging technology has been proposed as a method to avoid on-target off-tumour toxicities (446).

Capsomidis et al. 2018 used a second-generation CAR (CD3ζ and CD28) also targeting GD2 to transfect Vδ1 and Vγ9Vδ2 T-cells. They showed that CAR-modified γδ T-cells could enhance their cytotoxicity by CAR engagement while also retaining their functionality as APC. Their APC function would be expected to help promote the intratumoral immune response by the presentation of tumour antigens in their MHC to αβ T-cells (447).

Furthermore, non-signalling CARs have also been used in γδ T-cells, enhancing cytotoxicity unlike when used in αβ T-cells. The introduction of a high-affinity interaction mediated by CAR and the native γδ T-cell cytotoxicity leads to a boost of the anti-tumour activity without CAR activation (448).

1.2.9.5 CAR macrophages

Klichinsky et al. 2020 have modified macrophages with a first-generation anti-HER2/neu CAR with a CD3ζ endodomain. CD3ζ has three ITAMs highly homologous to the single ITAM present in FcεRIγ, a signalling molecule involved in antibody-dependent cellular phagocytosis (ADCP) in macrophages. CAR macrophages showed pro-inflammatory M1 phenotype polarisation (pro-inflammatory

phenotype with pathogen-killing abilities) (449), antigen-specific phagocytosis, and tumour clearance in culture. The efficacy was also tested *in vivo* in xenograft and humanised mouse models, showing M1 macrophage phenotype in the TME that leads to Th1 polarization of $CD4^+$ T-cells, the production of pro-inflammatory antitumor cytokines and chemokines, upregulation of the antigen presentation machinery and a boost of the anti-tumour T-cell activity (450).

1.2.10 CAR T-cell to treat EBV-associated malignancies

CAR T-cells have been used in preclinical studies with xenograft mouse models to treat EBV-associated malignancy, targeting the viral TAAs LMP1 and LMP2A. In the first study, a second-generation CAR with the endodomains CD3ζ and CD28 was generated using an anti-LMP1 antibody, specific for an unknown extracellular loop of LMP1, reformatted to scFv. These CAR T-cells displayed LMP1 specific cytotoxicity and produced IFN-γ and IL-2 in response to NPC cells (HNE2) expressing LMP1 in culture. Also, a significant reduction in tumour growth was observed when the CAR T-cells were injected intratumorally into a subcutaneous NPC xenograft model using SUNE1 cells expressing LMP1 (123,124). This CAR was also used as a third-generation CAR with the endodomain CD28 and 4-1BB to enhance the antitumor activity, exhibiting better antitumor activity and longer survival *in vivo* compared with the second-generation format (451).

Another antibody targeting an unknown extracellular loop of LMP2A was reformatted to scFv and used for similar studies using a third-generation CAR with the endodomains CD3ζ, C28 and 4-1BB. It showed cytotoxicity to NPC cells expressing LMP2A (C666-1) and partial inhibition of tumour growth in a xenograft model using CNE1 cell expressing LMP2A (125,126). Targeting LMP1 and LMP2A with a CAR is an especially attractive approach to treat EBV-associated malignancies since they are viral TAAs with epitopes located on the surface of the infected cell. Therefore, there should not be on-target off-tumour related toxicities associated with the therapy.

A second-generation CAR targeting the lytic viral protein gp350 has been also designed with scFvs derived from the neutralising antibody clone 72A1 and the endodomains CD28 and CD3ζ to treat PTLD. These CAR T-cells showed *in vitro* cytotoxicity against the cell line EBV^+ B95-8 and prophylactic and therapeutic

action in a humanized mouse model of EBV infection, controlling or reducing EBV spread and impeding EBV^+ lymphoproliferation and lymphomagenesis (452).

CARs targeting EBV peptide-HLA complexes have also been developed. Dragon et al. 2020 designed an anti-EBNA3C fourth-generation CAR with the endodomains 4-1BB and CD3ζ and an scFv derived from the monoclonal antibody TU165, able to recognise the EBNA3C-derived peptide LPPHDITPY in complex with HLA-B*35, and an IL-12 inducible system under CAR activation. The authors demonstrated *in vitro* cytotoxicity against peptide-loaded K562-B*35 cells and improved function and recruitment and activation of immune cells by incorporating the IL12 inducible system, proposing a new possible approach to treat PTLD (453).

Furthermore, B7H4 has also shown potential as a TAA to treat EBV-associated malignancies with CAR T-cell therapy. Smith et al. 2016 demonstrated that their second-generation anti-B7H4 CAR using the CD28 and CD3ζ intracellular domains induced CAR-driven cytotoxicity against an EBV-transformed B-cell line (named EBV-B) in culture (297).

1.3 Display technologies for the selection of antibody fragments

Since 1975 it has been possible to isolate and produce mAbs, thanks to the development of hybridoma technology by César Milstein and Georges J. F. Köhler (454). By injecting an animal with an antigen of interest, a humoral immune reaction is elicited. Then, the B-cells are harvested and fused with a myeloma cell line, a non-antibody producing immortal B-cell line. The resulting cells are termed hybridomas and have the antibody-producing ability of the primary B-cell and the longevity and the reproductive capacity of the myeloma cell line. Individual hybridoma cell clones can be isolated, and their antibodies characterised. In 1984, Köhler and Milstein were awarded a Nobel Prize in physiology or medicine for the development of hybridoma technology. This technology is still extensively used to develop mAbs for clinical and research use and other applications.

In 1985, the first mAb was approved for immunosuppression to reduce acute rejection in patients with organ transplants. Muromonab (OKT3) is a mouse IgG2a CD3-specific antibody (455,456). However, mouse antibodies are highly

immunogenic in humans and the use of Muromonab was associated with development of neutralising antibodies (457). Muromonab was withdrawn from the market in 2010 due to the substantial risk of infection, severe cytokine release, the high immunogenicity of mouse antibodies in humans and the availability of alternative therapies.

In 1994, the FDA approved the second mAb for clinical use. Abciximab is a chimeric human/mouse Fab fragment specific to the glycoprotein IIb/IIIa indicated as a platelet aggregation inhibitory drug. It was the first humanised mouse antibody obtained from a hybridoma. The constant regions of the mouse antibody were replaced with equivalent regions from a human antibody to reduce immunogenicity (458,459).

Meanwhile, in 1990, an alternative method to obtain mAbs was developed by Greg Winter and John McCafferty. This method is based on a technology previously developed by George P. Smith in 1985, where a library of peptides is created and displayed on the filamentous phage M13 by fusion with a virus capsid protein (460). Winter and McCafferty generated a phage library to display human scFvs created from antibody sequences obtained from human B-cells. Specific scFvs can be selected from the library based on their interaction with a specific antigen (174,175,461,462). This technology, called antibody phage display, enabled the isolation of the third mAb approved by the FDA in 2002 for clinical use and the first humanised antibody. Adalimumab was obtained by humanisation guided by phage display selection. This humanised antibody acts as an anti-TNF-α and it is used to treat inflammatory diseases and is currently the world's best-selling drug due to its wide range of applications (463,464). Smith and Winter received a shared Nobel Prize in chemistry in 2018 for the phage display of peptides and antibodies together with Frances H. Arnold for the directed evolution of enzymes.

Since then, other technologies have been developed for the display of antibodies or antibody fragments. The most prominent are yeast display, mammalian display and ribosome display. Together with hybridoma technology, antibody humanisation and the development of antibody humanised transgenic mice they have enabled the isolation and production of a large repertoire of clinical antibodies currently in the market.

1.3.1 Phage display of human scFvs

Phage display uses a modified filamentous bacteriophage M13 as a mediator between the protein displayed at the surface of the phage and the DNA sequence inside the phage and encoding this protein. Therefore, by recovering a selected phage or an infected bacterium, the amino acid sequence of the displayed protein can be determined by sequencing the phage's DNA. By protein-protein interaction, the phage displaying a protein of interest can be selected and isolated and the protein DNA and amino acids sequences obtained (460–462). The phage M13 is a filamentous phage with a 6407 nt long circular single-stranded DNA genome. The main protein comprising its capsid is termed PVIII. In a modified phage, the length of the genome determines the dimensions of the phage, which depends on the number of PVIII units assembled. Structurally, at the first end of the phage (first assembled end during the phage synthesis in *E. coli*) there are five copies of the protein PIX and five copies of the less exposed PVII. At the second end, five copies of the PIII protein and five copies of the less accessible PVI are located (figure 1.11).

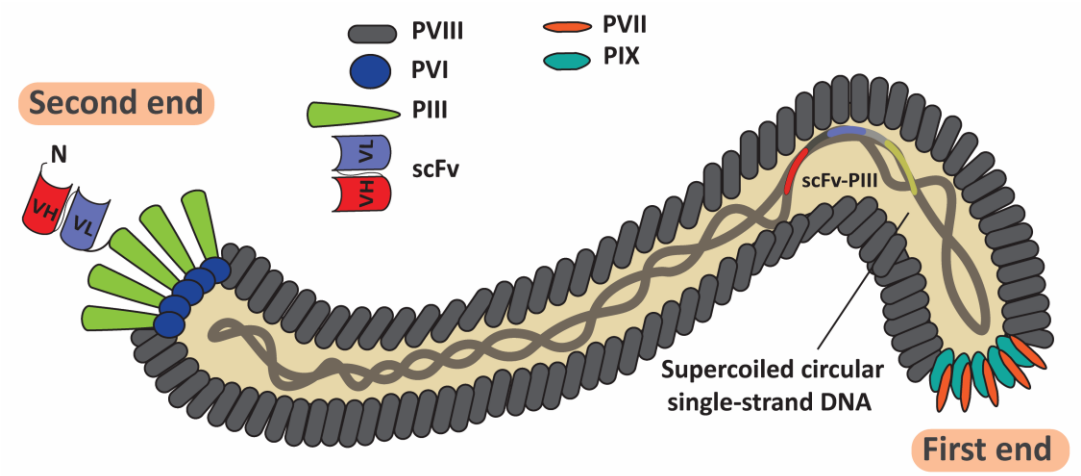

Figure 1.11 Diagrammatic structure of M13 phage from a phagemid library displaying scFv. At the first end of the phage (first assembled end during phage synthesis in E. coli), there are five copies of PIX (dark green) and five copies of PVII (orange). At the second end of the phage, there are five copies of PVI (blue) and five copies of PIII (clear green) one of them linked to an scFv. The rest of the capsid is composed of copies of PVIII comprising. The phage particle packages the phagemid supercoiled circular single-stranded DNA.

PIII is required for a two-step infection. The first interaction of the phage with the bacterium is via PIII and the bacterial F pilus. Then the complex interacts with the bacterial proteins TolQ, TolR and TolA and mediate an uncoating DNA

penetration (465). Attaching another protein to the N-terminus of PIII does not appear to affect the infection. Hence, PIII is the protein commonly used in phage display to create fusion proteins, with the recombinant protein segment at the N-terminus of PIII (figure 1.11).

1.3.1.1 Phage libraries versus phagemid libraries

There are two kinds of phage display libraries, distinguished by the vector system used: phage libraries and phagemid libraries (466). The plasmid used for phage libraries contains all the information for assembly of a functional M13 phage and at the N-terminus of PIII a cloning site for the creation of recombinant fusion proteins. Once the bacterial host is transfected with the plasmid, it produces functional phage with all five PIII copies displaying the foreign protein.

A phagemid contains an f1 origin of replication (for DNA package into the phage particle) and a bacteria origin of replication as pMB1 or pUC (for phagemid synthesis). The plasmid for phagemid libraries encodes only one phage protein, the PIII, with a cloning site for the recombinant fusion protein. Bacteria transfected with this vector are unable to produce functional phage. For the production of functional phage the bacteria need to be infected with a helper phage. The helper phage provides the rest of the elements to create a functional M13 phage, including the native PIII. As such, not all the PIII proteins on the produced phage display the recombinant protein. One of the most commonly used helper phage is M13KO7, which carries two modifications: a mutation Met40Ile in PII (a nickase involved in replication) and the origin of replication from p15A along with a kanamycin-resistance gene inserted within the M13 origin of replication. The insertion of the p15A origin and the kanamycin-resistance gene create a less efficient M13 origin working in conjunction with the mutated PII. Together with the high copy number of the phagemid, this leads to the preferential packaging of phagemid DNA, over helper phage DNA, into viral particles. The mutated PII functions sufficiently well with the altered M13 origin to produce a high enough titter of helper phage when grown alone, allowing for the expansion of the helper phage (467). Even so, virions prepared with M13KO7 have a phagemid/helper ratio of around 10:1.

The main difference between a phage library and a phagemid library is the number of copies of the fusion protein displayed. While the phage library displays five copies of the fusion protein (all the PIII are fused with the foreign protein), the phagemid library display fewer copies, since the helper phage also carries a wild type (wt) PIII (figure 1.11). The advantage of using phagemid libraries is that it results in a reduction of avidity during the selection, increasing the chances of isolation of candidates with higher binding affinities (468). The disadvantage is the presence in the phage library of some virions without fusion protein, but this can be overcome by increasing the number of phage used during the selection process.

1.3.1.1 Phage display libraries of antibody fragments

The phage libraries can be differentiated with respect to the displayed protein: peptides, scFv, Fab or single-domain antibody molecules such as VHH (variable heavy homodimers) or vNAR (variable new antigen receptor domain) (469). Antibody-based phage display libraries can be made in different ways giving rise to distinct libraries with different proprieties. Naïve libraries are generated using B-cells from a non-immunised source. These libraries contain antibodies able to bind to non-human antigens, but also to novel antibodies with binding possibilities including human antigens, since the reorganisation of VH and VL creates new specificities. The construction and production of non-immune phagemid library of human scFvs are described in figure 1.12. Immune libraries are created from B-cells from an immunised source, increasing the chances of obtaining a high-affinity antibody against a selected foreign antigen. Synthetic libraries are created from a specific antibody framework by *in vitro* randomisation of the CDRs, creating artificial loops that otherwise would probably not be part of the antibody repertoire of an individual. Semi-synthetic libraries consist of *in vitro* randomisation of CDRs of antibody chains obtained from B-cells from non-immunised donors. The diversity is primarily obtained from natural sources, while the CDR randomisation introduces extra diversity and new specificities. Each library has its advantages and disadvantages, and the use of one or another should be considered in each situation (470).

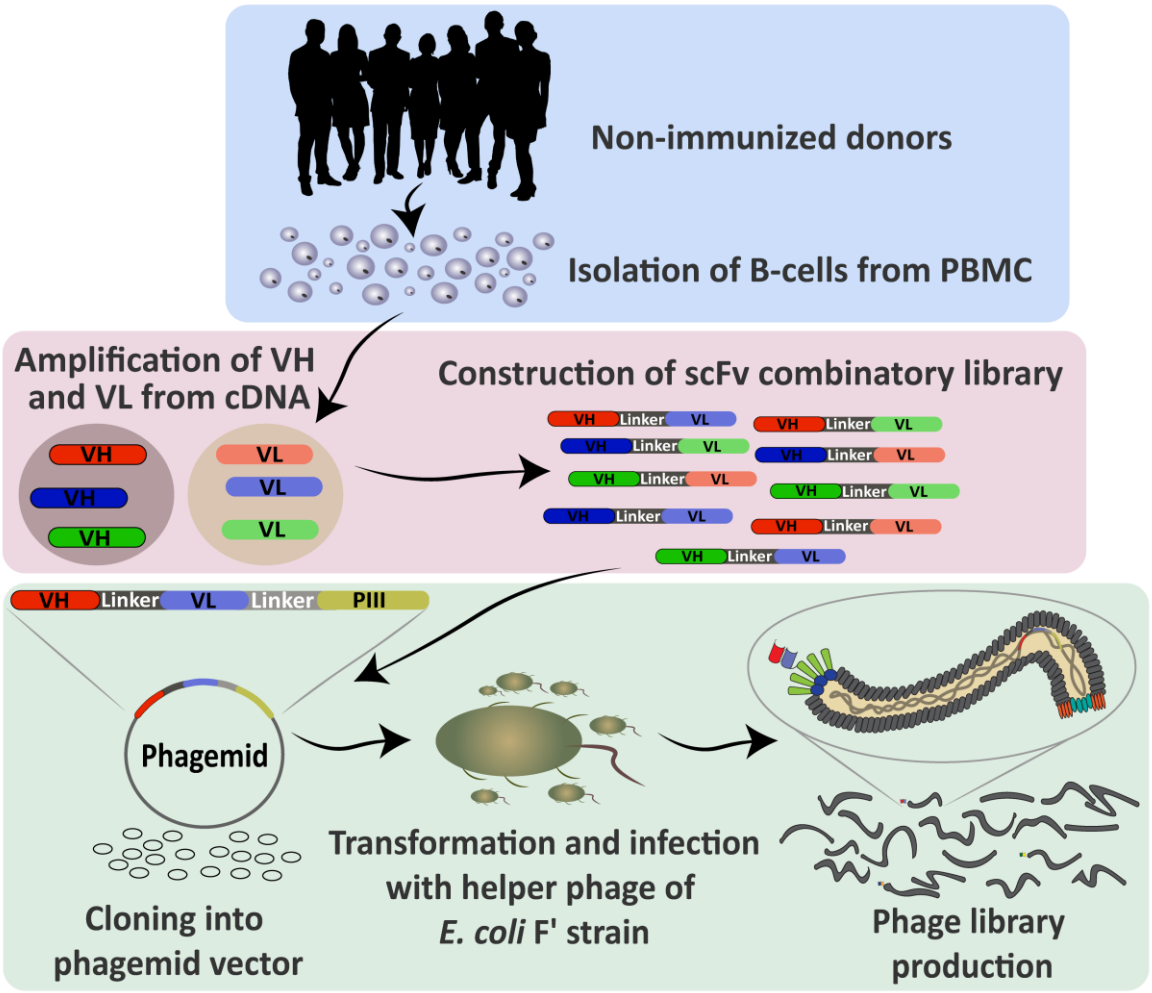

Figure 1.12 Construction and production of non-immune phagemid library of human scFvs. B-cells are isolated from PBMC obtained from non-immunized human donors, the RNA extracted, and the cDNA synthesized. The VH and VL segments are amplified from the cDNA and linked by PCR (Polymerase Chain Reaction) with a linking peptide for subsequent cloning into a phagemid vector. The phagemid vector is transfected into *Escherichia coli* F' to produce the bacterial library. To produce the phage library, the bacteria is infected with a helper phage.

1.3.2 Yeast display

In 1997, Boder and Wittrup developed a new display method using *Saccharomyces cerevisiae* EBY100 where the foreign protein is fused to the a-agglutinin adhesion receptor of the yeast. A-agglutinin is a cell wall-associated glycoprotein that interacts with α-agglutinin on the yeast wall and is involved in cell adhesion during mating in *S. cerevisiae* (471). A-agglutinin is composed of two subunits, Aga1 is a GPI anchored glycoprotein in the cell wall that creates a heterodimer with the Aga2 protein through two disulphide bonds. Aga2 is presented from the cell wall by its interaction with Aga1 and used to generate fusion proteins in the yeast display system (472). *S. cerevisiae* EBY100 is a Leu- and Trp- strain developed explicitly for yeast display. It has a genomic insertion of the gene *AGA1* regulated

by the GAL promoter with a URA3 selectable marker. Most of the plasmids used for yeast display use the C-terminal end of Aga2 as a cloning site to display the foreign protein. The fusion gene *AGA2* is controlled in these plasmids by a GAL promoter, the same promoter controlling the gene AGA1 inserted in *S. cerevisiae* EBY100. The yeast display system Aga1-Aga2-fusion proteins are inducible by the presence of galactose in the growing medium. The most commonly used and first developed plasmid for yeast display is pYD1 (473). A derived plasmid has been generated from pYD1 for fusion at the N-terminal region of Aga2, this plasmid was named pYD5 (474) (figure 1.13).

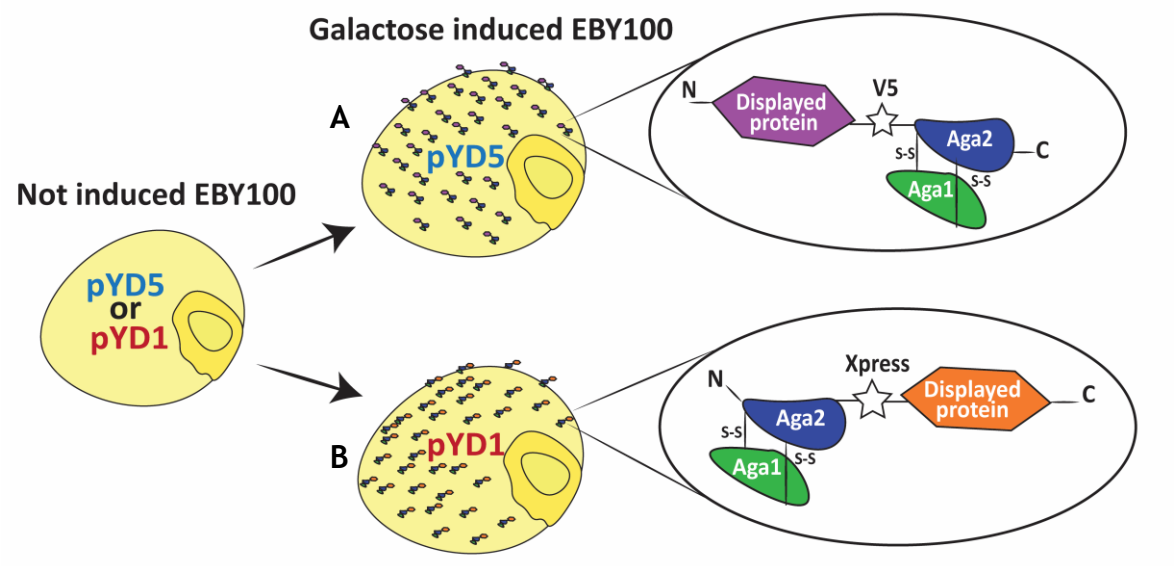

Figure 1.13 Galactose induction of pYD5 and pYD1 yeast display systems. A) N-terminal display of protein with the pYD5 yeast display system. B) C-terminal display of protein with the pYD1 yeast display system.

1.3.3 Yeast display versus phage display

Yeast display has been mainly used to create libraries of antibody fragments, having different features compared with phage display libraries. In phage display, the foreign protein is limited to prokaryotic post-translational modifications. Therefore, some mammalian proteins are not well expressed or appropriately modified in the system. In yeast display, post-translational modifications are closer to mammalian. Yeast display also allows detection of low-affinity binders due to the expression of thousands of antibodies on the surface of the yeast working together by avidity. Phage display expresses a maximum of five antibodies per phage with phage vectors or as few as one with phagemid vectors. Depending

on the objective of the antibody selection (level of affinity and diversity of antibodies desired), the use of phage display or yeast display need to be considered in each situation. Phage display, and especially phage display with a phagemid library, generally selects for high-affinity antibodies, although some of low affinity can also be promoted in the selection. With yeast display, selection of low-affinity antibodies together with high-affinity ones is possible. This system gives a competitive chance in the selection to the low-affinity antibodies due to enhanced avidity.

The main advantage of phage display over yeast display is the library complexity. Transformation of bacteria is relatively easy, creating large phage libraries with more than 10^{10} different clones. Working with a high number of phage (ten times the diversity of the library) is possible in a low volume of library sample (just a few µl of the library preparation). Yeast transformation is less efficient compared to bacterial, making it harder to create a complex yeast display library, therefore, typical library clone number are closer to 10^9. Additionally, working with more than 10^9 different yeast clones requires a high volume of library sample (hundreds of ml), making the first round of selection challenging when working with high complexity libraries.

1.4 Aims of the project

EBV-associated malignancies are a diverse group of cancers with different characteristics, some with low patient survival rates (39). The host immune system controls EBV infection and viral load and plays an essential role in defence against malignancy (68). By boosting the host immune response against viral factors, or other factors associated with EBV infection, it might be possible to improve patient outcome in the treatment of EBV-associated malignancies, offering an alternative therapy to patients that are not responding to first-line treatment. One of the most novel approach in cancer immunotherapy is CAR T-cell therapy. CAR T-cell therapies are producing outstanding results in clinical trials, mainly for the treatment of refractory haematological malignancies (184,186,234). The success of this type of therapy in clinical trials and the fact that there is a clear T-cell response of the body to EBV infection makes developing a CAR T-cell therapy to treat EBV-associated malignancies a worthwhile route to investigate. In

addition, this therapy could also be applied to other diseases associated with EBV infection, such as MS (117–119).

Aside from the viral proteins, the human protein B7H4 is an attractive target candidate to treat EBV-associated malignancies (164–169). Even though Smith et al. 2016 reported onset toxicity with anti-B7H4 CAR T-cell therapy (297), the possibility of using low-affinity scFvs for the CAR design keeps a door open to this approach (301–305). To do this, it would be necessary to test a pool of scFv targeting human B7H4 with different affinities and differentiate the ones able to functionally discriminate *in vitro* high expressing cells from low and medium expressing cells. Another approach is the targeting of viral TAAs. Theoretically, few on-target off-tumour toxicities should be associated with such therapy. The main targets selected in this study for this approach are the viral proteins LMP1 and LMP2, since they have extracellular loops that could be potentially recognised by an antibody (123,125) and used in CARs (124,126). Therefore, the project aimed to isolate human scFvs targeting B7H4, LMP1 and LMP2A for their use in developing potential CAR T-cell therapies to treat EBV-associated malignancies. The goal of the project (beyond the work described herein) was the expression of these scFvs in CAR format in a human reporter T-cell line to study their functionality with the ultimate goal of developing a CAR T-cell therapy to treat EBV-associated malignancies.

1.5 Approach

For the isolation of the human scFv, a naïve phagemid phage display library of 10^{10} human heavy chain linked to kappa light chain scFvs has been used. For the selection of the scFv candidates from this library, a novel method was established during this research. A conventional phage display selection consists of using a soluble recombinant antigen with a protein tag. The use of the recombinant antigens during the initial stages of the selection can be problematic due to the presence of immunogenic tags that can promote selection of unwanted scFvs. In the case of membrane proteins, the quality of the recombinant preparation is a concern, with the creation of new unwanted epitopes due to protein aggregation. The cost of production or the price of a commercial antigen is also an important limitation. Furthermore, membrane proteins with several transmembrane domains tend not to conserve their native structure in solution.

To overcome these difficulties and to establish an economically viable approach, we used a yeast display system to display the antigen. In the first stage of the selection, the phage library was the source of scFvs and the yeast display the source of antigens (475). In this way, the strength of the large size of a phage display library was used for the selections. The phage selections were conducted with several rounds of library depletion against wt yeast surface proteins followed by selection against yeast expressing the antigen (figure 1.14).

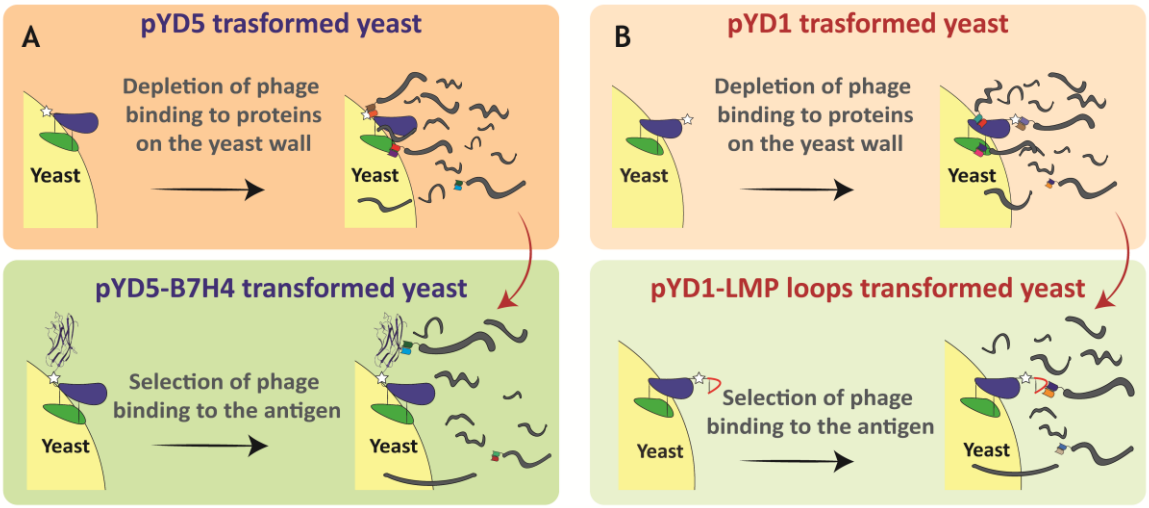

Figure 1.14 Phage depletion and selection. A) Phage depletion with induced pYD5 yeast following by selection with yeast expressing B7H4. B) Phage depletion with induced pYD1 yeast following by selection with yeast expressing LMP loops.

Then, after the completion of the first rounds of selections, the scFvs were transferred from the phagemid vector to a yeast display vector for their expression in a yeast display system, taking advantage of the strength of the yeast display of antibodies (476) (figure 1.15).

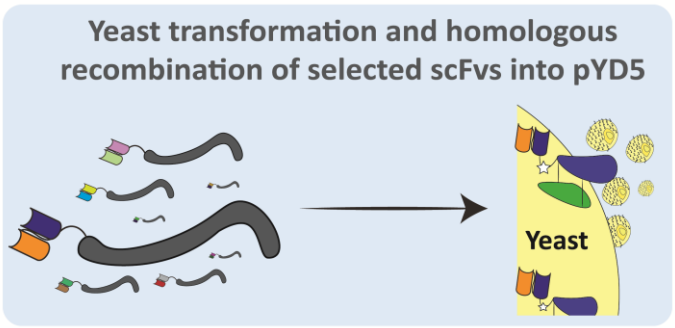

Figure 1.15 Yeast transformation and scFv homologous recombination into pYD5.

The yeast expressing the selected scFvs were exposed to interaction with mammalian cells expressing the antigen and selected by yeast-cell interaction (477–479). Thus, yeast mimicked the CAR T-cell recognising the antigen in native conformation expressed on the surface of mammalian cells (figure 1.16).

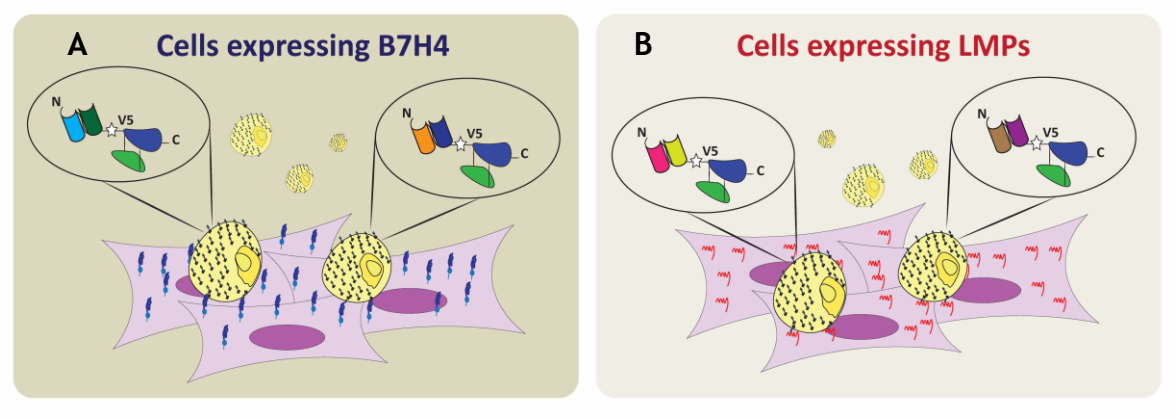

Figure 1.16 Selection of yeast expressing scFv by interaction with cells expressing B7H4 (A) or LMPs (B).

Next, the selected scFvs binding specifically to the target could be identified by two methods, by fluorescence-activated cell sorting (FACS), using a commercial recombinant antigen when possible, or by next-generation sequencing (NGS), where no recombinant antigen is available. Finally, the identified scFvs were used for the design of CARs. To test the functionality of these CARs, a reporter T-cell line has been used to assess the levels of antigen-driven CAR activation (figure 1.17).

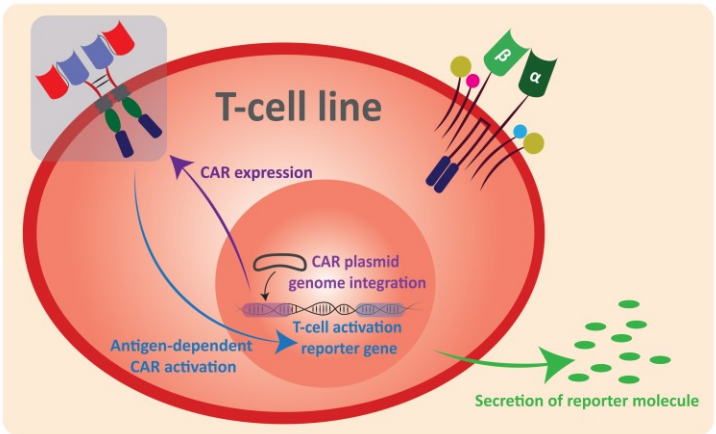

Figure 1.17 Reporter T-cell line expressing CAR to study antigen-driven CAR activation. An NF-κB reporter human T-cell line modified to express a second-generation CAR. CAR antigen-dependent stimulation leads to the activation of the reporter gene and secretion of a molecule to the medium. The quantity of the reporter molecule present in the media is directly related to the level of T-cell activation.

2. Materials and methods

2.1 Table of reagents

Table 2.1 Antibiotics for bacteria, yeast and mammalian cell culture.

Antibiotic	Working concentration	Company	Catalogue
Ampicillin	100 µg/ml	Sigma Aldrich	A0166-5G
Kanamycin	50 µg/ml	Sigma Aldrich	K1377-5G
Tetracycline	10 µg/ml	Sigma Aldrich	T7660-5G
Penicillin-streptomycin	100 U/ml	Sigma Aldrich	P4333-100ML
Zeocin	100 µg/ml	InvivoGen	ant-zn-05
Blasticidin	15 and 10 µg/ml	InvivoGen	ant-bl-05
Hygromycin B	400 and 200 µg/ml	InvivoGen	ant-hg-1

Table 2.2 Antibodies used in flow cytometry and western blotting.

Antibody	Host	Woking dilution	Company	Catalogue
Anti-Xpress tag	Mouse	1:250 (FC)	TFS	R910-25
Anti-mouse IgG Alexa 488	Goat	1:250 (FC)	TFS	A28175
Anti-V5 tag FITC	Mouse	1:500 (FC)	TFS	R963-25
Anti-V5 tag Alexa 647	Mouse	1:250 (FC)	TFS	451098
Anti-human Fc FITC	Mouse	1:40 (FC)	Bio-Rad	MCA647F
Anti-5HIS tag Alexa 647	Mouse	1:250 (FC)	Qiagen	35370
Anti-human B7H4 PE	Mouse	1:20 (FC)	BD	562507
Mouse IgG1 kappa isotype PE	Mouse	1:40 (FC)	BD	554680
Hybridoma supernatant Anti-LMP1 clone 1G6	Rat	1:25 (WB)	In-house	-
Hybridoma supernatant Anti-LMP2 clone 14B6	Rat	1:25 (WB)	In-house	-
Anti-rat IgG HRP	Goat	1:2000 (WB)	CTS	7077S
Anti-human ß-actin	Rabbit	1:4000 (WB)	CTS	8457S
Anti-rabbit IgG HRP	Goat	1:4000 (WB)	CTS	7074S

*FC= Flow cytometry, WB= Western Blot, TFS= Thermo Fisher Scientific, CST= Cell Signaling Technology, BD=Becton Dickinson

Table 2.3 Recombinant proteins.

Recombinant protein	Company	Catalogue
human B7H4-human Fc	R&D Systems	8870-B7-050
human Fc	R&D Systems	110-HG-100
mouse B7H4-mouse Fc	R&D Systems	4206-B7-100
human B7H4-10HIS	R&D Systems	6576-B7-050
mouse B7H4-10HIS	R&D Systems	2154-B7-050

Table 2.4 DNA Oligonucleotides.

Name	DNA sequence	Tm (˚C)
(-)NheI-F	TGG TTC TGA TAG CAT GAC T	48
(-)NheI-R	AGT CAT GCT ATC AGA ACC A	43

(+)NheI-F	TCA ATA TTT TCT GTT ATT GCT AGC GTT TTA GCA CAG GAA CTG ACA ACT ATA TGC	60
(+)NheI-R	GCA TAT AGT TGT CAG TTC CTG TGC TAA AAC GCT AGC AAT AAC AGA AAA TAT TGA	59
pYDN Cassette-F	AAA CTG CAT AAC CAC TTT AAC	50
pYDN Cassette-R	AAG TAT ATT GTA TTT TGT ACG AGC	50
pYDN Check-F	AGA TGC AGT TAC TTC GCT G	53
pYDN Check-R	AAG TAC AGT GGG AAC AAA GTC	53
pYD1 Check-F	AGT AAC GTT TGT CAG TAA TTG C	53
pYD1 Check-R	GTC GAT TTT GTT ACA TCT ACA C	51
HR-F	TGT TTT TCA ATA TTT TCT GTT ATT GCT AGC GTT TTA GCA GCT GGT CAG CCG GCC ATG GC	72
HR-R	TAG AGT CCA AAC CCA ACA ATG GAT TTG GAA TTG GTT TAC CAG AAC CAC CGC CTT GGC C	73
HR amp-F	CTT CGC TGT TTT TCA ATA TTT TCT G	53
HR amp-R	AGT AGA GTC CAA ACC CAA CAA TGG	58
pcDNA5/FRT Check-F	CGC AAA TGG GCG GTA GGC GTG	65
pcDNA5/FRT Check-R	CGG CGA ACG TGG CGA GAA AGG	64
SeqB7H4-F	TGC CGG AAG TGA ATG TGG AC	58
LMP1-F	GAT GCA AGC TTG CCG CCA CCA TGG AAC ACG ACC TTG AGA G	73
LMP1-R	CAT GTG CGG CCG CCC ATC TCG AGA GTG AGG CAC	73
SeqLMP1-F	ATT ACC ATG GAC AAC GAC ACA G	56
Seq2LMP1-F	CAC CAC ACA GGT AGC AAG GAC	58
LMP2A-F	GAA TGC AAG CTT GCC GCC ACC ATG GGG TCC CTA GAA ATG GTG	73
LMP2A-R	CAT GTG CGG CCG CTT ATT ATA CAG TGT TGC GAT ATG GGG	69
SeqLMP2A-F	TAG TAC CGT TGT GAC CGC C	57
Seq2LMP2A-F	GGA CAC TTG GTA AGT TTT CCC TTC C	58
ClnHR 1-F	ATT GCT AGC GTT TTA GCA CAG GTG CAG CTG GTG CAG T	70
ClnHR 2-F	ATT GCT AGC GTT TTA GCA CAG GTG CAG CTG CAG GAG T	69
ClnHR 3-5-F	ATT GCT AGC GTT TTA GCA CAG ATC ACC TTG AAG GAG	70
ClnHR 4-6-7-8-9-10-11-F	ATT GCT AGC GTT TTA GCA GAG GTG CAG CTG GTG GAG	70
ClnHR 1-2-4-5-6-8-9-11-R	ATT TGG AAT TGG TTT ACC TTT GAT CTC CAG CTT GGT CCC	71
ClnHR 3-10-R	ATT TGG AAT TGG TTT ACC GCC GAG GAC GGT CAG CTG G	70
ClnHR 7-R	ATT TGG AAT TGG TTT ACC TTT GAT TTC CAC CTT GGT CCC	71
ClnHR amp-F	CTG TTT TTC AAT ATT TTC TGT TAT TGC TAG CGT TTT AGC A	61
ClnHR amp-R	TAG AGT CCA AAC CCA ACA ATG GAT TTG GAA TTG GTT TAC C	61

pcDNA3.1 Hygr Check-F	GCC CAG TTC CGC CCA TTC TC	61
pcDNA3.1 Hygr Check-R	CCG ACT GGA AAG CGG GCA G	62
SeqHygr-F	CAT CCG GAG CTT GCA GGA TC	59
pcDNA3.1 Check-F	GAG AAC CCA CTG CTT ACT GGC	58
pcDNA3.1 Check-R	GAG TGG CAC CTT CCA GGG TC	60
IgG4CAR seq-F	GGT GCG AAC TGA GGG TCA AG	59
EF1a Check-F	GGG AGA GAA TGC AGG TCA GAG	57
EF1a Check-R	GCT ATC GTT GGA GCT GGT GTC	59
ClnCAR 1-F	CTC CAT GCG GCG CGC CCG CAG GTG CAG CTG GTG CAG	80
ClnCAR 2-F	CTC CAT GCG GCG CGC CCG CAG GTG CAG CTG CAG GAG	80
ClnCAR 3-5 -F	CTC CAT GCG GCG CGC CCG CAG ATC ACC TTG AAG GAG	79
ClnCAR 4-6-7-8-9-10-11-F	CTC CAT GCG GCG CGC CCG GAG GTG CAG CTG GTG GAG	81
ClnCARCD8 1-2-4-5-6-8-9-11-R	GTC TAG GCG CCG GCG TTG TTG TTT TGA TCT CCA GCT TGG TCC C	74
ClnCARCD8 3-10-R	GTC TAG GCG CCG GCG TTG TTG TGC CGA GGA CGG TCA GCT G	75
ClnCARCD8 7-R	GTC TAG GCG CCG GCG TTG TTG TTT TGA TTT CCA CCT TGG TCC C	75
ClnCARCD8 1lmp-R	GTC TAG GCG CCG GCG TTG TTG TTT TAA TCT CCA GTC GTG TCC C	75
ClnCARIgG4 4-R	GAC ACG GGG GCC CGT ACT TAC TTT CTT TGA TCT CCA GCT TGG TCC C	73
ClnCARIgG4 1lmp-R	GAC ACG GGG GCC CGT ACT TAC TTT CTT TAA TCT CCA GTC GTG TCC C	75
ClnCAR amp-F	CTC CAT GCG GCG CGC CCG	65
ClnCARCD8 amp-R	GTC TAG GCG CCG GCG TTG TTG T	65
ClnCARIgG4 amp-R	GAC ACG GGG GCC CGT ACT TAC TTT C	64
CAR Check-F	GTC AGA TCG CCT GGA GAC G	58
pCD8-CAR Cl Check-R	CCT CCG GTC GCA AAG ACA AAG	59
pIgG4-CAR Cl Check-R	GTT ACC TCG GGG GTG CGA C	61
AAVS1 Check-F	GGC AGA GTG GTC AGC ACA GAG	60
AAVS1 Check-R	CGG TGC GAT GTC CGG AGA G	61
AAVS1 HDR Check-F	GCA AGA GGA TGG AGA GGT GGC	60
AAVS1 HDR Check-R	CGG TTA CAG GCA GGG CCA TG	61

*All the oligos were ordered from Sigma Aldrich and diluted to 10μM in deionised H_2O (dH_2O).

Table 2.5 DNA related reagents.

Reagent	Company	Catalogue
Q5 site-directed mutagenesis kit	NEB	E0554S
GoTaq G2 hot start green master mix	Promega	M7422
Q5 high-fidelity DNA polymerase	NEB	M0491S
Deoxynucleotide (dNTP) solution mix	NEB	N0447S
*Mss*I (*Pme*I) (5 U/μL)	TFS	ER1341
FastDigest *Nhe*I	TFS	FD0973
FastDigest *Eco*RI	TFS	FD0274
FastDigest *Acc*65I	TFS	FD0274

FastDigest *Hind*III	TFS	FD0504
FastDigest *Not*I	TFS	FD0593
*Xma*I	NEB	R0180S
*Bst*Z17I-HF	NEB	R3594S
FastDigest *Sgs*I	TFS	FD1894
FastDigest *Mre*I	TFS	FD2024
FastDigest *Apa*I	TFS	FD1414
FastDigest *Bgl*II	TFS	FD0083
FastDigest *Mlu*I	TFS	FD0564
Shrimp alkaline phosphatase (rSAP)	NEB	M0371S
T4 DNA ligase	TFS	15224/017
Monarch DNA gel extraction kit	NEB	T1020S
DNA clean & concentrator-5	Zymo Research	D4013
QIAquick PCR purification kit	Qiagen	28106
Sodium acetate solution (3M), pH 5.2	TFS	R1181
QIAprep spin Midi-prep kit	Qiagen	12143
UltraPure agarose	TFS	16500500
SYBR safe DNA gel stain	TFS	S33102
1 kb Plus DNA ladder	TFS	10787018
Gel loading dye, Orange (6X)	NEB	B7022S
DH5α competent *Escherichia coli*	TFS	18265017
QuickExtract DNA Extraction Solution	Lucigen	QE0905T
T7 Endonuclease I	NEB	M0302
40% Acrylamide (w/v) ratio 37.5:1	Severn Biotech	20-3600-05
Ammonium persulfate	Fisher	10020020
TEMED	GE	17-1312-01
UltraPure ethidium bromide	TFS	15585011
100 bp DNA ladder	NEB	N3231

*NEB= New England Biolabs

Table 2.6 Protein related reagents.

Reagent	Company	Catalogue
Mini EDTA-free protease inhibitor cocktail	Roche	11836170001
Pierce phosphatase inhibitor mini tablets	TFS	A32957
Protein assay dye reagent concentrate	Bio-Rad	5000006
10X NuPAGE sample reducing agent	TFS	NP0004
4X Bolt LDS Sample Buffer	TFS	B0007
SeeBlue Plus2 pre-stained protein standard	TFS	LC5925
NuPAGE 12% Bis-Tris Protein Gels, 1.0 mm, 10-well	TFS	NP0341BOX
20X NuPAGE MOPS SDS running buffer	TFS	NP0001
Whatman 3 MM CHR cellulose papers	GE	3030-917
PVDF Transfer Membrane, 0.45 µm	TFS	88518
20X Bolt transfer buffer	TFS	BT0006
Restore PLUS western blot stripping buffer	TFS	46428
Ponceau S	Sigma Aldrich	P3504-10G
Pierce ECL western blotting substrate	TFS	32106

Table 2.7 Phage display related reagents.

Reagent	Company	Catalogue
scFvs library and *E. coli* XL1-Blue	RX Biosciences	P06-PD001-10-kappa
IPTG	Melford	MB1008
PEG 8000	Sigma Aldrich	89510-250G-F
NaCl	VWR	27810.295
Tween20	Sigma Aldrich	P9416
Non-fat milk powder (NFM)	Marvel	---
Foetal bovine serum (FBS)	TFS	10500-056
0.2µm syringe filter	Sartorius	16534k
Nunc square bioassay dishes	TFS	240845

Table 2.8 Yeast display related reagents.

Reagent	Company	Catalogue
Saccharomyces cerevisiae Meyen ex E.C. Hansen (EBY100)	ATCC	MYA-4941
Deoxyribonucleic acid sodium salt from salmon testes	Sigma Aldrich	D1626-250MG
Lithium acetate dihydrate	Sigma Aldrich	450189-5G
PEG 3350	Sigma Aldrich	202444-250G
Lyticase from *Arthrobacter luteus*	Sigma Aldrich	L4025-50KU
DTT 1M in dH_2O	Sigma Aldrich	43816-10ML
BSA	GERBU Biotechnik	1501,0100
Poly-D-Lysine	Sigma Aldrich	P7886-10MG
DPBS Ca^{++} Mg^{++}	TFS	14040117

Table 2.9 Cell lines.

Cell line	Company	Catalogue
HEK293 Flp-In T-REx cells	TFS	R78007
Jurkat-Dual cells	InvivoGen	jktd-isnf

Table 2.10 Cell culture, transfection reagents and cell assay reagents.

Reagent	Company	Catalogue
Dulbecco's phosphate-buffered saline (DPBS)	TFS	14190144
Cell dissociation solution	Sigma Aldrich	C5914
Trypsin-EDTA (0.05%), phenol red	TFS	25300054
D-MEM (high Glucose)	Sigma Aldrich	D5671
Foetal bovine serum (FBS)	Sigma Aldrich	F9665
L-glutamine	Sigma Aldrich	G7513
FBS-Tet Free (Lot. 42G1079K)	TFS	10270-106
IMDM, 2 mM L-glutamine, 25 mM HEPES	TFS	12440061
Trypan blue stain (0.4%)	TFS	T10282
Countess chamber slides	TFS	C10228
PolyFect transfection reagent	Qiagen	301105
TransIT-Jurkat transfection reagent	Mirus Bio	MIR 2124
EnGen Spy Cas9 NLS	NEB	M0646T
CRISPR-Cas9 tracrRNA	IDT	1072532
CRISPR-Cas9 crRNA for AASV1	IDT	Hs.Cas9.PPP1R12C.1.AC

Nuclease-free duplex buffer	IDT	11-01-03-01
Opti-MEM I reduced serum medium	TFS	31985062
SCR7	Stemcell Technologies	74102
L755507	Stemcell Technologies	73992
Cell line nucleofector kit V	Lonza	VCA-1003
QUANTI-Luc Gold	InvivoGen	rep-qlcg2
Concanavalin A	TFS	00-4978-93

Table 2.11 Equipment.

Equipment	Company	Catalogue
Wide mini ready sub-cell GT cell	Bio-Rad	1704468EDU
PowerPac basic power supply	Bio-Rad	1645050
MiniGel tank and blot module set	TFS	NW2000
PowerEase 500 power supply	TFS	EI8675
Mini-PROTEAN tetra handcast systems	Bio-Rad	1658003FC
Mini Trans-Blot cell	Bio-Rad	1703930
Nucleofector I	Lonza	-

2.2 Buffers and broths

Buffers were prepared using dH_2O and the pH was adjusted with HCl or NaOH as appropriate. The broths were autoclaved 15 minutes at 121°C.

TAE

40 mM Tris
20 mM acetic acid
1 mM EDTA

RIPA buffer

150 mM NaCl
50 mM Tris-HCl pH7.5
1% (v/v) triton x-100
1% (w/v) deoxycholic acid
0.1% (w/v) SDS
Pierce phosphatase inhibitor mini tablets (1 tablet/10 ml each)
Mini EDTA-free protease inhibitor cocktail (1 tablet/10 ml each)

TBS

50 mM Tris-Cl, pH 7.5
150 mM NaCl

TBE

89 mM Tris, pH 7.6
89 mM H_3BO_3
2 mM EDTA

10X PCR custom buffer

45 mM Tris-HCL (pH 8.8 at 25°C)
11 mM Ammonium sulphate
4.5 mM $MgCl_2$
0.113 mg/ml BSA
4.4 µM EDTA
0.48 % (v/v) 2-Mercaptoethanol

Lysogeny broth (LB), pH 7.5

1% (w/v) tryptone
0.5% (w/v) yeast extract
1% (w/v) NaCl

Terrific broth, pH 7.2

2.4% (w/v) yeast extract
2% (w/v) tryptone
0.4% (v/v) glycerol
0.23% (w/v) potassium phosphate monobasic
1.25% (w/v) potassium phosphate dibasic

YPD broth, pH 6.5

1% (w/v) yeast extract
2% (w/v) peptone
2% (w/v) dextrose

SD-CAA and SG-CAA broths, pH 6

0.5% (w/v) bacto casamino acids
0.17% (w/v) yeast nitrogen base
0.53% (w/v) ammonium sulphate
0.86% (w/v) sodium phosphate monobasic monohydrate
1.02% (w/v) sodium phosphate dibasic heptahydrate
SD-CAA
2% (w/v) dextrose
SG-CAA
2% (w/v) galactose
0.2% (w/v) dextrose

2.3 Plasmid and phage vectors

Table 2.12 Vectors and source plasmids.

Name	Lab ID	Size (bp)	Host	Replication ori	Expression promoter	Resistance**	Company/cat or reference
pUC57	na	2579	*E. coli* DH5α	pBR322	na	Kan	GeneWiz
pYD1	861	5009	*E. coli* DH5α *S. cer* EBY100	pUC CEN/ARS	GAL1	Amp TRP1	Adgene/Add#73447
pRXB-100	na	3943	*E. coli* XL1-Blue	pMB1 f1	*lacZ*	Amp	RX Biosciences
M13KO7	na	8669	*E. coli* XL1-Blue	p15A mutated M13	na	Kan	NEB/ N0315S
pcDN5/FRT	834	5137	*E. coli* DH5α	pUC	CMV/TetO2	Amp Hyg*	TFS/V601020
pOG44	835	5785	*E. coli* DH5α	pUC	CMV	Amp	TFS/V600520
pPyLMP1	139	6600	*E. coli* DH5α	pBR322	Py early	Amp	Wilson *et al* 1990 (497)
pSG5-c/gLMP2A	182	6055	*E. coli* DH5α	pBR322	SV40	Amp	Caldwell *et al* 1998 (21)
pcDNA3.1 (+)	497	5428	*E. coli* DH5α	pUC	CMV	Amp and Neo	TFS/V79020
pmaxGFP	na	3486	-	pUC	CMV	Kan	Lonza/VCA-1003

**Kan=kanamycin, Amp = ampicillin, Hyg = hygromycin, Neo = Neomycin *for selection in mammalian cells. See below 2.2.1 to 2.2.9 for further details.

Table 2.13 pUC57-Kan derivatives used during this investigation.

Derivative vector	Lab ID	Size (bp)	Vector	Cloning sites	Synthetic gene carried
pUC57-pYDN-Cassette	na	2903	pUC57	5'*Nhe*I - 3'*Pme*I	DNA cassette for pYDN development
pB7H4-D1	864	2960	pUC57	5'*Acc*65I - 3'*Eco*RI	B7H4 IgG-like V-type 1 domain (aa Phe29-Gly148)
pLMP1-lp2F	868	2649	pUC57	5'*Acc*65I - 3'*Eco*RI	LMP1 Loop2 F variant (aa Ile95-Gly108)
pLMP1-lp2Y	869	2649	pUC57	5'*Acc*65I - 3'*Eco*RI	LMP1 Loop2 Y variant (aa Ile95-Gly108)
pLMP2-lp2	870	2664	pUC57	5'*Acc*65I - 3'*Eco*RI	LMP2 Loop2 (aa Thr198-Leu213)
pLMP2-lp5	871	2664	pUC57	5'*Acc*65I - 3'*Eco*RI	LMP2 Loop5 (aa Ser374-Pro390)
pB7H4	878	3454	pUC57	5'*Hind*III - 3'*Not*I	Human B7H4 cDNA
pHygr	na	3547	pUC57	5'*Xma*I - 3'*Bst*Z17I	Hygromycin resistance gene
pUC57-CD8CAR	893	3337	pUC57	5'*Hind*III - 3'*Pme*I	DNA cassette for pCD8-CAR development
pUC57-IgG4CAR	894	3898	pUC57	5'*Hind*III - 3'*Pme*I	DNA cassette for pIgG4-CAR development
pAAVS1-HR	na	3489	pUC57	5'*Bgl*II – 3'*Mlu*I	DNA cassette with HR regions in *AAVS1* locus for pCD8-CAR and pIgG4-CAR development
pEF1αP	na	3165	pUC57	5'*Mlu*I – 3'*Sgs*I	DNA cassette with EF1α promoter for pCD8-CAR and pIgG4-CAR development

Table 2.14 pYD1 derivatives generated during this investigation.

Derivative vector	Lab ID	Size (bp)	Vector	Cloning sites*	Insertion or modification
pY-LMP1-lp2F	873	5053	pYD1	5'*Acc*65I - 3'*Eco*RI	LMP1 Loop2 F variant from pUC57-LMP1-lp2F
pY-LMP1-lp2Y	874	5053	pYD1	5'*Acc*65I - 3'*Eco*RI	LMP1 Loop2 Y variant from pUC57-LMP1-lp2Y
pY-LMP2-lp2	875	5068	pYD1	5'*Acc*65I - 3'*Eco*RI	LMP2 Loop2 from pUC57-LMP2-lp2
pY-LMP2-lp5	876	5068	pYD1	5'*Acc*65I - 3'*Eco*RI	LMP2 Loop5 from pUC57-LMP2-lp5
pY-NheI-del	na	5009	pYD1	na	*Nhe*I site deleted
pY-NheI-mod	na	5009	pYD1	na	*Nhe*I site moved
pYDN	862	4846	pYD1-Nhe-mod	5'*Nhe*I - 3'*Pme*I	N-terminal AGA2 fusion expression
pY-B7H4	866	5212	pYDN	5'*Nhe*I - 3'*Eco*RI	B7H4 IgG-like V-type 1 domain from pUC57-B7H4-D1
pY-scFv	na	≅5620	pYDN	*Eco*RI	Pool of scFvs from phage display selections and individual scFv clone

Table 2.15 pcDNA5/FRT derivatives generated during this investigation.

Derivate vector	Lab ID	Size (bp)	Vector	Cloning sites	Insertion or modification
pB7H4-FRT	880	5937	pcDN5/FRT	5'*Hind*III - 3'*Not*I	Human B7H4 cDNA obtained from pUC57-B7H4
pLMP1-FRT	882	7077	pcDN5/FRT	5'*Hind*III - 3'*Not*I	Viral LMP1 obtained by PCR from pPyLMP-1
pLMP2A-FRT	883	7067	pcDN5/FRT	5'*Hind*III - 3'*Not*I	Viral LMP2A obtained by PCR from pSG5-c/gLMP2A

Table 2.16 pcDNA3.1 (+) derivatives generated during this investigation.

Derivate vector	Lab ID	Size (bp)	Vector	Resistance*	Cloning sites	Insertion or modification
pcDNA3.1-hygr	na	5298	pcDNA3.1 (+)	Amp and Hygr	5'*Xma*I - 3'*Bst*Z17I	Hygromycin resistance gene from pHygr
pCD8-Cassette	na	6073	pcDNA3.1-hygr	Amp and Hygr	5'*Hind*III - 3'*Pme*I	CD8 hinge-based CAR framework from pUC57-CD8CAR-Cassette
pIgG4-Cassette	na	6634	pcDNA3.1-hygr	Amp and Hygr	5'*Hind*III - 3'*Pme*I	IgG4 hinge-based CAR framework from pUC57-IgG4CAR-Cassette
pCD8-Cass-HR	na	7763	pCD8-Cassette	Amp and Hygr	5'*Bgl*II – 3'*Mlu*I	HR region in *AAVS1* locus from pAAVS1-HR
pIgG4-Cass-HR	na	8324	pIgG4-Cassette	Amp and Hygr	5'*Bgl*II – 3'*Mlu*I	HR region in *AAVS1* locus from pAAVS1-HR
pCD8-CAR	na	7599	pCD8-Cass-HR	Amp and Hygr	5'*Mlu*I – 3'*Sgs*I	CMV substitution for EFα1 from pEF1αP
pIgG4-CAR	na	8160	pIgG4-Cass-HR	Amp and Hygr	5'*Mlu*I – 3'*Sgs*I	CMV substitution for EFα1 from pEF1αP
pCD8-CAR Clone X	898-909	≈8359	pCD8-CAR	Amp and Hygr	5'*Sgs*I - 3'*Mre*I	scFv inserted in CD8 cassette
pIgG4-CAR Clone X	910	≈8920	pIgG4-CAR	Amp and Hygr	5'*Sgs*I - 3'- *Apa*I	scFv inserted in IgG4 cassette
CMV-modified pCD8-CAR Clone 4 B7H4	913	8524	pCD8-CAR Clone 4	Amp and Hygr	5'*Sgs*I - 3'*Mre*I	Modified pCD8-CAR Clone 4 B7H4 with the original CMV promoter
CMV-modified IgG4-CAR Clone 4 B7H4	914	9085	pCD8-CAR Clone 4	Amp and Hygr	5'*Sgs*I - 3'- *Apa*I	Modified pIgG4-CAR Clone 4 B7H4 with the original CMV promoter

*Hygr = hygromycin

2.3.1 pUC57

pUC57 is a bacterial cloning vector which is the backbone used by GeneWiz to supply the synthetic DNA used in several cloning experiments.

2.3.2 pYD1

pYD1 is a yeast expression vector designed for expression, secretion, and display of proteins on the extracellular surface of *Saccharomyces cerevisiae* EBY100 cells (for map and sequence see figure 1 in the appendix). pYD1 was used to display several peptides on the surface of yeast, including LMP1 loop 2F, LMP1 loop 2Y, LMP2 loop 2 and LMP2 loop 5. It was also used to derive pYDN. The GAL promoter drive the expression of AGA2 fusion protein. The cloning site to generate a fusion protein is at the C-terminus of AGA2. Between an AGA2 and the cloning site, a T7 encoded peptide, and an Xpress tag have been inserted which can be used to confirm the display of the recombinant fusion protein. pYD1 contains an ARS (autonomously replicating sequence) and a CEN (yeast centromere). It replicates like a chromosome with an average of a single plasmid per yeast cell. During this investigation, several plasmids were generated using pYD1 as the backbone (table 2.14).

2.3.3 pYDN

pYDN is a modification of pYD1 based in the previously described vector pYD5 (474) for N-terminal display of an AGA2 fusion protein (for map and sequence see figure 2 in the appendix). It was used to display B7H4 IgG-like V-type 1 domain and the scFvs selected by phage display, on the surface of the yeast (table 2.14). The cloning site for the fusion protein is at the N-terminus of AGA2, with an intervening V5 tag. The V5 tag can be used to confirm the display of the recombinant fusion protein. pYDN was developed by site-directed mutagenesis and cloning from pYD1.

2.3.4 pRXB-100

pRXB-100 is a phagemid vector used for phage display of antibody libraries (for map and sequence see figure 3 in the appendix). The phage display library used

was cloned into pRXB-100. It contains a cloning site at the N-terminus of the phage protein PIII.

2.3.5 M13KO7 helper phage

M13KO7 is a helper phage is used in conjunction with a phagemid vector (for map see figure 4 in the appendix). It contains all the elements necessary to produce functional M13 phage but has a mutation in the nickase pII gene and an insertion of the origin of replication p15A and a kanamycin resistance gene within the M13 origin of replication. In the presence of a phagemid pRXB-100, single-stranded phagemid DNA is packaged preferentially in the M13 phage capsids.

2.3.6 pcDNA5/FRT and derivatives

pcDNA5/FRT is a mammalian expression vector used to express recombinant proteins with a tetracycline-inducible system (for map and sequence see figure 5 in the appendix). pcDNA5/FRT was used to clone B7H4, LMP1 and LMP2A sequences to create tetracycline-inducible HEK293 expressing the antigens of interest (table 2.15). It contains an FLP recombination target (FRT) site for Flp recombinase-mediated integration of the vector into the HEK293 Flp-In T-REx. It contains a CMV promoter regulated by tetracycline for the expression of the introduced gene of interest. During this investigation, several plasmids were generate using pcDNA5/FRT as backbone (table 2.15).

2.3.7 pOG44

pOG44 is a mammalian expression vector which expresses the Flp recombinase (for map see figure 6 in the appendix). When co-transfected with pcDNA5/FRT into HEK293 Flp-In T-REx, the Flp recombinase mediates integration of the pcDNA5/FRT into FRT sites present in the genome.

2.3.8 pPyLMP1

pPyLMP1 is a mammalian expression vector containing the viral sequence of LMP1. It was used as DNA template for the amplification by PCR of the viral DNA sequence of LMP1 with the objective of cloning into pcDNA5/FRT (table 2.15).

2.3.9 pSG5-c/gLMP2A

pSG5-c/gLMP2A is a mammalian expression vector containing the viral sequence of LMP2A. It was used as DNA template for the amplification by PCR of the viral DNA sequence of LMP2A with the objective of cloning into pcDNA5/FRT (table 2.15).

2.3.10 pcDNA3.1 (+)

pcDNA3.1 (+) is a mammalian expression vector (for map and sequence see figure 7 in the appendix). It was used to obtain pcDNA3.1-hygr. Several plasmids were generated using pcDNA3.1 (+) as the backbone with the objective of the expressing CAR in Jurkat Dual cells.

2.3.10.1 pcDNA3.1-hygr

pcDNA3.1-hygr is a modification of the pcDNA3.1 (+) mammalian expression vector (table 2.16). The neomycin resistance gene was replaced by a hygromycin resistance gene (for map and sequence see figure 8 in the appendix).

2.3.10.2 pCD8-Cassette

pCD8-Cassette is a modification of pcDNA3.1-hygr (table 2.16). It incorporates a DNA cassette encoding the CD8 signal peptide, the hinge domain of CD8, the transmembrane domain of CD8 and the stimulation intracellular domains of 4-1BB and CD3ζ, together comprising a CAR. It also includes two restriction sites, 5'-*Sgs*I and 3'-*Mre*I, for the in-frame cloning of scFvs between the signal peptide and the hinge domain.

2.3.10.3 pIgG4-Cassette

pIgG4-Cassette is a modification of pcDNA3.1-hygr (table 2.16). It incorporates a DNA cassette encoding the CD8 signal peptide, the hinge domain of IgG4, the transmembrane domain of CD8 and the stimulation intracellular domains of 4-1BB and CD3ζ, together comprising a CAR. It also includes two restriction sites, 5'-*Sgs*I and 3'-*Apa*I, for the in-frame cloning of scFvs between the signal peptide and the hinge domain.

2.3.10.4 pCD8-Cass-HR

pCD8-Cass-HR is a modification of pCD8-Cassette (table 2.16). It incorporates a DNA cassette with 400 bp homology arms to the safe harbour gene Adeno-Associated virus integration site 1 (*AAVS1*) separated by the restriction site *Nhe*I. These homology arms were incorporate to knock-in the plasmid into the cell genome using Cas9 nuclease directed to *AAVS1*.

2.3.10.5 pIgG4-Cass-HR

pIgG4-Cass-HR is a modification of pIgG4-Cassette (table 2.16). It incorporates a DNA cassette with 400 bp homology arms to the safe harbour gene *AAVS1* separated by the restriction site *Nhe*I. These homology arms were incorporate to knock-in the plasmid into the cell genome using Cas9 nuclease directed to *AAVS1*.

2.3.10.6 pCD8-CAR

pCD8-CAR is a modification of pCD8-Cass-HR (table 2.16). The CMV promoter was replaced by the EF1α promoter. Several plasmids were generated using pCD8-CAR as the backbone, these plasmids consist in the in-frame cloning of an scFv (between the signal peptide and the hinge domain of the CAR) using the restriction sites 5'-*Sgs*I and 3'-*Mre*I (for map and sequence see figure 9 in the appendix).

2.3.10.7 pIgG4-CAR

pIgG4-CAR is a modification of pIgG4-Cass-HR (table 2.16). The CMV promoter was replaced by the EF1α promoter. Several plasmids were generated using pIgG4-CAR as the backbone, these plasmids consist in the in-frame cloning of an scFv (between the signal peptide and the hinge domain of the CAR) using the restriction sites 5'-*Sgs*I and 3'-*Apa*I (for map and sequence see figure 10 in the appendix).

2.4 Bacterial and yeast strains

2.4.1 *Escherichia coli* DH5α

Escherichia coli DH5α cells were used for expansion of plasmid DNA. The strain contains mutated endA1 and hsdR17 genes to inhibit plasmid degradation.

2.4.2 *Escherichia coli* XL1-Blue

Escherichia coli XL1-Blue were used to create phage display libraries and for the infection of phage outputs obtained from phage display selection. It contains the mutated endA1 and hsdR17 endonuclease genes which inhibit the degradation of plasmid DNA. It also contains the F pilus, required for phage infection, on a tetracycline-selectable episome.

2.4.3 *Saccharomyces cerevisiae* EBY100

Saccharomyces cerevisiae EBY100 was used for yeast display of fusion proteins when transformed with vectors encoding AGA2 regulated by a GAL promoter and with a TRP1 selectable marker, including, pYD1 and pYDN. The Leu- and Trp- strain has also a genomic insertion of AGA1 regulated by a GAL promoter with a URA3 selectable marker. This insertion is integrated in tandem with the endogenous AGA1. EBY100 conserves the endogenous AGA2.

2.5 Mammalian cell lines

2.5.1 HEK293 Flp-In T-REx and derivates

HEK293 Flp-In T-REx was established from the human embryonic kidney cell line HEK293 by stable integration in the genome of pFRT/lacZeo and pcDNA6/TR plasmid sequences. A single copy of pFRT/lacZeo is stably integrated at a transcriptionally active genomic locus and maintained by selection with zeocin. When HEK293 Flp-In T-REx cells are co-transfected with pcDNA5/FRT and pOG44 vectors, the Flp recombinase expressed by pOG44 mediates homologous recombination between the FRT sites of pcDNA5/FRT and the integrated pFRT/lacZeo. In so doing, the zeocin resistance gene is lost and a hygromycin resistance gene from pcDNA5/FRT incorporated. The genome integrated pcDNA6/TR is maintained by selection with blasticidin and it expresses a Tet repressor protein (TetR) under the CMV promoter. TetR represses the inducible CMV/TetO2 promoter of pcDNA5/FRT in the absence of tetracycline/doxycycline.

2.5.1.1 HEK293-B7H4

HEK293-B7H4 is a cell line established by co-transfection of HEK293 Flp-In T-REx with pOG44 and pcDNA5/FRT-B7H4 (table 2.15). The HEK293-B7H4 cells are resistant to blasticidin (15 µg/ml) and hygromycin (400 µg/ml) and expresses the membrane protein B7H4 when cultured with tetracycline.

2.5.1.2 HEK293-LMP1

HEK293-LMP1 is a cell line established by co-transfection of HEK293F lp-In T-REx with pOG44 and pcDNA5/FRT-LMP1 (table 2.15). The HEK293-LMP1 cells are resistant to blasticidin and hygromycin and expresses the membrane protein LMP1 when cultured in the presence of tetracycline.

2.5.1.3 HEK293-LMP2A

HEK293-LMP2A is a cell line established by co-transfection of HEK293 Flp-In T-REx with pOG44 and pcDNA5/FRT-LMP2A (table 2.15). The HEK293-LMP2A cells are resistant to blasticidin and hygromycin and expresses the membrane protein LMP2A when cultured in the presence of tetracycline.

2.5.2 Jurkat-Dual and derivates

The Jurkat-Dual cell line was derived from the Jurkat cell line established from human leukaemia T-cells, by stable integration of two inducible reporter constructs. It has a luciferase reporter gene controlled by the IFN-β promoter fused upstream to five copies of the NF-κB consensus transcriptional response element (kappa-B site) with three copies of the c-Rel binding site each. It also encodes a secreted embryonic alkaline phosphatase (SEAP) reporter gene under the control of an ISG54 promoter in conjunction with five IFN-stimulated response elements. Jurkat-Dual cells allow simultaneous study of the NF-κB pathway, by monitoring the activity of luciferase, and the interferon regulatory factor (IRF) pathway, by assessing the activity of SEAP. The reporter constructs are maintained by selection with blasticidin (10 µg/ml) and zeocin.

2.5.2.1 Jurkat-rep-CAR Clone X cell lines

Jurkat-rep-CAR are cell lines derived from Jurkat-Dual by stable integration of plasmids generated using pCD8-CAR Clone X plasmids or pIgG4-CAR Clone X plasmids (table 2.16). Jurka-rep-CAR are maintained by selection with blasticidin, zeocin and hygromycin. The activation through the CAR was examined by the activity of the Lucia luciferase reporter gene as described below.

2.6 DNA preparation and purification

2.6.1 Plasmid purification

In order to obtain plasmid DNA from *E. coli* DH5α or *E. coli* XL1-Blue, plasmid extraction was conducted using the QIAGEN plasmid midi kit. 50 ml overnight bacterial culture was centrifuged at 4,000 xg for 30 minutes at 4°C. The supernatant was discarded, and the bacterial pellet was resuspended in 4 ml of suspension buffer P1. 4 ml of lysis buffer P2 was added and mixed by inverting the tube gently. 4 ml of cool neutralising buffer P3 was added and mixed by inverting the tube gently followed by centrifugation at 20,000 xg for 30 minutes. During the centrifugation, a QIAGEN-tip-100 was equilibrated with 4 ml of buffer QBT, allowing it to move through the QIAGEN-tip by gravity flow. The supernatant was applied to the equilibrated QIAGEN-tip-100. The flow-through was discarded, and 10 ml of wash buffer QC was added to the column. This step was performed twice. Then the flow-through was discarded, and the column was placed onto a 50 ml falcon tube and eluted with 5 ml of buffer QF. The plasmid DNA was precipitated by adding 3.5 ml of room temperature isopropanol, vortexed and centrifuged at 4,000 xg, 1 hour at 4°C. The supernatant was removed, and the DNA pellet washed with 1 ml of 70% ethanol and vortexed. The sample was centrifuged in a microfuge at 16,000 xg for 10 minutes at 4°C and the supernatant removed. The DNA pellet was air-dried for 5–10 minutes and dissolved in a suitable volume of dH_2O (usually 100 µl).

2.6.2 Purification of DNA from agarose gels

Monarch DNA gel extraction kit was used to purify DNA from agarose gels previously used for DNA electrophoresis. The agarose gel slices were excised and weighed. Four volumes of Gel dissolving buffer were added to the gel slice (e.g.,

400 µl buffer per 100 mg agarose) and incubated at 50°C with periodic vortexing until the gel slice was completely dissolved. A column was inserted into a collection tube, and the sample loaded onto the column and centrifuged for 30 seconds at 10,000 xg, the flow-through was discarded. The column was placed into a new collection tube, and 200 µl of DNA wash buffer was added onto the column and centrifuged for 30 seconds at 10,000 xg, the flow-through was discarded and this step repeated. The column was transferred to a 1.5 ml microfuge tube, and 6-20 µl of dH_2O was added onto the column to elute the DNA. The column was centrifuged for 1 minute at 10,000 xg and the flow-through with the eluted DNA collected.

2.6.3 Purification and concentration of DNA

DNA clean & concentrator-5 was used to clean or concentrate the DNA for use in cloning. For DNA fragments larger than 2 kb two volumes of DNA binding buffer were added to the DNA sample, for fragments smaller than 2 kb five volumes were added. The solution was mixed briefly by vortexing. A column was inserted into a collection tube, and the sample loaded onto the column and centrifuged for 30 seconds at 10,000 xg, the flow-through was discarded. The column was placed into a new collection tube, and 200 µl of DNA wash buffer was added onto the column and centrifuged for 30 seconds at 10,000 xg, the flow-through was discarded and this step repeated. The column was transferred to a 1.5 ml microfuge tube, and 10 µl of dH_2O was added onto the column to elute the DNA. The column was centrifuged for 1 minute at 10,000 xg and the flow-through with the eluted DNA collected.

2.6.4 Purification of PCR products

QIAquick PCR purification kit was used to purify DNA from PCR products. Five volumes of Buffer PB and 10 µl of 3 M sodium acetate pH 5.0 were added to the PCR reaction mix. The solution was mixed briefly by vortexing. A column was inserted into a collection tube, and the sample loaded onto the column and centrifuged for 30 seconds at 10,000 xg, the flow-through was discarded. The column was placed into a new collection tube, and 750 µl of Buffer PE was added onto the column and centrifuged for 30 seconds at 10,000 xg, the flow-through was discarded. The column was placed into a new collection tube and centrifuged

for 1 minutes at 10,000 xg, and the remaining flow-through was discarded. The column was transferred to a 1.5 ml microfuge tube, and 50 µl of dH_2O was added onto the column to elute the DNA. The column was centrifuged for 1 minute at 10,000 xg and the flow-through with the elute DNA collected.

2.6.5 DNA precipitation with isopropanol and ethanol

For DNA precipitation of linearised vectors, after the endonuclease digestion, one volume of isopropanol was added to the digestion mix, followed by 15 seconds of vortexing. The solution was then centrifuged at 13000 xg for 10 minutes at room temperature and the supernatant removed. The DNA pellet was washed with 500 µl of 75% ethanol and centrifuged at 13000 xg for 10 minutes at room temperature. The supernatant was removed the DNA pellet air dry. Finally, the DNA pellet was resuspended in TE buffer and the DNA concentration was determined by Nanodrop.

2.6.6 Genomic DNA extraction

Approximately 10^6 cells were harvested for genomic DNA (gDNA) extraction with 60 µl of QuickExtract DNA extraction solution. The cells were lysed in the solution, vortexed for 15 seconds, heated at 65°C for 6 minutes (followed by another 15 seconds of vortexing), heated at 98°C for 2 minutes and cooled down to room temperature. Then, the solutions were diluted with 120 µl of TE buffer, centrifuged at 13000 xg for 3 minutes and the supernatants collected. The DNA concentration was determined by Nanodrop using as blank a solution composed of 60 µl of QuickExtract DNA extraction solution plus 120 µl of TE buffer. The samples were diluted to 100 ng/µl with TE buffer and stored at -80°C.

2.6.7 DNA quantification

The concentration and purity of double-stranded DNA obtained in the above protocols (2.6.1, 2.6.2, 2.6.3, 2.6.4, 2.6.5 and 2.6.6) were determined by measuring the OD_{260} and the ration OD_{260}/OD_{280} with a NanoDrop 1000. The DNA was stored at -20°C or -80°C until use.

2.7 Polymerase chain reaction (PCR)

2.7.1 pYD1 site-directed mutagenesis PCR

In order to obtain pYDN, pYD1 was modified by site-directed mutagenesis using Q5 site-directed mutagenesis kit to remove the endogenous *Nhe*I restriction site and introduce a new *Nhe*I restriction site. To remove the *Nhe*I restriction site in pYD1, PCR was first performed using pYD1 as DNA template and the primers (-)NheI-F and (-)NheI-R (table 2.4). The reaction mix was prepared with 12.5 µl of Q5 hot start 2X master mix, 1.25 µl of 10 µM solution of each primer, 10 ng of pYD1 and dH_2O up to 25 µl and PCR conducted (table 2.18). Next, a KLD (Kinase, Ligase and *Dpn*I) reaction was performed using 1 µl of the first PCR product, 5 µl of 2X KLD reaction buffer, 1 µl of 10X KLD enzyme mix and 3 µl of dH_2O. The KLD reaction mix was incubated 5 minutes at room temperature. *E. coli* DH5α were transformed (2.9.4) using 5 µl of the KLD reaction and plated onto a plate with 1% (w/v) agarose in LB with ampicillin (table 2.1) and incubated overnight at 37°C. pY-NheI-del was purified from a bacterial colony (2.6.1) and was used in a second PCR with the primers (+)NheI-F and (+)NheI-R (table 2.4). A second KLD reaction was performed with the second PCR product, and this then transformed into *E. coli* DH5α. The derived pY-NheI-mod was purified (2.6.1) and used to derive pYDN.

Table 2.17 PCR conditions for directed mutagenesis of pYD1.

Step	Temperature	Time
Initial denaturalisation	98°C	30 seconds
25 cycles	98°C	10 seconds
	Annealing temperature	20 seconds
	72°C	Extension time
Final extension	72°C	2 minutes
Hold	10°C	-
Oligo couples	Annealing temperature	Extension time
-NheI-F -NheI-R	42°C	2 minutes 30 seconds
+NheI-F +NheI-R	56°C	2 minutes 30 seconds

2.7.2 PCR for sequencing

In order to amplify DNA for sequencing, PCR was conducted using the GoTaq G2 hot start green master mix. The reactions were performed with 25 µl of 2X GoTaq hot start green master mix, 5 µl of each 10 µM forward and reverse oligos, 1-10 ng

of DNA or a bacterial colony as template and dH_2O up to 50 µl. The reaction parameters for each Taq PCR are detailed in table 2.18.

Table 2.18 Taq PCR conditions.

Step	Temperature	Time
Initial denaturalisation	95°C	2 minutes
30 cycles	95°C	20 seconds
	Annealing temperature	30 seconds
	72°C	Extension time
Final extension	72°C	5 minutes
Hold	10°C	-
Oligo couples	Annealing temperature	Extension time
pYDN Cassette-F pYDN Cassette-R	47°C	1 minute
pYDN Check-F pYDN Check-R	50°C	1 minute
pYD1 Check-F pYD1 Check-R	50°C	1 minute
pcDNA5/FRT Check-F pcDNA5/FRT Check-R	60°C	2 minutes
pcDNA3.1 Hygr Check-F pcDNA3.1 Hygr Check-R	58°C	1 minute
pcDNA3.1 Check-F pcDNA3.1 Check-R	57°C	1 minute
EF1a Check-F EF1a Check-R	56	1 minute
CAR Check-F pCD8-CAR Check-R	57°C	1 minute
CAR Check-F pIgG4-CAR Check-R	57°C	1 minute
AAVS1 HR Check-F AAVS1 HR Check-R	56	1 minute

2.7.3 High-fidelity PCR for cloning and homologous recombination

In order to amplify DNA for cloning including use in homologous recombination, PCR was conducted using Q5 high-fidelity DNA polymerase. The reaction mixtures comprised 5 µl of 10X PCR custom buffer, 1 µl of 10 mM dNTPs, 2.5 µl of each 10 µM forward and reverse oligos, 10 ng of DNA template, 0.5 µl of Q5 high-fidelity DNA polymerase and dH_2O up to 50 µl. The reaction parameters for each PCR performed with the Q5 high-fidelity DNA polymerase are detailed in table 2.19.

Table 2.19 High-fidelity PCR for cloning and homologous recombination.

Step	Temperature	Time
Initial denaturalisation	98˚C	30 seconds
34 cycles	98˚C	10 seconds
	Annealing temperature	30 seconds
	72˚C	Extension time
Final extension	72˚C	2 minutes
Hold	10˚C	-
Oligo couples	Annealing temperature	Extension time
HR-F HR-R	72˚C	30 seconds
HR amp-F HR amp-R	55˚C	40 seconds
LMP1-F LMP1-R	55˚C	1 minute
LMP2A-F LMP2A-R	55˚C	1 minute
ClnHR **1**-F ClnHR **1**-2-4-5-6-8-9-11-R	55˚C	40 seconds
ClnHR **2**-F ClnHR 1-**2**-4-5-6-8-9-11-R	55˚C	40 seconds
ClnHR **3**-5-F ClnHR **3**-10-R	55˚C	40 seconds
ClnHR 3-**5**-F ClnHR 1-2-4-**5**-6-8-9-11-R	55˚C	40 seconds
ClnHR **4**-**6**-7-**8**-**9**-10-**11**-F ClnHR 1-2-**4**-5-**6**-**8**-**9**-**11**-R	55˚C	40 seconds
ClnHR 4-6-7-8-9-**10**-11-F ClnHR 3-**10**-R	55˚C	40 seconds
ClnHR 4-6-**7**-8-9-10-11-F ClnHR -**7**-R	55˚C	40 seconds
ClnHR amp-F ClnHR amp-R	58˚C	40 seconds
ClnCAR **1**-F ClnCARCD8 **1**-2-4-5-6-8-9-11-R	55˚C	40 seconds
ClnCAR **2**-F ClnCARCD8 1-**2**-4-5-6-8-9-11-R	55˚C	40 seconds
ClnCAR **3**-5-F ClnCARCD8 **3**-10-R	55˚C	40 seconds
ClnCAR 3-**5**-F ClnCARCD8 1-2-4-**5**-6-8-9-11-R	55˚C	40 seconds
ClnCAR **4**-**6**-7-**8**-**9**-10-**11**-F ClnCARCD8 1-2-**4**-5-**6**-**8**-**9**-**11**-R	55˚C	40 seconds
ClnCAR 4-6-7-8-9-**10**-11-F ClnCARCD8 3-**10**-R	55˚C	40 seconds
ClnCAR 4-6-**7**-8-9-10-11-F ClnCARCD8 **7**-R	55˚C	40 seconds
ClnCAR 1-F ClnCARCD8 1lmp-R	55˚C	40 seconds
ClnCAR 1-F ClnCARIgG4 1lmp-R	55˚C	40 seconds

ClnCAR 4-6-7-8-9-10-11-F ClnCARIgG4 4-R	55°C	40 seconds
ClnCAR amp-F ClnCARCD8 amp-R	60°C	40 seconds
ClnCAR amp-F ClnCARIgG4 amp-R	60°C	40 seconds

2.7.4 PCR for T7EI mismatch detection assay and tracking of indels by decomposition (TIDE)

In order to amplify DNA for the T7EI mismatch detection assay and TIDE, PCR was conducted using Q5 high-fidelity DNA polymerase. The reaction mixtures comprised 10 µl of 5X Q5 reaction buffer, 1 µl of 10 mM dNTPs, 2.5 µl of each 10 µM forward and reverse oligos, 100 ng of gDNA, 0.5 µl of Q5 high-fidelity DNA polymerase and dH2O up to 50 µl. The reaction parameters are the same as the ones described in table 2.19. The primers used for this PCR, annealing temperature and extension time are described in table 2.20.

Table 2.20 Primers and conditions used in the high-fidelity PCR for T7EI mismatch detection assay and TIDE.

Oligo couples	Annealing temperature	Extension time
AAVS1 HDR Check-F AAVS1 HDR Check-R	72°C	20 seconds

2.8 DNA gel electrophoresis

2.8.1 Agarose gel electrophoresis

In order to separate DNA fragments according to size and visualise these, agarose gel electrophoresis was conducted using TAE buffer in a Wide mini ready sub-cell GT cell (Bio-Rad) connected to a PowerPac basic power supply (Bio-Rad). The 1% agarose was prepared and melted in TAE buffer and allowed to cool until handleable. Then, SYBR safe DNA gel stain was added at a ratio of 1:10,000 and mixed well. This was poured into a sealed gel tray with a comb a left to solidify. The gel was placed into the electrophoresis chamber with TAE buffer, the comb removed and loaded with the DNA ladder and samples. The DNA ladder sample was prepared with 2.5 µl of 1 kb Plus DNA ladder, 4 µl of Orange G loading dye and dH_2O to a final volume of 25 µl. 1X Orange G loading dye was added to the

DNA samples except those obtained by PCR with GoTaq G2 hot start green master mix. The DNA fragments were separated at 100 V for 1 hour, visualised using an LED blue light transilluminator (470 nm) and collected if required for further analysis.

2.8.2 Polyacrylamide gel electrophoresis

In order to separate DNA fragments according to size and visualise these after digestion with T7 endonuclease I for the T7EI mismatch detection assay, a polyacrylamide gel electrophoresis was performed. A 1 mm 8% DNA-PAGE gel was casted using Mini-PROTEAN tetra handcast systems (Bio-Rad). 1.2 ml of 40 % Acrylamide (37.5:1) (Severn Biotech) was diluted in 3.6 ml of dH_2O plus 1.2 ml of 5X TBE buffer and 100 µl of 10 % ammonium persulfate. Then, 5 µl of the polymerisation agent TEMED was added. The acrylamide was allowed to polymerise for at least 30 minutes at room temperature. The DNA fragments were separated at 70 V for 90 minutes using Mini Trans-Blot cell (Bio-Rad) and PowerPac basic power supply. For visualisation, the gel was incubated in a container with 200 µl of 0.5% TBE plus 4 µl of ethidium bromide in dark for 20 minutes with gently shaking and visualised using c600 imaging system (Azure biosystems).

2.9 DNA Cloning

2.9.1 Restriction endonucleases digestion

Restriction endonuclease reactions were performed with different enzymes during the investigation. For FastDigest, Buffer B and Cutsmart, reactions were set up in a total volume of 50 µl or 100 µl, using 1-5 µg DNA, the appropriate volume of 10X buffer (to a final 1X concentration) and generally 5 µl endonuclease, and incubated at 37°C for 10 minutes to 2 hours (table 2.21).

In the case of sequential digestion with two endonucleases, after inactivation of the first enzyme, an extra 50 µl of final volume with the appropriate buffer and endonuclease were added and incubated. Alternatively, 1 µl of the second endonuclease was added directly to the first reaction and incubated. In the case where different buffers were required, the first digestion was performed and the DNA purified (2.6.3) for its use in the second endonuclease reaction.

After the completing the digestion with restriction enzymes, the sample was electrophoresed and the DNA fragment of interest collected from the gel and purified (2.6.2).

Table 2.21 Endonucleases, buffers and conditions for digestion and inactivation.

Enzyme	Buffer	Digestion		Inactivation	
		Time	Temperature	Time	Temperature
*Acc*65I	FastDigest	10 minutes	37°C	5 minutes	65°C
*Apa*I	FastDigest	10 minutes	37°C	5 minutes	65°C
*Bst*Z17I	CutSmart	10 minutes	37°C	na	na
*Bgl*II	FastDigest	25 minutes	37°C	na	na
*Eco*RI	FastDigest	20 minutes	37°C	5 minutes	80°C
*Hind*III	FastDigest	20 minutes	37°C	10 minutes	80°C
*Mre*I	FastDigest	10 minutes	37°C	5 minutes	80°C
*Mlu*I	FastDigest	10 minutes	37°C	5 minutes	80°C
*Nhe*I	FastDigest	20 minutes	37°C	5 minutes	65°C
*Not*I	FastDigest	35 minutes	37°C	5 minutes	80°C
*Pme*I	Buffer B	2 hours	37°C	20 minutes	65°C
*Sgs*I	FastDigest	10 minutes	37°C	20 minutes	65°C
*Xma*I	CutSmart	10 minutes	37°C	20 minutes	65°C

2.9.2 DNA dephosphorylation

After plasmid digestion with endonucleases and prior to ligation, a dephosphorylation reaction was carried out to remove the 5´phosphates of each fragment end. The aim was to inhibit the recircularisation of the single cut vector in the sample during the ligation reaction. Shrimp alkaline phosphatase (rSAP) was used, incubated at 37°C overnight in a final volume of 60 µl with 6 µl of 10X CutSmart buffer and 3 µl of rSAP. rSAP was inactivated at 65°C for 5 minutes and then the DNA was purified (2.6.2).

2.9.3 DNA ligation

The digested and dephosphorylated vector and the DNA insert with compatible sticky ends, were ligated using T4 DNA ligase. The DNA inserts and vector were mixed at a molar ratio of 3:1 respectively, with 1 µl of T4 DNA ligase and 4 µl of 5X ligase reaction buffer in a final volume of 20 µl. The reaction was incubated at 14°C overnight, and then inactivated at 65°C for 20 minutes.

2.9.4 Bacterial transformation

In order to transform plasmid DNA into bacteria, *Escherichia coli* DH5α competent cells were thawed on ice and 10 ng of plasmid or 5 µl of the ligation reaction was added to 50 µl of competent cells. The cells were incubated on ice for 30 minutes followed by a heat shock at 42°C for 20 seconds and incubation on ice for 2 minutes. Then, 1 ml of LB was added to the cells followed by incubation at 37°C, with shaking at 200 rpm for 1 hour. 100 µl of the bacterial culture was spread on an LB agar plate containing the appropriate antibiotic and incubated at 37°C overnight.

2.10 Protein related procedures

2.10.1 Protein extraction with RIPA buffer

In order to extract proteins from mammalian cell pellets, 200 µl of RIPA buffer containing protease and phosphatase inhibitors was added to 10^7 cells. The cells were disrupted by vortex and kept on ice for 30 minutes. The tissue or cell lysate was then centrifuged at 14,000 xg, 4°C for 10 minutes. The supernatant was transferred to a fresh tube, and the protein concentration was determined by Bradford assay.

2.10.2 Bradford assay

In order to determine the protein concentration in cell lysates, a Bradford assay was performed using Protein assay dye reagent concentrate. The Bradford red dye solution contains an acidic (cationic) form of coomassie brilliant blue G-250. The dye is converted to the blue anionic form when it binds to arginine and aromatic amino acid residues, thus the OD_{595} can be determined and related to protein concentration. A standard curve was prepared by serial dilutions from a 2 mg/ml BSA (Bovine serum albumin) stock solution and RIPA buffer. 10 µl of each serial dilution was transferred into a flat bottom 96-well plate preparing three replicates. 10 µl of each protein lysate was also transferred to the plate in three replicates. The dye was prepared by diluting 1:4 the Protein assay dye reagent concentrate with dH_2O, vortexing and filtering to remove particles. 200 µl of the dye reagent was added to each well and mixed by pipetting up and down. The samples were left 5 minutes at room temperature for the reaction to take place.

Then, to avoid the presence of bubbles in the sample, 100 µl of the sample was transferred to a new flat-bottom 96-wells plate. The addition of the dye reagent, sample mixing and transfer were performed with a multichannel pipette. The values of OD_{595} for each well were obtained using a plate reader, the standard curve was plotted with GraphPad prism 6 and a linear regression performed. The OD_{595} values from the cell lysates were converted into protein concentration using the equation obtained from the linear regression.

2.10.3 Polyacrylamide gel electrophoresis

In order to separate proteins by size, a MiniGel tank and blot module set and a PowerEase 500 power supply were used with a 10-well NuPAGE 12% Bis-Tris protein gel. The protein samples were prepared using 10 µg of protein, 5 µl of 4X Bolt LDS sample buffer, 2.5 µl of 10X NuPAGE sample reducing agent and RIPA buffer up to a volume of 25 µl. The mix was vortexed, centrifuged 10,000 xg for 2 minutes and heated at 95°C for 1 minute. The Mini Gel Tank and 10-well NuPAGE 12% Bis-Tris gel were set up for electrophoresis and filled with 1X dilution in dH_2O of 20X NuPAGE MOPS SDS running buffer. 10 µl SeeBlue Plus2 pre-stained protein standard and 15 µl (6 µg of total protein) of the 25 µl of protein sample were loaded into the gel. The electrophoresis was run for 1 hour at 125 V, 100 mA and 18 W. The gel was removed for western blotting.

2.10.4 Western blotting

In order to transfer the proteins from a polyacrylamide gel to a PVDF membrane by electrophoresis, the MiniGel tank and blot module set and a PowerEase 500 power supply were used. The PVDF membrane was activated by soaking 1 minute in methanol. The blot module was set up with the PVDF membrane placed on top of the gel and filter paper, then sponge pad covering both sides of the gel/membrane. The blot module was placed into the MiniGel tank, filed with 1X dilution in dH_2O of 20X Bolt transfer buffer. Electrophoresis was run for 1 hour at 30 V, 300 mA and 25 W using a PowerEase 500 power supply.

2.10.5 Ponceau membrane staining for protein visualisation

In order to assess the successful protein transfer to the PVDF membrane, the blot was stained with Ponceau solution: 0.1% (w/v) ponceau S and 5% (v/v) acetic acid

in dH_2O. The membrane was incubated in 10-15 ml of Ponceau staining solution at room temperature until bands became visible. Then, the unbound stain was washed off the membrane with two washes of 1 minute with 15 ml of dH_2O. The photographic image was recorded. The membrane was then washed three times with 0.1% (v/v) Tween20 in TBS for 5 minutes with shaking before probing.

2.10.6 Membrane blocking and antibody probing

The membrane was blocked with 5% (w/v) non-fat milk powder (NFM) 0.1% Tween20 in TBS at room temperature for 1 hour with shaking. After the blocking, the membrane was incubated with the primary antibody (table 2.2) diluted in 2% NFM 0.1% Tween20 in TBS overnight 4°C with shaking. The following day, the membrane was washed three times for 5 minutes with shaking with 0.1% Tween20 in TBS. The membrane was then incubated with the secondary antibody diluted in 2% NFM 0.1% Tween20 in TBS for 1 hour at room temperature with shaking. After the incubation, the membrane was washed three times for 5 minutes with shaking with 0.1% Tween20 in TBS. The membrane was kept wet in TBS.

2.10.7 Protein chemiluminescence detection

In order to detect secondary antibodies linked to HRP (horseradish peroxidase enzyme), Pierce ECL western blotting substrate was used together with an ECL (enhanced chemiluminescence) system. Pierce ECL western blotting substrate is composed of two solutions, detection reagent 1 (peroxide solution) and detection reagent 2 (luminol enhancer). 12 ml of detection reagent was prepared by mixing detection reagent 1 and detection reagent 2 in equal parts at room temperature. The membrane was incubated with the detection reagent for 1 minute at room temperature and luminescence computed using a c600 imaging system.

2.10.8 Membrane stripping and reprobing

In order to detect a second protein in the membrane, the antibodies and detection reagent were removed by washing the membrane three times for 5 minutes with shaking with 0.1% Tween20 in TBS at room temperature, followed by incubating with Restore PLUS western blot stripping buffer 15 minutes at room temperature. The membrane was washed with three times for 5 minutes with shaking with 0.1%

Tween20 in TBS. The membrane could then be blocked and reprobed as described in sections 2.10.6 and 2.10.7 or stored sealed in plastic at 4°C until further use.

2.11 Yeast display related procedures

2.11.1 Yeast transformation

In order to transform *S. cerevisiae* EBY100, the lithium acetate/single-stranded carrier DNA/polyethylene glycol method was followed. *S. cerevisiae* EBY100 was spread on a plate with 1% agarose in YPD plus penicillin and streptomycin and incubated for 2 days at 30°C. A colony was picked and grown overnight in 5 ml of YPD broth plus penicillin and streptomycin at 30°C and 220 rpm. Next day, a 50 ml culture was prepared at a yeast density of OD_{600} 0.5 and was grown to a density of OD_{600} 1 equating to $2x10^7$ yeast cells/ml. The yeast were harvested by centrifugation at 2000 xg for 3 minutes, washed twice with sterile dH_2O and resuspended in 1 ml of sterile dH_2O. 100 µl of this yeast suspension was used for each transformation. The yeast sample was centrifuged at 2000 xg for 3 minutes, the supernatant removed and the pellet resuspended in 360 µl of transformation mix: 240 µl of 50% (w/v) PEG3350, 36 µl of 1M lithium acetate, 50 µl of 2 mg/ml boiled salmon sperm DNA, sample DNA and sterile dH_2O to a final volume of 360 µl. The sample DNA was 500 ng of circular plasmid DNA, or 1.4 µg of linearised plasmid plus 0.4 µg of DNA insert (when using homologous recombination mediated insertion). The yeast with the transformation mix were vortexed vigorously, then incubated at 42°C for 45 minutes. Next, the yeast were centrifuged at 2000 xg for 3 minutes and the supernatant removed. The yeast were resuspended in 1 ml of YPD and incubated 1 hour, 30°C and 220 rpm. After incubation, the yeast were pelleted by centrifugation at 2000 xg for 3 minutes and YPD broth was removed and the yeast were washed twice with sterile dH_2O and resuspended in 50 µl of SD-CAA selection broth supplemented with penicillin and streptomycin. The samples were finally plated in a Petri dish with 1% agarose in SD-CAA supplemented with penicillin and streptomycin or resuspended in SD-CAA broth with penicillin and streptomycin in the case of yeast transformation for homologous recombination of DNA insert into a pYDN. In both cases the yeast were incubated 2 days at 30°C.

In the case of yeast transformation for homologous recombination into pYDN, a titration was performed with serial dilutions of the selection both (undiluted and dilutions of 10^{-1}, 10^{-2}, 10^{-3}, 10^{-4}, 10^{-5}, 10^{-6} and 10^{-7}). 10 µl of each dilution were plated on 1% agarose in SD-CAA supplemented with penicillin and streptomycin SD-CAA and incubated at 2 days at 30°C. The colonies from the highest dilution with more than 20 colonies were counted for calculation of the total number of colony-forming units (CFU).

$$CFU/ml = \frac{N° \; of \; colonies}{Volume \; plated \; in \; ml} x \frac{1}{DF}$$

2.11.2 Preparation of yeast lysates

In preparation for PCR, *S. cerevisiae* EBY100 samples were lysed in yeast lysate buffer: 50 mM Tris-Cl (pH 8), 10 mM EDTA, 0.01 M DTT and 300 U/ml of lyticase. 10^6 yeast were resuspended in 100 µl of lysate buffer and incubated 40 minutes at 37°C, followed by 10 minutes at 80°C. The debris was pelleted at 10,000 xg for 10 minutes and 0.5 µl of the supernatant was used for a 50 µl PCR.

2.11.3 Yeast display: growth and induction

In order to expand the yeast and induce the expression of the recombinant fusion proteins on *S. cerevisiae* EBY100 transformed yeast, cultures were grown in 50 ml of SD-CAA broth with penicillin and streptomycin at 30°C and 220 rpm from a density of OD_{600} 0.5 to a final density of OD_{600} 1. Then, the yeast were centrifuged at 2000 xg for 3 minutes, the pellet resuspended in 50 ml of SG-CAA broth with penicillin and streptomycin and the yeast grown overnight at 20°C 220 rpm for the induction of the fusion protein. SG-CAA has the same formulation as SD-CAA with the exception that the carbon source is galactose instead dextrose, activating the GAL promoter and thus inducing the expression of the genomic AGA1 and the plasmid AGA2-fusion protein for subsequent display.

2.11.4 Yeast panning depletion prior to selection

In order to select yeast displaying scFvs able to interact with the target antigen on the surface of mammalian cells, the induced yeast display outputs obtained by transfer from the phage display selections were exposed to HEK293 cells

expressing the target antigen. Prior to this, to promote the antigen specificity, the induced yeast underwent two depletion steps, first with the surface of the flask (to remove any yeast-expressing flask-reactive scFv) and second with control HEK293 cells (to remove any yeast-expressing HEK293-reactive scFv). For the first depletion, the yeast were grown and the scFvs induced. BSA was used as a blocking agent to block non-specific binding. The yeast were pelleted, resuspended to a density of OD_{600} 3 in 2% (w/v) BSA in PBS and incubated 1 hour at room temperature with rocking. Then, $5x10^8$ yeast were resuspended in 15 ml of 2% BSA in PBS Ca^{++} Mg^{++} and exposed to the surface of a 150 cm^2 flask for 1 hour with gentle intermittent swirling. For the second depletion, to increase the adherence of the HEK293 cells to the flask, the 75 cm^2 flask were previously coated for 5 minutes with 5 ml of 0.2 mg/ml solution of Poly-D-Lysine in sterile dH_2O. Then, the solution was removed and the surface rinsed with sterile dH_2O and left to dry. HEK293 cells were seeded in 50% confluence and used for yeast-cell panning selection when the confluence reached 80-100%. The HEK293 cell were blocked with 10 ml of 2% BSA PBS Ca^{++} Mg^{++} for 1 hour. The blocking solution was removed from the flask and the yeast suspension was transferred from the first depletion flask to the flask with the HEK293. The yeast were incubated for 1.5 hours at room temperature with gentle swirling every 30 minutes.

2.11.5 Yeast selection and expansion

During the second depletion step, to prepare the selection step, a 75 cm^2 cell culture poly-D-lysine coated flask with 80-100% confluent HEK293 expressing the target antigen were blocked by replacing the medium with 10 ml of 2% BSA in PBS Ca++ Mg++ for 1 hour. Next, the blocking solution was removed from the antigen-expressing HEK293 cells, and the depleted yeast suspension was transferred to the flask, incubating for 1.5 hours at room temperature with gentle swirling every 30 minutes. The yeast suspension was removed and the HEK293 cells washed four times with 15 ml of 2% BSA in PBS Ca^{++} Mg^{++} and once with 15 ml of PBS with gentle swirling. The flask was examined under the microscope to detect the presence of yeast binding to the cells. The selected yeast and HEK293 cells were scraped from the surface of the flask in 15 ml of SD-CAA plus 100 U/ml of penicillin and streptomycin and transferred to a 250 ml flask were they were grown in a total volume of 50 ml medium for 2 days at 30°C and 220 rpm. Then, the culture was passed through a 40 µm cell strainer to remove the mammalian cell debris and

centrifuged at 2000 xg, 4°C for 3 minutes. The yeast pellet was resuspended in 4 ml of 15% glycerol in PBS and stored at -80°C for the next selection round.

2.12 Phage display related procedures

2.12.1 Phage library production

In order to produce the phage library, a bacterial glycerol stock of *E. coli* XL1-Blue transfected with the library cloned into a phagemid vector was purchased and used (table 2.7). 10^{11} *E. coli* XL1-Blue (ten times the library diversity) were grown at 37°C and 220 rpm from OD_{600} 0.3 to OD_{600} 0.6 (OD_{600} 1 with *E. coli* is equivalent to $8x10^8$ bacteria/ml) in Terrific broth supplemented with ampicillin, tetracycline and 0.1 M glucose. Then, $2x10^{11}$ M13KO7 helper phage were added, and the culture was incubated 30 minutes at 37°C without shaking for the infection. After the infection, the bacteria were centrifuged 4000 xg, 4°C for 30 minutes and the pellet was resuspended at a density of OD_{600} 1 in Terrific broth supplemented with ampicillin, tetracycline, kanamycin and 0.25 mM of IPTG. The infected bacteria were grown overnight at 30°C and 220 rpm. The bacteria were then centrifuged at 4000 xg, 4°C for 30 minutes and the phage containing supernatant collected. 10 ml of a solution composed of 20% (w/v) PEG8000 and 2.5 M NaCl was added to 40 ml of phage supernatant in a 50 ml falcon tube, mixed well and cooled on ice for 1 hour. Then, the phage suspension was centrifuged at 4000 xg, 4°C for 30 minutes. The supernatant was discarded, and the phage pellet resuspended in 1 ml of PBS. The phage suspension was centrifuged 10,000 xg, 4°C for 10 minutes and the supernatants collected and filtered through a 0.2 µm syringe filter. The phage density was determined using a NanoDrop 1000 by measuring OD_{268}. The value of OD_{268} 1 is equivalent to $5x10^{12}$ M13 phage/ml. This procedure was followed to produce the initial library for phage selection and the output phage obtained from each selection step.

2.12.2 Phage display selection using yeast expressing antigen

Several rounds of selection were performed and each round consisted of two steps, depletion and selection. In order to perform a phage display selection using yeast as a source of antigen, two different samples of induced yeast were prepared (2.11.3), $1.5x10^8$ induced yeast expressing the display system AGA1-

AGA2 and $1.5x10^8$ induced yeast expressing the display system with the fusion protein, AGA1-AGA2-fusion protein. Prior to the selection procedure, the yeast were blocked with 2% BSA in PBS at OD_{600} 3 and the phage in 1 ml of 2% NFM in 0.5% Tween20 in PBS, both for 1 hour at room temperature with rocking.

2.12.2.1 Phage depletion and selection

For the depletion step, the blocked phage were incubated with the blocked induced yeast expressing AGA1-AGA2, in phage blocking solution for 1.5 hours at room temperature with rocking. The yeast were pelleted at 10,000 xg for 5 minutes and the supernatant collected for the selection step. The supernatant was mixed with the blocked induced yeast expressing AGA1-AGA2-fusion protein for 1.5 hours at room temperature with rocking. The yeast were pelleted at 2000 xg for 3 minutes at room temperature, the supernatant discarded and the yeast collected for the washing steps. A total of eight washes were performed, seven with 1 ml of 0.1% of Tween20 in PBS and the last one with 1 ml of PBS. For every wash, the yeast were swirled in the tube then centrifuged at 2000 xg for 3 minutes at room temperature.

2.12.2.2 Phage elution

The phage were digested away from the yeast using 800 µl of 0.02 mM trypsin for 15 minutes at room temperature with rocking. After the incubation, the trypsin was blocked with 200 µl of FBS (Foetal bovine serum) and the 1 ml solution used for infection of *E. coli* XL1-Blue. Short trypsinisation treatments can elute the phage without affecting their infectivity.

2.12.2.3 *E. coli* infection, phage titration and expansion

To infect *E. coli* XL1-Blue with the selected phage, the day before the selection a colony was picked from an agar plate with LB supplemented with tetracycline and grown in 50 ml of Terrific broth supplemented with tetracycline overnight 37°C at 220 rpm. The next day, a new culture was prepared starting at $0D_{600}$ 0.1 and grown at 37°C at 220 rpm to OD_{600} 0.6. 5 ml of this culture was used for infection with the eluted phage. The eluted phage (1 ml) was added to the 5 ml of culture, and the total 6 ml of infection mix was incubated in a water bath for 30 minutes at 37°C with gentle mixing every 10 minutes. A titration was performed with serial

dilutions of the infection mix (undiluted and dilutions of 10^{-1}, 10^{-2}, 10^{-3}, 10^{-4}, 10^{-5}, 10^{-6} and 10^{-7}). 10 µl of each dilution were plated on LB plus 10 µg/ml tetracycline plus 100 µg/ml ampicillin plates and incubated at 37°C overnight. The colonies from the highest dilution with more than 20 colonies were counted for calculation of the total number of colony-forming units (CFU).

$$CFU/ml = \frac{N° \ of \ colonies}{Volume \ plated \ in \ ml} x \frac{1}{DF}$$

After the titration, the bacteria were pelleted from the infection mix by centrifugation at 4000 xg, 30 minutes at 4°C and resuspended in 1 ml of Terrific broth supplemented with tetracycline and ampicillin. Then, this was plated on a square bioassay plate with 1% agar in Terrific broth supplemented with tetracycline and ampicillin. The bioassay plate was incubated at 37°C overnight. Then, the bacteria were collected from the bioassay plate and resuspended in 4 ml of Terrific broth plus 25% of glycerol, generating four 1 ml glycerol stocks. The percentage of phage recovered in each round of selection was calculated by comparison between the number of phage obtained after selection with the number of phage used at the beginning of the selection. The results were plotted with GraphPad Prism 6.

2.13 Flow cytometry analysis

All flow cytometry data were analysed with FlowJo v10. In the case of working with yeast, the same volume was used for blocking, staining, washing and resuspension. This volume changes with the quantity of yeast needed for the analysis, but the yeast density was constant in all the steps (OD_{600} 3).

2.13.1 Yeast display expression

In order to analyse the expression of the displayed protein on the yeast surface, the transformed yeast were grown and induced, then blocked in 2% BSA in PBS for 1 hour at room temperature with rocking. To stain yeast transformed with pYD1-derived plasmids, a staining solution was prepared with the antibodies Mouse-anti-Xpress and Goat-anti-mouse Alexa 488 conjugated, both diluted 1:250 in 2% BSA in PBS. To stain yeast transformed with pYDN-derived plasmids, a staining solution was prepared with the antibody Mouse-anti-V5 FITC conjugated diluted 1:500 in

2% BSA in PBS. The yeast were resuspended in the staining solution and incubated for 1 hour at 4°C with rocking, covered with aluminium foil. The yeast were then centrifuged at 2000 xg, 4°C for 3 minutes and the pellet washed twice with cold 2% BSA in PBS. The yeast were finally resuspended in cold PBS and kept on ice till their analysis using MACSQuant analyser 10 (Miltenyi biotec).

2.13.2 B7H4 expression in HEK293-B7H4

In order to characterise the expression of B7H4 in HEK293 cells, a 75 cm^2 flask at 80-100% confluence with HEK293 cells was used and the cells detached with 10 minutes incubation in 5 ml of Cell dissociation solution, the dissociation reaction was stopped with 15 ml of PBS. The cells were collected and centrifuged for 5 minutes at 500 xg and 4°C, the pellet resuspended in 2 ml of cold PBS and filtered through a 40 µm cell strainer. The cell density was determined and adjusted to 10^7 cells/ml in PBS and kept on ice. 100 µl of the cell suspension was used for each cell staining. The staining was performed by adding 5 µl of Mouse-anti-B7H4 PE conjugated to 100 µl of cells (1:20 dilution). An isotype control was performed by adding 2.5 µl of Mouse IgG1 kappa isotype PE conjugated to 100 µl of cell suspension (1:40 dilution). Both samples were incubated for 1 hour at 4°C with rocking and covered by aluminium foil. After the incubation, the cells were washed twice with cold PBS, resuspended in 100 µl of cold PBS and kept on ice till their analysis using MACSQuant analyser 10.

2.13.3 Yeast Fluorescence-activated cell sorting (FACS)

In order to analyse and isolate scFvs binding to B7H4 after the yeast-cell panning selection, the interaction between the yeast displaying scFvs and recombinant antigen B7H4-Fc was examined by flow cytometry. B7H4-Fc is a recombinant fusion protein composed of the extracellular domain of B7-H4 and the Fc domain of an antibody (comprising the CH1 and CH2 domains) forming a homodimer.

The yeast from the different panning selection outputs were grown and induced, then blocked in 2% BSA in PBS for 1 hour at room temperature with rocking. The blocked yeast were resuspended in a solution of 100 nM of B7H4-Fc in 2% BSA in PBS and incubated for 1 hour at room temperature with rocking. Another sample of blocked yeast was used as control and incubated with 100 nM of Fc. Next, the

yeast were centrifuged at 2000 xg for 3 minutes and washed twice with 2% BSA in PBS. Then, they were incubated with a staining solution composed of 1:250 dilution of Mouse-anti-V5 Tag Alexa 647 conjugated and 1:40 dilution of Mouse-anti-human Fc FITC conjugated in 2% BSA in PBS. The samples were incubated for 1 hour at 4°C with rocking and covered by aluminium foil. After the incubation, they were washed twice with cold 2% BSA in PBS and finally resuspended in cold PBS and kept on ice until their analysis and sorting using BD FACSAria III (Becton Dickinson) and the software BD FACSDiva. The double-positive labelled yeast, $FITC^+$ and Alexa 647^+, were sorted into a 15 ml falcon tube containing 7 ml of SD-CAA supplemented with penicillin and streptomycin. They were transferred to a 250 ml flask for growth in a final volume of 50 ml for 2 days at 30°C and 220 rpm. A second sorting was performed and plated onto agar plates of SD-CAA supplemented with penicillin and streptomycin, sorting 96 double-positive single yeast. The plates were incubated for 2 days at 30°C for single colony growth.

2.13.4 Yeast single clone binding analysis

In order to study the interaction of single yeast clones expressing scFv with dimeric and monomeric recombinant B7H4, the yeast were exposed to the antigens and the binding assessed by flow cytometry. The individual yeast clones were grown and induced, then in 2% BSA in PBS for 1 hour at room temperature with rocking. To study the scFv expression, blocked yeast were incubated in a staining solution with 1:500 Mouse-anti-V5 tag FITC conjugated in 2% BSA in PBS for 1 hour at 4°C with rocking and covered in aluminium foil. Separately, blocked yeast were incubated in four different antigen solutions in 2% BSA in PBS for 1 hour at room temperature with rocking: [1] 100 nM of Human B7H4-humanFc, [2] 100 nM of Mouse B7H4-mouseFc, [3] 100 nM of Human B7H4- Polyhistidine tag and [4] 100 nM of Mouse B7H4-Polyhistidine tag. After the incubation with the recombinant antigens, the yeast were centrifuged at 2000 xg 3 minutes, washed twice with cold 2% BSA in PBS and stained with staining solution. The staining solutions were composed of 1:40 dilution in cold 2% BSA in PBS of Mouse-anti-human Fc FITC conjugated (in the case of yeast incubated with HumanB7H4-humanFc), 1:250 dilution in cold 2% BSA in PBS of Goat-anti-Mouse IgG Alexa 488 conjugated (in the case of MouseB7H4-mouseFc) or 1:250 dilution in cold 2% BSA in PBS of Mouse-anti-Polyhistidine Alexa 647 conjugated (in the cases of Human B7H4-Polyhistidine tag and Mouse B7H4-Polyhistidine tag). The yeast were incubated with the staining

solution 1 hour at 4°C with rocking and covered with aluminium foil. Next, the yeast were centrifuged at 2000 xg for 3 minutes and washed twice with cold 2% BSA in PBS and finally resuspended in cold PBS and kept on ice till their analysis using MACSQuant analyser 10.

2.13.5 CAR expression in Jurkat-rep-CAR Clone X cell lines

In order to study the level of expression of CARs in the established Jurkat-rep-CAR Clone X cell lines, the cells were exposed to dimeric recombinant B7H4 and the binding assessed by flow cytometry. 10^6 Jurkat-rep-CAR Clone X cells were incubated in 200 µl of 950 nM of Human B7H4-humanFc in PBS with 0.2% sodium azide, which blocks 80% to 90% of receptor internalisation, for 1 hour at 4°C. Next, the cells were centrifuged at 90 xg for 10 minutes and incubated in 200 µl of 1:40 dilution in PBS with 0.2% sodium azide of Mouse-anti-human Fc FITC conjugated for 1 hour at 4°C covered with aluminium foil. Finally, the cells were centrifuged at 90 xg for 10 minutes, washed twice with 200 µl PBS with 0.2% sodium azide and kept on ice until their analysis using MACSQuant analyser 10.

2.14 Cell culture related procedures

2.14.1 Cell culture and cell passaging conditions

2.14.1.1 HEK293 Flip-In T-REx

The HEK293 Flip-In T-REx cell line was grown in high glucose D-MEM supplemented with 10% inactivated FBS, 2 mM of L-glutamine, zeocin, 15 µg/ml of blasticidin and penicillin and streptomycin. The cells were incubated in tissue culture flasks at 37°C and 5% CO_2. HEK293 Flip-In T-REx are adherent cells which were passaged by trypsinisation. The medium was decanted from the flask and the cells were washed twice with sterile PBS. The PBS was decanted, and an appropriate volume of 0.02 mM trypsin was added to the flask to cover the growth surface completely. The flask was left 5 minutes at room temperature and gently shaken to detach the cells from the flask. The trypsin was diluted 1:3 with sterile PBS and the cells were centrifuged at 500 xg and 4°C for 5 minutes, the supernatant then discarded. The cell pellet was resuspended in 10 ml fresh medium and the cell viability and density determined. Cells were passaged to a new flask using $6x10^3$ viable cells/cm^2 and an appropriate volume of fresh medium.

2.14.1.2 HEK293-B7H4, HEK293-LMP1 and HEK293-LMP2A

HEK293-B7H4, HEK293-LMP1 and HEK293-LMP2A cells were grown in high glucose D-MEM supplemented with 10% inactivated tetracycline free FBS, 2 mM L-glutamine, blasticidin (15 µg/ml), hygromycin B (400 µg/ml), penicillin and streptomycin. The cells were incubated in tissue culture flasks at 37°C and 5% CO_2. For the induction of the tetracycline-inducible protein, the medium was supplemented with tetracycline. For B7H4 the induction was performed with 10 µg/ml tetracycline for 24 hours. For LMP1 and LMP2A, induction was for 16 hours with 0.5 µg/ml and 1 µg/ml tetracycline respectively, due to the toxicity of these proteins in HEK293 when expressed in high amounts. These cells were passaged as described above in section 2.14.1.1.

2.14.1.3 Jurkat-Dual

The Jurkat-Dual cell line was grown in IMDM, 2 mM L-glutamine, 25 mM HEPES supplemented with 10% inactivated FBS, zeocin, 10 µg/ml of blasticidin and penicillin and streptomycin. The cells were incubated in tissue culture flasks at 37°C and 5% CO_2. Jurkat-Dual cells are suspension cells, and they were passaged by dilution in fresh medium in a new flask at $2x10^5$ viable cells/ml, not allowing the cell density to exceed $2x10^6$ cells/ml.

2.14.1.4 Jurkat-rep-CAR Clone X cell lines

Jurkat-rep-CAR Clone X cell lines were grown in IMDM, 2 mM L-glutamine, 25 mM HEPES supplemented with 10% inactivated FBS, zeocin, blasticidin, hygromycin (200 µg/ml) and penicillin and streptomycin. The cells were incubated in tissue culture flasks at 37°C and 5% CO_2. The cells were passaged as described in section 2.14.1.3.

2.14.2 Cell counting with trypan blue

Trypan blue is a polar dye that can cross the membrane of necrotic and apoptotic cells but not the intact membrane of viable cells. This property allows dead cells to be distinguished from viable cells. Under the microscope, the viable cells appear clear white, whereas dead cells are blue in colour. The density of viable cells in a cell suspension was determined by diluting 10 µl of the cell suspension

in 10 µl of 0.4% trypan blue and loading 10 µl in a chamber slide. The cell viability and density were determined with Countess II automated cell counter (TFS).

2.14.3 Freezing and thawing of viable cells

Cells were centrifuged, and the supernatant was discarded. The cell pellet was resuspended with 1 ml of freezing medium composed of 10% (v/v) DMSO in FBS. The cell suspension was transferred to a labelled cryovial and placed in a Mr. Frosty freezing container (TFS, 5100-0001) filled with isopropanol at -80°C for 1 day. Then the tube was transferred to liquid nitrogen. In order to thaw the cells stored in liquid nitrogen, the cryovial was quickly transferred to a 37°C water bath and incubated until the ice disappeared. The cell suspension was transferred to 10 ml of fresh medium and centrifuged. The pellet was resuspended in fresh medium and incubated at 37°C and 5% CO_2.

2.14.4 Mammalian cell transfection and selection

2.14.4.1 HEK293 transfection

PolyFect transfection reagent was used to transfect HEK293 Flip-In T-REx with the plasmids pcDNA5/FRT derivatives and pOG44. The reagent consists of dendrimer molecules that assemble DNA into compact structures by charged amino groups interacting with negatively charged phosphate groups of nucleic acids. The DNA compact structures bind to the cell surface and are taken into the cell by nonspecific endocytosis. $2.6x10^6$ HEK293 Flip-In T-REx were seeded in a 25 cm^2 flask with 5 ml of growth medium (defined above). The culture was grown to 40-80% confluence and the medium removed and the cells washed with PBS. Then, 3 ml of high glucose D-MEM supplemented with 10% inactivated tetracycline free FBS was added to the cells. A transfection mix was prepared by diluting 3.6 µg of pOG44 plus 0.4 µg of pcDNA5/FRT derived vector in 150 µl of high glucose D-MEM, then vortexed. 40 µl of PolyFect transfection reagent was added to the mix and vortexed for 10 seconds (and briefly centrifuged to collect at the bottom of the tube). The mix was incubated 5-10 minutes at room temperature to allow the formation of the DNA complexes. After the incubation, 1 ml of high glucose D-MEM supplemented with 10% inactivated tetracycline free FBS was added to the mix, and the mix transferred to the 3 ml culture and swirled gently. The cells were incubated for 2 days at 37°C and 5% CO_2, replacing the medium after 1 day with

fresh D-MEM supplemented with 10% inactivated tetracycline free FBS. After 2 days, the cells were trypsinised and seeded in a new 25 cm^2 flask with 5 ml of fresh D-MEM supplemented with 10% inactivated tetracycline free FBS. The culture was incubated for 4 hours at 37°C and 5% CO_2 until the cells attached to the surface of the flask. Then, the medium was replaced with 5 ml of high glucose D-MEM supplemented with 10% inactivated tetracycline free FBS, 2 mM of L-glutamine, blasticidin, hygromycin B and penicillin and streptomycin. The antibiotic selection was established for several weeks changing the selection medium every 3 days until several resistant colonies established. Finally, the resistant clones were trypsinised together, and the cells expanded in the presence of antibiotic. Frozen cell stocks were made to preserve the newly establish cell lines. The cell population was isogenic as the pcDNA5/FRT derived plasmid integrates into the same locus in every clone.

2.14.4.2 Jurkat transfection and Cas9-mediated homology-directed repair (HDR) of pCD8-CAR Clone X and pIgG4-CAR Clone X plasmids

TransIT-Jurkat transfection reagent was used to transfect Jurkat-Dual with the *Nhe*I linearised plasmids pCD8-CAR Clone and pIgG4-CAR Clone plus the Cas9 ribonucleoprotein (RNP). A day before the transfection, 1 ml of Jurkat-Dual cells were seeded at a cell density of $3x10^5$ cells/ml in a 24-well cell culture plate in IMDM, 2 mM L-glutamine, 25 mM HEPES supplemented with 10% inactivated FBS. Four hours before the transfection, 20 µM of the SCR7, an inhibitor of the non-homologous end-joining DNA repair pathway, was added to the media. During these four hours, the crRNA (CRISPR RNA) and tracrRNA (trans-activating crispr RNA) were annealed to form the gRNA (guide RNA) by mixing both at 1 µM in Nuclease-free duplex buffer and heating them at 95°C for 5 minutes, and then slow cooling to room temperature. The 1 µM gRNA solution could be then stored at -20°C for future use. Before the transfection, a 3 µM solution of EnGen Spy Cas9 NLS was prepared in 1X NEB 3.1 Buffer. To form the Cas9 RNP, the Cas9 and the gRNA were mixed 6 nM to 12 nM in Opti-MEM I reduced serum medium. 12 µl of 1 µM gRNA solution were diluted in 86 µl of Opti-MEM I, mixed and incubated at room temperature for 10 minutes. Then, 2 µl of 3 µM Cas9 solution was added to the mix and incubated at room temperature for 10 minutes (1-to-2 ratio of Cas9 and gRNA, 6 nM:12 nM). Afterwards, 1 µg of linearised plasmid was added to the mix followed by 3 µl of TransIT-Jurkat transfection reagent. The final solution was

mixed gently and incubated for 25 minutes at room temperature. During the 25 minutes incubation, 5 µM of the DNA HDR enhancer L755507 was added to the culture and mixed gently. Then, the transfection mix was added drop by drop to the culture in different areas, and the plate gently rocked for better distribution. The culture was incubated for 3 days at 37°C and 5% CO_2. After 3 days, the transfection media was removed and the cells resuspended at $5x10^5$ cell/ml in IMDM, 2 mM L-glutamine, 25 mM HEPES supplemented with 10% inactivated FBS, penicillin and streptomycin, zeocin, blasticidin and hygromycin. The cells were expanded in the presence of antibiotics for several months until the cell growth and viability were similar to the parental cell line. Frozen cell stocks were made to preserve the newly established cell lines.

2.14.4.3 Jurkat electroporation for CAR transient expression

Cell line nucleofector kit V and Nucleofector I were used to transfect Jurkat-Dual with the pCD8-CAR Clone X and pIgG4-CAR Clone X plasmids. A culture of $2x10^5$ viable cells/ml was established prior to electroporation and grown for 2 days. Then, the viability was measured to ensure values higher than 80% and $1x10^6$ cells were used for each electroporation. The volume of medium containing $1x10^6$ cells was centrifuged at 90 xg for 10 minutes and the supernatant removed. The electroporation mix was prepared with 2 µg of plasmid DNA, 82 µl of Nucleofector solution V and 18 µl of Supplement solution, the mix was vortexed. The cells were resuspended in the electroporation mix and transferred into the electroporation cuvette. The program X-001 was selected in Nucleofector I and the electroporation was performed. The electroporated cells were resuspended gently in 500 µl of 37°C prewarmed IMDM, 2 mM L-glutamine, 25 mM HEPES supplemented with 10% inactivated FBS and transferred to a well in a 24-well cell culture plate with 500 µl of the same prewarmed medium and incubated 24 hours at 37°C and 5% CO_2.

2.14.5 Cas9 RNP activity assays

TransIT-Jurkat transfection reagent was used to transfect Jurkat-Dual with the Cas9 RNP as described in section 2.14.4.2. Note that the linearised plasmid and the SCR7 and L755507 reagents were not used for this transfection. As negative control, Jurkat-Dual cells were exposed to TransIT-Jurkat transfection reagent in

the same conditions, but without the presence of the Cas9 RNP. The cells (approximately 10^6 cells) were harvested after 2 days at 37°C and 5% CO_2 for gDNA extraction. The gDNA was used for PCR with the primers AAVS1 Check-F and AAVS1 Check-R (section 2.7.4).

2.14.5.1 T7EI mismatch detection assay

The T7EI mismatch detection assay was performed with the DNA obtained from the Cas9 RNP activity assays. First, a denaturation and annealing step was performed with 100 ng of purified PCR product in 3 µl, 1 µl of 10X NEB Buffer 2 and 6 µl of dH_2O. The mix was subjected to the thermocycler protocol described in table 2.22.

Table 2.22 Denaturation and annealing.

Temperature	Time
95°C	5 minutes
95°C – 85°C	-2°C/seconds
85°C – 25°C	-0.1°C/seconds
10°C	-

Then, the T7EI reaction was performed by adding to the previous 10 µl solution 1 µl of 10X NEB Buffer 2, 0.5 µl of T7EI and 8.5 µl of dH_2O. The final mix was incubated at 37°C for 30 minutes and used immediately for polyacrylamide gel electrophoresis (section 2.8.2) using the 100 bp DNA ladder.

2.14.5.2 Tracking of indels by decomposition (TIDE)

Non-templated repair pathways introduce indels (insertion or deletion of a nucleotide) at the target site. TIDE software identifies the predominant types of indels and quantifies the editing efficacy using the data from two standard capillary sequencing reactions. TIDE analysis for non-templated Cas9 editing was performed with .ab1 files from the sequencing of the previous PCR products with the primer AAVS1 Check-F (http://shinyapps.datacurators.nl/tide/) (480,481).

2.14.6 Co-culture NF-kB activation luciferase reporter assay

Jurkat-Dual cells transfected with CMV-modified pCD8-CAR Clone 4 B7H4 and pIgG4-CAR Clone 4 B7H4 plasmids for transient expression of CARs (section

2.14.4.3) were used for functional assessment of CARs by co-culture with tetracycline induced HEK293-B7H4 cells. Target cells (HEK293-B7H4 cells) were previously induced with 10 µg/ml of tetracycline and used for the co-culture assay 24 hours after induction, together with transfected Jurkat-dual cells after 24 hours of transfection. $5x10^5$ target cells were co-cultured with $1x10^6$ transfected Jurkat-Dual in IMDM, 2 mM L-glutamine, 25 mM HEPES supplemented with 10% inactivated FBS, penicillin and streptomycin and 10 µg/ml of tetracycline. HEK293 Flp-In T-REx were also incubated with 10 µg/ml of tetracycline and used antigen negative control cells (negative control). As a positive control, $1x10^6$ electroporated but no transfected Jurkat-Dual were incubated with 50 µg/ml of Concanavalin A. The co-culture was incubated 48 hours at 37°C and 5% CO_2. Then, 20 µl of the culture (including cells with the medium) were mixed with 50 µl of QUANTI-Luc Gold solution to assess Lucia luciferase activity by measuring the Relative Light Units (RLUs) with the multi-mode plate reader CLARIOstar Plus using the luminescence end-point readings settings. The data were finally analysed using GraphPad prism 6.

3. Results: Development of a yeast system for antigen display

3.1 Rationale

Soluble membrane protein preparations are commonly associated with the presence of aggregates. Aggregates could also be present in peptide preparation. The presence of these aggregates is a known handicap of recombinant protein for phage display selection, having a critical impact on the selection experiment. For this reason, the quality of the recombinant protein is one of the essential points for a successful phage display selection experiment. To avoid the presence of these aggregates and reduce the cost of the selection experiments, a yeast display approach to express the antigens was implemented.

Yeast display has been commonly used for the expression of antibodies and antibody fragment libraries, as well as the expression of antigens for phage display selection (475). The original yeast display system was based on the vector pYD1, designed for C-terminal expression of the foreign protein by fusion with the C-terminal region of Aga2 (472). However, the extracellular domains of some plasma membrane proteins are located within the N-terminal region, which would lead to a shift in the orientation when displayed using the pYD1 yeast display system. Ideally, these proteins should be displayed in the correct orientation at the N-terminus of the Aga2 fusion. Wang et at. 2005 developed the vector pYD5, a modification of pYD1, for N-terminal yeast display of proteins (474). The design of pYD5 from Wang et al. has been used in this project, but a different approach for developing the plasmid was applied.

Unlike the Wang et al. pYD5 vector, for the vector developed here, the nucleotide sequence coding for the Aga2 fusion protein was codon optimised for expression in S. *cerevisiae*. As a result, a vector functionally similar to pYD5 was generated but with different nucleotide sequence. This vector has been named pYDN (to reflect yeast display N-terminal). To circumvent the use of recombinant antigen of soluble peptides during the selection, pYDN has been used to display the B7H4 IgG-like V-type 1 domain at the N-terminus of Aga2 and pYD1 to display the LMPs extracellular loops at the C-terminus of Aga2.

B7H4 is a 282 amino acids protein acting as immunomodulatory ligand with an unknown receptor. In the B7 protein family, the Ig-like V-type 1 domain interacts with the receptor. It is the case for B7-1 (CD80), B7-2 (CD86), B7H1 (PD-L1), B7DC (PD-L2), B7H2 (ICOSL) and B7H6 (NCR3L1) (482–487), and there is evidence indicating that this is also the case for B7H4 (155). The Ig-like V-type 1 domain of B7H4 (Phe29 to Gly148) has been used for its fusion to the N-terminus of Aga2 with a yeast display system based on pYDN (figure 3.1.A).

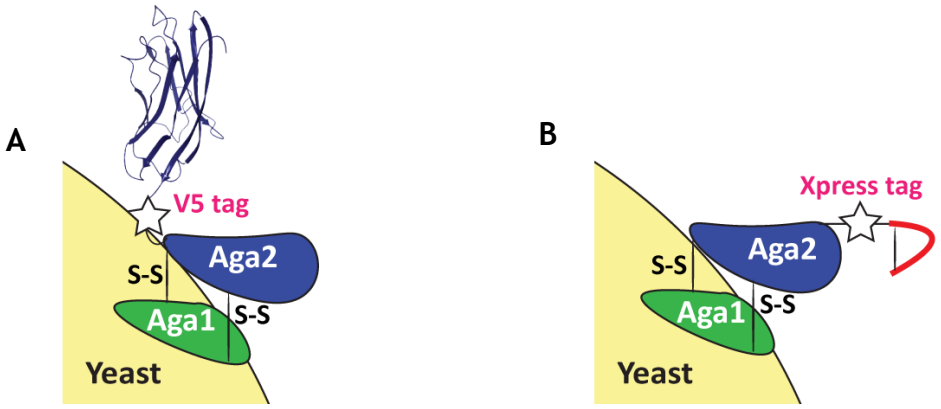

Figure 3.1 Yeast display of antigen. A) pYDN N-terminal display of B7H4 Ig-like V-type 1 domain by fusion with the heterodimer Aga1-Aga2. B) pYD1 C-terminal display of the extracellular loops of LMP1and LMP2 by fusion with the heterodimer Aga1-Aga2.

The goal using this construct is to obtain scFvs that target B7H4 and at the same time improve the chances of blocking of the ligand with its receptor, thereby avoiding a possible immunosuppressor signal to the CAR T-cell. The sequence of B7H4 Ig-like V-type 1 domain displayed at the N-terminus of Aga2 is shown in figure 3.2.

Figure 3.2 B7H4 Ig-like V-type 1 domain amino acid sequence displayed on yeast using pYDN.

B7H4 Ig-like V-type 1 domain
FGISGRHSITVTTVASAGNIGEDGILSCTFEPDIKLSDIVIQWLKEGVLGLVHEFKEGKDELSE QDEMFRGRTAVFADQVIVGNASLRLKNVQLTDAGTYKCYIITSKGKGNANLEYKTG

For LMP1 and LMP2A, the extracellular loops LMP1 loop 2F, LMP1 loop 2Y, LMP2 loop 2 and LMP2 loop 5 have been displayed at the C-terminus of Aga2 using pYD1 (figure 3.1.B). The loops have been chosen considering their size, using the largest of the extracellular loops of LMP1 and LMP2. LMP1 loop 2 is reported to comprise ten amino acids (Leu97 to Phe106), LMP2 loop 2 and LMP2 loop 5 each are thirteen

amino acids long (Arg199 to Ala211 and Leu376 to Phe388). There are two variants in different EBV strains of LMP1 loop 2 at the amino acid position 388 in different EBV strains, Phe388 or Tyr388. Therefore, two different LMP1 loops 2 versions were used: LMP1 loop 2F (Phe388) and LMP1 loop 2Y (Tyr388). The size of all the loops sequences used were extended by including one or two amino acids of the adjacent sequence at each end. Furthermore, to facilitate creating a loop structure (through potential disulphide bonds) two cysteines were added, one at each end. The final sequence of amino acids used for each loop is shown in table 3.2.

Table 3.1 Latent membrane proteins extracellular loops and finale amino acid sequence displayed on yeast using pYD1.

Loop	Amino acids	Final amino acid sequence
LMP1 loop 2F	Ile95-Gly108	CIALWNLHGQALFGC
LMP1 loop 2Y	Ile95-Gly108	CIALWNLHGQALYGC
LMP2 loop 2	Thr198-Leu213	CTWRIEDPPFNSLLFALLC
LMP2 loop 5	Ser374-Pro390	CSILQTNFKSLSSTEFIPC

3.2 Development of pYDN

To obtain pYDN from pYD1, the *Nhe*I restriction site present in pYD1 was removed by site-directed mutagenesis using the primers (-)NheI-F and (-)NheI-R (figure 3.3.A). The resulting vector was named pY-NheI-del. Next, pY-NheI-del was used for the second mutagenesis with the primers (+)NheI-F and (+)NheI-R (figure 3.3) to introduce a new *Nhe*I restriction site at the signal peptide of Aga2 (figure 3.3.B). A PCR with the primers pYD1 Check-F and pYD1 Check-R was performed and the amplicon purified and send for Sanger sequencing with the primer pYD1 Check-F. The sequence editing was confirmed, and the resulting vector named pY-NheI-mod.

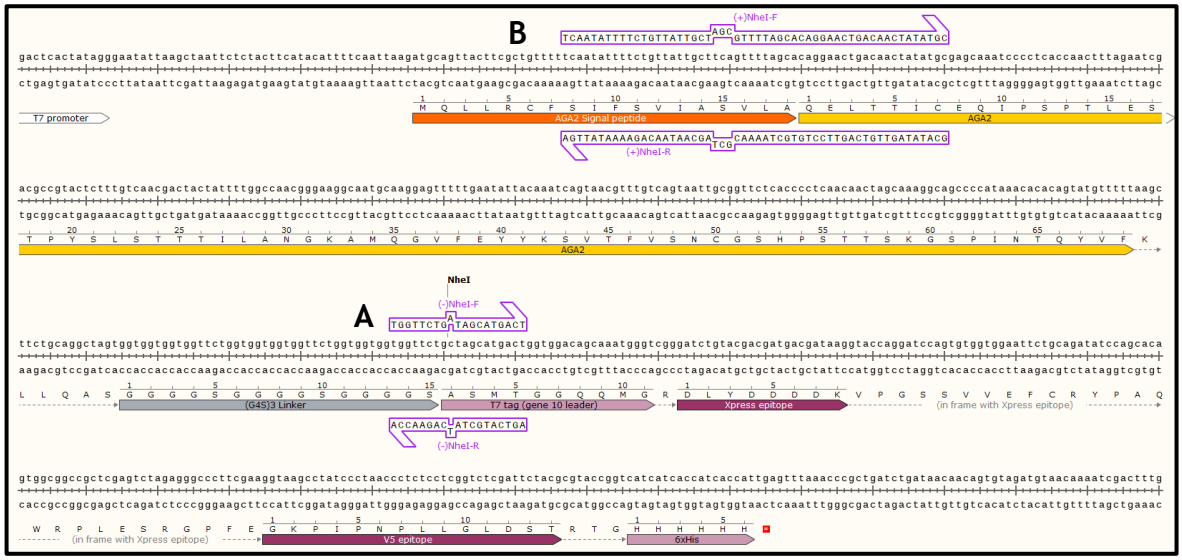

Figure 3.3 Site-directed mutagenesis strategy of pYD1 for the development of pY-NheI-mod. A) Primers for synthesis of pY-NheI-del using pYD1 as template. B) Primers for synthesis of pY-NheI-mod using pY-NheI-del as template. Plasmid features and open reading frames (ORFs) are coloured and denoted: white feature represent the end of the T7 promoter, the orange ORF represents AGA2 signal peptide DNA, yellow ORF AGA2 DNA, grey ORF (G4S)3 linker DNA and pink ORFs the T7 and Xpress tags DNA. Primers used for (+)NheI PCR and (-)NheI PCR denoted.

pY-NheI-mod was digested with *Nhe*I and *Pme*I (figure 3.4) and used for introducing a new DNA cassette including the DNA for a piece of the AGA2 signal peptide, the cloning sites *Nhe*I and *Eco*RI, the V5 tag, the (G4S)3 linker and AGA2 DNA (figure 3.5), giving rise to pYDN. This synthetic DNA cassette was obtained from GeneWiz and supplied in the pUC57 vector (plasmid pUC57-pYDN-Cassette). It was designed with a codon optimised sequence for its expression in *S. cerevisiae*. The DNA cassette was obtained by pUC57-pYDN-Cassette digestion with *Nhe*I and *Pme*I. Both digested plasmids DNA preparations, vector and insert, were electrophoresed and gel purified for their ligation (figure 3.6).

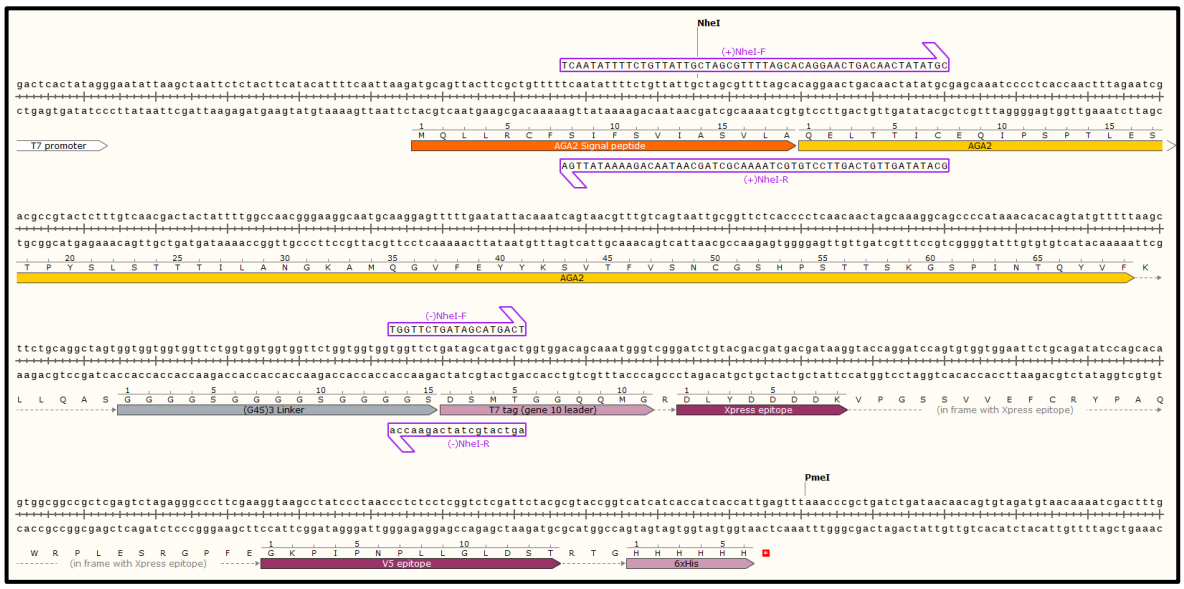

Figure 3.4 pY-NheI-mod. *Nhe*I and *Pme*I were used to remove the DNA fragment from pY-NheI-mod and the cloning of the new DNA cassette giving rise to pYDN. Plasmid features and ORFs are coloured and denoted: the white feature represent the end of the T7 promoter, the orange ORF represents AGA2 signal peptide, the yellow ORF AGA2, the grey ORF (G4S)3 linker, the pink ORFs the T7, Xpress tag, V5 and 6xHi tags and the red square the codon stop. Primers used for (+)NheI PCR and (-)NheI PCR denoted.

Figure 3.5 Synthetic DNA cassette used for the development of pYDN. *Nhe*I and *Pme*I restriction sequence highlighted in green.

DNA cassette for pYDN obtained from pUC57-pYDN-Cassette
GCT AGC GTT TTA GCA GAA TTC GGT AAA CCA ATT CCA AAT CCA TTG TTG GGT TTG GAC TCT ACT GGT GGT GGT GGT TCT GGT GGT GGT GGT TCT GGT GGT GGT GGT TCT CAG GAA TTG ACT ACT ATT TGC GAA CAA ATT CCA TCT CCA ACT TTG GAA TCT ACT CCA TAC TCT TTG TCT ACA ACT ACT ATT TTG GCT AAT GGT AAA GCT ATG CAA GGT GTT TTT GAA TAT TAT AAA TCT GTT ACT TTT GTT TCT AAT TGT GGT TCT CAC CCA TCT ACT ACT TCT AAA GGT TCT CCA ATT AAT ACT CAA TAT GTT TTT TGA TGA GTT TAA AC

After DNA ligation, *E. coli* transformation and plating onto LB agar plates containing ampicillin, three colonies were grown and used for colony PCR with the primers pYDN Cassette-F and pYDN Cassette-R. The PCR amplicons were purified and Sanger sequenced (by GATC, Eurofins) with the primer pYDN Cassette-F. All three sequencing reactions showed the correct sequence (figure 3.5), and one colony was used for subsequent plasmid production.

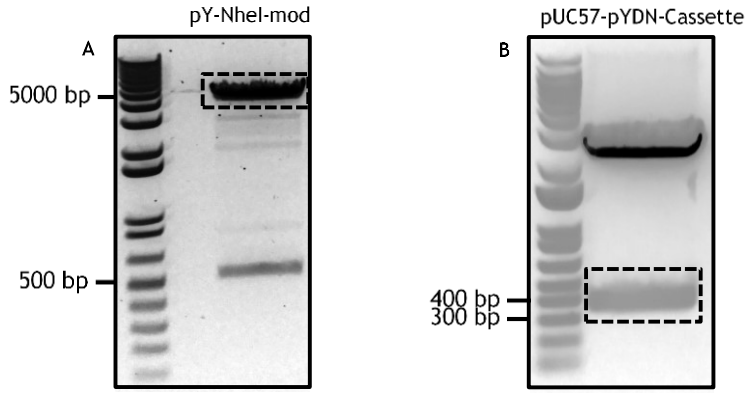

Figure 3.6 pYDN development. Digested plasmid DNA was electrophoresed through 1% agarose. A) Purification of the 4522 bp DNA band of *Nhe*I and *Pme*I digested pY-NheI-mod. B) Purification of the 329 bp DNA band of *Nhe*I and *Pme*I digested pUC57-pYDN-Cassette. The dashed boxes show DNA band excision for purification.

The cloning sites *Nhe*I and *Eco*RI were used to introduce the protein to be displayed by fusion with the N-terminal of Aga2 (figure 3.7).

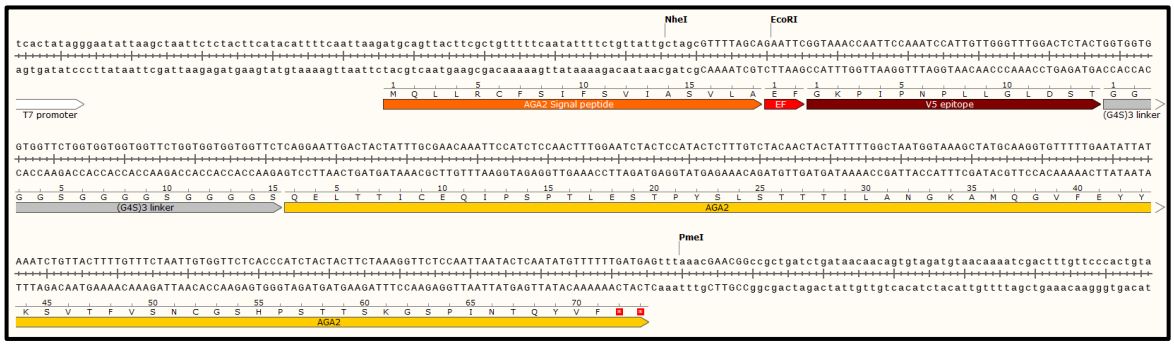

Figure 3.7 pYDN. The AGA2 fusion protein cassette with the cloning sites *Nhe*I and *Eco*RI is shown. Plasmid features and ORFs are coloured and denoted: the white feature represent the end of the T7 promoter, the orange ORF represents AGA2 signal peptide, the red ORF the restriction site *Eco*RI, the dark red ORF the V5 tag, the grey ORF the (G4S)3 linker, the yellow ORF AGA2 and the red squares the codon stop.

3.3 B7H4 Ig-like V-type 1 domain DNA cloning into pYDN to develop pY-B7H4

A synthetic gene cassette containing the codon optimised sequence of B7H4 Ig-like V-type 1 domain for *S. cerevisiae* was designed (obtained from GeneWiz) and named pB7H4-D1 (figure 3.8). It includes a fragment of the Aga2 signal peptide and also the amino acids alanine and glycine at the N-terminus of the B7H4 Ig-like V-type 1 domain (Phe29 to Gly148). These amino acids are required for optimal cleavage of the Aga2 signal peptide(474).

Figure 3.8 Synthetic DNA cassette used for the development of pY-B7H4. *Nhe*I and *Eco*RI restriction sequence highlighted in green.

DNA cassette for pY-B7H4 obtained from pB7H4-D1
GCT AGC GTT TTA GCA GCT GGT TTT GGT ATT TCT GGT AGA CAT TCT ATT ACT GTT ACT ACT GTT GCT TCT GCT GGT AAT ATT GGT GAA GAT GGT ATT TTG TCT TGT ACT TTT GAA CCA GAT ATT AAA TTG TCT GAT ATT GTT ATT CAA TGG TTG AAA GAA GGT GTT TTG GGT TTG GTT CAT GAA TTT AAA GAA GGT AAA GAT GAA TTG TCT GAA CAA GAT GAA ATG TTT AGA GGT AGA ACT GCT GTT TTT GCT GAT CAA GTT ATT GTT GGT AAT GCT TCT TTG AGA TTG AAA AAT GTT CAA TTG ACT GAT GCT GGT ACT TAT AAA TGT TAT ATT ATT ACT TCT AAA GGT AAA GGT AAT GCT AAT TTG GAA TAT AAA ACT GGT GAA TTC

The cassette was isolated from the vector by digestion with *Nhe*I and *Eco*RI (figure 3.9) and used for ligation with *Nhe*I and *Eco*RI digested pYDN to obtain the final plasmid pY-B7H4.

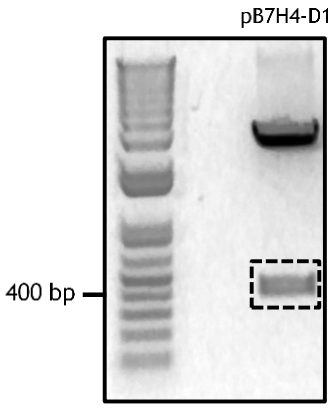

Figure 3.9 pY-B7H4 development. The digested plasmid DNA was electrophoresed through 1% agarose. *Nhe*I and *Eco*RI digested pB7H4-D1 and purification of the 387 bp DNA band for cloning into *Nhe*I and *Eco*RI digested pYDN, giving rise to pY-B7H4. The dashed box shows DNA band excision for purification.

After DNA ligation, *E. coli* transformation and plating onto LB agar plates containing ampicillin, three colonies were grown and used for colony PCR with the primers pYDN Check-F and pYDN Check-R. The PCR amplicons were purified and Sanger sequenced with the primers pYDN Check-F (GATC, Eurofins). All three sequencing reactions showed the correct sequence (figure 3.10), and one colony was used for subsequent plasmid production and experiments. pY-B7H4 was used for transformation of *S. cerevisiae* EBY100 and expression of the fusion protein (as depicted in figure 3.1.A).

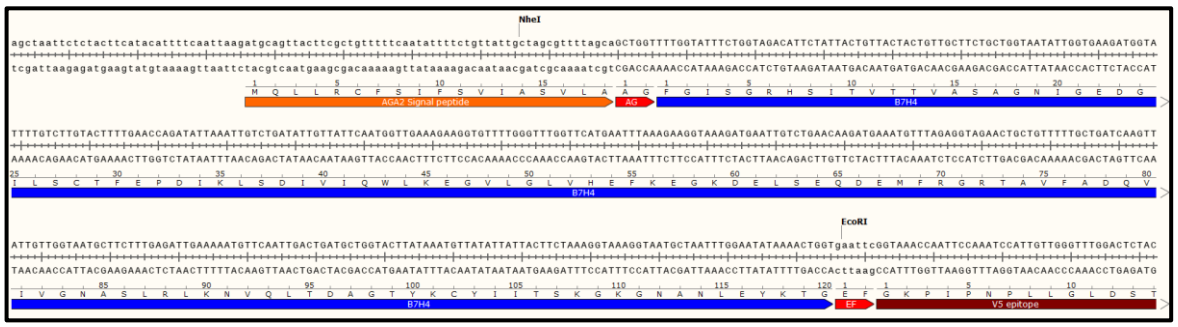

Figure 3.10 DNA sequence of pY-B7H4. B7H4 Ig-like V-type 1 domain fused with the N-terminal of Aga2. Plasmid features and ORFs are coloured and denoted: the orange ORF represents AGA2 signal peptide, the red ORF the amino acids AG and the restriction site *Eco*RI, the blue region the B7H4 Ig-like V-type 1 domain and the dark red ORF the V5 tag.

3.4 Cloning of LMP loops and development of pY-LMP1-lp2F, pY-LMP1-lp2Y, pY-LMP2-lp2 and pY-LMP2-lp5

Synthetic DNA codon optimised for *S. cerevisiae* expression of the extracellular LMP loops (table 3.2) were designed (cassette vectors obtained from GeneWiz) and termed plasmids pLMP1-lp2F, pLMP1-lp2Y, pLMP2-lp2 and pLMP2-lp5. The sequences were flanked by the restriction sites *Acc*65I and *Eco*RI for subsequent cloning into pYD1 (table 3.11).

Figure 3.11 DNA cassette for extracellular loops of the latent membrane proteins for cloning into pYD1. *Acc*65I and *Eco*RI restriction sequence highlighted in green.

DNA cassette for pY-LMP1-lp2F obtained from pLMP1-lp2F
GGT ACC ATG TAT TGC TTT GTG GAA TTT GCA TGG TCA AGC TTT GTT TTT GGG TTG TTA ATA AGT G GAA TTC
DNA cassette for pY-LMP1-lp2Y obtained from pLMP1-lp2Y
GGT ACC ATG TAT TGC TTT GTG GAA TTT GCA TGG TCA AGC TTT GTA TTT GGG TTG TTA ATA AGT G GAA TTC
DNA cassette for pY-LMP2-lp2 obtained from pLMP2-lp2
GGT ACC ATG TAC TTG GAG AAT TGA AGA TCC ACC ATT TAA TTC TTT GTT GTT TGC TTT GTT GTG TTA ATA AAA GCT TGT G GAA TTC
DNA cassette for pY-LMP2-lp5 obtained from pLMP2-lp5
GGT ACC ATG TTC TAT TTT GCA AAC TAA TTT TAA ATC TTT GTC TTC TAC TGA ATT TAT TCC ATG TTA ATA AAA GCT TGT G GAA TTC

The DNA cassettes were digested with *Acc*65I and *Eco*RI (figure 3.12) and used for ligation with *Acc*65I and *Eco*RI digested pYD1 to obtain the final plasmids LMP1-lp2F, LMP1-lp2Y, LMP2-lp2 and LMP2-lp5.

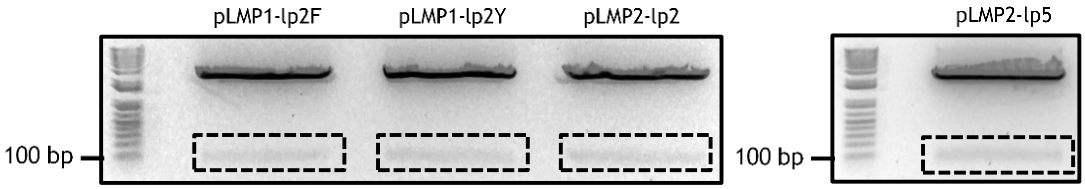

Figure 3.12 Development of pY-LMP1-lp2F, pY-LMP1-lp2Y, pY-LMP2-lp2 and pY-LMP2-lp5. The digested plasmid DNA was electrophoresed through 1% agarose. *Acc*65I and *Eco*RI digested LMPs loops for cloning into pYD1. The dashed boxes show DNA band excision for purification.

After DNA ligation, *E. coli* transformation and plating onto LB agar plates containing ampicillin, three colonies were grown and used for colony PCR with the primers pYD1 Check-F and pYD1 Check-R. The PCR amplicons were purified and Sanger sequenced with the primer pYD1 Check-F (GATC, Eurofins). All three sequencing reactions for each plasmid showed the correct sequence (figure 3.13), and one colony of each was used for DNA plasmid production and subsequent experiments.

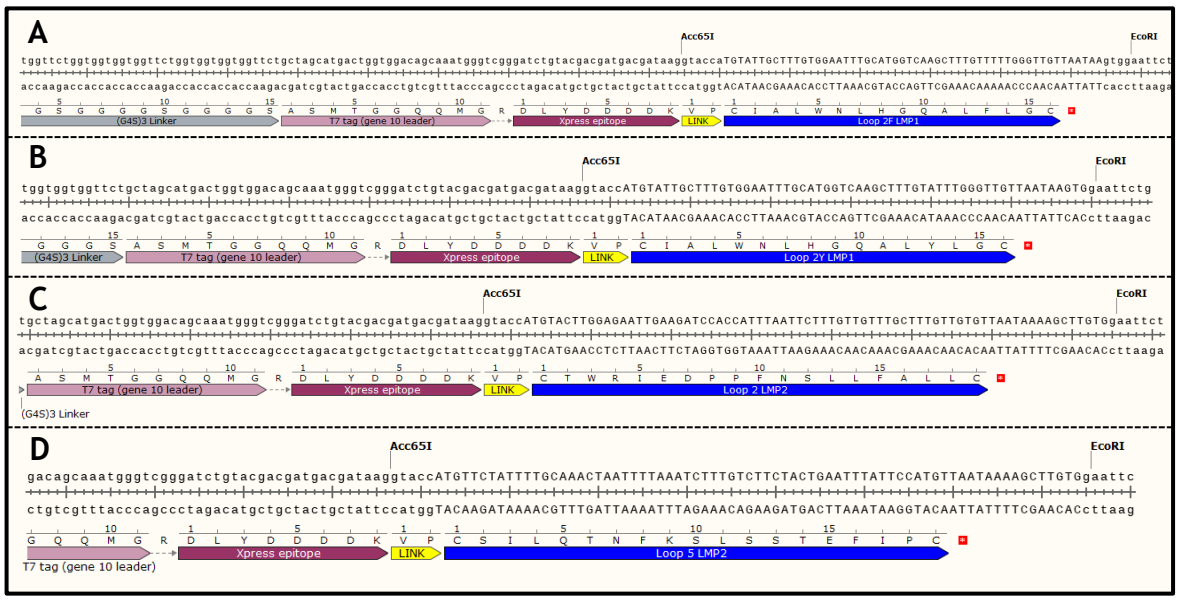

Figure 3.13 DNA sequence of pY-LMP1-lp2F, pY-LMP1-lp2Y, pY-LMP2-lp2 and pY-LMP2-lp5. A) pY-LMP1-lp2F with LMP1 loop 2F fused with the C-terminal of Aga2. B) pY-LMP1-lp2Y with LMP1 loop 2Y fused with the C-terminal of Aga2 C) pY-LMP2-lp2 with LMP2 loop 2 fused with the C-terminal of Aga2 D) pY-LMP2-lp5 with LMP2 loop 5 fused with the C-terminal of Aga2. Plasmid features and ORFs are coloured and denoted: the grey ORFs (G4S)3 linker, the pink ORFs the T7 tag, the dark red ORFs Xpress tag, the yellow ORFs the amino acids VP, the blue ORFs the LMP loops and red squares the codon stop.

pY-LMP1-lp2F, pY-LMP1-lp2Y, pY-LMP2-lp2 and pY-LMP2-lp5 were used for transformation of *S. cerevisiae* EBY100 and expression of the fusion protein (as depicted in figure 3.1.B).

3.5 Yeast clone transformation, selection and expression of the fusion proteins

To obtain single yeast clones for yeast display of B7H4 and the LMP loops, *S. cerevisiae* EBY100 cultures were separately transformed with pY-B7H4, pY-LMP1-lp2F, pY-LMP1-lp2Y, pY-LMP2-lp2 and pY-LMP2-lp5 using the lithium acetate/single-stranded carrier DNA/polyethylene glycol method(488) and selected in SD-CAA agar. EBY100 is a Trp- strain and pYD1 derived vectors have the selectable marker TRP1 for tryptophan biosynthesis. EBY100 transformed with these plasmids can grow in the SD-CAA is a selection media. Single colonies for each plasmid were then grown in SD-CAA broth and the yeast DNA isolated by treatment with lysate buffer containing lyticase. The lysate was used to perform a PCR with the primers pYDN Check-F and pYDN Check-R, in the case of yeast transformed with pY-B7H4, or pYD1 Check-F and pYD1 Check-R, in the cases of yeast transformed with pY-LMP1-lp2F, pY-LMP1-lp2Y, pY-LMP2-lp2 or pY-LMP2-lp5. The PCR amplicons were purified and Sanger sequenced with the primers pYDN Check-F and pYD1 Check-F (GATC, Eurofins). All sequencing reactions showed the presence of the correct sequence (as depicted in figures 3.8 and 3.11).

In order to express the fusion proteins, the yeast cultures were induced using SG-CAA broth, with the same formulation of SD-CAA but the carbon source is galactose instead of dextrose. Therefore, SG-CAA can induce the GAL promoters of the genomic AGA1 and the AGA2-fusion genes. During the induction, Aga1 forms a heterodimer with the Aga2 fusion protein in the yeast wall. pYDN and pYD1 based expression of the Aga2 fusion protein can be assessed using antibodies specific for the amino acid tag present into the fusion protein: V5 tag in the case of pYDN and Xpress tag in the case of pYD1 (as depicted in figure 3.1). The expression of the B7H4 fusion protein was assessed by flow cytometry with the antibody mouse anti-V5 Tag FITC conjugated, which recognises the V5 tag present within the Aga2 fusion protein of pYDN and pY-B7H4 (as depicted in figure 3.1.A). Expression of the LMP loops was assessed using a combination of mouse anti-Xpress and goat anti-mouse IgG Alexa488 conjugated, which recognises the Xpress tag present in the Aga2 fusion protein of pYD1, pY-LMP1-lp2F, pY-LMP1-lp2Y, pY-LMP2-lp2 and pY-LMP2-lp5 (as depicted in figure 3.1.B). Yeast were stained and analysed. In each case, the percentage of yeast showing positive surface expression of the fusion Aga2 fusion protein was at least 76% (figure 3.14).

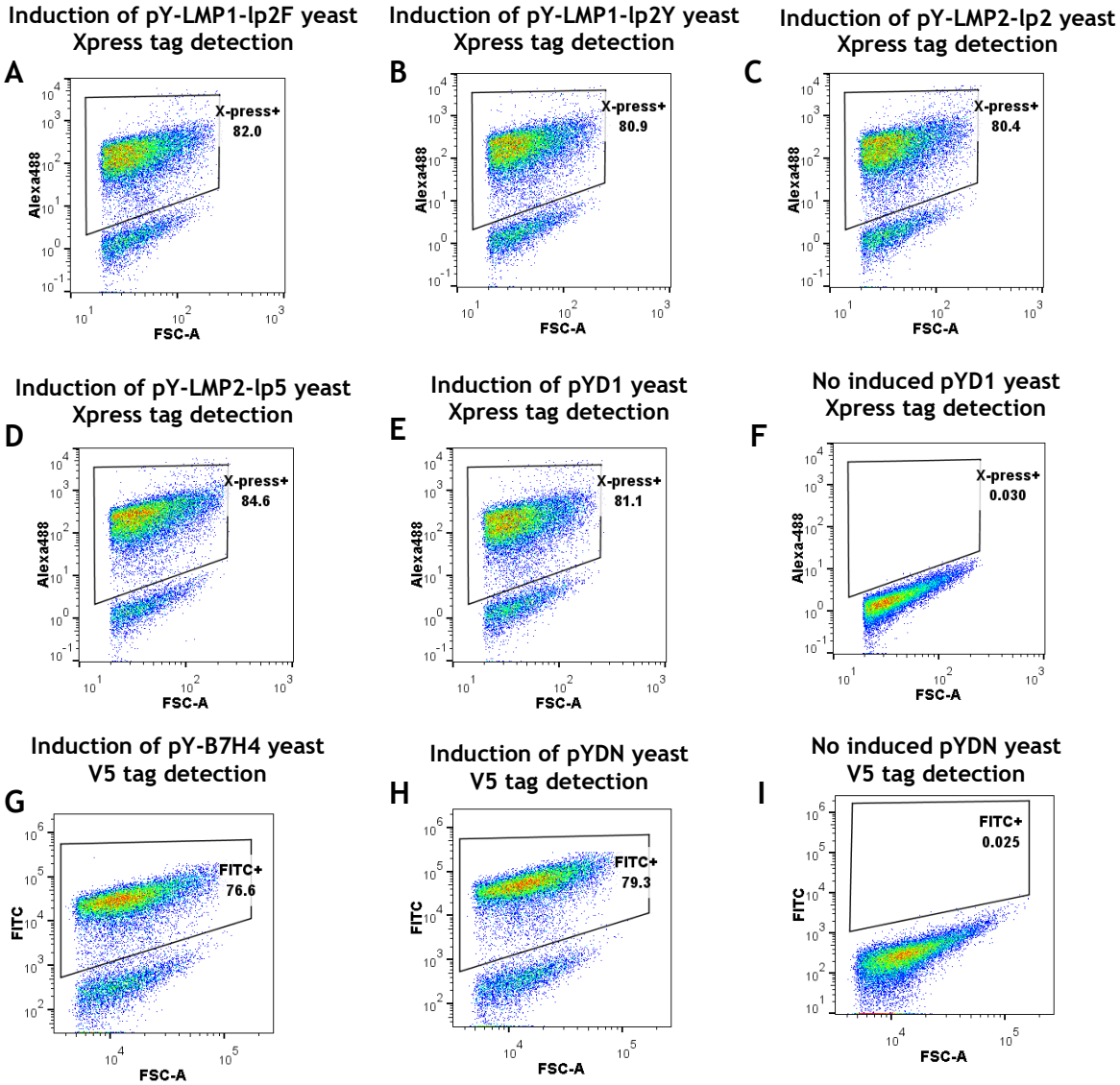

Figure 3.14 Aga2 fusion protein expression. Flow cytometry dot plots of Aga2 fusion protein expression. Aga2 fusion protein was detected with mouse anti-Xpress plus anti-mouse Alexa 488 in A to F and with mouse anti-V5 FITC in G to I. A) Induced yeast transformed with pY-LMP1-lp2F. B) Induced yeast transformed with pY-LMP1-lp2Y. C) Induced yeast transformed with pY-LMP2-lp2. D) Induced yeast transformed with pY-LMP2-lp5. E) Induced yeast transformed with pYD1. F) No induced yeast transformed with pYD1. G) Induced yeast transformed with pY-B7H4. H) Induced yeast transformed with pYDN. I) No induced yeast transformed with pYDN.

3.6 Conclusion

Yeast displaying the antigens on the surface were obtained successfully, including control yeast displaying Aga2 fused with the described tags, but without the additional fused antigens. Previous use of pYD5 was restricted to scFv N-terminal expression. In this chapter, it has been proved efficient Aga2 N-terminal display of antigens using pYDN (similar to pYD5).

4. Results: Phage display selection using a non-immune library and yeast expressing antigens

4.1 Introduction

A phage display library with a diversity of 10^{10} human scFvs was used for screening using yeast displaying the antigens described in chapter 3. The phage scFv library comprises VH and κVL (kappa variable light chain) sequences linked by a 20 amino acid peptide (VH-linker-κVL) cloned into the *Sfi*I restriction sites of the phagemid vector pRXB-100, which carries an ampicillin-resistant gene. A *lacZ* promoter controls the expression of the fusion protein scFv-PIII. The amino acid sequence of the linker between VH and κVL is GSSGSSSGTSSGGSSSSGSG. The non-immune phagemid library was made from human B-cells obtained from non-immunised donors (figure 1.15). The library was transfected into *E. coli* XL1-Blue, which contains the F pilus, required for phage infection, on a tetracycline-selectable episome.

To produce the phage, the phagemid system requires the coinfection with helper phage. The M13KO7 helper phage was used for library production. When M13KO7 infects the *E. coli* XL1-Blue carrying the phagemid vector, it delivers a helper phage vector coding for the proteins necessary to produce functional phage and a kanamycin resistance gene. *E. coli* XL1-Blue carrying the phagemid vector and infected with M13KO7 able to produce the phage display library when they are growing in broth with tetracycline, ampicillin and kanamycin.

First, to remove non-specific clones that might bind to yeast but not the desired antigens, the phage display library was panned against yeast expressing the display system but not the antigen. This process was denoted library depletion. Then, for selection of the scFvs able to bind to the antigen, the depleted library was selected against the yeast expressing the display system with the antigen fused with Aga2. The recovered phage were used to infect bacteria with objective of expanding them before being used in the next round. Several rounds of depletion and selection were performed as described below.

4.2 Cleavage of the displayed protein from the yeast surface with trypsin

After the incubation in the selection step, the phage that have interacted with the yeast need to be eluted from the yeast surface for subsequent *E. coli* XL1-Blue infection and phagemid propagation. The infected *E. coli* are then used to produce the phage for the next round. The elution was conducted by treatment with trypsin, cleaving the antigen from the surface of the yeast.

To determine the optimal concentration of trypsin and time of digestion to digest 100% of the Aga2 fusion protein displayed, a flow cytometry analysis was performed. First, the trypsin treatment was performed with pY-LMP1-lp2F induced yeast. The yeast were incubated in a solution with 0.02 mM trypsin for 15 minutes at room temperature with rotation. After the incubation, FBS was added to stop the trypsinisation, and the yeast were washed twice with PBS. Then, the yeast were stained with mouse anti-Xpress and goat anti-mouse IgG Alexa488 conjugated to detect the Xpress tag present in the Aga2 fusion protein. 81.8% of induced pY-LMP1-lp2F yeast expressed Aga2 fusion protein, after 15 minutes of trypsinisation, just 0.21% maintain the presence of induced Aga2 fusion protein in the yeast wall (figure 4.1). This result indicates that this protocol is an effective method of eluting the phage interacting with the Aga2 fusion protein. However, to avoid the negative effect of trypsinisation in phage infectivity, the incubation should not last more than 20 minutes (489).

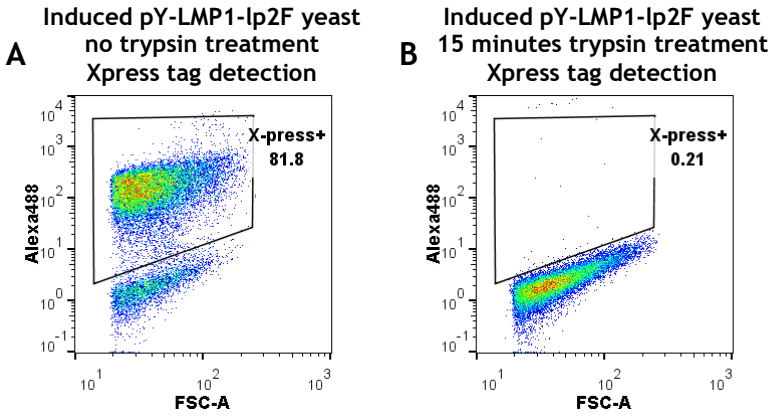

Figure 4.1 Flow cytometry dot plot of trypsin digested pY-LMP1-lp2F induced yeast. A) Control induced yeast without trypsinisation and stained with mouse anti-Xpress and goat anti-mouse Alexa488. B) Trypsinised induced yeast stained with mouse anti-Xpress and goat anti-mouse Alexa488.

4.3 Phage production for phage display selection

The library was produced from a commercially supplied bacteria glycerol stock of *E. coli* XL1-Blue transfected with the phagemid library. Ten times the diversity (10^{11} bacteria) was grown, infected with the M13KO7 helper phage and incubated overnight for phage production. The phage were then isolated from the culture supernatant and the complete library was used for the first round of selection. The subsequent rounds of selection were performed with the phage output obtained from the previous round using a convenient number of phage for each. For each round, the number and the % of phage recovered were calculated and increase in the phage recovery at the end of the selection indicating that the selection process was working.

4.3.1 Phage display selection using B7H4 Ig-like V-type 1 domain expressing yeast

Two different samples of induced yeast were prepared for each round of selection: pYDN expressing yeast and pY-B7H4 yeast. Each round of selection consisted of two steps, depletion and selection (Figure 4.2).

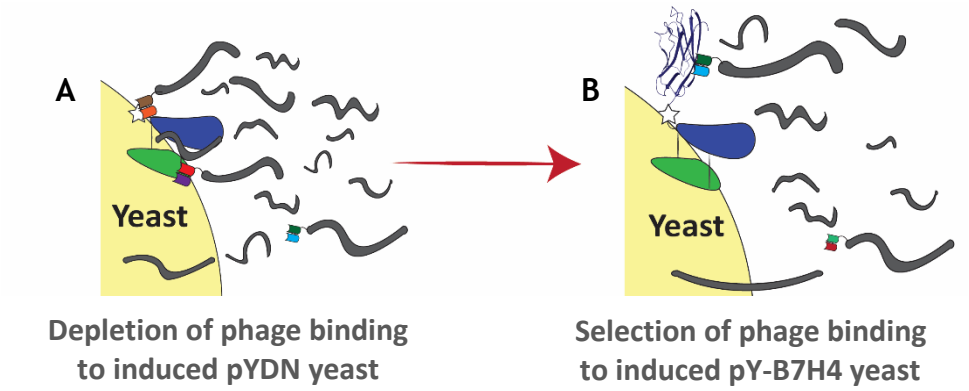

Figure 4.2 Depletion and selection steps during the phage selection with induced pY-B7H4 yeast. A) Phage depletion using induced pYDN yeast. B) Phage selection using induced pY-B7H4 yeast.

During the depletion, the phage were incubated with the pYDN yeast, the yeast removed and the supernatant collected for the selection round. For the selection, the supernatant was mixed with the blocked pY-B7H4 yeast. The unbound phage were removed and the yeast collected for the eight washing steps. Then, the elution step was performed with trypsin as described above. The yeast were

removed and the eluted phage used for infection of *E. coli* XL1-Blue. For each round, the recovered phage were used to infect bacteria. The resulting culture was titrated, and the serial dilution plated in LB agar plus the correspondent antibiotics. The value of CFU obtained after infection (designated as output) was used to calculate the % of phage recovered based in the phage input used for each round of selection (table 4.1). A sharp increase in phage recovery was observed in Round 4 (figure 4.3), suggesting enrichment in phage interacting with B7H4 Ig-like V-type 1 domain.

Table 4.1 Phage selection using induced pY-B7H4 yeast as a source of antigen.

Phage display selection using B7H4 Ig-like V-type 1 domain expressing yeast			
Round (R)	Phage input	Output (CFU)	Recovery (%)
Phage R1 B7H4	$5x10^{12}$	$3.9x10^{7}$	0.00078
Phage R2 B7H4	10^{12}	$1.32x10^{5}$	0.0000132
Phage R3 B7H4	10^{12}	$9x10^{5}$	0.00009
Phage R4 B7H4	$5x10^{10}$	$8.4x10^{6}$	0.0168

*The selection outputs have been named using the following format: Platform (Phage or Yeast) RX (round number) Antigen (B7H4 or LMP loops).

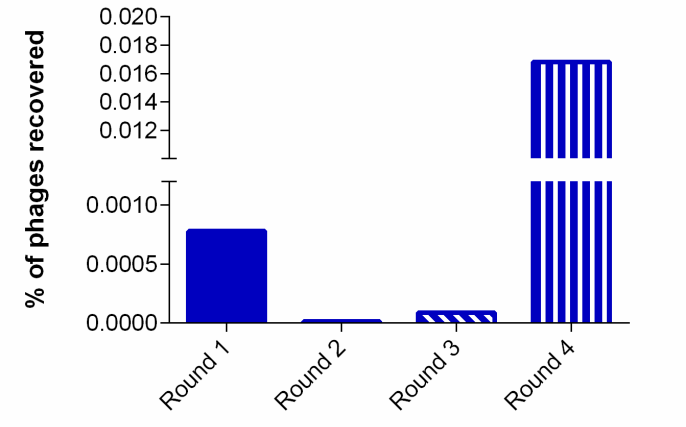

Figure 4.3 Percetange of phage recovery from the four rounds of phage selection using induced pY-B7H4 yeast as source of antigen.

4.3.2 Phage display selection using LMP1 loop 2F, LMP1 loop 2Y, LMP2A loop 2 or LMP2A loop 5 expressing yeast

As for B7H4, each round of selection consisted of two steps, depletion and selection (figure 4.4).

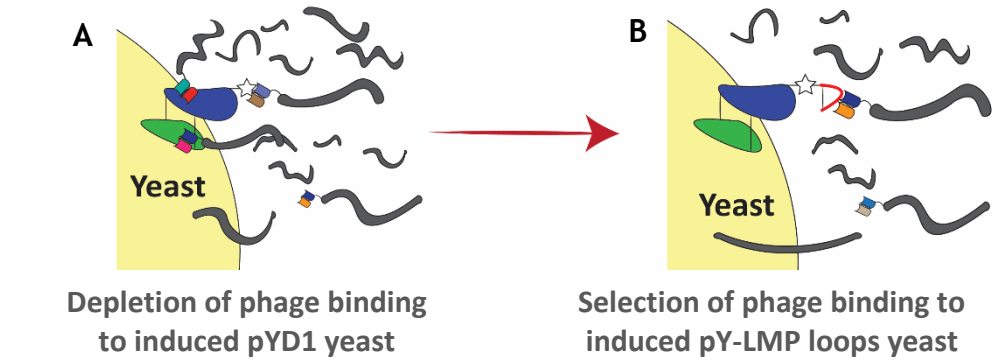

Figure 4.4 Depletion and selection steps during the phage selection with induced yeast expressing the extracellular loops of LMP1 and LMP2A. A) Phage depletion using induced pYD1 yeast. B) Phage selection using induced pY-LMP1-lp2F, pY-LMP1-lp2Y, pY-LMP2-lp2 or pY-LMP2-lp5 yeast.

4.3.2.1 Phage display selection for LMP1 loop 2F

As with B7H4, pYD1 yeast were used as the control for the LMP1 loop 2F selection (table 4.2). A sharp increase in phage recovery was observed in Round 4 (figure 4.5), suggesting enrichment in phage interacting with LMP1 loop 2F.

Table 4.2 Phage selection using induced pY-LMP1-lp2F yeast as a source of antigen.

Phage display selection using LMP1 loop 2F expressing yeast			
Round (R)	Phage input	Output (CFU)	Recovery (%)
Phage R1 LMP1-l2F	10^{12}	$3.9x10^{5}$	0.000039
Phage R2 LMP1-l2F	10^{12}	$9x10^{5}$	0.00009
Phage R3 LMP1-l2F	$5x10^{10}$	$2x10^{5}$	0.0004
Phage R4 LMP1-l2F	$5x10^{10}$	$6x10^{7}$	0.12

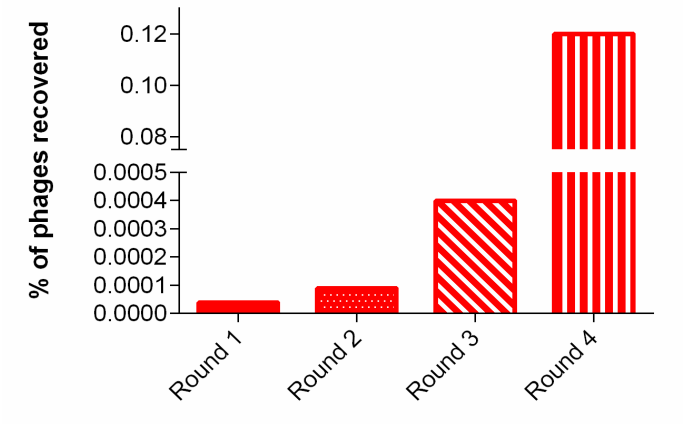

Figure 4.5 Percetange of phage recovery during the different rounds of phage selection using induced pY-LMP1-lp2F yeast as source of antigen.

4.3.2.2 Phage display selection for LMP1 loop 2Y

The same process was used for the LMP1 loop 2Y selection (table 4.3). A sharp increase in phage recovery was observed in Round 3 (figure 4.6), suggesting enrichment in phage interacting with LMP1 loop 2Y.

Table 4.3 Phage selection using induced pY-LMP1-lp2Y yeast as a source of antigen.

Phage display selection using LMP1 loop 2Y expressing yeast			
Round (R)	Phage input	Output (CFU)	Recovery (%)
Phage R1 LMP1-l2Y	10^{12}	$3.6x10^{4}$	0.0000036
Phage R2 LMP1-l2Y	10^{12}	$6x10^{4}$	0.000006
Phage R3 LMP1-l2Y	$5x10^{10}$	$6x10^{7}$	0.12

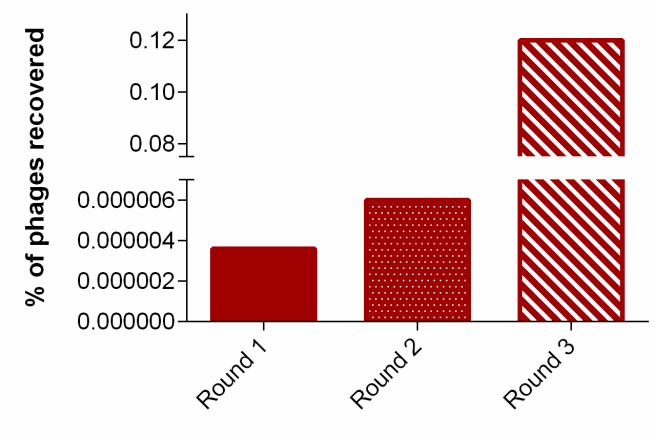

Figure 4.6 Percetange of phage recovery during the different rounds of phage selection using induced pY-LMP1-lp2Y yeast as source of antigen.

4.3.2.3 Phage display selection for LMP2 loop 2

The same process was used for the LMP2 loop 2 selection (table 4.4). A sharp increase in phage recovery was observed in Round 3 (figure 4.7), suggesting enrichment in phage interacting with LMP2 loop 2.

Table 4.4 Phage selection using induced pY-LMP2-lp2 yeast as a source of antigen.

Phage display selection using LMP2A loop 2 expressing yeast			
Round (R)	Phage input	Output (CFU)	Recovery (%)
Phage R1 LMP2-l2	10^{12}	$2x10^{5}$	0.00002
Phage R2 LMP2-l2	10^{12}	$5.1x10^{4}$	0.0000051
Phage R3 LMP2-l2	$5x10^{10}$	$1.3x10^{6}$	0.0026

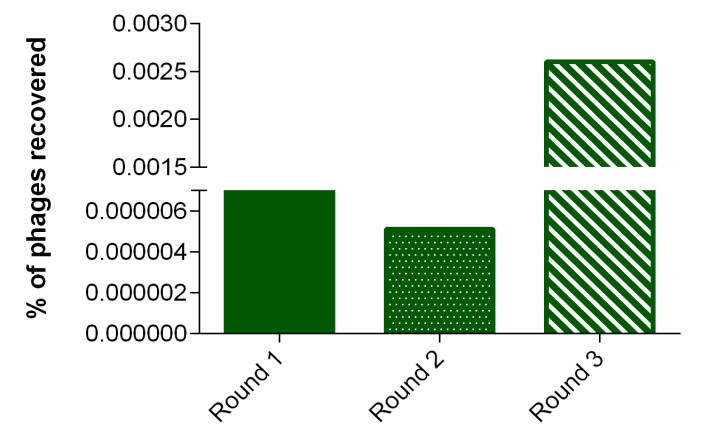

Figure 4.7 Percetange of phage recovery during the different rounds of phage selection using induced pY-LMP2-lp2 yeast as source of antigen.

4.3.2.4 Phage display selection for LMP2 loop 5

The same process was used for the LMP2A loop 5 selection (table 4.5). An increase in phage recovery was observed in Round 4 (figure 4.8), suggesting enrichment in phage interacting with LMP2 loop 5.

Table 4.5 Phage selection using induced pY-LMP2-lp5 yeast as a source of antigen.

Phage display selection using LMP2A loop 5 expressing yeast			
Round (R)	Phage input	Output (CFU)	Recovery (%)
Phage R1 LMP2-l5	10^{12}	$1.7x10^{5}$	0.000017
Phage R2 LMP2-l5	10^{12}	$1.74x10^{6}$	0.000174
Phage R3 LMP2-l5	10^{12}	$6x10^{6}$	0.0006
Phage R4 LMP2-l5	$5x10^{10}$	$1.26x10^{6}$	0.00252

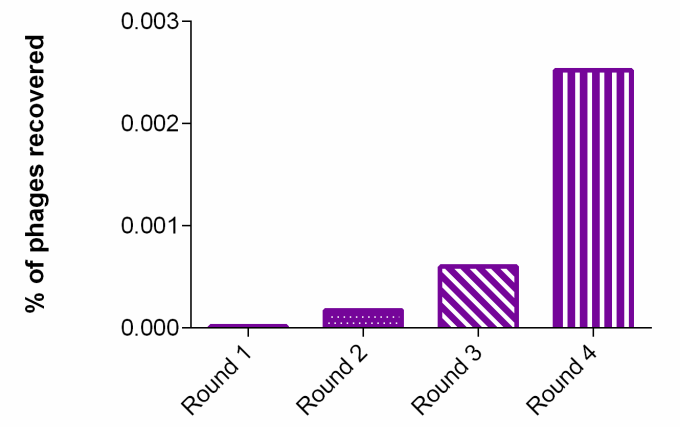

Figure 4.8 Percetange of phage recovery during the different rounds of phage selection using induced pY-LMP2-lp5 yeast as source of antigen.

4.4 Conclusion

All the phage selections performed showed a substantial increase in the phage recovery in the third or fourth round. This suggested that the selection from the library was working and that the output of each selection could be assessed further. The following format have been stablished to name the selection outputs obtained during this research: Platform (Phage or Yeast) RX (round number) Antigen (B7H4 or LMP loops).

5. Results: Transfer of selected scFvs to the yeast display system

5.1 Introduction

The selection in the phage display system is biased towards scFvs with better expression in a prokaryotic system and with more stable fusion with the protein PIII. Therefore, the promotion of very few clones can mask the full diversity of the binders in the library. The expression of scFvs in a eukaryotic system would allow us to overcome this bias of the phage display platform. It provides outputs in an organism with protein posttranslational modifications closer to the mammals. Furthermore, the yeast mimics the final display of the scFvs in a CAR T-cell, acting by avidity with the target and making it possible to select the scFv clones by interaction with the antigen expressed on the surface of mammalian cells (figure 5.1). For these reasons, to continue selecting scFvs, the sequence from the penultimate round (rather than the final round) of each phage selection (described in chapter 4) was transferred to the vector pYDN for expression on the yeast surface at the N-terminus of Aga2.

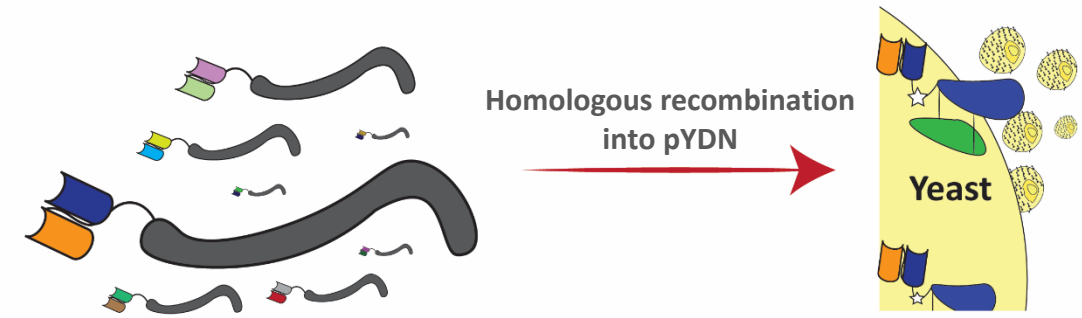

Figure 5.1 Transfer of phage display selected scFv sequences to N-terminal yeast display system by homologous recombination into the vector pYDN. scFvs are represented by coloured tags on the end of the filamentous phage (shown to the left) which are then transferred to the surface of the yeast fused to N-terminus of Aga2 (blue) which associates with Aga1 (green).

To do this, the scFv sequences from the phage selection outputs were amplified with primers with tags that introduced (at the ends of the selected scFv sequences) 40 nt of complementarity with the vector pYDN to allow homologous recombination into the pYDN vector in *S. cerevisiae* EBY100.

5.2 Output amplification and homologous recombination into pYDN

The homologous recombination pathway is activated in eukaryotes for error-free repair of double-stranded DNA when single or double-strand breaks occur (490). We can take advantage of homologous recombination to introduce inserts into yeast plasmids without using restriction endonucleases. Therefore, we can create libraries in yeast with highly diverse inserts, where the presence of endonuclease restriction sites in the inserts is probable and thus the use of these enzymes for cloning would affect diversity. For efficient homologous recombination of inserts into a yeast plasmid, at least 40 bp of homology are required between the insert and the linearised yeast plasmid (491).

5.2.1 Output amplification by homologous recombination PCR

With the aim of transferring the scFvs selected by phage display to an N-terminal yeast display system (figure 5.1), two sequential PCRs were required to obtain the DNA to be inserted by homologous recombination into pYDN. The phagemid vector DNA, pRXB-100 with scFvs, from the penultimate round of each phage selection was purified by midi-prep to be used as the template for the first PCR with the primers HR-F and HR-R (figure 5.2 and 5.3).

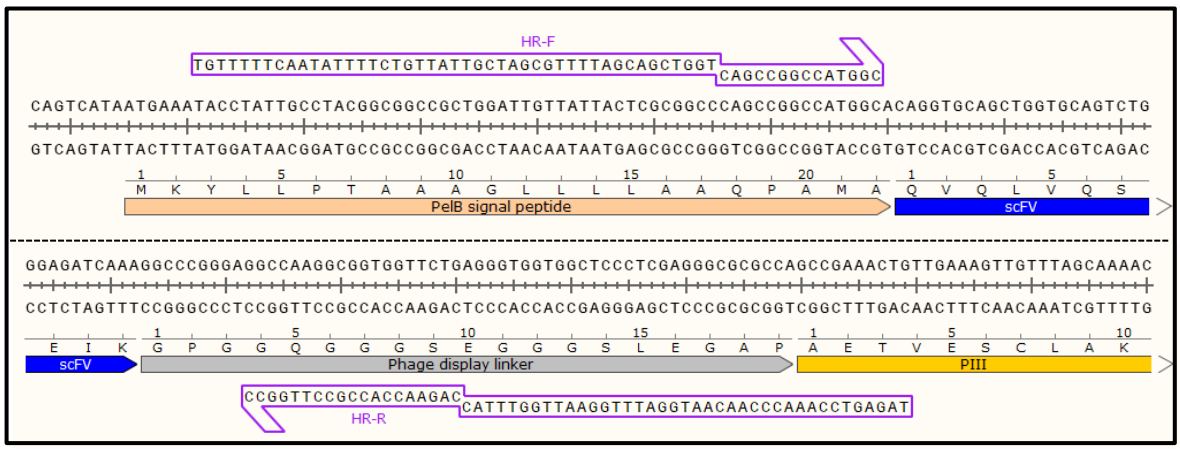

Figure 5.2 First homologous recombination PCR. The primers HR-F and HR-R, complementary to pRXB-100, were used to amplify the scFvs selected during phage display experiments. Plasmid ORFs are coloured and denoted: the light orange ORF represents the PelB signal peptide, blue ORF the scFv, grey ORF the linker between the scFv and the PIII, yellow ORF the PIII phage protein. Primers used for HR PCR are indicated. The middle dashed line represents the diagrammatic discontinuity between the 5' end (shown above) and the 3' end (shown below) of the fragment. The full fragment size is expected to be approximately 850 bp.

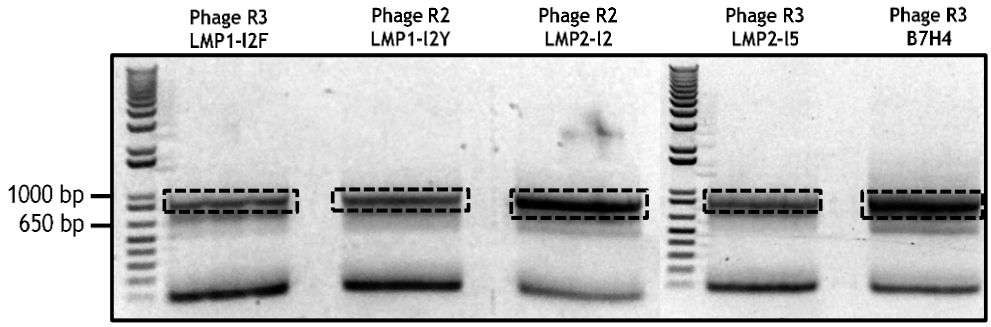

Figure 5.3 First homologous recombination PCRs with the primers HR-F and HR-R. PCR products were electrophoresed through 1% agarose. The dashed boxes show DNA band excision for purification of the ≈850 bp DNA fragments. Note: primer-dimers can be seen at the bottom of each track.

Part of HR-F is complementary to a sequence coding for the signal peptide used for the expression of scFv-PIII in pRXB-100. This complementary region introduces the extra amino acid sequence QPAMA at the N-terminus of the scFv. Furthermore, nucleotides coding for the amino acid AG were introduced at the N-terminus of QPAMA for improved digestion of the Aga2 signal peptide when recombined in pYDN and expressed in yeast (474). Therefore, the extra amino acid sequence at the N-terminus when expressed in yeast is AGQPAMA. HR-R is complementary to a nucleotide sequence of the linker between the scFv and PIII. The sequence codes for the amino acids GPGGQGGGS. It was postulated that these extra amino acids would have no, or little, impact on the binding of the selected scFvs to their targets (figure 5.2).

The second PCR (figure 5.4) was performed using as template the purified DNA band (around 850 bp) obtained from the first recombination PCR (figure 5.3) and the primers HR amp-F and HR amp-R (figure 5.5). The main objective of this PCR was to amplify the quantity of DNA and reduce primer dimers by suing smaller primers. The product obtained from the second PCR was purified and used for yeast transformation together with *Eco*RI digested pYDN. The final homologous recombination product in pYDN is shown in figure 5.5.

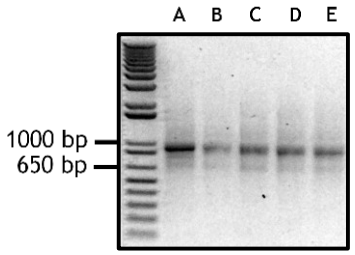

Figure 5.4 Second homologous recombination PCRs with the primers HR amp-F and HR amp-R primers. PCR products were electrophoresed through 1% agarose. A) Phage R3 LMP1-I2F. B) Phage R2 LMP1-I2Y. C) Phage R2 LMP2-I2. D) Phage R3 LMP2-I5. E) Phage R3 B7H4. Note: the absence of primer dimers in this amplification.

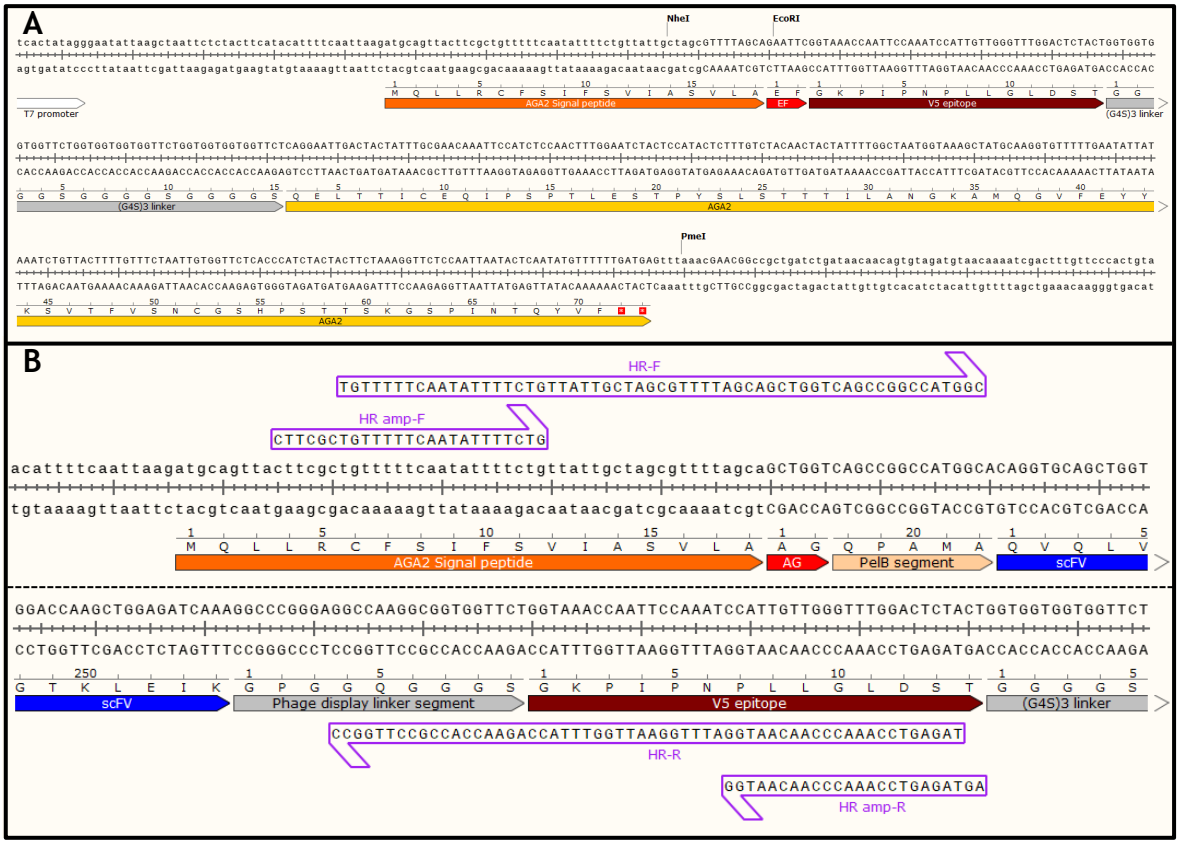

Figure 5.5 Recombination of scFv into pYDN. A) pYDN vector. pYDN was linearised by digestion with *Eco*RI to be used for homologous recombination. B) Homologous recombined scFv into pYDN. Primers used for first and second homologous recombination PCRs complementary to the recombined fragment are shown. Plasmid ORFs are coloured and denoted: the orange ORF represents the AGA2 signal peptide, red ORF the linking amino acids AG, light orange ORF the segment of the PelB signal peptide complementary to the primer HR-F, blue ORF the scFv, grey ORFs the fragment of phage display linker complementary to the primer HR-R and the linker with the AGA2 protein and dark red ORF the V5 epitope. Primers used for HR PCR and HR amp PCR indicated. The middle dashed line represent the diagrammatic discontinuity between the 5' end (shown above) and the 3' end (shown below) of the fragment.

5.2.2 Yeast transformation, homologous recombination and scFv expression

5.2.2.1 Yeast transformation, homologous recombination and selection

Samples of *S. cerevisiae* EBY100 were transformed with *Eco*RI digested pYDN, cleaving between the Aga2 ORF and the V5 epitope (figure 5.5.A), and the purified PCR product following the lithium acetate/single-stranded carrier DNA/polyethylene glycol method (488). Within the yeast cell, the inserts recombine into the plasmid via the host error-free repair of double-strand breaks system (ie through homologous recombination) (490) to generated a recombinant circularised plasmid. After the transformation, the yeast were selected in SD-CAA broth, selection for circularised pYDN as with any linearised fragment (unlike the yeast chromosomes with telomers at the end), the linearised pYDN cannot be stably maintained. Several transformations were performed to obtain a satisfactory number of CFU (table 5.1). Glycerol stocks were generated with each yeast output.

Table 5.1 Number of colony forming units (CFU) and % of homologous recombination (HR).

Output*	CFU	% of HR
Yeast *EcoR*I digested pYDN without insert	$6x10^4$	-
Yeast R3 B7H4	$1.83x10^6$	96.78%
Yeast R3 LMP1-l2F	$2.1x10^6$	97.17%
Yeast R2 LMP1-l2Y	$1.17x10^6$	94.88%
Yeast R2 LMP2-l2	$1.77x10^6$	96.62%
Yeast R3 LMP2-l5	$1.41x10^6$	95.75%

*R=Round

$6x10^4$ CFU were obtained in Yeast *Eco*RI digested pYDN without insert. This could be due to remaining undigested plasmid or to plasmid recirculation by cell DNA repair mechanism. Even so, the percentage of homologous recombination obtained in each output was satisfactory.

5.2.2.2 Yeast display of scFv fusions

The yeast from the different outputs were grown and the scFv fusions induced to explore the expression of the fusion proteins scFv-Aga2 by flow cytometry, using the antibody anti-V5 Tag FITC-conjugated, which bind to the V5 tag present in the

fusion protein expressed by pYDN (figure 5.6). Roughly 2x10^4 yeast were analysed (figure 5.7).

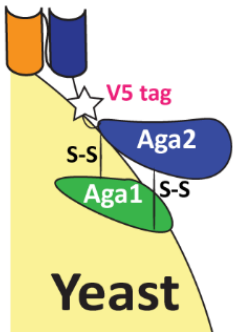

Figure 5.6 Yeast display of scFv obtained from the phage section and recombined into pYDN. pYDN N-terminal display of scFv (orange and blue tags) by fusion with the heterodimer Aga1-Aga2. The white star represent the V5 tag used to detect expression by flow cytometry with the antibody anti-V5 Tag FITC-conjugated.

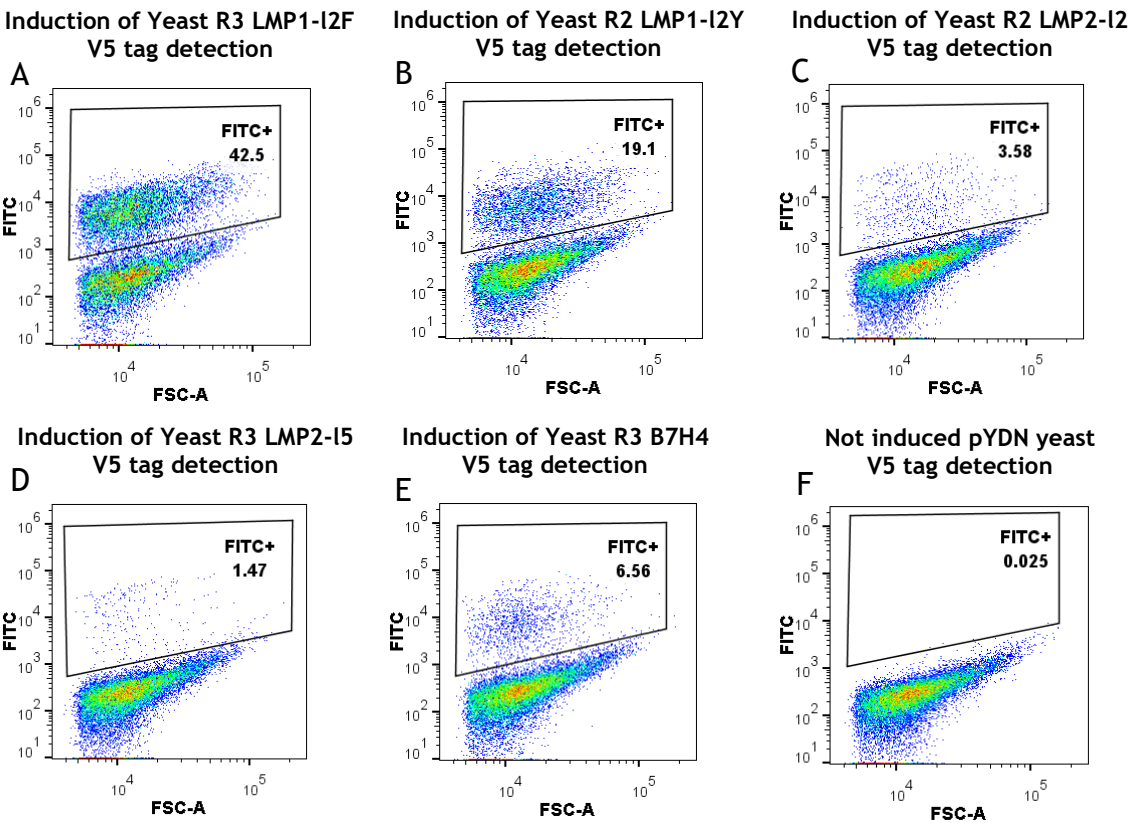

Figure 5.7 scFv-Aga2 expression. Flow cytometry dot plots of scFv-Aga2 protein expression. Aga2 fusion protein was detected with mouse anti V5 FITC. A) Induced yeast expressing the scFvs selected after Phage R3 LMP1-I2F. B) Induced yeast expressing the scFv selected after Phage R2 LMP1-I2Y. C) Induced yeast expressing the scFvs selected after Phage R2 LMP2-I2. D) Induced yeast expressing the scFvs selected after Phage R3 LMP2-I5. E) Induced yeast expressing the scFvs selected after Phage R3 B7H4. F) No induced pYDN yeast. The % positive cells (as shown in the gated section) is indicated in each case. Induced pYDN yeast can be found in figure 3.10.H with 79.3% of positive cells.

It might be anticipated that 100% of the transformed yeast would express the Aga2 fusion protein, expressed from the recombinant pYDN. However, the level of display of each output varied, with as low as 1.47% in one case. This could be due, in part, to linear pYDN that were closed/repaired aberrantly in the yeast without an insert. Alternatively, the presence in the outputs of scFv sequences with codon stops in the ORF could lead to the disrupted expression of the Aga2 fusion protein when they are transferred to the yeast display system. The promotion of these sequences during the phage selection is due to the presence of polyphages. This effect would have a different impact on each selection depending on the target protein, which explains the variability in the percentage of displayed Aga2 fusion protein for each analysed output.

To investigate this possibility, ten PCRs from each output were performed with the primers pYDN Check-F and pYDN Check-R from single colony yeast lysates and Sanger sequenced with the primer pYDN Check-F. For Yeast R2 LMP2-l2, Yeast R3 LMP2-l5 and Yeast R3 B7H4, all the sequence colonies had codon stops on the scFv ORF (figure 5.8).

Figure 5.8 DNA and amino acid sequence of a non-ORF scFv found during yeast colony screening. The DNA and amino acid sequence of the linker has been highlighted in grey. The codon stop has been coloured in red.

Example of a non-ORF scFv
CAG GTG CAG CTG GTG CAG GGA GCG CAG GCA GAG CGG AGG AGA GCT CCC CAA ACC CAA ATG CGT GGG TCA CAC GGC CAG TCC TTC CCC GGA GCT CAG CGT GGA CAG AGG GAA GGG ACC TCA GGC AGA GAC ACC TGC CCC ACG CCC TCA CCA GGT GCC CTT GGC CCA AGA AGA CAG GAC AAC AGG GTC CTC CCG CCC AGG GTC CTC CAC CCA AAA CTC CTG CCC CAG TCT GAG GAA ACA CCA GCC CGA CTA CTC CAG GGC ATC CAC ACC ACC CGA CCA GCC CCA AGG TCG GCA GCA GCG GCA GCA GCA GCG GTA CCA GCA GCG GCG GCA GCA GCA GCA GCG GCA GCG GCG AGC TCA CAC TCA CGC AGT CTC CAG GCA CCC TGT CTT TGT CTC CAG GGG AAA GAG CCA CCC TCT CCT GCA GGG CCA GTC AGA GTG TCA GCA GCA ACT ACT TAG CCT GGT ACC AGC AGA CAC CTG GCC AGG CTC CCA GGC TCC TCA TTT ATG GTG CGT CCA GTA GGG CCA CTG GTG TCC CAG ACA GGT TCG GTG GCA GTG GGT CTG GGA CAG ACT TCA CTC TCA CCA TCA ACA GAC TGG AGC CGG AAG ATT CTG CAG TGT ATT ACT GTC AGC ACT ATG GTA GTT ATT CGT GGA CGT TCG GCC AAG GGA CCA AGC TGG AGA TCA AAG

QVQLVQGAQAERRRAPQTQMRGSHGQSFPGAQRGQREGTSGRDTCPTPSPGALGPRRQD NRVLPPRVLHPKLLPQSEETPARLLQGIHTTRPAPRSAAAAAAAVPAAAAAAAAAAASSHSR SLQAPCLCLQGKEPPSPAGPVRVSAATT*PGTSRHLARLPGSSFMVRPVGPLVSQTGSVAVG LGQTSLSPSTDWSRKILQCITVSTMVVIRGRSAKGPSWRSK

For Yeast R3 LMP1-l2F and Yeast R2 LMP1-l2Y, the majority of the sequences had codon stops on the scFv ORF, but also a functional scFv with no codon stops was detected among the sequences in both outputs. The same scFv promoted during the phage selection in both selections. This could be indicative of a possible *bona fide* LMP1 loop 2 binder, as the loop displayed by pY-LMP1-lp2F yeast and pY-LMP1-lp2Y yeast are highly similar and just differ in one amino acid. The scFv was named Clone 1 LMP1, and the DNA and the amino acids sequence is described in figure 11 in the appendix.

5.3 Conclusion

Following yeast transformation and using homologous recombination to incorporate scFv sequences into an Aga2 fusion, a fraction of the yeast expressed the Aga2 fusion protein and with different proportions in each case: 42.5% in Yeast R3 LMP1-l2F, 19.1% in Yeast R2 LMP1-l2Y, 3.58% in Yeast R2 LMP2-l2, 1.47% of Yeast R3 LMP2-l5 and 6.56% in Yeast R3 B7H4.

Codon stops may have been introduced in the scFv DNA during the original library synthesis by shift in the ORF during the PCR, giving rise after cloning to phagemid without an ORF through the scFv-PIII due to the presence of in-frame codon stop. We have named these sequences as non-ORF scFvs. Non-ORF scFvs could have been present in the original phage display library. Alternatively, some may have been generated during the PCR cloning described above. The promotion of such sequences during the phage selection is usually observed when working with phagemid libraries based on the fusion of scFv with PIII (492–494). This bias is related to the promotion of polyphage during phage selection (as described below). Even so, the N-terminal yeast display system permitted the isolation of a proportion of ORF scFvs in the phage display outputs and continued selection without being affected by this bias.

Nevertheless, a functional scFv could be identified by sequencing in the outputs Yeast R3 LMP1-l2F and Yeast R2 LMP1-l2Y. The selection of this sequence in two different phage selection using yeast displaying very similar loops could be indicative of a *bona fide* LMP1 loop 2 binder.

5.3.1 Polyphage bias during phage selection

A polyphage is an extra-long M13 phage able to package a high quantity of single-stranded DNA, being able to pack more than one genome. The PIII is essential for assembly; a low level of PIII increases the phage assembly time, increasing the size of the filamentous phage. In a phagemid system, the wt PIII is expressed at low levels from the helper phage. The expression is complemented by the scFv-PIII expressed from the phagemid, the combination being sufficient to produce functional phage. If the scFv-PIII expression fails, it leads to the production of polyphage with several phagemids packaged inside (492–494).

The promotion of polyphage carrying a non-ORF scFv in their phagemid during phage display selection is not currently well described in the scientific literature. A possible hypothesis is related to the metabolic cost of the scFv expressed in the bacteria host. Since polyphage can only promote during the phage selection by binding to the target antigen, the promoted polyphage must have scFv-PIII on their surface (able to bind to the antigen). These polyphage (with scFv-PIII in their surface but carrying a non-ORF scFv in its phagemid) could have been produced in bacteria carrying two different phagemids (the non-ORF scFv phagemid plus an ORF scFv phagemid, required for scFv-PIII expression). The presence of bacteria carrying both kinds of phagemids can be explained by the metabolic cost that scFv-PIII is to the bacteria. As the non-ORF scFv phagemid have less metabolic cost to the bacteria, it may be produced in higher copy number than the ORF scFv phagemid. Therefore, the phenotype needed from antibiotic resistance gene is provided by high copies number non-ORF scFv phagemid, while the low copy number ORF scFv phagemid express low level of scFv-PIII (required in the polyphage to promote during the phage display selection). Higher copies of non-ORF scFv phagemid would also lead to packaging advantage in the polyphage.

If the polyphage effect described above is occurring, it is difficult to avoid when using phagemid libraries. Working with the basal activity of the *LacZ* promoter (not using IPTG) could reduce the scFv expression in the bacteria reducing it metabolic cost and, therefore, this bias. However, the use of IPTG could also promote the selection of more stable expressed scFvs. The library design, especially the linker between VH and VL in the scFv, could also have an impact on

the promotion of polyphages, as GC-rich linkers can increase burden of the plasmid on the bacterial host (plasmid fitness cost) (495).

6. Results: Development of antigen-expressing mammalian cells

6.1 Introduction

Adherent antigen-expressing mammalian cells were developed to be used during the scFv selection and for CAR functional characterisation. A tetracycline-inducible system was chosen because it enables modulation of the level of expression of the antigen by the addition of tetracycline. Antigen expression modulation is especially useful to facilitate the development of LMP1 and LMP2A expressing cells, as the overexpression of these oncogenic proteins could have a toxic effect on the cells making it difficult to select positive clones (496). Moreover, by regulating the expression of the antigen, low, medium and high expressing cells can be used for CAR functional characterisation. Therefore, HEK293 Flip-In T-REx cells and pcDNA5/FRT were used for cell line development and three cell lines were developed: HEK293-B7H4, HEK293-LMP1 and HEK293-LMP2A (figure 6.1).

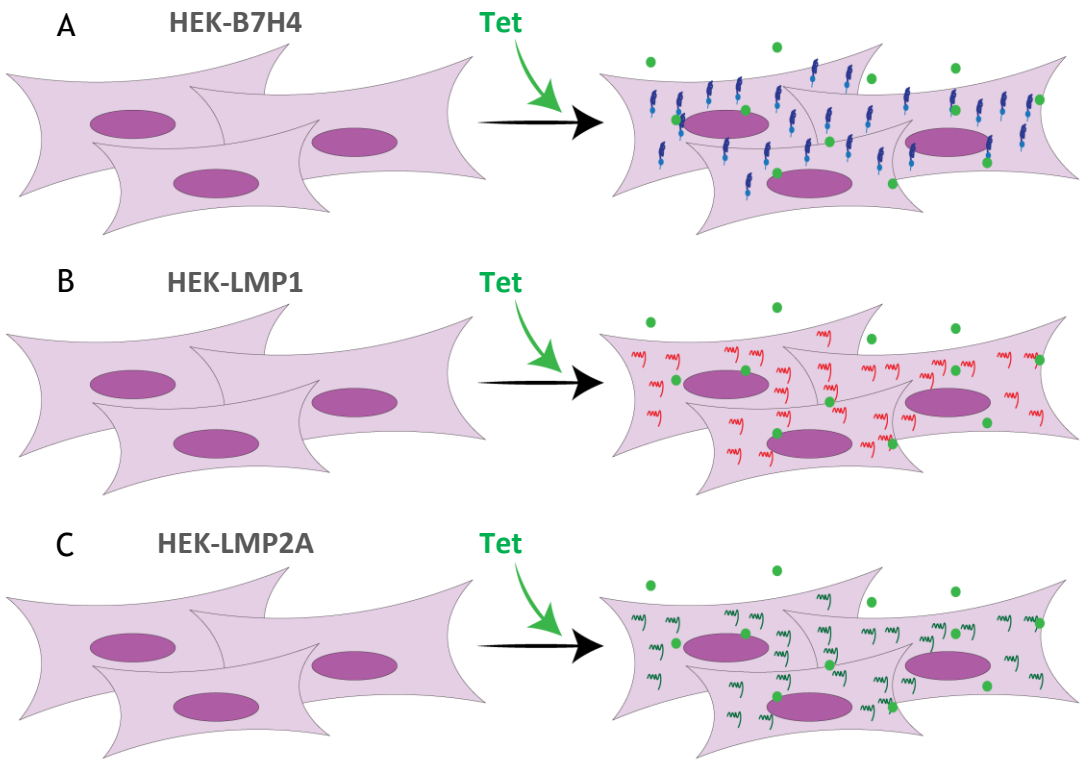

Figure 6.1 HEK293-B7H4, HEK293-LMP1 and HEK293-LMP2A cell lines. The cell lines were developed using HEK293 Flip-In T-REx cells which has stable integration in the genome of pFRT/lacZeo and pcDNA6/TR. Co-transfection with pcDNA5/FRT derived vectors and pOG44 leads to homologous recombination of the pcDNA5/FRT based vector into the genome integrated pFRT/lacZeo. Addition of tetracycline to the media leads to expression of the gene of interest cloned

into pcDNA5/FRT. Diagrammatic representation of the plasmid Flip-In system is shown in figures 5 and 6 in the appendix.

6.2 Development of pB7H4-FRT, pLMP1-FRT and pLMP2A-FRT

To create the tetracycline-inducible antigen-expressing HEK293 the complete cDNA sequence of B7H4 and the viral DNA sequences of LMP1 and LMP2A (including introns) were cloned into pcDNA5/FRT giving rise to pB7H4-FRT, pLMP1-FRT and pLMP2A-FRT. Each of these plasmids was co-transfected with the plasmid pOG44 into HEK293 Flip-In T-REx cells.

6.2.1 Cloning of B7H4 into pcDNA5/FRT

A synthetic DNA cassette was ordered from GeneWiz containing the complete cDNA sequence of human B7H4 (Uniprot Q7Z7D3). In addition, the sequence GCCGCCACC was added before the first ATG (methionine) of the signal peptide to generate a consensus Kozak sequence (GCCGCCACCATGG) to promote the initiation of protein translation. The sequence was flanked by *Hind*III and *Not*I for cloning into pcDNA5/FRT (figure 6.2). The DNA sequence (figure 6.2) was provided by the manufacturer in a plasmid (pB7H4) and codes for the amino acid sequence which encompasses the complete protein (figure 6.3).

Figure 6.2 Synthetic DNA cassette used for the development of pB7H4-FRT by cloning into pcDNA5/FRT. *Hind*III and *Not*I restriction sequence highlighted in grey and extra sequence for Kozak's sequence highlighted in yellow.

B7H4 DNA cassette for pB7H4-FRT obtained by digestion from pB7H4
AAG CTT GCC GCC ACC ATG GCT TCC CTG GGG CAG ATC CTC TTC TGG AGC ATA ATT AGC ATC ATC ATT ATT CTG GCT GGA GCA ATT GCA CTC ATC ATT GGC TTT GGT ATT TCA GGG AGA CAC TCC ATC ACA GTC ACT ACT GTC GCC TCA GCT GGG AAC ATT GGG GAG GAT GGA ATC CTG AGC TGC ACT TTT GAA CCT GAC ATC AAA CTT TCT GAT ATC GTG ATA CAA TGG CTG AAG GAA GGT GTT TTA GGC TTG GTC CAT GAG TTC AAA GAA GGC AAA GAT GAG CTG TCG GAG CAG GAT GAA ATG TTC AGA GGC CGG ACA GCA GTG TTT GCT GAT CAA GTG ATA GTT GGC AAT GCC TCT TTG CGG CTG AAA AAC GTG CAA CTC ACA GAT GCT GGC ACC TAC AAA TGT TAT ATC ATC ACT TCT AAA GGC AAG GGG AAT GCT AAC CTT GAG TAT AAA ACT GGA GCC TTC AGC ATG CCG GAA GTG AAT GTG GAC TAT AAT GCC AGC TCA GAG ACC TTG CGG TGT GAG GCT CCC CGA TGG TTC CCC CAG CCC ACA GTG GTC TGG GCA TCC CAA GTT GAC CAG GGA GCC AAC TTC TCG GAA GTC TCC AAT ACC AGC TTT GAG CTG AAC TCT GAG AAT GTG ACC ATG AAG GTT GTG TCT GTG CTC TAC AAT GTT ACG ATC AAC AAC ACA TAC TCC TGT ATG ATT GAA AAT GAC ATT GCC AAA GCA ACA GGG GAT ATC AAA GTG ACA GAA TCG GAG ATC AAA AGG CGG AGT CAC CTA CAG CTG CTA AAC TCA AAG GCT TCT CTG TGT GTC TCT TCT TTC TTT GCC

ATC AGC TGG GCA CTT CTG CCT CTC AGC CCT TAC CTG ATG CTA AAA TAA GCG GCC GC

Figure 6.3 Amino acid sequence synthesised from the mRNA coded by B7H4 DNA cassette.

Amino acid sequence of LMP1
MASLGQILFWSIISIIIILAGAIALIIGFGISGRHSITVTTVASAGNIGEDGILSCTFEPDIKLSDIVIQ WLKEGVLGLVHEFKEGKDELSEQDEMFRGRTAVFADQVIVGNASLRLKNVQLTDAGTYKCY IITSKGKGNANLEYKTGAFSMPEVNVDYNASSETLRCEAPRWFPQPTVVWASQVDQGANFS EVSNTSFELNSENVTMKVVSVLYNVTINNTYSCMIENDIAKATGDIKVTESEIKRRSHLQLLNS KASLCVSSFFAISWALLPLSPYLMLK

The DNA cassette released from the plasmid pB7H4 with *Hind*III and *Not*I digestion (figure 6.4) and used for ligation with *Hind*III and *Not*I digested pcDNA5/FRT to obtain the final plasmid pB7H4-FRT.

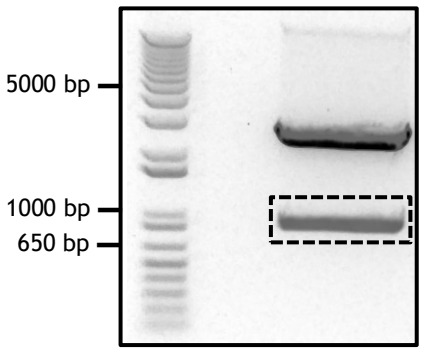

Figure 6.4 pB7H4-FRT development. Digested plasmid pB7H4 DNA was electrophoresed through 1% agarose. The *Hind*III and *Not*I fragment (872 bp DNA band) was purified and cloned into *Hind*III and *Not*I digested pcDNA5/FRT, giving rise to pB7H4-FRT. The dashed box shows the 872 bp DNA band excised for DNA purification.

After *E. coli* transformation, three colonies were grown and used for colony PCR with the primers pcDNA5/FRT-F and pcDNA5/FRT-R. The PCR amplicons were purified and sequenced with the primers pcDNA5/FRT-F and SeqB7H4-F. The sequencing showed the correct sequence (figure 6.2) inserted in pcDNA5/FRT, giving rise to the plasmid pB7H4-FRT (figure 6.5). One colony was used for DNA plasmid production and glycerol stocks.

Figure 6.5 pB7H4-FRT. Plasmid features and ORFs are coloured and denoted: the white arrow represents the CMV promoter, green boxes the Tet operator, yellow box the Kozak sequence, blue box the B7H4 ORF, grey BOX the poly(A) signal and the red square shows the codon stop. The middle dashed line represents the diagrammatic discontinuity between the 5' end (shown above) and the 3' end (shown below) of the fragment.

6.2.2 PCR amplification of LMP1 and cloning into pcDNA5/FRT

The DNA containing the complete viral DNA sequence of LMP1 (including introns) with Phe388 and additional 3' sequences was amplified from the plasmid pPyLMP1 (497) with the primers LMP1-F and LMP1-R. LMP1-F introduces the restriction site *Hind*III and the sequence GCCGCCACC (to form a Kozak consensus sequence) at the 5' end. LMP1-R introduces the restriction site *Not*I in the 3' end. Five extra nucleotides were added at each end for the subsequent digestion with *Hind*III and *Not*I. The sequence of the resulting amplicon (figure 6.8) is shown in figure 6.6. The encoded amino acid sequence of LMP1 is shown in figure 6.7.

Figure 6.6 DNA amplicon used for the development of pLMP1-FRT by cloning into pcDNA5/FRT. *Hind*III and *Not*I restriction sequence highlighted in grey, an extra sequence for Kozak sequence highlighted in yellow and extra EBV genome in grey.

LMP1 DNA for pLMP1-FRT obtained by PCR from pPyLMP-1
GAT GCA AGC TTG CCG CCA CCA TGG AAC ACG ACC TTG AGA GGG GCC CAC CGG GCC CGC GAC GGC CCC CTC GAG GAC CCC CCC TCT CCT CTT CCC TAG GCC TTG CTC TCC TTC TCC TCC TCT TGG CGC TAC TGT TTT GGC TGT ACA TCG TTA TGA GTG ACT GGA CTG GAG GAG CCC TCC TTG TCC TCT ATT CCT TTG CTC TCA TGC TTA TAA TTA TAA TTT TGA TCA TCT TTA TCT TCA GAA GAG ACC TTC TCT GTC CAC TTG GAG CCC TTT GTA TAC TCC TAC TGA TGA GTA AGT ATT ACA CCC TTT GCC CCA CAC CCC CTT TCC CTT ACT CTT CCT TCT CTA ACG CAC TTT CTC CTC TTT CCC CAG TCA CCC TCC TGC TCA TCG CTC TCT GGA ATT TGC ACG GAC AGG CAT TGT TCC TTG GAA TTG TGC TGT TCA TCT TCG GGT GCT TAC TTG GTA AGA TCT AAC ATT CCC TAG GAA TTA TTT ACC ACA CCC CCA CTT TTC CAA CCC TAA CAC TCT TTT TTC AAC GCA GTC TTA GGT ATC TGG ATC TAC TTA TTG GAG ATG

CTC TGG CGA CTT GGT GCC ACC ATC TGG CAG CTT TTG GCC TTC TTC CTA GCC
TTC TTC CTA GAC CTC ATC CTG CTC ATT ATT GCT CTC TAT CTA CAA CAA AAC
TGG TGG ACT CTA TTG GTT GAT CTC CTT TGG CTC CTC CTG TTT CTG GCG ATT
TTA ATC TGG ATG TAT TAC CAT GGA CAA CGA CAC AGT GAT GAA CAC CAC CAC
GAT GAC TCC CTC CCG CAC CCT CAA CAA GCT ACC GAT GAT TCT GGC CAT GAA
TCT GAC TCT AAC TCC AAC GAG GGC AGA CAC CAC CTG CTC GTG AGT GGA GCC
GGC GAC GGA CCC CCA CTC TGC TCT CAA AAC CTA GGC GCA CCT GGA GGT GGT
CCT GAC AAT GGC CCA CAG GAC CCT GAC AAC ACT GAT GAC AAT GGC CCA CAG
GAC CCT GAC AAC ACT GAT GAC AAT GGC CCA CAT GAC CCG CTG CCT CAG GAC
CCT GAC AAC ACT GAT GAC AAT GGC CCA CAG GAC CCT GAC AAC ACT GAT GAC
AAT GGC CCA CAT GAC CCG CTG CCT CAT AGC CCT AGC GAC TCT GCT GGA AAT
GAT GGA GGC CCT CCA CAA TTG ACG GAA GAG GTT GAA AAC AAA GGA GGT GAC
CAG GGC CCG CCT TTG ATG ACA GAC GGA GGC GGC GGT CAT AGT CAT GAT
TCC GGC CAT GGC GGC GGT GAT CCA CAC CTT CCT ACG CTG CTT TTG GGT TCT
TCT GGT TCC GGT GGA GAT GAT GAC GAC CCC CAC GGC CCA GTT CAG CTA AGC
TAC TAT GAC TAA CCT TTC TTT ACT TCT AGG CAT TAC CAT GTC ATA GGC TTG
CCT GAC TGA CTC TCC CTC CAT TTA CTG GGA ATG CCT TAG CTA ATC ACC TTA
ACT GG CAC ACA CTC CCT TAG CCA CAC TGT CTG TCT AGG CTG AAA AGC CAC
ATT CAT ATT CTA TTT CAA AAC AAG GGG AAA GGA GGA CAT GCG AGA ATT GGC
AGA CAC CTT TAC CCA GCC CTT AAC ACA CCA CAC AGG TAG CAA GGA CCC GGG
CGT TGC CAG ACT CCG CCA CCA ACG CCC CTG CGT TGA ACC CAC CCC TCC TAC
ACA CAT CAG ACC TCT GCA CAA CAC AAC TAC CAG GCA GAT GAG GCC CCT TAC
TTC CAC AGG GTA CTG GCA TAC CAG CGG GGG ACC ACA TAC ATC CCT GTC TCC
CAC CCA GTA ACT CCA GCA ACT TTG CTT TCC ATC TTG TGC CAA TAC ACA TTT
GGA TTC AGC CCA AGC CAC ACC TAA CTC ATG CCA GCA GAG GCA GGA ACA CCT
GTT GTT GAC ACA TTC TTT GCG CAT AAG CAC TTT AAT CCC TCT CTC ACA CCC
AGA AAC TAA GAG CTA GCC CAA AAC CTC CAC ACC TGT CCT CGC TCA TCT TTC
CAC ATT CCT CTG GCC TTC TTT CCT TGT CCT TAC TGT ATA AAA GTC CAC GAA
AAC AGC TGT GCC TCA CTC TCG AGA TGG GCG GCC GCA CAT G

Figure 6.7 Amino acid sequence synthesised from the mature mRNA coded by LMP1 PCR amplicon after pre-mRNA processing.

Amino acid sequence of LMP1
MEHDLERGPPGPRRPPRGPPLSSSLGLALLLLLLALLFWLYIVMSDWTGGALLVLYSFALMLI IIILIIFIFRRDLLCPLGALCILLLMITLLLIALWNLHGQALFLGIVLFIFGCLLVLGIWIYLLEMLW RLGATIWQLLAFFLAFFLDLILLIIALYLQQNWWTLLVDLLWLLLFLAILIWMYYHGQRHSDE HHHDDSLPHPQQATDDSGHESDSNSNEGRHHLLVSGAGDGPPLCSQNLGAPGGGPDNGP QDPDNTDDNGPQDPDNTDDNGPQDPDNTDDNGPHDPLPHSPSDSAGNDGGPPQLTEEVE NKGGDQGPPLMTDGGGGHSHDSGHGGGDPHLPTLLLGSSGSGGDDDDPHGPVQLSYYD

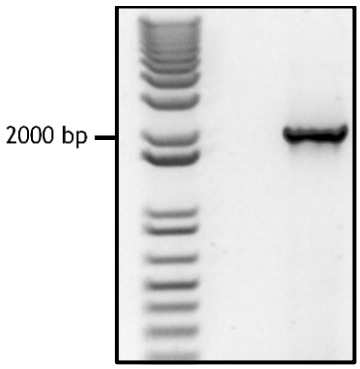

Figure 6.8 pLMP1-FRT development. The PCR was conducted with the primers LMP1-F and LMP1-R and pPyLMP-1 as a template. The product was electrophoresed through 1% agarose. The 2025 bp band was purified, digested with *Hind*III and *Not*I and used to generate pLMP1-FRT.

The LMP1 PCR amplicon and the pcDNA5/FRT plasmid were digested with *Hind*III and *Not*I and ligated. Several resulting bacterial colonies were used for colony PCR with the primers pcDNA5/FRT-F and pcDNA5/FRT-R, correct ones selected, and sequenced with the primers pcDNA5/FRT-F, SeqLMP1-F and Seq2LMP1-F. A correct colony was selected and used for glycerol stock and plasmid production (figure 6.9).

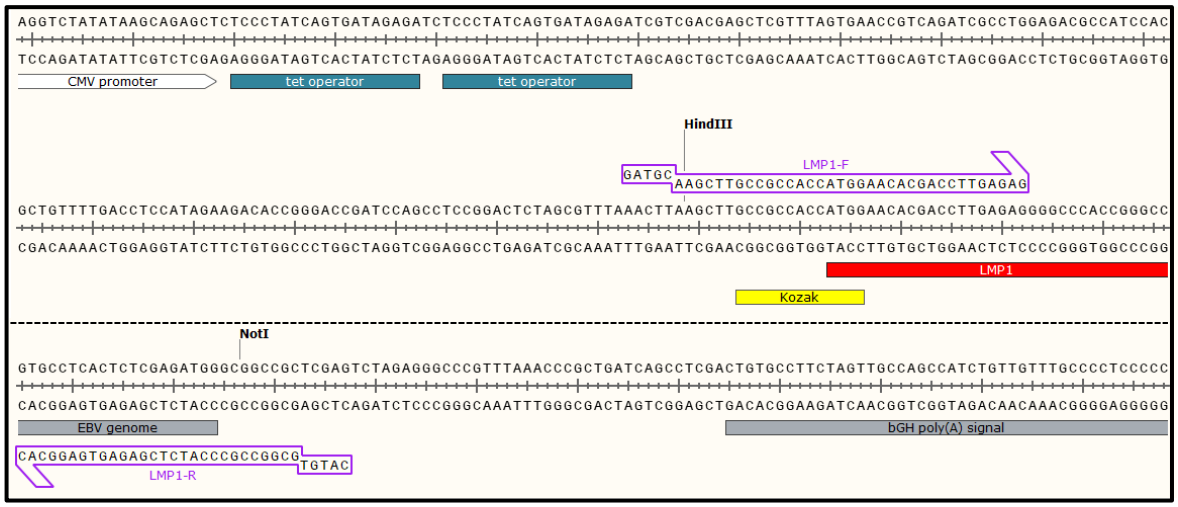

Figure 6.9 pLMP1-FRT. Primers LMP1-F and LMP1-R were used to amplify LMP1 from pPyLMP1. Plasmid features and ORFs are coloured and denoted: the white arrow represents the CMV promoter, green boxes the Tet operator, yellow box the Kozak sequence, red box the LMP1 ORF and grey box the poly(A). The middle dashed line represents the diagrammatic discontinuity between the 5' end (shown above) and the 3' end (shown below) of the fragment.

6.2.3 PCR amplification of LMP2A and cloning into pcDNA5/FRT

The DNA containing the complete viral sequence of LMP2A (including introns) was amplified from the plasmid pSG5-c/gLMP2A (21) with the primers LMP2A-F and

LMP2A-R. LMP2A-F introduces the restriction site *Hind*III and the sequence GCCGCCACC (to form a Kozak consensus sequence) at the 5' end. LMP2A-R introduces the restriction site *Not*I in the 3' end. Five extra nucleotides were added at each end for the subsequent digestion with *Hind*III and *Not*I. The sequence of the resulting amplicon (figure 6.12) is shown in figure 6.10. The amino acid sequence of LMP2A encoded by the DNA sequence is shown in figure 6.11.

Figure 6.10 PCR DNA amplicon used for the development of pLMP2A-FRT by cloning into pcDNA5/FRT. *Hind*III and *Not*I restriction sequence highlighted in grey and extra sequence for Kozak sequence highlighted in yellow.

LMP2A DNA for pLMP2A-FRT obtained by PCR from pSG5-c/gLMP2A
GAA TGC AAG CTT GCC GCC ACC ATG GGG TCC CTA GAA ATG GTG CCA ATG GGC
GCG GGT CCC CCT AGC CCC GGC GGG GAT CCG GAT GGG TAC GAT GGC GGA
AAC AAC TCC CAA TAT CCA TCT GCT TCT GGC TCT TCT GGG AAC ACC CCC ACC
CCA CCG AAC GAT GAG GAA CGT GAA TCT AAT GAA GAG CCC CCA CCG CCT TAT
GAG GAC CCA TAT TGG GGC AAT GGC GAC CGT CAC TCG GAC TAT CAA CCA CTA
GGA ACC CAA GAT CAA AGT CTG TAC TTG GGA TTG CAA CAC GAC GGG AAT GAC
GGG CTC CCT CCC CCT CCC TAC TCT CCA CGG GAT GAC TCA TCT CAA CAC ATA
TAC GAA GAA GCG GGC AGA GGA AGT ATG AAT CCA GTA TGC CTG CCT GTA ATT
GTT GCG CCC TAC CTC TTT TGG CTG GCG GCT ATT GCC GCC TCG TGT TTC ACG
GCC TCA GTT AGT ACC GTT GTG ACC GCC ACC GGC TTG GCC CTC TCA CTT CTA
CTC TTG GCA GCA GTG GCC AGC TCA TAT GCC GCT GCA CAA AGG AAA CTG CTG
ACA CCG GTG ACA GTG CTT ACT GCG GTT GTC ACT TGT GAG TAC ACA CGC ACC
ATT TAC AAT GCA TGA TGT TCG TGA GAT TGA TCT GTC TCT AAC AGT TCA CTT
CCT CTG CTT TTC TCC TCA GTC TTT GCA ATT TGC CTA ACA TGG AGG ATT GAG
GAC CCA CCT TTT AAT TCT CTT CTG TTT GCA TTG CTG GCC GCA GCT GGC GGA
CTA CAA GGC ATT TAC GGT TAG TGT GCC TCT GTT ATG AAA TGC AGG TTT GAC
TTC ATA TGT ATG CCT TGG CAT GAC GTC AAC TTT ACT TTT ATT TCA GTT CTG
GTG ATG CTT GTG CTC CTG ATA CTA GCG TAC AGA AGG AGA TGG CGC CGT TTG
ACT GTT TGT GGC GGC ATC ATG TTT TTG GCA TGT GTA CTT GTC CTC ATC GTC
GAC GCT GTT TTG CAG CTG AGT CCC CTC CTT GGA GCT GTA ACT GTG GTT TCC
ATG ACG CTG CTG CTA CTG GCT TTC GTC CTC TGG CTC TCT TCG CCA GGG GGC
CTA GGT ACT CTT GGT GCA GCC CTT TTA ACA TTG GCA GCA GGT AAG CCA CAC
GTG TGA CAT TGC TTG CCT TTT TGC CAC ATG TTT TCT GGA CAC AGG ACT AAC
CAT GCC ATC TCT GAT TAT AGC TCT GGC ACT GCT AGC GTC ACT GAT TTT GGG
CAC ACT TAA CTT GAC TAC AAT GTT CCT TCT CAT GCT CCT ATG GAC ACT TGG
TAA GTT TTC CCT TCC TTT AAC TCA TTA CTT GTT CTT TTG TAA TCG CAG CTC
TAA CTT GGC ATC TCT TTT ACA GTG GTT CTC CTG ATT TGC TCT TCG TGC TCT
TCA TGT CCA CTG AGC AAG ATC CTT CTG GCA CGA CTG TTC CTA TAT GCT CTC
GCA CTC TTG TTG CTA GCC TCC GCG CTA ATC GCT GGT GGC AGT ATT TTG CAA
ACA AAC TTC AAG AGT TTA AGC AGC ACT GAA TTT ATA CCC AGT GAG TAT CTA
TTT GTT ACT CCT GTT TAG TTG AAG AAA ACA AGC TAT TGG ATT GTA ACA CAC
ATT TTA CGC TTT GTT CCT TAG ATT TGT TCT GCA TGT TAT TAC TGA TTG TCG
CTG GCA TAC TCT TCA TTC TTG CTA TCC TGA CCG AAT GGG GCA GTG GAA ATA
GAA CAT ACG GTC CAG TTT TTA TGT GCC TCG GTG GCC TGC TCA CCA TGG TAG
CCG GCG CTG TGT GGC TGA CGG TGA TGT CTA ACA CGC TTT TGT CTG CCT GGA
TTC TTA CAG CAG GAT TCC TGA TTT TCC TCA TTG GTA AGT GTG ACA CCA ACA
GGT GTT GCC TTG TTA TGT CAC CGT TCT GAC ACA TGA CTT ACA TGG GTT TGG
CTT TTG TAG GCT TTG CCC TCT TTG GGG TCA TTA GAT GCT GCC GCT ACT GCT

GCT ACT ACT GCC TTA CAC TGG AAA GTG AGG AGC GCC CAC CGA CCC CAT ATC GCA ACA CTG TAT AAT AAG CGG CCG CAC ATG

Figure 6.11 Amino acid sequence synthesised from the mature mRNA coded by LMP2A PCR amplicon after pre-mRNA processing.

Amino acid sequence of LMP2A
MGSLEMVPMGAGPPSPGGDPDGYDGGNNSQYPSASGSSGNTPTPPNDEERESNEEPPPPY EDPYWGNGDRHSDYQPLGTQDQSLYLGLQHDGNDGLPPPPYSPRDDSSQHIYEEAGRGSM NPVCLPVIVAPYLFWLAAIAASCFTASVSTVVTATGLALSLLLLAAVASSYAAAQRKLLTPVTV LTAVVTFFAICLTWRIEDPPFNSLLFALLAAAGGLQGIYVLVMLVLLILAYRRRWRRLTVCGG IMFLACVLVLIVDAVLQLSPLLGAVTVVSMTLLLLAFVLWLSSPGGLGTLGAALLTLAAALAL LASLILGTLNLTTMFLLMLLWTLVVLLICSSCSSCPLSKILLARLFLYALALLLLASALIAGGSIL QTNFKSLSSTEFIPNLFCMLLLIVAGILFILAILTEWGSGNRTYGPVFMCLGGLLTMVAGAVW LTVMSNTLLSAWILTAGFLIFLIGFALFGVIRCCRYCCYYCLTLESEERPPTPYRNTV

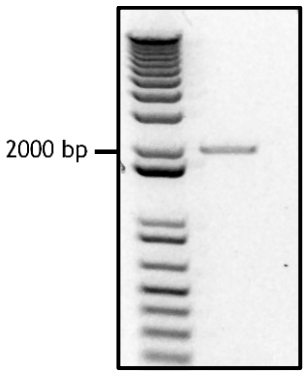

Figure 6.12 pLMP2A-FRT development. The PCR product was electrophoresed through 1% agarose in TAE and stained with SYBR Safe. LMP2A PCR with the primers LMP2A-F and LMP2A-R and pSG5-c/gLMP2A as a template. The 2016 bp band correspond with the DNA sequence described in table 6.3. The DNA obtained from the PCR reaction was purified, digested with *Hind*III and *Not*I and used for the development of pLMP2A-FRT.

The cloning into pcDNA5/FRT was conducted exactly as described above for LMP1 (figure 6.13).

Figure 6.13 pLMP2A-FRT. Primers LMP2A-F and LMP2A-R were used to amplify LMP2A from pSG5-c/gLMP2A. Plasmid features and ORFs are coloured and denoted: the white arrow represents the CMV promoter, green boxes the Tet operator, yellow box the Kozak sequence and the green box the LMP2A ORF. The middle dashed line represents the diagrammatic discontinuity between the 5' end (shown above) and the 3' end (shown below) of the fragment.

6.3 HEK293 Flip-In T-REx transfection and antigen expression

HEK293 Flip-In T-REx cells were co-transfected with one of the pcDNA5/FRT derived plasmids (pB7H4-FRT, pLMP1-FRT or pLMP2A-FRT) plus pOG44 (encoding the Flp recombinase). Three transfections with each plasmid pair (with polyfectamine) were performed to develop the cell lines HEK293-B7H4, HEK293-LMP1 and HEK293-LMP2A. During the transfection tetracycline free and tested FBS was used (due to traces of tetracycline in standard commercial FBS) when required to avoid the induction of expression of the plasmid sequences.

The HEK293 Flip-In T-REx system is designed to obtain an isogenic cell modification, leading to similar levels of protein expression by all modified clones. Therefore, the obtained antibiotic resistant colonies (resistant to hygromycin B and sensitive to zeocin) were collected as a pool of clones, expanded and stored in liquid nitrogen for their use in yeast-cell panning selections and functional characterisation of CARs.

6.3.1 B7H4 expression by tetracycline induction of HEK293-B7H4

HEK293-B7H4 cell were cultured to 80% confluence in media with standard FBS and then supplemented with 10 µg/ml of tetracycline for 24 hours for the

induction of the B7H4 expression. The cells were then detached and dissociated for their analysis by flow cytometry (figure 6.14). Low expression of B7H4 on uninduced HEK293-B7H4 (figure 6.14.B) is likely due to the trace presence of tetracycline in standard FBS.

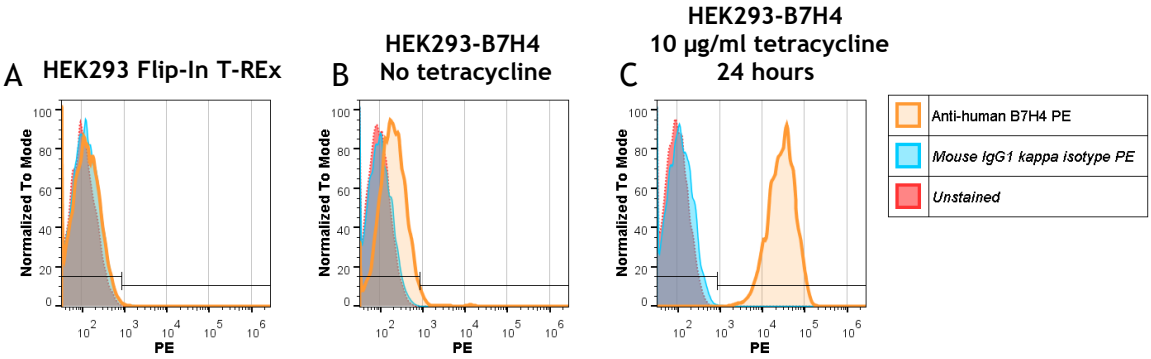

Figure 6.14 Tetracycline inducible expression of B7H4 in HEK293-B7H4 cells. Flow cytometry histograms of HEK293 cells unstained, stained with isotype control and stained with anti-human B7H4 (as indicated in the key). A) HEK293 Flip-In T-REx. B) Uninduced HEK294-B7H4. C) Tetracycline induced HEK293-B7H4.

6.3.2 LMP1 expression by tetracycline induction of HEK293-LMP1

HEK293-LMP1 cells were cultured to 80% confluence in media with tetracycline-free FBS and then supplemented with 10 µg/ml of tetracycline for 24 hours for the induction of expression of LMP1. This protocol of induction proved to be highly toxic, with all the cells dying. Therefore, the induction of LMP1 was performed with 0.5 µg/ml tetracycline for 16 hours. 0.5 µg/ml was the maximum concentration of tetracycline that allows having variable cells attached to the flask after 16 hours of incubation. The cells were then detached and lysed for protein analysis. Lysates were also prepared from HEK293 Flip-In T-REx control cells (A) and uninduced HEK293-LMP1 (B) and samples were separated by SDS-PAGE and western blotted (figure 6.15).

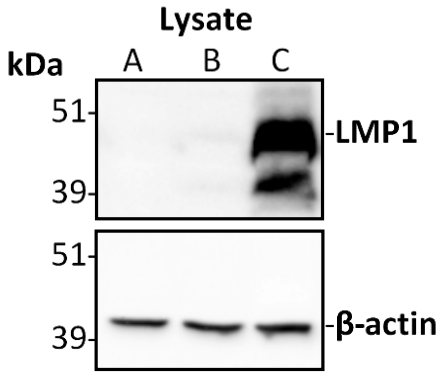

Figure 6.15 Western blot result of LMP1 expression under tetracycline induction in HEK293-LMP1 cells. 6 µg of protein lysates were separated by NuPAGE (Gel 4-12% polyacrylamide gradient Bis-Tris run in MOPS buffer). The gel was blotted and probed with antibody anti-LMP1 clone 1G6 and secondary anti-rat HRP conjugated. The blot was then stripped and re-probed with antibody anti-β-actin and secondary anti-rabbit HRP conjugated, as a loading control. The marker ladder sizes in kDa are shown. Lysate from HEK293 Flip-In T-REx control cells loaded in track A, lysate from uninduced HEK293-LMP1 loaded in track B and sample lysate loaded in track C. Full size western blots, including the protein ladder, are shown in figure 12 in the appendix.

6.3.3 LMP2A expression by tetracycline induction of HEK293-LMP2A

HEK293-LMP2A cells were cultured and analysed exactly as above for HEK293-LMP1 cells. Induction with 10 µg/ml of tetracycline for 24 hours also proved to be highly toxic. Therefore, the induction of LMP2A was performed with 1 µg/ml of tetracycline for 16 hours. 1 µg/ml was maximum concentration of tetracycline that allows having attached viable cells after 16 hours incubation. Lysates were also prepared from HEK293 Flip-In T-REx control cells (A) and uninduced HEK293-LMP2A (D) and samples were separated by SDS-PAGE and western blotted (figure 6.16).

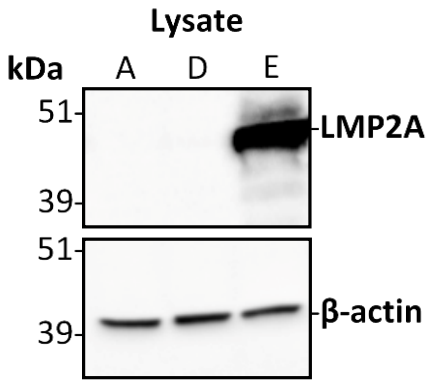

Figure 6.16 Western blot result of LMP2A expression under tetracycline induction in HEK293-LMP2A cells. 6 µg of protein lysates were separated by NuPAGE (Gel 4-12% polyacrylamide gradient Bis-Tris run in MOPS buffer). The gel was first blotted and probed with antibody anti-LMP2A

clone 14B6 and secondary anti-rat HRP conjugated. The blot was then, stripped and re-probed with antibody anti-β-actin and secondary anti-rabbit HRP conjugated, as a loading control. The marker ladder sizes in kDa are shown. Lysate from HEK293 Flip-In T-REx control cells loaded in track A, lysate from uninduced HEK293-LMP2A loaded in track D and sample lysate loaded in track E. Full size western blots, including the protein ladder, are shown in figure 13 in the appendix.

6.4 Conclusions

HEK293-B7H4, HEK293-LMP1 and HEK293-LMP2A were successfully developed, and expression confirmed. Cells were stored in lN2 for subsequent use. Due to the toxicity of high level of expression of LMP1 and LMP2A, the uninduced cells must be cultured in media with tetracycline-free FBS.

The induction conditions chosen for subsequent experiments were: 10 μg/ml of tetracycline for 24 hours for HEK293-B7H4, 0.5 μg/ml of tetracycline for 16 hours for HEK293-LMP1 and 1 μg/ml of tetracycline for 16 hours for HEK293-LMP2A. Even though the expression of B7H4, LMP1 and LMP2A in this inducible mammalian expression system is most probably far higher than in EBV-associated tumour cell lines, overexpressing cells are more convenient for scFv selection and the first assessment of CAR functionality. Then, after confirming CAR activation, EBV-associated tumour cell lines should be used for a final functional assessment of CAR activity.

7. Results: scFv selection by yeast panning using mammalian cells

7.1 Introduction

To continue with the selection of specific scFvs, the phage display outputs transferred to yeast display were used in yeast against mammalian cell panning experiments, using antigen-expressing tetracycline-inducible HEK293 cells (figure 7.1). During the phage display selection, non-specific scFvs binding to the yeast surface were promoted, even though depletion was performed. Theoretically, the only identical protein shared between the surfaces of the yeast and mammalian cells in this system is the target antigen overexpressed in both. Therefore, these non-specific scFvs should not promote when using mammalian cells for the next selection steps. Together with the depletion steps performed during both selection process (phage selection using yeast as a source of antigen and yeast-mammalian cell panning), the swap between antigen-expressing platforms during the selection should ensure the enrichment of scFvs binding specifically to the expressed target antigen.

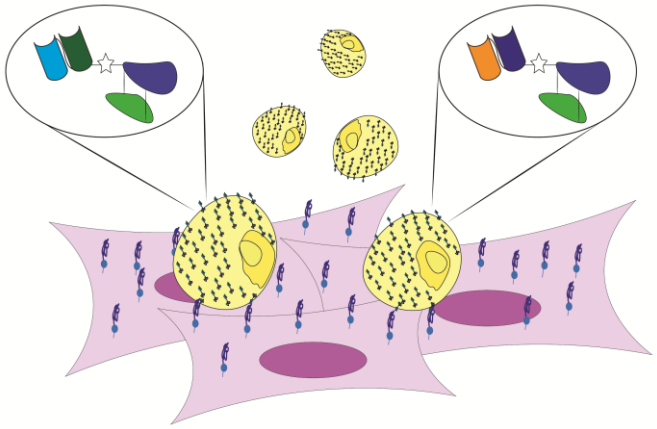

Figure 7.1 Yeast-mammalian cell panning. Yeast outputs expressing the fusion protein scFv-Aga2 (yellow) are exposed to adherent mammalian cells (purple) expressing the target antigen. The yeast expressing scFvs able to interact with the antigen and adhere to the cells while the non-interacting yeast can be washed off.

In the yeast-mammalian cell panning experiments and prior to every selection step, two depletion steps were performed: first to remove yeast with a tendency to interact with the surface of the flask, then to remove yeast with a tendency to interact with the surface of the mammalian cells. HEK293 Flip-In T-REx cells were

used for the second depletion steps. These cells do not express B7H4, LMP1 or LMP2A and were named as control HEK293. For the selection steps, tetracycline induced HEK293-B7H4, HEK293-LMP1, HEK293-LMP2A were used (as described in chapter 6). HEK293-LMP1 expresses the LMP1 variant with Phe388, and it was used for LMP1 loop 2F and LMP1 loop 2Y selections. LMP1 loop 2Y selection was performed to isolate scFvs reactive to both LMP1 variants found in the different strains of EBV (Phe388 and Tyr388).

The number of rounds of selection performed was decided after assessing by light microscopy the number of non-specific binding yeast following each depletion (as low as possible) and comparing this to the number of binding yeast during the selection (as high as possible). At least three rounds of selection were conducted to ensure the promotion of scFvs binding to the antigen.

7.2 Continuation of the B7H4 Ig-like V-type 1 domain selection by yeast-mammalian cell panning using HEK293-B7H4

Induced Yeast R3 B7H4 (figure 5.7.E) were used as the first input for the yeast-mammalian cell panning selection with tetracycline induced HEK293-B7H4 (induction conditions described in chapter 6). Three rounds of induced yeast vs. induced HEK293-B7H4 selection were performed, giving rise to the yeast outputs Yeast R4 B7H4, Yeast R5 B7H4 and Yeast R6 B7H4. The yeast-mammalian cell interactions were not always evident when observed by light microscopy, being difficult to differentiate between yeast interacting with the cells from other morphological structures developed by HEK293 cells.

Yeast interactions with the surface of the flask and the control HEK293 were observed during the depletion steps in Yeast R5 B7H4 and Yeast R6 B7H4 (figure 7.2.A and 7.2.B) but not in Yeast R4 B7H4. During the selection step of Yeast R6 B7H4, some clusters of yeast binding to the induced HEK293-B7H4 cells were observed (figure 7.2.C). However, due to the presence of yeast binding non-specifically to the surface of the flask and the cells, it could not be concluded that these were yeast expressing scFvs with specific binding to B7H4.

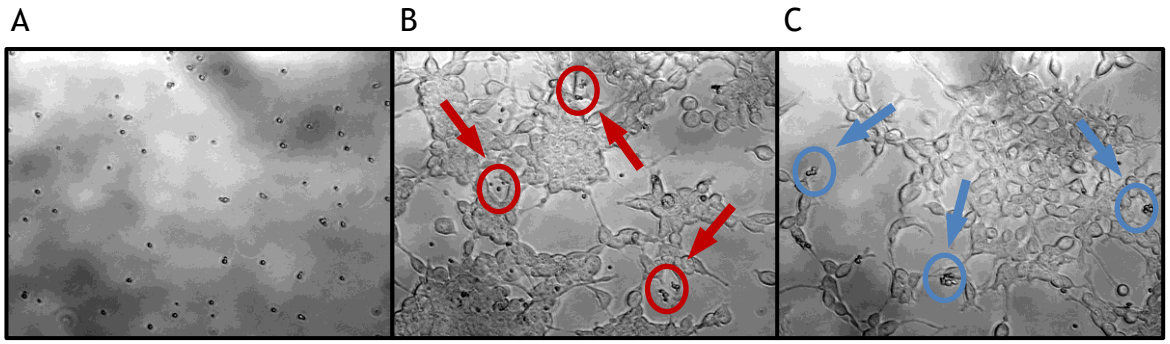

Figure 7.2 Yeast-mammalian cell panning B7H4 Ig-like V-type 1 domain selection round 6. A) Flask depletion of Yeast R5 B7H4 showing yeast binding to the flask. B) Control HEK293 depletion of flask depleted Yeast R5 B7H4. Red arrows and circles indicate yeast binding to the control cells. C) Selection with tetracycline induced HEK293-B7H4 of flask and control HEK293 depleted Yeast R5 B7H4 giving rise to Yeast R6 B7H4. Blue arrows and circles indicate yeast binding to the antigen-expressing cells.

7.2.1 Aga2 fusion protein enrichment after yeast-mammalian cell panning

Following the selection and enrichment of Aga2 fusion protein by yeast-mammalian cell panning, the expression of the Aga2 fusion protein was studied by flow cytometry with anti-V5 Tag FITC conjugated and compared between the first input for yeast-mammalian cell panning (Yeast R3 B7H4) and the outputs Yeast R4 B7H4 and Yeast R6 B7H4.

Enrichment of yeast expressing the Aga2 fusion protein was observed through the rounds of yeast-mammalian cell panning, increasing from 6.54% of the original input (figure 7.3.A) to 15% after one round (figure 7.3.B) and 81% after three rounds (figure 7.3.C). This yeast-mammalian cell panning effectively provided a means to overcome the polyphage bias of the phage display selection.

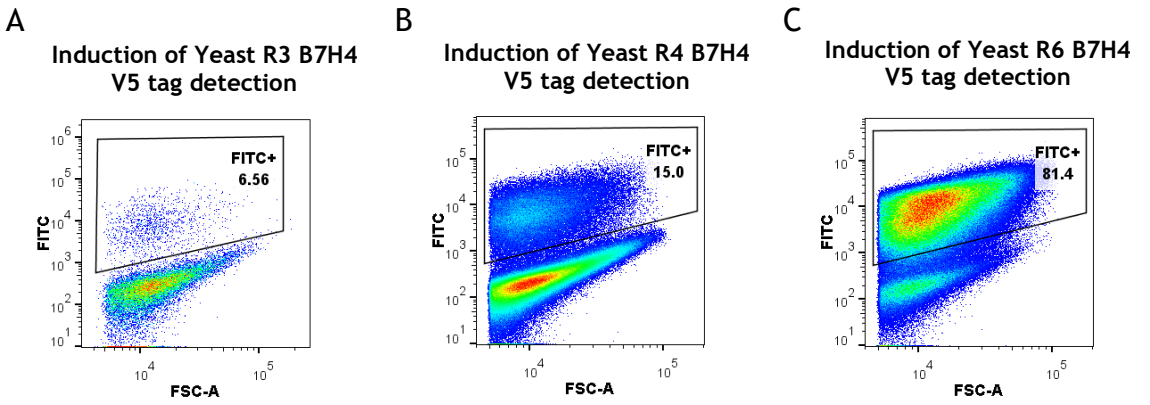

Figure 7.3 Enrichment of Aga2 fusion protein expressing yeast after yeast-mammalian cell panning. Flow cytometry dot plots of induced yeast stained with mouse anti-V5 FITC. A) Induced Yeast R3 B7H4. B) Induced Yeast R4 B7H4. C) Induced Yeast R6 B7H4. Note: Difference in population density between dot plots is due to the number of events acquired during the experiment: 20,000 events for R3 while for R4 and R5 100,000 were acquired.

7.3 Continuation of LMP1 loop 2 selection by yeast-mammalian cell panning using HEK293-LMP1

Induced Yeast R3 LMP1-l2F and Yeast R2 LMP1-l2Y scFv expressing yeast (figures 5.7.A and 5.7.B) were used as the first input for the yeast-mammalian cells panning selection with tetracycline induced HEK293-LMP1. Four rounds of yeast-induced HEK293-LMP1 panning were performed for each selection. The resulting outputs for the LMP1 loop 2F selection were named Yeast R4 LMP1-l2F, Yeast R5 LMP1-l2F, Yeast R6 LMP1-l2F and Yeast R7 LMP1-l2F. For the LMP1 loop 2Y selection, the resulting outputs were Yeast R3 LMP1-l2Y, Yeast R4 LMP1-l2Y, Yeast R5 LMP1-l2Y and Yeast R6 LMP1-l2Y. Fewer yeast binding to the flask and the control HEK293 were detected during both selections compared with the B7H4 Ig-like V-type 1 domain selection. However, no apparent interaction between yeast and the antigen-expressing mammalian cells was detected by light microscopy (figures 7.4 and 7.5).

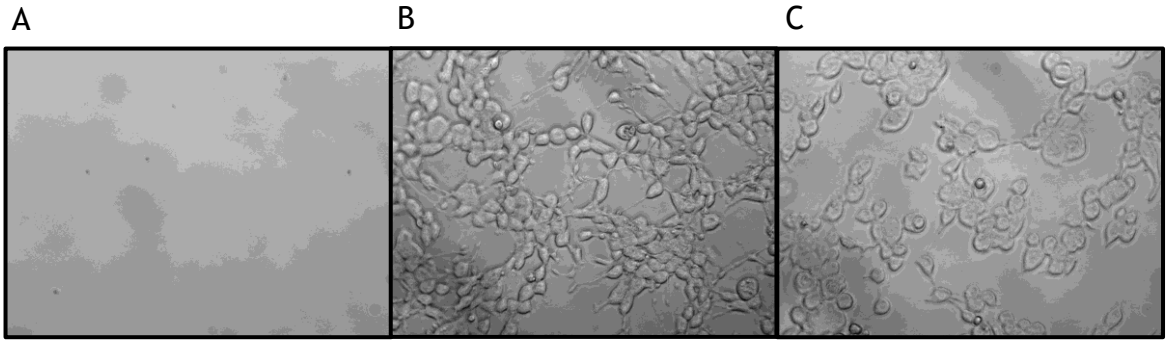

Figure 7.4 Yeast-mammalian cell panning LMP1 loop 2F selection round 7. A) Flask depletion of Yeast R6 LMP1-l2F. B) Control HEK293 depletion of flask depleted Yeast R6 LMP1-l2F. C) Selection with tetracycline induced HEK293-LMP1 of flask and control HEK293 depleted Yeast R6 LMP1-l2F giving rise to Yeast R7 LMP1-l2F.

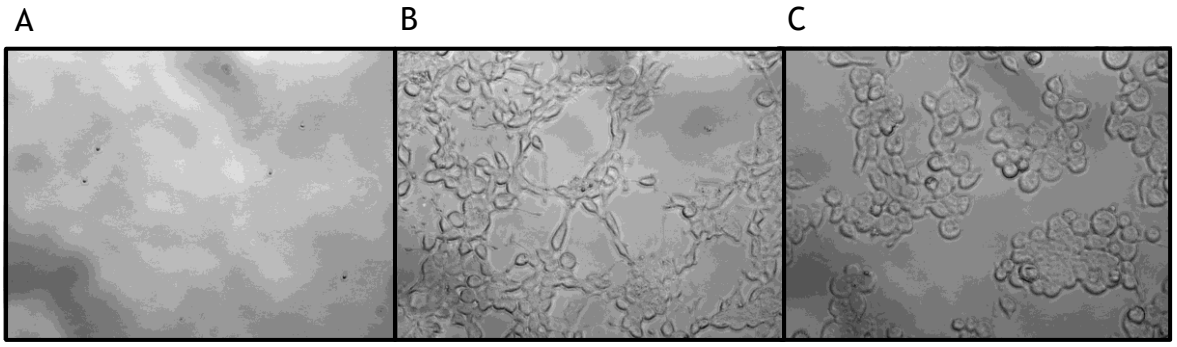

Figure 7.5 Yeast-mammalian cell panning LMP1 loop 2Y selection round 6. A) Flask depletion of Yeast R5 LMP1-l2Y. B) Control HEK293 depletion of flask depleted Yeast R5 LMP1-l2Y. C) Selection with tetracycline induced HEK293-LMP1 of flask and control HEK293 depleted Yeast R5-LMP1-l2Y giving rise to Yeast R6 LMP1-l2Y.

7.4 Continuation of LMP2 loop 2 and loop 5 selection by yeast-mammalian cells panning using HEK293-LMP2A

Induced Yeast R2 LMP2-l2 and Yeast R3 LMP2-l5 scFv expressing yeast (figures 5.7.C and 5.7.D) were used as the first input for the yeast-mammalian cells panning selection with tetracycline induced HEK293-LMP2A. Five rounds of yeast-induced HEK293-LMP2A panning were performed for each selection. The resulting outputs for the LMP2 loop 2 selection were named Yeast R3 LMP2-l2, Yeast R4 LMP2-l2, Yeast R5 LMP2-l2, Yeast R6 LMP2-l2 and Yeast R7 LMP2-l2. For the LMP2 loop 5 selection, the resulting outputs were Yeast R4 LMP2-l5, Yeast R5 LMP2-l5, Yeast R6 LMP2-l5, Yeast R7 LMP2-l5 and Yeast R8 LMP2-l5. A high level of yeast binding to the flask was detected by light microscopy during the selection.

Moreover, no clear interaction between the yeast and mammalian cells was detected (figures 7.6 and 7.7).

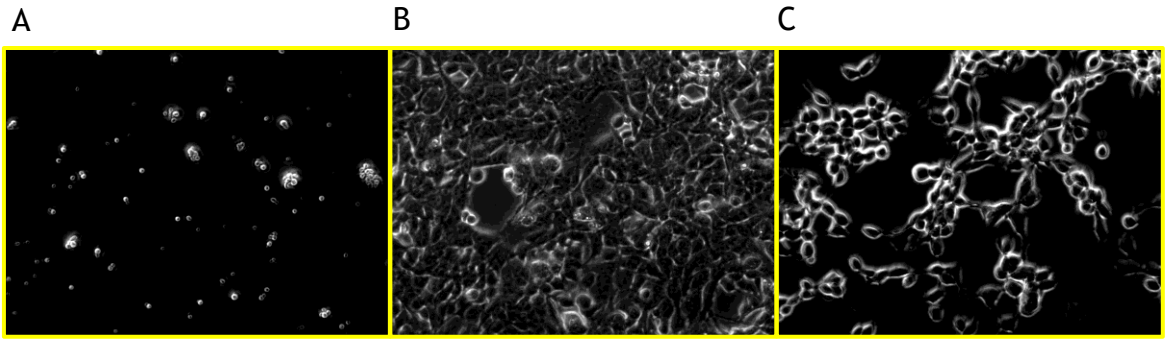

Figure 7.6 Yeast-mammalian cell panning LMP2 loop 2 selection round 7. A) Flask depletion of Yeast R6 LMP2-l2. B) Control HEK293 depletion of flask depleted Yeast R6 LMP2-l2. C) Selection with tetracycline induced HEK293-LMP2A of flask and control HEK293 depleted Yeast R6 LMP2-l2 giving rise to Yeast R7 LMP2-l2. Note: Different view than previous pictures due to inability to change the microscope setting at this moment.

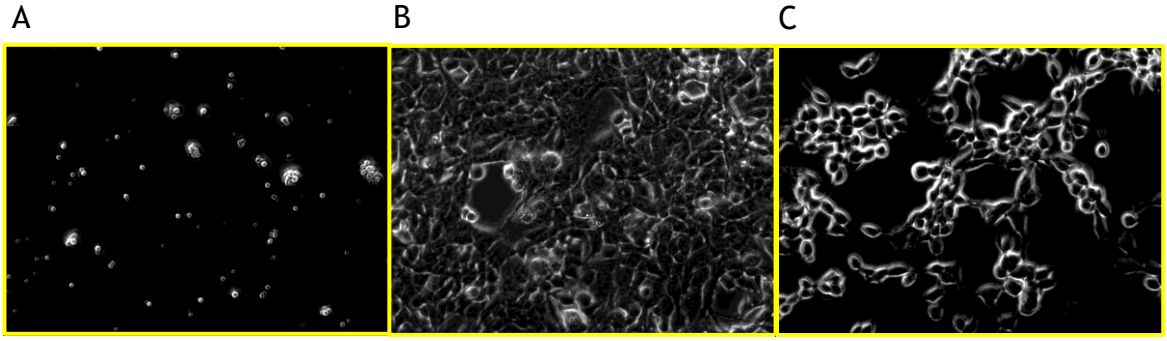

Figure 7.7 Yeast-mammalian cell panning LMP2 loop 5 selection round 8. A) Flask depletion of Yeast R7 LMP2-l5. B) Control HEK293 depletion of flask depleted Yeast R7 LMP2-l5. C) Selection with tetracycline induced HEK293-LMP2A of flask and control HEK293 depleted Yeast R7 LMP2 -l5 giving rise to Yeast R8 LMP2-l5.

7.5 Non-specific binding of yeast to the flask surface and control HEK293

To investigate the characteristic of the yeast showing binding to the flask, the yeast in the flask used in figure 7.2.A were grown. Ten colonies were used for single colony yeast lysate, PCR with the primers pYDN Check-F and pYDN Check-R and Sanger sequencing with the primer pYDN Check-F. Such yeast have been detected in all the selection performed and they competed with the possible *bona fide* antigen-specific yeast during the selection, possibly having a strong negative effect in the final outcome.

The analysis showed that all the sequenced yeast clones carried an Aga2 fusion protein with a non-functional scFv, composed of an aberrant VH chain (different amino acids than a VH chain) linked to a functional VL chain and Aga2 fusion. The presence of non-functional scFv can be explained by two frameshift mutations in the ORF during the library synthesis PCRs, one at the 5' end of the VH and another at the 3' end of the VH or the linker. The second shift in the reading frame returns the ORF to the original reading frame. While the frameshift resulting in the ending of the reading frame (with stop codons) within the scFv leads to no expression of the fusion protein (described in chapter 5), the two ORF shifts in non-functional scFvs seen here lead to an aberrant VH chain linked to an in-frame VL-Aga2 fusion (figure 7.8). These sequences appear to interact non-specifically and are promoted during the phage and yeast selection even though depletion was performed in every step.

Figure 7.8 DNA and amino acid sequence of a non-functional scFv found after yeast panning. The DNA and amino acid sequence of the linker has been highlighted in grey. The amino acids of the non-functional VH chain are coloured in red. The CDRs follow a colour code for identification: CDR1L in orange, CDR2L in pink and CDR3L golden yellow.

Example of a non-functional scFv
CAG GTG CAG CTA CAG CAG TGG GGT GGT GAG GGT CTG CAC AGC GCT CCG GGG TGG TCC GCC TCT CCC CTC CCC CAG GAC AAC TCC CGG CCG GGC CGG GAG CGC TCA CCG TCG AAA CGC TTC CTC CAG CAG GGT GCA GGA GGG GCC CGC CGT GGA ATT GGG GCT GTG GCT GAT GTA GAA GTT CTC CGG GGC GAG ATG CAG CAG GTT CGG GGT CAT CTT CAC CGA GAG CGG CAG GGG CCA CAG CGC CGG CCC CGG CTT GGC CGA GAC GCT CGG GGC CCG AGC CGC CTC CGC CAC CTG CAC CAC CAG CGC CAC CTG AGT CAG CAG CGC CAA CAT CCC CGA CCA GCC CCA AGG TCG GCA GCA GCG GCA GCA GCA GCG GTA CCA GCA GCG CGC AGC AGC AGC AGC GGC AGC GGC GAG CTC GTG ATG ACC CAG TCT CCA TCA TCC CTG TCT GCA TCT GTA GGA GAC AGA GTT AGA ATC ACT TGC CGG GCA AGT CAG AGC ATT GGC ACC TCT TTA AAA TGG ATT CAA CAG AAA CCC GGG AAA GCC CCT AGG CTC CTG ATC TAC GAT GCA TCT AAA TTG CAA AGT GGG GTC CCG TCT CGA TTC AGT GGC AGT GGA TCT GGG ACA GAT TTC TCT CTC ACC ATC CGC ACT CTG CAA CCT GAA GAT TTT GCG ACT TAC TTC TGC CTA CAG ACT TAC AGA ACC CCT CGA ACG TTC GGC CAA GGG ACC AAG GTG GAG ATC AAA

QVQLQQWGGEGLHSAPGWSASPLPQDNSRPGRERSPSKRFLQQGAGGARRGIGAVADVE VLRGEMQQVRGHLHRERQGPQRRPRLGRDARGPSRLRHLHHQRHLSQQRQHPRPAPRSA AAAAAAVPAARSSSSGSGELVMTQSPSSLSASVGDRVRITCRASQSIGTSLKWIQQKPGKAPR LLIYDASKLQSGVPSRFSGSGSGTDFSLTIRTLQPEDFATYFCLQTYRTPRTFGQGTKVEIK

7.6 Conclusions

The characteristics and utility of a phagemid library depend on its design and the molecular biology techniques applied during its creation. The chosen linker could have a substantial impact on the PCRs needed for DNA amplification of the VH and VL and their linking as scFv (figure 1.15). Furthermore, the rate of mutation of the DNA polymerase should be as low as possible. The scFv assembly PCR during the phage library synthesis could lead to changes in the ORF and the introduction of codon stops (and the production of polyphage), or the presence of non-functional scFv (and their promotion during the selection by non-specific binding). Selecting scFvs from a phagemid library carrying PCR mutations is a complicated and not always successful endeavour. Table 7.1 describes the different biases found in the scFv sequences of the phage display library used in these studies.

Table 7.1 Library biases encountered during the scFv selection process.

Library bias	Description	Effect
Non-ORF scFvs (described in chapter 5)	Shift in the ORF of the scFv leading to in frame stop codon and no expression of the fusion protein scFv-PIII in the phage display system.	Polyphage promotion
Non-functional scFvs	Shift in the ORF of the scFv leading to an aberrant VH chain fused with a functional VL and Aga2 in the yeast display system. These were also present in the phage display system fused with PIII, but they were detected during yeast panning.	Non-specific binding

The transfer of the scFv selected by phage display to a yeast display system allowed the problem with polyphage to be solved and permitted enrichment of the Aga2 fusion expressing yeast population. However, non-functional scFvs were detected during the yeast-mammalian cell panning affecting the selection of scFv through non-specific binding to the surface of the flask and the cells. Despite this, functional scFvs could be present in the outputs obtained from yeast-mammalian

cell panning. Therefore, they were further studied for the presence of functional scFv binding specifically to the antigen.

Furthermore, the possibilities of antigen-specific binding of non-functional scFv through their functional VL chain are reduced. The main driver of binding in the integration antibody-antigen usually is CDR3H motif. But further conclusion will be disclosed in the next chapter.

8. Results: FACS selection of single yeast binding to the B7H4 Ig-like V-type 1 domain

8.1 Introduction

Unlike LMP1 and LMP2A, B7H4 is a membrane protein with only one transmembrane domain. The recombinant soluble extracellular domain of B7H4 can be produced without aggregation and conserving its biological activity and presumably its native structure. These preparations can be commercially acquired and used to screen for binding to B7H4. This is an advantage for the scFv selection process compared to proteins with several transmembrane domains like LMP1 and LMP2A, where no commercial recombinant preparation is available.

A commercial recombinant antigen B7H4-Fc was used to study the presence of scFvs binding to B7H4 in the yeast outputs obtained by yeast panning using HEK293-B7H4 selection. The IgG fragment crystallizable region (Fc region) serves as a dimerization structure for the recombinant antigen and also as tag for the detection of the interaction with scFv-B7H4, by staining with an anti-Fc FITC conjugated antibody. Using a dimeric B7H4 recombinant antigen enhances the avidity of the interaction with the scFvs, increasing the sensitivity of detection. By FACS single yeast expressing scFvs and with positive binding to B7H4-Fc can be detected by double staining (figure 8.1) and isolated for colony growth and Sanger sequencing, allowing us to identify the DNA sequence of scFvs able to bind B7H4.

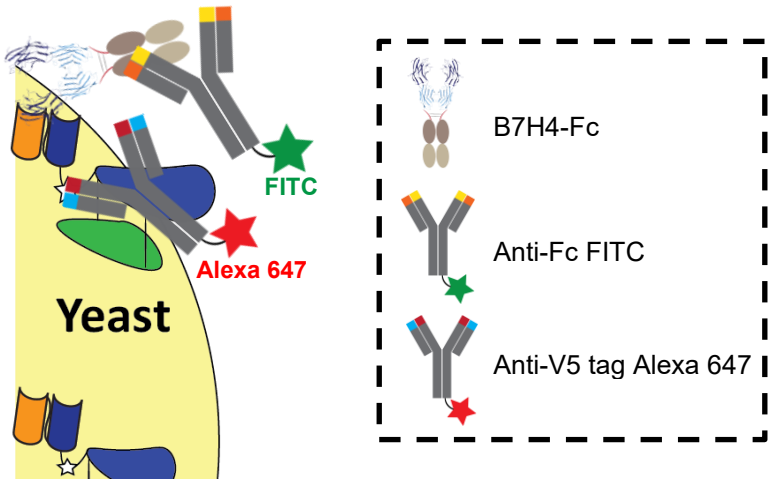

Figure 8.1 Yeast display antigen-binding staining. Yeast expressing scFv-Aga2 fusion proteins are exposed to dimeric B7H4-Fc, and then stained with the antibodies anti-Fc FITC and anti-V5 tag Alexa 647. FITC fluorescence determinates the level of antigen binding to the scFvs. Alexa 647

fluorescence determinates the level of scFv expression. Double positives FITC-Alexa 647 represent yeast expressing scFvs which bind to B7H4-Fc.

8.2 Antigen binding analysis and FACS of B7H4 outputs

Induced Yeast R4 B7H4 and Yeast R6 B7H4 were analysed by flow cytometry for antigen binding using B7H4-Fc, anti-Fc FITC and anti-V5 tag Alexa 647 (figures 8.2.B and 8.2.D). Recombinant Fc was used as a control to study the presence of yeast binding to the Fc tag of the B7H4-Fc antigen (figures 8.2.A and 8.2.C).

Yeast binding to the antigen were detected from both rounds of selection (R4 and R6) with no binding to the Fc tag (figure 8.2). Even though the percentage of double-positive yeast is equivalent between Yeast R4 B7H4 and Yeast R6 B7H4 (3.5% and 3.4% respectively), a clear difference in the binding characteristics of the two populations was detected when comparing the obtained dot plots (figures 8.2.B and 8.2.D).

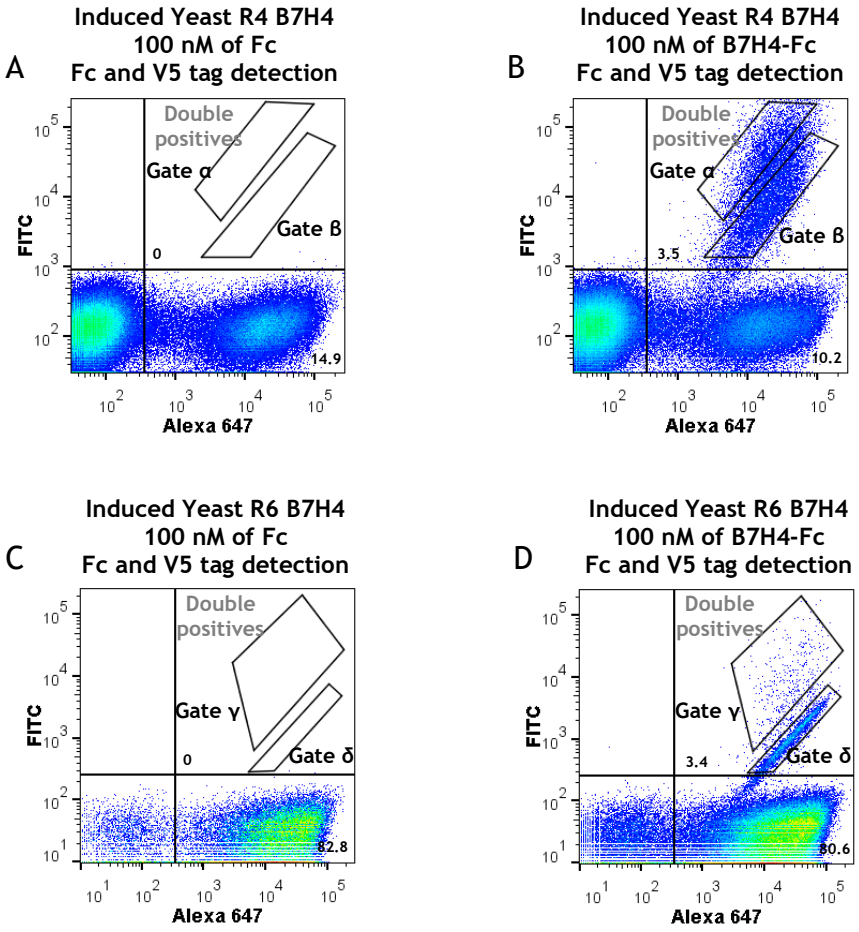

Figure 8.2 Yeast display antigen-binding FACS. Flow cytometry dot plots of yeast expressing scFv-Aga2 exposed to antigen binding and stained with anti-Fc FITC and anti-V5 tag Alexa 647.

Gates α, β, γ, and δ were used for single colony sorting. A) Induced Yeast R4 B7H4 incubated with 100 nM of Fc. B) Induced Yeast R4 B7H4 incubated with 100 nM of B7H4-Fc. C) Induced Yeast R6 B7H4 incubated with 100 nM of Fc. D) Induced Yeast R6 B7H4 incubated with 100 nM of B7H4-Fc.

8.3 Single colony Sanger sequencing

Ninety-six single yeast cells were directly sorted from gates α, ß, γ and δ (figure 8.2) onto independent SD-CAA agar plates. Ten colonies were picked and cultured from each plate for yeast lysate, PCR with the primers pYDN Check-F and pYDN Check-R, followed by Sanger sequencing with the primer pYDN Check-F. All DNA sequences obtained coded for functional scFvs. All the twenty colonies sorted from gates α and ß showed the same sequence. This clone, named Clone 3 B7H4, is dominant in the Yeast R4 B7H4 output. However, from gates γ and δ, ten different scFvs sequences were obtained from the twenty sequenced colonies. This might suggest that the yeast panning using HEK293-B7H4 re-diversified the population of scFvs binding to B7H4 from Yeast R4 B7H4 to Yeast R6 B7H4, unmasking the scFvs hidden by the dominant clone identified in Yeast R4 B7H4. A total of eleven sequences were isolated from both outputs and are detailed in figure 14 in the appendix.

8.4 Identities of the isolated VHs and VLs

The sequences of the VH and VL components of the 11 scFvs isolated were compared, revealing assortment between the two components. Five different VH and ten different VL were identified. Each of them was given an identifying number (as H_number and L_number). The gene family of each unique VH and VL sequences were determined by comparing similarities with the sequences deposited in the Ig gene repertoire of the IMGT (ImMunoGeneTics) database. Six of the identified VL sequences were placed into the sub-group L_2 due to their similarities regarding gene family and CDRs (table 8.1). The amino acid sequence for each CRD of the VH and VL chains are described in tables 8.2 and 8.3.

Table 8.1 Identified VHs and VLs and their gene family.

Clone	VH name	VH gene family	VL name	VL gene family
Clone 1 B7H4	H_1	IGHV1-69	L_1	IGKV4-1
Clone 2 B7H4	H_2	IGHV4-30-2	L_2-1*	IGKV1-12
Clone 3 B7H4	H_3	IGHV3-23	L_3	IGLV3-21
Clone 4 B7H4	H_4	IGHV3-23	L_2-2*	IGKV1-12
Clone 5 B7H4	H_4	IGHV3-23	L_2-3*	IGKV1-12
Clone 6 B7H4	H_4	IGHV3-23	L_2-4*	IGKV1-12
Clone 7 B7H4	H_4	IGHV3-23	L_2-5*	IGKV1-12
Clone 8 B7H4	H_4	IGHV3-23	L_4	IGKV3-20
Clone 9 B7H4	H_4	IGHV3-23	L_2-6*	IGKV1-12
Clone 10 B7H4	H_5	IGHV3-23	L_3	IGLV3-21
Clone 11 B7H4	H_5	IGHV3-23	L_5	IGKV3-11

*L_2 sequences have been sub-grouped due to their similarities regarding gene family and CDRs.

Table 8.2 HCRDs of identified VH chains.

VH name	HCDR1	HCDR2	HCDR3
H_1	GTFSSYAIS	WMGGIIPIFGTANY	RDSRLLRHD
H_2	GSISSGGYYWS	WIGYIYHTGTTYY	RGDLRYSDSWSDRYWYFDL
H_3	FTFSSYAMS	WVSAISGSGGSTYY	KGGGYFYFDY
H_4	FTFSSYAMS	WVSAISGSGGSTYY	RFGWFGSIDY
H_5	FTFSSYAMS	WVSAISGSGGSTYY	KISVIDYYYGMDV

Table 8.3 LCDRs of identified VL chains.

VL name	LCDR1	LCDR2	LCDR3
L_1	KSSQSVLYSSNNKNYLA	YWASTRES	QQYYSTPPT
L_2-1	RASQGISNSLA	YAASSLQS	QQSYSTPLT
L_2-2	RTSQDISTWLA	YAASNLLS	QQSYSTPQT
L_2-3	RASQGISSWLA	YAASSLQS	QQSYSTPLT
L_2-4	RASQGISSWLA	YAASSLQS	QQSYSTPHT
L_2-5	RASQGISSWLA	YAASSLQS	QQFDGSLWT
L_2-6	RASQGISSWLA	YAASSLKS	QQSYSRPT
L_3	GGNNIGSKSVH	YDDSDRPS	QVWDSSSDQ
L_4	RASQSVSSNYLA	YGASSRAT	QHYGSYPWT
L_5	RASQSVSNYLA	YDASSRAT	QQRSNWPLYT

8.5 Conclusions

The yeast clones isolated by FACS did not bind to recombinant Fc and appeared to bind specifically to B7H4. The lack of the expected increase in the percentage of double-positive yeast between Yeast R4 B7H4 and Yeast R6 B7H4 could have been due to the presence of yeast expressing non-functional scFvs (described in chapter 7) with the ability to interact with the surface of the flask and the cells.

These non-functional scFvs could have competed in binding during the yeast panning. Even though the percentage of double-positive yeast is equivalent between the R4 and R6 selections, a clear difference in the binding characteristics was observed in the dot plots (figures 8.2.B and 8.2.D), suggesting that yeast panning with HEK293-B7H4 had a positive impact in the selection of scFvs, resulting in diversification of the population of *bona fide* binders. This was supported by sequencing of single colonies sorted from both outputs.

All the sequenced clones from gates α, β, γ and δ carried functional scFvs, indicating that the non-functional scFvs, with the ability to bind the surface of the flask and the cells, were not able to bind to B7H4-Fc, even though they carry a functional VL chain. Eleven scFvs were obtained with a non-extensive screening, a further exploration of the Yeast R6 B7H4 output might reveal higher numbers of scFvs binding to B7H4.

9. Results: Antigen-binding characterisation of isolated anti-B7H4 scFvs

9.1 Introduction

To study the capacity of each isolated scFv to interact with B7H4 and the specificity of this interaction, the yeast expressing scFv clones were exposed to different B7H4 recombinant proteins: dimeric human B7H4 (human B7H4-human Fc), dimeric mouse B7H4 (mouse B7H4-mouse Fc), monomeric human B7H4 (human B7H4-10HIS) and monomeric mouse B7H4 (mouse B7H4-10HIS). Prior to this experiment, the scFv DNA was transferred again into pYDN with the objective of removing the extra amino acids AG (introduced for improving expression in pYDN), QPAMA (PelB segment at the N-terminus of the scFv) and GPGGQGGGS (phage display linker segment at the C-terminus of the scFv). These extra amino acids (described in Chapter 5) resulted from the transfer of the scFv output from the phagemid vector to pYDN (figure 9.1). The resulting pYDN-scFv vectors were used for yeast transformation. These yeast displaying the scFvs without the extra amino acids were used for binding characterisation.

Figure 9.1 Nucleotide removal from yeast clones isolated by FACS. The scFvs of each isolated yeast clone were amplified with primers to introduce 40 bp of homology with the AGA2 signal peptide (forward) and the V5 epitope (reverse) and at the same time remove the DNA coding for the AG, the "PelB segment" and the "Phage display linker segment" (green squares with a cross). The amplicons were used for yeast homologous recombination into digested pYDN, giving rise to yeast clones displaying scFvs-AGA2 fusion proteins without boxed segments. Plasmid ORFs are coloured and denoted: orange ORF AGA2 signal peptide, red AG, clear orange PelB segment, blue the scFv Clone 4 B7H4, grey the phage display linker segment and the linker with the AGA2 protein and dark red the V5 epitope. Primers used for ClnHR PCR are depicted. The middle dashed line represents the diagrammatic discontinuity between the 5' end (shown above) and the 3' end (shown below) of the fragment.

9.2 Single-clone homologous recombination into pYDN and yeast transformation

The aim of this experiment was to transfer the scFvs selected by FACS to a new pYDN vector to remove the extra amino acids that remained from the cloning process. Two PCR were required to obtain the DNA to be inserted by homologous recombination into pYDN. Each clone was grown in SD-CAA broth and the yeast DNA isolated. The lysate was used to perform a PCR with the primers ClnHR X-F and ClnHR X-R, with "X" being the clone number. Some of the ClnHR primers are shared between clones. For example, Clone 4 B7H4 shares the ClnHR forward primer with clones 6, 7, 8, 9, 10 and 11, and the ClnHR reverse primers with clones 1, 2, 5, 6, 8, 9 and 11. A second PCR with the primers ClnHR amp-F and ClnHR amp-R was needed to increase the size of the homologous recombination region. This PCR was standard for all the different clones (figure 9.2 and 9.3).

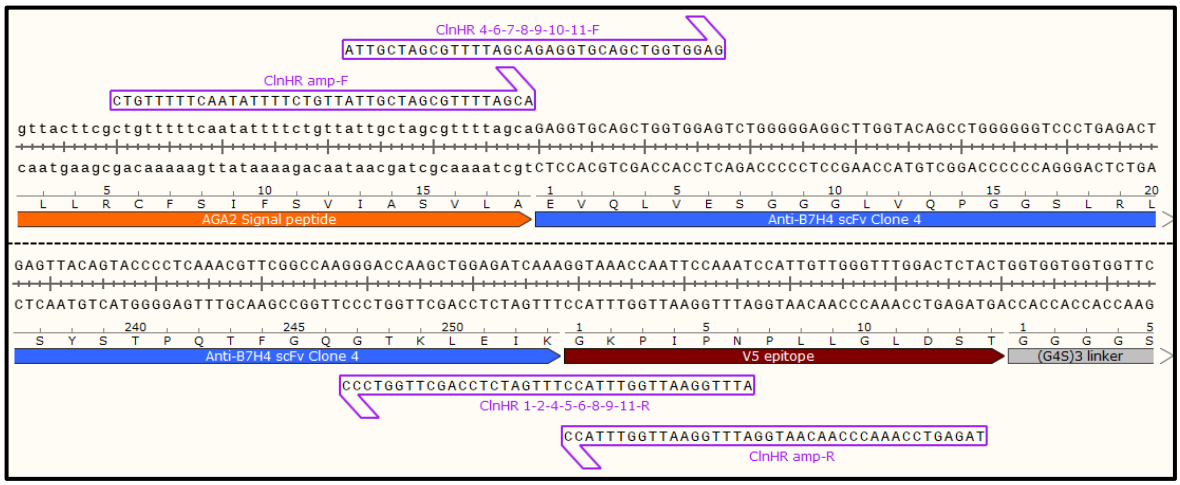

Figure 9.2 Homologous recombined Clone 4 scFvs into pYDN for binding characterisation. Plasmid ORFs are coloured and denoted: orange ORF represents the AGA2 signal peptide, blue the scFv Clone 4 B7H4, dark red the V5 epitope and grey the linker with the AGA2 protein. Primers used for ClnHR PCR and ClnHR amp PCR depicted. The middle dashed line represents the diagrammatic discontinuity between the 5' end (shown above) and the 3' end (shown below) of the fragment.

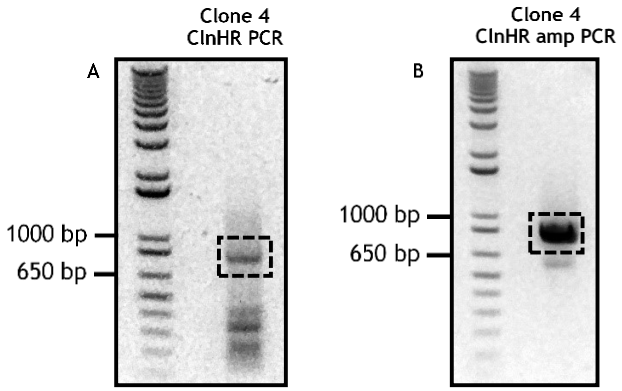

Figure 9.3 ClnHR and ClnHR amp PCRs for the scFv Clone 4 B7H4. PCR products were electrophoresed through 1% agarose. The dashed boxes show DNA band excision for purification of the ≈850 bp DNA fragments.

9.2.1 Yeast transformation, homologous recombination and selection

Yeast *S. cerevisiae* EBY100 was transformed (following the lithium acetate/single-stranded carrier DNA/polyethylene glycol method) with *Eco*RI digested pYDN and the gel-purified PCR products from each ClnHR amp PCR of each isolated scFv clone. After the transformation, the yeast were selected in SD-CAA agar. Single colonies from each clone transformation were grown in SD-CAA and the yeast DNA isolated by treatment with lysate buffer containing lyticase. The lysates were used to perform PCRs with the primers pYDN Check-F and pYDN Check-R. The PCR amplicons were sent for Sanger sequencing together with the primer pYDN Check-F to confirm the scFvs sequences.

9.3 Single-clone yeast antigen-binding analysis by flow cytometry

Each yeast clone obtained (transformed with each isolated scFv-Aga2 fusion without the extra amino acids resulting from the transference from phage display to yeast display) was grown and induced to explore the expression of the fusion proteins. The V5 tag, present in the fusion protein expressed by pYDN, was detected by flow cytometry with the antibody anti-V5 tag FITC conjugated. The binding to dimeric human B7H4 was assessed by incubating the yeast with 100 nM of human B7H4-human Fc followed by incubation with anti-human Fc FITC conjugated. Furthermore, the specificity was evaluated by incubation with 100 nM of mouse B7H4-mouse Fc followed by incubation with anti-mouse IgG Alexa

488. The binding to monomeric human B7H4 was assessed by incubation with 100 nM of human B7H4-10HIS followed by incubation with anti-HIS tag Alexa 647. The specificity was also evaluated by incaution with mouse B7H4-10HIS followed by incubation with anti-HIS tag Alexa 647 (figure 9.4).

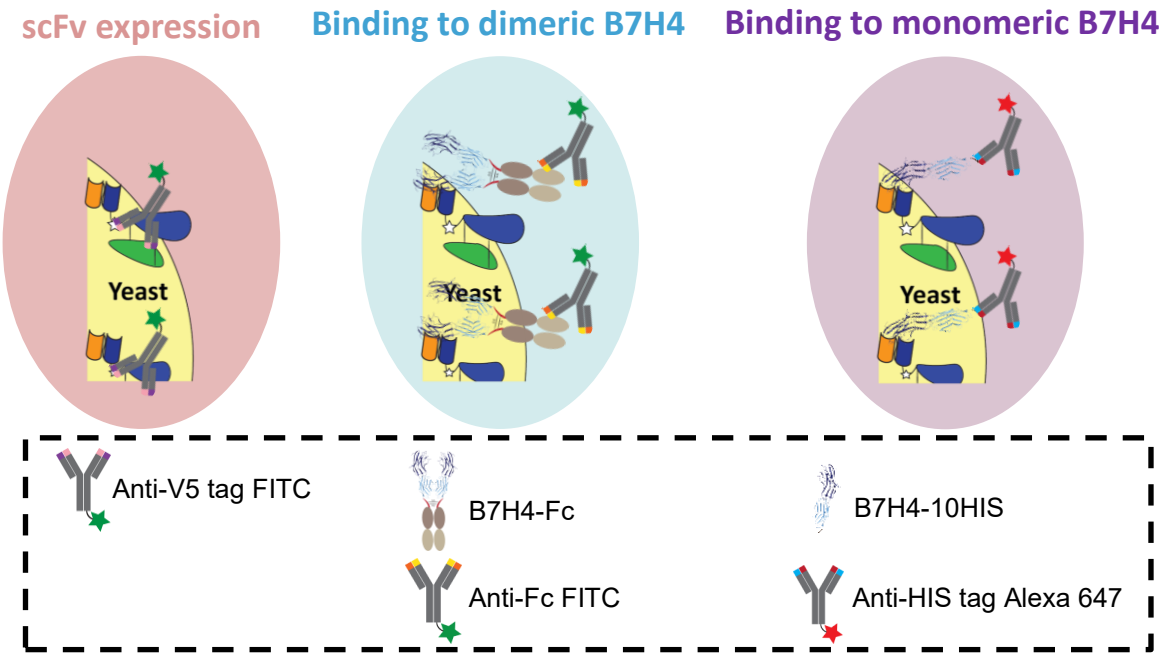

Figure 9.4 Schematic representation of the flow cytometry approaches for antigen-binding analysis. scFv expression assessed with the use of anti-V5 tag FITC conjugated. Binding to dimeric B7H4 was studied by incubation with B7H4-Fc fusion protein and subsequent detection with anti-Fc FITC or Alexa 488 conjugated. Binding to monomeric B7H4 was determined by incubation with B7H4-10HIS and subsequent detection with anti-HIS tag Alexa 647.

The samples were analysed by flow cytometry to assess the binding (figures 9.5 to 9.16). The percentages of positive binding to each antigen for each yeast clone is summarised in table 9.1. scFv clones binding to dimeric B7H4 but not to monomeric B7H4 were classified as very low-affinity binders, when the population binding to dimeric B7H4 was below 20%, and low-affinity binders when the population binding to dimeric B7H4 was above 20%. scFv clones binding to dimeric B7H4 and monomeric B7H4 were classified as medium-affinity binders, when the population binding to monomeric B7H4 was below 20%, and high-affinity binders when the population binding to monomeric B7H4 was above 20% (table 9.1).

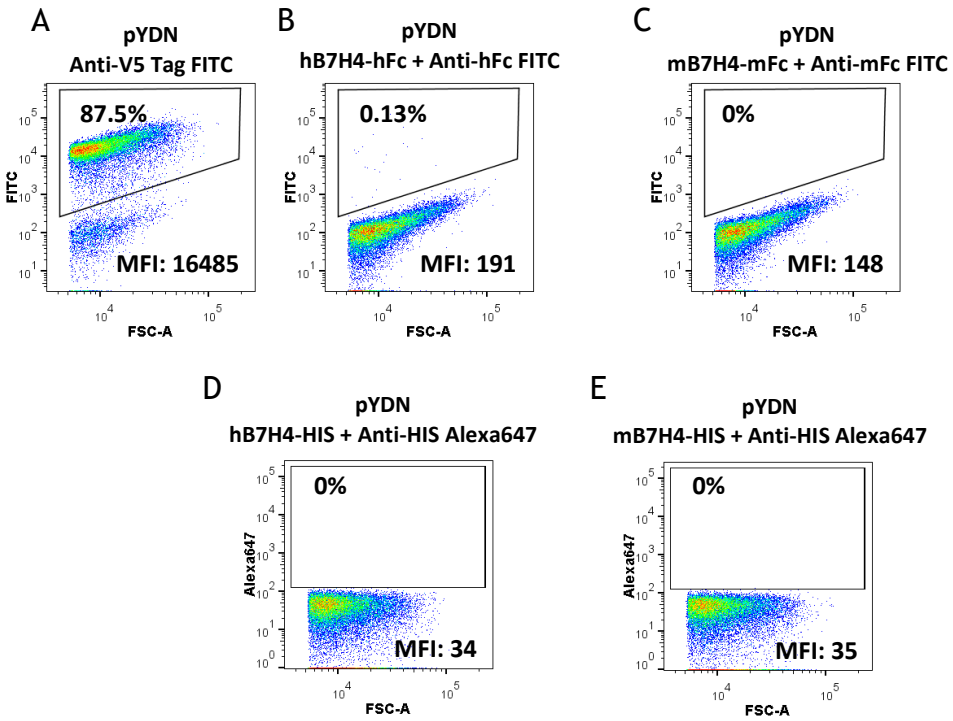

Figure 9.5 Induced control pYDN yeast stained and analysed by flow cytometry following antigen-binding. pYDN Anti-V5 Tag FITC dot plot represents AGA2 fusion protein expression. pYDN hB7H4-hFc + Anti-hFc FITC dot plot represents the analysis of binding to dimeric human B7H4. pYDN mB7H4-mFc + Anti-mFc FITC dot plot represent the analysis of binding to dimeric mouse B7H4. pYDN hB7H4-HIS + Anti-HIS Alexa647 dot plot represents the analysis of binding to monomeric human B7H4. pYDN mB7H4-HIS + Anti-HIS Alexa647 dot plot represents the analysis of binding to monomeric mouse B7H4. Dot plots in figures 9.6 to 9.16 follow the same pattern.

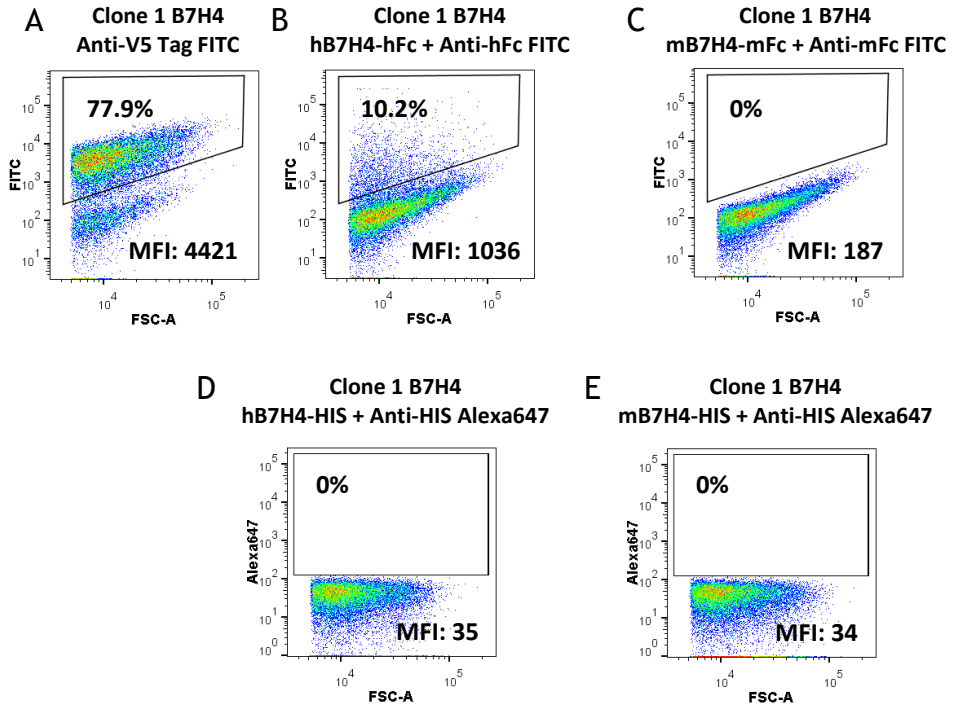

Figure 9.6 Induced Clone 1 B7H4 yeast stained and analysed by flow cytometry following antigen-binding. Refer to figure 9.5 for dot plots description.

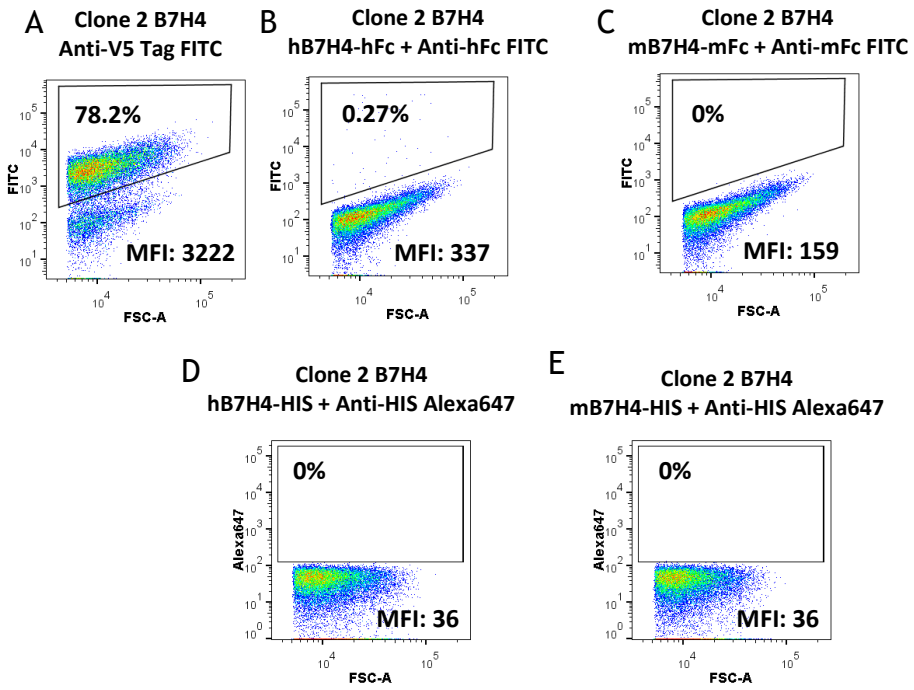

Figure 9.7 Induced Clone 2 B7H4 yeast stained and analysed by flow cytometry following antigen-binding. Refer to figure 9.5 for dot plot description.

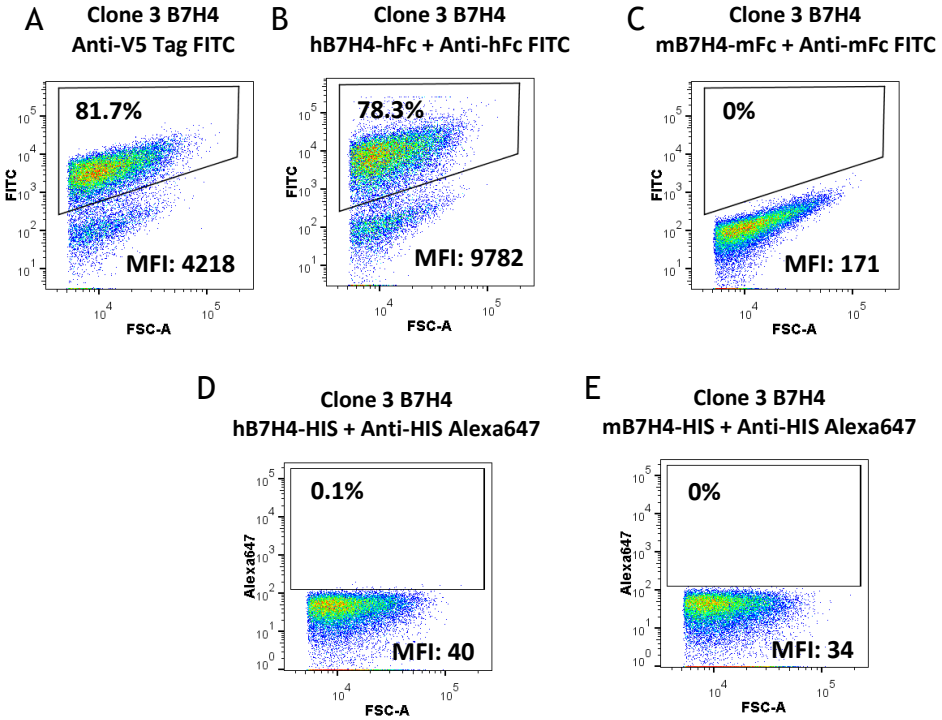

Figure 9.8 Induced Clone 3 B7H4 yeast stained and analysed by flow cytometry following antigen-binding. Refer to figure 9.5 for dot plots description.

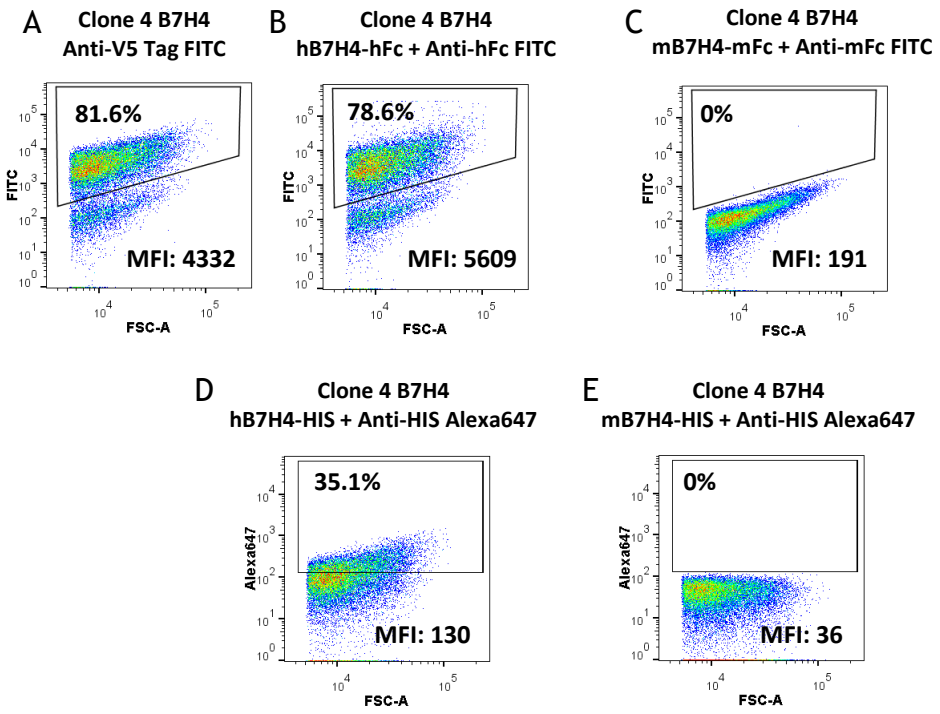

Figure 9.9 Induced Clone 4 B7H4 yeast stained and analysed by flow cytometry following antigen-binding. Refer to figure 9.5 for dot plots description.

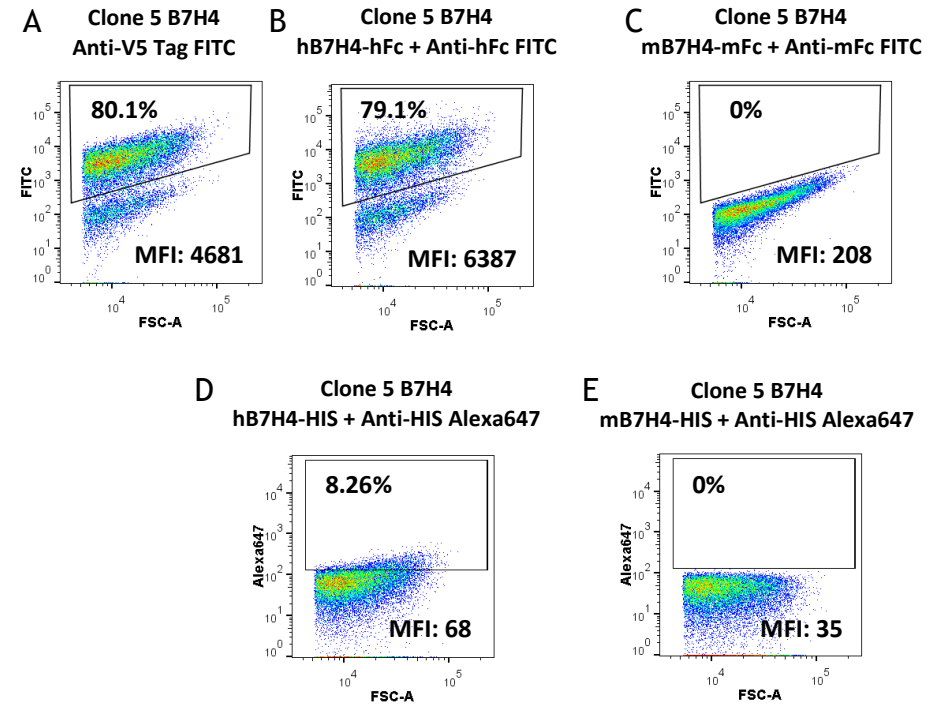

Figure 9.10 Induced Clone 5 B7H4 yeast stained and analysed by flow cytometry following antigen-binding. Refer to figure 9.5 for dot plots description.

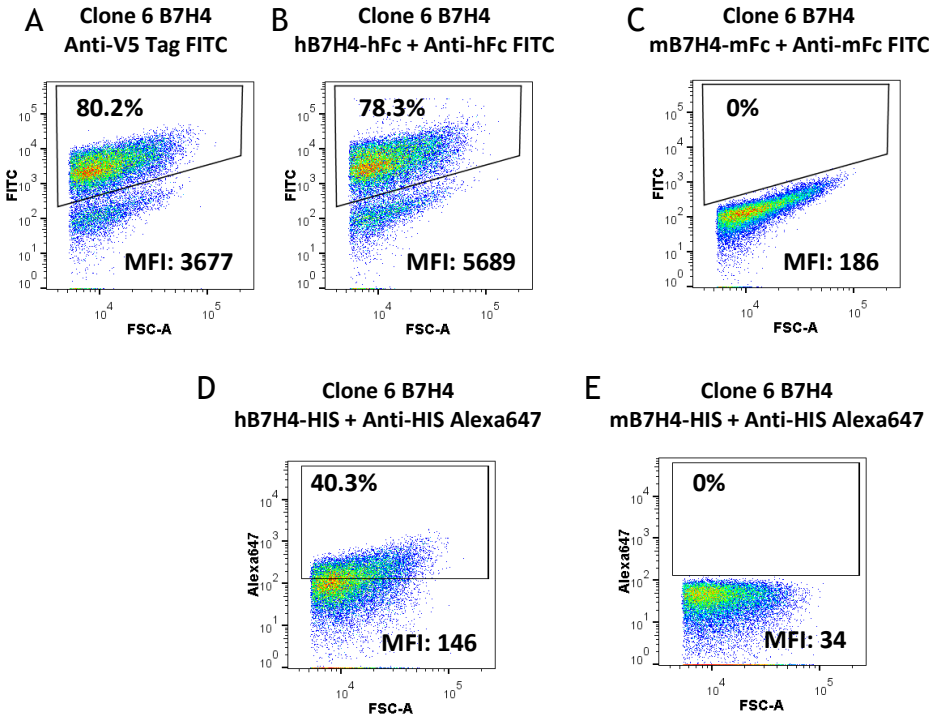

Figure 9.11 Induced Clone 6 B7H4 yeast stained and analysed by flow cytometry following antigen-binding. Refer to figure 9.5 for dot plots description.

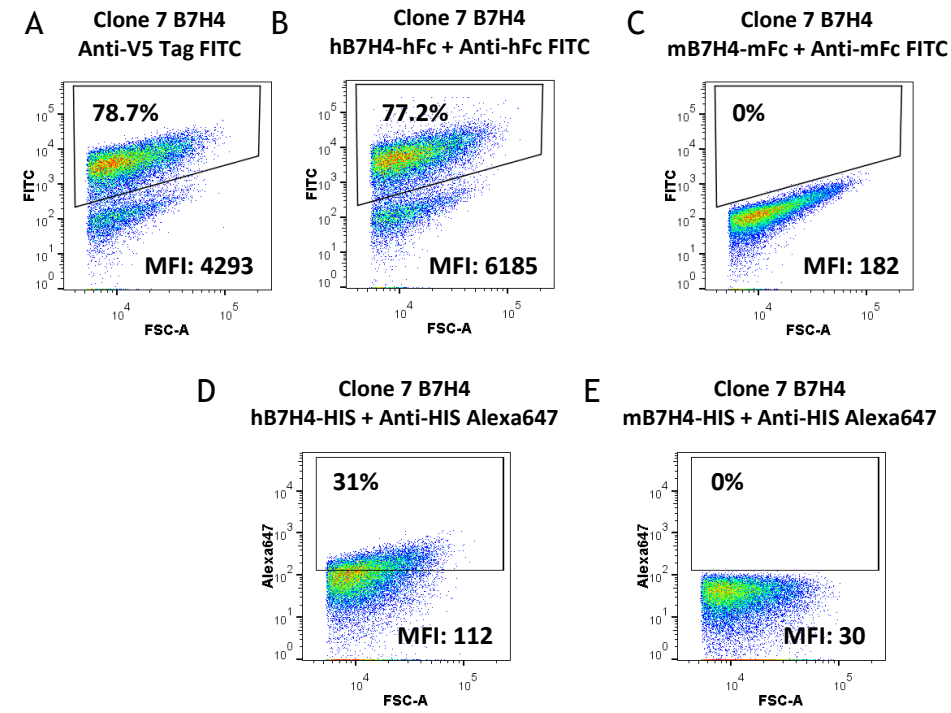

Figure 9.12 Induced Clone 7 B7H4 yeast stained and analysed by flow cytometry following antigen-binding. Refer to figure 9.5 for dot plots description.

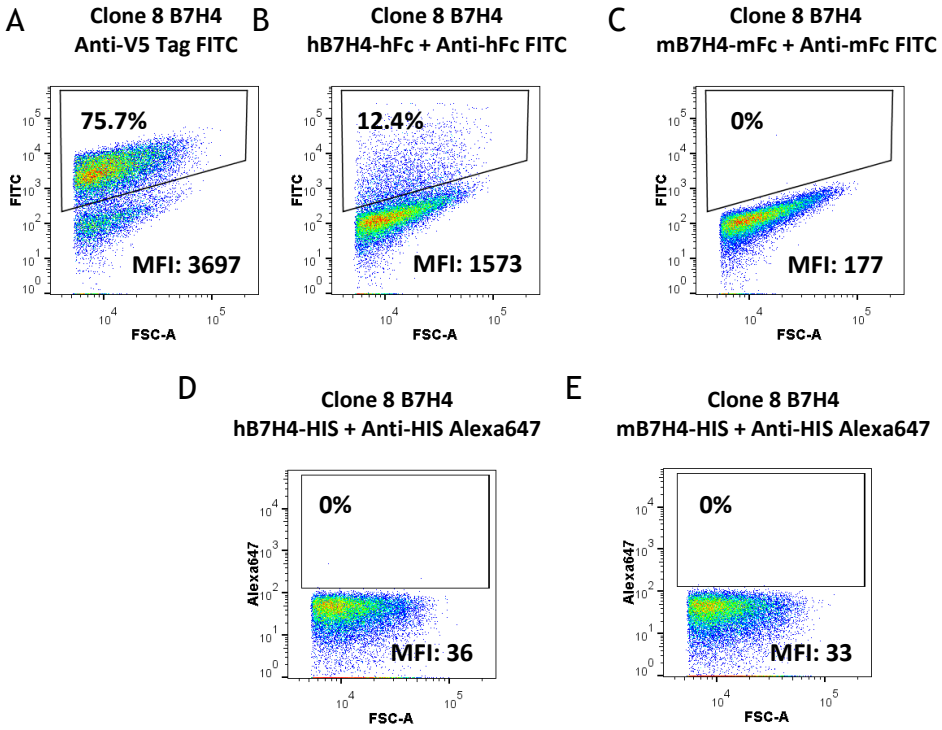

Figure 9.13 Induced Clone 8 B7H4 yeast stained and analysed by flow cytometry following antigen-binding. Refer to figure 9.5 for dot plots description.

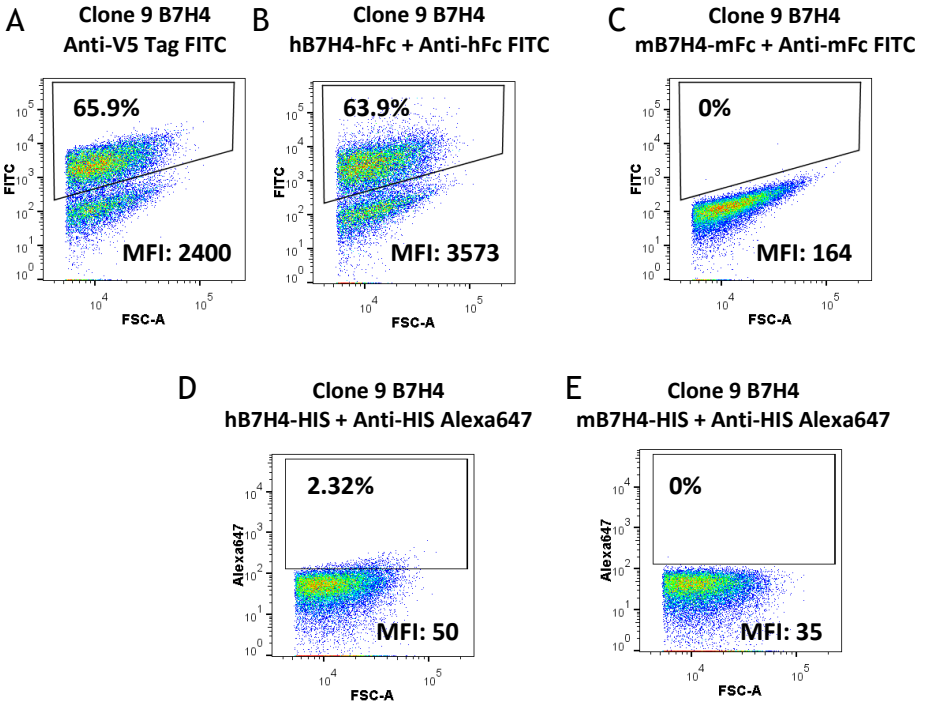

Figure 9.14 Induced Clone 9 B7H4 yeast stained and analysed by flow cytometry following antigen-binding. Refer to figure 9.5 for dot plots description.

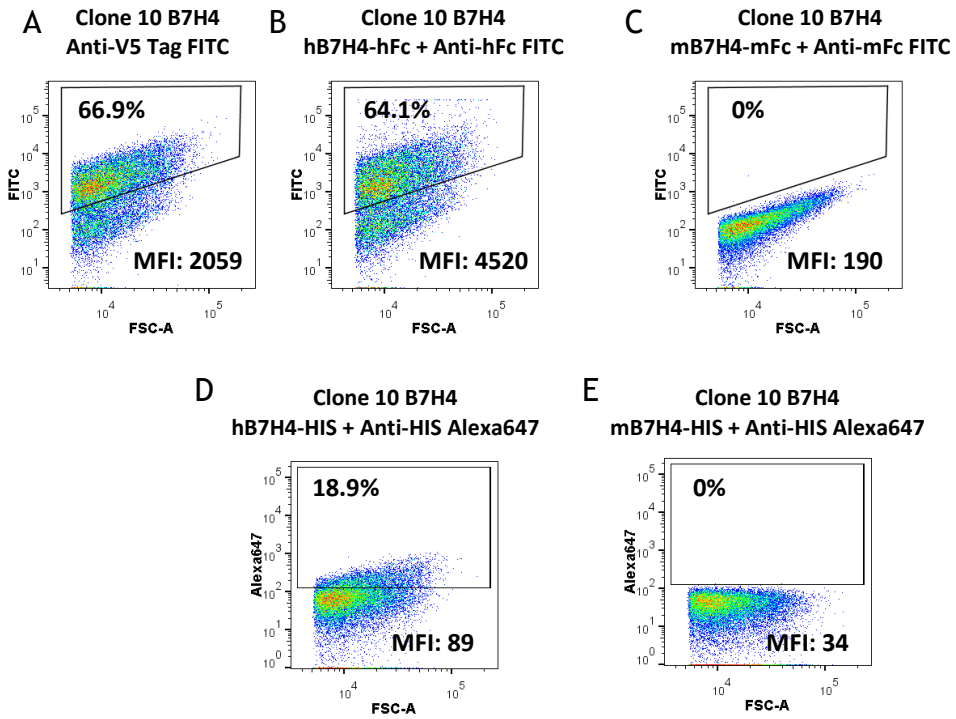

Figure 9.15 Induced Clone 10 B7H4 yeast stained and analysed by flow cytometry following antigen-binding. Refer to figure 9.5 for dot plots description.

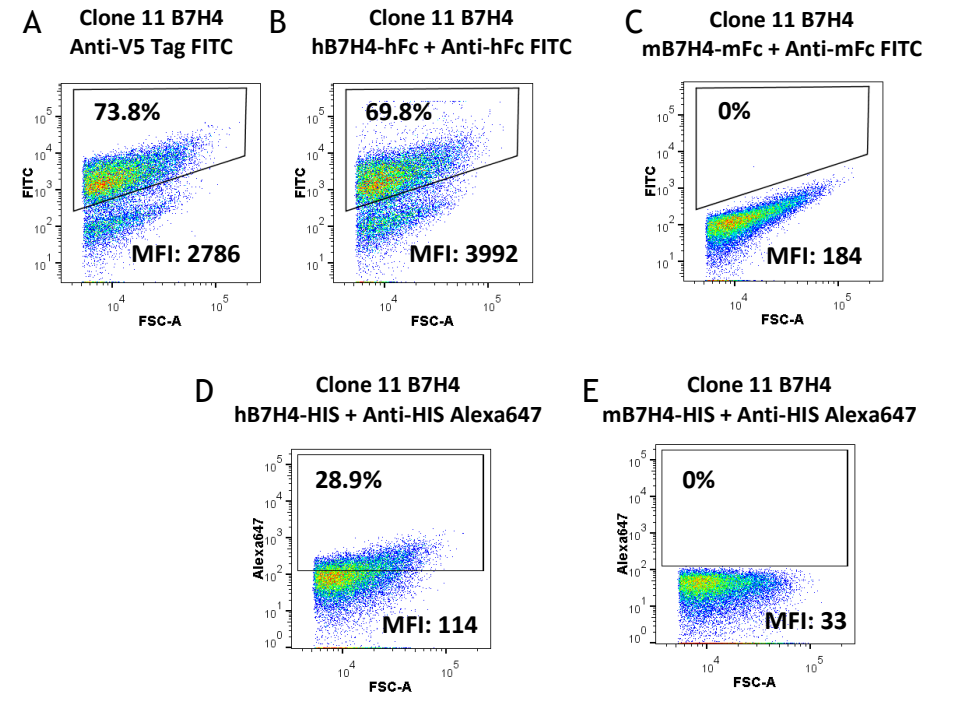

Figure 9.16 Induced Clone 11 B7H4 yeast stained and analysed by flow cytometry following antigen-binding. Refer to figure 9.5 for dot plots description.

9.4 Conclusions

The expression of the isolated scFvs was characterised in scFv-AGA2 fusion protein format on the yeast surface. Wang et al. 2005 reported that the amino acids "AG" (at the N-terminus of the scFv and before the AGA2 signal peptide) were necessary for the processing of the Aga2 signal peptidase when expressing scFv-Aga2 in VL-VH format with pYD5 (474). In this experiment, it has been observed that VH-VL scFv-Aga2 are properly expressed with pYDN (similar to pYD5) without requiring the incorporation of the amino acids "AG" at the N-terminus. All the scFv isolated showed good levels of expression on yeast in the scFv-Aga2 format.

The binding to different recombinant antigens was also studied. All the isolated scFvs showed specific binding to human B7H4, even though both proteins share a very similar amino acid sequence with 87% identity. However, a positive control for binding to mouse B7H4 would be needed to confirm that they are not false negatives.

The binding was characterised using 100 nM of dimeric or monomeric human B7H4. The use of dimeric B7H4 allows identification of low-affinity binding due to the cooperative strength of multiple affinities (avidity) when binding to the two proximal B7H4 arms present in the homodimer. Differences in the level of binding to the same concentration of human B7H4 antigens (dimeric and monomeric) was observed between the different scFvs. This could be indicative of binding with different affinities. Nevertheless, different detection reagents were used for dimeric and monomeric antigens, and further binding kinetic analysis of the scFvs is needed to confirm this. The low levels of fluorescence obtained in the staining with monomeric antigen (compared with the dimeric antigen) may be due to the nature of the staining. In the case of the dimeric antigen, more B7H4 dimeric molecules may bind to the yeast surface. Commonly, the two B7H4 arms of the dimer would lead to interaction with scFvs. Still, it is possible that in some cases, just one arm interacts, leading to a higher number of Fc tags on the yeast surface compared with the number of HIS tags obtained with the monomer staining. Even though the monomeric antigen has a ten-histidine tail and the antibody used is an anti-5HIS (recognising five histidines), most probably only one antibody can bind this tag, masking the remaining histidines for further binding.

Regarding the binding of Clone 1 B7H4 and Clone 8 B7H4 to dimeric human B7H4, despite good homogeneity in surface expression, according to the anti-V5 staining, some yeast show a high level of binding while most of them none. This can be due to the low binding affinity at this antigen concentration or the tendency to aggregate the scFvs displayed. Further binding analysis with higher concentrations of dimeric B7H4 antigen could be performed to discard the latter.

A summary of the obtained Mean fluorescent intensities (MFI) is shown in table 9.1. Based on the binding characterisation and the sequence diversity, four scFv sequences, Clone 3 B7H4, Clone 5 B7H4, Clone 7 B7H4 and Clone 11 B7H4, were taken forward by TC Biopharm Ltd. to use them in the construction of Chimeric Co-stimulatory Receptors (Co-Stim CARs), express them in Vγ9Vδ2 T-cells and investigate their efficacy.

Table 9.1 Summary of MFIs obtained from the flow cytometry analysis of expression and binding.

Anti-B7H4 scFv clone	Expression levels (MFI) FITC	Yeast binding at 100 nM (MFI)				Delivered to TC Biopharm
		Dimeric hB7H4 FITC	Monomeric hB7H4 Alexa 647	Dimeric mB7H4 FITC	Monomeric mB7H4 Alexa 647	
pYDN	16487	191	34	148	35	Control
Clone 1	4421	1036	35	198	34	X
Clone 2	3222	337	36	159	36	X
Clone 3	4218	9782	40	171	34	Selected
Clone 4	4332	5609	130	191	36	X
Clone 5	4681	6387	68	208	35	Selected
Clone 6	3677	5689	146	186	34	X
Clone 7	4293	6185	112	182	30	Selected
Clone 8	3697	1573	36	177	33	X
Clone 9	2400	3573	50	164	35	X
Clone 10	2059	4520	89	190	34	X
Clone 11	2786	3992	114	184	33	Selected

10. Results: Functional characterisation of CARs

10.1 Introduction and plan

The original plan for functional characterisation of the isolated scFvs as CAR was to deliver Co-Stim CARs constructs by lentivirus into Vγ9Vδ2 T-cells. Four scFvs were selected (Clone 3 B7H4, Clone 5 B7H4, Clone 7 B7H4 and Clone 11 B7H4) and sent to TC Biopharm Ltd. to generate the vectors and the cells for this purpose. The vectors were generated, but then several issues and the COVID-19 pandemic impacted this work and an alternative plan within the lab setting was actioned to assess functionality.

To study the functionality of each isolated scFv in CAR format, the NF-κB reporter cell line Jurkat-Dual was acquired from InvivoGen. This cell line has a luciferase reporter gene controlled by NF-κB consensus transcriptional response elements (kappa-B sites), allowing the study of NF-κB pathway activation by monitoring the production and activity of luciferase. Two different second-generation CAR constructs were chosen for the scFv candidates. The hinge-space domain defines the distance between the antigen-binding domain and the plasma membrane. The extracellular length of the CAR, together with the position of the target epitope, has been shown to be critical for optimal delivery of an activation signal (182,183). Therefore, a short construct (using the CD8 hinge-spacer domain and CD8 transmembrane domain) (185) and a long construct (using the hinge, CH2 and CH3 domains of IgG4 and the CD28 transmembrane domain) (180) have been used to test the functionality of our CARs (figure 10.1). Both constructs have been generated with a Kozak consensus sequence around the starting methionine codon (ATG), the CD8 signal peptide, and the 4-1BB and CD3ζ endodomains. 4-1BB costimulation endodomain was chosen for the CAR constructs over other endodomains (such as CD28 or OX40) because its costimulation signal leads to the activation of both the canonical and non-canonical NF-κB pathways (498–501). Therefore, it was postulated that this would be optimal to assess the functionality of second-generation CARs in the Jurkat-Dual cell system.

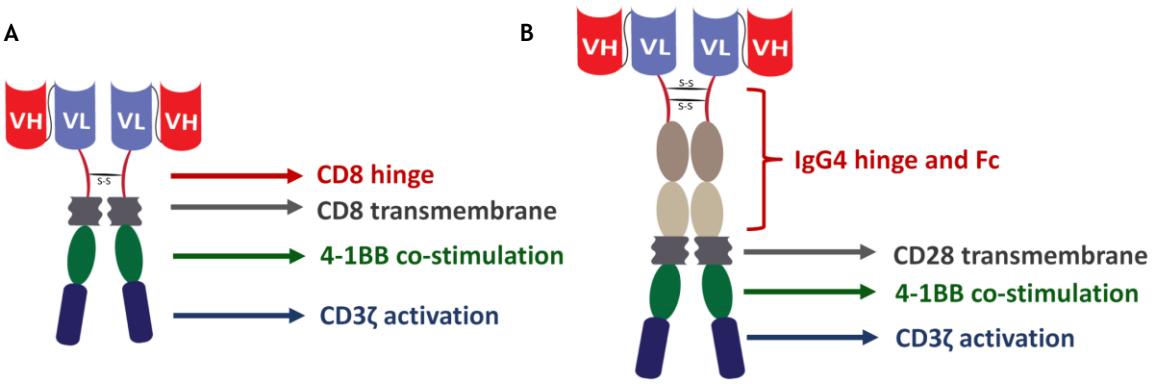

A) Short CAR DNA
Kozak - CD8 SP - **scFv** - CD8 HS - CD8 TM - 4-1BB ED - CD3ζ ED
B) Long CAR DNA
Kozak - CD8 SP - **scFv** - IgG4 HS - CD28 TM - 4-1BB ED - CD3ζ ED

*SP=Signal peptide; HS=Hinge-spacer; TM=Transmembrane; ED=Endodomain.

Figure 10.1 Second-generation CAR constructs used to functionally characterise the isolated scFvs. A) Short CAR based on the CD8 hinge and transmembrane domains. B) Long CAR based on the IgG4 hinge and Fc and the CD28 transmembrane domains.

Initially, the Jurkat-Dual cells were exposed to 1 µg/ml of G418 to assess the effectivity of the antibiotic when using the plasmid pcDNA3.1 (+). After 3 weeks, around 80% of the cells were still viable. The same experiment was performed with 200 µg/ml of hygromycin, and after two weeks, 100% of the cells were dead. Therefore, it was decided to change the NeoR gene for the HygR gene, giving rise to pcDNA3.1-hygr (section 10.2.1). After the development of pCD8-Cassette (sections 10.2.2), the scFv Clone 4 B7H4 was cloned, and the resulting plasmid used in an attempt to integrate it randomly into the genome by nucleofection and hygromycin selection. However, after four weeks of hygromycin selection, there were not viable cells detected. Consequently, the plasmids pCD8-Cassette and pIgG4-Cassette were modified to knock-in the constructs into the genome using Cas9-mediated homology-directed repair (HDR) (figure 10.2) giving rise to the plasmids pCD8-CAR and pIgG4-CAR (section 10.2.4). Finally, the plasmids pCD8-CAR and pIgG4-CAR were used to obtain the plasmids pCD8-CAR Clone X and pIgG4-CAR Clone X, where X is the name of the scFv, by cloning the scFv into the cassette (section 10.2.5). pCD8-CAR Clone X and pIgG4-CAR Clone X were the plasmids used to guide the integration of the plasmids, by Cas9-mediated HDR, into the safe harbour genetic locus *AAVS1* within the *PPP1R12C* gene (502) (figure 10.3).

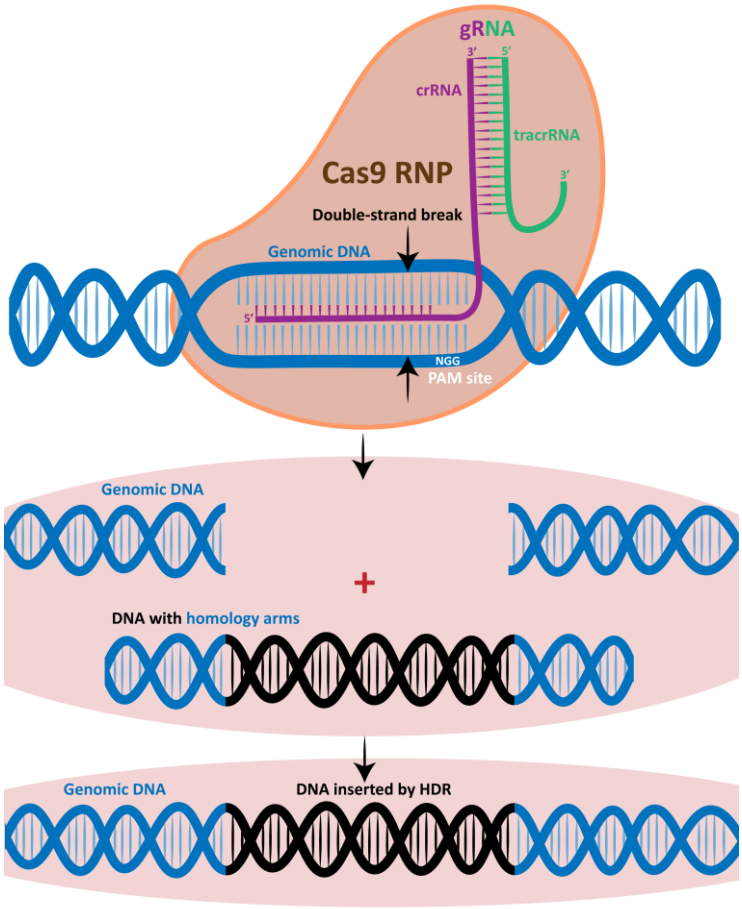

Figure 10.2 Cas9-mediated homology-directed repair (HDR). CRISPR associated protein 9 (Cas9) is a 160 kDa dual RNA-guided DNA endonuclease enzyme that can be directed to produce double-strand breaks in a specific part of the genome. To do this, Cas9 requires a guide RNA (gRNA) composed of two associated RNAs: the CRISPR RNA (crRNA) and the trans-activating crRNA (tracrRNA). Furthermore, the DNA sequence immediately following the targeted DNA, known as the protospacer adjacent motif (PAM), must be the canonical sequence 5'-NGG-3'. Lack of the PAM sequence would lead to unsuccessful binding and cleavage of the target DNA. A double-standard break of the genomic DNA can lead to HDR in the presence of a DNA template with homology arms adjacent to the digested genomic DNA. Therefore, foreign DNA can be inserted into the genome by Cas9-mediated HDR.

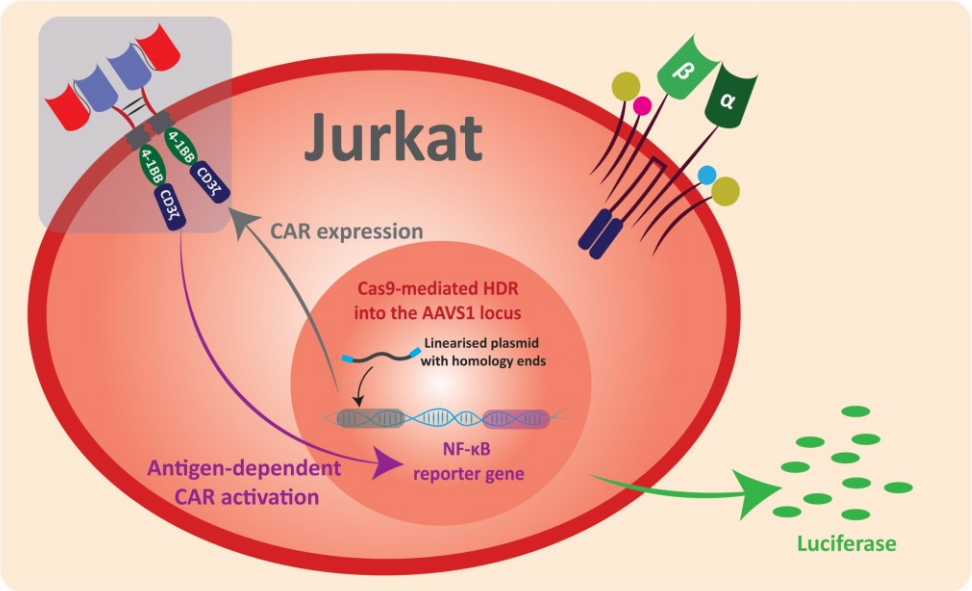

Figure 10.3 Jurkat reporter CAR T-cell line to study antigen-driven CAR activation. The Jurkat-Dual cell line (an NF-κB reporter human T-cell line) is depicted as modified cell expressing a second-generation CAR with the endodomains of 4-1BB and CD3ζ. The plasmids pCD8-CAR Clone X or pIgG4-CAR Clone X, carrying the sequence coding for the CARs under the promoter EF-1α, would be integrated by Cas9 mediated HDR into the safe harbour locus *AAVS1* and cells would then be resistant to hygromycin for selection and expansion. CAR antigen-dependent stimulation would lead to the activation of the NF-κB pathway and the luciferase reporter gene controlled by kappa-B sites. Luciferase is secreted to the medium in proportion to the level of T-cell activation. A non-functional CAR would be expected to show no such activation compared to control.

10.2 Development of pCD8-CAR Clone X and pIgG4-CAR Clone X plasmids

To express the CARs derived from the isolated scFvs, two mammalian expression vectors were designed with two different CAR cassettes (short construct and long construct) into which the DNA sequence of each isolated scFvs could be cloned, as detailed below. These plasmids were derived from the backbone plasmid pcDNA 3.1 (+) with the neomycin resistance gene. Due to the resistance of Jurkat-Dual cells to high concentrations of the antibiotic G418, the antibiotic resistance gene of pcDNA 3.1 (+) was swapped with a hygromycin resistance gene, giving rise to pcDNA3.1-hygr. Next, the CAR DNA cassettes were cloned into pcDNA3.1-hygr giving rise to the plasmids pCD8-Cassette and pIgG4-Cassette. Then, pCD8-Cassette and pIgG4-Cassette were modified by cloning the homology arms to the safe harbour locus *AAVS1*, giving rise to pCD8-Cass-HR and pIgG4-Cass-HR. Finally, the original CMV promoter was replaced by the EF-1α promoter, more suitable for CAR expression (201,503), giving rise to the plasmids pCD8-CAR and pIgG4-CAR. pCD8-CAR and pIgG4-CAR were finally used to incorporate the isolated scFvs and

the resulting plasmids (pCD8-CAR Clone X and pIgG4-CAR Clone X) were transfected into Jurkat-Dual with the Cas9 RBP.

10.2.1 Development of pcDNA3.1-hygr

To replace the neomycin resistance gene of pcDNA3.1 (+) with a hygromycin resistance gene, a synthetic DNA cassette was obtained from GeneWiz containing the sequences of the gene hph, coding for hygromycin B phosphotransferase (HPH), flanked by *Xma*I and *Bst*Z17I sites for cloning into pcDNA3.1 (+). The DNA sequence (figure 15 in the appendix) was provided by the manufacturer in a plasmid (pHygr) and codes for the amino acid sequence shown in figure 10.4.

Figure 10.4 Amino acid sequence encoded by the hph DNA cassette.

Amino acid sequence of hygromycin B phosphotransferase
MKKPELTATSVEKFLIEKFDSVSDLMQLSEGEESRAFSFDVGGRGYVLRVNSCADGFYKDRY VYRHFASAALPIPEVLDIGEFSESLTYCISRRAQGVTLQDLPETELPAVLQPVAEAMDAIAAAD LSQTSGFGPFGPQGIGQYTTWRDFICAIADPHVYHWQTVMDDTVSASVAQALDELMLWAE DCPEVRHLVHADFGSNNVLTDNGRITAVIDWSEAMFGDSQYEVANIFFWRPWLACMEQQT RYFERRHPELAGSPRLRAYMLRIGLDQLYQSLVDGNFDDAAWAQGRCDAIVRSGAGTVGRT QIARRSAAVWTDGCVEVLADSGNRRPSTRPRAKE

The DNA cassette was released from the plasmid pHygr with *Xma*I and *Bst*Z17I digestion and used for ligation with *Xma*I and *Bst*Z17I digested pcDNA3.1 (+) (figure 10.4) to obtain the final plasmid pcDNA3.1-hygr.

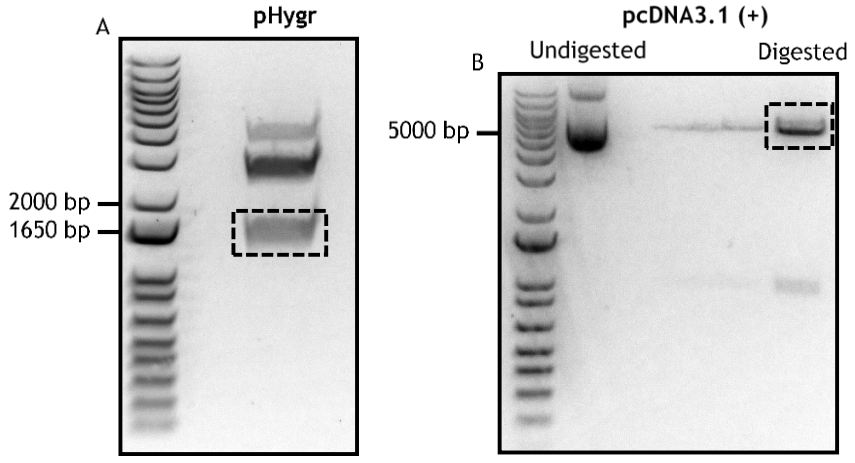

Figure 10.5 Development of pcDNA3.1-hygr. A) Digested plasmid pHygr DNA was electrophoresed through 1% agarose. The *Xma*I and *Bst*Z17I fragment was purified. B) *Xma*I and *Bst*Z17I digested plasmid pcDNA3.1 (+) DNA was electrophoresed through 1% agarose. The vector was purified and used to clone the purified fragment obtained from pHygr, giving rise to pcDNA3.1-hygr. The dashed boxes show the 1395 bp and 4326 bp DNA bands excised for DNA purification.

After *E. coli* transformation, three colonies were grown and used for colony PCR with the primers pcDNA3.1 Hygr Check-F and pcDNA3.1 Hygr Check-R. The PCR amplicons were purified and sequenced with the primers pcDNA3.1 Hygr Check-F and SeqHygr-F. The three colonies showed the correct sequence, giving rise to the plasmid pcDNA3.1-hygr (figure 10.6). One colony was used for DNA plasmid production and glycerol stocks.

Figure 10.6 pcDNA3.1-hygr. Plasmid features and ORFs are coloured and denoted: the white arrow represents the SV40 promoter, light green box the hph ORF and the grey box the SV40 poly(A) signal. The middle dashed line represents the diagrammatic discontinuity between the 5' end (shown above) and the 3' end (shown below) of the fragment. Primers for PCR and sequencing denoted. SeqHygr-F is complementary to and internal sequence of the HygR gene (not shown).

10.2.2 Development of pCD8-Cassette and pIgG4-Cassette

To introduce a CAR cassette into pcDNA3.1-hygr, two synthetic DNA cassettes were designed, the CD8 CAR cassette and the IgG4 CAR cassette (figure 10.1), and obtained from GeneWiz, flanked by *Hind*III and *Pme*I sites for cloning into pcDNA3.1-hygr. For the IgG4 CAR cassette hinge the CH2 and CH3 domains were included in the hinge-spacer domain. In addition, two mutations previously used by Hudecek et al. 2015 were introduced to eliminate the binding of the IgG4 CH2 domain (UniProtKB-P01861) to FcγRI and to eliminate a glycosylation site that contributes to interactions with other Fcγ receptors. The amino acids 113-116 (EFLG) were replaced with the amino acids 113-115 (PVA) of IgG2 CH2 domain (UniProtKB-P01859), a modification known as 4/2 substitution, and the N177Q mutation was introduced to eliminate the glycosylation site (180).

The DNA sequences (figure 16 in the appendix) were provided by the manufacturer in two plasmids (pUC57-CD8CAR and pUC57-IgG4CAR). In order to subsequently clone scFvs into both cassettes, the restriction site *Sgs*I was introduced at the CD8 signal peptide of both plasmids. In the DNA cassette obtained from pUC57-CD8CAR, a second restriction site *Mre*I was introduced at the CD8 hinge-spacer, while for the one obtained from pUC57-IgG4CAR, a second restriction site, *Apa*I was introduced at the IgG4 hinge-spacer domain. These DNA cassettes code for the amino acid sequences shown in figures 10.7.A and 10.7.B.

Figure 10.7 Amino acid sequences encoded by the CD8-CAR and IgG4-CAR DNA cassettes. A) Amino acid sequence of CD8-CAR. CD8 signal peptide in yellow, position of the scFv indicated in bold black, CD8 hinge-spacer domain in green, CD8 transmembrane domain in orange, 4-1BB costimulatory endodomain in blue and CD3ζ activation endodomain in red. B) Amino acid sequence of IgG4-CAR. CD8 signal peptide in yellow, position of the scFv indicated in bold black, IgG4 hinge-spacer domain in green (4/2 substitution and N177Q mutation in bold green and underlined), CD28 transmembrane domain in orange, 4-1BB costimulatory endodomain in blue and CD3ζ activation endodomain in red.

A) Amino acid sequence of Short CAR (CD8-CAR)
MALPVTALLLPLALLLHAARP**scFv**TTTPAPRPPTPAPTIASQPLSLRPEACRPAAGGAVHTR GLDFACDIYIWAPLAGTCGVLLLSLVITLYCKRGRKKLLYIFKQPFMRPVQTTQEEDGCSCRF PEEEEGGCELRVKFSRSADAPAYQQGQNQLYNELNLGRREEYDVLDKRRGRDPEMGGKPR RKNPQEGLYNELQKDKMAEAYSEIGMKGERRRGKGHDGLYQGLSTATKDTYDALHMQALP PR
B) Amino acid sequence of Long CAR (IgG4-CAR)
MALPVTALLLPLALLLHAARP**scFv**ESKYGPPCPPCPAP**PVA**GPSVFLFPPKPKDTLMISRTP EVTCVVVDVSQEDPEVQFNWYVDGVEVHNAKTKPREEQF**Q**STYRVVSVLTVLHQDWLNGK EYKCKVSNKGLPSSIEKTISKAKGQPREPQVYTLPPSQEEMTKNQVSLTCLVKGFYPSDIAVE WESNGQPENNYKTTPPVLDSDGAFFLYSRLTVDKSRWQEGNVFSCSVMHEALHNHYTQKS LSLSLGKMFWVLVVVGGVLACYSLLVTVAFIIFWVKRGRKKLLYIFKQPFMRPVQTTQEEDG CSCRFPEEEEGGCELRVKFSRSADAPAYQQGQNQLYNELNLGRREEYDVLDKRRGRDPEMG GKPRRKNPQEGLYNELQKDKMAEAYSEIGMKGERRRGKGHDGLYQGLSTATKDTYDALHM QALPPR

The DNA cassettes were released from the plasmids pUC57-CD8CAR and pUC57-IgG4CAR with *Hind*III and *Pme*I digestion and used for ligation with *Hind*III and *Pme*I digested pcDNA3.1-hygr (figure 10.8) to obtain the final plasmids pCD8-Cassette and pIgG4-Cassette.

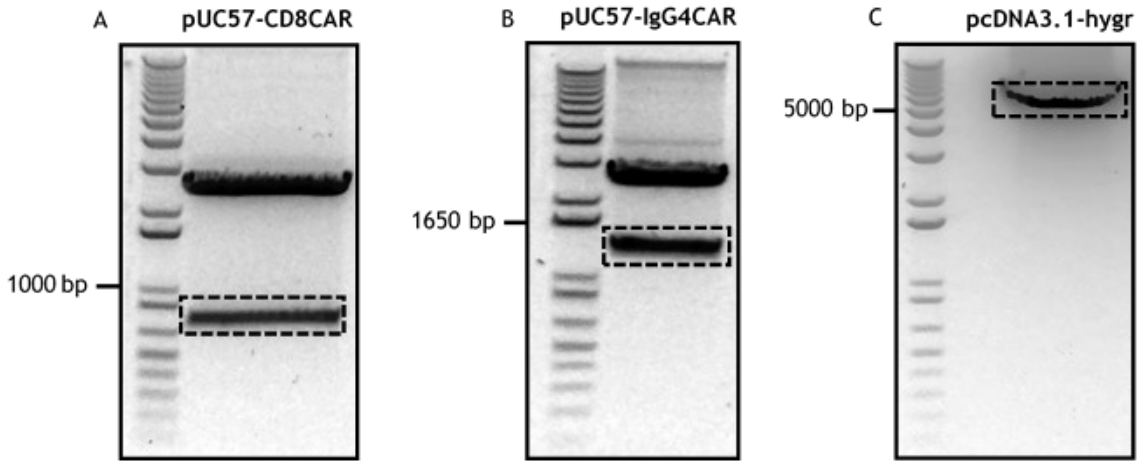

Figure 10.8 Development of pCD8-Cassette and pIgG4-Cassette. A) Digested plasmid pUC57-CD8CAR DNA was electrophoresed through 1% agarose. The *Hind*III and *Pme*I fragment was purified. B) Digested plasmid pUC57-IgG4CAR DNA was electrophoresed through 1% agarose. The *Hind*III and *Pme*I fragment was purified. C) *Hind*III and *Pme*I digested plasmid pcDNA3.1-hygr DNA was electrophoresed through 1% agarose. The vector was purified and used to clone separately the purified fragments obtained from pUC57-CD8CAR and pUC57-IgG4CAR, giving rise to pCD8-Cassette and pIgG4-Cassette. The dashed boxes show the 758 bp (A), 1319 bp (B) and 5552 bp (C) DNA bands excised for DNA purification.

Following *E. coli* transformation and growth, three colonies were used for colony PCR with the primers pcDNA3.1 Check-F and pcDNA3.1 Check-R. The PCR amplicons were purified and sequenced with the primers pcDNA3.1 Check-F and IgG4CAR seq-F (in the case of the PCR obtained from pIgG4-Cassette). The colonies showed the correct sequences and the restriction sites introduced for scFv cloning (figure 10.9), giving rise to the plasmids pCD8-Cassette and pIgG4-Cassette. One colony from each transformation was used for DNA plasmid production and glycerol stocks.

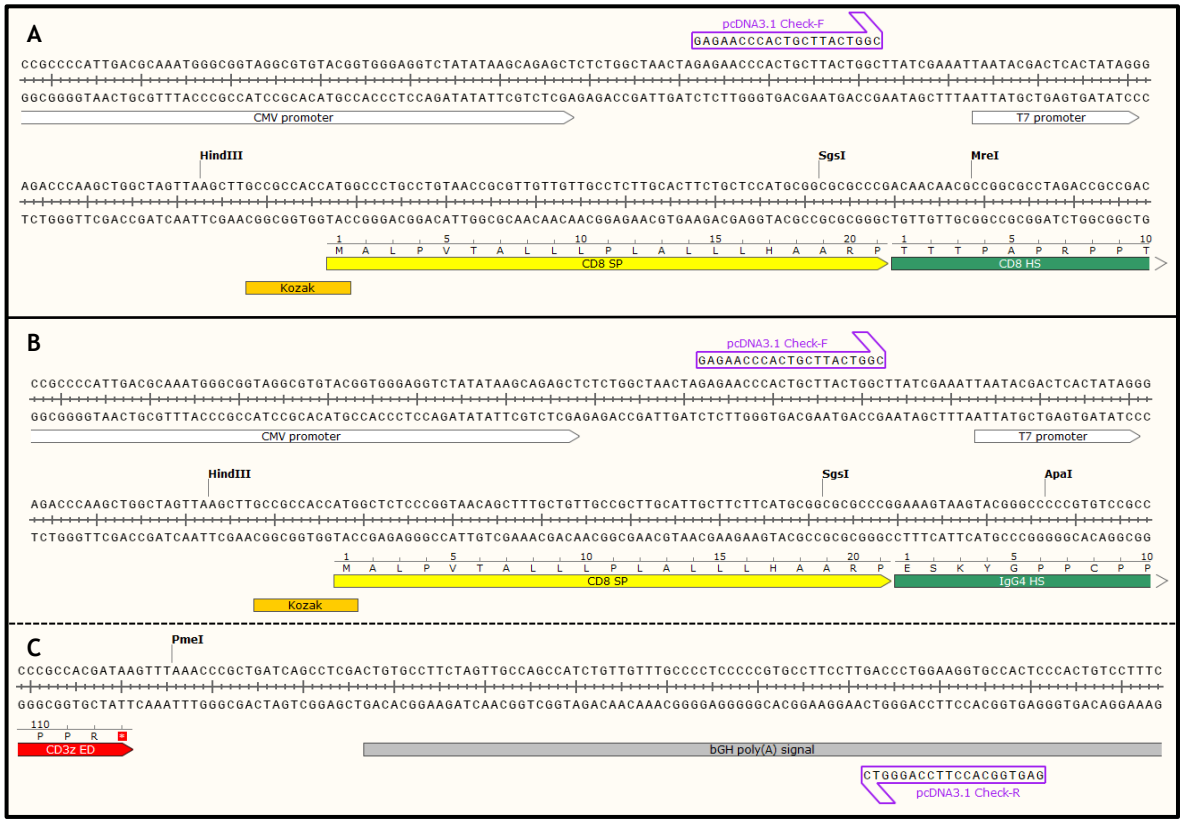

Figure 10.9 pCD8-Cassette and pIgG4-Cassette. A) pCD8-Cassette. Plasmid features and ORFs are coloured and denoted: the yellow arrow represents the CD8 signal peptide and the green arrow the CD8 hinge-spacer domain. *Sgs*I and *Mre*I are indicated and used for scFv cloning. B) IgG4-Cassette. Plasmid features and ORFs are coloured and denoted: the yellow arrow represents the CD8 signal peptide and the green arrow the IgG4 hinge-spacer domain. *Sgs*I and *Apa*I are indicated and used for scFv cloning. C) pCD8-Cassette or IgG4-Cassette. Plasmid features and ORFs are coloured and denoted: the red arrow represents the CD3ζ activation domain signal and the green feature the poly(A) signal. The middle dashed line represents the diagrammatic discontinuity between the 5' end (A or B shown above) and the 3' end (C shown below) for each fragment (pCD8-Cassette or IgG4-Cassette). Primers for PCR and sequencing denoted.

10.2.3 Development of pCD8-Cass-HR and pIgG4-Cass-HR

After the development of pCD8-Cassette and pIgG4-Cassette and with the objective of increasing the chances of plasmid integration into the genome, 400 bp homology arms to the safe harbour locus *AAVS1* were incorporated into both plasmids separated by the restriction site *Nhe*I for plasmid linearisation. The homology arm size 400 bp was chosen to avoid an excessive increase in the vector size but nevertheless being sufficient for HDR, while also being cost-effective. HDR in mammalian cells has been reported to be functional with as little as 200 bp (504). The linearised plasmid delivered together with Cas9 RNP, acting with a crRNA directed to a genomic sequence located in the middle of the DNA sequence complementary to the homology arms (figure 10.10), should facilitate the genomic integration of the plasmid by HDR.

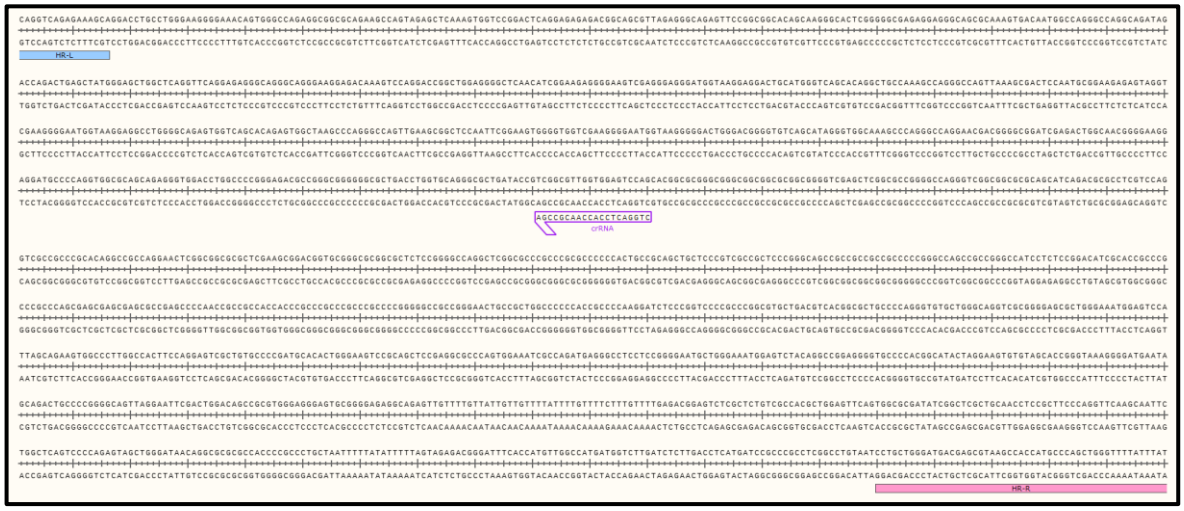

Figure 10.10 DNA segment of the *AAVS1* locus (GenBank-AC010327.8). Features are coloured and denoted: the light blue box represents the edge of the left homology arm incorporated into pCD8-Cassette and pIgG4-Cassette and the pink box the edge of the right homology arm incorporated into pCD8-Cassette and pIgG4-Cassette. The DNA sequence equivalent to the crRNA used to from the Cas9 RNP (5'-CUGGACUCCACCAACGCCGA-3') is indicated.

A synthetic HR DNA cassette was designed (figure 17 in the appendix) and obtained from GeneWiz flanked by *Bgl*II and *Mlu*I sites for cloning into the pCD8-Cassette and pIgG4-Cassette.

The DNA cassette was released from the plasmid pAAVS1-HR with *Bgl*II and *Mlu*I digestion and used for ligation with *Bgl*II and *Mlu*I digested pCD8-Cassette and pIgG4-Cassette (figure 10.11) to obtain the final plasmids pCD8-Cass-HR and pIgG4-Cass-HR.

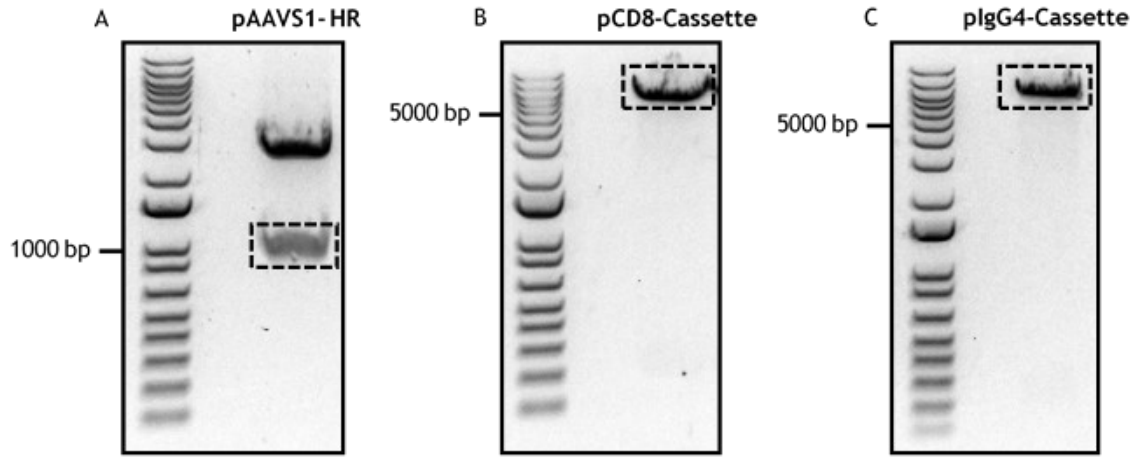

Figure 10.11 Development of pCD8-Cass-HR and pIgG4-Cass-HR. A) Digested plasmid pAAVS1-HR DNA was electrophoresed through 1% agarose. The *Bgl*II and *Mlu*I fragment was purified. B) *Bgl*II and *Mlu*I digested plasmid pCD8-Cassette DNA was electrophoresed through 1% agarose. The vector was purified and used to clone separately the purified fragments obtained from pAAVS1-HR, giving rise to pCD8-Cass-HR. C) *Bgl*II and *Mlu*I digested plasmid pIgG4-Cassette DNA was electrophoresed through 1% agarose. The vector was purified and used to clone separately the

purified fragments obtained from pAAVS1-HR, giving rise to pIgG4-Cass-HR. The dashed boxes show the 916 bp (A), 6088 bp (B) and 6649 bp (C) DNA bands excised for DNA purification.

After *E. coli* transformation, three colonies from each transformation were grown and used for colony PCR with the primers AAVS1 HR Check-F and AAVS1 HR Check-R. The PCR amplicons were purified and sequenced with the primer AAVS1 HR Check-F. The colonies showed the correct sequences for both plasmids and the *Nhe*I restriction sites for plasmid linearisation (figure 10.12), giving rise to the plasmids pCD8-Cass-HR and pIgG4-Cass-HR. One colony from each transformation was used for DNA plasmid production and glycerol stocks.

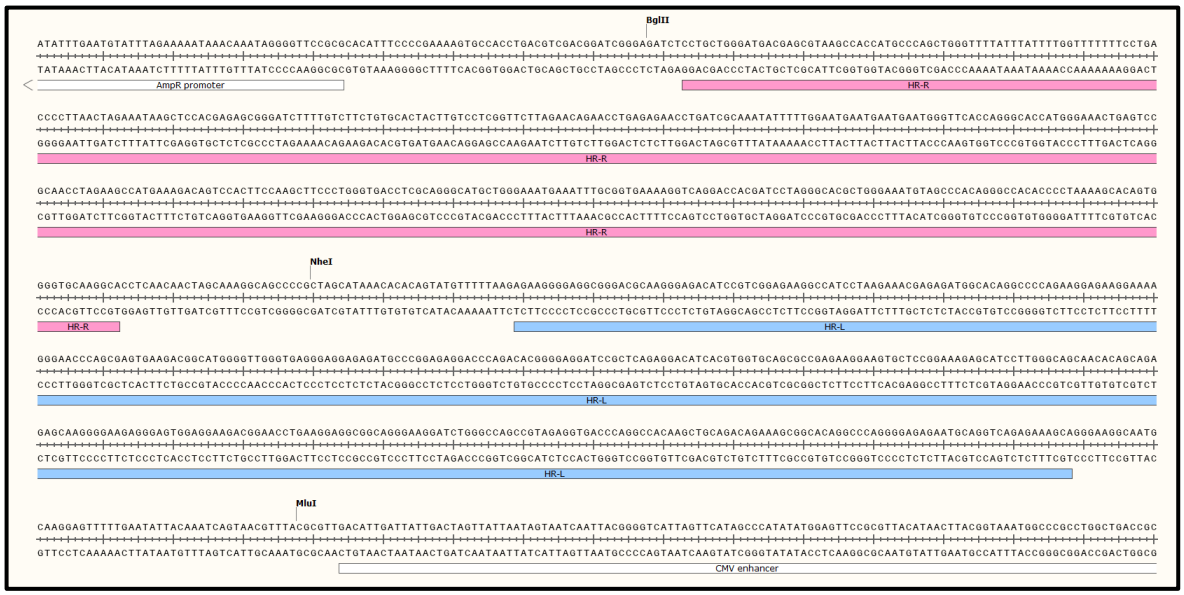

Figure 10.12 pCD8-Cass-HR and pIgG4-Cass-HR. Plasmid features are coloured and denoted: the white arrows represents the AmpR promoter and CMV enhancer, pink box the right homology arm with respect to the *AAVS1* locus (HR-R) and the light blue box the left homology arm to the *AAVS1* locus (HR-L).

After plasmid purification, the next step was to linearise the plasmid with *Nhe*I prior to the cell transformation. The linear plasmid would have the homology arms appropriately situated for HDR into the *AAVS1* locus. *Nhe*I digestion was carried out to examine the linearisation with pCD8-Cass-HR and pIgG4-Cass-HR (figure 10.13). The linear structure of both plasmids is shown in figure 10.14.

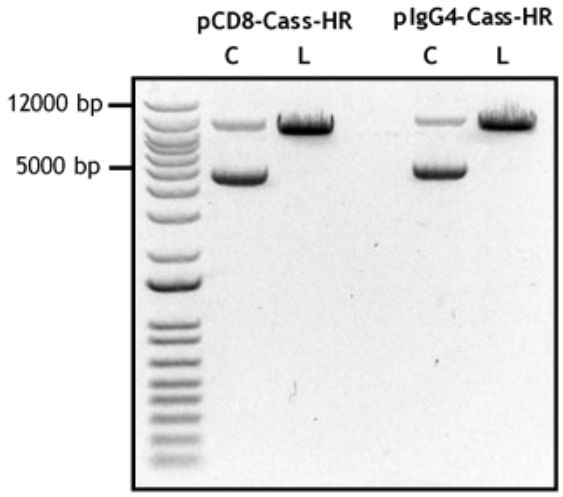

Figure 10.13 *Nhe*I linearisation of pCD8-Cass-HR and pIgG4-Cass-HR. *Nhe*I digested pCD8-Cass-HR and pIgG4-Cass-HR plasmids (L) were compared with the undigested preparation (C). pCD8-Cass-HR plasmid size: 7004 bp. pIgG4-Cass-HR plasmid size: 7565 bp. Due to the higher amount of DNA loaded of the samples compared to the ladder, the sample DNA bands ran slower and therefore, the sizes look bigger.

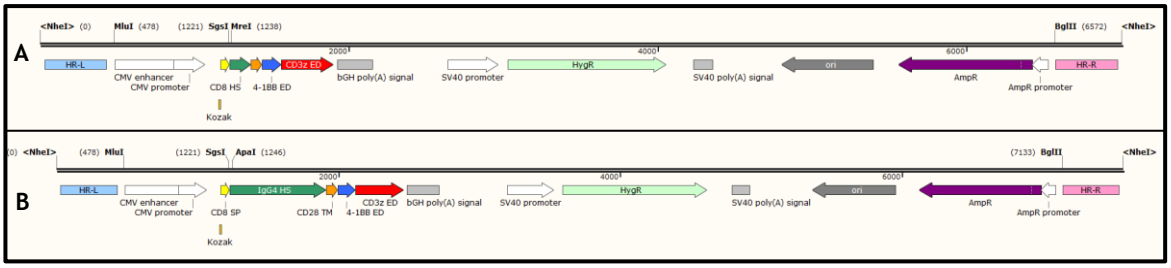

Figure 10.14 *Nhe*I linearised pCD8-Cass-HR and pIgG4-Cass-HR. A) 7004 bp pCD8-Cass-HR *Nhe*I linearised plasmid. B) 7565 bp pIgG4-Cass-HR *Nhe*I linearised plasmid. Plasmid features are coloured and denoted: the light blue box represents the left homology arm to the *AAVS1* locus, white arrows the CMV enhance and promoter, the SV40 promoter and AmpR promoter, yellow arrow the CD8 signal peptide, green arrow the CD8 hinge-spacer domain, orange arrow the CD8 transmembrane domain, blue arrow the 4-1BB costimulatory endodomain, red arrow the CD3ζ activation endodomain, clear grey boxes the Poly(A) signals, clear green arrow the hygromycin resistance gene (hph), grey arrow the pUC Ori, purple arrow the ampicillin resistance gene and pink box the right homology arm to the *AAVS1* locus.

10.2.4 Development of pCD8-CAR and pIgG4-CAR

After developing pCD8-Cass-HR and pIgG4-Cass-HR, based on evidence from the literature and in the design of the first CAR T-cell product approved for clinical use, it was decided to change the promoter that controls the expression of the CAR in the plasmids. The original backbone of these plasmids (pcDNA3.1 (+)) uses the CMV promoter for mammalian expression of proteins. However, the CMV promoter may not be optimal to obtain high expression of a protein in hematopoietic cells (505) and thus for CAR expression (201,503). Therefore, it was

decided to replace the CMV promoter with the EF-1α promoter, previously used with success in CAR T-cells (201) and the promoter which drives the expression in the approved CAR T-cell product Tisagenlecleucel. A synthetic DNA cassette was designed using the sequence of the EF-1α promoter described in the vector pSMPUW-Hygro (figure 18 in the appendix) and obtained from GeneWiz flanked by *Mlu*I and *Sgs*I sites for cloning into pCD8-Cass-HR and pIgG4-Cass-HR.

The DNA cassette was released from the plasmid pEF1αP with *Mlu*I and *Sgs*I digestion and used for ligation with *Mlu*I and *Sgs*I digested pCD8-Cass-HR and pIgG4-Cass-HR (figure 10.15) to obtain the final plasmids pCD8-CAR and pIgG4-CAR (figure 10.16).

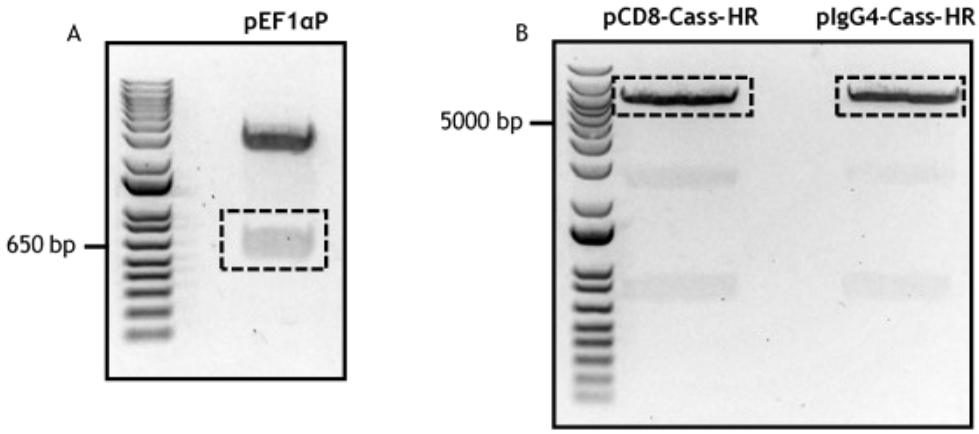

Figure 10.15 Development of pCD8-CAR and pIgG4-CAR. A) Digested plasmid pEF1αP DNA was electrophoresed through 1% agarose. The *Mlu*I and *Sgs*I fragment was purified. B) *Mlu*I and *Sgs*I digested plasmids pCD8-Cass-HR and pIgG4-Cass-HR DNA was electrophoresed through 1% agarose. The vectors were purified and used to clone separately the purified fragments obtained from pEF1αP, giving rise to pCD8-CAR and pIgG4-CAR. The dashed boxes show the 586 bp (A), 6261 bp (B) and 6822 bp (B) DNA bands excised for DNA purification.

After *E. coli* transformation and growth, three colonies from each transformation were used for colony PCR with the primers EF1a Check-F and EF1a Check-R. The PCR amplicons were purified and sequenced with the primer EF1a Check-F. The colonies showed the correct sequences for both plasmids, giving rise to the plasmids pCD8-CAR and pIgG4-CAR (figure 10.16). One colony from each transformation was used for DNA plasmid production and glycerol stocks.

Figure 10.16 pCD8-CAR and pIgG4-CAR. Plasmid features are coloured and denoted: the clear blue box represents the left homology arm to the *AAVS1* locus (HR-L), white arrow the EF-1α promoter, orange box the Kozak sequence and yellow arrow the CD8 signal peptide.

10.2.5 Cloning of scFv into pCD8-CAR and pIgG4-CAR

To transfer the scFvs expressed in the yeast display system to the pCD8-CAR and pIgG4 vectors, two PCRs were required using yeast lysate as DNA template. The lysate was used to perform a PCR with the primers ClnCAR X-F, ClnCARCD8 X-R and ClnCARIgG4 X-R, "X" being the clone number. Some of the ClnCAR primers are shared between clones, as previously described in the example in chapter 9, section 9.2. A second PCR with the primers ClnCAR amp-F, ClnCARCD8 amp-R and ClnCARIgG4 amp-R was needed to amplify the material and eliminate primer dimmers by using smaller primers. This PCR was standard for all the different clones. The PCR strategy is described in figure 10.17.

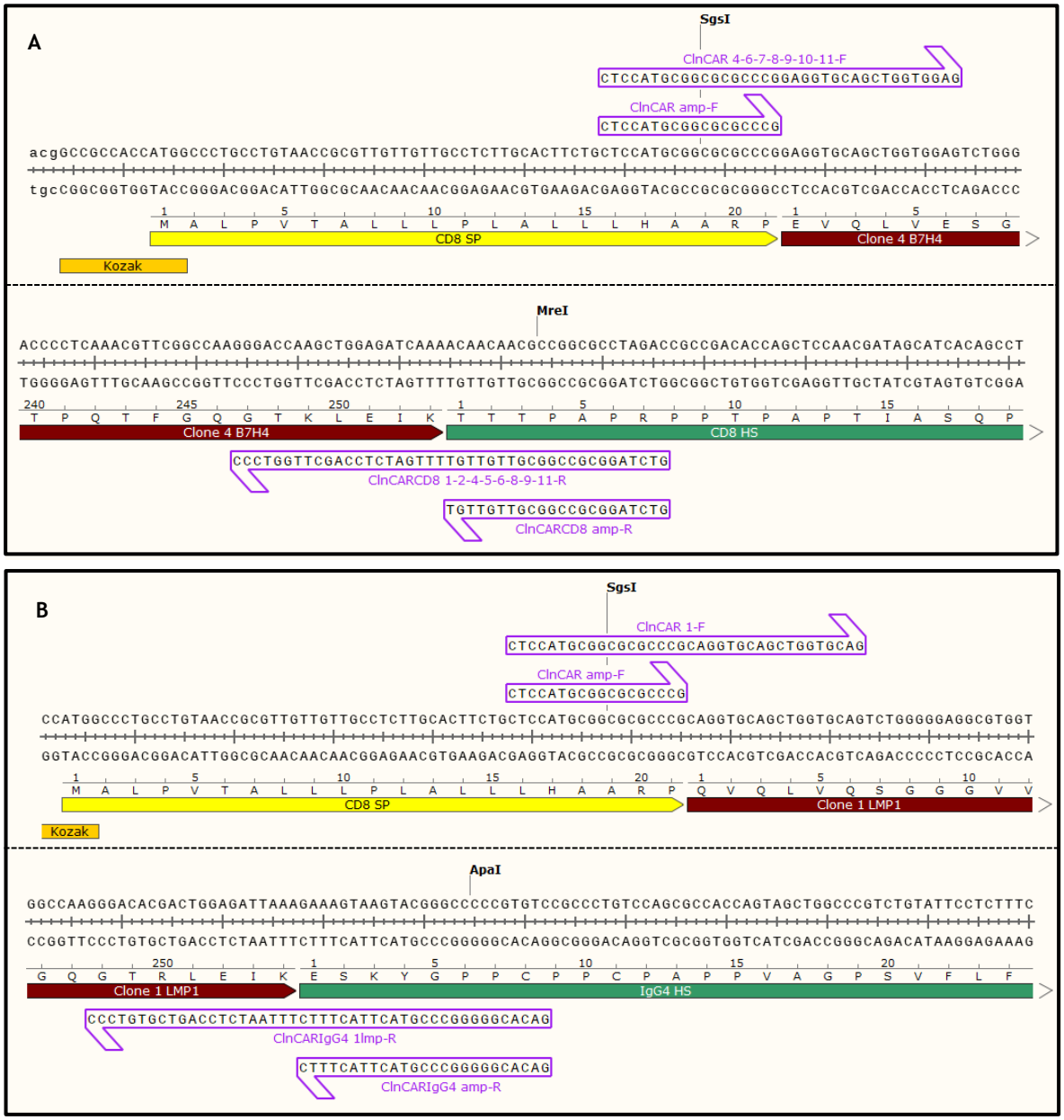

Figure 10.17 PCR strategy for scFv cloning into pCD8-CAR (ClnCAR-CD8 PCR) and pIgG4-CAR (ClnCAR-IgG4 PCR). Plasmid ORFs and features are coloured and denoted: the orange feature represents the Kozak sequence, yellow ORF the CD8 signal peptide, dark red ORF the scFv and green ORF the IgG4 hinge-spacer domain. Primers used for the ClnCAR PCR and the ClnCAR amp PCR denoted. The middle dashed line represents the diagrammatic discontinuity between the 5' end (shown above) and the 3' end (shown below) of the fragment. A) ClnCAR-CD8 PCR strategy. Clone 4 B7H4 scFv cloned into pCD8-CAR, giving rise to the plasmid pCD8-CAR Clone 4. B) ClnCAR-IgG4 PCR strategy. Clone 1 LMP1 scFv cloned into pIgG4-CAR, giving rise to the plasmid pIgG4-CAR Clone 1 LMP1.

The PCR products from the ClnCAR PCR were electrophoresed and excised at the correct band size (figure 10.18.A). Then, they were used for the ClnCAR amp PCR second PCR (figure 10.18.B) and digested with the correspondent enzymes (*Sgs*I and *Mre*I for ClnCARCD8 PCRs and *Sgs*I and *Apa*I for ClnCARIgG4 PCR) for their use in cloning into digested pCD8-CAR or pIgG4-CAR (figure 10.18.C) to finally obtain the plasmids pCD8-CAR Clone X and pIgG4-CAR Clone X, "X" being the clone

number, that can be digested with *Nhe*I for linearisation and cell transformation for Cas9-mediated HDR (figure 10.19).

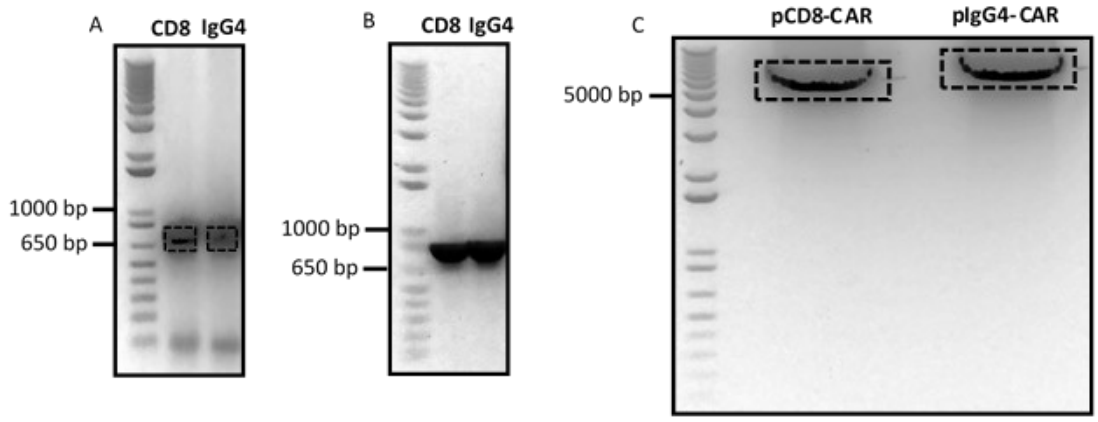

Figure 10.18 ClnCAR and ClnCAR amp PCRs for scFvs Clone 4 B7H4 (CD8) and Clone 1 LMP1 (IgG4) for their cloning into digested pCD8-CAR and pIgG4-CAR, respectively. PCR products were electrophoresed through 1% agarose. CD8 represents the Clone 4 B7H4 scFv amplified ClnCAR-CD8 PCR strategy. IgG4 represent the Clone 1 LMP1 scFv amplified by the ClnCAR-IgG4 PCR strategy. Dashed boxes show DNA band excision to purify the ≈800 bp DNA fragments (figure A) and 6831 bp and 7387 bp (figure C).

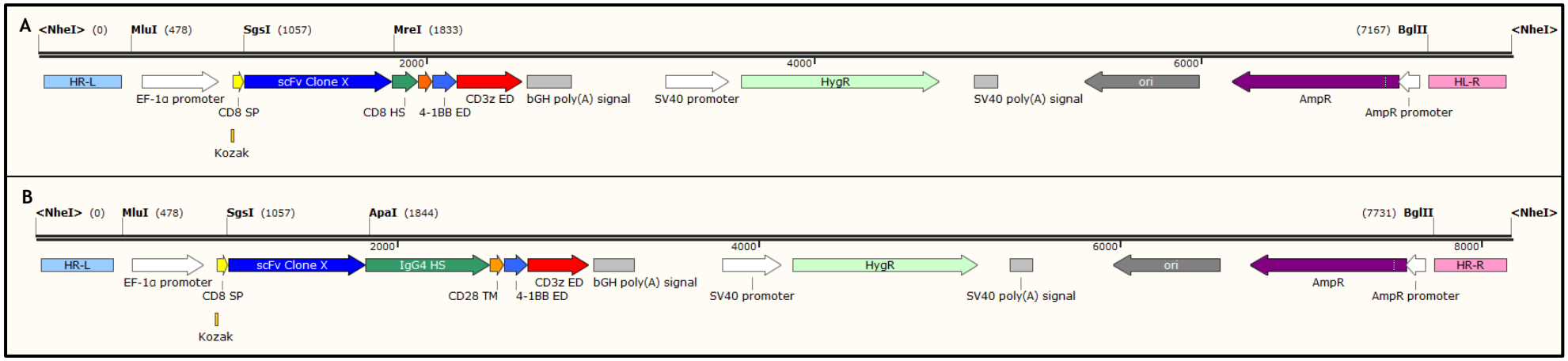

Figure 10.19 *Nhe*I linearised pCD8-CAR Clone X and pIgG4-CAR Clone X. A) ≈ 7600 bp pCD8-CAR Clone X *Nhe*I linearised plasmid. B) ≈ 8165 bp pIgG4-CAR Clone X *Nhe*I linearised plasmid. Plasmid features are coloured and denoted as in figure 10.13 with two differences: The CVM enhancer and promoted were replace by the EF-1α promoter (first white arrow) and the scFv have been cloned into the sites *Sgs*I and *Mre*I (dark blue arrow).

All the B7H4 scFvs were cloned into pCD8-CAR following the ClnCAR-CD8 PCR strategy, while just Clone 1 LMP1 was cloned into pIgG4-CAR following the ClnCAR-IgG4 PCR strategy. The LMP1 loop 2 is small (approximately 13 amino acids) and close to the cell membrane, while the B7H4 Ig-like V-type 1 domain is located at the extracellular N-terminus of the protein separated from the cell membrane by the B7H4 Ig-like V-type 2 domain. It was decided to use short (CD8 CAR) and long (IgG4 CAR) CARs to test the activity of the scFv Clone 1 LMP1. Moreover, scFv Clone 4 B7H4 was also cloned into the IgG4 CAR vector.

After *E. coli* transformation and growth, three colonies from each transformation were used for colony PCR with the primers CAR Check-F and pCD8-CAR Cl Check-R or pIgG4-CAR Cl Check-R. The PCR amplicons were purified and sequenced with the primer CAR Check-F. The colonies showed the correct scFv sequences for both plasmids (figures 5.9 and 8.3), giving rise to the plasmids pCD8-CAR Clone X and pIgG4-CAR X (where X is the clone number). One colony from each transformation was used for DNA plasmid production and glycerol stocks. The plasmid preparations were linearised with *Nhe*I before cell transformation.

10.3 Cas9-mediated HDR for development of reporter CAR cell lines

To determine the level of activity of the designed gRNA (duplex crRNA and tracrRNA) in complex with Cas9 (Cas9 RNP), two different assays were used: the T7EI mismatch detection assay and tracking of indels by decomposition (TIDE). For these assays (explained below), the cell line Jurkat-Dual was transfected with the Cas9 RNP using the transfection reagent TransIT-Jurkat from Mirus Bio. Therefore, before the transfection, the efficacy of TransIT-Jurkat was assessed after 48 hours using the plasmid pmaxGFP, which uses the CMV promoter to control GFP (Green fluorescent protein) expression (figure 10.20).

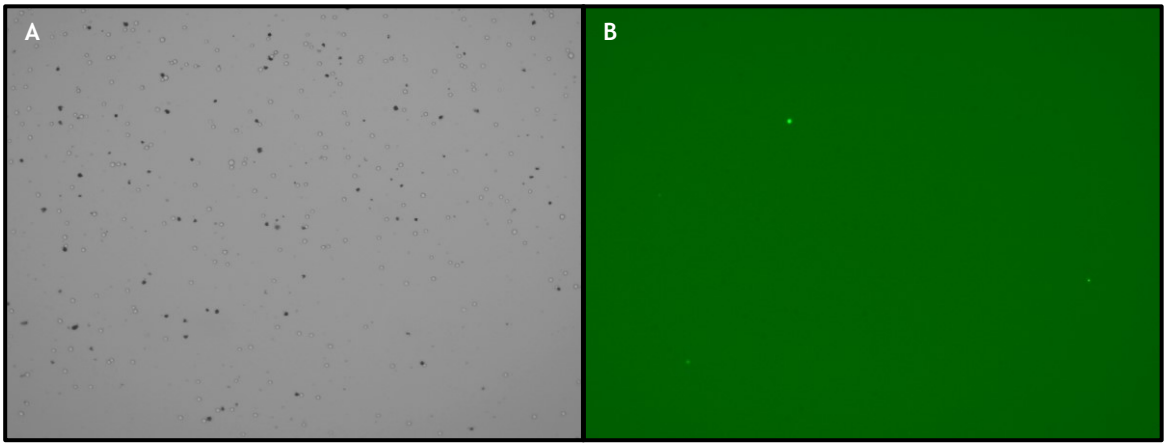

Figure 10.20 pmaxGFP transfection with TransIT-Jurkat. Fluorescence observed with Countess II FL. A) Bright field. B) Green fluorescence.

Fluorescent cells were observed (figure 10.20.B), meaning that the plasmid has been taken up and was sufficiently expressed in some cells. However, the proportion of fluorescent cells was low (1.5%). Nevertheless, the same transfection method was subsequently used for Cas9 RNP together with the linearised plasmids pCD8-CAR Clone X and pIgG4-CAR Clone X.

After transfection with the Cas9 RNP using TransIT-Jurkat, the cells were collected and the gDNA isolated for PCR with the primers AAVS1 Check-F and AAVS1 Check-R to amplify a 570 bp region of the *AAVS1* locus that included the double-strand break produced by the Cas9 RNP in the middle of the amplicon (figure 10.21). Therefore, the sample transfected with Cas9 RNP would show indels in this position that can be detected by T7EI mismatch detection assay and TIDE.

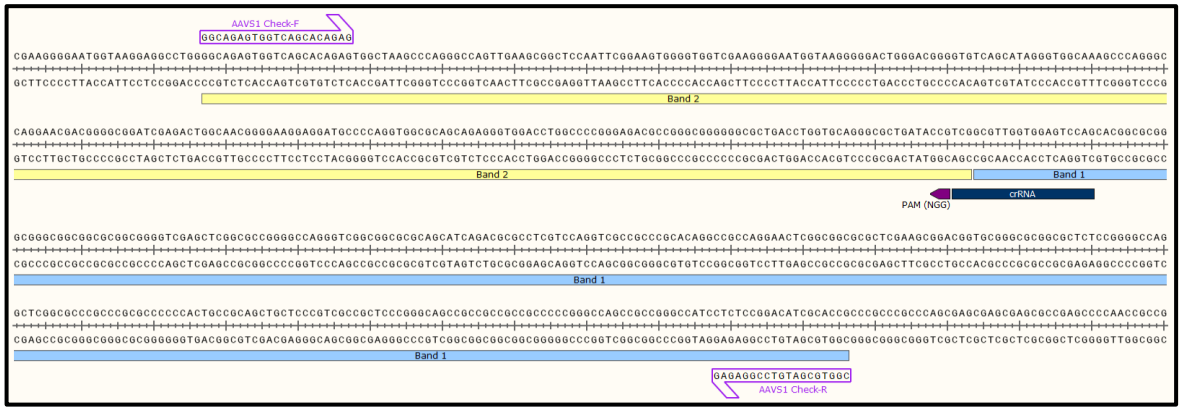

Figure 10.21 *AAVS1* Locus with the primers for AAVS1 Check PCR denoted. The AAVS1 Check primers flank a 570 bp region of the *AAVS1* locus, including the double-strand break produced by the Cas9 RNP. Features are coloured and denoted: the yellow feature represents Band 2 of 267 bp and the light blue feature the Band 1 of 303 bp, both separate by the site of double-strand break produced by the Cas9 RNP. The dark blue feature represents the DNA sequence equivalent to the

crRNA used to form the Cas9 RNP (5'-CUGGACUCCACCAACGCCGA-3') and the purple arrow the PAM region.

The product of the two PCRs were electrophoresed to confirm the size before their use in the T7EI mismatch detection assay and TIDE (figure 10.22).

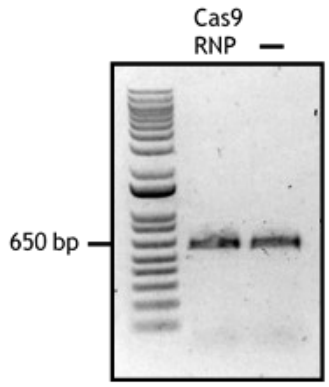

Figure 10.22 PCR amplicons obtained from the AAVS1 Check PCR. Cas9 RNP represents the PCR amplicon of 570 bp obtained from cells transfected with the Cas9 RNP targeting the *AAVS1* locus. The negative control represents the PCR amplicon of 570 bp obtained from cells exposed to the transfection reagent but not to the Cas9 RNP.

10.3.1 T7EI mismatch detection assay

The PCR product was then subjected to a denaturing and annealing step before a T7EI reaction. Cas9 digestion of genomic DNA leads to double-strand breaks in the target location. Cells principally repair these breaks by Non-homologous end joining (NHEJ) and Microhomology-mediated end joining (MMEJ) pathways, which are error-prone and random, and sometimes they introduce mismatched repairs (insertions or deletions of DNA in the target place, also known as indels). This a common way to obtain knock-out cells using Cas9. The objective of the denaturing and annealing step in this assay is to allow the hybridisation of the DNA strands from different DNA molecules present in the final amplicon solution.

Therefore, the denaturing and annealing step would lead to non-perfectly matched DNA molecules in the mix due to mismatched repairs. T7EI catalyses the cleavage of DNA mismatches giving rise to a double-strand break and two separate DNA molecules. The T7EI mismatch detection assay allows an assessment of the level of activity of the gRNA by examining the DNA band of the T7EI digested DNA

in a DNA-PAGE gel and comparing it with a control sample (sample not treated with the Cas9 RNP) (figure 10.23).

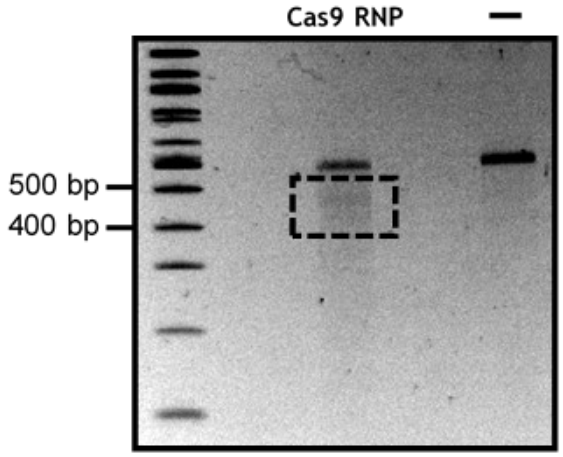

Figure 10.23 T7EI mismatch detection assay. The previous PCR products (570 bp) were subjected to T7EI treatment and electrophoresed through 8% polyacrylamide. Dashed boxes highlight faint DNA bands between 400 bp and 500 bp present in the sample but not in the control sample.

The smear of bands observed in the gel track from the positive sample after T7EI mismatch detection, with sizes between 400 bp and 500 bp, does not correspond with the expected band of 303 bp (band 1) and 267 bp (band 2) after T7EI digestion of DNA mismatches (figure 10.21). However, a difference is observed from the control sample, which may indicate indel production. Therefore, it was decided to perform a TIDE analysis with the amplicons.

10.3.2 TIDE

The TIDE test is based on two PCRs and two Sanger sequencing reactions and a sequencing trace decomposition algorithm developed by Brinkman EK et al. (2014) (480,481). TIDE software identifies the predominant types of indels and quantifies the editing efficacy using the data from two standard capillary sequencing reactions, providing accurate and sensitive calculation of indel frequency.

The PCR products (figure 10.22) were purified and sequenced with the primer AAVS1 Check-F. The obtained sequencing files were then used for TIDE analysis together with the sequence of the crRNA. The total efficiency of 34.1% was estimated for this CRISPR/Cas9 digestion experiment, meaning that 34.1% of the readings have deletions or insertions (figure 10.24).

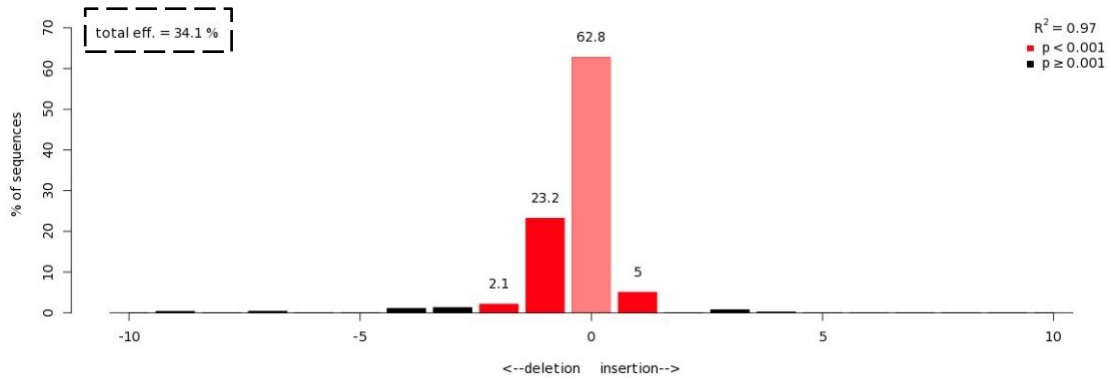

Figure 10.24 Indel spectrum obtained by TIDE. The Cas9 RNP sample and the negative control sample were sequenced with the primer AAVS1 Check-F and the .ab1 sequencing files were used for analysis with TIDE, together with the DNA sequence equivalent to the crRNA used for the Cas9 RNP complex. 62.8% of the sequences showed 0 indels, and 30.3% showed deletions or insertions, both estimations with p<0.001. The total efficiency estimated (indels with p<0.001 plus indels with p≥0.001) was 34.1%.

After performing the T7EI mismatch detection assay and the TIDE test, the results obtained were considered acceptable to continue with the co-transfection of the Cas9 RNP with the plasmids pCD8-CAR Clone X or pIgG4-CAR Clone X.

10.3.3 Co-transfection and selection of Jurkat-rep-CAR cell lines

The plasmids pCD8-CAR Clone X and pIgG4-CAR Clone X were linearised with *Nhe*I (figure 10.25) and purified by isopropanol and ethanol precipitation.

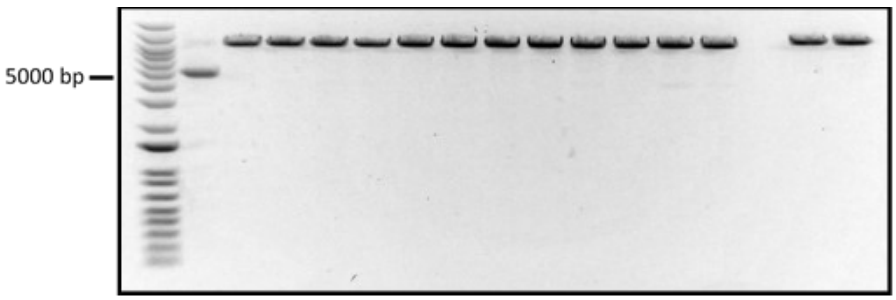

Figure 10.25 *Nhe*I linearisation of pCD8-CAR Clone X and pIgG4-CAR Clone X plasmids. Plasmid order from left to right: Undigested control, pCD8-CAR Clone 1 B7H4, pCD8-CAR Clone 2 B7H4, pCD8-CAR Clone 3 B7H4, pCD8-CAR Clone 4 B7H4, pIgG4-CAR Clone 4 B7H4, pCD8-CAR Clone 5 B7H4, pCD8-CAR Clone 6 B7H4, pCD8-CAR Clone 7 B7H4, pCD8-CAR Clone 8 B7H4, pCD8-CAR Clone 9 B7H4, pCD8-CAR Clone 10 B7H4, pCD8-CAR Clone 11 B7H4, pCD8-CAR Clone 1 LMP1 and pIgG4-CAR Clone 1 LMP1. No sample loaded in track 15 (intended empty track).

Jurkat-Dual cells were transfected with each linearised plasmid and the Cas9 RBP, and the selection with hygromycin was performed for several months until cell growth and viability were similar to the parental cells (passage number 14), giving

rise to the cell lines Jurkat-rep-CAR Clone X. After selection, just four cell lines were able to give rise to viable clones with the other dying off, all of them with Short CARs (CD8-based CARs): Jurkat-rep-ShortCAR Clone 8 B7H4, Jurkat-rep-ShortCAR Clone 10 B7H4, Jurkat-rep-ShortCAR Clone 11 B7H4 and Jurkat-rep-ShortCAR Clone 1 LMP1.

The cells were collected and the gDNA extracted to study the integration of the plasmid by HDR into the *AAVS1* locus. First, the integration of the plasmid into the genome was assessed by PCR with the primers CAR Check-F and pCD8-CAR Cl Check-R (Clone PCR), a band of ≈ 950 bp would be expected in the case of positive plasmid integration. Then, the HDR was also assessed by PCR (AAVS1 HDR PCR) with the primers AAVS1 HDR Check-F (complementary to a region in the *AAVS1* locus upstream of the HDR region) and AAVS1 HDR Check-R (complementary to a region of the plasmid), a band of ≈ 1100 bp would be expected in the case of positive HDR into the *AAVS1* locus. The results of these PCRs are shown in figure 10.26.

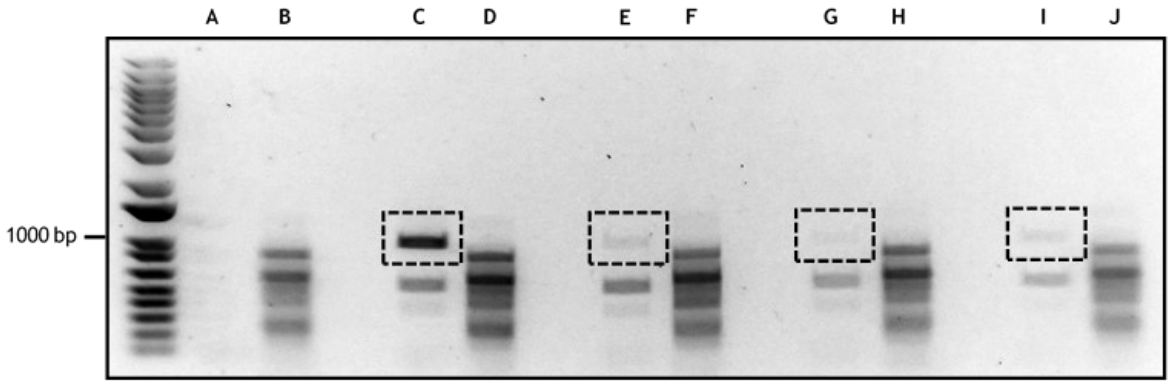

Figure 10.26 Clone PCRs and AAVS1 HDR PCRs for Jurkat-rep-CAR Clone 8 B7H4, Jurkat-rep-CAR Clone 10 B7H4, Jurkat-rep-CAR Clone 11 B7H4 and Jurkat-rep-CAR Clone 1 LMP1. Clone PCRs for Jurkat-Dual (A), Jurkat-rep-CAR Clone 8 B7H4 (C), Jurkat-rep-CAR Clone 10 B7H4 (E), Jurkat-rep-CAR Clone 11 B7H4 (G) and Jurkat-rep-CAR Clone 1 LMP1 (I). Dashed boxes highlight the DNA bands of ≈ 950 bp indicative of the presence of plasmids pCD8-CAR Clone X in the genome. AAVS1 HDR PCRs for Jurkat-Dual (B), Jurkat-rep-CAR Clone 8 B7H4 (D), Jurkat-rep-CAR Clone 10 B7H4 (F), Jurkat-rep-CAR Clone 11 B7H4 (H) and Jurkat-rep-CAR Clone 1 LMP1 (J). The absence of the expected band of ≈ 1100 bp is indicative of ineffective HDR.

The band at ≈ 950 bp in the Clone PCR (figures 10.26.C, 10.26.E, 10.26.G and 10.26.I) is indicative of plasmid integration. However, smaller bands (e.g., around 700 bp) were observed. None of these bands were observed in the Jurkat-Dual control (figure 10.26.A). Regarding the AAVS1 HDR PCR, a band of ≈ 1100 bp was expected in the case of correct HDR into the *AAVS1* locus, but it was not observed.

Instead, smaller fragments were amplified similar to those found in the Jurkat-Dual control (figure 10.26.B). These data suggest plasmid integration had occurred in the obtained cell lines. However, it does not appear that this integration was mediated by HDR into the *AAVS1* locus. This raises the concern that if integration has been random, then plasmid sequence may have been lost in the process, although using a linearised plasmid reduce the chances of inappropriate integration.

To investigate if the CAR cassettes are expressed in each cell line, the cells were incubated with 950 nM of dimeric human B7H4 recombinant antigen followed by incubation with anti-human Fc FITC conjugated. If the CARs are expressed in these cells, they would be expected to bind to the dimeric human B7H4 antigen, and this binding would be detected with the anti-human Fc FITC. The samples were analysed by flow cytometry and the histograms obtained overlapped with the control cells indicating there was no expression of the CARs in any of the developed cell lines, detectable by this assay (figure 10.27).

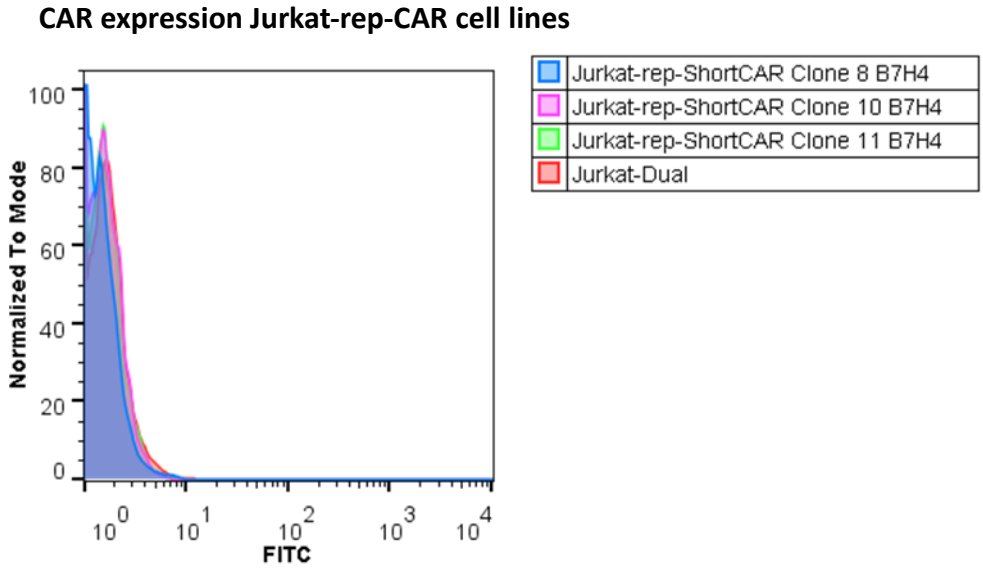

Figure 10.27 Flow cytometry histogram overlay of CAR expression in Jurkat-rep-CAR cell lines. Jurkat-Dual, Jurkat-rep-ShortCAR Clone 8 B7H4, Jurkat-rep-ShortCAR Clone 10 B7H4 and Jurkat-rep-ShortCAR Clone 11 B7H4 were incubated with hB7H4-hFc + Anti-hFc FITC to study CAR expression. The obtained histograms were overlapped for comparison.

10.4 Transient expression of CARs

As an alternative to develop expressing cell lines in an attempt to assess functionality, a transient expression experiment was performed with the plasmids

pCD8-CAR Clone 4 B7H4 and pIgG4-CAR Clone 4 B7H4 and their equivalents with the original CMV promoter. The equivalents with the CMV promoter were obtained after *Mlu*I and *Sgs*I digestion of pCD8-Cass-HR and pIgG4-Cass-HR, to get the DNA fragment with the CMV promoter. Then, pCD8-CAR Clone 4 B7H4 and pIgG4-CAR Clone 4 B7H4 were also digested with *Mlu*I and *Sgs*I, releasing the DNA fragment with the EF1-α promoter and living the *Mlu*I and *Sgs*I sites for cloning. The DNA fragment with the CMV promoter was finally cloned into *Mlu*I and *Sgs*I digested pCD8-CAR Clone 4 B7H4 and pIgG4-CAR Clone 4 B7H4.

Before the experiment, the efficacy of electroporation with the nucleofector kit V and Nucleofector I was assessed 48 hours after transfection using the plasmid pmaxGFP, and 5.5% of the cells showed fluorescence (figure 10.28).

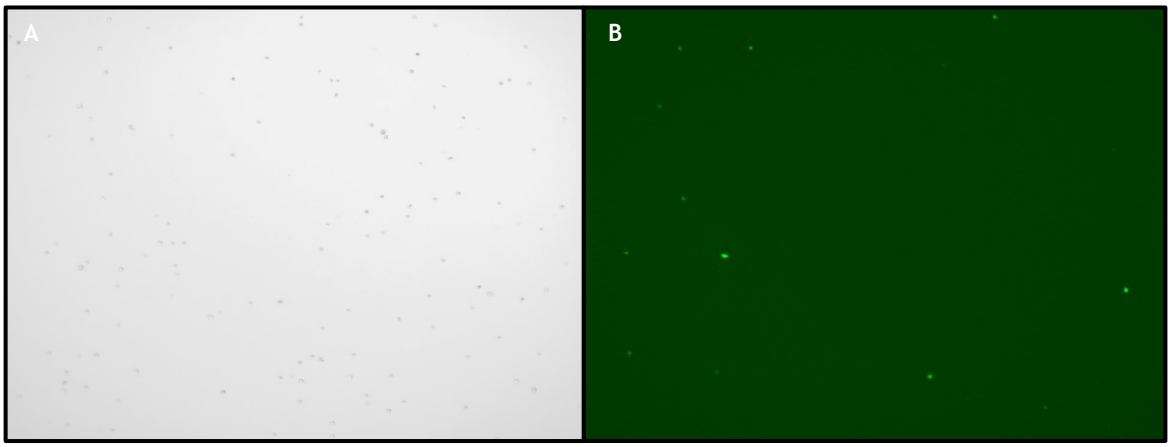

Figure 10.28 pmaxGFP transfection with Cell line nucleofector kit V and Nucleofector I. Fluorescence observed with Countess II FL. A) Bright field. B) Green fluorescence.

Transfection occurred, although at low frequency, therefore Jurkat-Dual cells were transfected with the plasmids pCD8-CAR Clone 4 B7H4 and pIgG4-CAR Clone 4 B7H4 (bearing the EF1-α promoter) and CMV-modified pCD8-CAR Clone 4 B7H4 and pIgG4-CAR Clone 4 B7H4 (bearing the CMV promoter). The CAR expression was then assessed by flow cytometry 48 hours after transfection by staining with dimeric human B7H4 recombinant antigen and anti-human Fc FITC conjugated. Cells transfected with pCD8-CAR Clone 4 B7H4 and pIgG4-CAR Clone 4 B7H4, which carry the EF-1α promoter, did not show any CAR expression (figure 10.29) while cells transfected with the CMV modified plasmids pCD8-CAR Clone 4 B7H4 and pIgG4-CAR Clone 4 B7H4 showed low expression. Higher expression was obtained with the Short CAR format (figure 10.30).

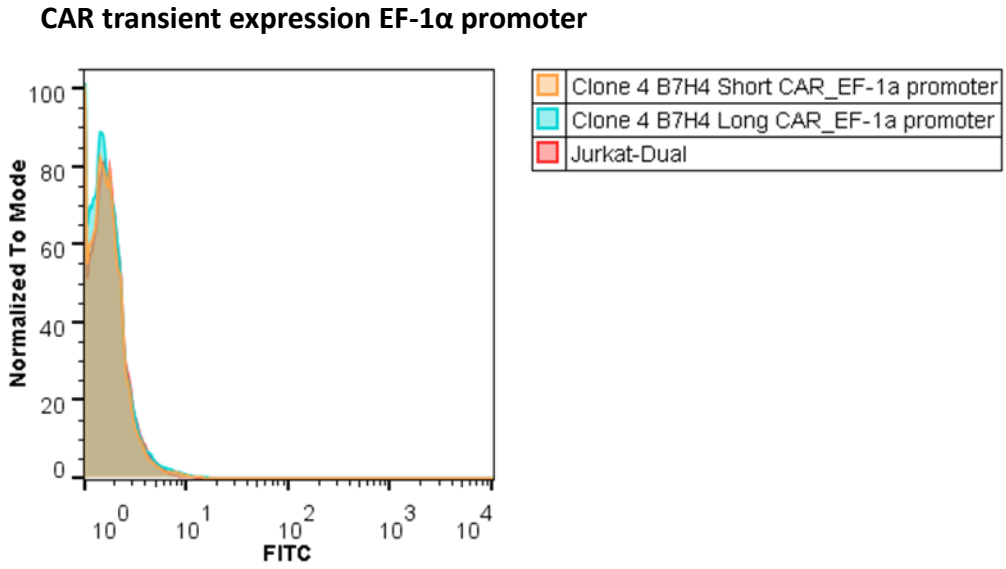

Figure 10.29 Flow cytometry histogram overlay of CAR transient expression under the EF-1α promoter in Jurkat-Dual cells transfected with pCD8-CAR Clone 4 B7H4 and pIgG4-CAR Clone 4 B7H4. Jurkat-Dual, Clone 4 B7H4 Short CAR and Clone 4 B7H4 Long CAR were incubated with hB7H4-hFc + Anti-hFc FITC to study CAR expression. The obtained histograms were overlapped for comparison.

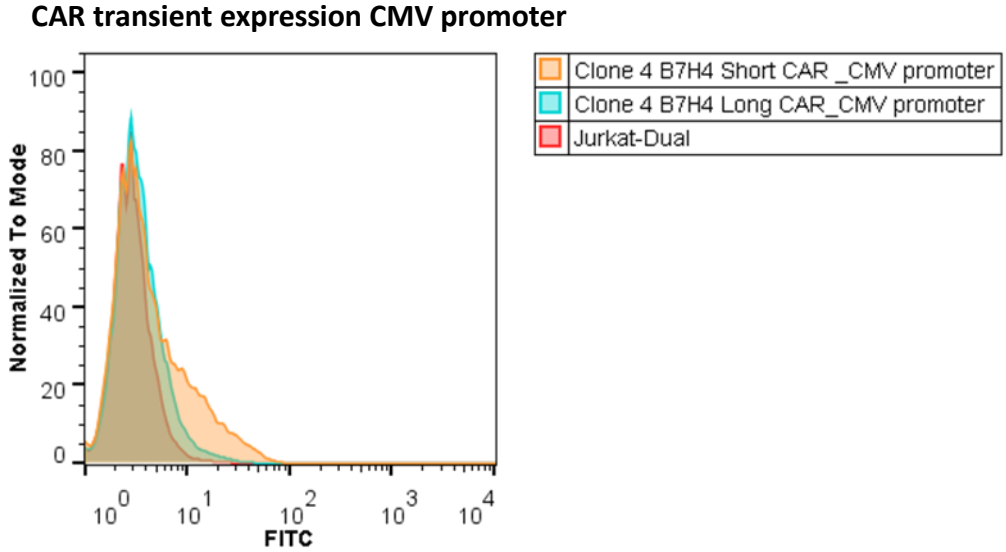

Figure 10.30 Flow cytometry histogram overlay of CAR transient expression under the CMV promoter in Jurkat-Dual cells transfected with CMV-modified pCD8-CAR Clone 4 B7H4 and pIgG4-CAR Clone 4 B7H4. Jurkat-Dual, Clone 4 B7H4 Short CAR and Clone 4 B7H4 Long CAR were incubated with hB7H4-hFc + Anti-hFc FITC to study CAR expression. The obtained histograms were overlapped for comparison.

10.5 Co-culture NF-kB activation luciferase reporter assay

Given that low expression of the CAR was detected with the CMV-modified pCD8-CAR Clone 4 B7H4 and pIgG4-CAR Clone 4 B7H4, an attempt to assess functionality

was conducted. For functional assessment of the CARs, CMV-modified pCD8-CAR Clone 4 B7H4 and pIgG4-CAR Clone 4 B7H4 were used to transiently express for the Short and Long CAR format of Clone 4 B7H4 in Jurkat-Dual cells. 24 hours after the transfection, these cells were co-cultured with tetracycline induced HEK293-B7H4 in a ratio of 2:1 (effector cells : target cells) for 48 hours. HEK293 (HEK293 Flp-In T-REx) were used as $B7H4^-$ target cells (figure 6.14), with electroporated but not transfected Jurkat-Dual cells as a negative control and Concanavalin A (Conc A) as a positive control of NF-kB activation. After 48 hours of co-culture, the cultures were analysed for the presence of Lucia luciferase in the medium, resulting from the activation of the NF-kB reporter pathway through CAR stimulation (figure 10.31).

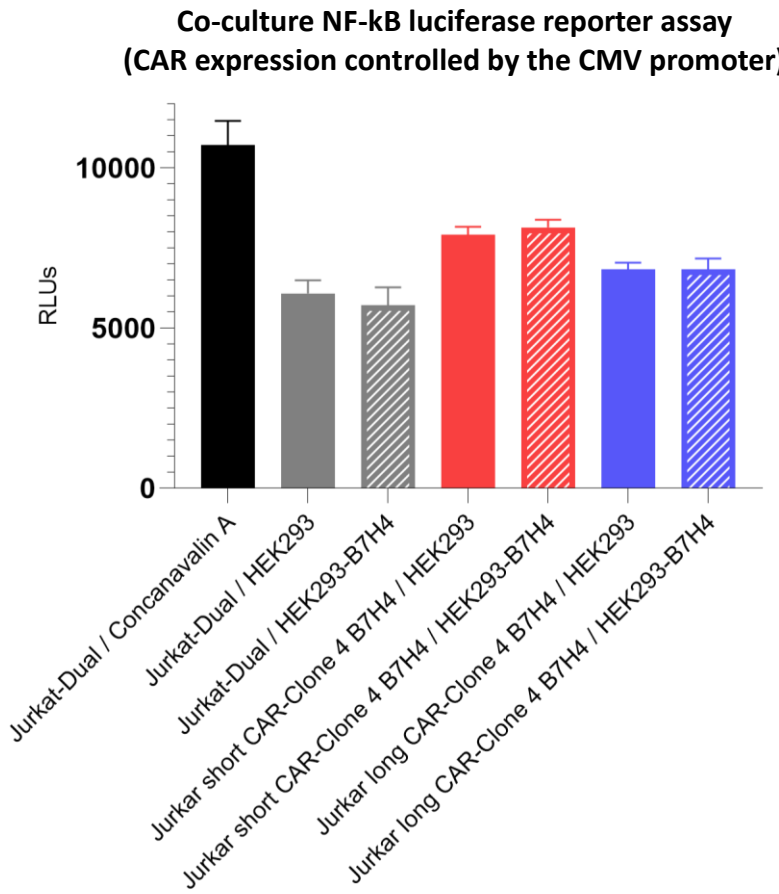

Figure 10.31 Co-culture NF-kB luciferase reporter assay with Clone 4 B7H4 scFv in Short and Long CAR format. Clone 4 B7H4 Short and Long CARs were transiently expressed in Jurkat-Dual cells under the control of the CMV promoter and the cells were co-cultured with tetracycline induced target cells (HEK293 and HEK293-B7H4). 50 µg/ml of Concanavalin A was used as a positive control of NF-kB activation. Three biological replicates were performed for each condition. Error bars mean with SD.

Even though Short and Long CAR showed apparently higher luciferase signals than Jurkat-Dual control cells, no increase in activity with the HEK293-B7H4 cells was detected with either of them compared to antigen-negative (HEK293) target cells ($p > 0.05$). The signal window was also low when compared with the positive control (Concanavalin A). The apparent lack of activity may reflect the low expression level of the CAR detected in these cells. As such, the potential activity of these sequences in a CAR is yet to be determined.

10.6 Conclusions

Jurkat-rep-CAR Clone 8 B7H4 Short CAR, Jurkat-rep-CAR Clone 10 B7H4 Short CAR, Jurkat-rep-CAR Clone 11 B7H4 Short CAR and Jurkat-rep-CAR Clone 1 LMP1 Short CAR were established. However, the plasmids appeared to be randomly integrated into the genome instead of directed to the *AAVS1* locus by Cas9-mediated HDR, as was intended.

Furthermore, the chosen EF1-α promoter for the plasmids pCD8-CAR and pIgG4-CAR oddly seems inactive, leading to no expression of CARs in the established cell lines. The EF-1α promoter has been previously used in CAR T-cells(201). In addition, this promoter drives the expression in the approved CAR T-cell product Tisagenlecleucel, as it is reported to be a stable and robust promoter in human T-cells. The DNA sequence for the EF1-α promoter was obtained from the commercial lentiviral vector pSMPUW-Hygro from Cell Biolabs Inc. (catalogue number VPK-214-PAN), which contains the core promoter region (around 200-300 bp) but not the full-size promoter (approximately 1100 bp containing an intronic sequence). However, Zheng et al. 2014 reported the difference regarding gene expression of the distinct versions of the human EF1-α promoter in different constructs (506), concluding that different forms of the EF1-α promoter are named similar in the literature. However, they are not equivalent, and the use of one or another could result in dramatically lower gene expression. It is possible that the EF-1α promoter of pSMPUW-Hygro works well in that plasmid setting but may not be optimal for the pCD8-CAR and pIgG4-CAR vectors designed here.

The plasmids pCD8-CAR Clone 4 B7H4 and pIgG4-CAR Clone 4 B7H4 were modified, replacing the EF1-α promoter with the original CMV promoter of pcDNA3.1 (+) for transient expression by nucleofection to assess the activity of Clone 4 B7H4 in

Short and Long CAR format. Low levels of CAR expression were observed with the plasmids pCD8-CAR Clone 4 B7H4, but no activity was detected in the co-culture NF-kB luciferase reporter assay, possibly due to the low level of expression. However, no expression was detected with pIgG4-CAR Clone 4 B7H4. This can be due to the low level of transfection, a more challenging expression of the Long CAR format by the cells or the lack of binding of scFv Clone 4 B7H4 as Long CAR. The reduced but present expression and binding of Clone 4 B7H4 as Short CAR when transiently expressed with CMV-modified pCD8-CAR Clone 4 B7H4 confirm the lack of activity of the EF1-α and the absence of expression in the established cell lines. Alternative approaches can be used to sustain the lack of activity of EF1-α in the context of pCD8-CAR Clone 4 B7H4 and to assess CAR expression, such RT-PCR, western blot with human B7H4-human Fc or the incorporation of a tag at the located at the N-terminal end of the CAR molecule for western blot or flow cytometry experiments.

Regarding the apparent antigen-independent increase in RLUs by “Jurkat short CAR-Clone 4 B7H4 / HEK293” compared to “Jurkat-Dual / HEK293”, the low signal window of the assay suggests that this effect is not real, since the positive control did not give a high increase of RLUs even though the concentration used of Concanavalin A is high. High antigen stimulation may be necessary to obtain a clear signal of activation and the background signal of the assay could be fluctuating in the levels observed for “Jurkat-Dual / HEK293”, “Jurkat short CAR-Clone 4 B7H4 / HEK293” and “Jurkat long CAR-Clone 4 B7H4 / HEK293”.

To conclude, the expression level after transfection with TransIT-Jurkat or nucleofection, the percentage of GFP positive cells was low with both methods (1.5 and 5.5 %, respectively). Nevertheless, weak fluorescence was detected in some of the positive cells, opening the possibility that more cells were transfected but the amount of plasmid introduced into the cells was insufficient to produce enough GFP to show fluorescence. Even though the low efficiency of transfection also impacted the level of CAR expression during the transient expression experiments.

11. Discussion

EBV infection is associated with cancers where the presence of the virus in latency is an essential factor for cell immortalisation. The group of malignancies associated with EBV infection is comprised mainly of lymphomas but also carcinomas. B7H4, LMP1 and LMP2A are membrane proteins expressed in these cancers, and therefore, potential targets for therapies to treat these diseases. B7H4 is a human protein that has been reported to be overexpressed in many cancers, among them EBV-associated malignancies. LMP1 and LMP2A are viral proteins that are expressed during the latency 2 and 3 of EBV infection and in EBV-associated malignancies such as NPC, HL or DLBCL.

CAR T-cell therapy provides a novel approach to treat cancers where T-cells are genetically modified to express an artificial receptor that can trigger T-cell activation through an interaction with a specific antigen and independently of HLA presentation. The domain that determines the specificity of the CAR receptor is based on an antibody fragment. Therefore, antibody fragments that recognise specifically B7H4, LMP1 or LMP2A can be potentially used for CAR T-cell therapies to treat EBV-associated malignancies. Regarding the anti-B7H4 CAR T-cell therapy, apart from possibly all EBV-associated malignancies, other malignancies could also benefit from this therapy, such as breast cancer, ovarian cancer, uterine endometrioid adenocarcinoma, prostate cancer, melanoma, oesophageal squamous cell carcinoma, gastric cancer, non-small cell lung cancer, pancreatic cancer, cervical carcinoma, oral squamous cell carcinoma, gallbladder carcinoma, non-Hodgkin lymphoma, pleural adenocarcinoma, hepatocellular carcinoma and colorectal cancer. As for the anti-LMP1 and anti-LMP2 CAR T-cell therapies, they could be used individually, in combination or as one therapy using a Tandem CAR. Anti-LMP1 and anti-LMP2 CAR T-cell therapies could treat EBV-associated malignancies where the virus is in the latency programs 2 or 3, such as diffuse large B-cell lymphoma, Hodgkin lymphoma, post-transplant lymphoproliferative disorder/lymphoma, AIDS-associated immunoblastic and primary central nervous system lymphoma, nasopharyngeal carcinoma and lymphoepithelioma-like carcinoma. Furthermore, they could also be possible therapies for MS, and other inflammatory diseases related to EBV infection. Anti-LMP2 CAR T-cell therapy

could also be used to treat nasal-type extranodal NK/T-cell lymphoma and gastric adenocarcinoma.

Currently, four CAR T-cell therapies have been approved for their clinical use: Tisagenlecleucel, Axicabtagene ciloleucel, Brexucabtagene autoleucel and Lisocabtagene maraleucel. These therapies target the TAA CD19 and are used to treat B-cell malignancies. All of them are based on the use of a mouse scFv formatted using the mouse antibody clone FMC63. The clinical use of mouse antibodies or antibody fragments is associated with immunogenicity that can impact the outcome of the safety of the therapies and limit the efficacy of second infusions of the treatment. Due to this, the therapies based on FMC63 target B-cell malignancies, and most of the patients suffer B-cell aplasia because of previous treatments. Therefore, the impact of the CAR immunogenicity has not been a concern. Even so, 90% of the patients have in their serum pre-existing anti-mouse scFv antibodies and 5% of these increase the titre after CAR T-cell infusion (507). However, the impact of the immunogenicity of CAR T-cells targeting non-B-cell cancers could be crucial, as such patients have an intact humoral immunity and could develop a robust humoral anti-mouse scFv response leading to CAR T-cell immunogenicity (508). In addition, CAR T-cells can also act as APCs, presenting immunogenic epitopes with their MHCs derived from the mouse scFv (232,509) and further increase the immunogenicity of the therapy. In conclusion, full human scFvs should provide the optimal binding domain for CAR T-cells to maximise the therapy's efficacy and safety (292).

The CAR's binding affinity to its antigen also seems to be key for the efficacy and safety of the therapy, and discrimination between malignant cells (overexpressing the antigen) and healthy cells (expressing physiological levels of antigen) (302–307). Thus, CAR T-cell therapies that have shown toxicities at the preclinical stage, for example, the anti-B7H4 CAR T-cell therapy designed by Smith et al. 2016, which showed tumour regression but also delayed onset toxicity (297). This therapy could be modified by affinity tuning of the scFv to avoid toxicity. Third-generation designs could be a good option for low affinity scFvs, as they could boost the activation signal and the anti-tumour cytotoxicity (308). In addition, the CAR interaction with its antigen must be specific. Specificity is a common issue with non-clinical antibodies, and also some clinical antibodies have shown

problems of non-specificity. For example, the anti-PD1 clinical antibody SHR-1210 was shown to bind with low affinity VEGFR2. This interaction leads to activation of the receptor, leading to capillary haemangioma (abnormal overgrowth of tiny blood vessels) (510). These problems could also be translated to CAR T-cell therapies leading to off-target off-tumour toxicities. Therefore, a full assessment of binding specificity is crucial before choosing the scFv for a CAR construct. Moreover, two different scFvs could form a dimeric molecule by the interaction between the VH and the VL of different scFvs. In CAR T-cells, scFv dimerisation leads to CAR clustering and tonic signalling, leading to exhausted phenotypes during CAR T-cell expansion and reduced therapy efficacy (199). The linker length between the VH chain and the VL chain is critical for dimer formation, with linkers longer than 20 amino acids being more suitable for the formation of scFv monomers (511).

Non-immunised scFv phage display libraries (aka naïve phage display libraries) were the first antibody-based libraries, synthesised by Greg Winter and John McCafferty (461). However, these libraries did not lead to the isolation of high affinity scFvs to be progressed into clinical antibodies. Furthermore, the reformatting from scFv to IgG1 also affected the affinity of the candidates. Soon after, to increase the affinity of the candidates isolated by phage display, a new generation of synthetic libraries of Fabs were developed by *in vitro* randomisation of the DNA coding for the CDRs (466). CAR discovery, where high affinity is unnecessary and could even be counterproductive, represents a new opportunity for naïve phage display libraries of scFvs. In addition, the use of phage display libraries follows the recent EURL ECVAM recommendation on non-animal derived antibodies (512).

During this research project, a novel discovery methodology has been developed for screening a human naïve phage display library of scFvs. This method allows the isolation of a high diversity of scFvs binding specifically to the desired antigen target, obtaining different variable chain families with a range of affinities of binding in a cost and time-efficient manner. The novel selection methodology described in this research uses three elements: phage display, yeast display and mammalian adherent target cells, expressing the antigen of interest.

The method can be divided into four steps. The first step consists of the scFvs selection from the phage library using the yeast display system as an antigen source. A pool of scFvs are selected from the diverse phage display library by exposure to the yeast antigen-display system and several rounds of depletion of non-specific phage and selection of specific phage are required to enrich the population of phage displaying the scFvs binding to the target antigen. In the second step, the enriched scFvs are transferred to the yeast display system. This is achieved by PCR amplification of the pool of selected scFvs from the phagemid vector and homologous recombination into the yeast display vector, where the scFvs are expressed on the yeast surface. During the third step, the pool of selected scFvs, expressed now on yeast, is exposed to mammalian adherent cells expressing the target membrane protein. Yeast expressing scFvs able to interact with the antigen are retained with the mammalian cells after several washes. The last step consists of isolating single yeast clones with positive binding to the target antigen from the final scFv pool. Several options for this final step can be considered, depending on the availability of commercial recombinant antigen. Membrane proteins with one transmembrane domain are often produced and commercialised in an Fc chimaera format. These preparations are expensive and sometimes not optimal for selection. However, they could be used as a detection tool to isolate single yeast with positive binding to the recombinant antigen by FACS. The amount of recombinant protein needed for this is low and it does not represent a high expense. In the case of no availability of commercial antigen preparations, random colony PCR and Sanger sequencing could reveal sequence diversity of the pool. An alternative approach could be to use PacBio Sequel sequencing to reveal the full diversity of the selected final population and identify VH family clusters that could indicate binding to the target antigen. scFvs from these clusters would be selected for further characterisation.

This new approach circumvents the need for recombinant protein preparations during the selection step by using yeast and mammalian cells expressing the antigen. Membrane proteins are frequently the desired target antigen in these selections. However, these proteins are often unstable in solution, leading to aggregates that can undergo conformational changes forming new epitopes and hiding *bona fide* epitopes. The presence of aggregates, even in small amounts, critically impact the phage display selection experiments, leading to the

accumulation and dominance of phage binding to these aggregates. Furthermore, commercially available recombinant proteins are frequently tagged at N- or C-terminus, which aids in the purification protocols and is also helpful during antibody selection. However, these tags can also form an immunogenic sequence that promotes dominant binders and masks the ones specific to the antigen. The cost of this preparation is also a handicap as a considerable quantity is needed. Additionally, no commercial preparations are available for many membrane proteins, often with multiple transmembrane domains, as they cannot be readily expressed or purified. These possible complications derived from recombinant proteins or peptides have been bypassed using the yeast display platform to present the antigen to the phage display library. Therefore, the antigen (domain or loop) is expressed as a fusion protein on the surface of the yeast, reducing the possibility of forming aggregates, having fresh antigen expressed the day of the selection and reducing the cost of the experiment. Then, the selection is completed by exposing the previously selected binders to the antigen expressed on mammalian cells. By changing from yeast expression of antigen to mammalian expression, the promotion of possible binder to the surface of the yeast is avoided, and the *bona fide* binders are exposed to the antigen on its natural conformation for the final selection rounds.

The method described here also overcomes two other problems associated with standard phage display selections. Phage display libraries are synthesised by PCR and the amplicons cloned cloning into a phagemid vector. In the final library, there are very low levels of non-recombinant phagemid vector (without scFvs) and truncated scFvs with stop-codons (produced by mutation during the PCR). These non-functional phagemid vectors have an advantage during the phage synthesis in the host bacteria while the phage is being assembled, as the copy number is maybe higher than the recombinant phagemid due to its lower metabolic charge. Therefore, these non-functional phagemids are enriched through the selection process together with functional phagemid in a phage entity known as polyphage, which contains several phagemids (functional and non-functional). As a result, at the end of the selection, most of the bacterial colonies carry a non-functional phagemid vector due to the advantage of the non-functional phagemid over the functional phagemid, making it hard to identify the real scFvs (coded by the functional phagemids) by colony PCR and Sanger sequencing. The transfer of the

selected pool of scFvs from the phage display system to a yeast display system eliminates polyphage promotion during the next selection steps. Moreover, the scFvs generated by phage display are the products of mRNA translation in a prokaryotic cell. The post-translational modifications that occur in prokaryotes and eukaryotes differ substantially. The former may compromise the ability of the scFvs to recognise the antigen as it would do in the eukaryote setting. Therefore, the transfer of the scFv pools to the yeast display system also provides the translated scFv products with post-translational modifications closer to the mammalian CAR T-cells. Another limitation of the standard phage display technology is the promotion of scFvs with a growth advantage in the phage display system. The phage display library could have bias promoting one or several scFvs with a metabolic advantage for the bacteria (for example, if it is easier to be synthesised) and unrelated to the strength of binding to the antigen. As a result, the observable diversity of scFvs at the end of the phage selection is low, and the selected scFvs may not reflect the most optimal or the highest affinity present in the original library. The transfer of the scFv pools to the yeast display system eliminates this possible problem. In addition, it introduces a component of avidity that boosts the binding of low affinity or low expressed scFvs. As a result, the yeast panning using mammalian cells allows obtaining a population of scFvs with higher diversity than the last round of phage display. This diversification of the output leads to identifying different families of scFv binding with low and high affinities and probably to different epitopes in the antigen. In the case of the phage display library used in this research, the phage display selection for scFvs binding to B7H4 only allowed to identify one scFv (Clone 3 B7H3). In contrast, by applying this approach, ten more scFvs were identified with a superficial screening of the output Yeast R6 B7H4. More scFvs binding to B7H4 could potentially be obtained with a deeper screening of this output.

The main weakness of this approach is the possible presence of non-functional scFv that can interact with the surface of the flask, competing with the *bona fide* scFvs during the yeast-mammalian cell panning. These non-functional scFvs could be present in the original phage display library due to changes in the ORF during the PCR that gives origin to the scFvs, subsequently cloned into the phagemid vector. Therefore, the design of the phage display library and the quality of molecular biology techniques used for its synthesis have an impact on the

selection's results, whether it is performed with classical phage display techniques or with the method described here. Although the phage display library used in this research had a high presence of non-functional scFvs, this bias was overcome by performing depletion steps with the surface of the flask before every round of yeast-mammalian cell panning.

In this project, eleven human scFvs targeting the Ig-like V-type 1 domain of the human protein B7H4 have been isolated from a naïve phage display library using the novel methodology of selection as described. These clones were prioritised for further characterisation. Additionally, an scFv targeting loop 2 of the viral protein LMP1 was also identified. This scFv was found to be dominant during the selections for LMP1 loop 2F and LMP1 loop 2Y, and in this case, the method did not unmask new candidates. This clone was not characterised further. PacBio Sequel sequencing could be used in future for the outputs obtained (Yeast R7 LMP1-l2F and Yeast R6 LMP1-l2Y) to identify other, possibly masked, candidates. Regarding the selections for LMP2 loop 2 and LMP2 loop 5, non-functional scFvs overtook the selection until the last round of yeast-mammalian cell panning. In future, screening by PacBio Sequel sequencing of the outputs Yeast R7 LMP2-l2 and Yeast R8 LMP2-l5 could be used to identify candidates among the dominant non-functional scFvs.

The aim of the B7H4 branch of the project was to obtain a wide range of B7H4-specific scFvs with different binding affinities. A future aim of the work will be to use one with lower affinity that still triggers functionality, in order to avoid the toxicity seen with anti-B7H4 CAR T-cells described by Smith et al. 2016 (297). Aside from the affinity issues, other approaches, such as Co-Stim CARs expressed in Vγ9Vδ2 T-cells, could be explored with the same objective. The DNA sequences of the scFvs Clone 3 B7H4, Clone 5 B7H4, Clone 7 B7H4 and Clone 11 B7H4 were shared with TC Biopharm Ltd. to generate lentiviral Co-Stim CAR expression constructs to subsequently transduce into Vγ9Vδ2 T-cells and investigate their therapeutic potential. However, a conflict related to the intellectual property of the scFvs isolated in this research and the recent COVID-19 pandemic impacted the development of this work. If this work can resume, the Vγ9Vδ2 T-cells modified with the generated Co-Stim CARs could be tested for CAR-driven co-

stimulation with a co-culture killing assay using pAgs-producing target cells expressing the target antigen.

As an alternative to the lentiviral platform, it was planned to develop Jurkat reporter cell lines (Jurkat-Dual) expressing second-generation CARs designed with the isolated scFvs, in order to test B7H4-induced functional signalling by the CARs. A Cas9-mediated HDR approach was designed to achieve this. A new plasmid was developed with this aim, introducing 400 bp regions of homology to the *AAVS1* locus and using the promoter EF-1α for CAR expression. After multiple rounds of transfection and selection, only four cell lines were established from this work. However, the plasmid integration in these four lines was not HDR-mediated and expression of the CAR (assessed by flow cytometry) via the EF-1α promoter was low or negative. NHEJ is the dominant DNA repair pathway in normal cells, and the rarity of HDR makes this gene-editing experiment highly inefficient. Even though the NHEJ inhibitor SCR7 and the HDR enhancer L755507 were used in the experiment, their efficacy could variable between cell lines. Other reagents could be considered to increase the efficiency of HDR in Jurkat cells.

Consequently, efforts to optimise Cas9-mediated HDR were abandoned, and instead, the two CAR formats (Short CAR and Long CAR) were designed with the scFv Clone 4 B7H4. The CAR vectors were introduced transiently by nucleofection into Jurkat-Dual cells using the original CMV promoter for CAR expression. The expression of the CARs was assessed after 48 hours, revealing low expression for the Short CAR format and very low expression for the Long CAR. These cells were used for an NF-kB activation luciferase reporter assay by co-culture with antigen-expressing cells. However, no difference was observed between the signal in the co-culture with cells expressing B7H4 compared with non-expressing cells. This could be due to the low transfection efficiency, the low CAR expression levels and/or low signal window compared to the positive control (incubation with concanavalin A). Within the project time frame, it was not possible to explore this further. As such, whether the scFv Clone 4 B7H4 can act as a functional responder to B7H4 remains to be determined (as for the other scFv clones isolated). Alternative approaches to the assay used to assess CAR dependent activation could be to examine the upregulation of the early lymphocyte activation marker CD69

by flow cytometry or quantitatively determinate the concentration of human IL2 or IFN-γ concentrations in cell culture supernatants by ELISA.

A possible next step for this project regarding the Cas9-mediated HDR approach is the optimisation of pCD8-CAR and pIgG4-CAR in several ways: 1] by introducing longer HDR regions (800 bp) that could increase the efficiency of HDR, 2] optimising the Cas9:gRNA ratio to increase the level of activity of the RNP complex, 3] nucleofection could be used to transfect the cells and 4] the EF1-α promoter could be replaced (506). As an alternative to the Cas9-mediated HDR approach, mRNA electroporation could achieve a high level of CAR expression in Jurkat without lentiviral transduction and independent of promoter activity.

Furthermore, an in-depth characterisation of the affinity of binding of the anti-B7H4 scFvs would be required since a balance between the level of CAR expression and binding affinity to the antigen would be crucial to obtain the desired level of CAR activity against antigen-overexpressing cancer cells and to be able to discriminate antigen-expressing normal cells. The K_D (the equilibrium dissociation constant between an antibody and its antigen) of the isolated anti-B7H4 scFvs could be assessed by Surface plasmon resonance (SPR). Determining the K_D for each scFv would permit a more extensive comparison between the affinities of the isolated anti-B7H4 scFvs and the affinities of other scFvs used previously to generate low affinity CARs. However, production and purification of soluble scFvs would be required for this.

Additionally, and as mentioned previously, if a higher affinity of binding by the scFv is required for CAR activation, the output Yeast R6 B7H4 could be further screened by decreasing the concentration of B7H4 antigen during the FACS experiment. Thus, the yeast able to bind the recombinant antigen in low concentrations would be selected by FACS and, therefore, the scFvs binding with high affinity would be isolated. Furthermore, third-generation constructs could be used to boost the activation signal of low affinity scFvs and assess functionality.

During this project, the LMP1 and LMP2A selections were not fully completed due to the prioritisation of the B7H4 branch of the project. As a possible next steps to complete these selections a PacBio Sequel sequencing experiment could be performed with Yeast R7 LMP2-l2 and Yeast R8 LMP2-l5 to identify candidates

among the dominant non-functional scFvs, and with Yeast R7 LMP1-l2F and Yeast R6 LMP1-l2Y to identify candidates among the dominant Clone 1 LMP1. Then, the binding of these possible identified scFvs could be assessed by flow cytometry using biotinylated peptides mimicking the target loop and streptavidin conjugated with APC. However, the peptide production, purification and biotinylation would have to be performed in-house, as no commercial options are available. An alternative is to assess binding and functionality as CAR in a co-culture functional assay with cells expressing LMP1 or LMP2A, as it was intended with Clone 1 LMP1. The activation of these CARs with antigen-expressing cells but not with control cells would also implicate binding to the loop.

In conclusion, a new methodology to isolate scFvs from phage display libraries has been established, allowing the isolation of a wide diversity of scFvs with specific binding to an antigen. With this method, eleven anti-B7H4 scFvs and one potential anti-LMP1 scFv have been obtained. These scFvs could be potentially used as CAR components. Further characterisation in CAR format would assess their suitability and clinical potential for new CAR T-cell therapies.

References

1. de-Thé G, Day NE, Geser A, Lavoué MF, Ho JH, Simons MJ, Sohier R, Tukei P, Vonka V, Zavadova H. Sero-epidemiology of the Epstein-Barr virus: preliminary analysis of an international study - a review. IARC Sci Publ. 1975;(11 Pt 2):3-16. PMID: 191375.

2. Epstein MA, Achong BG, Barr YM. Virus particles in cultured lymphoblasts from Burkitt's lymphoma. Lancet. 1964 Mar 28;1(7335):702-3. doi: 10.1016/s0140-6736(64)91524-7. PMID: 14107961.

3. Henle W, Diehl V, Kohn G, Zur Hausen H, Henle G. Herpes-type virus and chromosome marker in normal leukocytes after growth with irradiated Burkitt cells. Science. 1967 Sep 1;157(3792):1064-5. doi: 10.1126/science.157.3792.1064. PMID: 6036237.

4. Kang MS, Kieff E. Epstein-Barr virus latent genes. Exp Mol Med. 2015 Jan 23;47(1):e131. doi: 10.1038/emm.2014.84. PMID: 25613728; PMCID: PMC4314583.

5. Thorley-Lawson DA, Hawkins JB, Tracy SI, Shapiro M. The pathogenesis of Epstein-Barr virus persistent infection. Curr Opin Virol. 2013 Jun;3(3):227-32. doi: 10.1016/j.coviro.2013.04.005. Epub 2013 May 15. PMID: 23683686; PMCID: PMC3789532.

6. Thorley-Lawson DA. EBV Persistence--Introducing the Virus. Curr Top Microbiol Immunol. 2015;390(Pt 1):151-209. doi: 10.1007/978-3-319-22822-8_8. PMID: 26424647; PMCID: PMC5125397.

7. Murata T. Encyclopedia of EBV-Encoded Lytic Genes: An Update. Adv Exp Med Biol. 2018;1045:395-412. doi: 10.1007/978-981-10-7230-7_18. PMID: 29896677.

8. Wagner HJ, Bein G, Bitsch A, Kirchner H. Detection and quantification of latently infected B lymphocytes in Epstein-Barr virus-seropositive, healthy individuals by polymerase chain reaction. J Clin Microbiol. 1992 Nov;30(11):2826-9. doi: 10.1128/jcm.30.11.2826-2829.1992. PMID: 1333480; PMCID: PMC270536.

9. Gires O, Zimber-Strobl U, Gonnella R, Ueffing M, Marschall G, Zeidler R, Pich

D, Hammerschmidt W. Latent membrane protein 1 of Epstein-Barr virus mimics a constitutively active receptor molecule. EMBO J. 1997 Oct 15;16(20):6131-40. doi: 10.1093/emboj/16.20.6131. PMID: 9359753; PMCID: PMC1326297.

10. Yasui T, Luftig M, Soni V, Kieff E. Latent infection membrane protein transmembrane FWLY is critical for intermolecular interaction, raft localization, and signaling. Proc Natl Acad Sci U S A. 2004 Jan 6;101(1):278-83. doi: 10.1073/pnas.2237224100. Epub 2003 Dec 26. PMID: 14695890; PMCID: PMC314176.

11. Soni V, Yasui T, Cahir-McFarland E, Kieff E. LMP1 transmembrane domain 1 and 2 (TM1-2) FWLY mediates intermolecular interactions with TM3-6 to activate NF-kappaB. J Virol. 2006 Nov;80(21):10787-93. doi: 10.1128/JVI.01214-06. Epub 2006 Aug 23. PMID: 16928765; PMCID: PMC1641781.

12. Li HP, Chang YS. Epstein-Barr virus latent membrane protein 1: structure and functions. J Biomed Sci. 2003 Sep-Oct;10(5):490-504. doi: 10.1007/BF02256110. PMID: 12928589.

13. Bentz GL, Whitehurst CB, Pagano JS. Epstein-Barr virus latent membrane protein 1 (LMP1) C-terminal-activating region 3 contributes to LMP1-mediated cellular migration via its interaction with Ubc9. J Virol. 2011 Oct;85(19):10144-53. doi: 10.1128/JVI.05035-11. Epub 2011 Jul 27. PMID: 21795333; PMCID: PMC3196420.

14. Gires O, Kohlhuber F, Kilger E, Baumann M, Kieser A, Kaiser C, Zeidler R, Scheffer B, Ueffing M, Hammerschmidt W. Latent membrane protein 1 of Epstein-Barr virus interacts with JAK3 and activates STAT proteins. EMBO J. 1999 Jun 1;18(11):3064-73. doi: 10.1093/emboj/18.11.3064. PMID: 10357818; PMCID: PMC1171388.

15. Hannigan A, Qureshi AM, Nixon C, Tsimbouri PM, Jones S, Philbey AW, Wilson JB. Lymphocyte deficiency limits Epstein-Barr virus latent membrane protein 1 induced chronic inflammation and carcinogenic pathology in vivo. Mol Cancer. 2011 Feb 3;10(1):11. doi: 10.1186/1476-4598-10-11. PMID: 21291541; PMCID: PMC3041781.

16. Charalambous CT, Hannigan A, Tsimbouri P, McPhee GM, Wilson JB. Latent

membrane protein 1-induced EGFR signalling is negatively regulated by TGF alpha prior to neoplasia. Carcinogenesis. 2007 Aug;28(8):1839-48. doi: 10.1093/carcin/bgm055. Epub 2007 Mar 14. PMID: 17361012.

17. Kieser A, Sterz KR. The Latent Membrane Protein 1 (LMP1). Curr Top Microbiol Immunol. 2015;391:119-49. doi: 10.1007/978-3-319-22834-1_4. PMID: 26428373.

18. Cen O, Longnecker R. Latent Membrane Protein 2 (LMP2). Curr Top Microbiol Immunol. 2015;391:151-80. doi: 10.1007/978-3-319-22834-1_5. PMID: 26428374.

19. Matskova L, Ernberg I, Pawson T, Winberg G. C-terminal domain of the Epstein-Barr virus LMP2A membrane protein contains a clustering signal. J Virol. 2001 Nov;75(22):10941-9. doi: 10.1128/JVI.75.22.10941-10949.2001. PMID: 11602734; PMCID: PMC114674.

20. Rovedo M, Longnecker R. Epstein-barr virus latent membrane protein 2B (LMP2B) modulates LMP2A activity. J Virol. 2007 Jan;81(1):84-94. doi: 10.1128/JVI.01302-06. Epub 2006 Oct 11. PMID: 17035319; PMCID: PMC1797235.

21. Caldwell RG, Wilson JB, Anderson SJ, Longnecker R. Epstein-Barr virus LMP2A drives B cell development and survival in the absence of normal B cell receptor signals. Immunity. 1998 Sep;9(3):405-11. doi: 10.1016/s1074-7613(00)80623-8. PMID: 9768760.

22. Mancao C, Hammerschmidt W. Epstein-Barr virus latent membrane protein 2A is a B-cell receptor mimic and essential for B-cell survival. Blood. 2007 Nov 15;110(10):3715-21. doi: 10.1182/blood-2007-05-090142. Epub 2007 Aug 6. PMID: 17682125; PMCID: PMC2077319.

23. Souza TA, Stollar BD, Sullivan JL, Luzuriaga K, Thorley-Lawson DA. Peripheral B cells latently infected with Epstein-Barr virus display molecular hallmarks of classical antigen-selected memory B cells. Proc Natl Acad Sci U S A. 2005 Dec 13;102(50):18093-8. doi: 10.1073/pnas.0509311102. Epub 2005 Dec 5. PMID: 16330748; PMCID: PMC1306799.

24. Engels N, Yigit G, Emmerich CH, Czesnik D, Schild D, Wienands J. Epstein-Barr virus LMP2A signaling in statu nascendi mimics a B cell antigen receptor-like activation signal. Cell Commun Signal. 2012 Apr 3;10:9. doi:

10.1186/1478-811X-10-9. PMID: 22472181; PMCID: PMC3352256.

25. Fotheringham JA, Raab-Traub N. Epstein-Barr virus latent membrane protein 2 effects on epithelial acinus development reveal distinct requirements for the PY and YEEA motifs. J Virol. 2013 Dec;87(24):13803-15. doi: 10.1128/JVI.02203-13. Epub 2013 Oct 9. PMID: 24109232; PMCID: PMC3838228.

26. Wu H, Kapoor P, Frappier L. Separation of the DNA replication, segregation, and transcriptional activation functions of Epstein-Barr nuclear antigen 1. J Virol. 2002 Mar;76(5):2480-90. doi: 10.1128/jvi.76.5.2480-2490.2002. PMID: 11836426; PMCID: PMC135949.

27. Kaiser C, Laux G, Eick D, Jochner N, Bornkamm GW, Kempkes B. The proto-oncogene c-myc is a direct target gene of Epstein-Barr virus nuclear antigen 2. J Virol. 1999 May;73(5):4481-4. doi: 10.1128/JVI.73.5.4481-4484.1999. PMID: 10196351; PMCID: PMC104340.

28. Wang F, Tsang SF, Kurilla MG, Cohen JI, Kieff E. Epstein-Barr virus nuclear antigen 2 transactivates latent membrane protein LMP1. J Virol. 1990 Jul;64(7):3407-16. doi: 10.1128/JVI.64.7.3407-3416.1990. PMID: 2352328; PMCID: PMC249594.

29. Gross H, Hennard C, Masouris I, Cassel C, Barth S, Stober-Grässer U, Mamiani A, Moritz B, Ostareck D, Ostareck-Lederer A, Neuenkirchen N, Fischer U, Deng W, Leonhardt H, Noessner E, Kremmer E, Grässer FA. Binding of the heterogeneous ribonucleoprotein K (hnRNP K) to the Epstein-Barr virus nuclear antigen 2 (EBNA2) enhances viral LMP2A expression. PLoS One. 2012;7(8):e42106. doi: 10.1371/journal.pone.0042106. Epub 2012 Aug 3. PMID: 22879910; PMCID: PMC3411732

30. Harada S, Kieff E. Epstein-Barr virus nuclear protein LP stimulates EBNA-2 acidic domain-mediated transcriptional activation. J Virol. 1997 Sep;71(9):6611-8. doi: 10.1128/JVI.71.9.6611-6618.1997. PMID: 9261383; PMCID: PMC191939.

31. Portal D, Zhou H, Zhao B, Kharchenko PV, Lowry E, Wong L, Quackenbush J, Holloway D, Jiang S, Lu Y, Kieff E. Epstein-Barr virus nuclear antigen leader protein localizes to promoters and enhancers with cell transcription factors and EBNA2. Proc Natl Acad Sci U S A. 2013 Nov 12;110(46):18537-42. doi:

10.1073/pnas.1317608110. Epub 2013 Oct 28. PMID: 24167291; PMCID: PMC3832032.

32. Styles CT, Paschos K, White RE, Farrell PJ. The Cooperative Functions of the EBNA3 Proteins Are Central to EBV Persistence and Latency. Pathogens. 2018 Mar 17;7(1):31. doi: 10.3390/pathogens7010031. PMID: 29562595; PMCID: PMC5874757.

33. Waltzer L, Perricaudet M, Sergeant A, Manet E. Epstein-Barr virus EBNA3A and EBNA3C proteins both repress RBP-J kappa-EBNA2-activated transcription by inhibiting the binding of RBP-J kappa to DNA. J Virol. 1996 Sep;70(9):5909-15. doi: 10.1128/JVI.70.9.5909-5915.1996. PMID: 8709211; PMCID: PMC190609.

34. Bazot Q, Deschamps T, Tafforeau L, Siouda M, Leblanc P, Harth-Hertle ML, Rabourdin-Combe C, Lotteau V, Kempkes B, Tommasino M, Gruffat H, Manet E. Epstein-Barr virus nuclear antigen 3A protein regulates CDKN2B transcription via interaction with MIZ-1. Nucleic Acids Res. 2014 Sep;42(15):9700-16. doi: 10.1093/nar/gku697. Epub 2014 Aug 4. PMID: 25092922; PMCID: PMC4150796.

35. Chen A, Divisconte M, Jiang X, Quink C, Wang F. Epstein-Barr virus with the latent infection nuclear antigen 3B completely deleted is still competent for B-cell growth transformation in vitro. J Virol. 2005 Apr;79(7):4506-9. doi: 10.1128/JVI.79.7.4506-4509.2005. PMID: 15767450; PMCID: PMC1061580.

36. White RE, Rämer PC, Naresh KN, Meixlsperger S, Pinaud L, Rooney C, Savoldo B, Coutinho R, Bödör C, Gribben J, Ibrahim HA, Bower M, Nourse JP, Gandhi MK, Middeldorp J, Cader FZ, Murray P, Münz C, Allday MJ. EBNA3B-deficient EBV promotes B cell lymphomagenesis in humanized mice and is found in human tumors. J Clin Invest. 2012 Apr;122(4):1487-502. doi: 10.1172/JCI58092. Epub 2012 Mar 12. PMID: 22406538; PMCID: PMC3314448.

37. Zhao B, Mar JC, Maruo S, Lee S, Gewurz BE, Johannsen E, Holton K, Rubio R, Takada K, Quackenbush J, Kieff E. Epstein-Barr virus nuclear antigen 3C regulated genes in lymphoblastoid cell lines. Proc Natl Acad Sci U S A. 2011 Jan 4;108(1):337-42. doi: 10.1073/pnas.1017419108. Epub 2010 Dec 20. PMID: 21173222; PMCID: PMC3017193.

38. Parker GA, Crook T, Bain M, Sara EA, Farrell PJ, Allday MJ. Epstein-Barr virus

nuclear antigen (EBNA)3C is an immortalizing oncoprotein with similar properties to adenovirus E1A and papillomavirus E7. Oncogene. 1996 Dec 19;13(12):2541-9. PMID: 9000128.

39. Hsu JL, Glaser SL. Epstein-barr virus-associated malignancies: epidemiologic patterns and etiologic implications. Crit Rev Oncol Hematol. 2000 Apr;34(1):27-53. doi: 10.1016/s1040-8428(00)00046-9. PMID: 10781747.

40. Molyneux EM, Rochford R, Griffin B, Newton R, Jackson G, Menon G, Harrison CJ, Israels T, Bailey S. Burkitt's lymphoma. Lancet. 2012 Mar 31;379(9822):1234-44. doi: 10.1016/S0140-6736(11)61177-X. Epub 2012 Feb 13. PMID: 22333947.

41. Leder P, Battey J, Lenoir G, Moulding C, Murphy W, Potter H, Stewart T, Taub R. Translocations among antibody genes in human cancer. Science. 1983 Nov 18;222(4625):765-71. doi: 10.1126/science.6356357. PMID: 6356357.

42. Klein G, Klein E. Myc/Ig juxtaposition by chromosomal translocations: some new insights, puzzles and paradoxes. Immunol Today. 1985 Jul;6(7):208-15. doi: 10.1016/0167-5699(85)90036-2. PMID: 25290182.

43. Dalla-Favera R, Martinotti S, Gallo RC, Erikson J, Croce CM. Translocation and rearrangements of the c-myc oncogene locus in human undifferentiated B-cell lymphomas. Science. 1983 Feb 25;219(4587):963-7. doi: 10.1126/science.6401867. PMID: 6401867.

44. Harabuchi Y, Takahara M, Kishibe K, Nagato T, Kumai T. Extranodal Natural Killer/T-Cell Lymphoma, Nasal Type: Basic Science and Clinical Progress. Front Pediatr. 2019 Apr 16;7:141. doi: 10.3389/fped.2019.00141. PMID: 31041299; PMCID: PMC6476925.

45. Kuze T, Nakamura N, Hashimoto Y, Sasaki Y, Abe M. The characteristics of Epstein-Barr virus (EBV)-positive diffuse large B-cell lymphoma: comparison between EBV(+) and EBV(-) cases in Japanese population. Jpn J Cancer Res. 2000 Dec;91(12):1233-40. doi: 10.1111/j.1349-7006.2000.tb00909.x. PMID: 11123421; PMCID: PMC5926305.

46. Ok CY, Li L, Xu-Monette ZY, Visco C, Tzankov A, Manyam GC, Montes-Moreno S, Dybkaer K, Chiu A, Orazi A, Zu Y, Bhagat G, Chen J, Richards KL, Hsi ED, Choi WW, van Krieken JH, Huh J, Ai W, Ponzoni M, Ferreri AJ, Farnen JP,

Møller MB, Bueso-Ramos CE, Miranda RN, Winter JN, Piris MA, Medeiros LJ, Young KH. Prevalence and clinical implications of epstein-barr virus infection in de novo diffuse large B-cell lymphoma in Western countries. Clin Cancer Res. 2014 May 1;20(9):2338-49. doi: 10.1158/1078-0432.CCR-13-3157. Epub 2014 Feb 28. Erratum in: Clin Cancer Res. 2014 Sep 15;20(18):4974. Dybaer, Karen [corrected to Dybkaer, Karen]. PMID: 24583797; PMCID: PMC4014309.

47. Park S, Lee J, Ko YH, Han A, Jun HJ, Lee SC, Hwang IG, Park YH, Ahn JS, Jung CW, Kim K, Ahn YC, Kang WK, Park K, Kim WS. The impact of Epstein-Barr virus status on clinical outcome in diffuse large B-cell lymphoma. Blood. 2007 Aug 1;110(3):972-8. doi: 10.1182/blood-2007-01-067769. Epub 2007 Mar 30. PMID: 17400912.

48. Beltran BE, Morales D, Quiñones P, Medeiros LJ, Miranda RN, Castillo JJ. EBV-positive diffuse large b-cell lymphoma in young immunocompetent individuals. Clin Lymphoma Myeloma Leuk. 2011 Dec;11(6):512-6. doi: 10.1016/j.clml.2011.07.003. Epub 2011 Sep 1. PMID: 21889434.

49. Hong JY, Yoon DH, Suh C, Huh J, Do IG, Sohn I, Jo J, Jung SH, Hong ME, Yoon H, Ko YH, Kim SJ, Kim WS. EBV-positive diffuse large B-cell lymphoma in young adults: is this a distinct disease entity? Ann Oncol. 2015 Mar;26(3):548-55. doi: 10.1093/annonc/mdu556. Epub 2014 Dec 4. PMID: 25475080.

50. Montes-Moreno S, Odqvist L, Diaz-Perez JA, Lopez AB, de Villambrosía SG, Mazorra F, Castillo ME, Lopez M, Pajares R, García JF, Mollejo M, Camacho FI, Ruiz-Marcellán C, Adrados M, Ortiz N, Franco R, Ortiz-Hidalgo C, Suarez-Gauthier A, Young KH, Piris MA. EBV-positive diffuse large B-cell lymphoma of the elderly is an aggressive post-germinal center B-cell neoplasm characterized by prominent nuclear factor-kB activation. Mod Pathol. 2012 Jul;25(7):968-82. doi: 10.1038/modpathol.2012.52. Epub 2012 Apr 27. PMID: 22538516.

51. Kato H, Karube K, Yamamoto K, Takizawa J, Tsuzuki S, Yatabe Y, Kanda T, Katayama M, Ozawa Y, Ishitsuka K, Okamoto M, Kinoshita T, Ohshima K, Nakamura S, Morishima Y, Seto M. Gene expression profiling of Epstein-Barr virus-positive diffuse large B-cell lymphoma of the elderly reveals alterations of characteristic oncogenetic pathways. Cancer Sci. 2014

May;105(5):537-44. doi: 10.1111/cas.12389. Epub 2014 Apr 9. PMID: 24581222; PMCID: PMC4317839.

52. Shanbhag S, Ambinder RF. Hodgkin lymphoma: A review and update on recent progress. CA Cancer J Clin. 2018 Mar;68(2):116-132. doi: 10.3322/caac.21438. Epub 2017 Dec 1. PMID: 29194581; PMCID: PMC5842098.

53. Glaser SL, Lin RJ, Stewart SL, Ambinder RF, Jarrett RF, Brousset P, Pallesen G, Gulley ML, Khan G, O'Grady J, Hummel M, Preciado MV, Knecht H, Chan JK, Claviez A. Epstein-Barr virus-associated Hodgkin's disease: epidemiologic characteristics in international data. Int J Cancer. 1997 Feb 7;70(4):375-82. doi: 10.1002/(sici)1097-0215(19970207)70:4<375::aid-ijc1>3.0.co;2-t. PMID: 9033642.

54. Reshef R, Vardhanabhuti S, Luskin MR, Heitjan DF, Hadjiliadis D, Goral S, Krok KL, Goldberg LR, Porter DL, Stadtmauer EA, Tsai DE. Reduction of immunosuppression as initial therapy for posttransplantation lymphoproliferative disorder(★). Am J Transplant. 2011 Feb;11(2):336-47. doi: 10.1111/j.1600-6143.2010.03387.x. Epub 2011 Jan 10. PMID: 21219573; PMCID: PMC3079420.

55. Loren AW, Porter DL, Stadtmauer EA, Tsai DE. Post-transplant lymphoproliferative disorder: a review. Bone Marrow Transplant. 2003 Feb;31(3):145-55. doi: 10.1038/sj.bmt.1703806. PMID: 12621474.

56. Knowles DM. Biologic aspects of AIDS-associated non-Hodgkin's lymphoma. Curr Opin Oncol. 1993 Sep;5(5):845-51. doi: 10.1097/00001622-199309000-00012. PMID: 8218497.

57. Hernandez AM, Shibata D. Epstein-Barr virus-associated non-Hodgkin's lymphoma in HIV-infected patients. Leuk Lymphoma. 1995 Jan;16(3-4):217-21. doi: 10.3109/10428199509049760. PMID: 7719229.

58. Nishikawa J, Yoshiyama H, Iizasa H, Kanehiro Y, Nakamura M, Nishimura J, Saito M, Okamoto T, Sakai K, Suehiro Y, Yamasaki T, Oga A, Yanai H, Sakaida I. Epstein-barr virus in gastric carcinoma. Cancers (Basel). 2014 Nov 7;6(4):2259-74. doi: 10.3390/cancers6042259. PMID: 25386788; PMCID: PMC4276965.

59. Chang ET, Adami HO. The enigmatic epidemiology of nasopharyngeal

carcinoma. Cancer Epidemiol Biomarkers Prev. 2006 Oct;15(10):1765-77. doi: 10.1158/1055-9965.EPI-06-0353. PMID: 17035381.

60. Tsao SW, Yip YL, Tsang CM, Pang PS, Lau VM, Zhang G, Lo KW. Etiological factors of nasopharyngeal carcinoma. Oral Oncol. 2014 May;50(5):330-8. doi: 10.1016/j.oraloncology.2014.02.006. Epub 2014 Mar 12. PMID: 24630258.

61. Tsao SW, Tsang CM, Lo KW. Epstein-Barr virus infection and nasopharyngeal carcinoma. Philos Trans R Soc Lond B Biol Sci. 2017 Oct 19;372(1732):20160270. doi: 10.1098/rstb.2016.0270. PMID: 28893937; PMCID: PMC5597737.

62. Lu SJ, Day NE, Degos L, Lepage V, Wang PC, Chan SH, Simons M, McKnight B, Easton D, Zeng Y, et al. Linkage of a nasopharyngeal carcinoma susceptibility locus to the HLA region. Nature. 1990 Aug 2;346(6283):470-1. doi: 10.1038/346470a0. PMID: 2377207.

63. Goldsmith DB, West TM, Morton R. HLA associations with nasopharyngeal carcinoma in Southern Chinese: a meta-analysis. Clin Otolaryngol Allied Sci. 2002 Feb;27(1):61-7. doi: 10.1046/j.0307-7772.2001.00529.x. PMID: 11903375.

64. Lu CC, Chen JC, Tsai ST, Jin YT, Tsai JC, Chan SH, Su IJ. Nasopharyngeal carcinoma-susceptibility locus is localized to a 132 kb segment containing HLA-A using high-resolution microsatellite mapping. Int J Cancer. 2005 Jul 10;115(5):742-6. doi: 10.1002/ijc.20946. PMID: 15729690.

65. Iezzoni JC, Gaffey MJ, Weiss LM. The role of Epstein-Barr virus in lymphoepithelioma-like carcinomas. Am J Clin Pathol. 1995 Mar;103(3):308-15. doi: 10.1093/ajcp/103.3.308. PMID: 7872253.

66. Spencer JM, Amonette RA. Tumors with smooth muscle differentiation. Dermatol Surg. 1996 Sep;22(9):761-8. doi: 10.1111/j.1524-4725.1996.tb00726.x. PMID: 8874523.

67. Dekate J, Chetty R. Epstein-Barr Virus-Associated Smooth Muscle Tumor. Arch Pathol Lab Med. 2016 Jul;140(7):718-22. doi: 10.5858/arpa.2015-0120-RS. PMID: 27362573.

68. Taylor GS, Long HM, Brooks JM, Rickinson AB, Hislop AD. The immunology of Epstein-Barr virus-induced disease. Annu Rev Immunol. 2015;33:787-821.

doi: 10.1146/annurev-immunol-032414-112326. Epub 2015 Feb 11. PMID: 25706097.

69. Blake N, Haigh T, Shaka'a G, Croom-Carter D, Rickinson A. The importance of exogenous antigen in priming the human CD8+ T cell response: lessons from the EBV nuclear antigen EBNA1. J Immunol. 2000 Dec 15;165(12):7078-87. doi: 10.4049/jimmunol.165.12.7078. PMID: 11120837.

70. Catalina MD, Sullivan JL, Bak KR, Luzuriaga K. Differential evolution and stability of epitope-specific CD8(+) T cell responses in EBV infection. J Immunol. 2001 Oct 15;167(8):4450-7. doi: 10.4049/jimmunol.167.8.4450. Erratum in: J Immunol 2001 Nov 15;167(10):6045. PMID: 11591771.

71. Hislop AD, Annels NE, Gudgeon NH, Leese AM, Rickinson AB. Epitope-specific evolution of human CD8(+) T cell responses from primary to persistent phases of Epstein-Barr virus infection. J Exp Med. 2002 Apr 1;195(7):893-905. doi: 10.1084/jem.20011692. PMID: 11927633; PMCID: PMC2193726.

72. Tangye SG, Palendira U, Edwards ES. Human immunity against EBV-lessons from the clinic. J Exp Med. 2017 Feb;214(2):269-283. doi: 10.1084/jem.20161846. Epub 2017 Jan 20. PMID: 28108590; PMCID: PMC5294862.

73. Azzi T, Lünemann A, Murer A, Ueda S, Béziat V, Malmberg KJ, Staubli G, Gysin C, Berger C, Münz C, Chijioke O, Nadal D. Role for early-differentiated natural killer cells in infectious mononucleosis. Blood. 2014 Oct 16;124(16):2533-43. doi: 10.1182/blood-2014-01-553024. Epub 2014 Sep 9. PMID: 25205117; PMCID: PMC4199955.

74. Hendricks DW, Balfour HH Jr, Dunmire SK, Schmeling DO, Hogquist KA, Lanier LL. Cutting edge: NKG2C(hi)CD57+ NK cells respond specifically to acute infection with cytomegalovirus and not Epstein-Barr virus. J Immunol. 2014 May 15;192(10):4492-6. doi: 10.4049/jimmunol.1303211. Epub 2014 Apr 16. PMID: 24740502; PMCID: PMC4013527.

75. Yokoyama WM, Plougastel BF. Immune functions encoded by the natural killer gene complex. Nat Rev Immunol. 2003 Apr;3(4):304-16. doi: 10.1038/nri1055. PMID: 12669021.

76. Lanier LL. NK cell recognition. Annu Rev Immunol. 2005;23:225-74. doi: 10.1146/annurev.immunol.23.021704.115526. PMID: 15771571.

77. Yuling H, Ruijing X, Li L, Xiang J, Rui Z, Yujuan W, Lijun Z, Chunxian D, Xinti T, Wei X, Lang C, Yanping J, Tao X, Mengjun W, Jie X, Youxin J, Jinquan T. EBV-induced human CD8+ NKT cells suppress tumorigenesis by EBV-associated malignancies. Cancer Res. 2009 Oct 15;69(20):7935-44. doi: 10.1158/0008-5472.CAN-09-0828. Epub 2009 Oct 6. PMID: 19808969.

78. Exley M, Garcia J, Balk SP, Porcelli S. Requirements for CD1d recognition by human invariant Valpha24+ CD4-CD8- T cells. J Exp Med. 1997 Jul 7;186(1):109-20. doi: 10.1084/jem.186.1.109. PMID: 9207002; PMCID: PMC2198960.

79. Spada FM, Koezuka Y, Porcelli SA. CD1d-restricted recognition of synthetic glycolipid antigens by human natural killer T cells. J Exp Med. 1998 Oct 19;188(8):1529-34. doi: 10.1084/jem.188.8.1529. PMID: 9782130; PMCID: PMC2213414.

80. Chung BK, Tsai K, Allan LL, Zheng DJ, Nie JC, Biggs CM, Hasan MR, Kozak FK, van den Elzen P, Priatel JJ, Tan R. Innate immune control of EBV-infected B cells by invariant natural killer T cells. Blood. 2013 Oct 10;122(15):2600-8. doi: 10.1182/blood-2013-01-480665. Epub 2013 Aug 23. PMID: 23974196.

81. Lam V, DeMars R, Chen BP, Hank JA, Kovats S, Fisch P, Sondel PM. Human T cell receptor-gamma delta-expressing T-cell lines recognize MHC-controlled elements on autologous EBV-LCL that are not HLA-A, -B, -C, -DR, -DQ, or -DP. J Immunol. 1990 Jul 1;145(1):36-45. PMID: 1694208.

82. Häcker G, Kromer S, Falk M, Heeg K, Wagner H, Pfeffer K. V delta 1+ subset of human gamma delta T cells responds to ligands expressed by EBV-infected Burkitt lymphoma cells and transformed B lymphocytes. J Immunol. 1992 Dec 15;149(12):3984-9. PMID: 1334108.

83. Herrmann T, Fichtner AS, Karunakaran MM. An Update on the Molecular Basis of Phosphoantigen Recognition by Vγ9Vδ2 T Cells. Cells. 2020 Jun 9;9(6):1433. doi: 10.3390/cells9061433. PMID: 32527033; PMCID: PMC7348870.

84. Rigau M, Ostrouska S, Fulford TS, Johnson DN, Woods K, Ruan Z, McWilliam HEG, Hudson C, Tutuka C, Wheatley AK, Kent SJ, Villadangos JA, Pal B, Kurts C, Simmonds J, Pelzing M, Nash AD, Hammet A, Verhagen AM, Vairo G, Maraskovsky E, Panousis C, Gherardin NA, Cebon J, Godfrey DI, Behren A,

Uldrich AP. Butyrophilin 2A1 is essential for phosphoantigen reactivity by γδ T cells. Science. 2020 Feb 7;367(6478):eaay5516. doi: 10.1126/science.aay5516. Epub 2020 Jan 9. PMID: 31919129.

85. De Paschale M, Clerici P. Serological diagnosis of Epstein-Barr virus infection: Problems and solutions. World J Virol. 2012 Feb 12;1(1):31-43. doi: 10.5501/wjv.v1.i1.31. PMID: 24175209; PMCID: PMC3782265.

86. Middeldorp JM. Epstein-Barr Virus-Specific Humoral Immune Responses in Health and Disease. Curr Top Microbiol Immunol. 2015;391:289-323. doi: 10.1007/978-3-319-22834-1_10. PMID: 26428379.

87. Ressing ME, van Gent M, Gram AM, Hooykaas MJ, Piersma SJ, Wiertz EJ. Immune Evasion by Epstein-Barr Virus. Curr Top Microbiol Immunol. 2015;391:355-81. doi: 10.1007/978-3-319-22834-1_12. PMID: 26428381.

88. van Zyl DG, Mautner J, Delecluse HJ. Progress in EBV Vaccines. Front Oncol. 2019 Feb 25;9:104. doi: 10.3389/fonc.2019.00104. PMID: 30859093; PMCID: PMC6398348.

89. Smith C, Khanna R. The Development of Prophylactic and Therapeutic EBV Vaccines. Curr Top Microbiol Immunol. 2015;391:455-73. doi: 10.1007/978-3-319-22834-1_16. PMID: 26428385.

90. Sokal EM, Hoppenbrouwers K, Vandermeulen C, Moutschen M, Léonard P, Moreels A, Haumont M, Bollen A, Smets F, Denis M. Recombinant gp350 vaccine for infectious mononucleosis: a phase 2, randomized, double-blind, placebo-controlled trial to evaluate the safety, immunogenicity, and efficacy of an Epstein-Barr virus vaccine in healthy young adults. J Infect Dis. 2007 Dec 15;196(12):1749-53. doi: 10.1086/523813. PMID: 18190254.

91. Cui X, Cao Z, Sen G, Chattopadhyay G, Fuller DH, Fuller JT, Snapper DM, Snow AL, Mond JJ, Snapper CM. A novel tetrameric gp350 1-470 as a potential Epstein-Barr virus vaccine. Vaccine. 2013 Jun 26;31(30):3039-45. doi: 10.1016/j.vaccine.2013.04.071. Epub 2013 May 9. PMID: 23665339; PMCID: PMC3700395.

92. Elliott SL, Suhrbier A, Miles JJ, Lawrence G, Pye SJ, Le TT, Rosenstengel A, Nguyen T, Allworth A, Burrows SR, Cox J, Pye D, Moss DJ, Bharadwaj M. Phase I trial of a CD8+ T-cell peptide epitope-based vaccine for infectious mononucleosis. J Virol. 2008 Feb;82(3):1448-57. doi: 10.1128/JVI.01409-07.

Epub 2007 Nov 21. PMID: 18032491; PMCID: PMC2224445.

93. Pavlova S, Feederle R, Gärtner K, Fuchs W, Granzow H, Delecluse HJ. An Epstein-Barr virus mutant produces immunogenic defective particles devoid of viral DNA. J Virol. 2013 Feb;87(4):2011-22. doi: 10.1128/JVI.02533-12. Epub 2012 Dec 12. PMID: 23236073; PMCID: PMC3571473.

94. Lin CL, Lo WF, Lee TH, Ren Y, Hwang SL, Cheng YF, Chen CL, Chang YS, Lee SP, Rickinson AB, Tam PK. Immunization with Epstein-Barr Virus (EBV) peptide-pulsed dendritic cells induces functional CD8+ T-cell immunity and may lead to tumor regression in patients with EBV-positive nasopharyngeal carcinoma. Cancer Res. 2002 Dec 1;62(23):6952-8. PMID: 12460912.

95. Chia WK, Wang WW, Teo M, Tai WM, Lim WT, Tan EH, Leong SS, Sun L, Chen JJ, Gottschalk S, Toh HC. A phase II study evaluating the safety and efficacy of an adenovirus-ΔLMP1-LMP2 transduced dendritic cell vaccine in patients with advanced metastatic nasopharyngeal carcinoma. Ann Oncol. 2012 Apr;23(4):997-1005. doi: 10.1093/annonc/mdr341. Epub 2011 Aug 4. PMID: 21821548; PMCID: PMC3314324.

96. Wilson JB, Bell JL, Levine AJ. Expression of Epstein-Barr virus nuclear antigen-1 induces B cell neoplasia in transgenic mice. EMBO J. 1996 Jun 17;15(12):3117-26. PMID: 8670812; PMCID: PMC450254.

97. Gurer C, Strowig T, Brilot F, Pack M, Trumpfheller C, Arrey F, Park CG, Steinman RM, Münz C. Targeting the nuclear antigen 1 of Epstein-Barr virus to the human endocytic receptor DEC-205 stimulates protective T-cell responses. Blood. 2008 Aug 15;112(4):1231-9. doi: 10.1182/blood-2008-03-148072. Epub 2008 Jun 2. PMID: 18519810; PMCID: PMC2515117.

98. Hui EP, Taylor GS, Jia H, Ma BB, Chan SL, Ho R, Wong WL, Wilson S, Johnson BF, Edwards C, Stocken DD, Rickinson AB, Steven NM, Chan AT. Phase I trial of recombinant modified vaccinia ankara encoding Epstein-Barr viral tumor antigens in nasopharyngeal carcinoma patients. Cancer Res. 2013 Mar 15;73(6):1676-88. doi: 10.1158/0008-5472.CAN-12-2448. Epub 2013 Jan 24. PMID: 23348421; PMCID: PMC6485495.

99. Taylor GS, Jia H, Harrington K, Lee LW, Turner J, Ladell K, Price DA, Tanday M, Matthews J, Roberts C, Edwards C, McGuigan L, Hartley A, Wilson S, Hui EP, Chan AT, Rickinson AB, Steven NM. A recombinant modified vaccinia

ankara vaccine encoding Epstein-Barr Virus (EBV) target antigens: a phase I trial in UK patients with EBV-positive cancer. Clin Cancer Res. 2014 Oct 1;20(19):5009-22. doi: 10.1158/1078-0432.CCR-14-1122-T. Epub 2014 Aug 14. PMID: 25124688; PMCID: PMC4340506.

100. Rühl J, Citterio C, Engelmann C, Haigh T, Dzionek A, Dreyer J, Khanna R, Taylor GS, Wilson JB, Leung CS, Münz C. Heterologous prime-boost vaccination protects against EBV antigen-expressing lymphomas. J Clin Invest. 2019 May 1;129(5):2071-2087. doi: 10.1172/JCI125364. Epub 2019 Apr 15. PMID: 31042161; PMCID: PMC6486346.

101. Tashiro H, Brenner MK. Immunotherapy against cancer-related viruses. Cell Res. 2017 Jan;27(1):59-73. doi: 10.1038/cr.2016.153. Epub 2016 Dec 23. PMID: 28008927; PMCID: PMC5223233.

102. Papadopoulos EB, Ladanyi M, Emanuel D, Mackinnon S, Boulad F, Carabasi MH, Castro-Malaspina H, Childs BH, Gillio AP, Small TN, et al. Infusions of donor leukocytes to treat Epstein-Barr virus-associated lymphoproliferative disorders after allogeneic bone marrow transplantation. N Engl J Med. 1994 Apr 28;330(17):1185-91. doi: 10.1056/NEJM199404283301703. PMID: 8093146.

103. Rooney CM, Smith CA, Ng CY, Loftin S, Li C, Krance RA, Brenner MK, Heslop HE. Use of gene-modified virus-specific T lymphocytes to control Epstein-Barr-virus-related lymphoproliferation. Lancet. 1995 Jan 7;345(8941):9-13. doi: 10.1016/s0140-6736(95)91150-2. PMID: 7799740.

104. Heslop HE, Slobod KS, Pule MA, Hale GA, Rousseau A, Smith CA, Bollard CM, Liu H, Wu MF, Rochester RJ, Amrolia PJ, Hurwitz JL, Brenner MK, Rooney CM. Long-term outcome of EBV-specific T-cell infusions to prevent or treat EBV-related lymphoproliferative disease in transplant recipients. Blood. 2010 Feb 4;115(5):925-35. doi: 10.1182/blood-2009-08-239186. Epub 2009 Oct 30. PMID: 19880495; PMCID: PMC2817637.

105. Apcher S, Komarova A, Daskalogianni C, Yin Y, Malbert-Colas L, Fåhraeus R. mRNA translation regulation by the Gly-Ala repeat of Epstein-Barr virus nuclear antigen 1. J Virol. 2009 Feb;83(3):1289-98. doi: 10.1128/JVI.01369-08. Epub 2008 Nov 19. PMID: 19019958; PMCID: PMC2620890.

106. Blake N, Lee S, Redchenko I, Thomas W, Steven N, Leese A, Steigerwald-

Mullen P, Kurilla MG, Frappier L, Rickinson A. Human CD8+ T cell responses to EBV EBNA1: HLA class I presentation of the (Gly-Ala)-containing protein requires exogenous processing. Immunity. 1997 Dec;7(6):791-802. doi: 10.1016/s1074-7613(00)80397-0. PMID: 9430224.

107. Levitskaya J, Coram M, Levitsky V, Imreh S, Steigerwald-Mullen PM, Klein G, Kurilla MG, Masucci MG. Inhibition of antigen processing by the internal repeat region of the Epstein-Barr virus nuclear antigen-1. Nature. 1995 Jun 22;375(6533):685-8. doi: 10.1038/375685a0. PMID: 7540727.

108. Levitskaya J, Sharipo A, Leonchiks A, Ciechanover A, Masucci MG. Inhibition of ubiquitin/proteasome-dependent protein degradation by the Gly-Ala repeat domain of the Epstein-Barr virus nuclear antigen 1. Proc Natl Acad Sci U S A. 1997 Nov 11;94(23):12616-21. doi: 10.1073/pnas.94.23.12616. PMID: 9356498; PMCID: PMC25057.

109. Yin Y, Manoury B, Fåhraeus R. Self-inhibition of synthesis and antigen presentation by Epstein-Barr virus-encoded EBNA1. Science. 2003 Sep 5;301(5638):1371-4. doi: 10.1126/science.1088902. PMID: 12958359.

110. Bollard CM, Gottschalk S, Torrano V, Diouf O, Ku S, Hazrat Y, Carrum G, Ramos C, Fayad L, Shpall EJ, Pro B, Liu H, Wu MF, Lee D, Sheehan AM, Zu Y, Gee AP, Brenner MK, Heslop HE, Rooney CM. Sustained complete responses in patients with lymphoma receiving autologous cytotoxic T lymphocytes targeting Epstein-Barr virus latent membrane proteins. J Clin Oncol. 2014 Mar 10;32(8):798-808. doi: 10.1200/JCO.2013.51.5304. Epub 2013 Dec 16. PMID: 24344220; PMCID: PMC3940538.

111. Bollard CM, Tripic T, Cruz CR, Dotti G, Gottschalk S, Torrano V, Dakhova O, Carrum G, Ramos CA, Liu H, Wu MF, Marcogliese AN, Barese C, Zu Y, Lee DY, O'Connor O, Gee AP, Brenner MK, Heslop HE, Rooney CM. Tumor-Specific T-Cells Engineered to Overcome Tumor Immune Evasion Induce Clinical Responses in Patients With Relapsed Hodgkin Lymphoma. J Clin Oncol. 2018 Apr 10;36(11):1128-1139. doi: 10.1200/JCO.2017.74.3179. Epub 2018 Jan 9. PMID: 29315015; PMCID: PMC5891126.

112. Lei X, Wang L, Yang J, Sun LZ. TGFbeta signaling supports survival and metastasis of endometrial cancer cells. Cancer Manag Res. 2009 Apr;2009(1):15-24. PMID: 20622970; PMCID: PMC2901109.

113. Colak S, Ten Dijke P. Targeting TGF-ß Signaling in Cancer. Trends Cancer. 2017 Jan;3(1):56-71. doi: 10.1016/j.trecan.2016.11.008. Epub 2017 Jan 3. PMID: 28718426.

114. Fogg MH, Wirth LJ, Posner M, Wang F. Decreased EBNA-1-specific CD8+ T cells in patients with Epstein-Barr virus-associated nasopharyngeal carcinoma. Proc Natl Acad Sci U S A. 2009 Mar 3;106(9):3318-23. doi: 10.1073/pnas.0813320106. Epub 2009 Feb 11. PMID: 19211798; PMCID: PMC2651339.

115. Lee SP, Brooks JM, Al-Jarrah H, Thomas WA, Haigh TA, Taylor GS, Humme S, Schepers A, Hammerschmidt W, Yates JL, Rickinson AB, Blake NW. CD8 T cell recognition of endogenously expressed epstein-barr virus nuclear antigen 1. J Exp Med. 2004 May 17;199(10):1409-20. doi: 10.1084/jem.20040121. PMID: 15148339; PMCID: PMC2211813.

116. Münz C. Epstein-barr virus nuclear antigen 1: from immunologically invisible to a promising T cell target. J Exp Med. 2004 May 17;199(10):1301-4. doi: 10.1084/jem.20040730. PMID: 15148332; PMCID: PMC2211815.

117. Moreno MA, Or-Geva N, Aftab BT, Khanna R, Croze E, Steinman L, Han MH. Molecular signature of Epstein-Barr virus infection in MS brain lesions. Neurol Neuroimmunol Neuroinflamm. 2018 Jun 7;5(4):e466. doi: 10.1212/NXI.0000000000000466. PMID: 29892607; PMCID: PMC5994704.

118. Hassani A, Corboy JR, Al-Salam S, Khan G. Epstein-Barr virus is present in the brain of most cases of multiple sclerosis and may engage more than just B cells. PLoS One. 2018 Feb 2;13(2):e0192109. doi: 10.1371/journal.pone.0192109. PMID: 29394264; PMCID: PMC5796799.

119. Bar-Or A, Pender MP, Khanna R, Steinman L, Hartung HP, Maniar T, Croze E, Aftab BT, Giovannoni G, Joshi MA. Epstein-Barr Virus in Multiple Sclerosis: Theory and Emerging Immunotherapies. Trends Mol Med. 2020 Mar;26(3):296-310. doi: 10.1016/j.molmed.2019.11.003. Epub 2019 Dec 17. Erratum in: Trends Mol Med. 2021 Apr;27(4):410-411. PMID: 31862243; PMCID: PMC7106557.

120. Pender MP, Csurhes PA, Smith C, Douglas NL, Neller MA, Matthews KK, Beagley L, Rehan S, Crooks P, Hopkins TJ, Blum S, Green KA, Ioannides ZA, Swayne A, Aftab BT, Hooper KD, Burrows SR, Thompson KM, Coulthard A,

Khanna R. Epstein-Barr virus-specific T cell therapy for progressive multiple sclerosis. JCI Insight. 2018 Nov 15;3(22):e124714. doi: 10.1172/jci.insight.124714. Erratum in: JCI Insight. 2020 Oct 15;5(20): PMID: 30429369; PMCID: PMC6302936.

121. Lai J, Choo JAL, Tan WJ, Too CT, Oo MZ, Suter MA, Mustafa FB, Srinivasan N, Chan CEZ, Lim AGX, Zhong Y, Chan SH, Hanson BJ, Gascoigne NRJ, MacAry PA. TCR-like antibodies mediate complement and antibody-dependent cellular cytotoxicity against Epstein-Barr virus-transformed B lymphoblastoid cells expressing different HLA-A*02 microvariants. Sci Rep. 2017 Aug 30;7(1):9923. doi: 10.1038/s41598-017-10265-6. PMID: 28855662; PMCID: PMC5577143.

122. Ahmed M, Lopez-Albaitero A, Pankov D, Santich BH, Liu H, Yan S, Xiang J, Wang P, Hasan AN, Selvakumar A, O'Reilly RJ, Liu C, Cheung NV. TCR-mimic bispecific antibodies targeting LMP2A show potent activity against EBV malignancies. JCI Insight. 2018 Feb 22;3(4):e97805. doi: 10.1172/jci.insight.97805. PMID: 29467338; PMCID: PMC5916246.

123. Chen R, Zhang D, Mao Y, Zhu J, Ming H, Wen J, Ma J, Cao Q, Lin H, Tang Q, Liang J, Feng Z. A human Fab-based immunoconjugate specific for the LMP1 extracellular domain inhibits nasopharyngeal carcinoma growth in vitro and in vivo. Mol Cancer Ther. 2012 Mar;11(3):594-603. doi: 10.1158/1535-7163.MCT-11-0725. Epub 2011 Dec 14. PMID: 22169768.

124. Tang X, Zhou Y, Li W, Tang Q, Chen R, Zhu J, Feng Z. T cells expressing a LMP1-specific chimeric antigen receptor mediate antitumor effects against LMP1-positive nasopharyngeal carcinoma cells in vitro and in vivo. J Biomed Res. 2014 Nov;28(6):468-75. doi: 10.7555/JBR.28.20140066. Epub 2014 Dec 1. PMID: 25469116; PMCID: PMC4250525.

125. Cao Q, Zhang D, Mao Y, Meng C, Zhu J, Feng Z, Chen R. A human Fab exclusively binding to the extracellular domain of LMP2A. Biochem Biophys Res Commun. 2017 Jan 8;482(2):226-231. doi: 10.1016/j.bbrc.2016.11.045. Epub 2016 Nov 11. PMID: 27845040.

126. Chen Y, Chen RJ, Huang XC, Tang GX, Kuai XW, Zhang MJ, Zhang DW, Tang Q, Zhu J, Feng ZQ. [Construction of latent membrane protein 2A chimeric antigen receptor-T cells and their lethal effects on nasopharyngeal

carcinoma cells]. Zhonghua Er Bi Yan Hou Tou Jing Wai Ke Za Zhi. 2018 Dec 7;53(12):925-930. Chinese. doi: 10.3760/cma.j.issn.1673-0860.2018.12.010. PMID: 30585005.

127. Jiao Y, Zhao P, Zhu J, Grabinski T, Feng Z, Guan X, Skinner RS, Gross MD, Hay RV, Tachibana H, Cao B. Construction of human naïve Fab library and characterization of anti-met Fab fragment generated from the library. Mol Biotechnol. 2005 Sep;31(1):41-54. doi: 10.1385/mb:31:1:041. PMID: 16118414.

128. Ammous-Boukhris N, Mosbah A, Ayadi W, Sahli E, Chevance S, Bondon A, Gargouri A, Baudy-Floc'h M, Mokdad-Gargouri R. B1.12: a novel peptide interacting with the extracellular loop of the EBV oncoprotein LMP1. Sci Rep. 2019 Mar 13;9(1):4389. doi: 10.1038/s41598-019-39732-y. PMID: 30867462; PMCID: PMC6416395.

129. Sica GL, Choi IH, Zhu G, Tamada K, Wang SD, Tamura H, Chapoval AI, Flies DB, Bajorath J, Chen L. B7-H4, a molecule of the B7 family, negatively regulates T cell immunity. Immunity. 2003 Jun;18(6):849-61. doi: 10.1016/s1074-7613(03)00152-3. PMID: 12818165.

130. Prasad DV, Richards S, Mai XM, Dong C. B7S1, a novel B7 family member that negatively regulates T cell activation. Immunity. 2003 Jun;18(6):863-73. doi: 10.1016/s1074-7613(03)00147-x. PMID: 12818166.

131. Zang X, Loke P, Kim J, Murphy K, Waitz R, Allison JP. B7x: a widely expressed B7 family member that inhibits T cell activation. Proc Natl Acad Sci U S A. 2003 Sep 2;100(18):10388-92. doi: 10.1073/pnas.1434299100. Epub 2003 Aug 14. PMID: 12920180; PMCID: PMC193571.

132. Paulick MG, Bertozzi CR. The glycosylphosphatidylinositol anchor: a complex membrane-anchoring structure for proteins. Biochemistry. 2008 Jul 8;47(27):6991-7000. doi: 10.1021/bi8006324. Epub 2008 Jun 17. PMID: 18557633; PMCID: PMC2663890.

133. Tringler B, Zhuo S, Pilkington G, Torkko KC, Singh M, Lucia MS, Heinz DE, Papkoff J, Shroyer KR. B7-h4 is highly expressed in ductal and lobular breast cancer. Clin Cancer Res. 2005 Mar 1;11(5):1842-8. doi: 10.1158/1078-0432.CCR-04-1658. PMID: 15756008.

134. Tringler B, Liu W, Corral L, Torkko KC, Enomoto T, Davidson S, Lucia MS,

Heinz DE, Papkoff J, Shroyer KR. B7-H4 overexpression in ovarian tumors. Gynecol Oncol. 2006 Jan;100(1):44-52. doi: 10.1016/j.ygyno.2005.08.060. Epub 2005 Oct 26. PMID: 16256178.

135. Miyatake T, Tringler B, Liu W, Liu SH, Papkoff J, Enomoto T, Torkko KC, Dehn DL, Swisher A, Shroyer KR. B7-H4 (DD-O110) is overexpressed in high risk uterine endometrioid adenocarcinomas and inversely correlated with tumor T-cell infiltration. Gynecol Oncol. 2007 Jul;106(1):119-27. doi: 10.1016/j.ygyno.2007.03.039. Epub 2007 May 16. PMID: 17509674.

136. Zang X, Thompson RH, Al-Ahmadie HA, Serio AM, Reuter VE, Eastham JA, Scardino PT, Sharma P, Allison JP. B7-H3 and B7x are highly expressed in human prostate cancer and associated with disease spread and poor outcome. Proc Natl Acad Sci U S A. 2007 Dec 4;104(49):19458-63. doi: 10.1073/pnas.0709802104. Epub 2007 Nov 27. PMID: 18042703; PMCID: PMC2148311.

137. Quandt D, Fiedler E, Boettcher D, Marsch WCh, Seliger B. B7-h4 expression in human melanoma: its association with patients' survival and antitumor immune response. Clin Cancer Res. 2011 May 15;17(10):3100-11. doi: 10.1158/1078-0432.CCR-10-2268. Epub 2011 Mar 4. PMID: 21378130.

138. Chen LJ, Sun J, Wu HY, Zhou SM, Tan Y, Tan M, Shan BE, Lu BF, Zhang XG. B7-H4 expression associates with cancer progression and predicts patient's survival in human esophageal squamous cell carcinoma. Cancer Immunol Immunother. 2011 Jul;60(7):1047-55. doi: 10.1007/s00262-011-1017-3. Epub 2011 Apr 26. PMID: 21519829.

139. Arigami T, Uenosono Y, Ishigami S, Hagihara T, Haraguchi N, Natsugoe S. Clinical significance of the B7-H4 coregulatory molecule as a novel prognostic marker in gastric cancer. World J Surg. 2011 Sep;35(9):2051-7. doi: 10.1007/s00268-011-1186-4. PMID: 21748517.

140. Geng Y, Wang H, Lu C, Li Q, Xu B, Jiang J, Wu C. Expression of costimulatory molecules B7-H1, B7-H4 and Foxp3+ Tregs in gastric cancer and its clinical significance. Int J Clin Oncol. 2015 Apr;20(2):273-81. doi: 10.1007/s10147-014-0701-7. Epub 2014 May 9. PMID: 24804867.

141. Li ZY, Zhang XH, Chen Y, Guo JG, Sai K, Yang QY, Chen ZP, Mou YG. Clinical significance of B7-H4 expression in matched non-small cell lung cancer brain

metastases and primary tumors. Onco Targets Ther. 2013 Jul 10;6:869-75. doi: 10.2147/OTT.S48085. PMID: 23874109; PMCID: PMC3711949.

142. Chen Y, Sun J, Zhao H, Zhu D, Zhi Q, Song S, Zhang L, He S, Kuang Y, Zhang Z, Li D. The coexpression and clinical significance of costimulatory molecules B7-H1, B7-H3, and B7-H4 in human pancreatic cancer. Onco Targets Ther. 2014 Aug 19;7:1465-72. doi: 10.2147/OTT.S66809. PMID: 25170273; PMCID: PMC4145732.

143. Wang X, Wang T, Xu M, Xiao L, Luo Y, Huang W, Zhang Y, Geng W. B7-H4 overexpression impairs the immune response of T cells in human cervical carcinomas. Hum Immunol. 2014 Dec;75(12):1203-9. doi: 10.1016/j.humimm.2014.10.002. Epub 2014 Oct 13. PMID: 25446402.

144. Wu L, Deng WW, Yu GT, Mao L, Bu LL, Ma SR, Liu B, Zhang WF, Sun ZJ. B7-H4 expression indicates poor prognosis of oral squamous cell carcinoma. Cancer Immunol Immunother. 2016 Sep;65(9):1035-45. doi: 10.1007/s00262-016-1867-9. Epub 2016 Jul 6. PMID: 27383830.

145. Liu CL, Zang XX, Huang H, Zhang H, Wang C, Kong YL, Zhang HY. The expression of B7-H3 and B7-H4 in human gallbladder carcinoma and their clinical implications. Eur Rev Med Pharmacol Sci. 2016 Nov;20(21):4466-4473. PMID: 27874953.

146. Che F, Heng X, Zhang H, Su Q, Zhang B, Chen Y, Zhang Z, Du Y, Wang L. Novel B7-H4-mediated crosstalk between human non-Hodgkin lymphoma cells and tumor-associated macrophages leads to immune evasion via secretion of IL-6 and IL-10. Cancer Immunol Immunother. 2017 Jun;66(6):717-729. doi: 10.1007/s00262-017-1961-7. Epub 2017 Feb 28. PMID: 28246881.

147. Chen C, Qu QX, Xie F, Zhu WD, Zhu YH, Huang JA. Analysis of B7-H4 expression in metastatic pleural adenocarcinoma and therapeutic potential of its antagonists. BMC Cancer. 2017 Sep 18;17(1):652. doi: 10.1186/s12885-017-3615-8. PMID: 28923053; PMCID: PMC5604341.

148. Kang FB, Wang L, Sun DX, Li HJ, Li D, Wang Y, Kang JW. B7-H4 overexpression is essential for early hepatocellular carcinoma progression and recurrence. Oncotarget. 2017 Sep 8;8(46):80878-80888. doi: 10.18632/oncotarget.20718. PMID: 29113351; PMCID: PMC5655246.

149. Cao H, Wang Q, Gao Z, Xu X, Lu Q, Wu Y. Clinical value of detecting IQGAP3, B7-H4 and cyclooxygenase-2 in the diagnosis and prognostic evaluation of colorectal cancer. Cancer Cell Int. 2019 Jun 14;19:163. doi: 10.1186/s12935-019-0881-3. PMID: 31223291; PMCID: PMC6570966.

150. Kryczek I, Zou L, Rodriguez P, Zhu G, Wei S, Mottram P, Brumlik M, Cheng P, Curiel T, Myers L, Lackner A, Alvarez X, Ochoa A, Chen L, Zou W. B7-H4 expression identifies a novel suppressive macrophage population in human ovarian carcinoma. J Exp Med. 2006 Apr 17;203(4):871-81. doi: 10.1084/jem.20050930. Epub 2006 Apr 10. PMID: 16606666; PMCID: PMC2118300.

151. Liu L, Li D, Chen S, Zhao R, Pang D, Li D, Fu Z. B7-H4 expression in human infiltrating ductal carcinoma-associated macrophages. Mol Med Rep. 2016 Sep;14(3):2135-42. doi: 10.3892/mmr.2016.5510. Epub 2016 Jul 13. PMID: 27430170.

152. Watanabe N, Gavrieli M, Sedy JR, Yang J, Fallarino F, Loftin SK, Hurchla MA, Zimmerman N, Sim J, Zang X, Murphy TL, Russell JH, Allison JP, Murphy KM. BTLA is a lymphocyte inhibitory receptor with similarities to CTLA-4 and PD-1. Nat Immunol. 2003 Jul;4(7):670-9. doi: 10.1038/ni944. Epub 2003 Jun 8. PMID: 12796776.

153. Sedy JR, Gavrieli M, Potter KG, Hurchla MA, Lindsley RC, Hildner K, Scheu S, Pfeffer K, Ware CF, Murphy TL, Murphy KM. B and T lymphocyte attenuator regulates T cell activation through interaction with herpesvirus entry mediator. Nat Immunol. 2005 Jan;6(1):90-8. doi: 10.1038/ni1144. Epub 2004 Nov 28. PMID: 15568026.

154. MacGregor HL, Ohashi PS. Molecular Pathways: Evaluating the Potential for B7-H4 as an Immunoregulatory Target. Clin Cancer Res. 2017 Jun 15;23(12):2934-2941. doi: 10.1158/1078-0432.CCR-15-2440. Epub 2017 Mar 21. PMID: 28325750.

155. Jeon H, Vigdorovich V, Garrett-Thomson SC, Janakiram M, Ramagopal UA, Abadi YM, Lee JS, Scandiuzzi L, Ohaegbulam KC, Chinai JM, Zhao R, Yao Y, Mao Y, Sparano JA, Almo SC, Zang X. Structure and cancer immunotherapy of the B7 family member B7x. Cell Rep. 2014 Nov 6;9(3):1089-98. doi: 10.1016/j.celrep.2014.09.053. Epub 2014 Oct 30. PMID: 25437562; PMCID:

PMC4250833.

156. Leong SR, Liang WC, Wu Y, Crocker L, Cheng E, Sampath D, Ohri R, Raab H, Hass PE, Pham T, Firestein R, Li D, Schutten M, Stagg NJ, Ogasawara A, Koppada N, Roth L, Williams SP, Lee BC, Chalouni C, Peng I, DeVoss J, Tremayne J, Polakis P, Polson AG. An anti-B7-H4 antibody-drug conjugate for the treatment of breast cancer. Mol Pharm. 2015 Jun 1;12(6):1717-29. doi: 10.1021/mp5007745. Epub 2015 Apr 23. PMID: 25853436.

157. Shields RL, Lai J, Keck R, O'Connell LY, Hong K, Meng YG, Weikert SH, Presta LG. Lack of fucose on human IgG1 N-linked oligosaccharide improves binding to human Fcgamma RIII and antibody-dependent cellular toxicity. J Biol Chem. 2002 Jul 26;277(30):26733-40. doi: 10.1074/jbc.M202069200. Epub 2002 May 1. PMID: 11986321.

158. Sakae Y, Satoh T, Yagi H, Yanaka S, Yamaguchi T, Isoda Y, Iida S, Okamoto Y, Kato K. Conformational effects of N-glycan core fucosylation of immunoglobulin G Fc region on its interaction with Fcγ receptor IIIa. Sci Rep. 2017 Oct 23;7(1):13780. doi: 10.1038/s41598-017-13845-8. PMID: 29062024; PMCID: PMC5653758.

159. Cartron G, Dacheux L, Salles G, Solal-Celigny P, Bardos P, Colombat P, Watier H. Therapeutic activity of humanized anti-CD20 monoclonal antibody and polymorphism in IgG Fc receptor FcgammaRIIIa gene. Blood. 2002 Feb 1;99(3):754-8. doi: 10.1182/blood.v99.3.754. PMID: 11806974.

160. Umaña P, Jean-Mairet J, Moudry R, Amstutz H, Bailey JE. Engineered glycoforms of an antineuroblastoma IgG1 with optimized antibody-dependent cellular cytotoxic activity. Nat Biotechnol. 1999 Feb;17(2):176-80. doi: 10.1038/6179. PMID: 10052355.

161. Yamane-Ohnuki N, Kinoshita S, Inoue-Urakubo M, Kusunoki M, Iida S, Nakano R, Wakitani M, Niwa R, Sakurada M, Uchida K, Shitara K, Satoh M. Establishment of FUT8 knockout Chinese hamster ovary cells: an ideal host cell line for producing completely defucosylated antibodies with enhanced antibody-dependent cellular cytotoxicity. Biotechnol Bioeng. 2004 Sep 5;87(5):614-22. doi: 10.1002/bit.20151. PMID: 15352059.

162. Kaplan CD, Houser D, Kemp F, Nielson N, Hsu A, Legris K, Brattich G, Xiang H, Ahene A, Jeffry U, Bellovin D, Borges L. FPA150, a novel B7-H4

therapeutic antibody with checkpoint blockade and ADCC activities. Ann Oncol. 2017 Sep 1;28(suppl_5). doi: 10.1093/annonc/mdx361.005.

163. Sachdev JC, Bauer TM, Chawla SP, Pant S, Patnaik A, Wainberg ZA, Inamdar SP, Marina N, Sun S, Schmidt M, Xiang H, LoRusso P. Phase 1a/1b study of first-in-class B7-H4 antibody, FPA150, as monotherapy in patients with advanced solid tumors. J Clin Oncol. 2019 May 20;37(15_suppl):2529–2529. doi: 10.1200/JCO.2019.37.15_suppl.2529.

164. Jiang Y, Lin J, Zhang J, Lu S, Wang C, Tong Y. Expression of co-inhibitory molecules B7-H4 and B7-H1 in Epstein-Barr virus positive diffuse large B-cell lymphoma and their roles in tumor invasion. Pathol Res Pract. 2019 Dec;215(12):152684. doi: 10.1016/j.prp.2019.152684. Epub 2019 Oct 7. PMID: 31679792.

165. Jiang Y, Cai G, Lin J, Zhang J, Bo Z, Li Y, Wang C, Tong Y. B7-H4 is highly expressed in aggressive Epstein-Barr virus positive diffuse large B-cell lymphoma and inhibits apoptosis through upregulating Erk1/2 and Akt signalling pathways. Infect Agent Cancer. 2019 Aug 8;14:20. doi: 10.1186/s13027-019-0234-9. PMID: 31406503; PMCID: PMC6686556.

166. Wang YQ, Zhang Y, Jiang W, Chen YP, Xu SY, Liu N, Zhao Y, Li L, Lei Y, Hong XH, Liang YL, Li JY, Zhang LL, Yun JP, Sun Y, Li YQ, Ma J. Development and validation of an immune checkpoint-based signature to predict prognosis in nasopharyngeal carcinoma using computational pathology analysis. J Immunother Cancer. 2019 Nov 13;7(1):298. doi: 10.1186/s40425-019-0752-4. PMID: 31722750; PMCID: PMC6854706.

167. Song H, Park G, Kim YS, Hur I, Kim H, Ryu JW, Lee HK, Cho DH, Choi IH, Lee WJ, Hur DY. B7-H4 reverse signaling induces the apoptosis of EBV-transformed B cells through Fas ligand up-regulation. Cancer Lett. 2008 Aug 8;266(2):227-37. doi: 10.1016/j.canlet.2008.02.067. Epub 2008 Apr 15. PMID: 18417276.

168. Song P, Zhang C, Peng T, Zhou XH. Roles of VTCN1 in apoptosis and invasion in nasopharyngeal carcinoma. Int J Clin Exp Pathol. 2016;9(10):10282–9.

169. Park GB, Song H, Kim YS, Sung M, Ryu JW, Lee HK, Cho DH, Kim D, Lee WJ, Hur DY. Cell cycle arrest induced by engagement of B7-H4 on Epstein-Barr virus-positive B-cell lymphoma cell lines. Immunology. 2009 Nov;128(3):360-

8. doi: 10.1111/j.1365-2567.2009.03111.x. PMID: 20067536; PMCID: PMC2770684.

170. Turatti F, Figini M, Balladore E, Alberti P, Casalini P, Marks JD, Canevari S, Mezzanzanica D. Redirected activity of human antitumor chimeric immune receptors is governed by antigen and receptor expression levels and affinity of interaction. J Immunother. 2007 Oct;30(7):684-93. doi: 10.1097/CJI.0b013e3180de5d90. PMID: 17893561.

171. Papapetrou EP, Kovalovsky D, Beloeil L, Sant'angelo D, Sadelain M. Harnessing endogenous miR-181a to segregate transgenic antigen receptor expression in developing versus post-thymic T cells in murine hematopoietic chimeras. J Clin Invest. 2009 Jan;119(1):157-68. doi: 10.1172/JCI37216. Epub 2008 Dec 1. PMID: 19033646; PMCID: PMC2613472.

172. Guest RD, Hawkins RE, Kirillova N, Cheadle EJ, Arnold J, O'Neill A, Irlam J, Chester KA, Kemshead JT, Shaw DM, Embleton MJ, Stern PL, Gilham DE. The role of extracellular spacer regions in the optimal design of chimeric immune receptors: evaluation of four different scFvs and antigens. J Immunother. 2005 May-Jun;28(3):203-11. doi: 10.1097/01.cji.0000161397.96582.59. PMID: 15838376.

173. Wilkie S, Picco G, Foster J, Davies DM, Julien S, Cooper L, Arif S, Mather SJ, Taylor-Papadimitriou J, Burchell JM, Maher J. Retargeting of human T cells to tumor-associated MUC1: the evolution of a chimeric antigen receptor. J Immunol. 2008 Apr 1;180(7):4901-9. doi: 10.4049/jimmunol.180.7.4901. PMID: 18354214.

174. Huston JS, Levinson D, Mudgett-Hunter M, Tai MS, Novotný J, Margolies MN, Ridge RJ, Bruccoleri RE, Haber E, Crea R, et al. Protein engineering of antibody binding sites: recovery of specific activity in an anti-digoxin single-chain Fv analogue produced in Escherichia coli. Proc Natl Acad Sci U S A. 1988 Aug;85(16):5879-83. doi: 10.1073/pnas.85.16.5879. PMID: 3045807; PMCID: PMC281868.

175. Bird RE, Hardman KD, Jacobson JW, Johnson S, Kaufman BM, Lee SM, Lee T, Pope SH, Riordan GS, Whitlow M. Single-chain antigen-binding proteins. Science. 1988 Oct 21;242(4877):423-6. doi: 10.1126/science.3140379. Erratum in: Science 1989 Apr 28;244(4903):409. PMID: 3140379.

176. Schneider D, Xiong Y, Hu P, Wu D, Chen W, Ying T, Zhu Z, Dimitrov DS, Dropulic B, Orentas RJ. A Unique Human Immunoglobulin Heavy Chain Variable Domain-Only CD33 CAR for the Treatment of Acute Myeloid Leukemia. Front Oncol. 2018 Nov 22;8:539. doi: 10.3389/fonc.2018.00539. PMID: 30524966; PMCID: PMC6262782.

177. Jamnani FR, Rahbarizadeh F, Shokrgozar MA, Mahboudi F, Ahmadvand D, Sharifzadeh Z, Parhamifar L, Moghimi SM. T cells expressing VHH-directed oligoclonal chimeric HER2 antigen receptors: towards tumor-directed oligoclonal T cell therapy. Biochim Biophys Acta. 2014 Jan;1840(1):378-86. doi: 10.1016/j.bbagen.2013.09.029. Epub 2013 Sep 27. PMID: 24076235.

178. Zhang T, Lemoi BA, Sentman CL. Chimeric NK-receptor-bearing T cells mediate antitumor immunotherapy. Blood. 2005 Sep 1;106(5):1544-51. doi: 10.1182/blood-2004-11-4365. Epub 2005 May 12. PMID: 15890688; PMCID: PMC1895219.

179. Zhang T, Lemoi BA, Sentman CL. Chimeric NK-receptor-bearing T cells mediate antitumor immunotherapy. Blood. 2005 Sep 1;106(5):1544-51. doi: 10.1182/blood-2004-11-4365. Epub 2005 May 12. PMID: 15890688; PMCID: PMC1895219.

180. Hudecek M, Sommermeyer D, Kosasih PL, Silva-Benedict A, Liu L, Rader C, Jensen MC, Riddell SR. The nonsignaling extracellular spacer domain of chimeric antigen receptors is decisive for in vivo antitumor activity. Cancer Immunol Res. 2015 Feb;3(2):125-35. doi: 10.1158/2326-6066.CIR-14-0127. Epub 2014 Sep 11. PMID: 25212991; PMCID: PMC4692801.

181. Guedan S, Calderon H, Posey AD Jr, Maus MV. Engineering and Design of Chimeric Antigen Receptors. Mol Ther Methods Clin Dev. 2018 Dec 31;12:145-156. doi: 10.1016/j.omtm.2018.12.009. PMID: 30666307; PMCID: PMC6330382.

182. James SE, Greenberg PD, Jensen MC, Lin Y, Wang J, Till BG, Raubitschek AA, Forman SJ, Press OW. Antigen sensitivity of CD22-specific chimeric TCR is modulated by target epitope distance from the cell membrane. J Immunol. 2008 May 15;180(10):7028-38. doi: 10.4049/jimmunol.180.10.7028. PMID: 18453625; PMCID: PMC2585549.

183. Hombach AA, Schildgen V, Heuser C, Finnern R, Gilham DE, Abken H. T cell

activation by antibody-like immunoreceptors: the position of the binding epitope within the target molecule determines the efficiency of activation of redirected T cells. J Immunol. 2007 Apr 1;178(7):4650-7. doi: 10.4049/jimmunol.178.7.4650. PMID: 17372024.

184. Maude SL, Laetsch TW, Buechner J, Rives S, Boyer M, Bittencourt H, Bader P, Verneris MR, Stefanski HE, Myers GD, Qayed M, De Moerloose B, Hiramatsu H, Schlis K, Davis KL, Martin PL, Nemecek ER, Yanik GA, Peters C, Baruchel A, Boissel N, Mechinaud F, Balduzzi A, Krueger J, June CH, Levine BL, Wood P, Taran T, Leung M, Mueller KT, Zhang Y, Sen K, Lebwohl D, Pulsipher MA, Grupp SA. Tisagenlecleucel in Children and Young Adults with B-Cell Lymphoblastic Leukemia. N Engl J Med. 2018 Feb 1;378(5):439-448. doi: 10.1056/NEJMoa1709866. PMID: 29385370; PMCID: PMC5996391.

185. Milone MC, Fish JD, Carpenito C, Carroll RG, Binder GK, Teachey D, Samanta M, Lakhal M, Gloss B, Danet-Desnoyers G, Campana D, Riley JL, Grupp SA, June CH. Chimeric receptors containing CD137 signal transduction domains mediate enhanced survival of T cells and increased antileukemic efficacy in vivo. Mol Ther. 2009 Aug;17(8):1453-64. doi: 10.1038/mt.2009.83. Epub 2009 Apr 21. Erratum in: Mol Ther. 2015 Jul;23(7):1278. PMID: 19384291; PMCID: PMC2805264.

186. Locke FL, Ghobadi A, Jacobson CA, Miklos DB, Lekakis LJ, Oluwole OO, Lin Y, Braunschweig I, Hill BT, Timmerman JM, Deol A, Reagan PM, Stiff P, Flinn IW, Farooq U, Goy A, McSweeney PA, Munoz J, Siddiqi T, Chavez JC, Herrera AF, Bartlett NL, Wiezorek JS, Navale L, Xue A, Jiang Y, Bot A, Rossi JM, Kim JJ, Go WY, Neelapu SS. Long-term safety and activity of axicabtagene ciloleucel in refractory large B-cell lymphoma (ZUMA-1): a single-arm, multicentre, phase 1-2 trial. Lancet Oncol. 2019 Jan;20(1):31-42. doi: 10.1016/S1470-2045(18)30864-7. Epub 2018 Dec 2. PMID: 30518502; PMCID: PMC6733402.

187. Kochenderfer JN, Feldman SA, Zhao Y, Xu H, Black MA, Morgan RA, Wilson WH, Rosenberg SA. Construction and preclinical evaluation of an anti-CD19 chimeric antigen receptor. J Immunother. 2009 Sep;32(7):689-702. doi: 10.1097/CJI.0b013e3181ac6138. PMID: 19561539; PMCID: PMC2747302.

188. Bridgeman JS, Hawkins RE, Bagley S, Blaylock M, Holland M, Gilham DE. The optimal antigen response of chimeric antigen receptors harboring the

CD3zeta transmembrane domain is dependent upon incorporation of the receptor into the endogenous TCR/CD3 complex. J Immunol. 2010 Jun 15;184(12):6938-49. doi: 10.4049/jimmunol.0901766. Epub 2010 May 17. PMID: 20483753.

189. Alabanza L, Pegues M, Geldres C, Shi V, Wiltzius JJW, Sievers SA, Yang S, Kochenderfer JN. Function of Novel Anti-CD19 Chimeric Antigen Receptors with Human Variable Regions Is Affected by Hinge and Transmembrane Domains. Mol Ther. 2017 Nov 1;25(11):2452-2465. doi: 10.1016/j.ymthe.2017.07.013. Epub 2017 Jul 27. PMID: 28807568; PMCID: PMC5675490.

190. Wan Z, Shao X, Ji X, Dong L, Wei J, Xiong Z, Liu W, Qi H. Transmembrane domain-mediated Lck association underlies bystander and costimulatory ICOS signaling. Cell Mol Immunol. 2020 Feb;17(2):143-152. doi: 10.1038/s41423-018-0183-z. Epub 2018 Dec 6. PMID: 30523347; PMCID: PMC7000777.

191. Ying Z, Huang XF, Xiang X, Liu Y, Kang X, Song Y, Guo X, Liu H, Ding N, Zhang T, Duan P, Lin Y, Zheng W, Wang X, Lin N, Tu M, Xie Y, Zhang C, Liu W, Deng L, Gao S, Ping L, Wang X, Zhou N, Zhang J, Wang Y, Lin S, Mamuti M, Yu X, Fang L, Wang S, Song H, Wang G, Jones L, Zhu J, Chen SY. A safe and potent anti-CD19 CAR T cell therapy. Nat Med. 2019 Jun;25(6):947-953. doi: 10.1038/s41591-019-0421-7. Epub 2019 Apr 22. PMID: 31011207; PMCID: PMC7518381.

192. Haynes NM, Snook MB, Trapani JA, Cerruti L, Jane SM, Smyth MJ, Darcy PK. Redirecting mouse CTL against colon carcinoma: superior signaling efficacy of single-chain variable domain chimeras containing TCR-zeta vs Fc epsilon RI-gamma. J Immunol. 2001 Jan 1;166(1):182-7. doi: 10.4049/jimmunol.166.1.182. PMID: 11123291.

193. Töpfer K, Cartellieri M, Michen S, Wiedemuth R, Müller N, Lindemann D, Bachmann M, Füssel M, Schackert G, Temme A. DAP12-based activating chimeric antigen receptor for NK cell tumor immunotherapy. J Immunol. 2015 Apr 1;194(7):3201-12. doi: 10.4049/jimmunol.1400330. Epub 2015 Mar 4. PMID: 25740942.

194. Billadeau DD, Leibson PJ. ITAMs versus ITIMs: striking a balance during cell

regulation. J Clin Invest. 2002 Jan;109(2):161-8. doi: 10.1172/JCI14843. PMID: 11805126; PMCID: PMC150845.

195. van der Stegen SJ, Hamieh M, Sadelain M. The pharmacology of second-generation chimeric antigen receptors. Nat Rev Drug Discov. 2015 Jul;14(7):499-509. doi: 10.1038/nrd4597. PMID: 26129802; PMCID: PMC6410718.

196. Abraham RT, Weiss A. Jurkat T cells and development of the T-cell receptor signalling paradigm. Nat Rev Immunol. 2004 Apr;4(4):301-8. doi: 10.1038/nri1330. PMID: 15057788.

197. Chen L, Flies DB. Molecular mechanisms of T cell co-stimulation and co-inhibition. Nat Rev Immunol. 2013 Apr;13(4):227-42. doi: 10.1038/nri3405. Epub 2013 Mar 8. Erratum in: Nat Rev Immunol. 2013 Jul;13(7):542. PMID: 23470321; PMCID: PMC3786574.

198. Condomines M, Arnason J, Benjamin R, Gunset G, Plotkin J, Sadelain M. Tumor-Targeted Human T Cells Expressing CD28-Based Chimeric Antigen Receptors Circumvent CTLA-4 Inhibition. PLoS One. 2015 Jun 25;10(6):e0130518. doi: 10.1371/journal.pone.0130518. PMID: 26110267; PMCID: PMC4482147.

199. Long AH, Haso WM, Shern JF, Wanhainen KM, Murgai M, Ingaramo M, Smith JP, Walker AJ, Kohler ME, Venkateshwara VR, Kaplan RN, Patterson GH, Fry TJ, Orentas RJ, Mackall CL. 4-1BB costimulation ameliorates T cell exhaustion induced by tonic signaling of chimeric antigen receptors. Nat Med. 2015 Jun;21(6):581-90. doi: 10.1038/nm.3838. Epub 2015 May 4. PMID: 25939063; PMCID: PMC4458184.

200. Pulè MA, Straathof KC, Dotti G, Heslop HE, Rooney CM, Brenner MK. A chimeric T cell antigen receptor that augments cytokine release and supports clonal expansion of primary human T cells. Mol Ther. 2005 Nov;12(5):933-41. doi: 10.1016/j.ymthe.2005.04.016. Epub 2005 Jun 23. PMID: 15979412.

201. Frigault MJ, Lee J, Basil MC, Carpenito C, Motohashi S, Scholler J, Kawalekar OU, Guedan S, McGettigan SE, Posey AD Jr, Ang S, Cooper LJ, Platt JM, Johnson FB, Paulos CM, Zhao Y, Kalos M, Milone MC, June CH. Identification of chimeric antigen receptors that mediate constitutive or inducible

proliferation of T cells. Cancer Immunol Res. 2015 Apr;3(4):356-67. doi: 10.1158/2326-6066.CIR-14-0186. Epub 2015 Jan 19. PMID: 25600436; PMCID: PMC4390458.

202. Song DG, Ye Q, Poussin M, Harms GM, Figini M, Powell DJ Jr. CD27 costimulation augments the survival and antitumor activity of redirected human T cells in vivo. Blood. 2012 Jan 19;119(3):696-706. doi: 10.1182/blood-2011-03-344275. Epub 2011 Nov 23. PMID: 22117050.

203. Zhao R, Cheng L, Jiang Z, Wei X, Li B, Wu Q, Wang S, Lin S, Long Y, Zhang X, Wu Y, Du X, Pei D, Liu P, Li Y, Cui S, Yao Y, Li P. DNAX-activating protein 10 co-stimulation enhances the anti-tumor efficacy of chimeric antigen receptor T cells. Oncoimmunology. 2018 Nov 2;8(1):e1509173. doi: 10.1080/2162402X.2018.1509173. PMID: 30546945; PMCID: PMC6287795.

204. Lai Y, Weng J, Wei X, Qin L, Lai P, Zhao R, Jiang Z, Li B, Lin S, Wang S, Wu Q, Tang Z, Liu P, Pei D, Yao Y, Du X, Li P. Toll-like receptor 2 costimulation potentiates the antitumor efficacy of CAR T Cells. Leukemia. 2018 Mar;32(3):801-808. doi: 10.1038/leu.2017.249. Epub 2017 Aug 3. PMID: 28841215.

205. Martín-Fontecha A, Moro M, Crosti MC, Veglia F, Casorati G, Dellabona P. Vaccination with mouse mammary adenocarcinoma cells coexpressing B7-1 (CD80) and B7-2 (CD86) discloses the dominant effect of B7-1 in the induction of antitumor immunity. J Immunol. 2000 Jan 15;164(2):698-704. doi: 10.4049/jimmunol.164.2.698. PMID: 10623812.

206. LaBelle JL, Hanke CA, Blazar BR, Truitt RL. Negative effect of CTLA-4 on induction of T-cell immunity in vivo to B7-1+, but not B7-2+, murine myelogenous leukemia. Blood. 2002 Mar 15;99(6):2146-53. doi: 10.1182/blood.v99.6.2146. PMID: 11877291.

207. Sansom DM, Manzotti CN, Zheng Y. What's the difference between CD80 and CD86? Trends Immunol. 2003 Jun;24(6):314-9. doi: 10.1016/s1471-4906(03)00111-x. PMID: 12810107.

208. Qureshi OS, Zheng Y, Nakamura K, Attridge K, Manzotti C, Schmidt EM, Baker J, Jeffery LE, Kaur S, Briggs Z, Hou TZ, Futter CE, Anderson G, Walker LS, Sansom DM. Trans-endocytosis of CD80 and CD86: a molecular basis for the cell-extrinsic function of CTLA-4. Science. 2011 Apr 29;332(6029):600-3.

doi: 10.1126/science.1202947. Epub 2011 Apr 7. PMID: 21474713; PMCID: PMC3198051.

209. Lee KM, Chuang E, Griffin M, Khattri R, Hong DK, Zhang W, Straus D, Samelson LE, Thompson CB, Bluestone JA. Molecular basis of T cell inactivation by CTLA-4. Science. 1998 Dec 18;282(5397):2263-6. doi: 10.1126/science.282.5397.2263. PMID: 9856951.

210. Knieke K, Lingel H, Chamaon K, Brunner-Weinzierl MC. Migration of Th1 lymphocytes is regulated by CD152 (CTLA-4)-mediated signaling via PI3 kinase-dependent Akt activation. PLoS One. 2012;7(3):e31391. doi: 10.1371/journal.pone.0031391. Epub 2012 Mar 6. PMID: 22412835; PMCID: PMC3295805.

211. Esensten JH, Helou YA, Chopra G, Weiss A, Bluestone JA. CD28 Costimulation: From Mechanism to Therapy. Immunity. 2016 May 17;44(5):973-88. doi: 10.1016/j.immuni.2016.04.020. PMID: 27192564; PMCID: PMC4932896.

212. Jang IK, Lee ZH, Kim YJ, Kim SH, Kwon BS. Human 4-1BB (CD137) signals are mediated by TRAF2 and activate nuclear factor-kappa B. Biochem Biophys Res Commun. 1998 Jan 26;242(3):613-20. doi: 10.1006/bbrc.1997.8016. PMID: 9464265.

213. Zapata JM, Perez-Chacon G, Carr-Baena P, Martinez-Forero I, Azpilikueta A, Otano I, Melero I. CD137 (4-1BB) Signalosome: Complexity Is a Matter of TRAFs. Front Immunol. 2018 Nov 15;9:2618. doi: 10.3389/fimmu.2018.02618. PMID: 30524423; PMCID: PMC6262405.

214. Croft M, So T, Duan W, Soroosh P. The significance of OX40 and OX40L to T-cell biology and immune disease. Immunol Rev. 2009 May;229(1):173-91. doi: 10.1111/j.1600-065X.2009.00766.x. PMID: 19426222; PMCID: PMC2729757.

215. So T, Choi H, Croft M. OX40 complexes with phosphoinositide 3-kinase and protein kinase B (PKB) to augment TCR-dependent PKB signaling. J Immunol. 2011 Mar 15;186(6):3547-55. doi: 10.4049/jimmunol.1003156. Epub 2011 Feb 2. PMID: 21289304; PMCID: PMC3079230.

216. Gross G, Gorochov G, Waks T, Eshhar Z. Generation of effector T cells expressing chimeric T cell receptor with antibody type-specificity.

Transplant Proc. 1989 Feb;21(1 Pt 1):127-30. PMID: 2784887.

217. Eshhar Z, Waks T, Gross G, Schindler DG. Specific activation and targeting of cytotoxic lymphocytes through chimeric single chains consisting of antibody-binding domains and the gamma or zeta subunits of the immunoglobulin and T-cell receptors. Proc Natl Acad Sci U S A. 1993 Jan 15;90(2):720-4. doi: 10.1073/pnas.90.2.720. PMID: 8421711; PMCID: PMC45737.

218. Brentjens RJ, Latouche JB, Santos E, Marti F, Gong MC, Lyddane C, King PD, Larson S, Weiss M, Rivière I, Sadelain M. Eradication of systemic B-cell tumors by genetically targeted human T lymphocytes co-stimulated by CD80 and interleukin-15. Nat Med. 2003 Mar;9(3):279-86. doi: 10.1038/nm827. Epub 2003 Feb 10. PMID: 12579196.

219. Hombach A, Heuser C, Marquardt T, Wieczarkowiecz A, Groneck V, Pohl C, Abken H. CD4+ T cells engrafted with a recombinant immunoreceptor efficiently lyse target cells in a MHC antigen- and Fas-independent fashion. J Immunol. 2001 Jul 15;167(2):1090-6. doi: 10.4049/jimmunol.167.2.1090. PMID: 11441120.

220. Maher J, Brentjens RJ, Gunset G, Rivière I, Sadelain M. Human T-lymphocyte cytotoxicity and proliferation directed by a single chimeric TCRzeta /CD28 receptor. Nat Biotechnol. 2002 Jan;20(1):70-5. doi: 10.1038/nbt0102-70. PMID: 11753365.

221. Haynes NM, Trapani JA, Teng MW, Jackson JT, Cerruti L, Jane SM, Kershaw MH, Smyth MJ, Darcy PK. Single-chain antigen recognition receptors that costimulate potent rejection of established experimental tumors. Blood. 2002 Nov 1;100(9):3155-63. doi: 10.1182/blood-2002-04-1041. Erratum in: Blood. 2003 May 15;101(10):3808. PMID: 12384413.

222. Finney HM, Akbar AN, Lawson AD. Activation of resting human primary T cells with chimeric receptors: costimulation from CD28, inducible costimulator, CD134, and CD137 in series with signals from the TCR zeta chain. J Immunol. 2004 Jan 1;172(1):104-13. doi: 10.4049/jimmunol.172.1.104. PMID: 14688315.

223. Brentjens RJ, Santos E, Nikhamin Y, Yeh R, Matsushita M, La Perle K, Quintás-Cardama A, Larson SM, Sadelain M. Genetically targeted T cells

eradicate systemic acute lymphoblastic leukemia xenografts. Clin Cancer Res. 2007 Sep 15;13(18 Pt 1):5426-35. doi: 10.1158/1078-0432.CCR-07-0674. Epub 2007 Sep 12. PMID: 17855649.

224. Haynes NM, Trapani JA, Teng MW, Jackson JT, Cerruti L, Jane SM, Kershaw MH, Smyth MJ, Darcy PK. Rejection of syngeneic colon carcinoma by CTLs expressing single-chain antibody receptors codelivering CD28 costimulation. J Immunol. 2002 Nov 15;169(10):5780-6. doi: 10.4049/jimmunol.169.10.5780. Erratum in: J Immunol. 2003 Mar 15;170(6):3440. PMID: 12421958.

225. Huang X, Guo H, Kang J, Choi S, Zhou TC, Tammana S, Lees CJ, Li ZZ, Milone M, Levine BL, Tolar J, June CH, Scott McIvor R, Wagner JE, Blazar BR, Zhou X. Sleeping Beauty transposon-mediated engineering of human primary T cells for therapy of CD19+ lymphoid malignancies. Mol Ther. 2008 Mar;16(3):580-9. doi: 10.1038/sj.mt.6300404. Epub 2008 Jan 29. PMID: 18227839; PMCID: PMC4539139.

226. Du H, Hirabayashi K, Ahn S, Kren NP, Montgomery SA, Wang X, Tiruthani K, Mirlekar B, Michaud D, Greene K, Herrera SG, Xu Y, Sun C, Chen Y, Ma X, Ferrone CR, Pylayeva-Gupta Y, Yeh JJ, Liu R, Savoldo B, Ferrone S, Dotti G. Antitumor Responses in the Absence of Toxicity in Solid Tumors by Targeting B7-H3 via Chimeric Antigen Receptor T Cells. Cancer Cell. 2019 Feb 11;35(2):221-237.e8. doi: 10.1016/j.ccell.2019.01.002. PMID: 30753824; PMCID: PMC6645919.

227. Smith EL, Harrington K, Staehr M, Masakayan R, Jones J, Long TJ, Ng KY, Ghoddusi M, Purdon TJ, Wang X, Do T, Pham MT, Brown JM, De Larrea CF, Olson E, Peguero E, Wang P, Liu H, Xu Y, Garrett-Thomson SC, Almo SC, Wendel HG, Riviere I, Liu C, Sather B, Brentjens RJ. GPRC5D is a target for the immunotherapy of multiple myeloma with rationally designed CAR T cells. Sci Transl Med. 2019 Mar 27;11(485):eaau7746. doi: 10.1126/scitranslmed.aau7746. PMID: 30918115; PMCID: PMC7508042.

228. Maude SL, Frey N, Shaw PA, Aplenc R, Barrett DM, Bunin NJ, Chew A, Gonzalez VE, Zheng Z, Lacey SF, Mahnke YD, Melenhorst JJ, Rheingold SR, Shen A, Teachey DT, Levine BL, June CH, Porter DL, Grupp SA. Chimeric antigen receptor T cells for sustained remissions in leukemia. N Engl J Med. 2014 Oct 16;371(16):1507-17. doi: 10.1056/NEJMoa1407222. Erratum in: N

Engl J Med. 2016 Mar 10;374(10):998. PMID: 25317870; PMCID: PMC4267531.

229. Lee DW, Kochenderfer JN, Stetler-Stevenson M, Cui YK, Delbrook C, Feldman SA, Fry TJ, Orentas R, Sabatino M, Shah NN, Steinberg SM, Stroncek D, Tschernia N, Yuan C, Zhang H, Zhang L, Rosenberg SA, Wayne AS, Mackall CL. T cells expressing CD19 chimeric antigen receptors for acute lymphoblastic leukaemia in children and young adults: a phase 1 dose-escalation trial. Lancet. 2015 Feb 7;385(9967):517-528. doi: 10.1016/S0140-6736(14)61403-3. Epub 2014 Oct 13. PMID: 25319501; PMCID: PMC7065359.

230. Gardner RA, Finney O, Annesley C, Brakke H, Summers C, Leger K, Bleakley M, Brown C, Mgebroff S, Kelly-Spratt KS, Hoglund V, Lindgren C, Oron AP, Li D, Riddell SR, Park JR, Jensen MC. Intent-to-treat leukemia remission by CD19 CAR T cells of defined formulation and dose in children and young adults. Blood. 2017 Jun 22;129(25):3322-3331. doi: 10.1182/blood-2017-02-769208. Epub 2017 Apr 13. PMID: 28408462; PMCID: PMC5482103.

231. Davila ML, Riviere I, Wang X, Bartido S, Park J, Curran K, Chung SS, Stefanski J, Borquez-Ojeda O, Olszewska M, Qu J, Wasielewska T, He Q, Fink M, Shinglot H, Youssif M, Satter M, Wang Y, Hosey J, Quintanilla H, Halton E, Bernal Y, Bouhassira DC, Arcila ME, Gonen M, Roboz GJ, Maslak P, Douer D, Frattini MG, Giralt S, Sadelain M, Brentjens R. Efficacy and toxicity management of 19-28z CAR T cell therapy in B cell acute lymphoblastic leukemia. Sci Transl Med. 2014 Feb 19;6(224):224ra25. doi: 10.1126/scitranslmed.3008226. PMID: 24553386; PMCID: PMC4684949.

232. Turtle CJ, Hanafi LA, Berger C, Gooley TA, Cherian S, Hudecek M, Sommermeyer D, Melville K, Pender B, Budiarto TM, Robinson E, Steevens NN, Chaney C, Soma L, Chen X, Yeung C, Wood B, Li D, Cao J, Heimfeld S, Jensen MC, Riddell SR, Maloney DG. CD19 CAR-T cells of defined CD4+:CD8+ composition in adult B cell ALL patients. J Clin Invest. 2016 Jun 1;126(6):2123-38. doi: 10.1172/JCI85309. Epub 2016 Apr 25. PMID: 27111235; PMCID: PMC4887159.

233. Park JH, Rivière I, Gonen M, Wang X, Sénéchal B, Curran KJ, Sauter C, Wang Y, Santomasso B, Mead E, Roshal M, Maslak P, Davila M, Brentjens RJ, Sadelain M. Long-Term Follow-up of CD19 CAR Therapy in Acute Lymphoblastic Leukemia. N Engl J Med. 2018 Feb 1;378(5):449-459. doi: 10.1056/NEJMoa1709919. PMID: 29385376; PMCID: PMC6637939.

234. Schuster SJ, Bishop MR, Tam CS, Waller EK, Borchmann P, McGuirk JP, Jäger U, Jaglowski S, Andreadis C, Westin JR, Fleury I, Bachanova V, Foley SR, Ho PJ, Mielke S, Magenau JM, Holte H, Pantano S, Pacaud LB, Awasthi R, Chu J, Anak Ö, Salles G, Maziarz RT; JULIET Investigators. Tisagenlecleucel in Adult Relapsed or Refractory Diffuse Large B-Cell Lymphoma. N Engl J Med. 2019 Jan 3;380(1):45-56. doi: 10.1056/NEJMoa1804980. Epub 2018 Dec 1. PMID: 30501490.

235. Wang J, Jensen M, Lin Y, Sui X, Chen E, Lindgren CG, Till B, Raubitschek A, Forman SJ, Qian X, James S, Greenberg P, Riddell S, Press OW. Optimizing adoptive polyclonal T cell immunotherapy of lymphomas, using a chimeric T cell receptor possessing CD28 and CD137 costimulatory domains. Hum Gene Ther. 2007 Aug;18(8):712-25. doi: 10.1089/hum.2007.028. PMID: 17685852.

236. Zhong XS, Matsushita M, Plotkin J, Riviere I, Sadelain M. Chimeric antigen receptors combining 4-1BB and CD28 signaling domains augment PI3kinase/AKT/Bcl-XL activation and CD8+ T cell-mediated tumor eradication. Mol Ther. 2010 Feb;18(2):413-20. doi: 10.1038/mt.2009.210. Epub 2009 Sep 22. PMID: 19773745; PMCID: PMC2839303.

237. Carpenito C, Milone MC, Hassan R, Simonet JC, Lakhal M, Suhoski MM, Varela-Rohena A, Haines KM, Heitjan DF, Albelda SM, Carroll RG, Riley JL, Pastan I, June CH. Control of large, established tumor xenografts with genetically retargeted human T cells containing CD28 and CD137 domains. Proc Natl Acad Sci U S A. 2009 Mar 3;106(9):3360-5. doi: 10.1073/pnas.0813101106. Epub 2009 Feb 11. PMID: 19211796; PMCID: PMC2651342.

238. Hombach AA, Heiders J, Foppe M, Chmielewski M, Abken H. OX40 costimulation by a chimeric antigen receptor abrogates CD28 and IL-2 induced IL-10 secretion by redirected CD4(+) T cells. Oncoimmunology. 2012 Jul 1;1(4):458-466. doi: 10.4161/onci.19855. PMID: 22754764; PMCID: PMC3382912.

239. Guedan S, Posey AD Jr, Shaw C, Wing A, Da T, Patel PR, McGettigan SE, Casado-Medrano V, Kawalekar OU, Uribe-Herranz M, Song D, Melenhorst JJ, Lacey SF, Scholler J, Keith B, Young RM, June CH. Enhancing CAR T cell persistence through ICOS and 4-1BB costimulation. JCI Insight. 2018 Jan

11;3(1):e96976. doi: 10.1172/jci.insight.96976. PMID: 29321369; PMCID: PMC5821198.

240. Kaiser AD, Assenmacher M, Schröder B, Meyer M, Orentas R, Bethke U, Dropulic B. Towards a commercial process for the manufacture of genetically modified T cells for therapy. Cancer Gene Ther. 2015 Mar;22(2):72-8. doi: 10.1038/cgt.2014.78. Epub 2015 Jan 23. PMID: 25613483; PMCID: PMC4356749.

241. Wang X, Rivière I. Clinical manufacturing of CAR T cells: foundation of a promising therapy. Mol Ther Oncolytics. 2016 Jun 15;3:16015. doi: 10.1038/mto.2016.15. PMID: 27347557; PMCID: PMC4909095.

242. Stock S, Schmitt M, Sellner L. Optimizing Manufacturing Protocols of Chimeric Antigen Receptor T Cells for Improved Anticancer Immunotherapy. Int J Mol Sci. 2019 Dec 10;20(24):6223. doi: 10.3390/ijms20246223. PMID: 31835562; PMCID: PMC6940894.

243. Das RK, Vernau L, Grupp SA, Barrett DM. Naïve T-cell Deficits at Diagnosis and after Chemotherapy Impair Cell Therapy Potential in Pediatric Cancers. Cancer Discov. 2019 Apr;9(4):492-499. doi: 10.1158/2159-8290.CD-18-1314. Epub 2019 Jan 10. PMID: 30630850; PMCID: PMC6676489.

244. Allen ES, Stroncek DF, Ren J, Eder AF, West KA, Fry TJ, Lee DW, Mackall CL, Conry-Cantilena C. Autologous lymphapheresis for the production of chimeric antigen receptor T cells. Transfusion. 2017 May;57(5):1133-1141. doi: 10.1111/trf.14003. Epub 2017 Feb 24. PMID: 28236305; PMCID: PMC5398918.

245. Fesnak A, Lin C, Siegel DL, Maus MV. CAR-T Cell Therapies From the Transfusion Medicine Perspective. Transfus Med Rev. 2016 Jul;30(3):139-45. doi: 10.1016/j.tmrv.2016.03.001. Epub 2016 Mar 28. PMID: 27067907; PMCID: PMC4914456.

246. Depil S, Duchateau P, Grupp SA, Mufti G, Poirot L. 'Off-the-shelf' allogeneic CAR T cells: development and challenges. Nat Rev Drug Discov. 2020 Mar;19(3):185-199. doi: 10.1038/s41573-019-0051-2. Epub 2020 Jan 3. PMID: 31900462.

247. Graham C, Jozwik A, Pepper A, Benjamin R. Allogeneic CAR-T Cells: More than Ease of Access? Cells. 2018 Oct 1;7(10):155. doi: 10.3390/cells7100155.

PMID: 30275435; PMCID: PMC6210057.

248. Hinrichs CS, Borman ZA, Gattinoni L, Yu Z, Burns WR, Huang J, Klebanoff CA, Johnson LA, Kerkar SP, Yang S, Muranski P, Palmer DC, Scott CD, Morgan RA, Robbins PF, Rosenberg SA, Restifo NP. Human effector CD8+ T cells derived from naive rather than memory subsets possess superior traits for adoptive immunotherapy. Blood. 2011 Jan 20;117(3):808-14. doi: 10.1182/blood-2010-05-286286. Epub 2010 Oct 22. PMID: 20971955; PMCID: PMC3035075.

249. Sommermeyer D, Hudecek M, Kosasih PL, Gogishvili T, Maloney DG, Turtle CJ, Riddell SR. Chimeric antigen receptor-modified T cells derived from defined CD8+ and CD4+ subsets confer superior antitumor reactivity in vivo. Leukemia. 2016 Feb;30(2):492-500. doi: 10.1038/leu.2015.247. Epub 2015 Sep 15. PMID: 26369987; PMCID: PMC4746098.

250. Cruz CR, Micklethwaite KP, Savoldo B, Ramos CA, Lam S, Ku S, Diouf O, Liu E, Barrett AJ, Ito S, Shpall EJ, Krance RA, Kamble RT, Carrum G, Hosing CM, Gee AP, Mei Z, Grilley BJ, Heslop HE, Rooney CM, Brenner MK, Bollard CM, Dotti G. Infusion of donor-derived CD19-redirected virus-specific T cells for B-cell malignancies relapsed after allogeneic stem cell transplant: a phase 1 study. Blood. 2013 Oct 24;122(17):2965-73. doi: 10.1182/blood-2013-06-506741. Epub 2013 Sep 12. Erratum in: Blood. 2014 May 22;123(21):3364. PMID: 24030379; PMCID: PMC3811171.

251. Curran KJ, Sauter CS, Kernan NA, Prockop SE, Boulad F, Perales M, Giralt SA, Riviere I, Wang X, Boelens J, Sadelain M, Brentjens R, O'Reilly RJ. Durable Remission Following "Off-the-Shelf" Chimeric Antigen Receptor (CAR) T-Cells in Patients with Relapse/Refractory (R/R) B-Cell Malignancies. Biol Blood Marrow Transplant. 2020;26(3):S89. doi: 10.1016/j.bbmt.2019.12.590.

252. Singh H, Figliola MJ, Dawson MJ, Olivares S, Zhang L, Yang G, Maiti S, Manuri P, Senyukov V, Jena B, Kebriaei P, Champlin RE, Huls H, Cooper LJ. Manufacture of clinical-grade CD19-specific T cells stably expressing chimeric antigen receptor using Sleeping Beauty system and artificial antigen presenting cells. PLoS One. 2013 May 31;8(5):e64138. doi: 10.1371/journal.pone.0064138. PMID: 23741305; PMCID: PMC3669363.

253. Fraietta JA, Nobles CL, Sammons MA, Lundh S, Carty SA, Reich TJ, Cogdill AP, Morrissette JJD, DeNizio JE, Reddy S, Hwang Y, Gohil M, Kulikovskaya I, Nazimuddin F, Gupta M, Chen F, Everett JK, Alexander KA, Lin-Shiao E, Gee MH, Liu X, Young RM, Ambrose D, Wang Y, Xu J, Jordan MS, Marcucci KT, Levine BL, Garcia KC, Zhao Y, Kalos M, Porter DL, Kohli RM, Lacey SF, Berger SL, Bushman FD, June CH, Melenhorst JJ. Disruption of TET2 promotes the therapeutic efficacy of CD19-targeted T cells. Nature. 2018 Jun;558(7709):307-312. doi: 10.1038/s41586-018-0178-z. Epub 2018 May 30. PMID: 29849141; PMCID: PMC6320248.

254. Nobles CL, Sherrill-Mix S, Everett JK, Reddy S, Fraietta JA, Porter DL, Frey N, Gill SI, Grupp SA, Maude SL, Siegel DL, Levine BL, June CH, Lacey SF, Melenhorst JJ, Bushman FD. CD19-targeting CAR T cell immunotherapy outcomes correlate with genomic modification by vector integration. J Clin Invest. 2020 Feb 3;130(2):673-685. doi: 10.1172/JCI130144. PMID: 31845905; PMCID: PMC6994131.

255. Thomas CE, Ehrhardt A, Kay MA. Progress and problems with the use of viral vectors for gene therapy. Nat Rev Genet. 2003 May;4(5):346-58. doi: 10.1038/nrg1066. PMID: 12728277.

256. Vargas JE, Chicaybam L, Stein RT, Tanuri A, Delgado-Cañedo A, Bonamino MH. Retroviral vectors and transposons for stable gene therapy: advances, current challenges and perspectives. J Transl Med. 2016 Oct 12;14(1):288. doi: 10.1186/s12967-016-1047-x. PMID: 27729044; PMCID: PMC5059932.

257. Kondo E, Akatsuka Y, Nawa A, Kuzushima K, Tsujimura K, Tanimoto M, Kodera Y, Morishima Y, Kuzuya K, Takahashi T. Retroviral vector backbone immunogenicity: identification of cytotoxic T-cell epitopes in retroviral vector-packaging sequences. Gene Ther. 2005 Feb;12(3):252-8. doi: 10.1038/sj.gt.3302406. PMID: 15496958.

258. Breckpot K, Escors D, Arce F, Lopes L, Karwacz K, Van Lint S, Keyaerts M, Collins M. HIV-1 lentiviral vector immunogenicity is mediated by Toll-like receptor 3 (TLR3) and TLR7. J Virol. 2010 Jun;84(11):5627-36. doi: 10.1128/JVI.00014-10. Epub 2010 Mar 17. PMID: 20237085; PMCID: PMC2876620.

259. Singh H, Huls H, Kebriaei P, Cooper LJ. A new approach to gene therapy

using Sleeping Beauty to genetically modify clinical-grade T cells to target CD19. Immunol Rev. 2014 Jan;257(1):181-90. doi: 10.1111/imr.12137. PMID: 24329797; PMCID: PMC4109051.

260. Srour SA, Singh H, McCarty J, de Groot E, Huls H, Rondon G, Qazilbash M, Ciurea S, Bardelli G, Buck J, Alousi A, Nieto Y, Rezvani K, Marin D, Popat U, Hosing C, Shpall EJ, Wierda WG, Kantarjian H, Champlin RE, Cooper LJ, Kebriaei P. Long-term outcomes of Sleeping Beauty-generated CD19-specific CAR T-cell therapy for relapsed-refractory B-cell lymphomas. Blood. 2020 Mar 12;135(11):862-865. doi: 10.1182/blood.2019002920. PMID: 31961918; PMCID: PMC8212349.

261. Beatty GL, Haas AR, Maus MV, Torigian DA, Soulen MC, Plesa G, Chew A, Zhao Y, Levine BL, Albelda SM, Kalos M, June CH. Mesothelin-specific chimeric antigen receptor mRNA-engineered T cells induce anti-tumor activity in solid malignancies. Cancer Immunol Res. 2014 Feb;2(2):112-20. doi: 10.1158/2326-6066.CIR-13-0170. Erratum in: Cancer Immunol Res. 2015 Feb;3(2):217. PMID: 24579088; PMCID: PMC3932715.

262. Cieri N, Camisa B, Cocchiarella F, Forcato M, Oliveira G, Provasi E, Bondanza A, Bordignon C, Peccatori J, Ciceri F, Lupo-Stanghellini MT, Mavilio F, Mondino A, Bicciato S, Recchia A, Bonini C. IL-7 and IL-15 instruct the generation of human memory stem T cells from naive precursors. Blood. 2013 Jan 24;121(4):573-84. doi: 10.1182/blood-2012-05-431718. Epub 2012 Nov 15. PMID: 23160470.

263. Xu Y, Zhang M, Ramos CA, Durett A, Liu E, Dakhova O, Liu H, Creighton CJ, Gee AP, Heslop HE, Rooney CM, Savoldo B, Dotti G. Closely related T-memory stem cells correlate with in vivo expansion of CAR.CD19-T cells and are preserved by IL-7 and IL-15. Blood. 2014 Jun 12;123(24):3750-9. doi: 10.1182/blood-2014-01-552174. Epub 2014 Apr 29. PMID: 24782509; PMCID: PMC4055922.

264. Gargett T, Brown MP. Different cytokine and stimulation conditions influence the expansion and immune phenotype of third-generation chimeric antigen receptor T cells specific for tumor antigen GD2. Cytotherapy. 2015 Apr;17(4):487-95. doi: 10.1016/j.jcyt.2014.12.002. Epub 2015 Jan 6. PMID: 25573334.

265. Hoffmann JM, Schubert ML, Wang L, Hückelhoven A, Sellner L, Stock S, Schmitt A, Kleist C, Gern U, Loskog A, Wuchter P, Hofmann S, Ho AD, Müller-Tidow C, Dreger P, Schmitt M. Differences in Expansion Potential of Naive Chimeric Antigen Receptor T Cells from Healthy Donors and Untreated Chronic Lymphocytic Leukemia Patients. Front Immunol. 2018 Jan 10;8:1956. doi: 10.3389/fimmu.2017.01956. PMID: 29375575; PMCID: PMC5767585.

266. Restifo NP. Big bang theory of stem-like T cells confirmed. Blood. 2014 Jul 24;124(4):476-7. doi: 10.1182/blood-2014-06-578989. PMID: 25061170; PMCID: PMC4110654.

267. Wherry EJ. T cell exhaustion. Nat Immunol. 2011 Jun;12(6):492-9. doi: 10.1038/ni.2035. PMID: 21739672.

268. Brudno JN, Lam N, Vanasse D, Shen YW, Rose JJ, Rossi J, Xue A, Bot A, Scholler N, Mikkilineni L, Roschewski M, Dean R, Cachau R, Youkharibache P, Patel R, Hansen B, Stroncek DF, Rosenberg SA, Gress RE, Kochenderfer JN. Safety and feasibility of anti-CD19 CAR T cells with fully human binding domains in patients with B-cell lymphoma. Nat Med. 2020 Feb;26(2):270-280. doi: 10.1038/s41591-019-0737-3. Epub 2020 Jan 20. Erratum in: Nat Med. 2020 May;26(5):803. PMID: 31959992; PMCID: PMC7781235.

269. Vedvyas Y, McCloskey JE, Yang Y, Min IM, Fahey TJ, Zarnegar R, Hsu YS, Hsu JM, Van Besien K, Gaudet I, Law P, Kim NJ, Hofe EV, Jin MM. Manufacturing and preclinical validation of CAR T cells targeting ICAM-1 for advanced thyroid cancer therapy. Sci Rep. 2019 Jul 23;9(1):10634. doi: 10.1038/s41598-019-46938-7. Erratum in: Sci Rep. 2020 Jul 27;10(1):12733. PMID: 31337787; PMCID: PMC6650612.

270. Cross PJ, Levine BL. Assays for the Release of Cellular Gene Therapy Products. In: Concepts in Genetic Medicine. eds Dropulic B and Carter BJ. 2007 Apr; p. 307–18. doi: 10.1002/9780470184585.ch26

271. Hollyman D, Stefanski J, Przybylowski M, Bartido S, Borquez-Ojeda O, Taylor C, Yeh R, Capacio V, Olszewska M, Hosey J, Sadelain M, Brentjens RJ, Rivière I. Manufacturing validation of biologically functional T cells targeted to CD19 antigen for autologous adoptive cell therapy. J Immunother. 2009 Feb-Mar;32(2):169-80. doi: 10.1097/CJI.0b013e318194a6e8. PMID: 19238016;

PMCID: PMC2683970.

272. Neelapu SS. CAR-T efficacy: is conditioning the key? Blood. 2019 Apr 25;133(17):1799-1800. doi: 10.1182/blood-2019-03-900928. PMID: 31023743.

273. Lee DW, Santomasso BD, Locke FL, Ghobadi A, Turtle CJ, Brudno JN, Maus MV, Park JH, Mead E, Pavletic S, Go WY, Eldjerou L, Gardner RA, Frey N, Curran KJ, Peggs K, Pasquini M, DiPersio JF, van den Brink MRM, Komanduri KV, Grupp SA, Neelapu SS. ASTCT Consensus Grading for Cytokine Release Syndrome and Neurologic Toxicity Associated with Immune Effector Cells. Biol Blood Marrow Transplant. 2019 Apr;25(4):625-638. doi: 10.1016/j.bbmt.2018.12.758. Epub 2018 Dec 25. PMID: 30592986.

274. Maude SL, Barrett D, Teachey DT, Grupp SA. Managing cytokine release syndrome associated with novel T cell-engaging therapies. Cancer J. 2014 Mar-Apr;20(2):119-22. doi: 10.1097/PPO.0000000000000035. PMID: 24667956; PMCID: PMC4119809.

275. Tanaka T, Narazaki M, Kishimoto T. Immunotherapeutic implications of IL-6 blockade for cytokine storm. Immunotherapy. 2016 Jul;8(8):959-70. doi: 10.2217/imt-2016-0020. PMID: 27381687.

276. Garbers C, Heink S, Korn T, Rose-John S. Interleukin-6: designing specific therapeutics for a complex cytokine. Nat Rev Drug Discov. 2018 Jun;17(6):395-412. doi: 10.1038/nrd.2018.45. Epub 2018 May 4. PMID: 29725131.

277. Kang S, Tanaka T, Narazaki M, Kishimoto T. Targeting Interleukin-6 Signaling in Clinic. Immunity. 2019 Apr 16;50(4):1007-1023. doi: 10.1016/j.immuni.2019.03.026. PMID: 30995492.

278. Heink S, Yogev N, Garbers C, Herwerth M, Aly L, Gasperi C, Husterer V, Croxford AL, Möller-Hackbarth K, Bartsch HS, Sotlar K, Krebs S, Regen T, Blum H, Hemmer B, Misgeld T, Wunderlich TF, Hidalgo J, Oukka M, Rose-John S, Schmidt-Supprian M, Waisman A, Korn T. Trans-presentation of IL-6 by dendritic cells is required for the priming of pathogenic TH17 cells. Nat Immunol. 2017 Jan;18(1):74-85. doi: 10.1038/ni.3632. Epub 2016 Nov 28. Erratum in: Nat Immunol. 2017 Mar 22;18(4):474. PMID: 27893700; PMCID: PMC5164931.

279. Brentjens RJ, Davila ML, Riviere I, Park J, Wang X, Cowell LG, Bartido S, Stefanski J, Taylor C, Olszewska M, Borquez-Ojeda O, Qu J, Wasielewska T, He Q, Bernal Y, Rijo IV, Hedvat C, Kobos R, Curran K, Steinherz P, Jurcic J, Rosenblat T, Maslak P, Frattini M, Sadelain M. CD19-targeted T cells rapidly induce molecular remissions in adults with chemotherapy-refractory acute lymphoblastic leukemia. Sci Transl Med. 2013 Mar 20;5(177):177ra38. doi: 10.1126/scitranslmed.3005930. PMID: 23515080; PMCID: PMC3742551.

280. Lee DW, Gardner R, Porter DL, Louis CU, Ahmed N, Jensen M, Grupp SA, Mackall CL. Current concepts in the diagnosis and management of cytokine release syndrome. Blood. 2014 Jul 10;124(2):188-95. doi: 10.1182/blood-2014-05-552729. Epub 2014 May 29. Erratum in: Blood. 2015 Aug 20;126(8):1048. Dosage error in article text. Erratum in: Blood. 2016 Sep 15;128(11):1533. PMID: 24876563; PMCID: PMC4093680.

281. Kochenderfer JN, Dudley ME, Feldman SA, Wilson WH, Spaner DE, Maric I, Stetler-Stevenson M, Phan GQ, Hughes MS, Sherry RM, Yang JC, Kammula US, Devillier L, Carpenter R, Nathan DA, Morgan RA, Laurencot C, Rosenberg SA. B-cell depletion and remissions of malignancy along with cytokine-associated toxicity in a clinical trial of anti-CD19 chimeric-antigen-receptor-transduced T cells. Blood. 2012 Mar 22;119(12):2709-20. doi: 10.1182/blood-2011-10-384388. Epub 2011 Dec 8. PMID: 22160384; PMCID: PMC3327450.

282. Grupp SA, Kalos M, Barrett D, Aplenc R, Porter DL, Rheingold SR, Teachey DT, Chew A, Hauck B, Wright JF, Milone MC, Levine BL, June CH. Chimeric antigen receptor-modified T cells for acute lymphoid leukemia. N Engl J Med. 2013 Apr 18;368(16):1509-1518. doi: 10.1056/NEJMoa1215134. Epub 2013 Mar 25. Erratum in: N Engl J Med. 2016 Mar 10;374(10):998. PMID: 23527958; PMCID: PMC4058440.

283. Chatenoud L, Ferran C, Legendre C, Thouard I, Merite S, Reuter A, Gevaert Y, Kreis H, Franchimont P, Bach JF. In vivo cell activation following OKT3 administration. Systemic cytokine release and modulation by corticosteroids. Transplantation. 1990 Apr;49(4):697-702. doi: 10.1097/00007890-199004000-00009. PMID: 2109379.

284. Wing MG, Moreau T, Greenwood J, Smith RM, Hale G, Isaacs J, Waldmann H, Lachmann PJ, Compston A. Mechanism of first-dose cytokine-release

syndrome by CAMPATH 1-H: involvement of CD16 (FcgammaRIII) and CD11a/CD18 (LFA-1) on NK cells. J Clin Invest. 1996 Dec 15;98(12):2819-26. doi: 10.1172/JCI119110. PMID: 8981930; PMCID: PMC507749.

285. Winkler U, Jensen M, Manzke O, Schulz H, Diehl V, Engert A. Cytokine-release syndrome in patients with B-cell chronic lymphocytic leukemia and high lymphocyte counts after treatment with an anti-CD20 monoclonal antibody (rituximab, IDEC-C2B8). Blood. 1999 Oct 1;94(7):2217-24. PMID: 10498591.

286. Suntharalingam G, Perry MR, Ward S, Brett SJ, Castello-Cortes A, Brunner MD, Panoskaltsis N. Cytokine storm in a phase 1 trial of the anti-CD28 monoclonal antibody TGN1412. N Engl J Med. 2006 Sep 7;355(10):1018-28. doi: 10.1056/NEJMoa063842. Epub 2006 Aug 14. PMID: 16908486.

287. Panelli MC, White R, Foster M, Martin B, Wang E, Smith K, Marincola FM. Forecasting the cytokine storm following systemic interleukin (IL)-2 administration. J Transl Med. 2004 Jun 2;2(1):17. doi: 10.1186/1479-5876-2-17. PMID: 15175100; PMCID: PMC434535.

288. Teachey DT, Rheingold SR, Maude SL, Zugmaier G, Barrett DM, Seif AE, Nichols KE, Suppa EK, Kalos M, Berg RA, Fitzgerald JC, Aplenc R, Gore L, Grupp SA. Cytokine release syndrome after blinatumomab treatment related to abnormal macrophage activation and ameliorated with cytokine-directed therapy. Blood. 2013 Jun 27;121(26):5154-7. doi: 10.1182/blood-2013-02-485623. Epub 2013 May 15. PMID: 23678006; PMCID: PMC4123427.

289. Topp MS, Gökbuget N, Stein AS, Zugmaier G, O'Brien S, Bargou RC, Dombret H, Fielding AK, Heffner L, Larson RA, Neumann S, Foà R, Litzow M, Ribera JM, Rambaldi A, Schiller G, Brüggemann M, Horst HA, Holland C, Jia C, Maniar T, Huber B, Nagorsen D, Forman SJ, Kantarjian HM. Safety and activity of blinatumomab for adult patients with relapsed or refractory B-precursor acute lymphoblastic leukaemia: a multicentre, single-arm, phase 2 study. Lancet Oncol. 2015 Jan;16(1):57-66. doi: 10.1016/S1470-2045(14)71170-2. Epub 2014 Dec 16. Erratum in: Lancet Oncol. 2015 Apr;16(4):e158. PMID: 25524800.

290. Parker KR, Migliorini D, Perkey E, Yost KE, Bhaduri A, Bagga P, Haris M, Wilson NE, Liu F, Gabunia K, Scholler J, Montine TJ, Bhoj VG, Reddy R,

Mohan S, Maillard I, Kriegstein AR, June CH, Chang HY, Posey AD Jr, Satpathy AT. Single-Cell Analyses Identify Brain Mural Cells Expressing CD19 as Potential Off-Tumor Targets for CAR-T Immunotherapies. Cell. 2020 Oct 1;183(1):126-142.e17. doi: 10.1016/j.cell.2020.08.022. Epub 2020 Sep 21. PMID: 32961131; PMCID: PMC7640763.

291. Maus MV, Haas AR, Beatty GL, Albelda SM, Levine BL, Liu X, Zhao Y, Kalos M, June CH. T cells expressing chimeric antigen receptors can cause anaphylaxis in humans. Cancer Immunol Res. 2013 Jul;1:26-31. PMID: 24432303; PMCID: PMC3888798.

292. Maude SL, Barrett DM, Rheingold SR, Aplenc R, Teachey DT, Callahan C, Baniewicz D, White C, Talekar MK, Shaw PA, Brogdon JL, Young RM, Scholler J, Marcucci KT, Levine BL, Frey N, Porter DL, Lacey SF, Melenhorst JJ, June CH, Grupp SA. Efficacy of Humanized CD19-Targeted Chimeric Antigen Receptor (CAR)-Modified T Cells in Children and Young Adults with Relapsed/Refractory Acute Lymphoblastic Leukemia. Blood (2016) 128 (22): 217. doi: 10.1182/blood.V128.22.217.217

293. Hacein-Bey-Abina S, Von Kalle C, Schmidt M, McCormack MP, Wulffraat N, Leboulch P, Lim A, Osborne CS, Pawliuk R, Morillon E, Sorensen R, Forster A, Fraser P, Cohen JI, de Saint Basile G, Alexander I, Wintergerst U, Frebourg T, Aurias A, Stoppa-Lyonnet D, Romana S, Radford-Weiss I, Gross F, Valensi F, Delabesse E, Macintyre E, Sigaux F, Soulier J, Leiva LE, Wissler M, Prinz C, Rabbitts TH, Le Deist F, Fischer A, Cavazzana-Calvo M. LMO2-associated clonal T cell proliferation in two patients after gene therapy for SCID-X1. Science. 2003 Oct 17;302(5644):415-9. doi: 10.1126/science.1088547. Erratum in: Science. 2003 Oct 24;302(5645):568. PMID: 14564000.

294. Lamers CH, Sleijfer S, Vulto AG, Kruit WH, Kliffen M, Debets R, Gratama JW, Stoter G, Oosterwijk E. Treatment of metastatic renal cell carcinoma with autologous T-lymphocytes genetically retargeted against carbonic anhydrase IX: first clinical experience. J Clin Oncol. 2006 May 1;24(13):e20-2. doi: 10.1200/JCO.2006.05.9964. PMID: 16648493.

295. Parkhurst MR, Yang JC, Langan RC, Dudley ME, Nathan DA, Feldman SA, Davis JL, Morgan RA, Merino MJ, Sherry RM, Hughes MS, Kammula US, Phan GQ, Lim RM, Wank SA, Restifo NP, Robbins PF, Laurencot CM, Rosenberg SA. T cells targeting carcinoembryonic antigen can mediate regression of

metastatic colorectal cancer but induce severe transient colitis. Mol Ther. 2011 Mar;19(3):620-6. doi: 10.1038/mt.2010.272. Epub 2010 Dec 14. PMID: 21157437; PMCID: PMC3048186.

296. Kochenderfer JN, Wilson WH, Janik JE, Dudley ME, Stetler-Stevenson M, Feldman SA, Maric I, Raffeld M, Nathan DA, Lanier BJ, Morgan RA, Rosenberg SA. Eradication of B-lineage cells and regression of lymphoma in a patient treated with autologous T cells genetically engineered to recognize CD19. Blood. 2010 Nov 18;116(20):4099-102. doi: 10.1182/blood-2010-04-281931. Epub 2010 Jul 28. PMID: 20668228; PMCID: PMC2993617.

297. Smith JB, Lanitis E, Dangaj D, Buza E, Poussin M, Stashwick C, Scholler N, Powell DJ Jr. Tumor Regression and Delayed Onset Toxicity Following B7-H4 CAR T Cell Therapy. Mol Ther. 2016 Nov;24(11):1987-1999. doi: 10.1038/mt.2016.149. Epub 2016 Jul 21. PMID: 27439899; PMCID: PMC5154474.

298. Chmielewski M, Hombach A, Heuser C, Adams GP, Abken H. T cell activation by antibody-like immunoreceptors: increase in affinity of the single-chain fragment domain above threshold does not increase T cell activation against antigen-positive target cells but decreases selectivity. J Immunol. 2004 Dec 15;173(12):7647-53. doi: 10.4049/jimmunol.173.12.7647. PMID: 15585893.

299. Schmid DA, Irving MB, Posevitz V, Hebeisen M, Posevitz-Fejfar A, Sarria JC, Gomez-Eerland R, Thome M, Schumacher TN, Romero P, Speiser DE, Zoete V, Michielin O, Rufer N. Evidence for a TCR affinity threshold delimiting maximal CD8 T cell function. J Immunol. 2010 May 1;184(9):4936-46. doi: 10.4049/jimmunol.1000173. Epub 2010 Mar 29. PMID: 20351194.

300. Thomas S, Xue SA, Bangham CR, Jakobsen BK, Morris EC, Stauss HJ. Human T cells expressing affinity-matured TCR display accelerated responses but fail to recognize low density of MHC-peptide antigen. Blood. 2011 Jul 14;118(2):319-29. doi: 10.1182/blood-2010-12-326736. Epub 2011 May 23. PMID: 21606483.

301. Ghorashian S, Kramer AM, Onuoha S, Wright G, Bartram J, Richardson R, Albon SJ, Casanovas-Company J, Castro F, Popova B, Villanueva K, Yeung J, Vetharoy W, Guvenel A, Wawrzyniecka PA, Mekkaoui L, Cheung GW, Pinner D, Chu J, Lucchini G, Silva J, Ciocarlie O, Lazareva A, Inglott S, Gilmour KC,

Ahsan G, Ferrari M, Manzoor S, Champion K, Brooks T, Lopes A, Hackshaw A, Farzaneh F, Chiesa R, Rao K, Bonney D, Samarasinghe S, Goulden N, Vora A, Veys P, Hough R, Wynn R, Pule MA, Amrolia PJ. Enhanced CAR T cell expansion and prolonged persistence in pediatric patients with ALL treated with a low-affinity CD19 CAR. Nat Med. 2019 Sep;25(9):1408-1414. doi: 10.1038/s41591-019-0549-5. Epub 2019 Sep 2. PMID: 31477906.

302. Caruso HG, Hurton LV, Najjar A, Rushworth D, Ang S, Olivares S, Mi T, Switzer K, Singh H, Huls H, Lee DA, Heimberger AB, Champlin RE, Cooper LJ. Tuning Sensitivity of CAR to EGFR Density Limits Recognition of Normal Tissue While Maintaining Potent Antitumor Activity. Cancer Res. 2015 Sep 1;75(17):3505-18. doi: 10.1158/0008-5472.CAN-15-0139. PMID: 26330164; PMCID: PMC4624228.

303. Liu X, Jiang S, Fang C, Yang S, Olalere D, Pequignot EC, Cogdill AP, Li N, Ramones M, Granda B, Zhou L, Loew A, Young RM, June CH, Zhao Y. Affinity-Tuned ErbB2 or EGFR Chimeric Antigen Receptor T Cells Exhibit an Increased Therapeutic Index against Tumors in Mice. Cancer Res. 2015 Sep 1;75(17):3596-607. doi: 10.1158/0008-5472.CAN-15-0159. PMID: 26330166; PMCID: PMC4560113.

304. Park S, Shevlin E, Vedvyas Y, Zaman M, Park S, Hsu YS, Min IM, Jin MM. Micromolar affinity CAR T cells to ICAM-1 achieves rapid tumor elimination while avoiding systemic toxicity. Sci Rep. 2017 Oct 30;7(1):14366. doi: 10.1038/s41598-017-14749-3. PMID: 29085043; PMCID: PMC5662687.

305. Drent E, Themeli M, Poels R, de Jong-Korlaar R, Yuan H, de Bruijn J, Martens ACM, Zweegman S, van de Donk NWCJ, Groen RWJ, Lokhorst HM, Mutis T. A Rational Strategy for Reducing On-Target Off-Tumor Effects of CD38-Chimeric Antigen Receptors by Affinity Optimization. Mol Ther. 2017 Aug 2;25(8):1946-1958. doi: 10.1016/j.ymthe.2017.04.024. Epub 2017 May 13. PMID: 28506593; PMCID: PMC5542711.

306. Arcangeli S, Rotiroti MC, Bardelli M, Simonelli L, Magnani CF, Biondi A, Biagi E, Tettamanti S, Varani L. Balance of Anti-CD123 Chimeric Antigen Receptor Binding Affinity and Density for the Targeting of Acute Myeloid Leukemia. Mol Ther. 2017 Aug 2;25(8):1933-1945. doi: 10.1016/j.ymthe.2017.04.017. Epub 2017 May 4. PMID: 28479045; PMCID: PMC5542631.

307. Castellarin M, Sands C, Da T, Scholler J, Graham K, Buza E, Fraietta JA, Zhao Y, June CH. A rational mouse model to detect on-target, off-tumor CAR T cell toxicity. JCI Insight. 2020 Jul 23;5(14):e136012. doi: 10.1172/jci.insight.136012. PMID: 32544101; PMCID: PMC7453898.

308. Drent E, Poels R, Ruiter R, van de Donk NWCJ, Zweegman S, Yuan H, de Bruijn J, Sadelain M, Lokhorst HM, Groen RWJ, Mutis T, Themeli M. Combined CD28 and 4-1BB Costimulation Potentiates Affinity-tuned Chimeric Antigen Receptor-engineered T Cells. Clin Cancer Res. 2019 Jul 1;25(13):4014-4025. doi: 10.1158/1078-0432.CCR-18-2559. Epub 2019 Apr 12. PMID: 30979735; PMCID: PMC7477921.

309. Subklewe M, von Bergwelt-Baildon M, Humpe A. Chimeric Antigen Receptor T Cells: A Race to Revolutionize Cancer Therapy. Transfus Med Hemother. 2019 Feb;46(1):15-24. doi: 10.1159/000496870. Epub 2019 Feb 5. PMID: 31244578; PMCID: PMC6558337.

310. Hawkes N. Childhood leukaemia: Novartis immunotherapy drug approved after deal with NHS. BMJ. 2018 Sep 5;362:k3799. doi: 10.1136/bmj.k3799. PMID: 30185629.

311. Paroder M, Le N, Pham HP, Thibodeaux SR. Important aspects of T-cell collection by apheresis for manufacturing chimeric antigen receptor T cells. Adv Cell Gene Ther. 2020;3(1):1–7. doi: 10.1002/acg2.75.

312. Davis MM, Fesnak A, Leskowitz RM, McKee JS, Ohayon Y, Corl CM, Malykhin A, Fraietta JA, Melenhorst JJ, June CH, Schuster S, Levine BL. Predictors of manufacturing (MFG) success for chimeric antigen receptor (CAR) T cells in Non-Hodgkin Lymphoma (NHL). Cytotherapy. 2017 May 1;19(5):S118–9. doi: 10.1016/j.jcyt.2017.02.190.

313. Apel M, Brüning M, Granzin M, Essl M, Stuth J, Blaschke J, Spiegel I, Müller S, Kabaha E, Fahrendorff E, Miltenyi D, Schmitz J, Balshüsemann D, Huppert V. Integrated clinical scale manufacturing system for cellular products derived by magnetic cell separation, centrifugation and cell culture. Chemie-Ingenieur-Technik. 2013;85(1–2):103–10. doi: 10.1002/cite.201200175.

314. Mock U, Nickolay L, Philip B, Cheung GW, Zhan H, Johnston ICD, Kaiser AD, Peggs K, Pule M, Thrasher AJ, Qasim W. Automated manufacturing of

chimeric antigen receptor T cells for adoptive immunotherapy using CliniMACS prodigy. Cytotherapy. 2016 Aug;18(8):1002-1011. doi: 10.1016/j.jcyt.2016.05.009. PMID: 27378344.

315. Lock D, Mockel-Tenbrinck N, Drechsel K, Barth C, Mauer D, Schaser T, Kolbe C, Al Rawashdeh W, Brauner J, Hardt O, Pflug N, Holtick U, Borchmann P, Assenmacher M, Kaiser A. Automated Manufacturing of Potent CD20-Directed Chimeric Antigen Receptor T Cells for Clinical Use. Hum Gene Ther. 2017 Oct;28(10):914-925. doi: 10.1089/hum.2017.111. PMID: 28847167.

316. Zhang W, Jordan KR, Schulte B, Purev E. Characterization of clinical grade CD19 chimeric antigen receptor T cells produced using automated CliniMACS Prodigy system. Drug Des Devel Ther. 2018 Oct 5;12:3343-3356. doi: 10.2147/DDDT.S175113. PMID: 30323566; PMCID: PMC6181073.

317. Castella M, Caballero-Baños M, Ortiz-Maldonado V, González-Navarro EA, Suñé G, Antoñana-Vidósola A, Boronat A, Marzal B, Millán L, Martín-Antonio B, Cid J, Lozano M, García E, Tabera J, Trias E, Perpiña U, Canals JM, Baumann T, Benítez-Ribas D, Campo E, Yagüe J, Urbano-Ispizua Á, Rives S, Delgado J, Juan M. Point-Of-Care CAR T-Cell Production (ARI-0001) Using a Closed Semi-automatic Bioreactor: Experience From an Academic Phase I Clinical Trial. Front Immunol. 2020 Mar 20;11:482. doi: 10.3389/fimmu.2020.00482. PMID: 32528460; PMCID: PMC7259426.

318. Qasim W. Allogeneic CAR T cell therapies for leukemia. Am J Hematol. 2019 May;94(S1):S50-S54. doi: 10.1002/ajh.25399. Epub 2019 Feb 1. PMID: 30632623.

319. Wei J, Han X, Bo J, Han W. Target selection for CAR-T therapy. J Hematol Oncol. 2019 Jun 20;12(1):62. doi: 10.1186/s13045-019-0758-x. PMID: 31221182; PMCID: PMC6587237.

320. Jiang H, Hegde S, DeNardo DG. Tumor-associated fibrosis as a regulator of tumor immunity and response to immunotherapy. Cancer Immunol Immunother. 2017 Aug;66(8):1037-1048. doi: 10.1007/s00262-017-2003-1. Epub 2017 Apr 27. PMID: 28451791; PMCID: PMC5603233.

321. Wang M, Zhao J, Zhang L, Wei F, Lian Y, Wu Y, Gong Z, Zhang S, Zhou J, Cao K, Li X, Xiong W, Li G, Zeng Z, Guo C. Role of tumor microenvironment in tumorigenesis. J Cancer. 2017 Feb 25;8(5):761-773. doi: 10.7150/jca.17648.

PMID: 28382138; PMCID: PMC5381164.

322. Martinez M, Moon EK. CAR T Cells for Solid Tumors: New Strategies for Finding, Infiltrating, and Surviving in the Tumor Microenvironment. Front Immunol. 2019 Feb 5;10:128. doi: 10.3389/fimmu.2019.00128. PMID: 30804938; PMCID: PMC6370640.

323. Chen PH, Lipschitz M, Weirather JL, Jacobson C, Armand P, Wright K, Hodi FS, Roberts ZJ, Sievers SA, Rossi J, Bot A, Go W, Rodig SJ. Activation of CAR and non-CAR T cells within the tumor microenvironment following CAR T cell therapy. JCI Insight. 2020 Jun 18;5(12):e134612. doi: 10.1172/jci.insight.134612. PMID: 32484797; PMCID: PMC7406247.

324. Liu Z, Chen O, Wall JBJ, Zheng M, Zhou Y, Wang L, Vaseghi HR, Qian L, Liu J. Systematic comparison of 2A peptides for cloning multi-genes in a polycistronic vector. Sci Rep. 2017 May 19;7(1):2193. doi: 10.1038/s41598-017-02460-2. PMID: 28526819; PMCID: PMC5438344.

325. Markley JC, Sadelain M. IL-7 and IL-21 are superior to IL-2 and IL-15 in promoting human T cell-mediated rejection of systemic lymphoma in immunodeficient mice. Blood. 2010 Apr 29;115(17):3508-19. doi: 10.1182/blood-2009-09-241398. Epub 2010 Feb 26. PMID: 20190192; PMCID: PMC2867264.

326. Chmielewski M, Kopecky C, Hombach AA, Abken H. IL-12 release by engineered T cells expressing chimeric antigen receptors can effectively Muster an antigen-independent macrophage response on tumor cells that have shut down tumor antigen expression. Cancer Res. 2011 Sep 1;71(17):5697-706. doi: 10.1158/0008-5472.CAN-11-0103. Epub 2011 Jul 8. PMID: 21742772.

327. Pegram HJ, Lee JC, Hayman EG, Imperato GH, Tedder TF, Sadelain M, Brentjens RJ. Tumor-targeted T cells modified to secrete IL-12 eradicate systemic tumors without need for prior conditioning. Blood. 2012 May 3;119(18):4133-41. doi: 10.1182/blood-2011-12-400044. Epub 2012 Feb 21. PMID: 22354001; PMCID: PMC3359735.

328. Hoyos V, Savoldo B, Quintarelli C, Mahendravada A, Zhang M, Vera J, Heslop HE, Rooney CM, Brenner MK, Dotti G. Engineering CD19-specific T lymphocytes with interleukin-15 and a suicide gene to enhance their anti-

lymphoma/leukemia effects and safety. Leukemia. 2010 Jun;24(6):1160-70. doi: 10.1038/leu.2010.75. Epub 2010 Apr 29. PMID: 20428207; PMCID: PMC2888148.

329. Zhao Z, Li Y, Liu W, Li X. Engineered IL-7 Receptor Enhances the Therapeutic Effect of AXL-CAR-T Cells on Triple-Negative Breast Cancer. Biomed Res Int. 2020 Jan 2;2020:4795171. doi: 10.1155/2020/4795171. PMID: 31998790; PMCID: PMC6970498.

330. Adachi K, Kano Y, Nagai T, Okuyama N, Sakoda Y, Tamada K. IL-7 and CCL19 expression in CAR-T cells improves immune cell infiltration and CAR-T cell survival in the tumor. Nat Biotechnol. 2018 Apr;36(4):346-351. doi: 10.1038/nbt.4086. Epub 2018 Mar 5. PMID: 29505028.

331. Batra SA, Rathi P, Guo L, Courtney AN, Fleurence J, Balzeau J, Shaik RS, Nguyen TP, Wu MF, Bulsara S, Mamonkin M, Metelitsa LS, Heczey A. Glypican-3-Specific CAR T Cells Coexpressing IL15 and IL21 Have Superior Expansion and Antitumor Activity against Hepatocellular Carcinoma. Cancer Immunol Res. 2020 Mar;8(3):309-320. doi: 10.1158/2326-6066.CIR-19-0293. Epub 2020 Jan 17. PMID: 31953246.

332. Hu B, Ren J, Luo Y, Keith B, Young RM, Scholler J, Zhao Y, June CH. Augmentation of Antitumor Immunity by Human and Mouse CAR T Cells Secreting IL-18. Cell Rep. 2017 Sep 26;20(13):3025-3033. doi: 10.1016/j.celrep.2017.09.002. PMID: 28954221; PMCID: PMC6002762.

333. Li X, Daniyan AF, Lopez AV, Purdon TJ, Brentjens RJ. Cytokine IL-36γ improves CAR T-cell functionality and induces endogenous antitumor response. Leukemia. 2021 Feb;35(2):506-521. doi: 10.1038/s41375-020-0874-1. Epub 2020 May 23. PMID: 32447345; PMCID: PMC7680719.

334. Batra SA, Rathi P, Guo L, Courtney AN, Fleurence J, Balzeau J, Shaik RS, Nguyen TP, Wu MF, Bulsara S, Mamonkin M, Metelitsa LS, Heczey A. Glypican-3-Specific CAR T Cells Coexpressing IL15 and IL21 Have Superior Expansion and Antitumor Activity against Hepatocellular Carcinoma. Cancer Immunol Res. 2020 Mar;8(3):309-320. doi: 10.1158/2326-6066.CIR-19-0293. Epub 2020 Jan 17. PMID: 31953246.

335. Shum T, Omer B, Tashiro H, Kruse RL, Wagner DL, Parikh K, Yi Z, Sauer T, Liu D, Parihar R, Castillo P, Liu H, Brenner MK, Metelitsa LS, Gottschalk S,

Rooney CM. Constitutive Signaling from an Engineered IL7 Receptor Promotes Durable Tumor Elimination by Tumor-Redirected T Cells. Cancer Discov. 2017 Nov;7(11):1238-1247. doi: 10.1158/2159-8290.CD-17-0538. Epub 2017 Aug 22. PMID: 28830878; PMCID: PMC5669830.

336. Kagoya Y, Tanaka S, Guo T, Anczurowski M, Wang CH, Saso K, Butler MO, Minden MD, Hirano N. A novel chimeric antigen receptor containing a JAK-STAT signaling domain mediates superior antitumor effects. Nat Med. 2018 Mar;24(3):352-359. doi: 10.1038/nm.4478. Epub 2018 Feb 5. PMID: 29400710; PMCID: PMC5839992.

337. Di Stasi A, De Angelis B, Rooney CM, Zhang L, Mahendravada A, Foster AE, Heslop HE, Brenner MK, Dotti G, Savoldo B. T lymphocytes coexpressing CCR4 and a chimeric antigen receptor targeting CD30 have improved homing and antitumor activity in a Hodgkin tumor model. Blood. 2009 Jun 18;113(25):6392-402. doi: 10.1182/blood-2009-03-209650. Epub 2009 Apr 17. PMID: 19377047; PMCID: PMC2710932.

338. Moon EK, Carpenito C, Sun J, Wang LC, Kapoor V, Predina J, Powell DJ Jr, Riley JL, June CH, Albelda SM. Expression of a functional CCR2 receptor enhances tumor localization and tumor eradication by retargeted human T cells expressing a mesothelin-specific chimeric antibody receptor. Clin Cancer Res. 2011 Jul 15;17(14):4719-30. doi: 10.1158/1078-0432.CCR-11-0351. Epub 2011 May 24. PMID: 21610146; PMCID: PMC3612507.

339. Whilding LM, Halim L, Draper B, Parente-Pereira AC, Zabinski T, Davies DM, Maher J. CAR T-Cells Targeting the Integrin αvß6 and Co-Expressing the Chemokine Receptor CXCR2 Demonstrate Enhanced Homing and Efficacy against Several Solid Malignancies. Cancers (Basel). 2019 May 14;11(5):674. doi: 10.3390/cancers11050674. PMID: 31091832; PMCID: PMC6563120.

340. Liu G, Rui W, Zheng H, Huang D, Yu F, Zhang Y, Dong J, Zhao X, Lin X. CXCR2-modified CAR-T cells have enhanced trafficking ability that improves treatment of hepatocellular carcinoma. Eur J Immunol. 2020 May;50(5):712-724. doi: 10.1002/eji.201948457. Epub 2020 Feb 10. PMID: 31981231.

341. Jin L, Tao H, Karachi A, Long Y, Hou AY, Na M, Dyson KA, Grippin AJ, Deleyrolle LP, Zhang W, Rajon DA, Wang QJ, Yang JC, Kresak JL, Sayour EJ, Rahman M, Bova FJ, Lin Z, Mitchell DA, Huang J. CXCR1- or CXCR2-modified

CAR T cells co-opt IL-8 for maximal antitumor efficacy in solid tumors. Nat Commun. 2019 Sep 5;10(1):4016. doi: 10.1038/s41467-019-11869-4. PMID: 31488817; PMCID: PMC6728370.

342. Dangaj D, Bruand M, Grimm AJ, Ronet C, Barras D, Duttagupta PA, Lanitis E, Duraiswamy J, Tanyi JL, Benencia F, Conejo-Garcia J, Ramay HR, Montone KT, Powell DJ Jr, Gimotty PA, Facciabene A, Jackson DG, Weber JS, Rodig SJ, Hodi SF, Kandalaft LE, Irving M, Zhang L, Foukas P, Rusakiewicz S, Delorenzi M, Coukos G. Cooperation between Constitutive and Inducible Chemokines Enables T Cell Engraftment and Immune Attack in Solid Tumors. Cancer Cell. 2019 Jun 10;35(6):885-900.e10. doi: 10.1016/j.ccell.2019.05.004. PMID: 31185212; PMCID: PMC6961655.

343. Zhao Z, Condomines M, van der Stegen SJC, Perna F, Kloss CC, Gunset G, Plotkin J, Sadelain M. Structural Design of Engineered Costimulation Determines Tumor Rejection Kinetics and Persistence of CAR T Cells. Cancer Cell. 2015 Oct 12;28(4):415-428. doi: 10.1016/j.ccell.2015.09.004. PMID: 26461090; PMCID: PMC5003056.

344. Curran KJ, Seinstra BA, Nikhamin Y, Yeh R, Usachenko Y, van Leeuwen DG, Purdon T, Pegram HJ, Brentjens RJ. Enhancing antitumor efficacy of chimeric antigen receptor T cells through constitutive CD40L expression. Mol Ther. 2015 Apr;23(4):769-78. doi: 10.1038/mt.2015.4. Epub 2015 Jan 13. PMID: 25582824; PMCID: PMC4395796.

345. Cherkassky L, Morello A, Villena-Vargas J, Feng Y, Dimitrov DS, Jones DR, Sadelain M, Adusumilli PS. Human CAR T cells with cell-intrinsic PD-1 checkpoint blockade resist tumor-mediated inhibition. J Clin Invest. 2016 Aug 1;126(8):3130-44. doi: 10.1172/JCI83092. Epub 2016 Jul 25. PMID: 27454297; PMCID: PMC4966328.

346. Kloss CC, Lee J, Zhang A, Chen F, Melenhorst JJ, Lacey SF, Maus MV, Fraietta JA, Zhao Y, June CH. Dominant-Negative TGF-β Receptor Enhances PSMA-Targeted Human CAR T Cell Proliferation And Augments Prostate Cancer Eradication. Mol Ther. 2018 Jul 5;26(7):1855-1866. doi: 10.1016/j.ymthe.2018.05.003. Epub 2018 May 8. PMID: 29807781; PMCID: PMC6037129.

347. Yamamoto TN, Lee PH, Vodnala SK, Gurusamy D, Kishton RJ, Yu Z, Eidizadeh

A, Eil R, Fioravanti J, Gattinoni L, Kochenderfer JN, Fry TJ, Aksoy BA, Hammerbacher JE, Cruz AC, Siegel RM, Restifo NP, Klebanoff CA. T cells genetically engineered to overcome death signaling enhance adoptive cancer immunotherapy. J Clin Invest. 2019 Feb 25;129(4):1551-1565. doi: 10.1172/JCI121491. PMID: 30694219; PMCID: PMC6436880.

348. Mohammed S, Sukumaran S, Bajgain P, Watanabe N, Heslop HE, Rooney CM, Brenner MK, Fisher WE, Leen AM, Vera JF. Improving Chimeric Antigen Receptor-Modified T Cell Function by Reversing the Immunosuppressive Tumor Microenvironment of Pancreatic Cancer. Mol Ther. 2017 Jan 4;25(1):249-258. doi: 10.1016/j.ymthe.2016.10.016. Epub 2017 Jan 4. PMID: 28129119; PMCID: PMC5363304.

349. Wang Y, Jiang H, Luo H, Sun Y, Shi B, Sun R, Li Z. An IL-4/21 Inverted Cytokine Receptor Improving CAR-T Cell Potency in Immunosuppressive Solid-Tumor Microenvironment. Front Immunol. 2019 Jul 19;10:1691. doi: 10.3389/fimmu.2019.01691. PMID: 31379876; PMCID: PMC6658891.

350. Liu X, Ranganathan R, Jiang S, Fang C, Sun J, Kim S, Newick K, Lo A, June CH, Zhao Y, Moon EK. A Chimeric Switch-Receptor Targeting PD1 Augments the Efficacy of Second-Generation CAR T Cells in Advanced Solid Tumors. Cancer Res. 2016 Mar 15;76(6):1578-90. doi: 10.1158/0008-5472.CAN-15-2524. PMID: 26979791; PMCID: PMC4800826.

351. Li C, Mei H, Hu Y. Applications and explorations of CRISPR/Cas9 in CAR T-cell therapy. Brief Funct Genomics. 2020 May 20;19(3):175-182. doi: 10.1093/bfgp/elz042. PMID: 31950135; PMCID: PMC7239310.

352. Torikai H, Reik A, Liu PQ, Zhou Y, Zhang L, Maiti S, Huls H, Miller JC, Kebriaei P, Rabinovich B, Lee DA, Champlin RE, Bonini C, Naldini L, Rebar EJ, Gregory PD, Holmes MC, Cooper LJ. A foundation for universal T-cell based immunotherapy: T cells engineered to express a CD19-specific chimeric-antigen-receptor and eliminate expression of endogenous TCR. Blood. 2012 Jun 14;119(24):5697-705. doi: 10.1182/blood-2012-01-405365. Epub 2012 Apr 24. Erratum in: Blood. 2015 Nov 26;126(22):2527. Rabinovitch, Brian [corrected to Rabinovich, Brian]. PMID: 22535661; PMCID: PMC3382929.

353. Torikai H, Reik A, Soldner F, Warren EH, Yuen C, Zhou Y, Crossland DL, Huls H, Littman N, Zhang Z, Tykodi SS, Kebriaei P, Lee DA, Miller JC, Rebar EJ,

Holmes MC, Jaenisch R, Champlin RE, Gregory PD, Cooper LJ. Toward eliminating HLA class I expression to generate universal cells from allogeneic donors. Blood. 2013 Aug 22;122(8):1341-9. doi: 10.1182/blood-2013-03-478255. Epub 2013 Jun 5. PMID: 23741009; PMCID: PMC3750336.

354. Toh BH, Kyaw T, Tipping P, Bobik A. Immune regulation by CD52-expressing CD4 T cells. Cell Mol Immunol. 2013 Sep;10(5):379-82. doi: 10.1038/cmi.2013.35. Epub 2013 Aug 12. PMID: 23934027; PMCID: PMC4003202.

355. Poirot L, Philip B, Schiffer-Mannioui C, Le Clerre D, Chion-Sotinel I, Derniame S, Potrel P, Bas C, Lemaire L, Galetto R, Lebuhotel C, Eyquem J, Cheung GW, Duclert A, Gouble A, Arnould S, Peggs K, Pule M, Scharenberg AM, Smith J. Multiplex Genome-Edited T-cell Manufacturing Platform for "Off-the-Shelf" Adoptive T-cell Immunotherapies. Cancer Res. 2015 Sep 15;75(18):3853-64. doi: 10.1158/0008-5472.CAN-14-3321. Epub 2015 Jul 16. PMID: 26183927.

356. Su S, Hu B, Shao J, Shen B, Du J, Du Y, Zhou J, Yu L, Zhang L, Chen F, Sha H, Cheng L, Meng F, Zou Z, Huang X, Liu B. CRISPR-Cas9 mediated efficient PD-1 disruption on human primary T cells from cancer patients. Sci Rep. 2016 Jan 28;6:20070. doi: 10.1038/srep20070. Erratum in: Sci Rep. 2017 Jan 19;7:40272. PMID: 26818188; PMCID: PMC4730182.

357. Rupp LJ, Schumann K, Roybal KT, Gate RE, Ye CJ, Lim WA, Marson A. CRISPR/Cas9-mediated PD-1 disruption enhances anti-tumor efficacy of human chimeric antigen receptor T cells. Sci Rep. 2017 Apr 7;7(1):737. doi: 10.1038/s41598-017-00462-8. PMID: 28389661; PMCID: PMC5428439.

358. Eyquem J, Mansilla-Soto J, Giavridis T, van der Stegen SJ, Hamieh M, Cunanan KM, Odak A, Gönen M, Sadelain M. Targeting a CAR to the TRAC locus with CRISPR/Cas9 enhances tumour rejection. Nature. 2017 Mar 2;543(7643):113-117. doi: 10.1038/nature21405. Epub 2017 Feb 22. PMID: 28225754; PMCID: PMC5558614.

359. Ren J, Liu X, Fang C, Jiang S, June CH, Zhao Y. Multiplex Genome Editing to Generate Universal CAR T Cells Resistant to PD1 Inhibition. Clin Cancer Res. 2017 May 1;23(9):2255-2266. doi: 10.1158/1078-0432.CCR-16-1300. Epub 2016 Nov 4. PMID: 27815355; PMCID: PMC5413401.

360. Liu X, Zhang Y, Cheng C, Cheng AW, Zhang X, Li N, Xia C, Wei X, Liu X, Wang H. CRISPR-Cas9-mediated multiplex gene editing in CAR-T cells. Cell Res. 2017 Jan;27(1):154-157. doi: 10.1038/cr.2016.142. Epub 2016 Dec 2. PMID: 27910851; PMCID: PMC5223227.

361. Zhang Y, Zhang X, Cheng C, Mu W, Liu X, Li N, Wei X, Liu X, Xia C, Wang H. CRISPR-Cas9 mediated LAG-3 disruption in CAR-T cells. Front Med. 2017 Dec;11(4):554-562. doi: 10.1007/s11684-017-0543-6. Epub 2017 Jun 17. PMID: 28625015.

362. Zhang W, Shi L, Zhao Z, Du P, Ye X, Li D, Cai Z, Han J, Cai J. Disruption of CTLA-4 expression on peripheral blood CD8 + T cell enhances anti-tumor efficacy in bladder cancer. Cancer Chemother Pharmacol. 2019 May;83(5):911-920. doi: 10.1007/s00280-019-03800-x. Epub 2019 Mar 8. PMID: 30848330.

363. Sterner RM, Cox MJ, Sakemura R, Kenderian SS. Using CRISPR/Cas9 to Knock Out GM-CSF in CAR-T Cells. J Vis Exp. 2019 Jul 22;(149). doi: 10.3791/59629. PMID: 31380838.

364. Tang N, Cheng C, Zhang X, Qiao M, Li N, Mu W, Wei XF, Han W, Wang H. TGF-ß inhibition via CRISPR promotes the long-term efficacy of CAR T cells against solid tumors. JCI Insight. 2020 Feb 27;5(4):e133977. doi: 10.1172/jci.insight.133977. PMID: 31999649; PMCID: PMC7101140.

365. Gomes-Silva D, Srinivasan M, Sharma S, Lee CM, Wagner DL, Davis TH, Rouce RH, Bao G, Brenner MK, Mamonkin M. CD7-edited T cells expressing a CD7-specific CAR for the therapy of T-cell malignancies. Blood. 2017 Jul 20;130(3):285-296. doi: 10.1182/blood-2017-01-761320. Epub 2017 May 24. PMID: 28539325; PMCID: PMC5520470.

366. Jung IY, Kim YY, Yu HS, Lee M, Kim S, Lee J. CRISPR/Cas9-Mediated Knockout of DGK Improves Antitumor Activities of Human T Cells. Cancer Res. 2018 Aug 15;78(16):4692-4703. doi: 10.1158/0008-5472.CAN-18-0030. Epub 2018 Jul 2. PMID: 29967261.

367. Wiede F, Lu KH, Du X, Liang S, Hochheiser K, Dodd GT, Goh PK, Kearney C, Meyran D, Beavis PA, Henderson MA, Park SL, Waithman J, Zhang S, Zhang ZY, Oliaro J, Gebhardt T, Darcy PK, Tiganis T. PTPN2 phosphatase deletion in T cells promotes anti-tumour immunity and CAR T-cell efficacy in solid

tumours. EMBO J. 2020 Jan 15;39(2):e103637. doi: 10.15252/embj.2019103637. Epub 2019 Dec 5. PMID: 31803974; PMCID: PMC6960448.

368. Chen J, López-Moyado IF, Seo H, Lio CJ, Hempleman LJ, Sekiya T, Yoshimura A, Scott-Browne JP, Rao A. NR4A transcription factors limit CAR T cell function in solid tumours. Nature. 2019 Mar;567(7749):530-534. doi: 10.1038/s41586-019-0985-x. Epub 2019 Feb 27. PMID: 30814732; PMCID: PMC6546093.

369. Seo H, Chen J, González-Avalos E, Samaniego-Castruita D, Das A, Wang YH, López-Moyado IF, Georges RO, Zhang W, Onodera A, Wu CJ, Lu LF, Hogan PG, Bhandoola A, Rao A. TOX and TOX2 transcription factors cooperate with NR4A transcription factors to impose CD8+ T cell exhaustion. Proc Natl Acad Sci U S A. 2019 Jun 18;116(25):12410-12415. doi: 10.1073/pnas.1905675116. Epub 2019 May 31. Erratum in: Proc Natl Acad Sci U S A. 2019 Sep 24;116(39):19761. PMID: 31152140; PMCID: PMC6589758.

370. Darowski D, Kobold S, Jost C, Klein C. Combining the best of two worlds: highly flexible chimeric antigen receptor adaptor molecules (CAR-adaptors) for the recruitment of chimeric antigen receptor T cells. MAbs. 2019 May/Jun;11(4):621-631. doi: 10.1080/19420862.2019.1596511. Epub 2019 Apr 17. PMID: 30892136; PMCID: PMC6601549.

371. Ochi F, Fujiwara H, Tanimoto K, Asai H, Miyazaki Y, Okamoto S, Mineno J, Kuzushima K, Shiku H, Barrett J, Ishii E, Yasukawa M. Gene-modified human α/ß-T cells expressing a chimeric CD16-CD3ζ receptor as adoptively transferable effector cells for anticancer monoclonal antibody therapy. Cancer Immunol Res. 2014 Mar;2(3):249-62. doi: 10.1158/2326-6066.CIR-13-0099-T. Epub 2014 Jan 3. PMID: 24778321.

372. Urbanska K, Lanitis E, Poussin M, Lynn RC, Gavin BP, Kelderman S, Yu J, Scholler N, Powell DJ Jr. A universal strategy for adoptive immunotherapy of cancer through use of a novel T-cell antigen receptor. Cancer Res. 2012 Apr 1;72(7):1844-52. doi: 10.1158/0008-5472.CAN-11-3890. Epub 2012 Feb 7. PMID: 22315351; PMCID: PMC3319867.

373. Lohmueller JJ, Ham JD, Kvorjak M, Finn OJ. mSA2 affinity-enhanced biotin-binding CAR T cells for universal tumor targeting. Oncoimmunology. 2017

Oct 26;7(1):e1368604. doi: 10.1080/2162402X.2017.1368604. PMID: 29296519; PMCID: PMC5739565.

374. Cho JH, Collins JJ, Wong WW. Universal Chimeric Antigen Receptors for Multiplexed and Logical Control of T Cell Responses. Cell. 2018 May 31;173(6):1426-1438.e11. doi: 10.1016/j.cell.2018.03.038. Epub 2018 Apr 26. PMID: 29706540; PMCID: PMC5984158.

375. Majzner RG, Mackall CL. Tumor Antigen Escape from CAR T-cell Therapy. Cancer Discov. 2018 Oct;8(10):1219-1226. doi: 10.1158/2159-8290.CD-18-0442. Epub 2018 Aug 22. PMID: 30135176.

376. Grada Z, Hegde M, Byrd T, Shaffer DR, Ghazi A, Brawley VS, Corder A, Schönfeld K, Koch J, Dotti G, Heslop HE, Gottschalk S, Wels WS, Baker ML, Ahmed N. TanCAR: A Novel Bispecific Chimeric Antigen Receptor for Cancer Immunotherapy. Mol Ther Nucleic Acids. 2013 Jul 9;2(7):e105. doi: 10.1038/mtna.2013.32. PMID: 23839099; PMCID: PMC3731887.

377. Martyniszyn A, Krahl AC, André MC, Hombach AA, Abken H. CD20-CD19 Bispecific CAR T Cells for the Treatment of B-Cell Malignancies. Hum Gene Ther. 2017 Dec;28(12):1147-1157. doi: 10.1089/hum.2017.126. PMID: 29207878.

378. Li D, Hu Y, Jin Z, Zhai Y, Tan Y, Sun Y, Zhu S, Zhao C, Chen B, Zhu J, Chen Z, Chen S, Li J, Liu H. TanCAR T cells targeting CD19 and CD133 efficiently eliminate MLL leukemic cells. Leukemia. 2018 Sep;32(9):2012-2016. doi: 10.1038/s41375-018-0212-z. Epub 2018 Jul 25. PMID: 30046161.

379. Jia H, Wang Z, Wang Y, Liu Y, Dai H, Tong C, Guo Y, Guo B, Ti D, Han X, Yang Q, Wu Z, Han W. Haploidentical CD19/CD22 bispecific CAR-T cells induced MRD-negative remission in a patient with relapsed and refractory adult B-ALL after haploidentical hematopoietic stem cell transplantation. J Hematol Oncol. 2019 Jun 10;12(1):57. doi: 10.1186/s13045-019-0741-6. PMID: 31182121; PMCID: PMC6558895.

380. Zhang H, Gao L, Liu L, Wang J, Wang S, Gao L, Zhang C, Liu Y, Kong P, Liu J, He J, Han Y, Shi H, He Y, Ye X, Zhao Y, Cao W, Shen L, Zhang X. A Bcma and CD19 Bispecific CAR-T for Relapsed and Refractory Multiple Myeloma. Blood. 2019;134(Supplement_1):3147. doi: 10.1182/blood-2019-131056.

381. Hegde M, Mukherjee M, Grada Z, Pignata A, Landi D, Navai SA, Wakefield A,

Fousek K, Bielamowicz K, Chow KK, Brawley VS, Byrd TT, Krebs S, Gottschalk S, Wels WS, Baker ML, Dotti G, Mamonkin M, Brenner MK, Orange JS, Ahmed N. Tandem CAR T cells targeting HER2 and IL13Rα2 mitigate tumor antigen escape. J Clin Invest. 2016 Aug 1;126(8):3036-52. doi: 10.1172/JCI83416. Epub 2016 Jul 18. PMID: 27427982; PMCID: PMC4966331.

382. Bielamowicz K, Fousek K, Byrd TT, Samaha H, Mukherjee M, Aware N, Wu MF, Orange JS, Sumazin P, Man TK, Joseph SK, Hegde M, Ahmed N. Trivalent CAR T cells overcome interpatient antigenic variability in glioblastoma. Neuro Oncol. 2018 Mar 27;20(4):506-518. doi: 10.1093/neuonc/nox182. Erratum in: J Clin Invest. 2021 Jul 1;131(13): PMID: 29016929; PMCID: PMC5909636.

383. Shah NN, Johnson BD, Schneider D, Zhu F, Szabo A, Keever-Taylor CA, Krueger W, Worden AA, Kadan MJ, Yim S, Cunningham A, Hamadani M, Fenske TS, Dropulić B, Orentas R, Hari P. Bispecific anti-CD20, anti-CD19 CAR T cells for relapsed B cell malignancies: a phase 1 dose escalation and expansion trial. Nat Med. 2020 Oct;26(10):1569-1575. doi: 10.1038/s41591-020-1081-3. Epub 2020 Oct 5. PMID: 33020647.

384. Li C, Mei H, Hu Y, Guo T, Liu L, Jiang H, Tang L, Wu Y, Ai L, Deng J, Jin D. A Bispecific CAR-T Cell Therapy Targeting Bcma and CD38 for Relapsed/Refractory Multiple Myeloma: Updated Results from a Phase 1 Dose-Climbing Trial. Blood. 2019 Nov 13;134(Supplement_1):930. doi: 10.1182/blood-2019-130340.

385. Kloss CC, Condomines M, Cartellieri M, Bachmann M, Sadelain M. Combinatorial antigen recognition with balanced signaling promotes selective tumor eradication by engineered T cells. Nat Biotechnol. 2013 Jan;31(1):71-5. doi: 10.1038/nbt.2459. Epub 2012 Dec 16. PMID: 23242161; PMCID: PMC5505184.

386. Fedorov VD, Themeli M, Sadelain M. PD-1- and CTLA-4-based inhibitory chimeric antigen receptors (iCARs) divert off-target immunotherapy responses. Sci Transl Med. 2013 Dec 11;5(215):215ra172. doi: 10.1126/scitranslmed.3006597. PMID: 24337479; PMCID: PMC4238416.

387. Clackson T, Yang W, Rozamus LW, Hatada M, Amara JF, Rollins CT, Stevenson LF, Magari SR, Wood SA, Courage NL, Lu X, Cerasoli F Jr, Gilman

M, Holt DA. Redesigning an FKBP-ligand interface to generate chemical dimerizers with novel specificity. Proc Natl Acad Sci U S A. 1998 Sep 1;95(18):10437-42. doi: 10.1073/pnas.95.18.10437. PMID: 9724721; PMCID: PMC27912.

388. Straathof KC, Pulè MA, Yotnda P, Dotti G, Vanin EF, Brenner MK, Heslop HE, Spencer DM, Rooney CM. An inducible caspase 9 safety switch for T-cell therapy. Blood. 2005 Jun 1;105(11):4247-54. doi: 10.1182/blood-2004-11-4564. Epub 2005 Feb 22. PMID: 15728125; PMCID: PMC1895037.

389. Li P, Zhou L, Zhao T, Liu X, Zhang P, Liu Y, Zheng X, Li Q. Caspase-9: structure, mechanisms and clinical application. Oncotarget. 2017 Apr 4;8(14):23996-24008. doi: 10.18632/oncotarget.15098. PMID: 28177918; PMCID: PMC5410359.

390. Di Stasi A, Tey SK, Dotti G, Fujita Y, Kennedy-Nasser A, Martinez C, Straathof K, Liu E, Durett AG, Grilley B, Liu H, Cruz CR, Savoldo B, Gee AP, Schindler J, Krance RA, Heslop HE, Spencer DM, Rooney CM, Brenner MK. Inducible apoptosis as a safety switch for adoptive cell therapy. N Engl J Med. 2011 Nov 3;365(18):1673-83. doi: 10.1056/NEJMoa1106152. PMID: 22047558; PMCID: PMC3236370.

391. Casucci M, Falcone L, Camisa B, Norelli M, Porcellini S, Stornaiuolo A, Ciceri F, Traversari C, Bordignon C, Bonini C, Bondanza A. Extracellular NGFR Spacers Allow Efficient Tracking and Enrichment of Fully Functional CAR-T Cells Co-Expressing a Suicide Gene. Front Immunol. 2018 Mar 21;9:507. doi: 10.3389/fimmu.2018.00507. PMID: 29619024; PMCID: PMC5871667.

392. Dey D, Evans GRD. Suicide Gene Therapy by Herpes Simplex Virus-1 Thymidine Kinase (HSV-TK). In: Targets in Gene Therapy. InTech; 2011. doi: 10.5772/18544.

393. Serafini M, Manganini M, Borleri G, Bonamino M, Imberti L, Biondi A, Golay J, Rambaldi A, Introna M. Characterization of CD20-transduced T lymphocytes as an alternative suicide gene therapy approach for the treatment of graft-versus-host disease. Hum Gene Ther. 2004 Jan;15(1):63-76. doi: 10.1089/10430340460732463. PMID: 14965378.

394. Wang X, Chang WC, Wong CW, Colcher D, Sherman M, Ostberg JR, Forman SJ, Riddell SR, Jensen MC. A transgene-encoded cell surface polypeptide for

selection, in vivo tracking, and ablation of engineered cells. Blood. 2011 Aug 4;118(5):1255-63. doi: 10.1182/blood-2011-02-337360. Epub 2011 Jun 7. PMID: 21653320; PMCID: PMC3152493.

395. Wu CY, Roybal KT, Puchner EM, Onuffer J, Lim WA. Remote control of therapeutic T cells through a small molecule-gated chimeric receptor. Science. 2015 Oct 16;350(6258):aab4077. doi: 10.1126/science.aab4077. Epub 2015 Sep 24. PMID: 26405231; PMCID: PMC4721629.

396. Juillerat A, Marechal A, Filhol JM, Valton J, Duclert A, Poirot L, Duchateau P. Design of chimeric antigen receptors with integrated controllable transient functions. Sci Rep. 2016 Jan 11;6:18950. doi: 10.1038/srep18950. PMID: 26750734; PMCID: PMC4707440.

397. Zhang RY, Wei D, Liu ZK, Yong YL, Wei W, Zhang ZY, Lv JJ, Zhang Z, Chen ZN, Bian H. Doxycycline Inducible Chimeric Antigen Receptor T Cells Targeting CD147 for Hepatocellular Carcinoma Therapy. Front Cell Dev Biol. 2019 Oct 11;7:233. doi: 10.3389/fcell.2019.00233. PMID: 31681766; PMCID: PMC6798074.

398. Morsut L, Roybal KT, Xiong X, Gordley RM, Coyle SM, Thomson M, Lim WA. Engineering Customized Cell Sensing and Response Behaviors Using Synthetic Notch Receptors. Cell. 2016 Feb 11;164(4):780-91. doi: 10.1016/j.cell.2016.01.012. Epub 2016 Jan 28. PMID: 26830878; PMCID: PMC4752866.

399. Steinbuck MP, Winandy S. A Review of Notch Processing With New Insights Into Ligand-Independent Notch Signaling in T-Cells. Front Immunol. 2018 Jun 1;9:1230. doi: 10.3389/fimmu.2018.01230. PMID: 29910816; PMCID: PMC5992298.

400. Hori K, Sen A, Artavanis-Tsakonas S. Notch signaling at a glance. J Cell Sci. 2013 May 15;126(Pt 10):2135-40. doi: 10.1242/jcs.127308. Epub 2013 May 31. PMID: 23729744; PMCID: PMC3672934.

401. Roybal KT, Rupp LJ, Morsut L, Walker WJ, McNally KA, Park JS, Lim WA. Precision Tumor Recognition by T Cells With Combinatorial Antigen-Sensing Circuits. Cell. 2016 Feb 11;164(4):770-9. doi: 10.1016/j.cell.2016.01.011. Epub 2016 Jan 28. PMID: 26830879; PMCID: PMC4752902.

402. Chillakuri CR, Sheppard D, Lea SM, Handford PA. Notch receptor-ligand

binding and activation: insights from molecular studies. Semin Cell Dev Biol. 2012 Jun;23(4):421-8. doi: 10.1016/j.semcdb.2012.01.009. Epub 2012 Feb 4. PMID: 22326375; PMCID: PMC3415683.

403. Srivastava S, Salter AI, Liggitt D, Yechan-Gunja S, Sarvothama M, Cooper K, Smythe KS, Dudakov JA, Pierce RH, Rader C, Riddell SR. Logic-Gated ROR1 Chimeric Antigen Receptor Expression Rescues T Cell-Mediated Toxicity to Normal Tissues and Enables Selective Tumor Targeting. Cancer Cell. 2019 Mar 18;35(3):489-503.e8. doi: 10.1016/j.ccell.2019.02.003. PMID: 30889382; PMCID: PMC6450658.

404. Roybal KT, Williams JZ, Morsut L, Rupp LJ, Kolinko I, Choe JH, Walker WJ, McNally KA, Lim WA. Engineering T Cells with Customized Therapeutic Response Programs Using Synthetic Notch Receptors. Cell. 2016 Oct 6;167(2):419-432.e16. doi: 10.1016/j.cell.2016.09.011. Epub 2016 Sep 29. PMID: 27693353; PMCID: PMC5072533.

405. Fritsche E, Volk HD, Reinke P, Abou-El-Enein M. Toward an Optimized Process for Clinical Manufacturing of CAR-Treg Cell Therapy. Trends Biotechnol. 2020 Oct;38(10):1099-1112. doi: 10.1016/j.tibtech.2019.12.009. Epub 2020 Jan 22. PMID: 31982150.

406. Adair PR, Kim YC, Zhang AH, Yoon J, Scott DW. Human Tregs Made Antigen Specific by Gene Modification: The Power to Treat Autoimmunity and Antidrug Antibodies with Precision. Front Immunol. 2017 Sep 21;8:1117. doi: 10.3389/fimmu.2017.01117. PMID: 28983300; PMCID: PMC5613123.

407. Kim YC, Bhairavabhotla R, Yoon J, Golding A, Thornton AM, Tran DQ, Shevach EM. Oligodeoxynucleotides stabilize Helios-expressing Foxp3+ human T regulatory cells during in vitro expansion. Blood. 2012 Mar 22;119(12):2810-8. doi: 10.1182/blood-2011-09-377895. Epub 2012 Jan 31. PMID: 22294730; PMCID: PMC3327459.

408. Hori S, Nomura T, Sakaguchi S. Control of regulatory T cell development by the transcription factor Foxp3. Science. 2003 Feb 14;299(5609):1057-61. doi: 10.1126/science.1079490. Epub 2003 Jan 9. PMID: 12522256.

409. Fontenot JD, Gavin MA, Rudensky AY. Foxp3 programs the development and function of CD4+CD25+ regulatory T cells. Nat Immunol. 2003 Apr;4(4):330-6. doi: 10.1038/ni904. Epub 2003 Mar 3. PMID: 12612578.

410. Fontenot JD, Rasmussen JP, Williams LM, Dooley JL, Farr AG, Rudensky AY. Regulatory T cell lineage specification by the forkhead transcription factor foxp3. Immunity. 2005 Mar;22(3):329-41. doi: 10.1016/j.immuni.2005.01.016. PMID: 15780990.

411. Sugimoto N, Oida T, Hirota K, Nakamura K, Nomura T, Uchiyama T, Sakaguchi S. Foxp3-dependent and -independent molecules specific for CD25+CD4+ natural regulatory T cells revealed by DNA microarray analysis. Int Immunol. 2006 Aug;18(8):1197-209. doi: 10.1093/intimm/dxl060. Epub 2006 Jun 13. PMID: 16772372.

412. Thornton AM, Korty PE, Tran DQ, Wohlfert EA, Murray PE, Belkaid Y, Shevach EM. Expression of Helios, an Ikaros transcription factor family member, differentiates thymic-derived from peripherally induced Foxp3+ T regulatory cells. J Immunol. 2010 Apr 1;184(7):3433-41. doi: 10.4049/jimmunol.0904028. Epub 2010 Feb 24. PMID: 20181882; PMCID: PMC3725574.

413. Fransson M, Piras E, Burman J, Nilsson B, Essand M, Lu B, Harris RA, Magnusson PU, Brittebo E, Loskog AS. CAR/FoxP3-engineered T regulatory cells target the CNS and suppress EAE upon intranasal delivery. J Neuroinflammation. 2012 May 30;9:112. doi: 10.1186/1742-2094-9-112. PMID: 22647574; PMCID: PMC3403996.

414. Zhang Q, Lu W, Liang CL, Chen Y, Liu H, Qiu F, Dai Z. Chimeric Antigen Receptor (CAR) Treg: A Promising Approach to Inducing Immunological Tolerance. Front Immunol. 2018 Oct 12;9:2359. doi: 10.3389/fimmu.2018.02359. PMID: 30369931; PMCID: PMC6194362.

415. Boardman DA, Philippeos C, Fruhwirth GO, Ibrahim MA, Hannen RF, Cooper D, Marelli-Berg FM, Watt FM, Lechler RI, Maher J, Smyth LA, Lombardi G. Expression of a Chimeric Antigen Receptor Specific for Donor HLA Class I Enhances the Potency of Human Regulatory T Cells in Preventing Human Skin Transplant Rejection. Am J Transplant. 2017 Apr;17(4):931-943. doi: 10.1111/ajt.14185. Epub 2017 Feb 1. PMID: 28027623.

416. Noyan F, Zimmermann K, Hardtke-Wolenski M, Knoefel A, Schulde E, Geffers R, Hust M, Huehn J, Galla M, Morgan M, Jokuszies A, Manns MP, Jaeckel E. Prevention of Allograft Rejection by Use of Regulatory T Cells With an MHC-

Specific Chimeric Antigen Receptor. Am J Transplant. 2017 Apr;17(4):917-930. doi: 10.1111/ajt.14175. Epub 2017 Feb 6. PMID: 27997080.

417. MacDonald KG, Hoeppli RE, Huang Q, Gillies J, Luciani DS, Orban PC, Broady R, Levings MK. Alloantigen-specific regulatory T cells generated with a chimeric antigen receptor. J Clin Invest. 2016 Apr 1;126(4):1413-24. doi: 10.1172/JCI82771. Epub 2016 Mar 21. PMID: 26999600; PMCID: PMC4811124.

418. Yoon J, Schmidt A, Zhang AH, Königs C, Kim YC, Scott DW. FVIII-specific human chimeric antigen receptor T-regulatory cells suppress T- and B-cell responses to FVIII. Blood. 2017 Jan 12;129(2):238-245. doi: 10.1182/blood-2016-07-727834. Epub 2016 Nov 15. PMID: 28064157; PMCID: PMC5234219.

419. Blat D, Zigmond E, Alteber Z, Waks T, Eshhar Z. Suppression of murine colitis and its associated cancer by carcinoembryonic antigen-specific regulatory T cells. Mol Ther. 2014 May;22(5):1018-28. doi: 10.1038/mt.2014.41. Epub 2014 Mar 6. PMID: 24686242; PMCID: PMC4015241.

420. Skuljec J, Chmielewski M, Happle C, Habener A, Busse M, Abken H, Hansen G. Chimeric Antigen Receptor-Redirected Regulatory T Cells Suppress Experimental Allergic Airway Inflammation, a Model of Asthma. Front Immunol. 2017 Sep 12;8:1125. doi: 10.3389/fimmu.2017.01125. PMID: 28955341; PMCID: PMC5600908.

421. Elinav E, Waks T, Eshhar Z. Redirection of regulatory T cells with predetermined specificity for the treatment of experimental colitis in mice. Gastroenterology. 2008 Jun;134(7):2014-24. doi: 10.1053/j.gastro.2008.02.060. Epub 2008 Mar 4. PMID: 18424268.

422. Elinav E, Adam N, Waks T, Eshhar Z. Amelioration of colitis by genetically engineered murine regulatory T cells redirected by antigen-specific chimeric receptor. Gastroenterology. 2009 May;136(5):1721-31. doi: 10.1053/j.gastro.2009.01.049. Epub 2009 Jan 27. PMID: 19208357.

423. Okkenhaug K, Wu L, Garza KM, La Rose J, Khoo W, Odermatt B, Mak TW, Ohashi PS, Rottapel R. A point mutation in CD28 distinguishes proliferative signals from survival signals. Nat Immunol. 2001 Apr;2(4):325-32. doi: 10.1038/86327. PMID: 11276203.

424. Nakaseko C, Miyatake S, Iida T, Hara S, Abe R, Ohno H, Saito Y, Saito T. Cytotoxic T lymphocyte antigen 4 (CTLA-4) engagement delivers an

inhibitory signal through the membrane-proximal region in the absence of the tyrosine motif in the cytoplasmic tail. J Exp Med. 1999 Sep 20;190(6):765-74. doi: 10.1084/jem.190.6.765. PMID: 10499915; PMCID: PMC2195638.

425. Dawson NAJ, Rosado-Sánchez I, Novakovsky GE, Fung VCW, Huang Q, McIver E, Sun G, Gillies J, Speck M, Orban PC, Mojibian M, Levings MK. Functional effects of chimeric antigen receptor co-receptor signaling domains in human regulatory T cells. Sci Transl Med. 2020 Aug 19;12(557):eaaz3866. doi: 10.1126/scitranslmed.aaz3866. PMID: 32817364.

426. Nianias A, Themeli M. Induced Pluripotent Stem Cell (iPSC)-Derived Lymphocytes for Adoptive Cell Immunotherapy: Recent Advances and Challenges. Curr Hematol Malig Rep. 2019 Aug;14(4):261-268. doi: 10.1007/s11899-019-00528-6. PMID: 31243643; PMCID: PMC6647376.

427. Takahashi K, Yamanaka S. Induction of pluripotent stem cells from mouse embryonic and adult fibroblast cultures by defined factors. Cell. 2006 Aug 25;126(4):663-76. doi: 10.1016/j.cell.2006.07.024. Epub 2006 Aug 10. PMID: 16904174.

428. Kennedy M, Awong G, Sturgeon CM, Ditadi A, LaMotte-Mohs R, Zúñiga-Pflücker JC, Keller G. T lymphocyte potential marks the emergence of definitive hematopoietic progenitors in human pluripotent stem cell differentiation cultures. Cell Rep. 2012 Dec 27;2(6):1722-35. doi: 10.1016/j.celrep.2012.11.003. Epub 2012 Dec 7. PMID: 23219550.

429. Nishimura T, Kaneko S, Kawana-Tachikawa A, Tajima Y, Goto H, Zhu D, Nakayama-Hosoya K, Iriguchi S, Uemura Y, Shimizu T, Takayama N, Yamada D, Nishimura K, Ohtaka M, Watanabe N, Takahashi S, Iwamoto A, Koseki H, Nakanishi M, Eto K, Nakauchi H. Generation of rejuvenated antigen-specific T cells by reprogramming to pluripotency and redifferentiation. Cell Stem Cell. 2013 Jan 3;12(1):114-26. doi: 10.1016/j.stem.2012.11.002. PMID: 23290140.

430. Vizcardo R, Masuda K, Yamada D, Ikawa T, Shimizu K, Fujii S, Koseki H, Kawamoto H. Regeneration of human tumor antigen-specific T cells from iPSCs derived from mature CD8(+) T cells. Cell Stem Cell. 2013 Jan 3;12(1):31-6. doi: 10.1016/j.stem.2012.12.006. PMID: 23290135.

431. Maeda T, Nagano S, Ichise H, Kataoka K, Yamada D, Ogawa S, Koseki H, Kitawaki T, Kadowaki N, Takaori-Kondo A, Masuda K, Kawamoto H. Regeneration of CD8αß T Cells from T-cell-Derived iPSC Imparts Potent Tumor Antigen-Specific Cytotoxicity. Cancer Res. 2016 Dec 1;76(23):6839-6850. doi: 10.1158/0008-5472.CAN-16-1149. Epub 2016 Nov 21. PMID: 27872100.

432. Themeli M, Kloss CC, Ciriello G, Fedorov VD, Perna F, Gonen M, Sadelain M. Generation of tumor-targeted human T lymphocytes from induced pluripotent stem cells for cancer therapy. Nat Biotechnol. 2013 Oct;31(10):928-33. doi: 10.1038/nbt.2678. Epub 2013 Aug 11. PMID: 23934177; PMCID: PMC5722218.

433. Kloess S, Kretschmer A, Stahl L, Fricke S, Koehl U. CAR-Expressing Natural Killer Cells for Cancer Retargeting. Transfus Med Hemother. 2019 Feb;46(1):4-13. doi: 10.1159/000495771. Epub 2019 Feb 5. PMID: 31244577; PMCID: PMC6558329.

434. Gong JH, Maki G, Klingemann HG. Characterization of a human cell line (NK-92) with phenotypical and functional characteristics of activated natural killer cells. Leukemia. 1994 Apr;8(4):652-8. PMID: 8152260.

435. Klingemann HG, Wong E, Maki G. A cytotoxic NK-cell line (NK-92) for ex vivo purging of leukemia from blood. Biol Blood Marrow Transplant. 1996 May;2(2):68-75. PMID: 9118301.

436. Tonn T, Schwabe D, Klingemann HG, Becker S, Esser R, Koehl U, Suttorp M, Seifried E, Ottmann OG, Bug G. Treatment of patients with advanced cancer with the natural killer cell line NK-92. Cytotherapy. 2013 Dec;15(12):1563-70. doi: 10.1016/j.jcyt.2013.06.017. Epub 2013 Oct 1. PMID: 24094496.

437. Tonn T, Becker S, Esser R, Schwabe D, Seifried E. Cellular immunotherapy of malignancies using the clonal natural killer cell line NK-92. J Hematother Stem Cell Res. 2001 Aug;10(4):535-44. doi: 10.1089/15258160152509145. PMID: 11522236.

438. Kriegsmann K, Kriegsmann M, von Bergwelt-Baildon M, Cremer M, Witzens-Harig M. NKT cells - New players in CAR cell immunotherapy? Eur J Haematol. 2018 Dec;101(6):750-757. doi: 10.1111/ejh.13170. Epub 2018 Oct 9. PMID: 30187578.

439. Marin V, Dander E, Biagi E, Introna M, Fazio G, Biondi A, D'Amico G. Characterization of in vitro migratory properties of anti-CD19 chimeric receptor-redirected CIK cells for their potential use in B-ALL immunotherapy. Exp Hematol. 2006 Sep;34(9):1219-29. doi: 10.1016/j.exphem.2006.05.004. PMID: 16939815.

440. Khairallah C, Chu TH, Sheridan BS. Tissue Adaptations of Memory and Tissue-Resident Gamma Delta T Cells. Front Immunol. 2018 Nov 27;9:2636. doi: 10.3389/fimmu.2018.02636. PMID: 30538697; PMCID: PMC6277633.

441. Himoudi N, Morgenstern DA, Yan M, Vernay B, Saraiva L, Wu Y, Cohen CJ, Gustafsson K, Anderson J. Human γδ T lymphocytes are licensed for professional antigen presentation by interaction with opsonized target cells. J Immunol. 2012 Feb 15;188(4):1708-16. doi: 10.4049/jimmunol.1102654. Epub 2012 Jan 16. PMID: 22250090.

442. Rischer M, Pscherer S, Duwe S, Vormoor J, Jürgens H, Rossig C. Human gammadelta T cells as mediators of chimaeric-receptor redirected anti-tumour immunity. Br J Haematol. 2004 Aug;126(4):583-92. doi: 10.1111/j.1365-2141.2004.05077.x. PMID: 15287953.

443. Deniger DC, Switzer K, Mi T, Maiti S, Hurton L, Singh H, Huls H, Olivares S, Lee DA, Champlin RE, Cooper LJ. Bispecific T-cells expressing polyclonal repertoire of endogenous γδ T-cell receptors and introduced CD19-specific chimeric antigen receptor. Mol Ther. 2013 Mar;21(3):638-47. doi: 10.1038/mt.2012.267. Epub 2013 Jan 8. PMID: 23295945; PMCID: PMC3589159.

444. Houchins JP, Yabe T, McSherry C, Bach FH. DNA sequence analysis of NKG2, a family of related cDNA clones encoding type II integral membrane proteins on human natural killer cells. J Exp Med. 1991 Apr 1;173(4):1017-20. doi: 10.1084/jem.173.4.1017. PMID: 2007850; PMCID: PMC2190798.

445. Lanier LL. NKG2D Receptor and Its Ligands in Host Defense. Cancer Immunol Res. 2015 Jun;3(6):575-82. doi: 10.1158/2326-6066.CIR-15-0098. PMID: 26041808; PMCID: PMC4457299.

446. Fisher J, Abramowski P, Wisidagamage Don ND, Flutter B, Capsomidis A, Cheung GW, Gustafsson K, Anderson J. Avoidance of On-Target Off-Tumor Activation Using a Co-stimulation-Only Chimeric Antigen Receptor. Mol

Ther. 2017 May 3;25(5):1234-1247. doi: 10.1016/j.ymthe.2017.03.002. Epub 2017 Mar 22. PMID: 28341563; PMCID: PMC5417796.

447. Capsomidis A, Benthall G, Van Acker HH, Fisher J, Kramer AM, Abeln Z, Majani Y, Gileadi T, Wallace R, Gustafsson K, Flutter B, Anderson J. Chimeric Antigen Receptor-Engineered Human Gamma Delta T Cells: Enhanced Cytotoxicity with Retention of Cross Presentation. Mol Ther. 2018 Feb 7;26(2):354-365. doi: 10.1016/j.ymthe.2017.12.001. Epub 2017 Dec 8. PMID: 29310916; PMCID: PMC5835118.

448. Fleischer LC, Becker SA, Ryan RE, Fedanov A, Doering CB, Spencer HT. Non-signaling Chimeric Antigen Receptors Enhance Antigen-Directed Killing by γδ T Cells in Contrast to αß T Cells. Mol Ther Oncolytics. 2020 Jun 4;18:149-160. doi: 10.1016/j.omto.2020.06.003. PMID: 32671190; PMCID: PMC7341062.

449. Murray PJ. Macrophage Polarization. Annu Rev Physiol. 2017 Feb 10;79:541-566. doi: 10.1146/annurev-physiol-022516-034339. Epub 2016 Oct 21. PMID: 27813830.

450. Klichinsky M, Ruella M, Shestova O, Lu XM, Best A, Zeeman M, Schmierer M, Gabrusiewicz K, Anderson NR, Petty NE, Cummins KD, Shen F, Shan X, Veliz K, Blouch K, Yashiro-Ohtani Y, Kenderian SS, Kim MY, O'Connor RS, Wallace SR, Kozlowski MS, Marchione DM, Shestov M, Garcia BA, June CH, Gill S. Human chimeric antigen receptor macrophages for cancer immunotherapy. Nat Biotechnol. 2020 Aug;38(8):947-953. doi: 10.1038/s41587-020-0462-y. Epub 2020 Mar 23. PMID: 32361713; PMCID: PMC7883632.

451. Tang X, Tang Q, Mao Y, Huang X, Jia L, Zhu J, Feng Z. CD137 Co-Stimulation Improves The Antitumor Effect Of LMP1-Specific Chimeric Antigen Receptor T Cells In Vitro And In Vivo. Onco Targets Ther. 2019 Nov 7;12:9341-9350. doi: 10.2147/OTT.S221040. PMID: 31807014; PMCID: PMC6847990.

452. Slabik C, Kalbarczyk M, Danisch S, Zeidler R, Klawonn F, Volk V, Krönke N, Feuerhake F, Ferreira de Figueiredo C, Blasczyk R, Olbrich H, Theobald SJ, Schneider A, Ganser A, von Kaisenberg C, Lienenklaus S, Bleich A, Hammerschmidt W, Stripecke R. CAR-T Cells Targeting Epstein-Barr Virus gp350 Validated in a Humanized Mouse Model of EBV Infection and Lymphoproliferative Disease. Mol Ther Oncolytics. 2020 Aug 8;18:504-524.

doi: 10.1016/j.omto.2020.08.005. PMID: 32953984; PMCID: PMC7479496.

453. Dragon AC, Zimmermann K, Nerreter T, Sandfort D, Lahrberg J, Klöß S, Kloth C, Mangare C, Bonifacius A, Tischer-Zimmermann S, Blasczyk R, Maecker-Kolhoff B, Uchanska-Ziegler B, Abken H, Schambach A, Hudecek M, Eiz-Vesper B. CAR-T cells and TRUCKs that recognize an EBNA-3C-derived epitope presented on HLA-B*35 control Epstein-Barr virus-associated lymphoproliferation. J Immunother Cancer. 2020 Oct;8(2):e000736. doi: 10.1136/jitc-2020-000736. PMID: 33127653; PMCID: PMC7604878.

454. Köhler G, Milstein C. Continuous cultures of fused cells secreting antibody of predefined specificity. Nature. 1975 Aug 7;256(5517):495-7. doi: 10.1038/256495a0. PMID: 1172191.

455. Kung P, Goldstein G, Reinherz EL, Schlossman SF. Monoclonal antibodies defining distinctive human T cell surface antigens. Science. 1979 Oct 19;206(4416):347-9. doi: 10.1126/science.314668. PMID: 314668.

456. Ortho Multicenter Transplant Study Group. A randomized clinical trial of OKT3 monoclonal antibody for acute rejection of cadaveric renal transplants. N Engl J Med. 1985 Aug 8;313(6):337-42. doi: 10.1056/NEJM198508083130601. PMID: 2861567.

457. Niaudet P, Jean G, Broyer M, Chatenoud L. Anti-OKT3 response following prophylactic treatment in paediatric kidney transplant recipients. Pediatr Nephrol. 1993 Jun;7(3):263-7. doi: 10.1007/BF00853215. PMID: 8518095.

458. Coller BS. A new murine monoclonal antibody reports an activation-dependent change in the conformation and/or microenvironment of the platelet glycoprotein IIb/IIIa complex. J Clin Invest. 1985 Jul;76(1):101-8. doi: 10.1172/JCI111931. PMID: 2991335; PMCID: PMC423718.

459. Knight DM, Wagner C, Jordan R, McAleer MF, DeRita R, Fass DN, Coller BS, Weisman HF, Ghrayeb J. The immunogenicity of the 7E3 murine monoclonal Fab antibody fragment variable region is dramatically reduced in humans by substitution of human for murine constant regions. Mol Immunol. 1995 Nov;32(16):1271-81. doi: 10.1016/0161-5890(95)00085-2. PMID: 8559151.

460. Smith GP. Filamentous fusion phage: novel expression vectors that display cloned antigens on the virion surface. Science. 1985 Jun 14;228(4705):1315-7. doi: 10.1126/science.4001944. PMID: 4001944.

461. McCafferty J, Griffiths AD, Winter G, Chiswell DJ. Phage antibodies: filamentous phage displaying antibody variable domains. Nature. 1990 Dec 6;348(6301):552-4. doi: 10.1038/348552a0. PMID: 2247164.

462. Marks JD, Hoogenboom HR, Bonnert TP, McCafferty J, Griffiths AD, Winter G. By-passing immunization. Human antibodies from V-gene libraries displayed on phage. J Mol Biol. 1991 Dec 5;222(3):581-97. doi: 10.1016/0022-2836(91)90498-u. PMID: 1748994.

463. Jespers LS, Roberts A, Mahler SM, Winter G, Hoogenboom HR. Guiding the selection of human antibodies from phage display repertoires to a single epitope of an antigen. Biotechnology (N Y). 1994 Sep;12(9):899-903. doi: 10.1038/nbt0994-899. PMID: 7521646.

464. Bain B, Brazil M. Adalimumab. Nat Rev Drug Discov. 2003 Sep;2(9):693-94. doi: 10.1038/nrd1182. PMID: 12953696.

465. Russel M. Moving through the membrane with filamentous phages. Trends Microbiol. 1995 Jun;3(6):223-8. doi: 10.1016/s0966-842x(00)88929-5. PMID: 7648030.

466. Carmen S, Jermutus L. Concepts in antibody phage display. Brief Funct Genomic Proteomic. 2002 Jul;1(2):189-203. doi: 10.1093/bfgp/1.2.189. PMID: 15239904.

467. Vieira J, Messing J. Production of single-stranded plasmid DNA. Methods Enzymol. 1987;153:3-11. doi: 10.1016/0076-6879(87)53044-0. PMID: 3323803.

468. O'Connell D, Becerril B, Roy-Burman A, Daws M, Marks JD. Phage versus phagemid libraries for generation of human monoclonal antibodies. J Mol Biol. 2002 Aug 2;321(1):49-56. doi: 10.1016/s0022-2836(02)00561-2. PMID: 12139932.

469. Wesolowski J, Alzogaray V, Reyelt J, Unger M, Juarez K, Urrutia M, Cauerhff A, Danquah W, Rissiek B, Scheuplein F, Schwarz N, Adriouch S, Boyer O, Seman M, Licea A, Serreze DV, Goldbaum FA, Haag F, Koch-Nolte F. Single domain antibodies: promising experimental and therapeutic tools in infection and immunity. Med Microbiol Immunol. 2009 Aug;198(3):157-74. doi: 10.1007/s00430-009-0116-7. Epub 2009 Jun 16. PMID: 19529959; PMCID: PMC2714450.

470. Ch'ng ACW, Choong YS, Lim TS. Phage Display-Derived Antibodies: Application of Recombinant Antibodies for Diagnostics. In: Proof and Concepts in Rapid Diagnostic Tests and Technologies. InTech; 2016. doi: 10.5772/63927.

471. Zhao H, Shen ZM, Kahn PC, Lipke PN. Interaction of alpha-agglutinin and a-agglutinin, Saccharomyces cerevisiae sexual cell adhesion molecules. J Bacteriol. 2001 May;183(9):2874-80. doi: 10.1128/JB.183.9.2874-2880.2001. PMID: 11292808; PMCID: PMC99505.

472. Boder ET, Wittrup KD. Yeast surface display for screening combinatorial polypeptide libraries. Nat Biotechnol. 1997 Jun;15(6):553-7. doi: 10.1038/nbt0697-553. PMID: 9181578.

473. Kieke MC, Cho BK, Boder ET, Kranz DM, Wittrup KD. Isolation of anti-T cell receptor scFv mutants by yeast surface display. Protein Eng. 1997 Nov;10(11):1303-10. doi: 10.1093/protein/10.11.1303. PMID: 9514119.

474. Wang Z, Mathias A, Stavrou S, Neville DM Jr. A new yeast display vector permitting free scFv amino termini can augment ligand binding affinities. Protein Eng Des Sel. 2005 Jul;18(7):337-43. doi: 10.1093/protein/gzi036. Epub 2005 Jun 23. PMID: 15976011.

475. Zhao L, Qu L, Zhou J, Sun Z, Zou H, Chen YY, Marks JD, Zhou Y. High throughput identification of monoclonal antibodies to membrane bound and secreted proteins using yeast and phage display. PLoS One. 2014 Oct 29;9(10):e111339. doi: 10.1371/journal.pone.0111339. PMID: 25353955; PMCID: PMC4213037.

476. Ferrara F, Naranjo LA, Kumar S, Gaiotto T, Mukundan H, Swanson B, Bradbury AR. Using phage and yeast display to select hundreds of monoclonal antibodies: application to antigen 85, a tuberculosis biomarker. PLoS One. 2012;7(11):e49535. doi: 10.1371/journal.pone.0049535. Epub 2012 Nov 14. PMID: 23166701; PMCID: PMC3498134.

477. Wang XX, Shusta EV. The use of scFv-displaying yeast in mammalian cell surface selections. J Immunol Methods. 2005 Sep;304(1-2):30-42. doi: 10.1016/j.jim.2005.05.006. PMID: 16099466.

478. Richman SA, Healan SJ, Weber KS, Donermeyer DL, Dossett ML, Greenberg PD, Allen PM, Kranz DM. Development of a novel strategy for engineering

high-affinity proteins by yeast display. Protein Eng Des Sel. 2006 Jun;19(6):255-64. doi: 10.1093/protein/gzl008. Epub 2006 Mar 20. PMID: 16549400.

479. Zorniak M, Clark PA, Umlauf BJ, Cho Y, Shusta EV, Kuo JS. Yeast display biopanning identifies human antibodies targeting glioblastoma stem-like cells. Sci Rep. 2017 Nov 20;7(1):15840. doi: 10.1038/s41598-017-16066-1. PMID: 29158489; PMCID: PMC5696472.

480. Brinkman EK, Chen T, Amendola M, van Steensel B. Easy quantitative assessment of genome editing by sequence trace decomposition. Nucleic Acids Res. 2014 Dec 16;42(22):e168. doi: 10.1093/nar/gku936. Epub 2014 Oct 9. PMID: 25300484; PMCID: PMC4267669.

481. Brinkman EK, Kousholt AN, Harmsen T, Leemans C, Chen T, Jonkers J, van Steensel B. Easy quantification of template-directed CRISPR/Cas9 editing. Nucleic Acids Res. 2018 Jun 1;46(10):e58. doi: 10.1093/nar/gky164. PMID: 29538768; PMCID: PMC6007333.

482. Lázár-Molnár E, Yan Q, Cao E, Ramagopal U, Nathenson SG, Almo SC. Crystal structure of the complex between programmed death-1 (PD-1) and its ligand PD-L2. Proc Natl Acad Sci U S A. 2008 Jul 29;105(30):10483-8. doi: 10.1073/pnas.0804453105. Epub 2008 Jul 18. PMID: 18641123; PMCID: PMC2492495.

483. Schwartz JC, Zhang X, Fedorov AA, Nathenson SG, Almo SC. Structural basis for co-stimulation by the human CTLA-4/B7-2 complex. Nature. 2001 Mar 29;410(6828):604-8. doi: 10.1038/35069112. PMID: 11279501.

484. Stamper CC, Zhang Y, Tobin JF, Erbe DV, Ikemizu S, Davis SJ, Stahl ML, Seehra J, Somers WS, Mosyak L. Crystal structure of the B7-1/CTLA-4 complex that inhibits human immune responses. Nature. 2001 Mar 29;410(6828):608-11. doi: 10.1038/35069118. Erratum in: Nature 2001 May 31;411(6837):617. PMID: 11279502.

485. Lin DY, Tanaka Y, Iwasaki M, Gittis AG, Su HP, Mikami B, Okazaki T, Honjo T, Minato N, Garboczi DN. The PD-1/PD-L1 complex resembles the antigen-binding Fv domains of antibodies and T cell receptors. Proc Natl Acad Sci U S A. 2008 Feb 26;105(8):3011-6. doi: 10.1073/pnas.0712278105. Epub 2008 Feb 14. PMID: 18287011; PMCID: PMC2268576.

486. Chattopadhyay K, Bhatia S, Fiser A, Almo SC, Nathenson SG. Structural basis of inducible costimulator ligand costimulatory function: determination of the cell surface oligomeric state and functional mapping of the receptor binding site of the protein. J Immunol. 2006 Sep 15;177(6):3920-9. doi: 10.4049/jimmunol.177.6.3920. PMID: 16951355.

487. Joyce MG, Tran P, Zhuravleva MA, Jaw J, Colonna M, Sun PD. Crystal structure of human natural cytotoxicity receptor NKp30 and identification of its ligand binding site. Proc Natl Acad Sci U S A. 2011 Apr 12;108(15):6223-8. doi: 10.1073/pnas.1100622108. Epub 2011 Mar 28. PMID: 21444796; PMCID: PMC3076882.

488. Gietz RD, Woods RA. Transformation of yeast by lithium acetate/single-stranded carrier DNA/polyethylene glycol method. Methods Enzymol. 2002;350:87-96. doi: 10.1016/s0076-6879(02)50957-5. PMID: 12073338.

489. Thomas WD, Smith GP. The case for trypsin release of affinity-selected phages. Biotechniques. 2010 Sep;49(3):651-4. doi: 10.2144/000113489. PMID: 20854266.

490. Krogh BO, Symington LS. Recombination proteins in yeast. Annu Rev Genet. 2004;38:233-71. doi: 10.1146/annurev.genet.38.072902.091500. PMID: 15568977.

491. Oldenburg KR, Vo KT, Michaelis S, Paddon C. Recombination-mediated PCR-directed plasmid construction in vivo in yeast. Nucleic Acids Res. 1997 Jan 15;25(2):451-2. doi: 10.1093/nar/25.2.451. PMID: 9016579; PMCID: PMC146432.

492. Salivar WO, Henry TJ, Pratt D. Purification and properties of diploid particles of coliphage M13. Virology. 1967 May;32(1):41-51. doi: 10.1016/0042-6822(67)90250-4. PMID: 5337710.

493. Crissman JW, Smith GP. Gene-III protein of filamentous phages: evidence for a carboxyl-terminal domain with a role in morphogenesis. Virology. 1984 Jan 30;132(2):445-55. doi: 10.1016/0042-6822(84)90049-7. PMID: 6608175.

494. Riechmann L, Holliger P. The C-terminal domain of TolA is the coreceptor for filamentous phage infection of E. coli. Cell. 1997 Jul 25;90(2):351-60. doi: 10.1016/s0092-8674(00)80342-6. PMID: 9244308.

495. Dietel AK, Merker H, Kaltenpoth M, Kost C. Selective advantages favour high

genomic AT-contents in intracellular elements. PLoS Genet. 2019 Apr 29;15(4):e1007778. doi: 10.1371/journal.pgen.1007778. PMID: 31034469; PMCID: PMC6519830.

496. Brocqueville G, Ndour PA, Ouk TS, Le Goff A, De Witte C, Mougel A, Coll J, Fafeur V, Le Bourhis X, Adriaenssens E. LMP1-induced cell death may contribute to the emergency of its oncogenic property. PLoS One. 2013 Apr 23;8(4):e60743. doi: 10.1371/journal.pone.0060743. PMID: 23637765; PMCID: PMC3634045.

497. Wilson JB, Weinberg W, Johnson R, Yuspa S, Levine AJ. Expression of the BNLF-1 oncogene of Epstein-Barr virus in the skin of transgenic mice induces hyperplasia and aberrant expression of keratin 6. Cell. 1990 Jun 29;61(7):1315-27. doi: 10.1016/0092-8674(90)90695-b. PMID: 1694724.

498. Kim JO, Kim HW, Baek KM, Kang CY. NF-kappaB and AP-1 regulate activation-dependent CD137 (4-1BB) expression in T cells. FEBS Lett. 2003 Apr 24;541(1-3):163-70. doi: 10.1016/s0014-5793(03)00326-0. PMID: 12706838.

499. Philipson BI, O'Connor RS, May MJ, June CH, Albelda SM, Milone MC. 4-1BB costimulation promotes CAR T cell survival through noncanonical NF-κB signaling. Sci Signal. 2020 Mar 31;13(625):eaay8248. doi: 10.1126/scisignal.aay8248. PMID: 32234960; PMCID: PMC7883633.

500. Li G, Boucher JC, Kotani H, Park K, Zhang Y, Shrestha B, Wang X, Guan L, Beatty N, Abate-Daga D, Davila ML. 4-1BB enhancement of CAR T function requires NF-κB and TRAFs. JCI Insight. 2018 Sep 20;3(18):e121322. doi: 10.1172/jci.insight.121322. PMID: 30232281; PMCID: PMC6237232.

501. Rydzek J, Nerreter T, Peng H, Jutz S, Leitner J, Steinberger P, Einsele H, Rader C, Hudecek M. Chimeric Antigen Receptor Library Screening Using a Novel NF-κB/NFAT Reporter Cell Platform. Mol Ther. 2019 Feb 6;27(2):287-299. doi: 10.1016/j.ymthe.2018.11.015. Epub 2018 Nov 20. PMID: 30573301; PMCID: PMC6369451.

502. Henckaerts E, Linden RM. Adeno-associated virus: a key to the human genome? Future Virol. 2010 Sep 1;5(5):555-574. doi: 10.2217/fvl.10.48. PMID: 21212830; PMCID: PMC3014576.

503. Rad S M AH, Poudel A, Tan GMY, McLellan AD. Promoter choice: Who should

drive the CAR in T cells? PLoS One. 2020 Jul 24;15(7):e0232915. doi: 10.1371/journal.pone.0232915. PMID: 32706785; PMCID: PMC7380635.

504. Rubnitz J, Subramani S. The minimum amount of homology required for homologous recombination in mammalian cells. Mol Cell Biol. 1984 Nov;4(11):2253-8. doi: 10.1128/mcb.4.11.2253-2258.1984. PMID: 6096689; PMCID: PMC369052.

505. Ramezani A, Hawley TS, Hawley RG. Lentiviral vectors for enhanced gene expression in human hematopoietic cells. Mol Ther. 2000 Nov;2(5):458-69. doi: 10.1006/mthe.2000.0190. PMID: 11082319.

506. Zheng C, Baum BJ. All human EF1α promoters are not equal: markedly affect gene expression in constructs from different sources. Int J Med Sci. 2014 Mar 7;11(5):404-8. doi: 10.7150/ijms.8033. PMID: 24688302; PMCID: PMC3970091.

507. Awasthi R, Pacaud L, Waldron E, Tam CS, Jäger U, Borchmann P, Jaglowski S, Foley SR, van Besien K, Wagner-Johnston ND, Kersten MJ, Schuster SJ, Salles G, Maziarz RT, Anak Ö, Del Corral C, Chu J, Gershgorin I, Pruteanu-Malinici I, Chakraborty A, Mueller KT, Waller EK. Tisagenlecleucel cellular kinetics, dose, and immunogenicity in relation to clinical factors in relapsed/refractory DLBCL. Blood Adv. 2020 Feb 11;4(3):560-572. doi: 10.1182/bloodadvances.2019000525. PMID: 32045475; PMCID: PMC7013261.

508. Wagner DL, Fritsche E, Pulsipher MA, Ahmed N, Hamieh M, Hegde M, Ruella M, Savoldo B, Shah NN, Turtle CJ, Wayne AS, Abou-El-Enein M. Immunogenicity of CAR T cells in cancer therapy. Nat Rev Clin Oncol. 2021 Jun;18(6):379-393. doi: 10.1038/s41571-021-00476-2. Epub 2021 Feb 25. PMID: 33633361.

509. Turtle CJ, Hanafi LA, Berger C, Hudecek M, Pender B, Robinson E, Hawkins R, Chaney C, Cherian S, Chen X, Soma L, Wood B, Li D, Heimfeld S, Riddell SR, Maloney DG. Immunotherapy of non-Hodgkin's lymphoma with a defined ratio of CD8+ and CD4+ CD19-specific chimeric antigen receptor-modified T cells. Sci Transl Med. 2016 Sep 7;8(355):355ra116. doi: 10.1126/scitranslmed.aaf8621. PMID: 27605551; PMCID: PMC5045301.

510. Finlay WJJ, Coleman JE, Edwards JS, Johnson KS. Anti-PD1 'SHR-1210' aberrantly targets pro-angiogenic receptors and this polyspecificity can be

ablated by paratope refinement. MAbs. 2019 Jan;11(1):26-44. doi: 10.1080/19420862.2018.1550321. Epub 2018 Dec 12. PMID: 30541416; PMCID: PMC6343799.

511. Plückthun A, Pack P. New protein engineering approaches to multivalent and bispecific antibody fragments. Immunotechnology. 1997 Jun;3(2):83-105. doi: 10.1016/s1380-2933(97)00067-5. PMID: 9237094.

512. Halder ME, Barroso J FV, Whelan M. EURL ECVAM recommendation on non-animal-derived antibodies. EUR 30185 EN, Publications Office of the European Union. 2020. doi:10.2760/091625.

Appendix

Figure 1. pYD1 plasmid map and sequence.

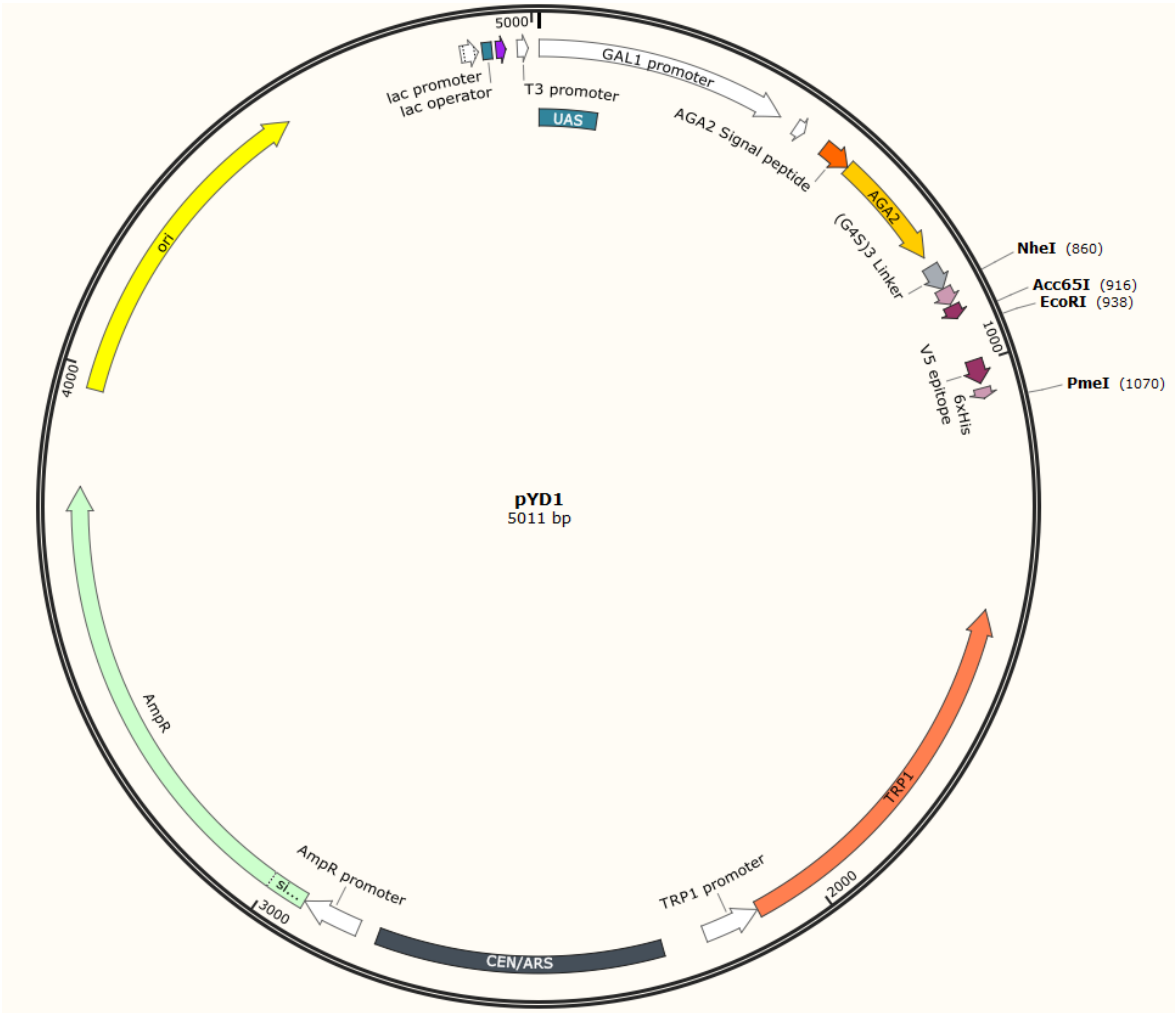

DNA sequence of pYD1
Signal peptide and AGA2 highlighted in their colours in the plasmid map.

acggattagaagccgccgagcgggtgacagccctccgaaggaagactctcctccgtgcgtcctcgtcttcacc
ggtcgcgttcctgaaacgcagatgtgcctcgcgccgcactgctccgaacaataaagattctacaatactagctt
ttatggttatgaagaggaaaaattggcagtaacctggccccacaaaccttcaaatgaacgaatcaaattaaca
accataggatgataatgcgattagttttttagccttatttctggggtaattaatcagcgaagcgatgatttttgat
ctattaacagatatataaatgcaaaaactgcataaccactttaactaatactttcaacattttcggtttgtatta
cttcttattcaaatgtaataaaagtatcaacaaaaaattgttaatatacctctatactttaacgtcaaggagaa
aaaaccccggatcggactactagcagctgtaatacgactcactatagggaatattaagctaattctctacttca
tacattttcaattaagatgcagttacttcgctgtttttcaatattttctgttattgcttcagttttagcacaggaac
tgacaactatatgcgagcaaatcccctcaccaactttagaatcgacgccgtactctttgtcaacgactactatt
tttggccaacgggaaggcaatgcaaggagtttttgaatattacaaatcagtaacgtttgtcagtaattgcggttct
caccctcaacaactagcaaaggcagccccataaacacacagtatgttttaagcttctgcaggctagtggtg
gtggtggttctggtggtggtggttctggtggtggtggttctgctagcatgactggtggacagcaaatgggtcggg
atctgtacgacgatgacgataaggtaccaggatccagtgtggtggaattctgcagatatccagcacagtggcg
gccgctcgagtctagagggcccttcgaaggtaagcctatccctaaccctctcctcggtctcgattctacgcgta
ccggtcatcatcaccatcaccattgagtttaaacccgctgatctgataacaacagtgtagatgtaacaaaatc
gactttgttcccactgtacttttagctcgtacaaaatacaatatacttttcatttctccgtaaacaacatgttttc
ccatgtaatatccttttctatttttcgttccgttaccaactttacacatactttatatagctattcacttctataca

ctaaaaaactaagacaattttaattttgctgcctgccatatttcaatttgttataaattcctataatttatcctat
tagtagctaaaaaaagatgaatgtgaatcgaatcctaagagaattgggcaagtgcacaaacaatacttaaat
aaatactactcagtaataacctatttcttagcatttttgacgaaatttgctattttgttagagtcttttacaccatt
tgtctccacacctccgcttacatcaacaccaataacgccatttaatctaagcgcatcaccaacattttctggcg
tcagtccaccagctaacataaaatgtaagctctcggggctctcttgccttccaacccagtcagaaatcgagttc
caatccaaaagttcacctgtcccacctgcttctgaatcaaacaagggaataaacgaatgaggtttctgtgaag
ctgcactgagtagtatgttgcagtcttttggaaatacgagtcttttaataactggcaaaccgaggaactcttggt
attcttgccacgactcatctccgtgcagttggacgatatcaatgccgtaatcattgaccagagccaaaacatcc
tccttaggttgattacgaaacacgccaaccaagtatttcggagtgcctgaactatttttatatgcttttacaaga
cttgaaattttccttgcaataaccgggtcaattgttctctttctattgggcacacatataatacccagcaagtca
gcatcggaatctagagcacattctgcggcctctgtgctctgcaagccgcaaactttcaccaatggaccagaac
tacctgtgaaattaataacagacatactccaagctgcctttgtgtgcttaatcacgtatactcacgtgctcaata
gtcaccaatgccctccctcttggccctctccttttctttttcgaccgaatttcttgaagacgaaagggcctcgtg
atacgcctatttttataggttaatgtcatgataataatggtttcttaggacggatcgcttgcctgtaacttacacg
cgcctcgtatcttttaatgatggaataatttgggaatttactctgtgtttatttatttttatgttttgtatttggattt
tagaaagtaaataaagaaggtagaagagttacggaatgaagaaaaaaaaataaacaaaggtttaaaaaattt
caacaaaaagcgtactttacatatatatttattagacaagaaaagcagattaaatagatatacattcgattaa
cgataagtaaaatgtaaaatcacaggattttcgtgtgtggtcttctacacagacaagatgaaacaattcggcat
taatacctgagagcaggaagagcaagataaaaggtagtatttgttggcgatccccctagagtcttttacatctt
cggaaaacaaaaactatttttttctttaatttctttttttacttttctatttttaatttatatatttatattaaaaaatt
taaattataattatttttatagcacgtgatgaaaaggacccaggtggcacttttcggggaaatgtgcgcggaac
ccctatttgtttatttttctaaatacattcaaatatgtatccgctcatgagacaataaccctgataaatgcttca
ataatattgaaaaaggaagagtatgagtattcaacatttccgtgtcgcccttattccctttttgcggcattttgc
cttcctgtttttgctcacccagaaacgctggtgaaagtaaaagatgctgaagatcagttgggtgcacgagtggg
ttacatcgaactggatctcaacagcggtaagatccttgagagttttcgccccgaagaacgttttccaatgatga
gcacttttaaagttctgctatgtggcgcggtattatcccgtgttgacgccgggcaagagcaactcggtcgccgc
atacactattctcagaatgacttggttgagtactcaccagtcacagaaaagcatcttacggatggcatgacagt
aagagaattatgcagtgctgccataaccatgagtgataacactgcggccaacttacttctgacaacgatcgga
ggaccgaaggagctaaccgcttttttgcacaacatgggggatcatgtaactcgccttgatcgttgggaaccgga
gctgaatgaagccataccaaacgacgagcgtgacaccacgatgcctgtagcaatggcaacaacgttgcgcaa
actattaactggcgaactacttactctagcttcccggcaacaattaatagactggatggaggcggataaagttg
caggaccacttctgcgctcggcccttccggctggctggtttattgctgataaatctggagccggtgagcgtgggt
ctcgcggtatcattgcagcactggggccagatggtaagccctcccgtatcgtagttatctacacgacgggcagt
caggcaactatggatgaacgaaatagacagatcgctgagataggtgcctcactgattaagcattggtaactgt
cagaccaagtttactcatatatactttagattgatttaaaacttcatttttaatttaaaaggatctaggtgaaga
tccttttgataatctcatgaccaaaatcccttaacgtgagttttcgttccactgagcgtcagaccccgtagaaa
agatcaaaggatcttcttgagatcctttttttctgcgcgtaatctgctgcttgcaaacaaaaaaaccaccgcta
ccagcggtggtttgtttgccggatcaagagctaccaactctttttccgaaggtaactggcttcagcagagcgca
gataccaaatactgtccttctagtgtagccgtagttaggccaccacttcaagaactctgtagcaccgcctacat
acctcgctctgctaatcctgttaccagtggctgctgccagtggcgataagtcgtgtcttaccgggttggactcaa
gacgatagttaccggataaggcgcagcggtcgggctgaacgggggttcgtgcacacagcccagcttggagc
gaacgacctacaccgaactgagatacctacagcgtgagcattgagaaagcgccacgcttcccgaagggagaa
aggcggacaggtatccggtaagcggcagggtcggaacaggagagcgcacgagggagcttccagggggaac
gcctggtatctttatagtcctgtcgggtttcgccacctctgacttgagcgtcgatttttgtgatgctcgtcagggg
ggccgagcctatggaaaaacgccagcaacgcggccttttacggttcctggccttttgctggccttttgctcac
atgttctttcctgcgttatcccctgattctgtggataaccgtattaccgcctttgagtgagctgataccgctcgcc
gcagccgaacgaccgagcgcagcgagtcagtgagcgaggaagcggaagagcgcccaatacgcaaaccgcct
ctccccgcgcgttggccgattcattaatgcagctggcacgacaggtttcccgactggaaagcgggcagtgagc
gcaacgcaattaatgtgagttacctcactcattaggcaccccaggctttacactttatgcttccggctcctatgt
tgtgtggaattgtgagcggataacaatttcacacaggaaacagctatgaccatgattacgccaagctcggaat
taaccctcactaaagggaacaaaagctggctagt

Figure 2. pYDN plasmid map and sequence.

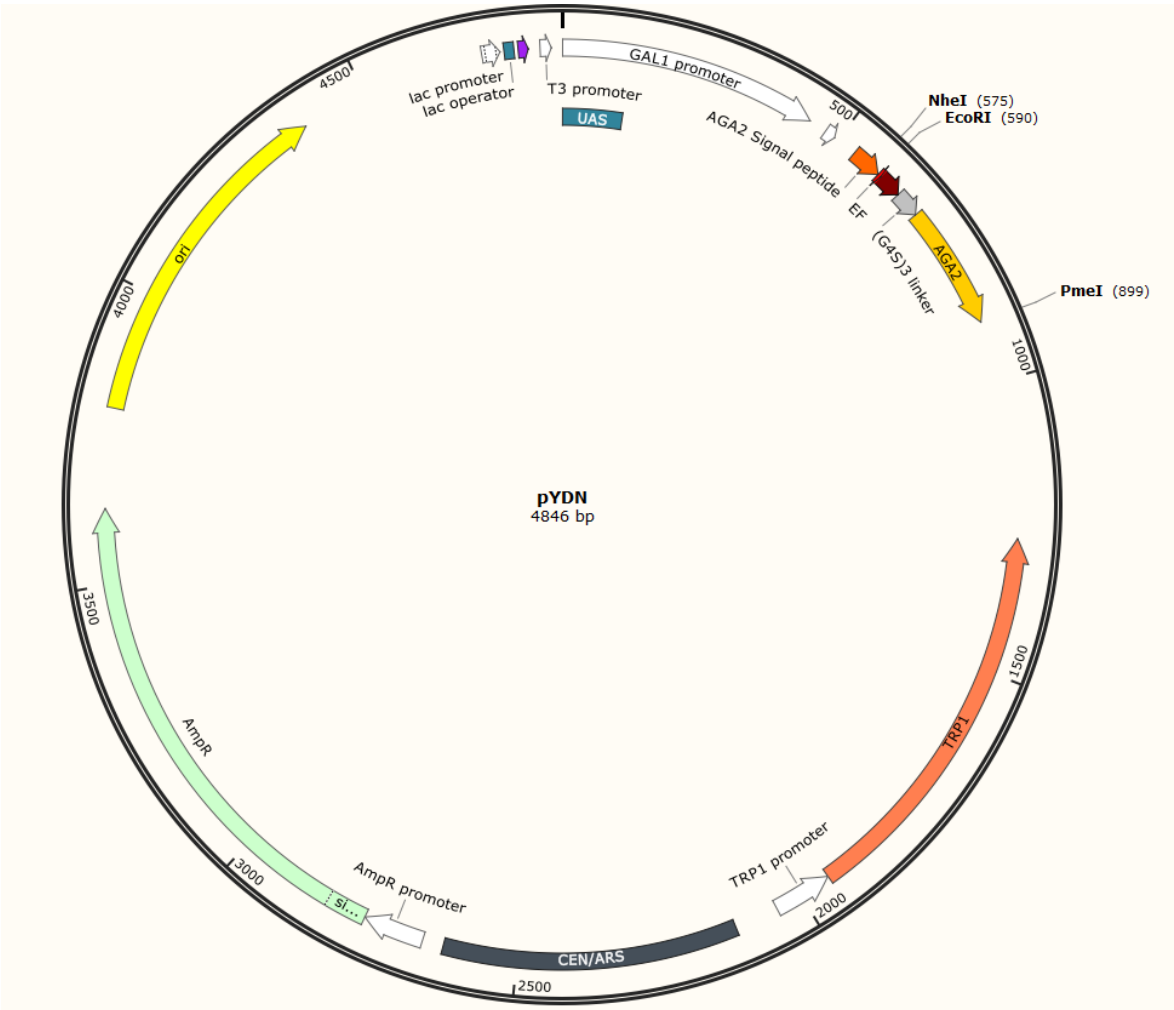

DNA sequence of pYDN
Signal peptide and AGA2 highlighted in their colours in the plasmid map.

acggattagaagccgccgagcgggtgacagccctccgaaggaagactctcctccgtgcgtcctcgtcttcacc
ggtcgcgttcctgaaacgcagatgtgcctcgcgccgcactgctccgaacaataaagattctacaatactagctt
ttatggttatgaagaggaaaaattggcagtaacctggccccacaaaccttcaaatgaacgaatcaaattaaca
accataggatgataatgcgattagttttttagccttatttctggggtaattaatcagcgaagcgatgattttgat
ctattaacagatatataaatgcaaaaactgcataaccactttaactaatactttcaacattttcggtttgtatta
cttcttattcaaatgtaataaaagtatcaacaaaaaattgttaatatacctctatactttaacgtcaaggagaa
aaaaccccggatcggactactagcagctgtaatacgactcactatagggaatattaagctaattctctacttca
tacattttcaattaagatgcagttacttcgctgtttttcaatattttctgttattgctagcgttttagcagaattcg
gtaaaccaattccaaatccattgttgggtttggactctactggtggtggtggttctggtggtggtggttctggtgg
tggtggttctcaggaattgactactatttgcgaacaaattccatctccaactttggaatctactccatactctttg
tctacaactactattttggctaatggtaaagctatgcaaggtgtttttgaatattataaatctgttacttttgtttc
taattgtggttctcacccatctactacttctaaaggttctccaattaatactcaatatgttttttgataggtttaa
acgaacggccgctgatctgataacaacagtgtagatgtaacaaaatcgactttgttcccactgtacttttagct
cgtacaaaatacaatatacttttcatttctccgtaaacaacatgttttcccatgtaatatccttttctatttttcgt
tccgttaccaactttacacatactttatatagctattcacttctatacactaaaaaactaagacaattttaatttt
gctgcctgccatatttcaatttgttataaattcctataatttatcctattagtagctaaaaaaagatgaatgtga
atcgaatcctaagagaattgggcaagtgcacaaacaatacttaaataaatactactcagtaataacctatttct
tagcatttttgacgaaatttgctattttgttagagtcttttacaccatttgtctccacacctccgcttacatcaac
accaataacgccatttaatctaagcgcatcaccaacattttctggcgtcagtccaccagctaacataaaatgt
aagctctcggggctctcttgccttccaacccagtcagaaatcgagttccaatccaaaagttcacctgtcccacc

tgcttctgaatcaaacaagggaataaacgaatgaggtttctgtgaagctgcactgagtagtatgttgcagtcttt
tggaaatacgagtcttttaataactggcaaaccgaggaactcttggtattcttgccacgactcatctccgtgca
gttggacgatatcaatgccgtaatcattgaccagagccaaaacatcctccttaggttgattacgaaacacgcc
aaccaagtatttcggagtgcctgaactatttttatatgcttttacaagacttgaaattttccttgcaataaccgg
gtcaattgttctctttctattgggcacacatataatacccagcaagtcagcatcggaatctagagcacattctg
cggcctctgtgctctgcaagccgcaaactttcaccaatggaccagaactacctgtgaaattaataacagacat
actccaagctgccttgtgtgcttaatcacgtatactcacgtgctcaatagtcaccaatgccctccctcttggcc
ctctccttttctttttcgaccgaatttcttgaagacgaaagggcctcgtgatacgcctatttttataggttaatgt
catgataataatggtttcttaggacggatcgcttgcctgtaacttacacgcgcctcgtatcttttaatgatggaa
taatttgggaatttactctgtgtttatttatttttatgttttgtatttggattttagaaagtaaataaagaaggtag
aagagttacggaatgaagaaaaaaaaataaacaaaggtttaaaaaatttcaacaaaaagcgtactttacata
tatatttattagacaagaaaagcagattaaatagatatacattcgattaacgataagtaaaatgtaaaatcac
aggattttcgtgtgtggtcttctacacagacaagatgaaacaattcggcattaatacctgagagcaggaagag
caagataaaaggtagtatttgttggcgatccccctagagtcttttacatcttcggaaaacaaaaactatttttc
tttaatttctttttttactttctatttttaatttatatatttatattaaaaaatttaaattataattatttttatagca
cgtgatgaaaaggacccaggtggcacttttcggggaaatgtgcgcggaacccctatttgtttatttttctaaata
cattcaaatatgtatccgctcatgagacaataaccctgataaatgcttcaataatattgaaaaaggaagagta
tgagtattcaacatttccgtgtcgcccttattccctttttgcggcattttgccttcctgtttttgctcacccagaa
acgctggtgaaagtaaaagatgctgaagatcagttgggtgcacgagtgggttacatcgaactggatctcaaca
gcggtaagatccttgagagttttcgccccgaagaacgttttccaatgatgagcacttttaaagttctgctatgtg
gcgcggtattatcccgtgttgacgccgggcaagagcaactcggtcgccgcatacactattctcagaatgacttg
gttgagtactcaccagtcacagaaaagcatcttacggatggcatgacagtaagagaattatgcagtgctgcca
taaccatgagtgataacactgcggccaacttacttctgacaacgatcggaggaccgaaggagctaaccgcttt
tttgcacaacatgggggatcatgtaactcgccttgatcgttgggaaccggagctgaatgaagccataccaaac
gacgagcgtgacaccacgatgcctgtagcaatggcaacaacgttgcgcaaactattaactggcgaactactta
ctctagcttcccggcaacaattaatagactggatggaggcggataaagttgcaggaccacttctgcgctcggc
ccttccggctggctggtttattgctgataaatctggagccggtgagcgtgggtctcgcggtatcattgcagcact
ggggccagatggtaagccctcccgtatcgtagttatctacacgacgggcagtcaggcaactatggatgaacga
aatagacagatcgctgagataggtgcctcactgattaagcattggtaactgtcagaccaagtttactcatatat
actttagattgatttaaaacttcatttttaatttaaaaggatctaggtgaagatccttttgataatctcatgacc
aaaatcccttaacgtgagttttcgttccactgagcgtcagaccccgtagaaaagatcaaaggatcttcttgaga
tccttttttttctgcgcgtaatctgctgcttgcaaacaaaaaaaccaccgctaccagcggtggtttgtttgccgga
tcaagagctaccaactctttttccgaaggtaactggcttcagcagagcgcagataccaaatactgtccttctag
tgtagccgtagttaggccaccacttcaagaactctgtagcaccgcctacatacctcgctctgctaatcctgtta
ccagtggctgctgccagtggcgataagtcgtgtcttaccgggttggactcaagacgatagttaccggataaggc
gcagcggtcgggctgaacgggggttcgtgcacacagcccagcttggagcgaacgacctacaccgaactgag
atacctacagcgtgagcattgagaaagcgccacgcttcccgaagggagaaaggcggacaggtatccggtaag
cggcagggtcggaacaggagagcgcacgagggagcttccagggggaacgcctggtatctttatagtcctgtc
gggtttcgccacctctgacttgagcgtcgattttgtgatgctcgtcaggggggccgagcctatggaaaaacgc
cagcaacgcggcctttttacggttcctggccttttgctggccttttgctcacatgttctttcctgcgttatcccctg
attctgtggataaccgtattaccgcctttgagtgagctgataccgctcgccgcagccgaacgaccgagcgcag
cgagtcagtgagcgaggaagcggaagagcgcccaatacgcaaaccgcctctccccgcgcgttggccgattca
ttaatgcagctggcacgacaggtttcccgactggaaagcgggcagtgagcgcaacgcaattaatgtgagttac
ctcactcattaggcaccccaggctttacactttatgcttccggctcctatgttgtgtggaattgtgagcggataa
caatttcacacaggaaacagctatgaccatgattacgccaagctcggaattaaccctcactaaagggaacaa
aagctggctagt

Figure 3. pRXB-100 plasmid map and sequence.

DNA sequence of pRXB-100

Pel B, an example of a cloned scFv and PIII highlighted in their colours in the plasmid map.

GCACTTTTCGGGGAAATGTGCGCGGAACCCCTATTTGTTTATTTTTCTAAATACATTCA
AATATGTATCCGCTCATGAGACAATAACCCTGATAAATGCTTCAATAATATTGAAAAAG
GAAGAGTATGAGTATTCAACATTTCCGTGTCGCCCTTATTCCCTTTTTTGCGGCATTTT
GCCTTCCTGTTTTTGCTCACCCAGAAACGCTGGTGAAAGTAAAAGATGCTGAAGATCA
GTTGGGTGCACGAGTGGGTTACATCGAACTGGATCTCAACAGCGGTAAGATCCTTGA
GAGTTTTCGCCCCGAAGAACGTTTTCCAATGATGAGCACTTTTAAAGTTCTGCTATGT
GGCGCGGTATTATCCCGTATTGACGCCGGGCAAGAGCAACTCGGTCGCCGCATACAC
TATTCTCAGAATGACTTGGTTGAGTACTCACCAGTCACAGAAAAGCATCTTACGGATG
GCATGACAGTAAGAGAATTATGCAGTGCTGCCATAACCATGAGTGATAACACTGCGGC
CAACTTACTTCTGACAACGATCGGAGGACCGAAGGAGCTAACCGCTTTTTTGCACAAC
ATGGGGGATCATGTAACTCGCCTTGATCGTTGGGAACCGGAGCTGAATGAAGCCATA
CCAAACGACGAGCGTGACACCACGATGCCTGTAGCAATGGCAACAACGTTGCGCAAAC
TATTAACTGGCGAACTACTTACTCTAGCTTCCCGGCAACAATTAATAGACTGGATGGA
GGCGGATAAAGTTGCAGGACCACTTCTGCGCTCGGCGCTTCCGGCTGGCTGGTTTAT
TGCTGATAAATCTGGAGCCGGTGAGCGTGGGTCTCGCGGTATCATTGCAGCACTGGG

GCCAGATGGTAAGCCCTCCCGTATCGTAGTTATCTACACGACGGGGAGTCAGGCAACT
ATGGATGAACGAAATAGACAGATCGCTGAGATAGGTGCCTCACTGATTAAGCATTGGT
AACTGTCAGACCAAGTTTACTCATATATACTTTAGATTGATTTAAAACTTCATTTTTAAT
TTAAAAGGATCTAGGTGAAGATCCTTTTTGATAATCTCATGACCAAAATCCCTTAACGT
GAGTTTTCGTTCCACTGAGCGTCAGACCCCGTAGAAAAGATCAAAGGATCTTCTTGAG
ATCCTTTTTTTCTGCGCGTAATCTGCTGCTTGCAAACAAAAAAACCACCGCTACCAGCG
GTGGTTTGTTTGCCGGATCAAGAGCTACCAACTCTTTTTCCGAAGGTAACTGGCTTCA
GCAGAGCGCAGATACCAAATACTGTTCTTCTAGTGTAGCCGTAGTTAGGCCACCACTT
CAAGAACTCTGTAGCACCGCCTACATACCTCGCTCTGCTAATCCTGTTACCAGTGGCT
GCTGCCAGTGGCGATAAGTCGTGTCTTACCGGGTTGGACTCAAGACGATAGTTACCG
GATAAGGCGCAGCGGTCGGGCTGAACGGGGGGTTCGTGCACACAGCCCAGCTTGGA
GCGAACGACCTACACCGAACTGAGATACCTACAGCGTGAGCTATGAGAAAGCGCCACG
CTTCCCGAAGGGAGAAAGGCGGACAGGTATCCGGTAAGCGGCAGGGTCGGAACAGGA
GAGCGCACGAGGGAGCTTCCAGGGGGAAACGCCTGGTATCTTTATAGTCCTGTCGGG
TTTCGCCACCTCTGACTTGAGCGTCGATTTTTGTGATGCTCGTCAGGGGGGCGGAGC
CTATGGAAAAACGCCAGCAACGCGGCCTTTTTACGGTTCCTGGCCTTTTGCTGGCCTT
TTGCTCACATGCGCCCAATACGCAAACCGCCTCTCCCCGCGCGTTGGCCGATTCATTA
ATGCAGCTGGCACGACAGGTTTCCCGACTGGAAAGCGGGCAGTGAGCGCAACGCAAT
TAATGTGAGTTAGCTCACTCATTAGGCACCCCAGGCTTTACACTTTATGCTTCCGGCT
CGTATGTTGTGTGGAATTGTGAGCGGATAACAATTTGAATTCAAGGAGACAGTCATAA
TGAAATACCTATTGCCTACGGCGGCCGCTGGATTGTTATTACTCGCGGCCCAGCCGGC
CATGGCACAGGTGCAGCTGGTGCAGTCTGGGGCTGAGGTGAAGAAGCCTGGGTCCTC
AGTGAAGGTCTCCTGCAAGGCTTCTGGAGGCACCTTCAGCAGCTATGCTATCAGCTG
GGTGCGACAGGCCCCTGGACAAGGGCTTGAGTGGATGGGAGGGATCATCCCTATCTT
TGGTACAGCAAACTACGCACAGAAGTTCCAGGGCAGAGTCACGATTACCGCGGACGAA
TCCACGAGCACAGCCTACATGGAGCTGAGCAGCCTGAGATCTGAGGACACGGCCGTG
TATTACTGTGCGAGAGGCACTGGTCCAGCTGCTATGAACTACTGGGGCCAGGGAACC
CTGGTCACCGTCTCCTCAGGGACTGCATCCACCCCAACCCTTGGCAGCAGCGGCAGCA
GCAGCGGTACCAGCAGCGGCGGCAGCAGCAGCAGCGGCAGCGGCGAGCTCACACTCA
CGCAGTCTCCAGGCACCCTGTCTTTGTCTCCAGGGGAAAGAGCCACCCTCTCCTGCAG
GGCTAGTCAGAGTGTTAGCAGCAGGTACTTAGCCTGGTACCAGCACAAACCTGGCCA
GGCTCCCAGGCTCCTCATCTACGGTGCATCCAGCAGGGCCACTGGCATCCCAGACAG
GTTCAGTGGCAGTGGGTCTGGGACAGACTTCACTCTCACCATCAGCAGACTGGAGCC
TGAAGATTTTGCAGTGTATTACTGTCAGCAGTATGGTAGCTCACCGTACAGTTTTGGC
CAGGGGACCAAGCTGGAGATCAAAGGCCCGGGAGGCCAAGGCGGTGGTTCTGAGGG
TGGTGGCTCCCTCGAGGGCGCGCCAGCCGAAACTGTTGAAAGTTGTTTAGCAAAACC
TCATACAGAAAATTCATTTACTAACGTCTGGAAAGACGACAAAACTTTAGATCGTTACG
CTAACTATGAGGGCTGTCTGTGGAATGCTACAGGCGTTGTGGTTTGTACTGGTGACG
AAACTCAGTGTTACGGTACATGGGTTCCTATTGGGCTTGCTATCCCTGAAAATGAGGG
TGGTGGCTCTGAGGGTGGCGGTTCTGAGGGTGGCGGTTCTGAGGGTGGCGGTACTA
AACCTCCTGAGTACGGTGATACACCTATTCCGGGCTATACTTATATCAACCCTCTCGAC
GGCACTTATCCGCCTGGTACTGAGCAAAACCCCGCTAATCCTAATCCTTCTCTTGAGG
AGTCTCAGCCTCTTAATACTTTCATGTTTCAGAATAATAGGTTCCGAAATAGGCAGGG
TGCATTAACTGTTTATACGGGCACTGTTACTCAAGGCACTGACCCCGTTAAAACTTATT
ACCAGTACACTCCTGTATCATCAAAAGCCATGTATGACGCTTACTGGAACGGTAAATTC
AGAGACTGCGCTTTCCATTCTGGCTTTAATGAGGATCCATTCGTTTGTGAATATCAAG
GCCAATCGTCTGACCTGCCTCAACCTCCTGTCAATGCTGGCGGCGGCTCTGGTGGTG
GTTCTGGTGGCGGCTCTGAGGGTGGCGGCTCTGAGGGTGGCGGTTCTGAGGGTGGC
GGCTCTGAGGGTGGCGGTTCCGGTGGCGGCTCCGGTTCCGGTGATTTTGATTATGAA
AAAATGGCAAACGCTAATAAGGGGGCTATGACCGAAAATGCCGATGAAAACGCGCTAC
AGTCTGACGCTAAAGGCAAACTTGATTCTGTCGCTACTGATTACGGTGCTGCTATCGA
TGGTTTCATTGGTGACGTTTCCGGCCTTGCTAATGGTAATGGTGCTACTGGTGATTTT

GCTGGCTCTAATTCCCAAATGGCTCAAGTCGGTGACGGTGATAATTCACCTTTAATGA
ATAATTTCCGTCAATATTTACCTTCTTTGCCTCAGTCGGTTGAATGTCGCCCTTATGTC
TTTGGCGCTGGTAAACCATATGAATTTTCTATTGATTGTGACAAAATAAACTTATTCCG
TGGTGTCTTTGCGTTTCTTTTATATGTTGCCACCTTTATGTATGTATTTTCGACGTTTG
CTAACATACTGCGTAATAAGGAGTCTTAAGCTAGCTAACAGTCACTATGAATCAACTAC
TTAGATGGTATTAGTGACCTGTAACAGAGCATTAGCGCAAGGTGATTTTTGTCTTCTT
GCGCTAATTTTTTGTCATCAAACCTGTCGCACTCCTTAATATTTTGTTAAAATTCGCGT
TAAATTTTTGTTAAATCAGCTCATTTTTTAACCAATAGGCCGAAATCGGCAAAATCCCT
TATAAATCAAAAGAATAGACCGAGATAGGGTTGAGTGTTGTTCCAGTTTGGAACAAGA
GTCCACTATTAAAGAACGTGGACTCCAACGTCAAAGGGCGAAAAACCGTCTATCAGGG
CGATGGCCCACTACGTGAACCATCACCCTAATCAAGTTTTTTGGGGTCGAGGTGCCGT
AAAGCACTAAATCGGAACCCTAAAGGGAGCCCCCGATTTAGAGCTTGACGGGGAAAGC
CGGCGAACGTGGCGAGAAAGGAAGGGAAGAAAGCGAAAGGAGCGGGCGCTAGGGCG
CTGGCAAGTGTAGCGGTCACGCTGCGCGTAACCACCACACCCGCCGCGCTTAATGCG
CCGCTACAGGGCGCGTCAGGTG

Figure 4. Helper phage M13K07 map.

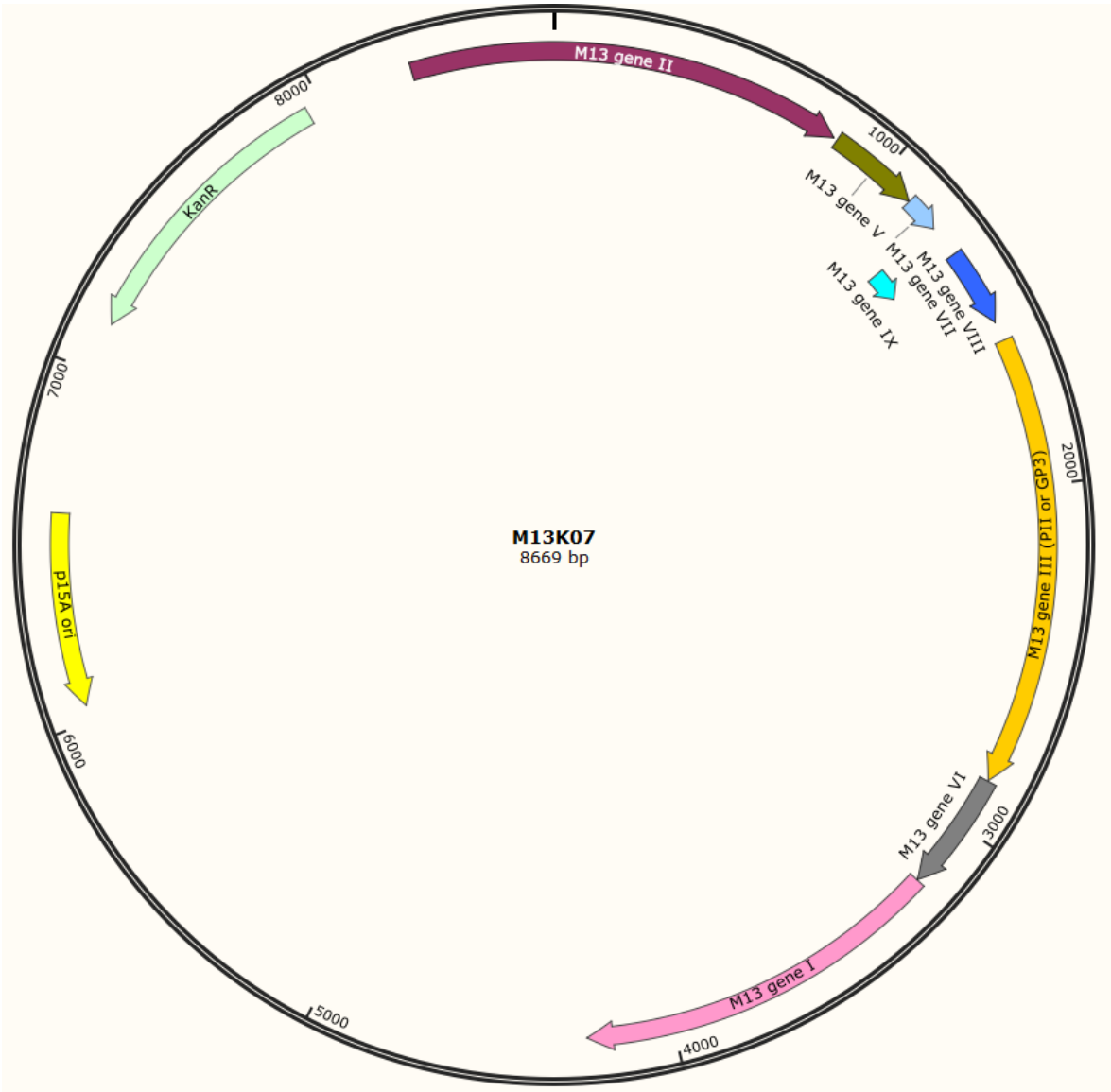

Figure 5. pcDNA5/FRT plasmid map and sequence.

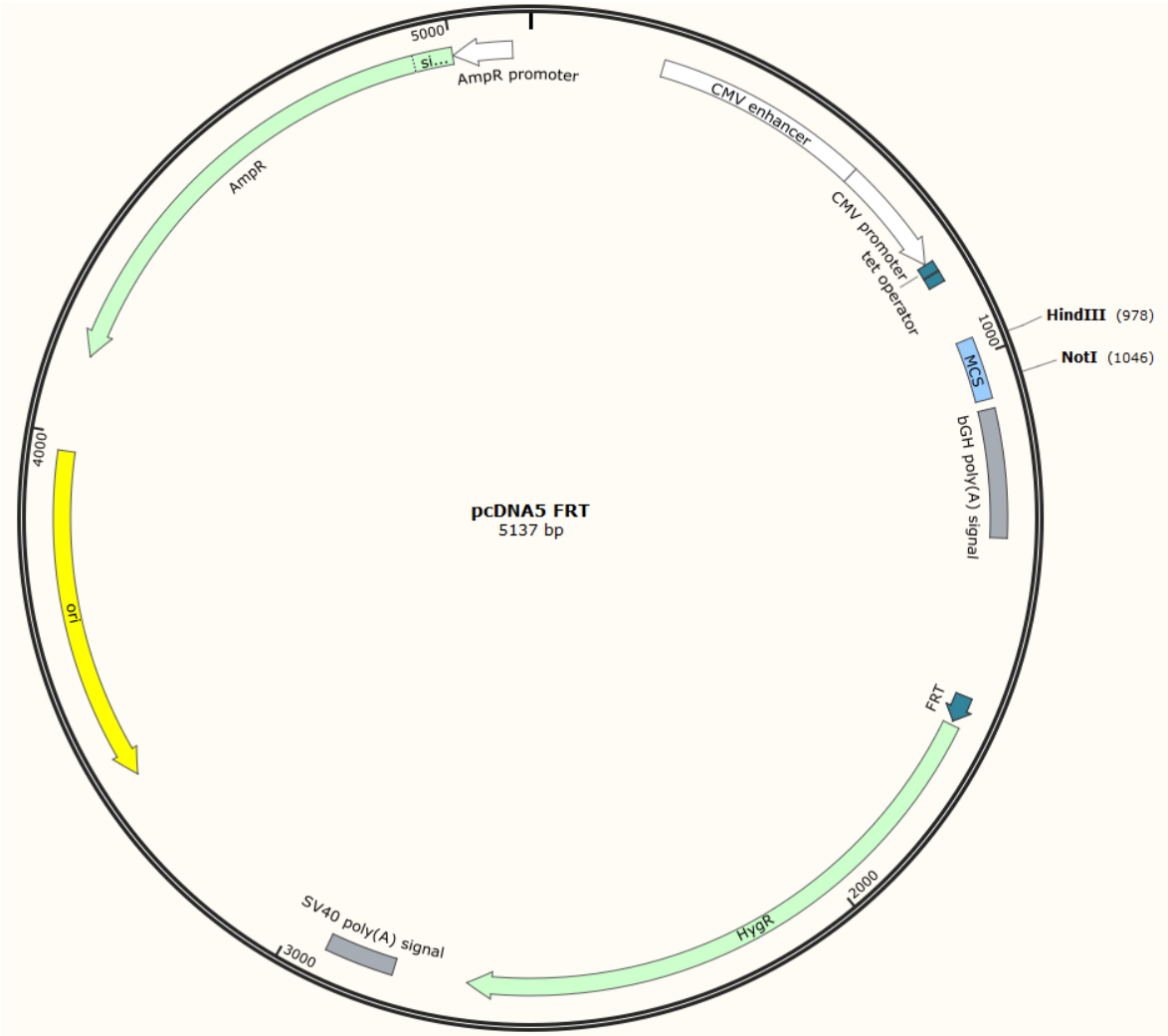

DNA sequence of pcDNA5/FRT
MCS and the bGH poly(A) signal highlighted in their colours in the plasmid map.

GACGGATCGGGAGATCTCCCGATCCCCTATGGTGCACTCTCAGTACAATCTGCTCTGA
TGCCGCATAGTTAAGCCAGTATCTGCTCCCTGCTTGTGTGTTGGAGGTCGCTGAGTA
GTGCGCGAGCAAAATTTAAGCTACAACAAGGCAAGGCTTGACCGACAATTGCATGAAG
AATCTGCTTAGGGTTAGGCGTTTTGCGCTGCTTCGCGATGTACGGGCCAGATATACG
CGTTGACATTGATTATTGACTAGTTATTAATAGTAATCAATTACGGGGTCATTAGTTCA
TAGCCCATATATGGAGTTCCGCGTTACATAACTTACGGTAAATGGCCCGCCTGGCTGA
CCGCCCAACGACCCCCGCCCATTGACGTCAATAATGACGTATGTTCCCATAGTAACGC
CAATAGGGACTTTCCATTGACGTCAATGGGTGGAGTATTTACGGTAAACTGCCCACTT
GGCAGTACATCAAGTGTATCATATGCCAAGTACGCCCCCTATTGACGTCAATGACGGT
AAATGGCCCGCCTGGCATTATGCCCAGTACATGACCTTATGGGACTTTCCTACTTGGC
AGTACATCTACGTATTAGTCATCGCTATTACCATGGTGATGCGGTTTTGGCAGTACAT
CAATGGGCGTGGATAGCGGTTTGACTCACGGGGATTTCCAAGTCTCCACCCCATTGAC
GTCAATGGGAGTTTGTTTTGGCACCAAAATCAACGGGACTTTCCAAAATGTCGTAACA
ACTCCGCCCCATTGACGCAAATGGGCGGTAGGCGTGTACGGTGGGAGGTCTATATAA
GCAGAGCTCTCCCTATCAGTGATAGAGATCTCCCTATCAGTGATAGAGATCGTCGACG
AGCTCGTTTAGTGAACCGTCAGATCGCCTGGAGACGCCATCCACGCTGTTTTGACCTC
CATAGAAGACACCGGGACCGATCCAGCCTCCGGACTCTAGCGTTTAAACTTAAGCTTG
GTACCGAGCTCGGATCCACTAGTCCAGTGTGGTGGAATTCTGCAGATATCCAGCACAG
TGGCGGCCGCTCGAGTCTAGAGGGCCCGTTTAAACCCGCTGATCAGCCTCGACTGTG
CCTTCTAGTTGCCAGCCATCTGTTGTTTGCCCCTCCCCCGTGCCTTCCTTGACCCTGG

AAGGTGCCACTCCCACTGTCCTTTCCTAATAAAATGAGGAAATTGCATCGCATTGTCT
GAGTAGGTGTCATTCTATTCTGGGGGGTGGGGTGGGGCAGGACAGCAAGGGGGAGG
ATTGGGAAGACAATAGCAGGCATGCTGGGGATGCGGTGGGCTCTATGGCTTCTGAGG
CGGAAAGAACCAGCTGGGGCTCTAGGGGGTATCCCCACGCGCCCTGTAGCGGCGCAT
TAAGCGCGGCGGGTGTGGTGGTTACGCGCAGCGTGACCGCTACACTTGCCAGCGCCC
TAGCGCCCGCTCCTTTCGCTTTCTTCCCTTCCTTTCTCGCCACGTTCGCCGGCTTTCCC
CGTCAAGCTCTAAATCGGGGGCTCCCTTTAGGGTTCCGATTTAGTGCTTTACGGCACC
TCGACCCCAAAAAACTTGATTAGGGTGATGGTTCACGTACCTAGAAGTTCCTATTCCG
AAGTTCCTATTCTCTAGAAAGTATAGGAACTTCCTTGGCCAAAAAGCCTGAACTCACCG
CGACGTCTGTCGAGAAGTTTCTGATCGAAAAGTTCGACAGCGTCTCCGACCTGATGCA
GCTCTCGGAGGGCGAAGAATCTCGTGCTTTCAGCTTCGATGTAGGAGGGCGTGGATA
TGTCCTGCGGGTAAATAGCTGCGCCGATGGTTTCTACAAAGATCGTTATGTTTATCGG
CACTTTGCATCGGCCGCGCTCCCGATTCCGGAAGTGCTTGACATTGGGGAATTCAGC
GAGAGCCTGACCTATTGCATCTCCCGCCGTGCACAGGGTGTCACGTTGCAAGACCTGC
CTGAAACCGAACTGCCCGCTGTTCTGCAGCCGGTCGCGGAGGCCATGGATGCGATCG
CTGCGGCCGATCTTAGCCAGACGAGCGGGTTCGGCCCATTCGGACCGCAAGGAATCG
GTCAATACACTACATGGCGTGATTTCATATGCGCGATTGCTGATCCCCATGTGTATCA
CTGGCAAACTGTGATGGACGACACCGTCAGTGCGTCCGTCGCGCAGGCTCTCGATGA
GCTGATGCTTTGGGCCGAGGACTGCCCCGAAGTCCGGCACCTCGTGCACGCGGATTT
CGGCTCCAACAATGTCCTGACGGACAATGGCCGCATAACAGCGGTCATTGACTGGAGC
GAGGCGATGTTCGGGGATTCCCAATACGAGGTCGCCAACATCTTCTTCTGGAGGCCG
TGGTTGGCTTGTATGGAGCAGCAGACGCGCTACTTCGAGCGGAGGCATCCGGAGCTT
GCAGGATCGCCGCGGCTCCGGGCGTATATGCTCCGCATTGGTCTTGACCAACTCTATC
AGAGCTTGGTTGACGGCAATTTCGATGATGCAGCTTGGGCGCAGGGTCGATGCGACG
CAATCGTCCGATCCGGAGCCGGGACTGTCGGGCGTACACAAATCGCCCGCAGAAGCG
CGGCCGTCTGGACCGATGGCTGTGTAGAAGTACTCGCCGATAGTGGAAACCGACGCC
CCAGCACTCGTCCGAGGGCAAAGGAATAGCACGTACTACGAGATTTCGATTCCACCGC
CGCCTTCTATGAAAGGTTGGGCTTCGGAATCGTTTTCCGGGACGCCGGCTGGATGAT
CCTCCAGCGCGGGGATCTCATGCTGGAGTTCTTCGCCCACCCCAACTTGTTTATTGCA
GCTTATAATGGTTACAAATAAAGCAATAGCATCACAAATTTCACAAATAAAGCATTTTT
TTCACTGCATTCTAGTTGTGGTTTGTCCAAACTCATCAATGTATCTTATCATGTCTGTA
TACCGTCGACCTCTAGCTAGAGCTTGGCGTAATCATGGTCATAGCTGTTTCCTGTGTG
AAATTGTTATCCGCTCACAATTCCACACAACATACGAGCCGGAAGCATAAAGTGTAAA
GCCTGGGGTGCCTAATGAGTGAGCTAACTCACATTAATTGCGTTGCGCTCACTGCCCG
CTTTCCAGTCGGGAAACCTGTCGTGCCAGCTGCATTAATGAATCGGCCAACGCGCGG
GGAGAGGCGGTTTGCGTATTGGGCGCTCTTCCGCTTCCTCGCTCACTGACTCGCTGC
GCTCGGTCGTTCGGCTGCGGCGAGCGGTATCAGCTCACTCAAAGGCGGTAATACGGT
TATCCACAGAATCAGGGGATAACGCAGGAAAGAACATGTGAGCAAAAGGCCAGCAAAA
GGCCAGGAACCGTAAAAAGGCCGCGTTGCTGGCGTTTTTCCATAGGCTCCGCCCCCCT
GACGAGCATCACAAAAATCGACGCTCAAGTCAGAGGTGGCGAAACCCGACAGGACTAT
AAAGATACCAGGCGTTTCCCCCTGGAAGCTCCCTCGTGCGCTCTCCTGTTCCGACCCT
GCCGCTTACCGGATACCTGTCCGCCTTTCTCCCTTCGGGAAGCGTGGCGCTTTCTCAT
AGCTCACGCTGTAGGTATCTCAGTTCGGTGTAGGTCGTTCGCTCCAAGCTGGGCTGT
GTGCACGAACCCCCCGTTCAGCCCGACCGCTGCGCCTTATCCGGTAACTATCGTCTTG
AGTCCAACCCGGTAAGACACGACTTATCGCCACTGGCAGCAGCCACTGGTAACAGGAT
TAGCAGAGCGAGGTATGTAGGCGGTGCTACAGAGTTCTTGAAGTGGTGGCCTAACTA
CGGCTACACTAGAAGAACAGTATTTGGTATCTGCGCTCTGCTGAAGCCAGTTACCTTC
GGAAAAAGAGTTGGTAGCTCTTGATCCGGCAAACAAACCACCGCTGGTAGCGGTGGT
TTTTTTGTTTGCAAGCAGCAGATTACGCGCAGAAAAAAAGGATCTCAAGAAGATCCTT
TGATCTTTTCTACGGGGTCTGACGCTCAGTGGAACGAAAACTCACGTTAAGGGATTTT
GGTCATGAGATTATCAAAAAGGATCTTCACCTAGATCCTTTTAAATTAAAAATGAAGTT
TTAAATCAATCTAAAGTATATATGAGTAAACTTGGTCTGACAGTTACCAATGCTTAATC

AGTGAGGCACCTATCTCAGCGATCTGTCTATTTCGTTCATCCATAGTTGCCTGACTCC
CCGTCGTGTAGATAACTACGATACGGGAGGGCTTACCATCTGGCCCCAGTGCTGCAAT
GATACCGCGAGACCCACGCTCACCGGCTCCAGATTTATCAGCAATAAACCAGCCAGCC
GGAAGGGCCGAGCGCAGAAGTGGTCCTGCAACTTTATCCGCCTCCATCCAGTCTATTA
ATTGTTGCCGGGAAGCTAGAGTAAGTAGTTCGCCAGTTAATAGTTTGCGCAACGTTGT
TGCCATTGCTACAGGCATCGTGGTGTCACGCTCGTCGTTTGGTATGGCTTCATTCAGC
TCCGGTTCCCAACGATCAAGGCGAGTTACATGATCCCCCATGTTGTGCAAAAAAGCGG
TTAGCTCCTTCGGTCCTCCGATCGTTGTCAGAAGTAAGTTGGCCGCAGTGTTATCACT
CATGGTTATGGCAGCACTGCATAATTCTCTTACTGTCATGCCATCCGTAAGATGCTTT
TCTGTGACTGGTGAGTACTCAACCAAGTCATTCTGAGAATAGTGTATGCGGCGACCGA
GTTGCTCTTGCCCGGCGTCAATACGGGATAATACCGCGCCACATAGCAGAACTTTAAA
AGTGCTCATCATTGGAAAACGTTCTTCGGGGCGAAAACTCTCAAGGATCTTACCGCTG
TTGAGATCCAGTTCGATGTAACCCACTCGTGCACCCAACTGATCTTCAGCATCTTTTAC
TTTCACCAGCGTTTCTGGGTGAGCAAAAACAGGAAGGCAAAATGCCGCAAAAAAGGGA
ATAAGGGCGACACGGAAATGTTGAATACTCATACTCTTCCTTTTTCAATATTATTGAAG
CATTTATCAGGGTTATTGTCTCATGAGCGGATACATATTTGAATGTATTTAGAAAAATA
AACAAATAGGGGTTCCGCGCACATTTCCCCGAAAAGTGCCACCTGACGTC

Figure 6. pOG44 plasmid map.

Figure 7. pCDNA3.1 (+) plasmid map and sequence.

DNA sequence of pcDNA3.1 (+)
CMV enhancer and promoter highlighted in grey. MCS, bGH poly(A) signal, NeoR/KanR and SV40 poly(A) signal highlighted in their colours in the plasmid map.

GACGGATCGGGAGATCTCCCGATCCCCTATGGTGCACTCTCAGTACAATCTGCTCTGA
TGCCGCATAGTTAAGCCAGTATCTGCTCCCTGCTTGTGTGTTGGAGGTCGCTGAGTA
GTGCGCGAGCAAAATTTAAGCTACAACAAGGCAAGGCTTGACCGACAATTGCATGAAG
AATCTGCTTAGGGTTAGGCGTTTTGCGCTGCTTCGCGATGTACGGGCCAGATATACG
CGTTGACATTGATTATTGACTAGTTATTAATAGTAATCAATTACGGGGTCATTAGTTCA
TAGCCCATATATGGAGTTCCGCGTTACATAACTTACGGTAAATGGCCCGCCTGGCTGA
CCGCCCAACGACCCCCGCCCATTGACGTCAATAATGACGTATGTTCCCATAGTAACGC
CAATAGGGACTTTCCATTGACGTCAATGGGTGGAGTATTTACGGTAAACTGCCCACTT
GGCAGTACATCAAGTGTATCATATGCCAAGTACGCCCCCTATTGACGTCAATGACGGT
AAATGGCCCGCCTGGCATTATGCCCAGTACATGACCTTATGGGACTTTCCTACTTGGC
AGTACATCTACGTATTAGTCATCGCTATTACCATGGTGATGCGGTTTTGGCAGTACAT
CAATGGGCGTGGATAGCGGTTTGACTCACGGGGATTTCCAAGTCTCCACCCCATTGAC
GTCAATGGGAGTTTGTTTTGGCACCAAAATCAACGGGACTTTCCAAAATGTCGTAACA
ACTCCGCCCCATTGACGCAAATGGGCGGTAGGCGTGTACGGTGGGAGGTCTATATAA
GCAGAGCTCTCTGGCTAACTAGAGAACCCACTGCTTACTGGCTTATCGAAATTAATAC
GACTCACTATAGGGAGACCCAAGCTGGCTAGTTAAGCTTGGTACCGAGCTCGGATCCA

CTAGTCCAGTGTGGTGGAATTCTGCAGATATCCAGCACAGTGGCGGCCGCTCGAGTC
TAGAGGGCCCTTCGAACAAAAACTCATCTCAGAAGAGGATCTGAATATGCATACCGGT
CATCATCACCATCACCATTGAGTTTAAACCCGCTGATCAGCCTCGACTGTGCCTTCTAG
TTGCCAGCCATCTGTTGTTTGCCCCTCCCCCGTGCCTTCCTTGACCCTGGAAGGTGCC
ACTCCCACTGTCCTTTCCTAATAAAATGAGGAAATTGCATCGCATTGTCTGAGTAGGT
GTCATTCTATTCTGGGGGGTGGGGTGGGGCAGGACAGCAAGGGGGAGGATTGGGAA
GACAATAGCAGGCATGCTGGGGATGCGGTGGGCTCTATGGCTTCTGAGGCGGAAAGA
ACCAGCTGGGGCTCTAGGGGGTATCCCCACGCGCCCTGTAGCGGCGCATTAAGCGCG
GCGGGTGTGGTGGTTACGCGCAGCGTGACCGCTACACTTGCCAGCGCCCTAGCGCCC
GCTCCTTTCGCTTTCTTCCCTTCCTTTCTCGCCACGTTCGCCGGCTTTCCCCGTCAAGC
TCTAAATCGGGGGCTCCCTTTAGGGTTCCGATTTAGTGCTTTACGGCACCTCGACCCC
AAAAAACTTGATTAGGGTGATGGTTCACGTAGTGGGCCATCGCCCTGATAGACGGTTT
TTCGCCCTTTGACGTTGGAGTCCACGTTCTTTAATAGTGGACTCTTGTTCCAAACTGG
AACAACACTCAACCCTATCTCGGTCTATTCTTTTGATTTATAAGGGATTTTGCCGATTT
CGGCCTATTGGTTAAAAAATGAGCTGATTTAACAAAAATTTAACGCGAATTAATTCTGT
GGAATGTGTGTCAGTTAGGGTGTGGAAAGTCCCCAGGCTCCCCAGCAGGCAGAAGTA
TGCAAAGCATGCATCTCAATTAGTCAGCAACCAGGTGTGGAAAGTCCCCAGGCTCCCC
AGCAGGCAGAAGTATGCAAAGCATGCATCTCAATTAGTCAGCAACCATAGTCCCGCCC
CTAACTCCGCCCATCCCGCCCCTAACTCCGCCCAGTTCCGCCCATTCTCCGCCCCATGG
CTGACTAATTTTTTTTATTTATGCAGAGGCCGAGGCCGCCTCTGCCTCTGAGCTATTC
CAGAAGTAGTGAGGAGGCTTTTTTGGAGGCCTAGGCTTTTGCAAAAAGCTCCCGGGA
GCTTGTATATCCATTTTCGGATCTGATCAAGAGACAGGATGAGGATCGTTTCGCATGA
TTGAACAAGATGGATTGCACGCAGGTTCTCCGGCCGCTTGGGTGGAGAGGCTATTCG
GCTATGACTGGGCACAACAGACAATCGGCTGCTCTGATGCCGCCGTGTTCCGGCTGT
CAGCGCAGGGGCGCCCGGTTCTTTTTGTCAAGACCGACCTGTCCGGTGCCCTGAATG
AACTGCAGGACGAGGCAGCGCGGCTATCGTGGCTGGCCACGACGGGCGTTCCTTGCG
CAGCTGTGCTCGACGTTGTCACTGAAGCGGGAAGGGACTGGCTGCTATTGGGCGAAG
TGCCGGGGCAGGATCTCCTGTCATCTCACCTTGCTCCTGCCGAGAAAGTATCCATCAT
GGCTGATGCAATGCGGCGGCTGCATACGCTTGATCCGGCTACCTGCCCATTCGACCAC
CAAGCGAAACATCGCATCGAGCGAGCACGTACTCGGATGGAAGCCGGTCTTGTCGAT
CAGGATGATCTGGACGAAGAGCATCAGGGGCTCGCGCCAGCCGAACTGTTCGCCAGG
CTCAAGGCGCGCATGCCCGACGGCGAGGATCTCGTCGTGACCCATGGCGATGCCTGC
TTGCCGAATATCATGGTGGAAAATGGCCGCTTTTCTGGATTCATCGACTGTGGCCGGC
TGGGTGTGGCGGACCGCTATCAGGACATAGCGTTGGCTACCCGTGATATTGCTGAAG
AGCTTGGCGGCGAATGGGCTGACCGCTTCCTCGTGCTTTACGGTATCGCCGCTCCCG
ATTCGCAGCGCATCGCCTTCTATCGCCTTCTTGACGAGTTCTTCTGAGCGGGACTCTG
GGGTTCGCGAAATGACCGACCAAGCGACGCCCAACCTGCCATCACGAGATTTCGATTC
CACCGCCGCCTTCTATGAAAGGTTGGGCTTCGGAATCGTTTTCCGGGACGCCGGCTG
GATGATCCTCCAGCGCGGGGATCTCATGCTGGAGTTCTTCGCCCACCCCAACTTGTTT
ATTGCAGCTTATAATGGTTACAAATAAAGCAATAGCATCACAAATTTCACAAATAAAGC
ATTTTTTTCACTGCATTCTAGTTGTGGTTTGTCCAAACTCATCAATGTATCTTATCATG
TCTGTATACCGTCGACCTCTAGCTAGAGCTTGGCGTAATCATGGTCATAGCTGTTTCC
TGTGTGAAATTGTTATCCGCTCACAATTCCACACAACATACGAGCCGGAAGCATAAAG
TGTAAAGCCTGGGGTGCCTAATGAGTGAGCTAACTCACATTAATTGCGTTGCGCTCAC
TGCCCGCTTTCCAGTCGGGAAACCTGTCGTGCCAGCTGCATTAATGAATCGGCCAACG
CGCGGGGAGAGGCGGTTTGCGTATTGGGCGCTCTTCCGCTTCCTCGCTCACTGACTC
GCTGCGCTCGGTCGTTCGGCTGCGGCGAGCGGTATCAGCTCACTCAAAGGCGGTAAT
ACGGTTATCCACAGAATCAGGGGATAACGCAGGAAAGAACATGTGAGCAAAAGGCCA
GCAAAAGGCCAGGAACCGTAAAAAGGCCGCGTTGCTGGCGTTTTTCCATAGGCTCCG
CCCCCCTGACGAGCATCACAAAAATCGACGCTCAAGTCAGAGGTGGCGAAACCCGACA
GGACTATAAAGATACCAGGCGTTTCCCCCTGGAAGCTCCCTCGTGCGCTCTCCTGTTC
CGACCCTGCCGCTTACCGGATACCTGTCCGCCTTTCTCCCTTCGGGAAGCGTGGCGCT

TTCTCATAGCTCACGCTGTAGGTATCTCAGTTCGGTGTAGGTCGTTCGCTCCAAGCTG
GGCTGTGTGCACGAACCCCCCGTTCAGCCCGACCGCTGCGCCTTATCCGGTAACTATC
GTCTTGAGTCCAACCCGGTAAGACACGACTTATCGCCACTGGCAGCAGCCACTGGTAA
CAGGATTAGCAGAGCGAGGTATGTAGGCGGTGCTACAGAGTTCTTGAAGTGGTGGCC
TAACTACGGCTACACTAGAAGAACAGTATTTGGTATCTGCGCTCTGCTGAAGCCAGTT
ACCTTCGGAAAAAGAGTTGGTAGCTCTTGATCCGGCAAACAAACCACCGCTGGTAGCG
GTGGTTTTTTTGTTTGCAAGCAGCAGATTACGCGCAGAAAAAAAGGATCTCAAGAAGA
TCCTTTGATCTTTTCTACGGGGTCTGACGCTCAGTGGAACGAAAACTCACGTTAAGGG
ATTTTGGTCATGAGATTATCAAAAAGGATCTTCACCTAGATCCTTTTAAATTAAAAATG
AAGTTTTAAATCAATCTAAAGTATATATGAGTAAACTTGGTCTGACAGTTACCAATGCT
TAATCAGTGAGGCACCTATCTCAGCGATCTGTCTATTTCGTTCATCCATAGTTGCCTG
ACTCCCCGTCGTGTAGATAACTACGATACGGGAGGGCTTACCATCTGGCCCCAGTGCT
GCAATGATACCGCGAGACCCACGCTCACCGGCTCCAGATTTATCAGCAATAAACCAGC
CAGCCGGAAGGGCCGAGCGCAGAAGTGGTCCTGCAACTTTATCCGCCTCCATCCAGT
CTATTAATTGTTGCCGGGAAGCTAGAGTAAGTAGTTCGCCAGTTAATAGTTTGCGCAA
CGTTGTTGCCATTGCTACAGGCATCGTGGTGTCACGCTCGTCGTTTGGTATGGCTTCA
TTCAGCTCCGGTTCCCAACGATCAAGGCGAGTTACATGATCCCCCATGTTGTGCAAAA
AAGCGGTTAGCTCCTTCGGTCCTCCGATCGTTGTCAGAAGTAAGTTGGCCGCAGTGTT
ATCACTCATGGTTATGGCAGCACTGCATAATTCTCTTACTGTCATGCCATCCGTAAGAT
GCTTTTCTGTGACTGGTGAGTACTCAACCAAGTCATTCTGAGAATAGTGTATGCGGCG
ACCGAGTTGCTCTTGCCCGGCGTCAATACGGGATAATACCGCGCCACATAGCAGAACT
TTAAAAGTGCTCATCATTGGAAAACGTTCTTCGGGGCGAAAACTCTCAAGGATCTTAC
CGCTGTTGAGATCCAGTTCGATGTAACCCACTCGTGCACCCAACTGATCTTCAGCATC
TTTTACTTTCACCAGCGTTTCTGGGTGAGCAAAAACAGGAAGGCAAAATGCCGCAAAA
AAGGGAATAAGGGCGACACGGAAATGTTGAATACTCATACTCTTCCTTTTTCAATATT
ATTGAAGCATTTATCAGGGTTATTGTCTCATGAGCGGATACATATTTGAATGTATTTA
GAAAAATAAACAAATAGGGGTTCCGCGCACATTTCCCCGAAAAGTGCCACCTGACGTC

Figure 8. pcDNA3.1-hygr plasmid map and sequence.

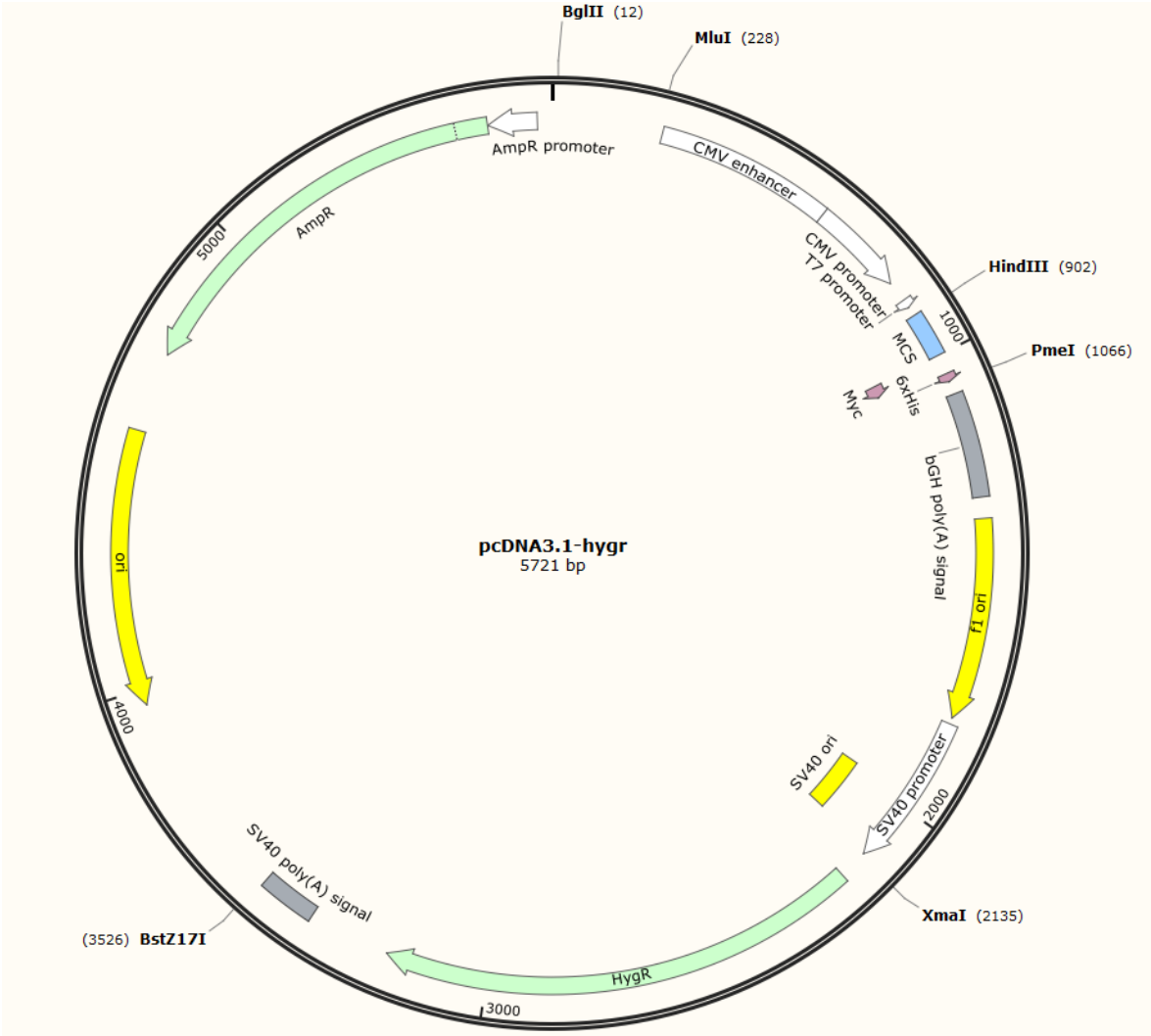

DNA sequence of pcDNA3.1-hygr
CMV enhancer and promoter highlighted in grey. MCS, bGH poly(A) signal, HygR and SV40 poly(A) signal highlighted in their colours in the plasmid map.

GACGGATCGGGAGATCTCCCGATCCCCTATGGTGCACTCTCAGTACAATCTGCTCTGA
TGCCGCATAGTTAAGCCAGTATCTGCTCCCTGCTTGTGTGTTGGAGGTCGCTGAGTA
GTGCGCGAGCAAAATTTAAGCTACAACAAGGCAAGGCTTGACCGACAATTGCATGAAG
AATCTGCTTAGGGTTAGGCGTTTTGCGCTGCTTCGCGATGTACGGGCCAGATATACG
CGTTGACATTGATTATTGACTAGTTATTAATAGTAATCAATTACGGGGTCATTAGTTCA
TAGCCCATATATGGAGTTCCGCGTTACATAACTTACGGTAAATGGCCCGCCTGGCTGA
CCGCCCAACGACCCCCGCCCATTGACGTCAATAATGACGTATGTTCCCATAGTAACGC
CAATAGGGACTTTCCATTGACGTCAATGGGTGGAGTATTTACGGTAAACTGCCCACTT
GGCAGTACATCAAGTGTATCATATGCCAAGTACGCCCCCTATTGACGTCAATGACGGT
AAATGGCCCGCCTGGCATTATGCCCAGTACATGACCTTATGGGACTTTCCTACTTGGC
AGTACATCTACGTATTAGTCATCGCTATTACCATGGTGATGCGGTTTTGGCAGTACAT
CAATGGGCGTGGATAGCGGTTTGACTCACGGGGATTTCCAAGTCTCCACCCCATTGAC
GTCAATGGGAGTTTGTTTTGGCACCAAAATCAACGGGACTTTCCAAAATGTCGTAACA
ACTCCGCCCCATTGACGCAAATGGGCGGTAGGCGTGTACGGTGGGAGGTCTATATAA
GCAGAGCTCTCTGGCTAACTAGAGAACCCACTGCTTACTGGCTTATCGAAATTAATAC
GACTCACTATAGGGAGACCCAAGCTGGCTAGTTAAGCTTGGTACCGAGCTCGGATCCA
CTAGTCCAGTGTGGTGGAATTCTGCAGATATCCAGCACAGTGGCGGCCGCTCGAGTC
TAGAGGGCCCTTCGAACAAAAACTCATCTCAGAAGAGGATCTGAATATGCATACCGGT

CATCATCACCATCACCATTGAGTTTAAACCCGCTGATCAGCCTCGACTGTGCCTTCTAG
TTGCCAGCCATCTGTTGTTTGCCCCTCCCCCGTGCCTTCCTTGACCCTGGAAGGTGCC
ACTCCCACTGTCCTTTCCTAATAAAATGAGGAAATTGCATCGCATTGTCTGAGTAGGT
GTCATTCTATTCTGGGGGGTGGGGTGGGGCAGGACAGCAAGGGGGAGGATTGGGAA
GACAATAGCAGGCATGCTGGGGATGCGGTGGGCTCTATGGCTTCTGAGGCGGAAAGA
ACCAGCTGGGGCTCTAGGGGGTATCCCCACGCGCCCTGTAGCGGCGCATTAAGCGCG
GCGGGTGTGGTGGTTACGCGCAGCGTGACCGCTACACTTGCCAGCGCCCTAGCGCCC
GCTCCTTTCGCTTTCTTCCCTTCCTTTCTCGCCACGTTCGCCGGCTTTCCCCGTCAAGC
TCTAAATCGGGGGCTCCCTTTAGGGTTCCGATTTAGTGCTTTACGGCACCTCGACCCC
AAAAAACTTGATTAGGGTGATGGTTCACGTAGTGGGCCATCGCCCTGATAGACGGTTT
TTCGCCCTTTGACGTTGGAGTCCACGTTCTTTAATAGTGGACTCTTGTTCCAAACTGG
AACAACACTCAACCCTATCTCGGTCTATTCTTTTGATTTATAAGGGATTTTGCCGATTT
CGGCCTATTGGTTAAAAAATGAGCTGATTTAACAAAAATTTAACGCGAATTAATTCTGT
GGAATGTGTGTCAGTTAGGGTGTGGAAAGTCCCCAGGCTCCCCAGCAGGCAGAAGTA
TGCAAAGCATGCATCTCAATTAGTCAGCAACCAGGTGTGGAAAGTCCCCAGGCTCCCC
AGCAGGCAGAAGTATGCAAAGCATGCATCTCAATTAGTCAGCAACCATAGTCCCGCCC
CTAACTCCGCCCATCCCGCCCCTAACTCCGCCCAGTTCCGCCCATTCTCCGCCCCATGG
CTGACTAATTTTTTTTATTTATGCAGAGGCCGAGGCCGCCTCTGCCTCTGAGCTATTC
CAGAAGTAGTGAGGAGGCTTTTTTGGAGGCCTAGGCTTTTGCAAAAAGCTCCCGGGA
GCTTGTATATCCATTTTCGGATCTGATCAAGAGACAGGATGAGGATCGTTTATGAAAA
AGCCTGAACTCACCGCGACGTCTGTCGAGAAGTTTCTGATCGAAAAGTTCGACAGCGT
CTCCGACCTGATGCAGCTCTCGGAGGGCGAAGAATCTCGTGCTTTCAGCTTCGATGTA
GGAGGGCGTGGATATGTCCTGCGGGTAAATAGCTGCGCCGATGGTTTCTACAAAGAT
CGTTATGTTTATCGGCACTTTGCATCGGCCGCGCTCCCGATTCCGGAAGTGCTTGACA
TTGGGGAATTCAGCGAGAGCCTGACCTATTGCATCTCCCGCCGTGCACAGGGTGTCA
CGTTGCAAGACCTGCCTGAAACCGAACTGCCCGCTGTTCTGCAGCCGGTCGCGGAGG
CCATGGATGCGATTGCTGCGGCCGATCTTAGCCAGACGAGCGGGTTCGGCCCATTCG
GACCGCAAGGAATCGGTCAATACACTACATGGCGTGATTTCATATGCGCGATTGCTGA
TCCCCATGTGTATCACTGGCAAACTGTGATGGACGACACCGTCAGTGCGTCCGTCGCG
CAGGCTCTCGATGAGCTGATGCTTTGGGCCGAGGACTGCCCCGAAGTCCGGCACCTC
GTGCACGCGGATTTCGGCTCCAACAATGTCCTGACGGACAATGGCCGCATAACAGCG
GTCATTGACTGGAGCGAGGCGATGTTCGGGGATTCCCAATACGAGGTCGCCAACATC
TTCTTCTGGAGGCCGTGGTTGGCTTGTATGGAGCAGCAGACGCGCTACTTCGAGCGG
AGGCATCCGGAGCTTGCAGGATCGCCGCGGCTCCGGGCGTATATGCTCCGCATTGGT
CTTGACCAACTCTATCAGAGCTTGGTTGACGGCAATTTCGATGATGCAGCTTGGGCGC
AGGGTCGATGCGACGCAATCGTCCGATCCGGAGCCGGGACTGTCGGGCGTACACAAA
TCGCCCGCAGAAGCGCGGCCGTCTGGACCGATGGCTGTGTAGAAGTACTCGCCGATA
GTGGAAACCGACGCCCCAGCACTCGTCCGAGGGCAAAGGAATAGGCGGGACTCTGGG
GTTCGCGAAATGACCGACCAAGCGACGCCCAACCTGCCATCACGAGATTTCGATTCCA
CCGCCGCCTTCTATGAAAGGTTGGGCTTCGGAATCGTTTTCCGGGACGCCGGCTGGA
TGATCCTCCAGCGCGGGGATCTCATGCTGGAGTTCTTCGCCCACCCCAACTTGTTTAT
TGCAGCTTATAATGGTTACAAATAAAGCAATAGCATCACAAATTTCACAAATAAAGCAT
TTTTTTCACTGCATTCTAGTTGTGGTTTGTCCAAACTCATCAATGTATCTTATCATGTC
TGTATACCGTCGACCTCTAGCTAGAGCTTGGCGTAATCATGGTCATAGCTGTTTCCTG
TGTGAAATTGTTATCCGCTCACAATTCCACACAACATACGAGCCGGAAGCATAAAGTG
TAAAGCCTGGGGTGCCTAATGAGTGAGCTAACTCACATTAATTGCGTTGCGCTCACTG
CCCGCTTTCCAGTCGGGAAACCTGTCGTGCCAGCTGCATTAATGAATCGGCCAACGCG
CGGGGAGAGGCGGTTTGCGTATTGGGCGCTCTTCCGCTTCCTCGCTCACTGACTCGC
TGCGCTCGGTCGTTCGGCTGCGGCGAGCGGTATCAGCTCACTCAAAGGCGGTAATAC
GGTTATCCACAGAATCAGGGGATAACGCAGGAAAGAACATGTGAGCAAAAGGCCAGC
AAAAGGCCAGGAACCGTAAAAAGGCCGCGTTGCTGGCGTTTTTCCATAGGCTCCGCCC
CCCTGACGAGCATCACAAAAATCGACGCTCAAGTCAGAGGTGGCGAAACCCGACAGGA

CTATAAAGATACCAGGCGTTTCCCCCTGGAAGCTCCCTCGTGCGCTCTCCTGTTCCGA
CCCTGCCGCTTACCGGATACCTGTCCGCCTTTCTCCCTTCGGGAAGCGTGGCGCTTTC
TCATAGCTCACGCTGTAGGTATCTCAGTTCGGTGTAGGTCGTTCGCTCCAAGCTGGGC
TGTGTGCACGAACCCCCCGTTCAGCCCGACCGCTGCGCCTTATCCGGTAACTATCGTC
TTGAGTCCAACCCGGTAAGACACGACTTATCGCCACTGGCAGCAGCCACTGGTAACAG
GATTAGCAGAGCGAGGTATGTAGGCGGTGCTACAGAGTTCTTGAAGTGGTGGCCTAA
CTACGGCTACACTAGAAGAACAGTATTTGGTATCTGCGCTCTGCTGAAGCCAGTTACC
TTCGGAAAAAGAGTTGGTAGCTCTTGATCCGGCAAACAAACCACCGCTGGTAGCGGT
GGTTTTTTTGTTTGCAAGCAGCAGATTACGCGCAGAAAAAAAGGATCTCAAGAAGATC
CTTTGATCTTTTCTACGGGGTCTGACGCTCAGTGGAACGAAAACTCACGTTAAGGGAT
TTTGGTCATGAGATTATCAAAAAGGATCTTCACCTAGATCCTTTTAAATTAAAAATGAA
GTTTTAAATCAATCTAAAGTATATATGAGTAAACTTGGTCTGACAGTTACCAATGCTTA
ATCAGTGAGGCACCTATCTCAGCGATCTGTCTATTTCGTTCATCCATAGTTGCCTGAC
TCCCCGTCGTGTAGATAACTACGATACGGGAGGGCTTACCATCTGGCCCCAGTGCTGC
AATGATACCGCGAGACCCACGCTCACCGGCTCCAGATTTATCAGCAATAAACCAGCCA
GCCGGAAGGGCCGAGCGCAGAAGTGGTCCTGCAACTTTATCCGCCTCCATCCAGTCTA
TTAATTGTTGCCGGGAAGCTAGAGTAAGTAGTTCGCCAGTTAATAGTTTGCGCAACGT
TGTTGCCATTGCTACAGGCATCGTGGTGTCACGCTCGTCGTTTGGTATGGCTTCATTC
AGCTCCGGTTCCCAACGATCAAGGCGAGTTACATGATCCCCCATGTTGTGCAAAAAAG
CGGTTAGCTCCTTCGGTCCTCCGATCGTTGTCAGAAGTAAGTTGGCCGCAGTGTTATC
ACTCATGGTTATGGCAGCACTGCATAATTCTCTTACTGTCATGCCATCCGTAAGATGC
TTTTCTGTGACTGGTGAGTACTCAACCAAGTCATTCTGAGAATAGTGTATGCGGCGAC
CGAGTTGCTCTTGCCCGGCGTCAATACGGGATAATACCGCGCCACATAGCAGAACTTT
AAAAGTGCTCATCATTGGAAAACGTTCTTCGGGGCGAAAACTCTCAAGGATCTTACCG
CTGTTGAGATCCAGTTCGATGTAACCCACTCGTGCACCCAACTGATCTTCAGCATCTTT
TACTTTCACCAGCGTTTCTGGGTGAGCAAAAACAGGAAGGCAAAATGCCGCAAAAAAG
GGAATAAGGGCGACACGGAAATGTTGAATACTCATACTCTTCCTTTTTCAATATTATTG
AAGCATTTATCAGGGTTATTGTCTCATGAGCGGATACATATTTGAATGTATTTAGAAA
AATAAACAAATAGGGGTTCCGCGCACATTTCCCCGAAAAGTGCCACCTGACGTC

Figure 9. pCD8-CAR plasmid map and sequence.

DNA sequence of pCD8-CAR

EF1-α promoter highlighted in grey. HL-R, HR-L, CD8 SP, CD8 HS, CD8 TM, 4-1BB ED, CD3ζ ED and bGH poly(A) signal highlighted in their colours in the plasmid map.

CTAGCATAAACACACAGTATGTTTTTAAGAGAAGGGGAGGCGGGACGCAAGGGAGAC
ATCCGTCGGAGAAGGCCATCCTAAGAAACGAGAGATGGCACAGGCCCCAGAAGGAGA
AGGAAAAGGGAACCCAGCGAGTGAAGACGGCATGGGGTTGGGTGAGGGAGGAGAGA
TGCCCGGAGAGGACCCAGACACGGGGAGGATCCGCTCAGAGGACATCACGTGGTGCA
GCGCCGAGAAGGAAGTGCTCCGGAAAGAGCATCCTTGGGCAGCAACACAGCAGAGAG
CAAGGGGAAGAGGGAGTGGAGGAAGACGGAACCTGAAGGAGGCGGCAGGGAAGGAT
CTGGGCCAGCCGTAGAGGTGACCCAGGCCACAAGCTGCAGACAGAAAGCGGCACAGG
CCCAGGGGAGAGAATGCAGGTCAGAGAAAGCAGGGAAGGCAATGCAAGGAGTTTTTG
AATATTACAAATCAGTAACGTTTACGCGTTTTTTTTAGCGCGTGCGCCAATTCTGCAGA
CATGAATCAACCTCTGGATTCCGCCTCCCCGTCACCACCCCCCCCAACCCGCCCCGACC
GGAGCTGAGAGTAATTCATACAAAAGGACTCGCCCCTGCCTTGGGGAATCCCAGGGA
CCGTCGTTAAACTCCCACTAACGTAGAACCCAGAGATCGCTGCGTTCCCGCCCCCTCA
CCCGCCCGCTCTCGTCATCACTGAGGTGGAGAAGAGCATGCGTGAGGCTCCGGTGCC
CGTCAGTGGGCAGAGCGCACATCGCCCACAGTCCCCGAGAAGTTGGGGGGAGGGGT
CGGCAATTGAACCGGTGCCTAGAGAAGGTGGCGCGGGGTAAACTGGGAAAGTGATGT
CGTGTACTGGCTCCGCCTTTTTCCCGAGGGTGGGGGAGAACCGTATATAAGTGCAGT
AGTCGCCGTGAACGTTCCTCTGGCTAACTAGAGAACCCACTGTAGTGAACCGTCAGAT

CGCCTGGAGACGCCATCCACGGCCGCCACCATGGCCCTGCCTGTAACCGCGTTGTTG
TTGCCTCTTGCACTTCTGCTCCATGCGGCGCGCCCGACAACAACGCCGGCGCCTAGAC
CGCCGACACCAGCTCCAACGATAGCATCACAGCCTTTGTCTTTGCGACCGGAGGCGTG
TAGACCAGCTGCGGGTGGCGCGGTTCATACCAGGGGTTTGGATTTTGCGTGCGATAT
TTACATATGGGCGCCGCTGGCAGGTACGTGTGGGGTGCTTCTGTTGAGCCTCGTCAT
AACTCTCTATTGCAAGCGGGGACGGAAAAAACTTTTGTATATATTTAAACAACCCTTTA
TGCGGCCTGTCCAAACGACGCAGGAGGAAGACGGGTGCTCTTGTAGGTTTCCCGAAG
AAGAGGAAGGTGGTTGTGAGCTGAGAGTGAAGTTCTCAAGATCAGCGGACGCTCCCG
CGTACCAGCAGGGTCAAAATCAGTTGTACAATGAACTTAATCTGGGAAGGCGAGAAGA
ATACGATGTACTTGATAAGAGGAGGGGGAGGGATCCAGAAATGGGCGGGAAGCCGC
GCCGAAAGAATCCACAGGAGGGGCTGTATAATGAACTCCAAAAGGATAAAATGGCTGA
GGCTTACTCAGAGATTGGCATGAAGGGTGAGCGGAGGAGAGGAAAGGGTCACGACG
GCTTGTATCAGGGCCTCTCTACTGCGACGAAGGATACGTATGACGCGCTCCACATGCA
AGCCCTCCCGCCACGATAAGTTTAAACCCGCTGATCAGCCTCGACTGTGCCTTCTAGT
TGCCAGCCATCTGTTGTTTGCCCCTCCCCCGTGCCTTCCTTGACCCTGGAAGGTGCCA
CTCCCACTGTCCTTTCCTAATAAAATGAGGAAATTGCATCGCATTGTCTGAGTAGGTG
TCATTCTATTCTGGGGGGTGGGGTGGGGCAGGACAGCAAGGGGGAGGATTGGGAAG
ACAATAGCAGGCATGCTGGGGATGCGGTGGGCTCTATGGCTTCTGAGGCGGAAAGAA
CCAGCTGGGGCTCTAGGGGGTATCCCCACGCGCCCTGTAGCGGCGCATTAAGCGCGG
CGGGTGTGGTGGTTACGCGCAGCGTGACCGCTACACTTGCCAGCGCCCTAGCGCCCG
CTCCTTTCGCTTTCTTCCCTTCCTTTCTCGCCACGTTCGCCGGCTTTCCCCGTCAAGCT
CTAAATCGGGGGCTCCCTTTAGGGTTCCGATTTAGTGCTTTACGGCACCTCGACCCCA
AAAAACTTGATTAGGGTGATGGTTCACGTAGTGGGCCATCGCCCTGATAGACGGTTTT
TCGCCCTTTGACGTTGGAGTCCACGTTCTTTAATAGTGGACTCTTGTTCCAAACTGGA
ACAACACTCAACCCTATCTCGGTCTATTCTTTTGATTTATAAGGGATTTTGCCGATTTC
GGCCTATTGGTTAAAAAATGAGCTGATTTAACAAAAATTTAACGCGAATTAATTCTGTG
GAATGTGTGTCAGTTAGGGTGTGGAAAGTCCCCAGGCTCCCCAGCAGGCAGAAGTAT
GCAAAGCATGCATCTCAATTAGTCAGCAACCAGGTGTGGAAAGTCCCCAGGCTCCCCA
GCAGGCAGAAGTATGCAAAGCATGCATCTCAATTAGTCAGCAACCATAGTCCCGCCCC
TAACTCCGCCCATCCCGCCCCTAACTCCGCCCAGTTCCGCCCATTCTCCGCCCCATGGC
TGACTAATTTTTTTTATTTATGCAGAGGCCGAGGCCGCCTCTGCCTCTGAGCTATTCC
AGAAGTAGTGAGGAGGCTTTTTTGGAGGCCTAGGCTTTTGCAAAAAGCTCCCGGGAG
CTTGTATATCCATTTTCGGATCTGATCAAGAGACAGGATGAGGATCGTTTATGAAAAA
GCCTGAACTCACCGCGACGTCTGTCGAGAAGTTTCTGATCGAAAAGTTCGACAGCGTC
TCCGACCTGATGCAGCTCTCGGAGGGCGAAGAATCTCGTGCTTTCAGCTTCGATGTAG
GAGGGCGTGGATATGTCCTGCGGGTAAATAGCTGCGCCGATGGTTTCTACAAAGATC
GTTATGTTTATCGGCACTTTGCATCGGCCGCGCTCCCGATTCCGGAAGTGCTTGACAT
TGGGGAATTCAGCGAGAGCCTGACCTATTGCATCTCCCGCCGTGCACAGGGTGTCAC
GTTGCAAGACCTGCCTGAAACCGAACTGCCCGCTGTTCTGCAGCCGGTCGCGGAGGC
CATGGATGCGATTGCTGCGGCCGATCTTAGCCAGACGAGCGGGTTCGGCCCATTCGG
ACCGCAAGGAATCGGTCAATACACTACATGGCGTGATTTCATATGCGCGATTGCTGAT
CCCCATGTGTATCACTGGCAAACTGTGATGGACGACACCGTCAGTGCGTCCGTCGCGC
AGGCTCTCGATGAGCTGATGCTTTGGGCCGAGGACTGCCCCGAAGTCCGGCACCTCG
TGCACGCGGATTTCGGCTCCAACAATGTCCTGACGGACAATGGCCGCATAACAGCGGT
CATTGACTGGAGCGAGGCGATGTTCGGGGATTCCCAATACGAGGTCGCCAACATCTT
CTTCTGGAGGCCGTGGTTGGCTTGTATGGAGCAGCAGACGCGCTACTTCGAGCGGAG
GCATCCGGAGCTTGCAGGATCGCCGCGGCTCCGGGCGTATATGCTCCGCATTGGTCT
TGACCAACTCTATCAGAGCTTGGTTGACGGCAATTTCGATGATGCAGCTTGGGCGCAG
GGTCGATGCGACGCAATCGTCCGATCCGGAGCCGGGACTGTCGGGCGTACACAAATC
GCCCGCAGAAGCGCGGCCGTCTGGACCGATGGCTGTGTAGAAGTACTCGCCGATAGT
GGAAACCGACGCCCCAGCACTCGTCCGAGGGCAAAGGAATAGGCGGGACTCTGGGGT
TCGCGAAATGACCGACCAAGCGACGCCCAACCTGCCATCACGAGATTTCGATTCCACC

GCCGCCTTCTATGAAAGGTTGGGCTTCGGAATCGTTTTCCGGGACGCCGGCTGGATG
ATCCTCCAGCGCGGGGATCTCATGCTGGAGTTCTTCGCCCACCCCAACTTGTTTATTG
CAGCTTATAATGGTTACAAATAAAGCAATAGCATCACAAATTTCACAAATAAAGCATTT
TTTTCACTGCATTCTAGTTGTGGTTTGTCCAAACTCATCAATGTATCTTATCATGTCTG
TATACCGTCGACCTCTAGCTAGAGCTTGGCGTAATCATGGTCATAGCTGTTTCCTGTG
TGAAATTGTTATCCGCTCACAATTCCACACAACATACGAGCCGGAAGCATAAAGTGTAA
AGCCTGGGGTGCCTAATGAGTGAGCTAACTCACATTAATTGCGTTGCGCTCACTGCCC
GCTTTCCAGTCGGGAAACCTGTCGTGCCAGCTGCATTAATGAATCGGCCAACGCGCG
GGGAGAGGCGGTTTGCGTATTGGGCGCTCTTCCGCTTCCTCGCTCACTGACTCGCTG
CGCTCGGTCGTTCGGCTGCGGCGAGCGGTATCAGCTCACTCAAAGGCGGTAATACGG
TTATCCACAGAATCAGGGGATAACGCAGGAAAGAACATGTGAGCAAAAGGCCAGCAAA
AGGCCAGGAACCGTAAAAAGGCCGCGTTGCTGGCGTTTTTCCATAGGCTCCGCCCCCC
TGACGAGCATCACAAAAATCGACGCTCAAGTCAGAGGTGGCGAAACCCGACAGGACTA
TAAAGATACCAGGCGTTTCCCCCTGGAAGCTCCCTCGTGCGCTCTCCTGTTCCGACCC
TGCCGCTTACCGGATACCTGTCCGCCTTTCTCCCTTCGGGAAGCGTGGCGCTTTCTCA
TAGCTCACGCTGTAGGTATCTCAGTTCGGTGTAGGTCGTTCGCTCCAAGCTGGGCTG
TGTGCACGAACCCCCCGTTCAGCCCGACCGCTGCGCCTTATCCGGTAACTATCGTCTT
GAGTCCAACCCGGTAAGACACGACTTATCGCCACTGGCAGCAGCCACTGGTAACAGGA
TTAGCAGAGCGAGGTATGTAGGCGGTGCTACAGAGTTCTTGAAGTGGTGGCCTAACT
ACGGCTACACTAGAAGAACAGTATTTGGTATCTGCGCTCTGCTGAAGCCAGTTACCTT
CGGAAAAAGAGTTGGTAGCTCTTGATCCGGCAAACAAACCACCGCTGGTAGCGGTGG
TTTTTTTGTTTGCAAGCAGCAGATTACGCGCAGAAAAAAAGGATCTCAAGAAGATCCT
TTGATCTTTTCTACGGGGTCTGACGCTCAGTGGAACGAAAACTCACGTTAAGGGATTT
TGGTCATGAGATTATCAAAAAGGATCTTCACCTAGATCCTTTTAAATTAAAAATGAAGT
TTTAAATCAATCTAAAGTATATATGAGTAAACTTGGTCTGACAGTTACCAATGCTTAAT
CAGTGAGGCACCTATCTCAGCGATCTGTCTATTTCGTTCATCCATAGTTGCCTGACTC
CCCGTCGTGTAGATAACTACGATACGGGAGGGCTTACCATCTGGCCCCAGTGCTGCAA
TGATACCGCGAGACCCACGCTCACCGGCTCCAGATTTATCAGCAATAAACCAGCCAGC
CGGAAGGGCCGAGCGCAGAAGTGGTCCTGCAACTTTATCCGCCTCCATCCAGTCTATT
AATTGTTGCCGGGAAGCTAGAGTAAGTAGTTCGCCAGTTAATAGTTTGCGCAACGTTG
TTGCCATTGCTACAGGCATCGTGGTGTCACGCTCGTCGTTTGGTATGGCTTCATTCAG
CTCCGGTTCCCAACGATCAAGGCGAGTTACATGATCCCCCATGTTGTGCAAAAAAGCG
GTTAGCTCCTTCGGTCCTCCGATCGTTGTCAGAAGTAAGTTGGCCGCAGTGTTATCAC
TCATGGTTATGGCAGCACTGCATAATTCTCTTACTGTCATGCCATCCGTAAGATGCTT
TTCTGTGACTGGTGAGTACTCAACCAAGTCATTCTGAGAATAGTGTATGCGGCGACCG
AGTTGCTCTTGCCCGGCGTCAATACGGGATAATACCGCGCCACATAGCAGAACTTTAA
AAGTGCTCATCATTGGAAAACGTTCTTCGGGGCGAAAACTCTCAAGGATCTTACCGCT
GTTGAGATCCAGTTCGATGTAACCCACTCGTGCACCCAACTGATCTTCAGCATCTTTTA
CTTTCACCAGCGTTTCTGGGTGAGCAAAAACAGGAAGGCAAAATGCCGCAAAAAAGGG
AATAAGGGCGACACGGAAATGTTGAATACTCATACTCTTCCTTTTTCAATATTATTGAA
GCATTTATCAGGGTTATTGTCTCATGAGCGGATACATATTTGAATGTATTTAGAAAAA
TAAACAAATAGGGGTTCCGCGCACATTTCCCCGAAAAGTGCCACCTGACGTCGACGGA
TCGGGAGATCTCCTGCTGGGATGACGAGCGTAAGCCACCATGCCCAGCTGGGTTTTA
TTTATTTTGGTTTTTTTCCTGACCCCTTAACTAGAAATAAGCTCCACGAGAGCGGGATC
TTTTGTCTTCTGTGCACTACTTGTCCTCGGTTCTTAGAACAGAACCTGAGAGAACCTG
ATCGCAAATATTTTTGGAATGAATGAATGAATGGGTTCACCAGGGCACCATGGGAAAC
TGAGTCCGCAACCTAGAAGCCATGAAAGACAGTCCACTTCCAAGCTTCCCTGGGTGAC
CTCGCAGGGCATGCTGGGAAATGAAATTTGCGGTGAAAAGGTCAGGACCACGATCCT
AGGGCACGCTGGGAAATGTAGCCCACAGGGCCACACCCCTAAAAGCACAGTGGGGTG
CAAGGCACCTCAACAACTAGCAAAGGCAGCCCCG

Figure 10. pIgG4-CAR plasmid map and sequence.

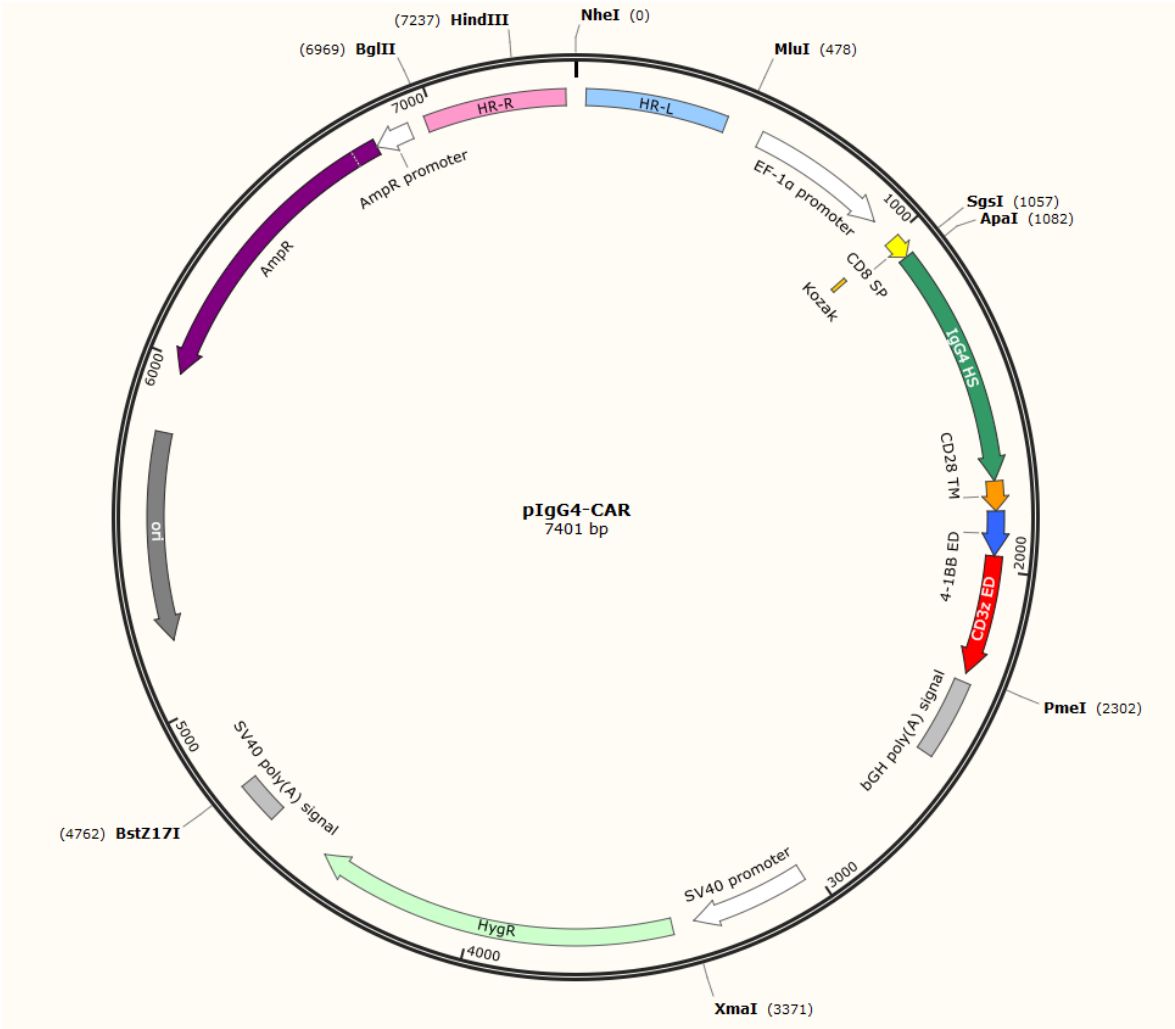

DNA sequence of pIgG4-CAR

EF1-α promoter highlighted in grey. HL-R, HR-L, CD8 SP, IgG4 HS, CD28 TM, 4-1BB ED, CD3ζ ED and bGH poly(A) signal highlighted in their colours in the plasmid map.

CTAGCATAAACACACAGTATGTTTTTAAGAGAAGGGGAGGCGGGACGCAAGGGAGAC
ATCCGTCGGAGAAGGCCATCCTAAGAAACGAGAGATGGCACAGGCCCCAGAAGGAGA
AGGAAAAGGGAACCCAGCGAGTGAAGACGGCATGGGGTTGGGTGAGGGAGGAGAGA
TGCCCGGAGAGGACCCAGACACGGGGAGGATCCGCTCAGAGGACATCACGTGGTGCA
GCGCCGAGAAGGAAGTGCTCCGGAAAGAGCATCCTTGGGCAGCAACACAGCAGAGAG
CAAGGGGAAGAGGGAGTGGAGGAAGACGGAACCTGAAGGAGGCGGCAGGGAAGGAT
CTGGGCCAGCCGTAGAGGTGACCCAGGCCACAAGCTGCAGACAGAAAGCGGCACAGG
CCCAGGGGAGAGAATGCAGGTCAGAGAAAGCAGGGAAGGCAATGCAAGGAGTTTTTG
AATATTACAAATCAGTAACGTTTACGCGTTTTTTTTAGCGCGTGCGCCAATTCTGCAGA
CATGAATCAACCTCTGGATTCCGCCTCCCCGTCACCACCCCCCCCAACCCGCCCCGACC
GGAGCTGAGAGTAATTCATACAAAAGGACTCGCCCCTGCCTTGGGGAATCCCAGGGA
CCGTCGTTAAACTCCCACTAACGTAGAACCCAGAGATCGCTGCGTTCCCGCCCCCTCA
CCCGCCCGCTCTCGTCATCACTGAGGTGGAGAAGAGCATGCGTGAGGCTCCGGTGCC
CGTCAGTGGGCAGAGCGCACATCGCCCACAGTCCCCGAGAAGTTGGGGGGAGGGGT
CGGCAATTGAACCGGTGCCTAGAGAAGGTGGCGCGGGGTAAACTGGGAAAGTGATGT
CGTGTACTGGCTCCGCCTTTTTCCCGAGGGTGGGGGAGAACCGTATATAAGTGCAGT
AGTCGCCGTGAACGTTCCTCTGGCTAACTAGAGAACCCACTGTAGTGAACCGTCAGAT
CGCCTGGAGACGCCATCCACGGCCGCCACCATGGCCCTGCCTGTAACCGCGTTGTTG

TTGCCTCTTGCACTTCTGCTCCATGCGGCGCGCCCGGAAAGTAAGTACGGGCCCCCGT
GTCCGCCCTGTCCAGCGCCACCAGTAGCTGGCCCGTCTGTATTCCTCTTTCCCCCCAA
ACCTAAGGATACACTTATGATAAGTCGCACCCCCGAGGTAACTTGCGTAGTGGTTGAC
GTGAGCCAAGAAGACCCGGAAGTTCAATTTAACTGGTATGTGGACGGTGTTGAAGTT
CATAATGCGAAAACGAAACCCAGAGAAGAACAATTTCAGTCCACCTATAGGGTCGTGT
CCGTTCTTACCGTGCTTCATCAGGACTGGTTGAATGGGAAGGAATATAAGTGCAAGGT
GAGTAACAAAGGCTTGCCCTCTAGCATTGAAAAGACGATTTCTAAGGCCAAAGGTCAA
CCGAGGGAACCGCAGGTGTACACCCTCCCTCCAAGCCAAGAAGAGATGACCAAAAATC
AGGTGTCTTTGACATGTTTGGTTAAGGGCTTTTATCCGAGCGACATTGCGGTAGAGT
GGGAATCTAACGGTCAACCCGAAAACAATTACAAGACCACACCGCCAGTACTCGATTC
TGACGGGGCTTTTTTTTTGTATTCACGACTCACAGTGGACAAAAGCAGATGGCAGGAA
GGTAACGTGTTCTCATGCAGCGTTATGCACGAAGCACTGCACAACCACTACACACAAA
AGTCCCTTTCTTTGAGTTTGGGCAAAATGTTCTGGGTTCTTGTAGTAGTGGGTGGCG
TATTGGCATGCTACTCTCTCCTTGTGACGGTAGCTTTCATAATCTTTTGGGTGAAACG
GGGAAGAAAGAAGCTGCTGTACATATTTAAGCAGCCCTTCATGCGGCCGGTTCAGACA
ACGCAGGAAGAGGACGGTTGTAGCTGCCGGTTTCCTGAAGAGGAAGAAGGGGGGTG
CGAACTGAGGGTCAAGTTTTCTCGCAGCGCCGACGCCCCTGCCTATCAACAGGGACAA
AATCAACTGTACAACGAATTGAATTTGGGTCGCAGAGAAGAGTACGACGTGTTGGATA
AACGGCGGGGCCGAGACCCGGAGATGGGAGGCAAGCCTAGGCGAAAAAATCCGCAG
GAGGGTTTGTATAATGAACTCCAGAAGGATAAGATGGCTGAGGCCTATTCCGAGATT
GGAATGAAGGGAGAGCGCAGGCGGGGAAAAGGCCATGATGGACTGTATCAGGGCTT
GTCAACAGCTACGAAAGACACTTACGATGCCCTGCACATGCAGGCCCTCCCCCCGCGG
TAAGTTTAAACCCGCTGATCAGCCTCGACTGTGCCTTCTAGTTGCCAGCCATCTGTTG
TTTGCCCCTCCCCCGTGCCTTCCTTGACCCTGGAAGGTGCCACTCCCACTGTCCTTTC
CTAATAAAATGAGGAAATTGCATCGCATTGTCTGAGTAGGTGTCATTCTATTCTGGGG
GGTGGGGTGGGGCAGGACAGCAAGGGGGAGGATTGGGAAGACAATAGCAGGCATGC
TGGGGATGCGGTGGGCTCTATGGCTTCTGAGGCGGAAAGAACCAGCTGGGGCTCTA
GGGGGTATCCCCACGCGCCCTGTAGCGGCGCATTAAGCGCGGCGGGTGTGGTGGTT
ACGCGCAGCGTGACCGCTACACTTGCCAGCGCCCTAGCGCCCGCTCCTTTCGCTTTCT
TCCCTTCCTTTCTCGCCACGTTCGCCGGCTTTCCCCGTCAAGCTCTAAATCGGGGGCT
CCCTTTAGGGTTCCGATTTAGTGCTTTACGGCACCTCGACCCCAAAAAACTTGATTAG
GGTGATGGTTCACGTAGTGGGCCATCGCCCTGATAGACGGTTTTTCGCCCTTTGACG
TTGGAGTCCACGTTCTTTAATAGTGGACTCTTGTTCCAAACTGGAACAACACTCAACCC
TATCTCGGTCTATTCTTTTGATTTATAAGGGATTTTGCCGATTTCGGCCTATTGGTTAA
AAAATGAGCTGATTTAACAAAAATTTAACGCGAATTAATTCTGTGGAATGTGTGTCAG
TTAGGGTGTGGAAAGTCCCCAGGCTCCCCAGCAGGCAGAAGTATGCAAAGCATGCAT
CTCAATTAGTCAGCAACCAGGTGTGGAAAGTCCCCAGGCTCCCCAGCAGGCAGAAGTA
TGCAAAGCATGCATCTCAATTAGTCAGCAACCATAGTCCCGCCCCTAACTCCGCCCATC
CCGCCCCTAACTCCGCCCAGTTCCGCCCATTCTCCGCCCCATGGCTGACTAATTTTTTT
TATTTATGCAGAGGCCGAGGCCGCCTCTGCCTCTGAGCTATTCCAGAAGTAGTGAGGA
GGCTTTTTTGGAGGCCTAGGCTTTTGCAAAAAGCTCCCGGGAGCTTGTATATCCATTT
TCGGATCTGATCAAGAGACAGGATGAGGATCGTTTATGAAAAAGCCTGAACTCACCGC
GACGTCTGTCGAGAAGTTTCTGATCGAAAAGTTCGACAGCGTCTCCGACCTGATGCAG
CTCTCGGAGGGCGAAGAATCTCGTGCTTTCAGCTTCGATGTAGGAGGGCGTGGATAT
GTCCTGCGGGTAAATAGCTGCGCCGATGGTTTCTACAAAGATCGTTATGTTTATCGGC
ACTTTGCATCGGCCGCGCTCCCGATTCCGGAAGTGCTTGACATTGGGGAATTCAGCG
AGAGCCTGACCTATTGCATCTCCCGCCGTGCACAGGGTGTCACGTTGCAAGACCTGCC
TGAAACCGAACTGCCCGCTGTTCTGCAGCCGGTCGCGGAGGCCATGGATGCGATTGC
TGCGGCCGATCTTAGCCAGACGAGCGGGTTCGGCCCATTCGGACCGCAAGGAATCGG
TCAATACACTACATGGCGTGATTTCATATGCGCGATTGCTGATCCCCATGTGTATCAC
TGGCAAACTGTGATGGACGACACCGTCAGTGCGTCCGTCGCGCAGGCTCTCGATGAG
CTGATGCTTTGGGCCGAGGACTGCCCCGAAGTCCGGCACCTCGTGCACGCGGATTTC

GGCTCCAACAATGTCCTGACGGACAATGGCCGCATAACAGCGGTCATTGACTGGAGC
GAGGCGATGTTCGGGGATTCCCAATACGAGGTCGCCAACATCTTCTTCTGGAGGCCG
TGGTTGGCTTGTATGGAGCAGCAGACGCGCTACTTCGAGCGGAGGCATCCGGAGCTT
GCAGGATCGCCGCGGCTCCGGGCGTATATGCTCCGCATTGGTCTTGACCAACTCTATC
AGAGCTTGGTTGACGGCAATTTCGATGATGCAGCTTGGGCGCAGGGTCGATGCGACG
CAATCGTCCGATCCGGAGCCGGGACTGTCGGGCGTACACAAATCGCCCGCAGAAGCG
CGGCCGTCTGGACCGATGGCTGTGTAGAAGTACTCGCCGATAGTGGAAACCGACGCC
CCAGCACTCGTCCGAGGGCAAAGGAATAGGCGGGACTCTGGGGTTCGCGAAATGACC
GACCAAGCGACGCCCAACCTGCCATCACGAGATTTCGATTCCACCGCCGCCTTCTATG
AAAGGTTGGGCTTCGGAATCGTTTTCCGGGACGCCGGCTGGATGATCCTCCAGCGCG
GGGATCTCATGCTGGAGTTCTTCGCCCACCCCAACTTGTTTATTGCAGCTTATAATGG
TTACAAATAAAGCAATAGCATCACAAATTTCACAAATAAAGCATTTTTTTCACTGCATTC
TAGTTGTGGTTTGTCCAAACTCATCAATGTATCTTATCATGTCTGTATACCGTCGACCT
CTAGCTAGAGCTTGGCGTAATCATGGTCATAGCTGTTTCCTGTGTGAAATTGTTATCC
GCTCACAATTCCACACAACATACGAGCCGGAAGCATAAAGTGTAAAGCCTGGGGTGCC
TAATGAGTGAGCTAACTCACATTAATTGCGTTGCGCTCACTGCCCGCTTTCCAGTCGG
GAAACCTGTCGTGCCAGCTGCATTAATGAATCGGCCAACGCGCGGGGAGAGGCGGTT
TGCGTATTGGGCGCTCTTCCGCTTCCTCGCTCACTGACTCGCTGCGCTCGGTCGTTCG
GCTGCGGCGAGCGGTATCAGCTCACTCAAAGGCGGTAATACGGTTATCCACAGAATCA
GGGGATAACGCAGGAAAGAACATGTGAGCAAAAGGCCAGCAAAAGGCCAGGAACCGT
AAAAAGGCCGCGTTGCTGGCGTTTTTCCATAGGCTCCGCCCCCCTGACGAGCATCACA
AAAATCGACGCTCAAGTCAGAGGTGGCGAAACCCGACAGGACTATAAAGATACCAGGC
GTTTCCCCCTGGAAGCTCCCTCGTGCGCTCTCCTGTTCCGACCCTGCCGCTTACCGGA
TACCTGTCCGCCTTTCTCCCTTCGGGAAGCGTGGCGCTTTCTCATAGCTCACGCTGTA
GGTATCTCAGTTCGGTGTAGGTCGTTCGCTCCAAGCTGGGCTGTGTGCACGAACCCC
CCGTTCAGCCCGACCGCTGCGCCTTATCCGGTAACTATCGTCTTGAGTCCAACCCGGT
AAGACACGACTTATCGCCACTGGCAGCAGCCACTGGTAACAGGATTAGCAGAGCGAG
GTATGTAGGCGGTGCTACAGAGTTCTTGAAGTGGTGGCCTAACTACGGCTACACTAG
AAGAACAGTATTTGGTATCTGCGCTCTGCTGAAGCCAGTTACCTTCGGAAAAAGAGTT
GGTAGCTCTTGATCCGGCAAACAAACCACCGCTGGTAGCGGTGGTTTTTTTGTTTGCA
AGCAGCAGATTACGCGCAGAAAAAAAGGATCTCAAGAAGATCCTTTGATCTTTTCTAC
GGGGTCTGACGCTCAGTGGAACGAAAACTCACGTTAAGGGATTTTGGTCATGAGATT
ATCAAAAAGGATCTTCACCTAGATCCTTTTAAATTAAAAATGAAGTTTTAAATCAATCT
AAAGTATATATGAGTAAACTTGGTCTGACAGTTACCAATGCTTAATCAGTGAGGCACC
TATCTCAGCGATCTGTCTATTTCGTTCATCCATAGTTGCCTGACTCCCCGTCGTGTAG
ATAACTACGATACGGGAGGGCTTACCATCTGGCCCCAGTGCTGCAATGATACCGCGAG
ACCCACGCTCACCGGCTCCAGATTTATCAGCAATAAACCAGCCAGCCGGAAGGGCCGA
GCGCAGAAGTGGTCCTGCAACTTTATCCGCCTCCATCCAGTCTATTAATTGTTGCCGG
GAAGCTAGAGTAAGTAGTTCGCCAGTTAATAGTTTGCGCAACGTTGTTGCCATTGCTA
CAGGCATCGTGGTGTCACGCTCGTCGTTTGGTATGGCTTCATTCAGCTCCGGTTCCCA
ACGATCAAGGCGAGTTACATGATCCCCCATGTTGTGCAAAAAAGCGGTTAGCTCCTTC
GGTCCTCCGATCGTTGTCAGAAGTAAGTTGGCCGCAGTGTTATCACTCATGGTTATGG
CAGCACTGCATAATTCTCTTACTGTCATGCCATCCGTAAGATGCTTTTCTGTGACTGG
TGAGTACTCAACCAAGTCATTCTGAGAATAGTGTATGCGGCGACCGAGTTGCTCTTGC
CCGGCGTCAATACGGGATAATACCGCGCCACATAGCAGAACTTTAAAAGTGCTCATCA
TTGGAAAACGTTCTTCGGGGCGAAAACTCTCAAGGATCTTACCGCTGTTGAGATCCAG
TTCGATGTAACCCACTCGTGCACCCAACTGATCTTCAGCATCTTTTACTTTCACCAGCG
TTTCTGGGTGAGCAAAAACAGGAAGGCAAAATGCCGCAAAAAAGGGAATAAGGGCGA
CACGGAAATGTTGAATACTCATACTCTTCCTTTTTCAATATTATTGAAGCATTTATCAG
GGTTATTGTCTCATGAGCGGATACATATTTGAATGTATTTAGAAAAATAAACAAATAG
GGGTTCCGCGCACATTTCCCCGAAAAGTGCCACCTGACGTCGACGGATCGGGAGATC
TCCTGCTGGGATGACGAGCGTAAGCCACCATGCCCAGCTGGGTTTTATTTATTTTGGT

TTTTTTCCTGACCCCTTAACTAGAAATAAGCTCCACGAGAGCGGGATCTTTTGTCTTCT
GTGCACTACTTGTCCTCGGTTCTTAGAACAGAACCTGAGAGAACCTGATCGCAAATAT
TTTTGGAATGAATGAATGAATGGGTTCACCAGGGCACCATGGGAAACTGAGTCCGCAA
CCTAGAAGCCATGAAAGACAGTCCACTTCCAAGCTTCCCTGGGTGACCTCGCAGGGCA
TGCTGGGAAATGAAATTTGCGGTGAAAAGGTCAGGACCACGATCCTAGGGCACGCTG
GGAAATGTAGCCCACAGGGCCACACCCCTAAAAGCACAGTGGGGTGCAAGGCACCTC
AACAACTAGCAAAGGCAGCCCCG

Figure 11. DNA and amino acid sequence of the scFv identified during the LMP1 loop 2F and LMP1 loop 2Y phage selections. The DNA and amino acid sequence of the linker has been highlighted in grey. The CDRs follow a colour code for identification: CDR1H in blue, CDR2H in green, CDR3H in red, CDR1L in orange, CDR2L in pink and CDR3L golden yellow.

Clone 1 LMP1
CAG GTG CAG CTG GTG CAG TCT GGG GGA GGC GTG GTC CAG CCT GGG AGG TCC CTG AGA CTC TCC TGT GCA GCC TCT GGA TTC ACC TTC AGT AGC TAT GCT ATG CAC TGG GTC CGC CAG GCT CCA GGC AAG GGG CTG GAG TGG GTG GCA GTT ATA TCA TAT GAT GGA AGT AAT AAA TAC TAC GCA GAC TCC GTG AAG GGC CGA TTC ACC ATC TCC AGA GAC AAT TCC AAG AAC ACG CTG TAT CTG CAA ATG AAC AGC CTG AGA GCC GAG GAC ACG GCC GTG TAT TAC TGT GCG AGA GGC CAC TTC CTT GAC TAC TGG GGC CAG GGA ACC CTG GTC ACC GTC TCC TCA GCA CCC ACC AAG GCT CCG GAT GTG GGC AGC AGC GGC AGC AGC AGC GGT ACC AGC AGC GGC GGC AGC AGC AGC AGC GGC AGC GGC GAG CTC GTG ATG ACT CAG TCT CCA CTC TCC CTG CCC GTC ACC CCT GGA GAG CCG GCC TCC ATC TCC TGC AGG TCT AGT CAG AGC CTC CTG CAT AGT AAT GGA TAC AAC TAT TTG GAT TGG TAC CTG CAG AAG CCA GGG CAG TCT CCA CAG CTC CTG ATC TAT TTG GGT TCT AAT CGG GCC TCC GGG GTC CCT GAC AGG TTC AGT GGC AGT GGA TCA GGC ACA GAT TTT ACA CTG AAA ATC AGC AGA GTG GAG GCT GAG GAT GTT GGC ATT TAC TAC TGC ATG CAG GCT ATA CAT CGT CTC ACC TTC GGC CAA GGG ACA CGA CTG GAG ATT AAA

QVQLVQSGGGVVQPGRSLRLSCAASGFTFSSYAMHWVRQAPGKGLEWVAVISYDGSNKYY ADSVKGRFTISRDNSKNTLYLQMNSLRAEDTAVYYCARGHFLDYWGQGTLVTVSSAPTKAP DVGSSGSSSGTSSGGSSSSGSGELVMTQSPLSLPVTPGEPASISCRSSQSLLHSNGYNYLDWY LQKPGQSPQLLIYLGSNRASGVPDRFSGSGSGTDFTLKISRVEAEDVGIYYCMQAIHRLTFGQ GTRLEIK

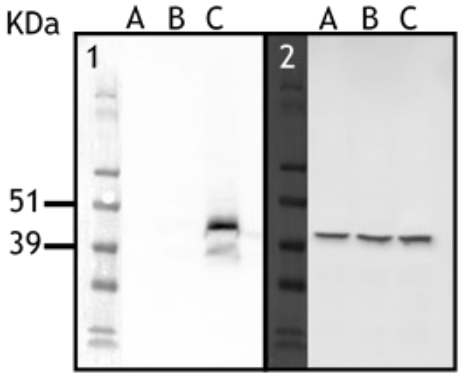

Figure 12 Western blot result of LMP1 expression under tetracycline induction in HEK293-LMP1 cells. 6 µg of protein lysates were separated by NuPAGE (Gel 4-12% polyacrylamide gradient Bis-Tris run in MOPS buffer). The gel was blotted and probed with antibody anti-LMP1 clone 1G6 and secondary anti-rat HRP conjugated (1). The blot was then stripped and re-probed with antibody anti-β-actin and secondary anti-rabbit HRP conjugated, as a loading control (2). Lysate from HEK293 Flip-In T-REx control cells loaded in track A, lysate from uninduced HEK293-LMP1 loaded in track B and sample lysate loaded in track C. The marker ladder sizes in kDa are shown.

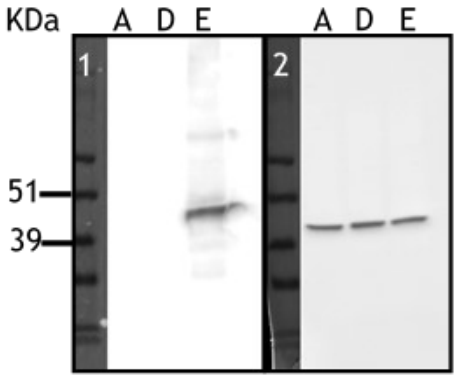

Figure 13 Western blot result of LMP2A expression under tetracycline induction in HEK293-LMP2A cells. 6 µg of protein lysates were separated by NuPAGE (Gel 4-12% polyacrylamide gradient Bis-Tris run in MOPS buffer). The gel was first blotted and probed with antibody anti-LMP2A clone 14B6 and secondary anti-rat HRP conjugated (1). The blot was then, stripped and re-probed with antibody anti-β-actin and secondary anti-rabbit HRP conjugated, as a loading control (2). Lysate from HEK293 Flip-In T-REx control cells loaded in track A, lysate from uninduced HEK293-LMP2A loaded in track D and sample lysate loaded in track E. The marker ladder sizes in kDa are shown.

Figure 14. DNA and amino acid sequence of scFvs identified during the B7H4 Ig-like V-type 1 domain selection. The DNA and amino acid sequence of the linker have been highlighted in grey. The CDRs follow a colour code for identification: CDR1H in blue, CDR2H in green, CDR3H in red, CDR1L in orange, CDR2L in pink and CDR3L golden yellow.

Clone 1 B7H4 (Gate δ in figure 8.2.D)
CAG GTG CAG CTG GTG CAG TCT GGG GCT GAG GTG AAG AAG CCT GGG TCC TCG GTG AAG GTC TCC TGC AAG GCT TCT GGA GGC ACC TTC AGC AGC TAT GCT ATC AGC TGG GTG CGA CAG GCC CCT GGA CAA GGG CTT GAG TGG ATG GGA GGG ATC ATC CCT ATC TTT GGT ACA GCA AAC TAC GCA CAG AAG TTC CAG GGC AGA GTC ACG ATT ACC GCG GAC GAA TCC ACG AGC ACA GCC TAC ATG GAG CTG AGC AGC CTG AGA TCT GAG GAC ACG GCC GTG TAT TAC TGT GCG AGA GAT TCC CGG TTA TTA CGG CAC GAT TGG GGC CAG GGA ACC CTG GTC ACC GTC TCC TCA GCA CCC ACC AAG GCT CCG GAT GTG GGC AGC AGC GGC AGC AGC AGC GGT

ACC AGC AGC GGC GGC AGC AGC AGC AGC GGC AGC GGC GAG CTC CAG ATG
ACC CAG TCT CCA GAC TCC CTG GCT GTG TCT CTG GGC GAG AGG GCC ACC ATC
AAC TGC AAG TCC AGC CAG AGT GTT TTA TAC AGC TCC AAC AAT AAG AAC TAC
TTA GCT TGG TAC CAG CAG AAA CCA GGA CAG CCT CCT AAG CTG CTC ATT TAC
TGG GCA TCT ACC CGG GAA TCC GGG GTC CCT GAC CGA TTC AGT GGC AGC
GGG TCT GGG ACA GAT TTC ACT CTC ACC ATC AGC AGC CTG CAG GCT GAA GAT
GTG GCA GTT TAT TAC TGT CAG CAA TAT TAT AGT ACT CCT CCC ACT TTC GGC
GGA GGG ACC AAG CTG GAG ATC AAA

QVQLVQSGAEVKKPGSSVKVSCKASGGTFSSYAISWVRQAPGQGLEWMGGIIPIFGTANYA
QKFQGRVTITADESTSTAYMELSSLRSEDTAVYYCARDSRLLRHDWGQGTLVTVSSAPTKAP
DVGSSGSSSGTSSGGSSSSGSGELQMTQSPDSLAVSLGERATINCKSSQSVLYSSNNKNYLAW
YQQKPGQPPKLLIYWASTRESGVPDRFSGSGSGTDFTLTISSLQAEDVAVYYCQQYYSTPPT
FGGGTKLEIK

Clone 2 B7H4 (Gate δ in figure 8.2.D)

CAG GTG CAG CTG CAG GAG TCG GGC ACA GGA CTG GTG AAG CCT TCA CAG
ACC CTG TCC GTC ACC TGC ACT GTC TCT GGT GGC TCC ATC AGC AGT GGT GGT
TAC TAC TGG AGC TGG ATC CGC CAG TAC CCA GGG AAG GGC CTG GAG TGG
ATT GGG TAC ATC TAT CAC ACT GGG ACC ACC TAC TAC AGC TCG TCC CTC AAG
AGT CGA GTT TCC ATA TCA GTA GAC ACC TCT AAG AAC CAG TTC TCC CTG GAG
CTG AGT TCT GTC ACT GCC GCG GAC ACG GCC GTG TAT TAC TGT GCG AGA GGC
GAC CTC CGA TAT AGC GAC AGC TGG TCC GAC CGC TAC TGG TAC TTC GAT CTC
TGG GGC CGT GGC ACC CTG GTC ACT GTC TCC TCA GCC TCC ACC AAG GGA CCA
TCG GTC GGC AGC AGC GGC AGC AGC AGC GGT ACC AGC AGC GGC GGC AGC
AGC AGC AGC AGC GGC AGC GGC GAG CTC GTG ATG ACT CAG TCT CCA TCC TCC CTG
TCT GCA TCT GTA GGA GAC AGA GTC ACC ATC ACT TGC CGG GCG AGT CAG GGC
ATT AGC AAT TCT TTA GCC TGG TAT CAG CAG AAA CCA GGG AAA GCC CCT AAG
CTC CTG CTC TAT GCT GCA TCC AGT TTG CAA AGT GGG GTC CCA TCA AGG TTC
AGT GGC AGT GGA TCT GGG ACA GAT TTC ACT CTC ACC ATC AGC AGT CTG CAA
CCT GAA GAT TTT GCA ACT TAC TAC TGT CAA CAG AGT TAC AGT ACC CCT CTC
ACT TTC GGC GGA GGG ACC AAG CTC GAG ATC AAA

QVQLQESGPGLVKPSQTLSVTCTVSGGSISSGGYYWSWIRQYPGKGLEWIGYIYHTGTTYY
SSSLKSRVSISVDTSKNQFSLELSSVTAADTAVYYCARGDLRYSDSWSDRYWYFDLWGRGTL
VTVSSASTKGPSVGSSGSSSGTSSGGSSSSGSGELVMTQSPSSLSASVGDRVTITCRASQGISN
SLAWYQQKPGKAPKLLLYAASSLQSGVPSRFSGSGSGTDFTLTISSLQPEDFATYYCQQSYST
PLTFGGGTKLEIK

Clone 3 B7H4 (Gates α and β in figure 8.2.B)

CAG ATC ACC TTG AAG GAG TCT GGG GGA GGC TTG GTA CAG CCT GGG GGG
TCC CTG AGA CTC TCC TGT GCA GCC TCT GGA TTC ACC TTT AGC AGC TAT GCC
ATG AGC TGG GTC CGC CAG GCT CCA GGG AAG GGG CTG GAG TGG GTC TCA
GCT ATT AGT GGT AGT GGT GGT AGC ACA TAC TAC GCA GAC TCC GTG AAG GGC
CGG TTC ACC ATC TCC AGA GAC AAT TCC AAG AAC ACG CTG TAT CTG CAA ATG
AAC AGC CTG AGA GCC GAG GAC ACG GCC GTA TAT TAC TGT GCG AAA GGT GGT
GGT TAT TTC TAC TTT GAC TAC TGG GGC CAG GGA ACC CTG GTC ACC GTC TCC
TCA GCA CCC ACC AAG GCT CCG GAT GTG GGC AGC AGC GGC AGC AGC AGC
GGT ACC AGC AGC GGC GGC AGC AGC AGC AGC GGC AGC GGC GAG CTC GTG
CTG ACT CAG CCA CCT TCG GTG TCA GTG GCC CCA GGA CAG ACG GCC AGG ATT
ACC TGT GGG GGA AAC AAC ATT GGA AGT AAA AGT GTG CAC TGG TAC CAG CAG
AAG CCA GGC CAG GCC CCT GTG CTG GTC GTC TAT GAT GAT AGC GAC CGG CCC
TCA GGG ATC CCT GAG CGA TTC TCT GGC TCC AAC TCT GGG AAC ACG GCC ACC
CTG ACC ATC AGC AGG GTC GAA GCC GGG GAT GAG GCC GAC TAT TAC TGT CAG

GTG TGG GAT AGT AGT AGT GAT CAA TTC GGC GGA GGC ACC CAG CTG ACC GTC CTC GGC

QITLKESGGGLVQPGGSLRLSCAASGFTFSSYAMSWVRQAPGKGLEWVSAISGSGGSTYYA DSVKGRFTISRDNSKNTLYLQMNSLRAEDTAVYYCAKGGGYFYFDYWGQGTLVTVSSAPTK APDVGSSGSSSGTSSGGSSSSGSGELVLTQPPSVSVAPGQTARITCGGNNIGSKSVHWYQQK PGQAPVLVVYDDSDRPSGIPERFSGSNSGNTATLTISRVEAGDEADYYCQVWDSSSDQFGG GTQLTVLG

Clone 4 B7H4 (Gate γ in figure 8.2.D)

GAG GTG CAG CTG GTG GAG TCT GGG GGA GGC TTG GTA CAG CCT GGG GGG TCC CTG AGA CTC TCC TGT GCA GCC TCT GGA TTC ACC TTT AGC AGC TAT GCC ATG AGC TGG GTC CGC CAG GCT CCA GGG AAG GGG CTG GAG TGG GTC TCA GCT ATT AGT GGT AGT GGT GGT AGC ACA TAC TAC GCA GAC TCT GTG AAG GGC CGA TTC ACC ATC TCC AGA GAC AAT GCC AAG AAC TCA CTG TAT CTG CAA ATG AAC AGC CTG AGA GAC GAG GAC ACG GCT GTG TAT TAC TGT GCG AGA TTC GGG TGG TTC GGG TCA ATT GAC TAC TGG GGC CAG GGA ACC CTG GTC ACC GTC TCC TCA GGG ACT GCA TCC GCC CCA ACC CTT GGC AGC AGC GGC AGC AGC AGC GGT ACC AGC AGC GGC GGC AGC AGC AGC AGC GGC AGC GGC GAG CTC CAG ATG ACC CAG TCT CCT TCT TCC GTG TCT GCA TCT GTG GGA GAC AGA GTC ACC ATC ACT TGT CGG ACG AGT CAG GAT ATT AGC ACC TGG TTA GCC TGG TAT CAA CAG AAA CCA GGG GAA GCC CCT AAG CTC CTG ATC TAT GCT GCA TCC AAT TTG CTA AGT GGG GTC CCA TCA AGG TTT AGC GGC AGT GGA TCT GGG ACA CAG TTC ACA CTC ACC ATC AAT GGC CTG CAG CCT GAA GAT TTT GCA ACT TAC TAC TGT CAA CAG AGT TAC AGT ACC CCT CAA ACG TTC GGC CAA GGG ACC AAG CTG GAG ATC AAA

EVQLVESGGGLVQPGGSLRLSCAASGFTFSSYAMSWVRQAPGKGLEWVSAISGSGGSTYYA DSVKGRFTISRDNAKNSLYLQMNSLRDEDTAVYYCARFGWFGSIDYWGQGTLVTVSSGTAS APTLGSSGSSSGTSSGGSSSSGSGELQMTQSPSSVSASVGDRVTITCRTSQDISTWLAWYQQ KPGEAPKLLIYAASNLLSGVPSRFSGSGSGTQFTLTINGLQPEDFATYYCQQSYSTPQTFGQ GTKLEIK

Clone 5 B7H4 (Gate γ in figure 8.2.D)

CAG ATC ACC TTG AAG GAG TCT GGG GGA GGC TTG GTA CAG CCT GGG GGG TCC CTG AGA CTC TCC TGT GCA GCC TCT GGA TTC ACC TTT AGC AGC TAT GCC ATG AGC TGG GTC CGC CAG GCT CCA GGG AAG GGG CTG GAG TGG GTC TCA GCT ATT AGT GGT AGT GGT GGT AGC ACA TAC TAC GCA GAC TCT GTG AAG GGC CGA TTC ACC ATC TCC AGA GAC AAT GCC AAG AAC TCA CTG TAT CTG CAA ATG AAC AGC CTG AGA GAC GAG GAC ACG GCT GTG TAT TAC TGT GCG AGA TTC GGG TGG TTC GGG TCA ATT GAC TAC TGG GGC CAG GGA ACC CTG GTC ACC GTC TCC TCA GGG ACT GCA TCC GCC CCA ACC CTT GGC AGC AGC GGC AGC AGC AGC GGT ACC AGC AGC GGC GGC AGC AGC AGC AGC GGC AGC GGC GAG CTC GTG TTG ACG CAG TCT CCA TCT TCC GTG TCT GCA TCT GTA GGA GAC AGA GTC ACC ATC ACT TGT CGG GCG AGT CAG GGT ATT AGC AGC TGG TTA GCC TGG TAT CAG CAG AAA CCA GGG AAA GCC CCT AAG CTC CTG ATC TAT GCT GCA TCC AGT TTG CAA AGT GGG GTC CCA TCA AGG TTC AGC GGC AGT GGA TCT GGG ACA GAT TTC ACT CTC ACC ATC AGC AGC CTG CAG CCT GAA GAT TTT GCA ACT TAC TAT TGT CAA CAG AGT TAC AGT ACC CCT CTG ACG TTC GGC CAA GGG ACC AAG CTG GAG ATC AAA

QITLKESGGGLVQPGGSLRLSCAASGFTFSSYAMSWVRQAPGKGLEWVSAISGSGGSTYYA DSVKGRFTISRDNAKNSLYLQMNSLRDEDTAVYYCARFGWFGSIDYWGQGTLVTVSSGTAS APTLGSSGSSSGTSSGGSSSSGSGELVLTQSPSSVSASVGDRVTITCRASQGISSWLAWYQQK

PGKAPKLLIYAASSLQSGVPSRFSGSGSGTDFTLTISSLQPEDFATYYCQQSYSTPLTFGQGT
KLEIK

Clone 6 B7H4 (Gate δ in figure 8.2.D)

GAG GTG CAG CTG GTG GAG TCT GGG GGA GGC TTG GTA CAG CCT GGG GGG
TCC CTG AGA CTC TCC TGT GCA GCC TCT GGA TTC ACC TTT AGC AGC TAT GCC
ATG AGC TGG GTC CGC CAG GCT CCA GGG AAG GGG CTG GAG TGG GTC TCA
GCT ATT AGT GGT AGT GGT GGT AGC ACA TAC TAC GCA GAC TCT GTG AAG GGC
CGA TTC ACC ATC TCC AGA GAC AAT GCC AAG AAC TCA CTG TAT CTG CAA ATG
AAC AGC CTG AGA GAC GAG GAC ACG GCT GTG TAT TAC TGT GCG AGA TTC GGG
TGG TTC GGG TCA ATT GAC TAC TGG GGC CAG GGA ACC CTG GTC ACC GTC TCC
TCA GGG ACT GCA TCC GCC CCA ACC CTT GGC AGC AGC GGC AGC AGC AGC GGT
ACC AGC AGC GGC GGC AGC AGC AGC AGC GGC AGC GGC GAG CTC GTG TTG
ACG CAG TCT CCA TCT TCC GTG TCT GCA TCT GTA GGA GAC AGA GTC ACC ATC
ACT TGT CGG GCG AGT CAG GGT ATT AGC AGC TGG TTA GCC TGG TAT CAG
CAG AAA CCA GGG AAA GCC CCT AAG CTC CTG ATC TAT GCT GCA TCC AGT TTG
CAA AGT GGG GTC CCA TCA AGG TTC AGC GGC AGT GGA TCT GGG ACA GAT TTC
ACT CTC ACC ATC AGC AGC CTG CAG CCT GAA GAT TTT GCA ACT TAC TTC TGT
CAA CAG AGT TAC AGT ACT CCT CAC ACT TTT GGC CAG GGG ACC AAG CTG GAG
ATC AAA

EVQLVESGGGLVQPGGSLRLSCAASGFTFSSYAMSWVRQAPGKGLEWVSAISGSGGSTYYA
DSVKGRFTISRDNAKNSLYLQMNSLRDEDTAVYYCARFGWFGSIDYWGQGTLVTVSSGTAS
APTLGSSGSSSGTSSGGSSSSGSGELVLTQSPSSVSASVGDRVTITCRASQGISSWLAWYQQK
PGKAPKLLIYAASSLQSGVPSRFSGSGSGTDFTLTISSLQPEDFATYFCQQSYSTPHTFGQGT
KLEIK

Clone 7 B7H4 (Gate δ in figure 8.2.D)

GAG GTG CAG CTG GTG GAG TCT GGG GGA GGC TTG GTA CAG CCT GGG GGG
TCC CTG AGA CTC TCC TGT GCA GCC TCT GGA TTC ACC TTT AGC AGC TAT GCC
ATG AGC TGG GTC CGC CAG GCT CCA GGG AAG GGG CTG GAG TGG GTC TCA
GCT ATT AGT GGT AGT GGT GGT AGC ACA TAC TAC GCA GAC TCT GTG AAG GGC
CGA TTC ACC ATC TCC AGA GAC AAT GCC AAG AAC TCA CTG TAT CTG CAA ATG
AAC AGC CTG AGA GAC GAG GAC ACG GCT GTG TAT TAC TGT GCG AGA TTC GGG
TGG TTC GGG TCA ATT GAC TAC TGG GGC CAG GGA ACC CTG GTC ACC GTC TCC
TCA GGG ACT GCA TCC GCC CCA ACC CTT GGC AGC AGC GGC AGC AGC AGC GGT
ACC AGC AGC GGC GGC AGC AGC AGC AGC GGC AGC GGC GAG CTC GTG TTG
ACG CAG TCT CCA TCT TCC GTG TCT GCA TCT GTA GGA GAC AGA GTC ACC ATC
ACT TGT CGG GCG AGT CAG GGT ATT AGC AGC TGG TTA GCC TGG TAT CAG
CAG AAA CCA GGG AAA GCC CCT AAG CTC CTG ATC TAT GCT GCA TCC AGT TTG
CAA AGT GGG GTC CCA TCA AGG TTC AGC GGC AGT GGA TCT GGG ACA GAT TTC
ACT CTC ACC ATC AGC AGC CTG CAG CCT GAC GAT TTT GCA GTG TAT TAC TGT
CAG CAG TTT GAT GGC TCA CTG TGG ACG TTC GGC CAA GGG ACC AAG GTG
GAA ATC AAA

EVQLVESGGGLVQPGGSLRLSCAASGFTFSSYAMSWVRQAPGKGLEWVSAISGSGGSTYYA
DSVKGRFTISRDNAKNSLYLQMNSLRDEDTAVYYCARFGWFGSIDYWGQGTLVTVSSGTAS
APTLGSSGSSSGTSSGGSSSSGSGELVLTQSPSSVSASVGDRVTITCRASQGISSWLAWYQQK
PGKAPKLLIYAASSLQSGVPSRFSGSGSGTDFTLTISSLQPDDFAVYYCQQFDGSLWTFGQG
TKVEIK

Clone 8 B7H4 (Gate δ in figure 8.2.D)

GAG GTG CAG CTG GTG GAG TCT GGG GGA GGC TTG GTA CAG CCT GGG GGG
TCC CTG AGA CTC TCC TGT GCA GCC TCT GGA TTC ACC TTT AGC AGC TAT GCC
ATG AGC TGG GTC CGC CAG GCT CCA GGG AAG GGG CTG GAG TGG GTC TCA

GCT ATT AGT GGT AGT GGT GGT AGC ACA TAC TAC GCA GAC TCT GTG AAG GGC CGA TTC ACC ATC TCC AGA GAC AAT GCC AAG AAC TCA CTG TAT CTG CAA ATG AAC AGC CTG AGA GAC GAG GAC ACG GCT GTG TAT TAC TGT GCG AGA TTC GGG TGG TTC GGG TCA ATT GAC TAC TGG GGC CAG GGA ACC CTG GTC ACC GTC TCC TCA GGG ACT GCA TCC GCC CCA ACC CTT GGC AGC AGC GGC AGC AGC AGC GGT ACC AGC AGC GGC GGC AGC AGC AGC AGC GGC AGC GGC GAG CTC ACA CTC ACG CAG TCT CCA GGC ACC CTG TCT TTG TCT CCA GGG GAA AGA GCC ACC CTC TCC TGC AGG GCC AGT CAG AGT GTC AGC AGC AAC TAC TTA GCC TGG TAC CAG CAG ACA CCT GGC CAG GCT CCC AGG CTC CTC ATT TAT GGT GCG TCC AGT AGG GCC ACT GGT GTC CCA GAC AGG TTC GGT GGC AGT GGG TCT GGG ACA GAC TTC ACT CTC ACC ATC AAC AGA CTG GAG CCG GAA GAT TCT GCA GTG TAT TAC TGT CAG CAC TAT GGT AGT TAT CCG TGG ACG TTC GGC CAA GGG ACC AAG CTG GAG ATC AAA

EVQLVESGGGLVQPGGSLRLSCAASGFTFSSYAMSWVRQAPGKGLEWVSAISGSGGSTYYA DSVKGRFTISRDNAKNSLYLQMNSLRDEDTAVYYCARFGWFGSIDYWGQGTLVTVSSGTAS APTLGSSGSSSGTSSGGSSSSGSGELTLTQSPGTLSLSPGERATLSCRASQSVSSNYLAWYQQ TPGQAPRLLIYGASSRATGVPDRFGGSGSGTDFTLTINRLEPEDSAVYYCQHYGSYPWTFG QGTKLEIK

Clone 9 B7H4 (Gate γ in figure 8.2.D)

GAG GTG CAG CTG GTG GAG TCT GGG GGA GGC TTG GTA CAG CCT GGG GGG TCC CTG AGA CTC TCC TGT GCA GCC TCT GGA TTC ACC TTT AGC AGC TAT GCC ATG AGC TGG GTC CGC CAG GCT CCA GGG AAG GGG CTG GAG TGG GTC TCA GCT ATT AGT GGT AGT GGT GGT AGC ACA TAC TAC GCA GAC TCT GTG AAG GGC CGA TTC ACC ATC TCC AGA GAC AAT GCC AAG AAC TCA CTG TAT CTG CAA ATG AAC AGC CTG AGA GAC GAG GAC ACG GCT GTG TAT TAC TGT GCG AGA TTC GGG TGG TTC GGG TCA ATT GAC TAC TGG GGC CAG GGA ACC CTG GTC ACC GTC TCC TCA GGG ACT GCA TCC GCC CCA ACC CTT GGC AGC AGC GGC AGC AGC AGC GGT ACC AGC AGC GGC GGC AGC AGC AGC AGC GGC AGC GGC GAG CTC GTG TTG ACG CAG TCT CCA TCT TCC GTG TCT GCA TCT GTA GGA GAC AGA GTC ACC ATC ACT TGT CGG GCG AGT CAG GGT ATT AGC AGC TGG TTA GCC TGG TAT CAG CAG AAA CCA GGG AAA GCC CCT AAG CTC CTG ATT TAT GCT GCA TCT AGT TTG AAA AGT GGG GTC CCA CCA AGG TTC AGT GGC AGT GGA TCC GGG ACA GAT TTC ACT CTC ACC ATC AGC AGT CTG CAA CCT GAG GAT TTT GCA ACT TAC TTT TGT CAA CAG AGT TAC AGT AGG CCG ACG TTC GGC CAA GGG ACC AAG CTG GAG ATC AAA

EVQLVESGGGLVQPGGSLRLSCAASGFTFSSYAMSWVRQAPGKGLEWVSAISGSGGSTYYA DSVKGRFTISRDNAKNSLYLQMNSLRDEDTAVYYCARFGWFGSIDYWGQGTLVTVSSGTAS APTLGSSGSSSGTSSGGSSSSGSGELVLTQSPSSVSASVGDRVTITCRASQGISSWLAWYQQK PGKAPKLLIYAASSLKSGVPPRFSGSGSGTDFTLTISSLQPEDFATYFCQQSYSRPTFGQGTK LEIK

Clone 10 B7H4 (Gate γ in figure 8.2.D)

GAG GTG CAG CTG GTG GAG TCT GGG GGA GGC GTG GTC CAG CCT GGG AGG TCC CTG AGA CTC TCC TGT GCA GCC TCT GGA TTC ACC TTT AGC AGC TAT GCC ATG AGC TGG GTC CGC CAG GCT CCA GGG AAG GGG CTG GAG TGG GTC TCA GCT ATT AGT GGT AGT GGT GGT AGC ACA TAC TAC GCA GAC TCC GTG AAG GGC CGG TTC ACC ATC TCC AGA GAC AAT TCC AAG AAC ACG CTG TAT CTG CAA ATG AAC AGC CTG AGA GCC GAG GAC ACG GCC GTA TAT TAC TGT GCG AAA ATT TCT GTT ATC GAC TAC TAC TAC GGT ATG GAC GTC TGG GGC CAA GGG ACC ACG GTC ACC GTC TCC TCA GGG AGT GCA TCC GCC CCA ACC CTT GGC AGC AGC GGC AGC AGC AGC AGC GGT ACC AGC AGC GGC GGC AGC AGC AGC AGC GGC AGC GGC GAG

CTC GTG CTG ACT CAG CCA CCT TCG GTG TCA GTG GCC CCA GGA CAG ACG GCC AGG ATT ACC TGT GGG GGA AAC AAC ATT GGA AGT AAA AGT GTG CAC TGG TAC CAG CAG AAG CCA GGC CAG GCC CCT GTG CTG GTC GTC TAT GAT GAT AGC GAC CGG CCC TCA GGG ATC CCT GAG CGA TTC TCT GGC TCC AAC TCT GGG AAC ACG GCC ACC CTG ACC ATC AGC AGG GTC GAA GCC GGG GAT GAG GCC GAC TAT TAC TGT CAG GTG TGG GAT AGT AGT AGT GAT CAA TTC GGC GGA GGC ACC CAG CTG ACC GTC CTC GGC

EVQLVESGGGVVQPGRSLRLSCAASGFTFSSYAMSWVRQAPGKGLEWVSAISGSGGSTYYA DSVKGRFTISRDNSKNTLYLQMNSLRAEDTAVYYCAKISVIDYYYGMDVWGQGTTVTVSSGS ASAPTLGSSGSSSGTSSGGSSSSGSGELVLTQPPSVSVAPGQTARITCGGNNIGSKSVHWYQ QKPGQAPVLVVYDDSDRPSGIPERFSGSNSGNTATLTISRVEAGDEADYYCQVWDSSSDQFG GGTQLTVLG

Clone 11 B7H4 (Gate δ in figure 8.2.D)

GAG GTG CAG CTG GTG GAG TCT GGG GGA GGC GTG GTC CAG CCT GGG AGG TCC CTG AGA CTC TCC TGT GCA GCC TCT GGA TTC ACC TTT AGC AGC TAT GCC ATG AGC TGG GTC CGC CAG GCT CCA GGG AAG GGG CTG GAG TGG GTC TCA GCT ATT AGT GGT AGT GGT GGT AGC ACA TAC TAC GCA GAC TCC GTG AAG GGC CGG TTC ACC ATC TCC AGA GAC AAT TCC AAG AAC ACG CTG TAT CTG CAA ATG AAC AGC CTG AGA GCC GAG GAC ACG GCC GTA TAT TAC TGT GCG AAA ATT TCT GTT ATC GAC TAC TAC TAC GGT ATG GAC GTC TGG GGC CAA GGG ACC ACG GTC ACC GTC TCC TCA GGG AGT GCA TCC GCC CCA ACC CTT GGC AGC AGC GGC AGC AGC AGC GGT ACC AGC AGC GGC GGC AGC AGC AGC AGC GGC AGC GGC GAG CTC ACA CTC ACG CAG TCT CCA GCC ACC CTG TAT GTG TCT CCA GGG GAA AGA GCC ACC CTC TCC TGC AGG GCC AGT CAG AGT GTT AGC AAC TAC TTA GCC TGG TAC CAG CAG AGA CCT GGC CTG GCG CCC AGG CTC CTC ATC TAT GAT GCA TCC AGC AGG GCC ACT GGC ATC CCA GAC AGG TTC AGT GGC AGT GGG TCT GGG ACA GAC TTC ACT CTC ACC ATC AGC AGA CTG GAG CCT GAA GAT TTT GCA GTG TAT TAC TGT CAG CAG CGT AGC AAC TGG CCT CTG TAC ACT TTT GGC CAG GGG ACC AAG CTG GAG ATC AAA

EVQLVESGGGVVQPGRSLRLSCAASGFTFSSYAMSWVRQAPGKGLEWVSAISGSGGSTYYA DSVKGRFTISRDNSKNTLYLQMNSLRAEDTAVYYCAKISVIDYYYGMDVWGQGTTVTVSSGS ASAPTLGSSGSSSGTSSGGSSSSGSGELTLTQSPATLYVSPGERATLSCRASQSVSNYLAWYQ QRPGLAPRLLIYDASSRATGIPDRFSGSGSGTDFTLTISRLEPEDFAVYYCQQRSNWPLYTFG QGTKLEIK

Figure 15. Synthetic DNA cassette used for the development of pcDNA3.1-hygr by cloning into pcDNA3.1 (+). *Xma*I and *BstZ*17I restriction sequences highlighted in green. Hygromycin B phosphotransferase's ORF highlighted in dark grey. SV40 poly(A) signal highlighted in light grey.

hph DNA cassette for pcDNA3.1-hygr obtained by digestion from pHygr

CCC GGG AGC TTG TAT ATC CAT TTT CGG ATC TGA TCA AGA GAC AGG ATG AGG ATC GTT TAT GAA AAA GCC TGA ACT CAC CGC GAC GTC TGT CGA GAA GTT TCT GAT CGA AAA GTT CGA CAG CGT CTC CGA CCT GAT GCA GCT CTC GGA GGG CGA AGA ATC TCG TGC TTT CAG CTT CGA TGT AGG AGG GCG TGG ATA TGT CCT GCG GGT AAA TAG CTG CGC CGA TGG TTT CTA CAA AGA TCG TTA TGT TTA TCG GCA CTT TGC ATC GGC CGC GCT CCC GAT TCC GGA AGT GCT TGA CAT TGG GGA ATT CAG CGA GAG CCT GAC CTA TTG CAT CTC CCG CCG TGC ACA GGG TGT CAC GTT GCA AGA CCT GCC TGA AAC CGA ACT GCC CGC TGT TCT GCA GCC GGT CGC GGA GGC CAT GGA TGC GAT TGC TGC GGC CGA TCT TAG CCA GAC GAG CGG GTT CGG CCC ATT CGG ACC GCA AGG AAT CGG TCA ATA CAC TAC ATG GCG TGA TTT

CAT ATG CGC GAT TGC TGA TCC CCA TGT GTA TCA CTG GCA AAC TGT GAT GGA CGA CAC CGT CAG TGC GTC CGT CGC GCA GGC TCT CGA TGA GCT GAT GCT TTG GGC CGA GGA CTG CCC CGA AGT CCG GCA CCT CGT GCA CGC GGA TTT CGG CTC CAA CAA TGT CCT GAC GGA CAA TGG CCG CAT AAC AGC GGT CAT TGA CTG GAG CGA GGC GAT GTT CGG GGA TTC CCA ATA CGA GGT CGC CAA CAT CTT CTT CTG GAG GCC GTG GTT GGC TTG TAT GGA GCA GCA GAC GCG CTA CTT CGA GCG GAG GCA TCC GGA GCT TGC AGG ATC GCC GCG GCT CCG GGC GTA TAT GCT CCG CAT TGG TCT TGA CCA ACT CTA TCA GAG CTT GGT TGA CGG CAA TTT CGA TGA TGC AGC TTG GGC GCA GGG TCG ATG CGA CGC AAT CGT CCG ATC CGG AGC CGG GAC TGT CGG GCG TAC ACA AAT CGC CCG CAG AAG CGC GGC CGT CTG GAC CGA TGG CTG TGT AGA AGT ACT CGC CGA TAG TGG AAA CCG ACG CCC CAG CAC TCG TCC GAG GGC AAA GGA ATA GGC GGG ACT CTG GGG TTC GCG AAA TGA CCG ACC AAG CGA CGC CCA ACC TGC CAT CAC GAG ATT TCG ATT CCA CCG CCG CCT TCT ATG AAA GGT TGG GCT TCG GAA TCG TTT TCC GGG ACG CCG GCT GGA TGA TCC TCC AGC GCG GGG ATC TCA TGC TGG AGT TCT TCG CCC ACC CCA ACT TGT TTA TTG CAG CTT ATA ATG GTT ACA AAT AAA GCA ATA GCA TCA CAA ATT TCA CAA ATA AAG CAT TTT TTT CAC TGC ATT CTA GTT GTG GTT TGT CCA AAC TCA TCA ATG TAT CTT ATC ATG TCT GTA TAC

Figure 16. Synthetic DNA cassette used for the development of pCD8-cassette and pIgG4-cassette. A) DNA digested from pUC57-CD8CAR. *Hind*III and *Pme*I restriction sequences highlighted in green. CD8-CAR ORF highlighted in clear grey. *Sgs*I and *Mre*I for scFv cloning highlighted in dark grey. B) DNA digested from pUC57-IgG4CAR. *Hind*III and *Pme*I restriction sequences highlighted in green. IgG4-CAR ORF highlighted in clear grey. *Sgs*I and *Apa*I for scFv cloning highlighted in dark grey.

A) DNA sequence digested from pUC57-CD8CAR and used to obtain pCD8-Cassette

AAG CTT GCC GCC ACC ATG GCC CTG CCT GTA ACC GCG TTG TTG TTG CCT CTT GCA CTT CTG CTC CAT GCG GCG CGC CCG ACA ACA ACG CCG GCG CCT AGA CCG CCG ACA CCA GCT CCA ACG ATA GCA TCA CAG CCT TTG TCT TTG CGA CCG GAG GCG TGT AGA CCA GCT GCG GGT GGC GCG GTT CAT ACC AGG GGT TTG GAT TTT GCG TGC GAT ATT TAC ATA TGG GCG CCG CTG GCA GGT ACG TGT GGG GTG CTT CTG TTG AGC CTC GTC ATA ACT CTC TAT TGC AAG CGG GGA CGG AAA AAA CTT TTG TAT ATA TTT AAA CAA CCC TTT ATG CGG CCT GTC CAA ACG ACG CAG GAG GAA GAC GGG TGC TCT TGT AGG TTT CCC GAA GAA GAG GAA GGT GGT TGT GAG CTG AGA GTG AAG TTC TCA AGA TCA GCG GAC GCT CCC GCG TAC CAG CAG GGT CAA AAT CAG TTG TAC AAT GAA CTT AAT CTG GGA AGG CGA GAA GAA TAC GAT GTA CTT GAT AAG AGG AGG GGG AGG GAT CCA GAA ATG GGC GGG AAG CCG CGC CGA AAG AAT CCA CAG GAG GGG CTG TAT AAT GAA CTC CAA AAG GAT AAA ATG GCT GAG GCT TAC TCA GAG ATT GGC ATG AAG GGT GAG CGG AGG AGA GGA AAG GGT CAC GAC GGC TTG TAT CAG GGC CTC TCT ACT GCG ACG AAG GAT ACG TAT GAC GCG CTC CAC ATG CAA GCC CTC CCG CCA CGA TAA GTT TAA AC

B) DNA sequence digested from pUC57-IgG4CAR and used to obtain pIgG4-Cassette

AAG CTT GCC GCC ACC ATG GCT CTC CCG GTA ACA GCT TTG CTG TTG CCG CTT GCA TTG CTT CTT CAT GCG GCG CGC CCG GAA AGT AAG TAC GGG CCC CCG TGT CCG CCC TGT CCA GCG CCA CCA GTA GCT GGC CCG TCT GTA TTC CTC TTT CCC CCC AAA CCT AAG GAT ACA CTT ATG ATA AGT CGC ACC CCC GAG GTA ACT TGC GTA GTG GTT GAC GTG AGC CAA GAA GAC CCG GAA GTT CAA TTT AAC TGG TAT GTG GAC GGT GTT GAA GTT CAT AAT GCG AAA ACG AAA CCC AGA GAA GAA CAA

TTT CAG TCC ACC TAT AGG GTC GTG TCC GTT CTT ACC GTG CTT CAT CAG GAC
TGG TTG AAT GGG AAG GAA TAT AAG TGC AAG GTG AGT AAC AAA GGC TTG CCC
TCT AGC ATT GAA AAG ACG ATT TCT AAG GCC AAA GGT CAA CCG AGG GAA CCG
CAG GTG TAC ACC CTC CCT CCA AGC CAA GAA GAG ATG ACC AAA AAT CAG GTG
TCT TTG ACA TGT TTG GTT AAG GGC TTT TAT CCG AGC GAC ATT GCG GTA GAG
TGG GAA TCT AAC GGT CAA CCC GAA AAC AAT TAC AAG ACC ACA CCG CCA GTA
CTC GAT TCT GAC GGG GCT TTT TTT TTG TAT TCA CGA CTC ACA GTG GAC AAA
AGC AGA TGG CAG GAA GGT AAC GTG TTC TCA TGC AGC GTT ATG CAC GAA GCA
CTG CAC AAC CAC TAC ACA CAA AAG TCC CTT TCT TTG AGT TTG GGC AAA ATG
TTC TGG GTT CTT GTA GTA GTG GGT GGC GTA TTG GCA TGC TAC TCT CTC CTT
GTG ACG GTA GCT TTC ATA ATC TTT TGG GTG AAA CGG GGA AGA AAG AAG CTG
CTG TAC ATA TTT AAG CAG CCC TTC ATG CGG CCG GTT CAG ACA ACG CAG GAA
GAG GAC GGT TGT AGC TGC CGG TTT CCT GAA GAG GAA GAA GGG GGG TGC
GAA CTG AGG GTC AAG TTT TCT CGC AGC GCC GAC GCC CCT GCC TAT CAA CAG
GGA CAA AAT CAA CTG TAC AAC GAA TTG AAT TTG GGT CGC AGA GAA GAG TAC
GAC GTG TTG GAT AAA CGG CGG GGC CGA GAC CCG GAG ATG GGA GGC AAG
CCT AGG CGA AAA AAT CCG CAG GAG GGT TTG TAT AAT GAA CTC CAG AAG GAT
AAG ATG GCT GAG GCC TAT TCC GAG ATT GGA ATG AAG GGA GAG CGC AGG
CGG GGA AAA GGC CAT GAT GGA CTG TAT CAG GGC TTG TCA ACA GCT ACG AAA
GAC ACT TAC GAT GCC CTG CAC ATG CAG GCC CTC CCC CCG CGG TAA GTT TAA
AC

Figure 17. Synthetic DNA cassette used for the development of pCD8-Cass-HR and pIgG4-Cass-HR. *Bgl*II and *Mlu*I restriction sequences highlighted in green. Homology arms to the *AAVS1* locus highlighted in clear grey. *Nhe*I for plasmid linearisation highlighted in dark grey.

DNA sequence digested from pAAVS1-HR and used to obtain pCD8-Cass-HR and pIgG4-Cass-HR

AGA TCT CCT GCT GGG ATG ACG AGC GTA AGC CAC CAT GCC CAG CTG GGT TTT
ATT TAT TTT GGT TTT TTT CCT GAC CCC TTA ACT AGA AAT AAG CTC CAC GAG
AGC GGG ATC TTT TGT CTT CTG TGC ACT ACT TGT CCT CGG TTC TTA GAA CAG
AAC CTG AGA GAA CCT GAT CGC AAA TAT TTT TGG AAT GAA TGA ATG AAT GGG
TTC ACC AGG GCA CCA TGG GAA ACT GAG TCC GCA ACC TAG AAG CCA TGA AAG
ACA GTC CAC TTC CAA GCT TCC CTG GGT GAC CTC GCA GGG CAT GCT GGG AAA
TGA AAT TTG CGG TGA AAA GGT CAG GAC CAC GAT CCT AGG GCA CGC TGG GAA
ATG TAG CCC ACA GGG CCA CAC CCC TAA AAG CAC AGT GGG GTG CAA GGC ACC
TCA ACA ACT AGC AAA GGC AGC CCC GCT AGC ATA AAC ACA CAG TAT GTT TTT
AAG AGA AGG GGA GGC GGG ACG CA AGG GAG ACA TCC GTC GGA GAA GGC CAT
CCT AAG AAA CGA GAG ATG GCA CAG GCC CCA GAA GGA GAA GGA AAA GGG
AAC CCA GCG AGT GAA GAC GGC ATG GGG TTG GGT GAG GGA GGA GAG ATG
CCC GGA GAG GAC CCA GAC ACG GGG AGG ATC CGC TCA GAG GAC ATC ACG
TGG TGC AGC GCC GAG AAG GAA GTG CTC CGG AAA GAG CAT CCT TGG GCA
GCA ACA CAG CAG AGA GCA AGG GGA AGA GGG AGT GGA GGA AGA CGG AAC
CTG AAG GAG GCG GCA GGG AAG GAT CTG GGC CAG CCG TAG AGG TGA CCC
AGG CCA CAA GCT GCA GAC AGA AAG CGG CAC AGG CCC AGG GGA GAG AAT
GCA GGT CAG AGA AAG CAG GGA AGG CAA TGC AAG GAG TTT TTG AAT ATT ACA
AAT CAG TAA CGT TTA CGC GT

Figure 18. Synthetic DNA cassette used for the development of pCD8-CAR and pIgG4-CAR. *Mlu*I and *Sgs*I restriction sequences highlighted in green. EF-1α promoter highlighted in clear grey. Kozak and CD8 SP highlighted in dark grey.

DNA sequence digested from pEF1αP and used to obtain pCD8-CAR and pIgG4-CAR
ACG CGT TTT TTT TAG CGC GTG CGC CAA TTC TGC AGA CAT GAA TCA ACC TCT GGA TTC CGC CTC CCC GTC ACC ACC CCC CCC AAC CCG CCC CGA CCG GAG CTG AGA GTA ATT CAT ACA AAA GGA CTC GCC CCT GCC TTG GGG AAT CCC AGG GAC CGT CGT TAA ACT CCC ACT AAC GTA GAA CCC AGA GAT CGC TGC GTT CCC GCC CCC TCA CCC GCC CGC TCT CGT CAT CAC TGA GGT GGA GAA GAG CAT GCG TGA GGC TCC GGT GCC CGT CAG TGG GCA GAG CGC ACA TCG CCC ACA GTC CCC GAG AAG TTG GGG GGA GGG GTC GGC AAT TGA ACC GGT GCC TAG AGA AGG TGG CGC GGG GTA AAC TGG GAA AGT GAT GTC GTG TAC TGG CTC CGC CTT TTT CCC GAG GGT GGG GGA GAA CCG TAT ATA AGT GCA GTA GTC GCC GTG AAC GTT CCT CTG GCT AAC TAG AGA ACC CAC TGT AGT GAA CCG TCA GAT CGC CTG GAG ACG CCA TCC ACG GCC GCC ACC ATG GCC CTG CCT GTA ACC GCG TTG TTG TTG CCT CTT GCA CTT CTG CTC CAT GCG GCG CGC C